UARL REPORT J-970802-12

FRA-RT-71-63

HEAT-ASSISTED TUNNEL BORING MACHINES

Jeffrey P. Carstens, W. Richard Davison,
Choate A. Brown, Alan R. Smith, Frederick J. McGarry

United Aircraft Research Laboratories
East Hartford, Connecticut 06108

SEPTEMBER 1970

FINAL REPORT

Prepared for
FEDERAL RAILROAD ADMINISTRATION
and
URBAN MASS TRANSPORTATION ADMINISTRATION
Department of Transportation
Washington, D.C. 20591

The contents of this report reflect the views of the United Aircraft Research Laboratories which are responsible for the facts and the accuracy of the data presented herein. The contents do not necessarily reflect the official views or policy of the Department of Transportation. This report does not constitute a standard, specification or regulation.

TECHNICAL REPORT STANDARD TITLE PAGE

1. Report No.	2. Government Accession No.	3. Recipient's Catalog No.
FRA-RT-71-63	PB 197 243	

4. Title and Subtitle	5. Report Date
HEAT-ASSISTED TUNNEL BORING MACHINES	September 1970
	6. Performing Organization Code

7. Author(s)	8. Performing Organization Report No.
J. P. Carstens, W. R. Davison, C. A. Brown, A. R. Smith (Fenix & Scisson), F. J. McGarry (MIT)	J-970802-12

9. Performing Organization Name and Address	10. Work Unit No.
United Aircraft Research Laboratories, Corporation, East Hartford, Connecticut 06108	11. Contract or Grant No. FR-9-0035
	13. Type of Report and Period Covered Final Report February 1969 to April 1970
12. Sponsoring Agency Name and Address Federal Railroad Administration and Urban Mass Transportation Administration Department of Transportation Washington, D. C.	14. Sponsoring Agency Code OHSGT

15. Supplementary Notes

16. Abstract

A study was performed to determine: a) the increase in tunneling machine performance in hard rock resulting from heat weakening of the rock in advance of the tunneling machine, b) the increase in hourly cost incurred by the heating system, and c) the net effect of the increased performance and the increased hourly cost on the cost of the finished tunnel. Rock-cutting experiments were performed on Barre granite using a 1-kw CO_2-N_2-He gas laser for rock heating and disc-type cutters of various diameters. Analytical work included the preparation of specific heat-assisted tunneler designs and their expected performance and economics. An alternative form of using heat for tunneling was also investigated in which slots were melted in the rock instead of merely heating it. The study concludes that the operation of tunneling machines incorporating lasers to provide the heat weakening is technically feasible but economically unattractive. Radiant heaters have insufficient power density to effectively heat the rock, and high-temperature jets create serious environmental problems. However, the test program indicated that a more effective way to assist mechanical cutters would be to use concentrated thermal energy to melt shallow slots in the rock between cutter paths.

17. Key Words	18. Distribution Statement
Tunneling, Tunneling Machines, Lasers Radiant Heaters, Rock Cutting, Heat Weakening	Available for distribution by National Technical Information Service Operations Division Springfield, Virginia 22151

19. Security Classif. (of this report)	20. Security Classif. (of this page)	21. No. of Pages	22. Price
UNCL	UNCL	408	

Form DOT F 1700.7 (8-69)

FOREWORD

This is a final report on United Aircraft Research Laboratories Project No. 970802 entitled "Heat-Assisted Tunnel Boring Machines," covering work during the period February 1969 to April 1970. This program was performed under Contract No. FR-9-0035 with the United States Department of Transportation, Office of High Speed Ground Transportation and Urban Mass Transportation Administration, under the technical direction of Mr. W. N. Lucke.

The work performed under this contract was managed by the United Aircraft Research Laboratories (UARL). Subcontractors to UARL were the Materials Division of the Department of Civil Engineering at the Massachusetts Institute of Technology (MIT), who performed a rock-cutting test program on laser-heated rock, and Fenix & Scisson, Inc. (F&S), who provided data on penetration rates, cutter costs, and overall excavation costs of present-day mechanical boring machines. The Hamilton Standard Division (HSD) of United Aircraft also provided information on electron beam machine design and performed rock-kerfing experiments with their 25-kw non-vacuum electron beam machine.

Contributions to the study were made as follows:

UARL

Jeffrey P. Carstens	Program Manager, Kerfing Analysis, Economic Analysis
W. Richard Davison	Environmental Control System Analysis, Heat Transfer of Gas Jet Systems
Choate A. Brown	Design of Laser and Radiant Heater Systems, Radiant Heat Transfer, Kerfing Analysis
Antonio B. Caruolo	Layout of Laser Tunneler
Leons Bramanis	Layout of Laser Tunneler, Electron Beam Machine Design

MIT

Frederick J. McGarry	Rock-Cutting Test Program
P. F. Rad	Rock-Cutting Test Program
R. W. Pratt	Rock-Cutting Test Program

F&S

Alan R. Smith	Costs of Nonheat-Assisted Mechanical Boring
Ronald B. Stone	Determination of Cutter Costs

TABLE OF CONTENTS

	Page
INTRODUCTION	1
CHAPTER I - LASER-ASSISTED ROCK-CUTTING TESTS	5
CHAPTER II - GENERAL ANALYSIS OF HEATER SYSTEM DESIGN	69
CHAPTER III - DESIGN AND ANALYSIS OF HEATER SYSTEMS	141
CHAPTER IV - PERFORMANCE AND ECONOMICS OF PRESENT-DAY TUNNEL BORING MACHINES	215
CHAPTER V - ALTERNATE MODES OF THERMAL ROCK FRACTURE	249
CHAPTER VI - ECONOMIC ANALYSIS OF HEAT-ASSISTED TUNNEL BORING MACHINES	277
CONCLUSIONS	307
RECOMMENDATIONS	311
APPENDIX A - TEMPERATURE PROFILES IN ROCK	313
APPENDIX B - ROCK TEMPERATURE PROFILE PROGRAM	317
APPENDIX C - MAXIMUM PERMISSIBLE EXPOSURE LEVELS TO LASER RADIATION	319
APPENDIX D - DESIGN CONSIDERATIONS FOR ELECTRON BEAM MACHINES	321
REFERENCES	325

INTRODUCTION

Background

Rock tunneling machines have been developed in the last decade to the point where they are being extensively used in both soft and medium-hard rock conditions with performance and cost advantages over traditional drill-and-blast methods (e.g., Ref. 1). Although these machines have clearly demonstrated the advantages of continuous operation and smooth-wall tunneling, they have not yet been found capable of economic operation in the relatively hard rock types. This limitation is due mainly to the inability to penetrate these rocks economically with present-day mechanical cutters.

To promote the development of rock-boring machines which will extend the range of rock types which can be economically bored into the range of very hard rocks, several new types of rock-destruction mechanisms have been considered. Basically three modes of using heat for rock destruction have been under investigation. Heat can be used to: (a) weaken, (b) spall, and (c) melt and/or vaporize rock. The last method has been shown to involve tremendous quantities of energy and has not seriously been considered as a primary method for rock excavation. The second method, that of thermal spalling, has been the subject of a prior study by United Aircraft (Ref. 2) and does appear to offer promise for very hard rock situations where the rock demonstrates good spallability. However, the development of systems required to exploit the spalling method involves the application of new technology in machine design and methods of life support for crew protection and operation in a hot and toxic environment.

The first method of using heat to weaken rock in conjunction with mechanical tunneling machines is the subject of this study.

Basic Concept of Heat Weakening

The basic phenomenon of weakening a rock mass by the application of heat has been under study at the Massachusetts Institute of Technology since 1965 (e.g., Refs. 3 through 8). This work has demonstrated that the application of heat to rock causes a significant decrease in mechanical strength. This weakening is associated with an increase in the microcrack structure caused by heat flow and resulting tensile stress field. Reference 5 contains some quantitative information on heat weakening in terms of the amount of energy applied to a piece of rock, the power level of the energy being applied, and the resulting decrease in the modulus of rupture of a small beam of rock. This modulus is measured in a three-point bending test of the rock beam which has been subjected to laser radiation. A summary of the results of these tests on blocks of granite is shown in Fig. 1.

Referring to Fig. 1, an increase in the energy supplied to the rock beam results in a significant decrease in the modulus of rupture, to the point where, with a large amount of heat added, the rock has lost over 90% of its original strength.

The basic objective of the present study is to determine whether the phenomenon which is quantitatively described by the tests resulting in the data shown in Fig. 1 can be successfully (i.e., both technically and economically) applied to the design and operation of a full-scale tunnel boring machine. This machine would incorporate a heating system to preweaken the rock by heating it in advance of the otherwise normal mechanical cutters mounted on the tunneling machine face. The attainment of this objective involves (a) a test program to evaluate the effects of heat in terms of increased borability, by boring the rock in the same manner it would be bored by a mechanical tunneling machine (rather than failing the rock in a bending test), (b) the gathering of information on present-day mechanical tunnel boring machines and determining the economic limitations thereon as a function of the strength and borability of rock, (c) the design and analysis of various types of potential heating systems that could be added to a tunnel boring machine to make it a heat-assisted tunnel boring machine, and (d) the performance and economic analysis of such a heat-assisted tunnel boring machine. These four tasks comprise the approach to this program.

Organization of This Report

The main body of this report consists of six chapters. Chapter I contains a complete discussion of the test program wherein rocks were irradiated with a laser beam and bored in a manner similar to the boring action of a full-scale tunneling machine to determine the effects of heat weakening rocks in a quantitative manner. This test program was conducted by the Massachusetts Institute of Technology, Civil Engineering Department, under the general direction of Professor F. J. McGarry. In Chapter II is presented a preliminary analysis of heating power requirements for full-scale tunnel boring machines in the diameter range of 10 to 20 ft, and a preliminary analysis of the various possible systems and problems of heating rock in advance of a tunnel boring machine. In Chapter III particular attention is given to the detailed design of several specific heater types, with the greatest emphasis given to a laser-assisted tunnel boring machine. The economics of present-day tunnel boring machines without heat-assist is considered in Chapter IV. This material was developed by Fenix & Scisson, Inc., under the general direction of Messrs. A. Smith and R. B. Stone. Work done on the heat-assisted mode of hard rock tunneling led, during the course of the study, to the formulation of a basically different method of applying heat in advance of mechanical cutters. This mode, in which a physical kerf is made by the melting and vaporization of rock, is analyzed in Chapter V. Finally, in Chapter VI the economics of heat-assisted tunnel boring machines are explored based on the data developed in Chapters I through V.

HEAT INPUT OVER 7.1 CM^2

SOURCE: REF. 5

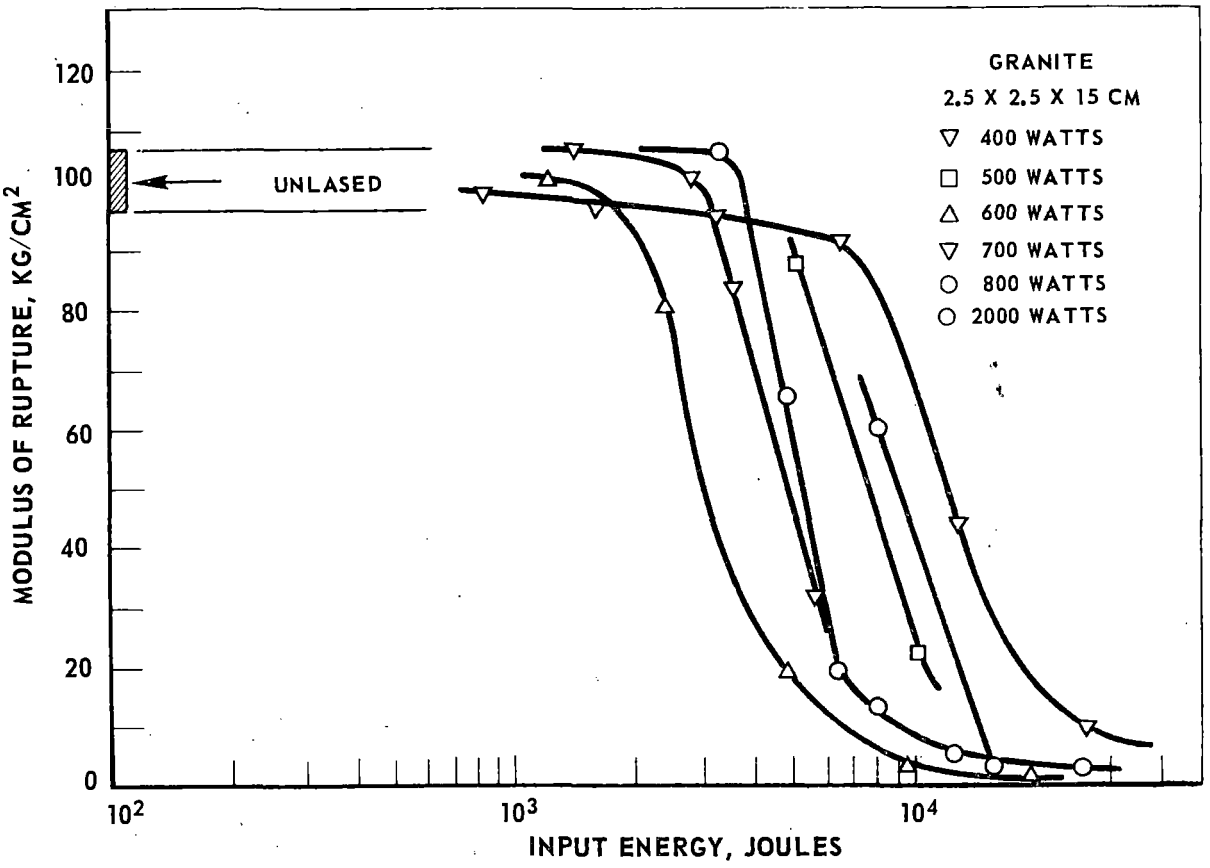

FIGURE 1 REDUCTION IN STRENGTH OF HEATED ROCK

CHAPTER I - LASER-ASSISTED ROCK-CUTTING TESTS

This chapter presents the results of a rock-cutting test program performed at MIT to yield quantitative results on the effect of heat weakening hard rock in advance of a mechanical cutter. The research discussed here is a continuation of work done previously in which it had been established that radiation from a continuous, one-kilowatt gas laser drastically reduced the strength of hard sound rock (Refs. 3 through 8).

MATERIALS, APPARATUS, AND TEST PROCEDURES

Figure 2 shows the rock cutter testing device which was lent to MIT by the Ingersoll-Rand Research Laboratory. The device consists of a fixed vertical frame which can hold various cutters which bear on rock samples placed on the horizontal, hydraulically driven table. Modifications to the device were made to allow the following modes of operation and test characteristics:

Cutter Thrust:	0 to 3000 lb, held constant by hydraulic cylinder 0 to 10,000 lb, held constant by hydraulic cylinder Variable, under fixed cutter displacement conditions
Work Table Velocity:	0.10 to 5.0 in./sec
Disk Cutter Diameters:	3, 4, 5, and 11½ in. nominal 60 deg included angle
Force Measurements:	Vertical, on cutter, versus time; Horizontal, on cutter, versus time.
Recorder:	Integrates horizontal force versus displacement to indicate work expended by the cutter.

The rock material chosen as a standard was Barre (Vermont) granite quarried by the Rock of Ages Corporation. The characteristics of Barre granite are given in Table 1. Sample size was 4 by 13 by 14 in.; the surfaces were in the sawed condition with no coarse irregularities or ridges. All (approximately 220 samples) were cut at one time from a single quarry block, with the grain orientation held constant to ensure uniformity. For testing with the 11½-in. cutter and also with higher thrust forces, a limited number of larger-size blocks (8 by 13 by 20 in.) was obtained.

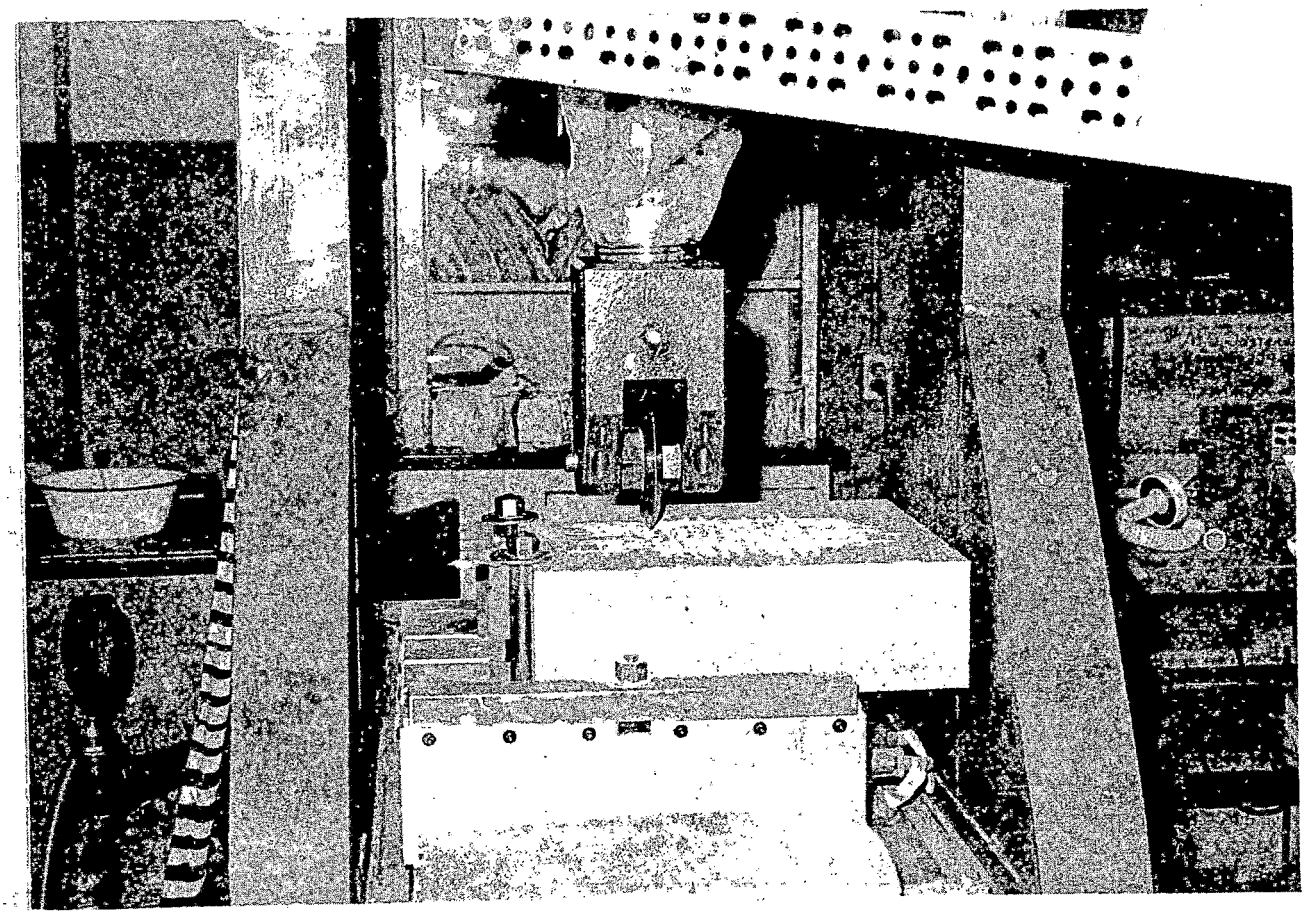

FIGURE 2. ROCK CUTTER TESTING DEVICE WITH 5–INCH–DIAMETER DISK CUTTER

TABLE 1

PROPERTIES OF BARRE GRANITE

Source	Rock of Ages Quarry, Graniteville, Vermont
Color	Blue-gray
Rock Type	Quartz monzonite
Density	165.5 lb/ft^3
Specific Gravity	2.64
Grain Texture	Fine grained 3 mm
Compressive Strength	32,000 psi
Young's Modulus of Elasticity	
Head grain on top	3.5 to 4.0 x 10^6 psi
Head grain on the side	5.0 x 10^6 psi
Head grain on the end	7.0 x 10^6 psi
Modulus of Rupture	2000 psi
Hardness	
Scleroscope	102
Rockwell C scale	72
Moh's Scale	Quartz - 7 Feldspar - 6 Mica - 3
Thermal coefficient of expansion	
inch/inch/degree F	4 x 10^{-6}
inch/inch/degree C	6.2 x 10^{-6}
Water Absorption	
% by weight	0.23
Petrographic analysis	
% by volume	65 Feldspar 27 Quartz 8 Mica

TABLE 1 (Continued)

PROPERTIES OF BARRE GRANITE

Dominating Mineralogical Constituents

Mineral	Formula	Weight %
Quartz	SiO_2	23.2
Orthoclase	$KAlSi_3O_8$	2.7
Microline	$KAlSi_3O_8$	26.4
Plagioclase	$8NaAlSi_3O_8$	
(Oligoclase $Ab_{80}An_{20}$)	$2CaAl_2Si_2O_8$	31.7
Muscovite	$KAl_2(OH)$	6.4
	$(AlSi_3O_{10})$	
Biotite	$K_2(Mg,Fe)_2(OH)_2$	4.5
	$(AlSi_3O_{10})$	
Chlorite (Penninite)	$Mg_5(Al, Fe)(OH)_8$ $(Al, Si)_4)_{10}$	2.1
Calcite	$CaCO_3$	1.6
Sphene	$CaTiSiO_5$	0.7
Magnetite	Fe_3O_4	0.4
Leucoxene	$TiO_2 \cdot H_2O$	trace
Zircon	$ZrSi \cdot O_4$	0.1
Apatite	$3Ca_3(PO_4)_2 \cdot CaF_2$	trace
Pyrite	FeS_2	trace
		99.9

Chemical Composition

SiO_2	68.1
TiO_2	0.3
Al_2O_3	16.5
Fe_2O_3	0.3
FeO	1.3
MgO	0.8
CaO	2.4
Na_2O	3.6
K_2O	5.3
H_2O	0.6
CO_2	0.7
ZrO_2	0.1 (-)
P_2O_5	trace
F	trace
ThO_2	trace
UO_2	trace
S	trace
	100.0

The laser used for the heating was a CO_2-N_2-He continuous laser with a rated output of 1 kw. The laser beam was reflected by two mirrors onto the surface of the specimen (Fig. 3). Immediately in front of the laser was an optically flat mirror (Fig. 4); the second mirror (Fig. 5) is also flat for investigating the effect of the unfocused beam. In other tests this second mirror was replaced by a concave focusing mirror whose focal length was such that the focal point of the beam fell on the specimen surface.

The operating mode of the cutting device was modified to one of constant vertical thrust for the purposes of this study. Holding the vertical thrust at a fixed value, tests were run with different diameter disk cutters, with varying distances between cutter paths. The muck produced by each pass of the cutter was gathered by a hand-held vacuum cleaner and then weighed to the nearest 0.10 gram on a laboratory scale. Two channels of a strip chart recorder made continuous records of horizontal and vertical loads on the cutter for each pass; a disk integrator measured the work done by the cutter in each pass.

To find the effects of cutting pattern on specific energy, in one type of test the cuts were made by repeated passes over the same path. In another, the cuts were performed with different lateral distances between adjacent grooves or paths.

With the $11\frac{1}{2}$-in. cutter, splitting of the blocks was encountered on many occasions. Some data were obtained, but these experiments were generally unsatisfactory.

The gas laser was used in two ways. For "cold" tests each block was passed repeatedly under the reflected laser beam at a specified speed, producing parallel lased paths at equal intervals. The energy input per linear inch of beam travel was therefore inversely proportional to the table speed. The actual cutting of the specimens was done after they had cooled completely; the disk cutter traveled directly in the center of the lased paths.

In the "hot" tests the cutting was performed simultaneously with the lasing. The beam was aimed 5 inches ahead of the cutter, and therefore the time lag between lasing and cutting as well as the heat input were determined by table speed. Some tests in this series were run with the focusing mirror; cutting in this case was done directly on the lased path and also 0.5 in. to one side of it. The cutting in all the unfocused hot tests was done directly on the lased path, as shown schematically in Fig. 6.

With the focusing mirror in place, the heated strip of rock was about 3/8 in. wide. With the flat nonfocusing mirror, the heated path was about 1 in. wide.

The results of the experiments are reported by mean value and standard deviation for each set of data points. Where possible and appropriate, a linear regression curve has been calculated using the least squares technique. The

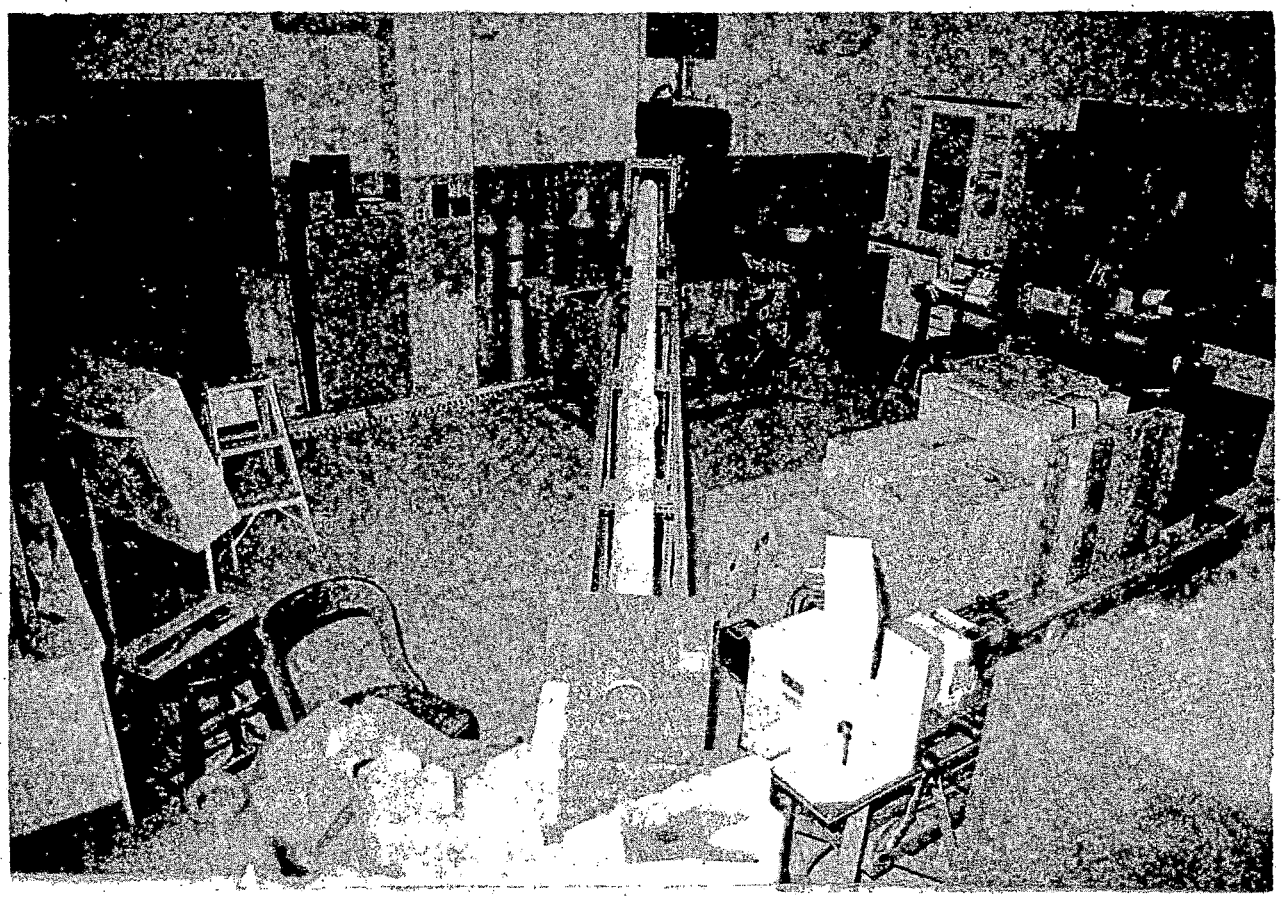

FIGURE 3. OUTPUT END OF THE GAS LASER, PROTECTIVE PIPE, AND TESTING DEVICE

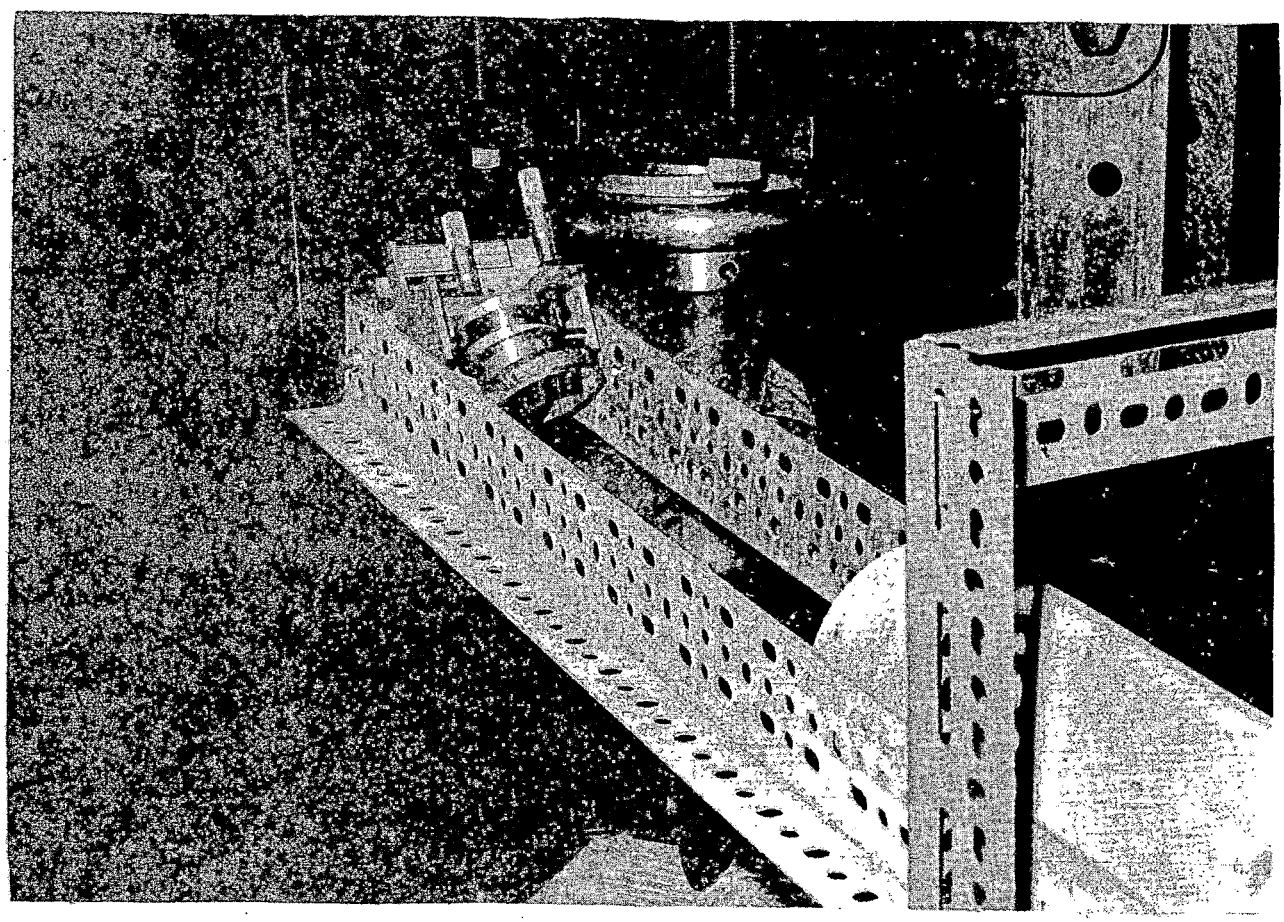

FIGURE 5. HOLDER FOR SECOND MIRROR TOGETHER WITH TESTING DEVICE

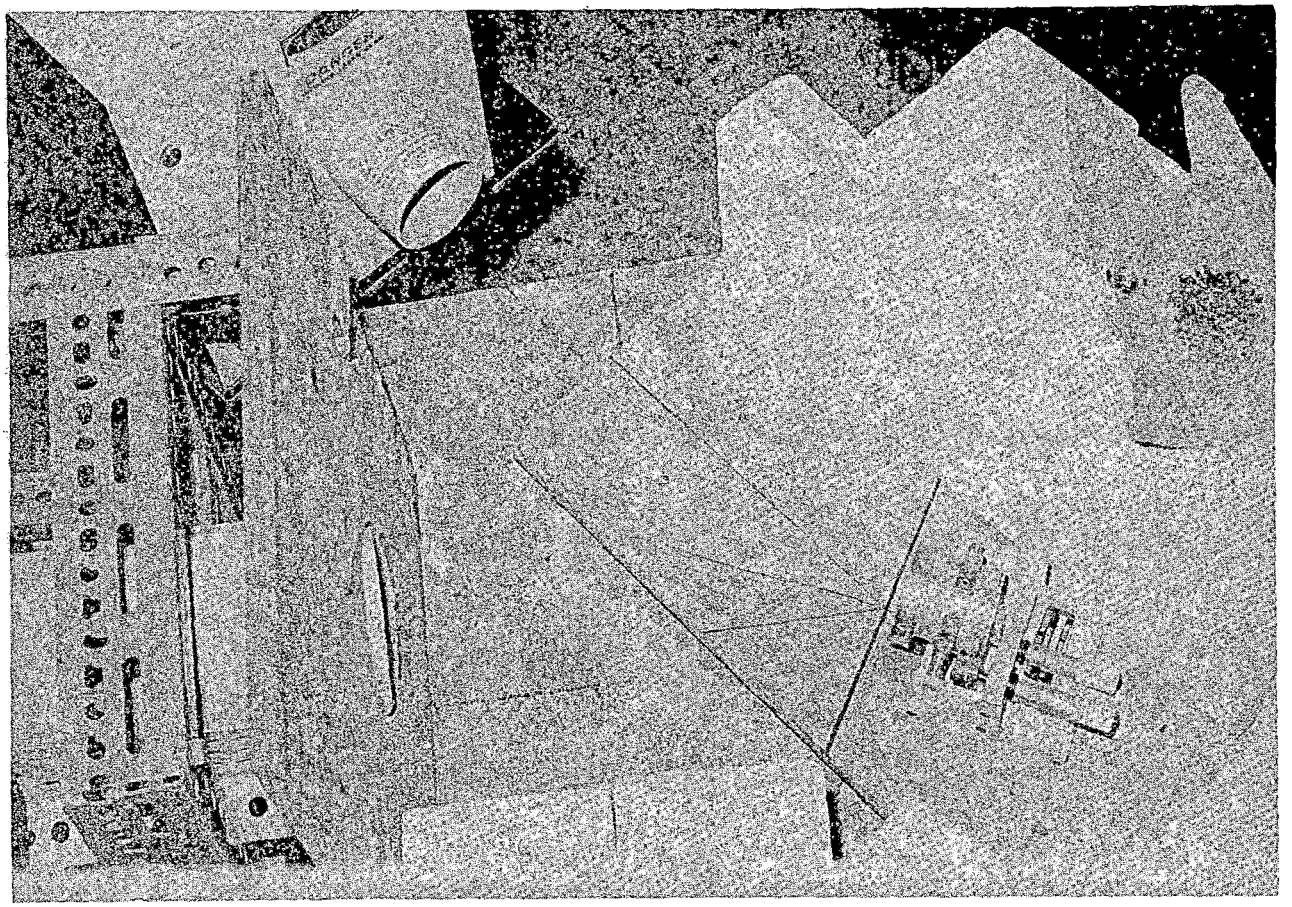

FIGURE 4. OUTPUT END OF GAS LASER, HOLDER, AND REFLECTING FLAT MIRROR

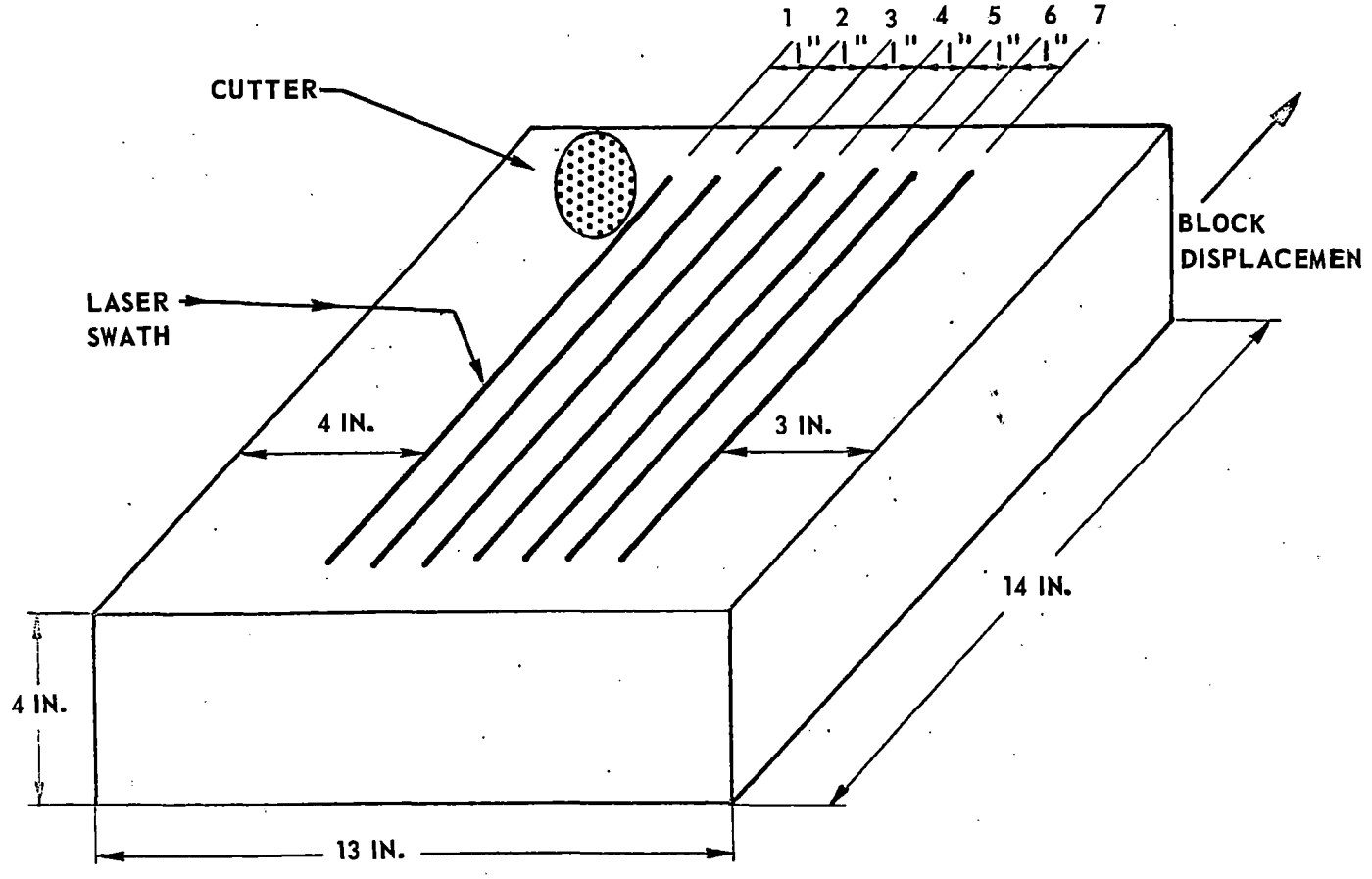

FIGURE 6. CUTTING PATTERNS AND SCHEMATIC OF HEATING AND CUTTING ARRANGEMENT

scatter of the data points about the curve was also calculated, indicating the reliability of each fit. In general, the regression correlation coefficient for the specific energy data was 0.95 or better and for muck removal data was 0.70 or better.

In the following three sections, the results of the test program are presented in detail. The first section contains the results of all the tests done on rock that had not been lased. All tests involving rock heating with the laser are presented in the second section, and the final section is a summary of the data in the form to be used in the economic analysis.

TEST RESULTS - UNTREATED ROCK

Single Cuts on a Smooth Surface

Groove Spacing

For a fixed cutter force and diameter, there exists a "critical spacing" for parallel cuts; at larger spacings the cuts are independent, and at smaller, there is chipping between adjacent grooves. The chips formed in this manner are considerably larger than the powdery debris produced by independent cuts; the amount of muck produced per cut is greater, and the specific energy is generally lower than for the wider spacings. This reflects the fact that the specific energy is related to the fracture surface energy required to produce the debris, and the amount of surface area per unit volume is lower for large chips.

As the groove spacing is decreased below the critical value, the average chip size increases and then diminishes again since the maximum chip width is seldom larger than the groove spacing. Thus there also exists an "optimum spacing" with regard to specific energy and muck. Figures 7 and 8 show the variation of these quantities as the groove spacing increases through the optimum value, 3/8 in., and the critical value, 1 in. For values larger than 1 in., the cuts do not intersect, and the test results become independent of spacing. The samples with spacings of $\frac{1}{2}$ and $\frac{3}{4}$ in. were turned 90 deg after cutting and another series of cuts was made in the perpendicular direction. The greatly reduced specific energy so obtained is in keeping with the concept of fracture surface energy; perpendicular cutting forms large chips, as the muck values indicate. The critical and optimum spacings vary with cutter diameter, cutter thrust, and cutter speed.

Cutter Diameter

With thrust held constant, critical and optimum spacings decrease as the cutter diameter increases in the range tested (3, 4, and 5 in.) because a small cutter has a smaller contact area on the specimen and hence a higher local stress

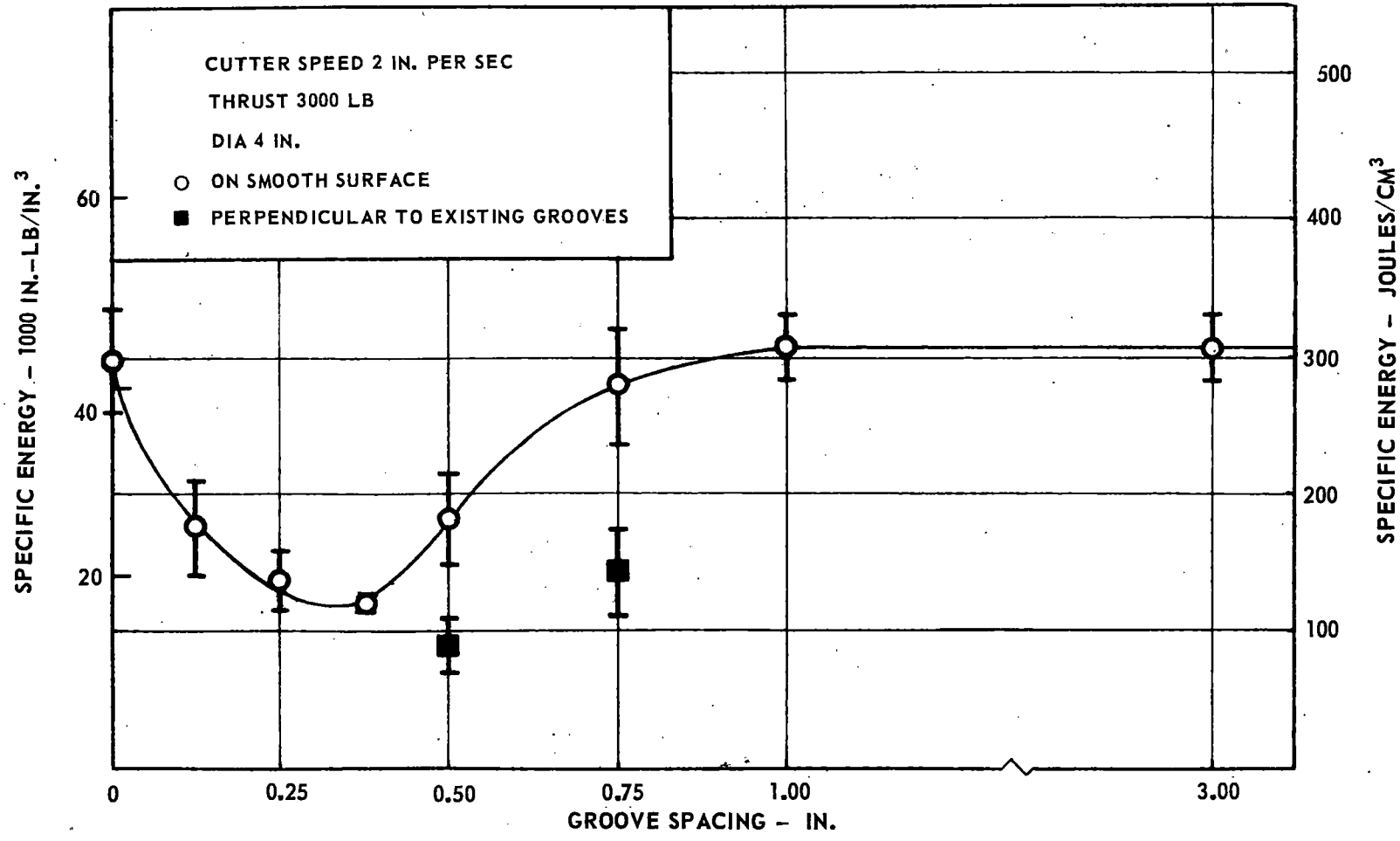

FIGURE 7. SPECIFIC ENERGY VERSUS GROOVE SPACING

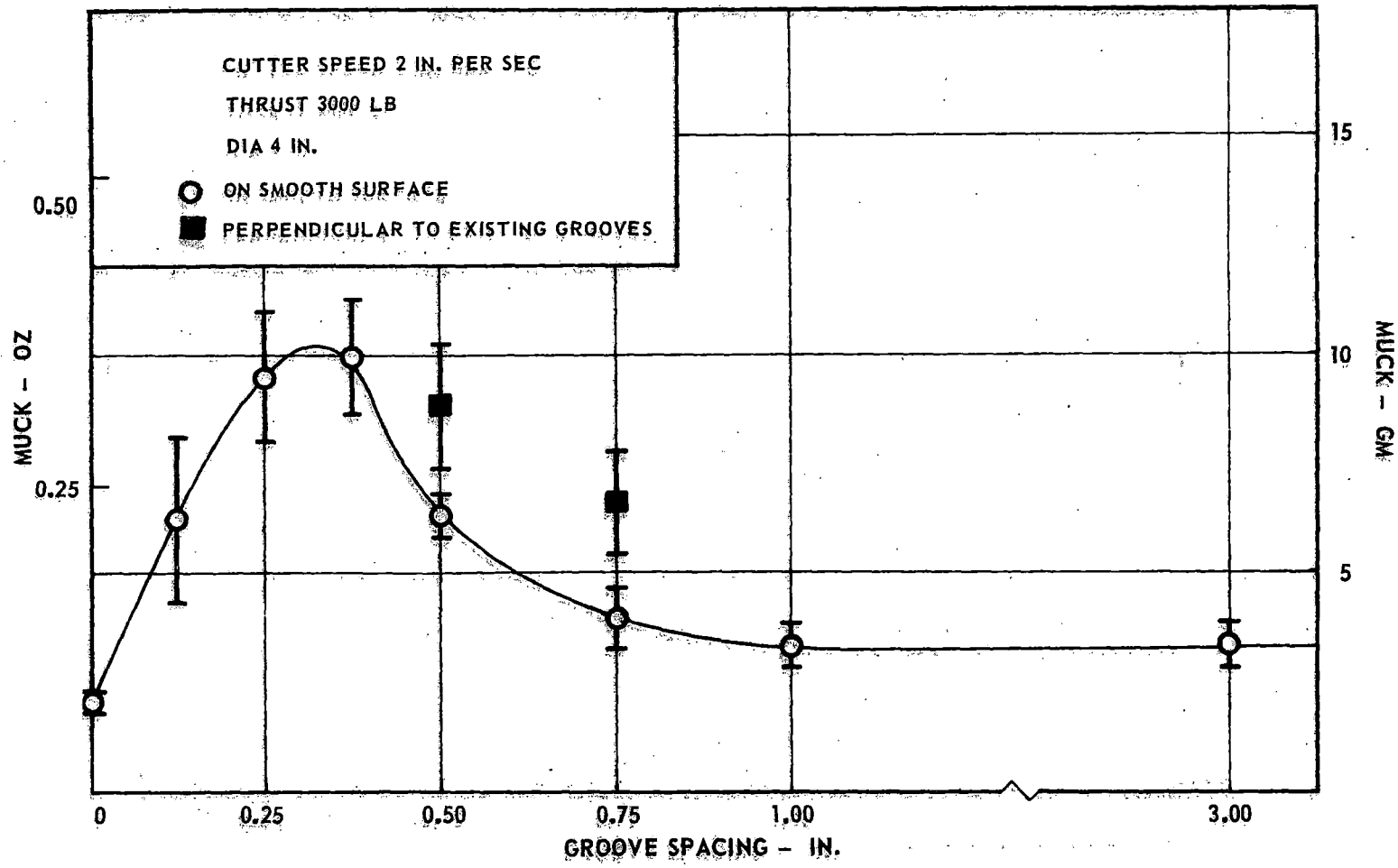

FIGURE 8. MUCK VERSUS GROOVE SPACING

which produces more chipping, to greater distances, than the large cutters. Figures 9 and 10 show that the larger tools give poor results compared to the three-inch one; at the spacing of $\frac{1}{2}$ inch the larger cutters appear to be operating away from their respective optimum spacings.

Thrust

Increasing the cutter thrust has the same effect as reducing the diameter: the critical and optimum spacings are increased, because of the higher contact stresses. The data in Fig. 11 were obtained with a full-size, $11\frac{1}{2}$-in.-diameter, tunneling machine cutter at a thrust of 12,500 lb. The critical spacing, approximately $2\frac{1}{2}$ in., is much larger than for the 3000-lb thrust results of Fig. 7, even though the increased diameter tends to decrease the critical spacing. Data points at small spacings could not be obtained for Fig. 11 due to equipment limitations which make high-thrust tests very difficult; the optimum spacing is estimated to be about one inch for these conditions.

Figure 12 shows some effects of increasing the thrust for independent cuts with a 4-in. tool. Muck values increase smoothly, in a nonlinear manner, up to about 6000 lb. The results for higher thrust values are not reliable since the horizontal forces encountered were sufficient to stop the specimen table completely several times during each cut; it could be freed only by lifting the cutter temporarily, resulting in greatly reduced values of muck. Data for thrusts greater than 6000 lb with a 4-in. cutter could not be obtained for the same reason.

To provide detailed information for subsequent comparison with heated tests, experiments were run at a cutter thrust of 5000 lb for cutter diameters of four and six inches. Due to limitations in the test equipment, cutter drag forces could not be measured at these thrust levels, and specific energy could not be measured. The resulting muck was measured, however, and is presented in Fig. 13.

Cutter Speed

Granite, like most other minerals, is rate sensitive; i.e., its strength and other mechanical properties change if the rate of load application is changed (Ref. 9). The load rate in the cutting tests is directly related to the linear cutter speed, so the cutter speed may affect all results: muck, specific energy, and optimum and critical spacings. Figure 14 shows the variation of specific energy with cutter speed for cuts on a smooth surface. The fact that the observed ratio of crushed material to chips is greater at high speeds helps explain the increase of specific energy, since, as shown in Fig. 15, the corresponding values of muck removed are independent of cutter speed.

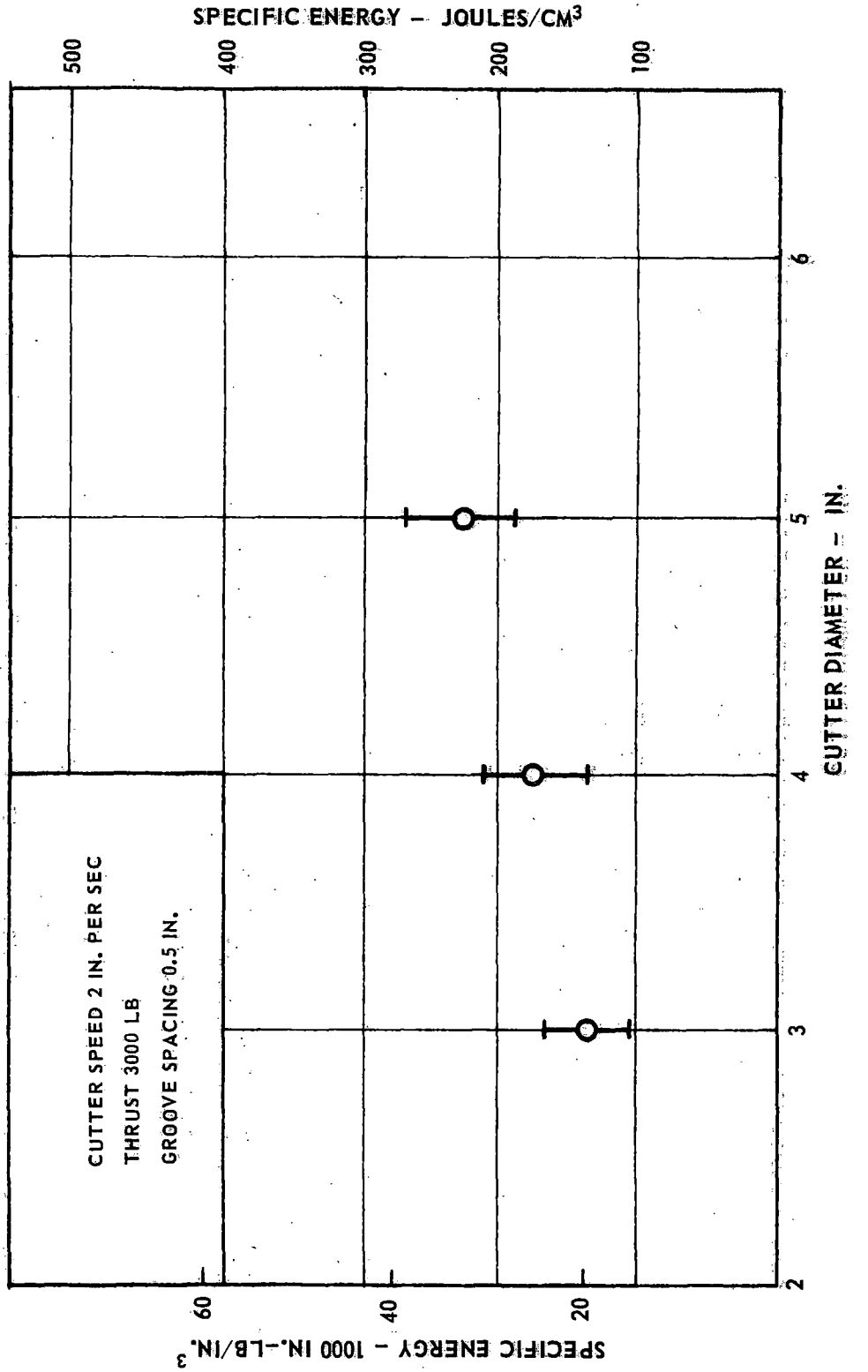

FIGURE 9. SPECIFIC ENERGY VERSUS CUTTER DIAMETER

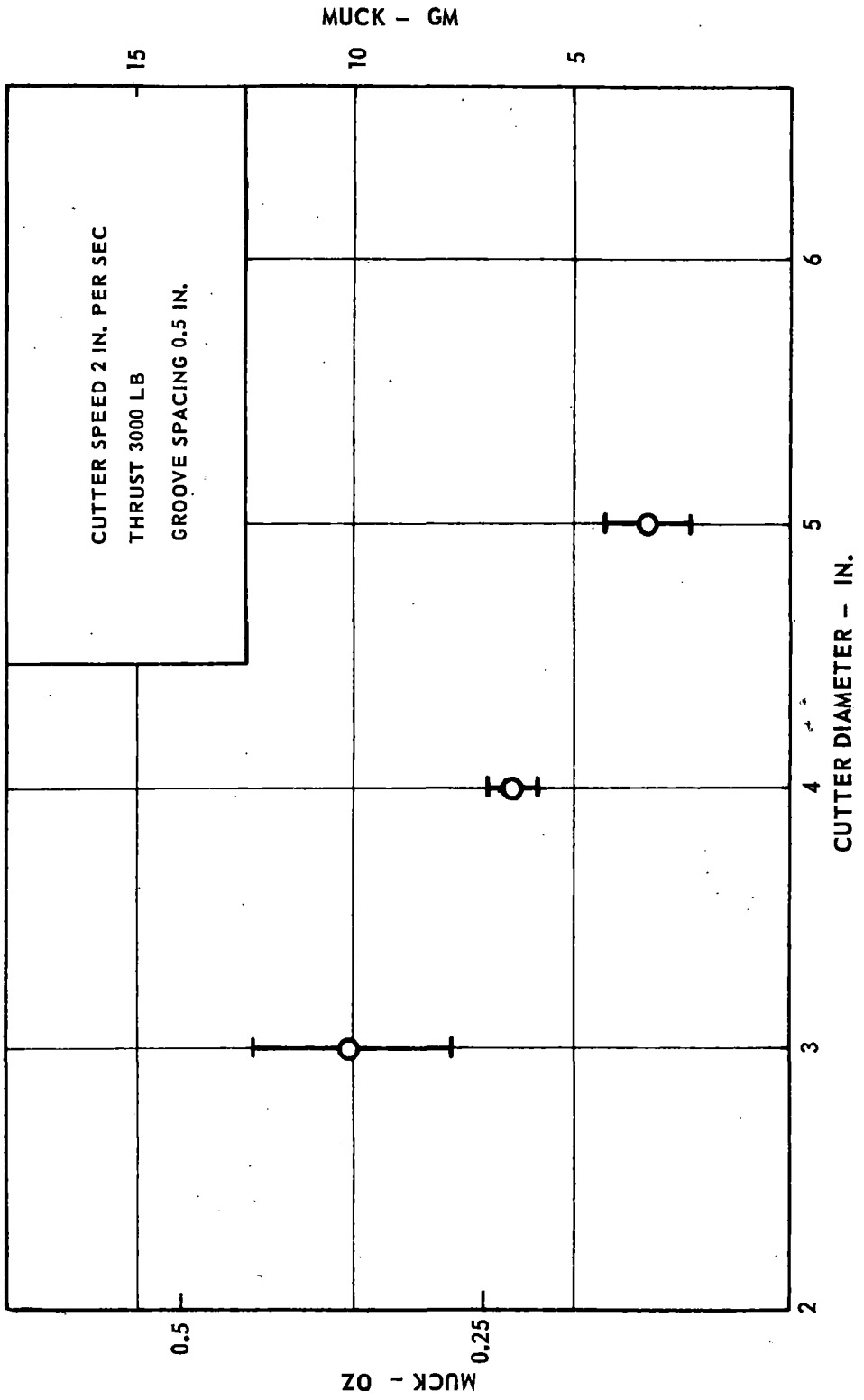

FIGURE 10. MUCK VERSUS CUTTER DIAMETER

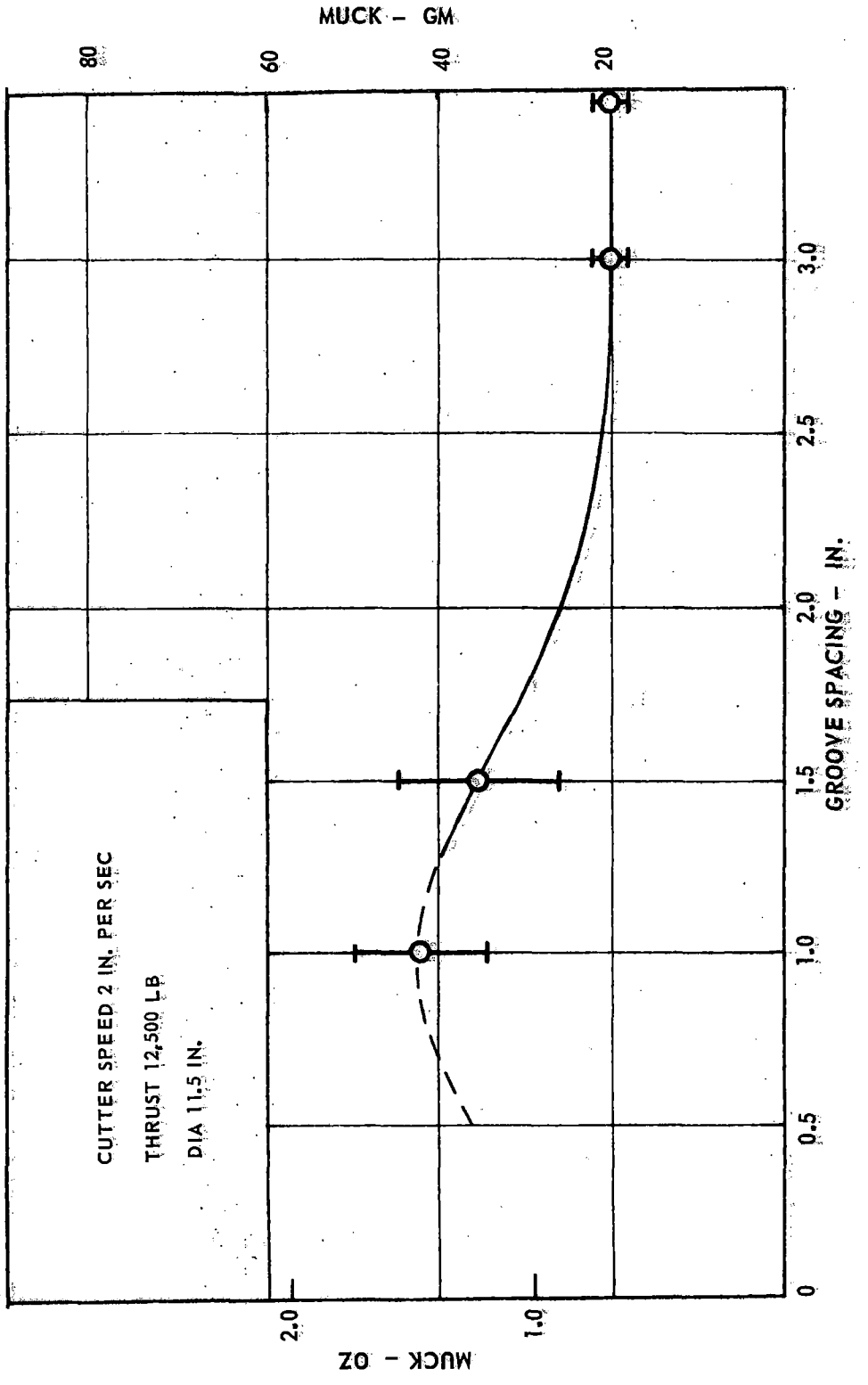

FIGURE 11. EFFECT OF GROOVE SPACING ON MUCK REMOVED FROM A SMOOTH SURFACE AT HIGH CUTTER THRUST

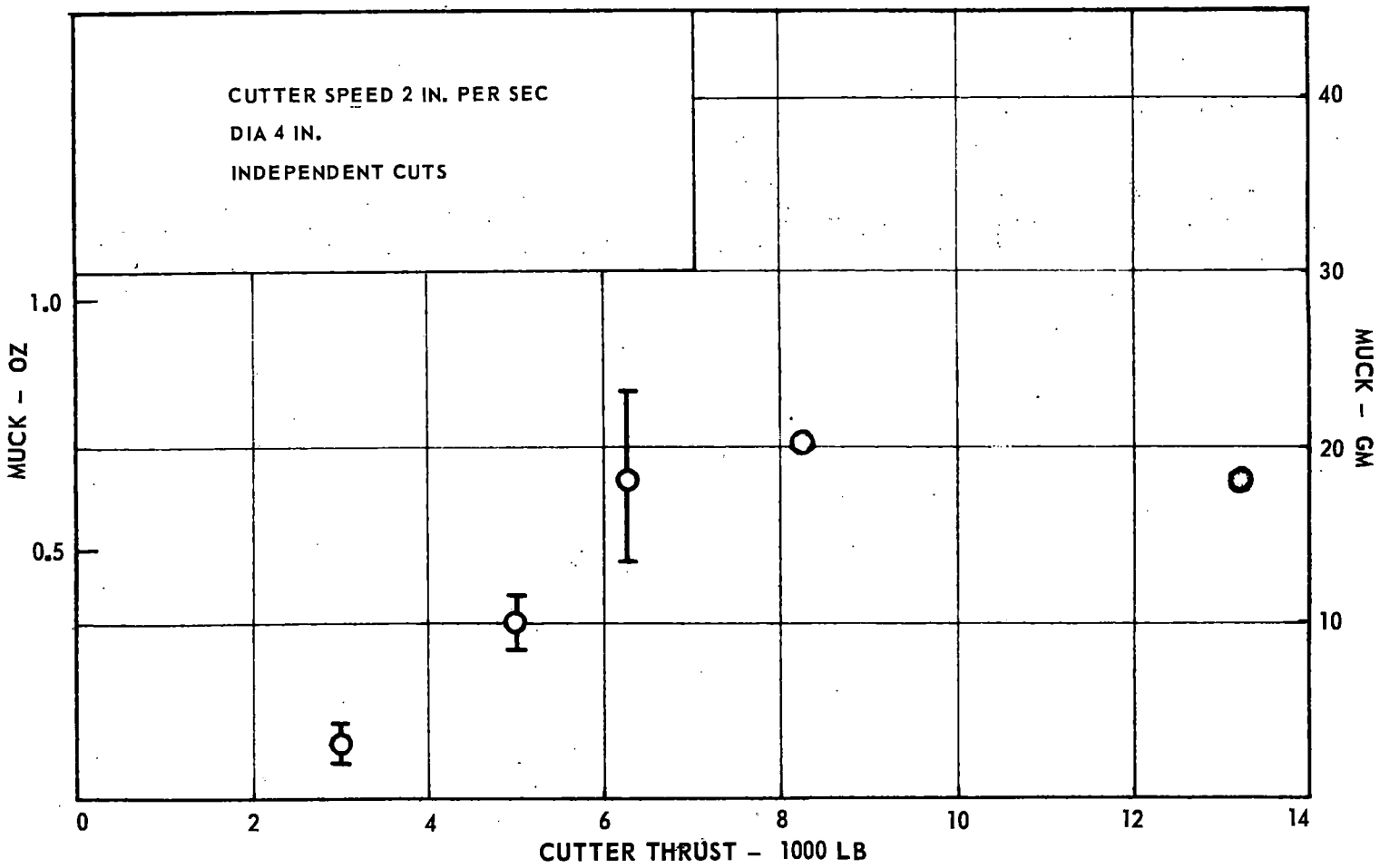

FIGURE 12. MUCK VERSUS CUTTER THRUST

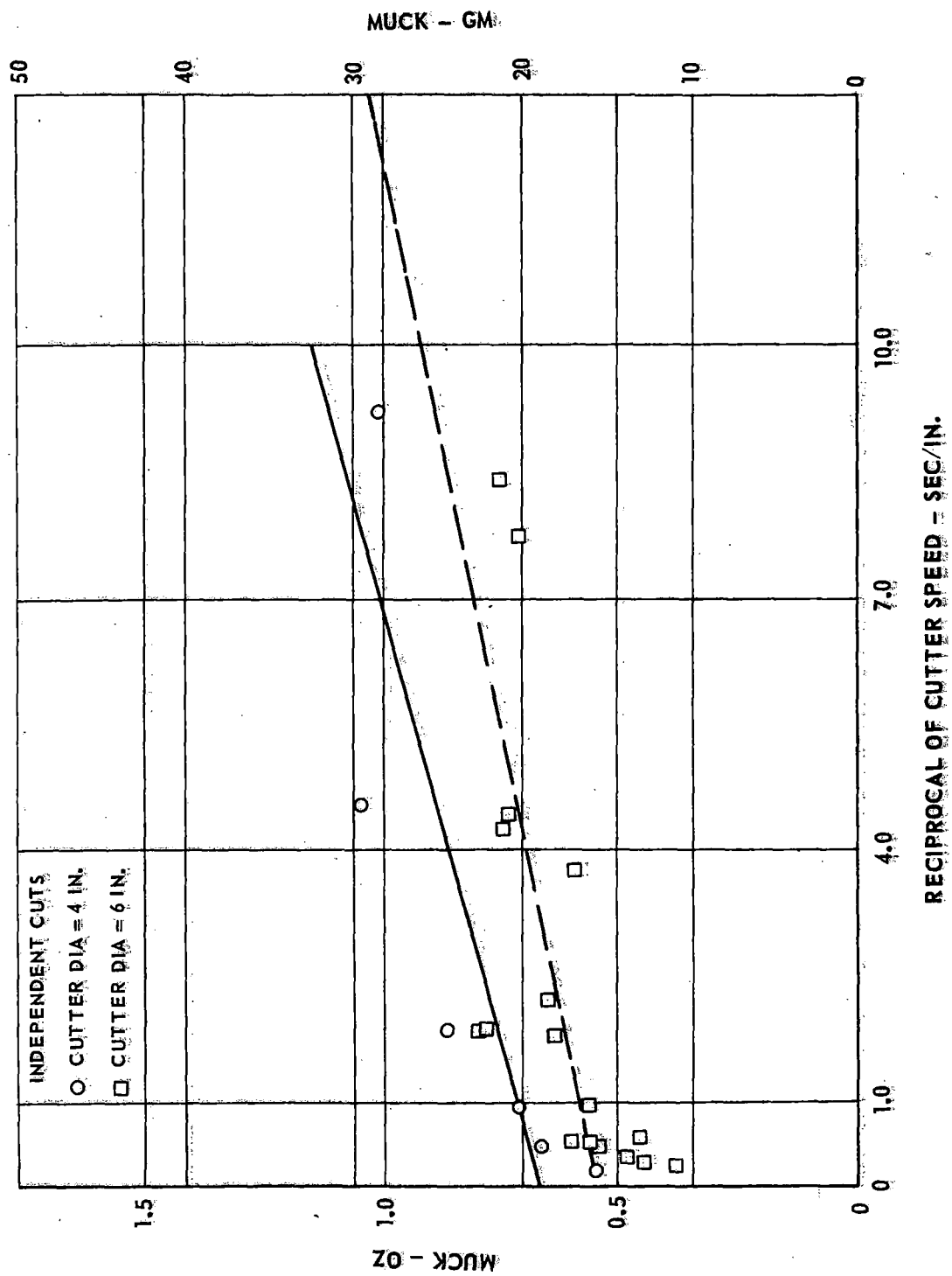

FIGURE 13. MUCK REMOVAL AT 5000 LB CUTTER THRUST

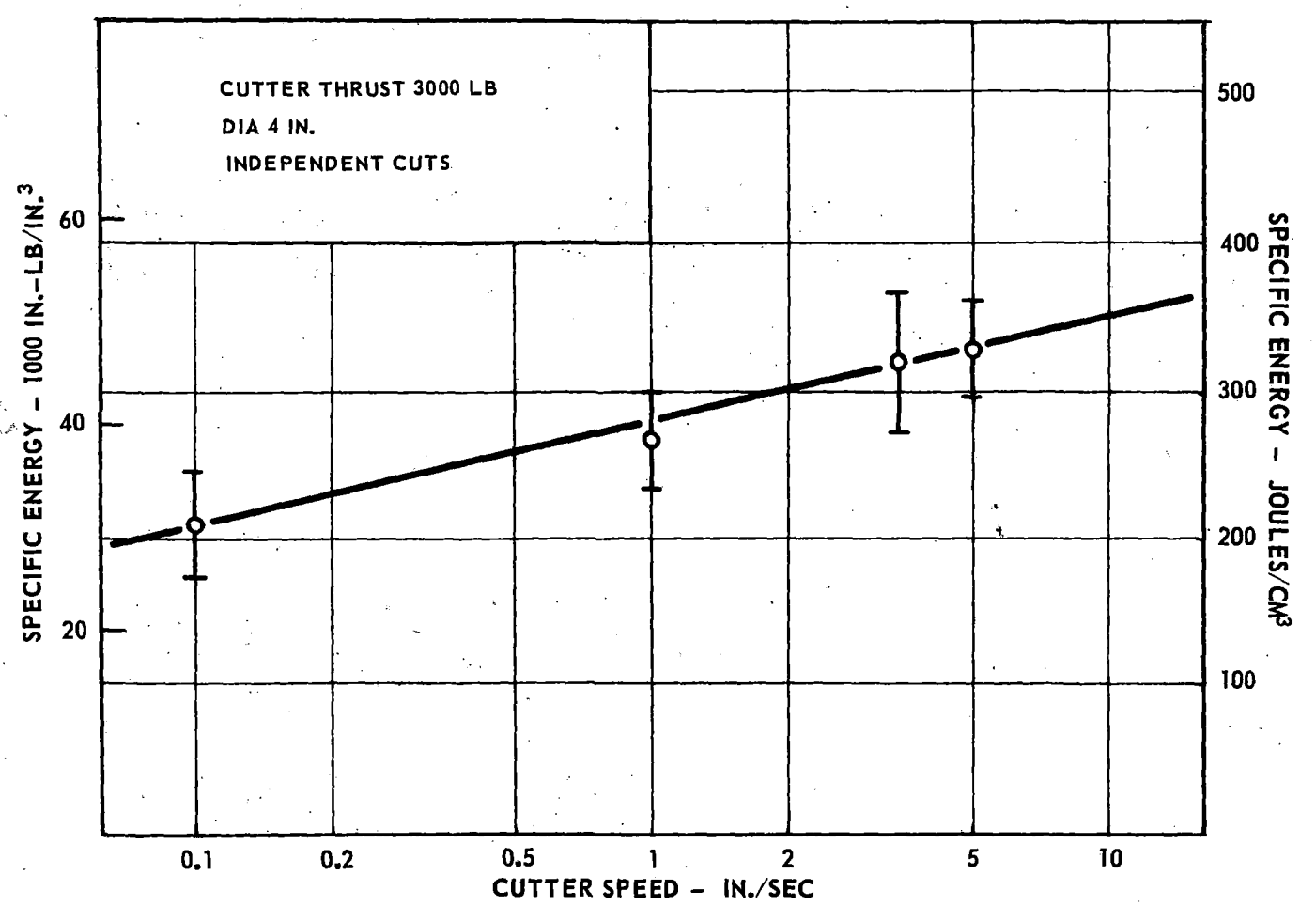

FIGURE 14. SPECIFIC ENERGY VERSUS CUTTER SPEED

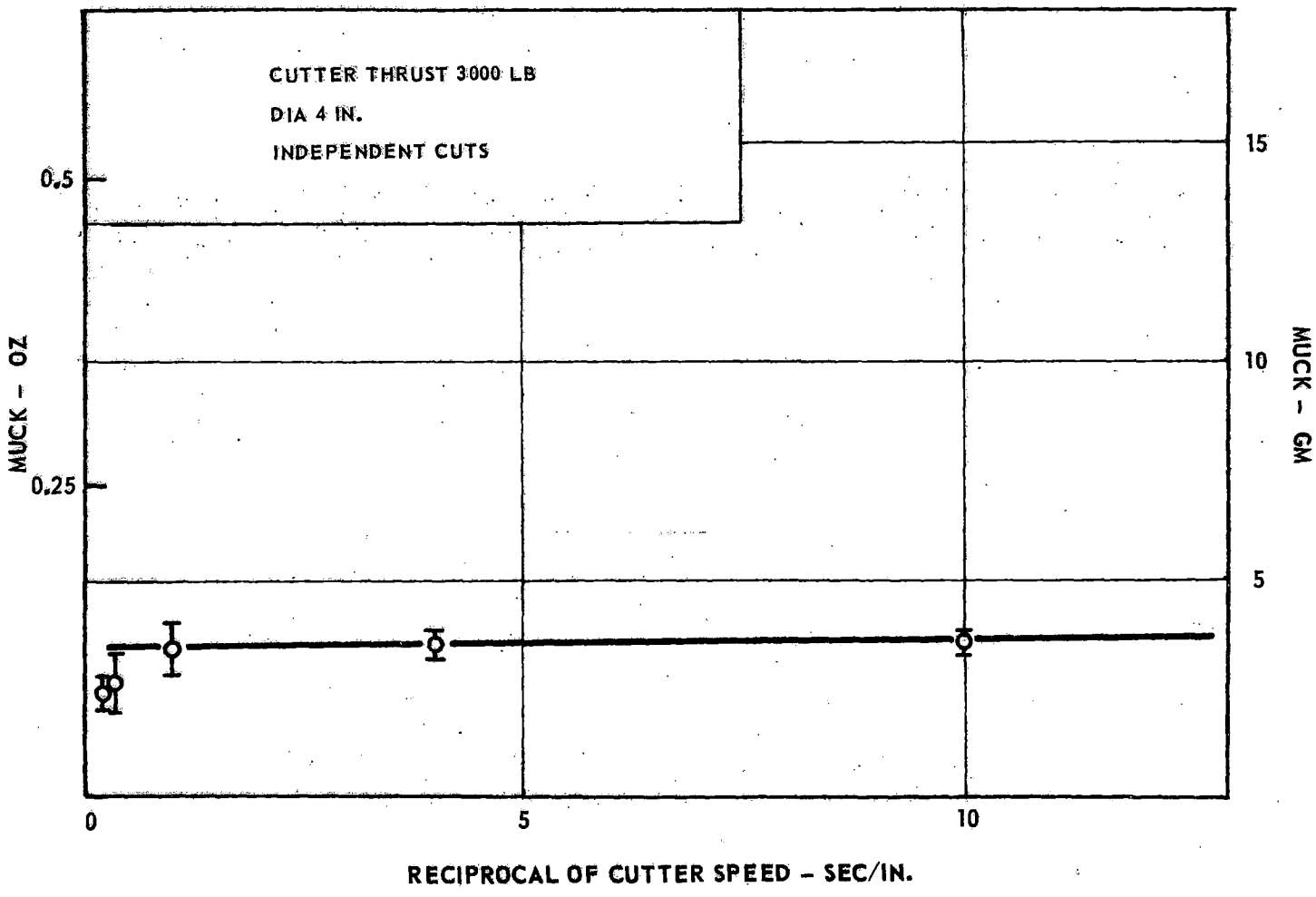

FIGURE 15. MUCK VERSUS CUTTER SPEED

Multiplicity of Cuts

All of the above data are based on cutting an initially smooth surface. However, tunneling machine cutters usually travel on circular paths continuously, and therefore work on a roughened tunnel face. There are two factors which contribute to muck removal in this multiple pass situation: the cutters continue to penetrate further into the groove each pass by removing additional muck from the groove, and neighboring grooves interact with each other, causing chips as large as the groove spacing to be formed. The efficiency of this process depends on choosing the correct groove spacing for the particular operating conditions: rock type, thrust, cutter diameter, and speed. This section concerns the effects of cutting repeatedly over the same path, both independently (i.e., with the distance between cutter passes greater than the "critical" distance) and with interactions between neighboring grooves.

Multiple Independent Cuts

When the 3-in.-diameter cutter was passed over the surface of the rock with a thrust of 300 lb, the resulting groove was roughly 0.1 inch deep. Subsequent passes increase the depth, although by decreasing increments. Figure 16 shows the results obtained from three repeated cuts in an independent groove. The results are compared with data from a single cut using the same cutter, but at a $\frac{1}{2}$-in. groove spacing, for which case the interaction between grooves was high. The muck decreases for successive passes, as does the observed size of the chips produced. After the third pass the groove was about 0.2 inches deep, and the wedging action of the cutter was sufficient to split the specimen completely in two if a fourth pass was attempted. Block splitting was avoided if conditions allow removal of a significant amount of muck with each pass, such as when there is groove interaction. Hence repeated, isolated cuts are not considered useful for obtaining valid data.

Multiple Interacting Cuts

In actual field conditions the cutters traverse the same path repeatedly and continuously remove the muck. The major portion of the muck is removed through the interaction of the neighboring grooves. After a certain number of cutter passes on an initially smooth surface, the values of specific energy and muck removed will reach "steady-state" conditions. The groove, or cutter path, spacing is of prime importance, and if it is chosen at an optimum value, best results are obtained. This optimum spacing for steady-state conditions is different from that for a single pass on a smooth surface.

Figure 17 shows the specific energy results obtained from multiple passes on grooves with a spacing between grooves of $\frac{3}{4}$ in. A series of parallel grooves was made consecutively with this spacing across the surface of the block; this series comprised one pass. Subsequent passes were made by repeating the process,

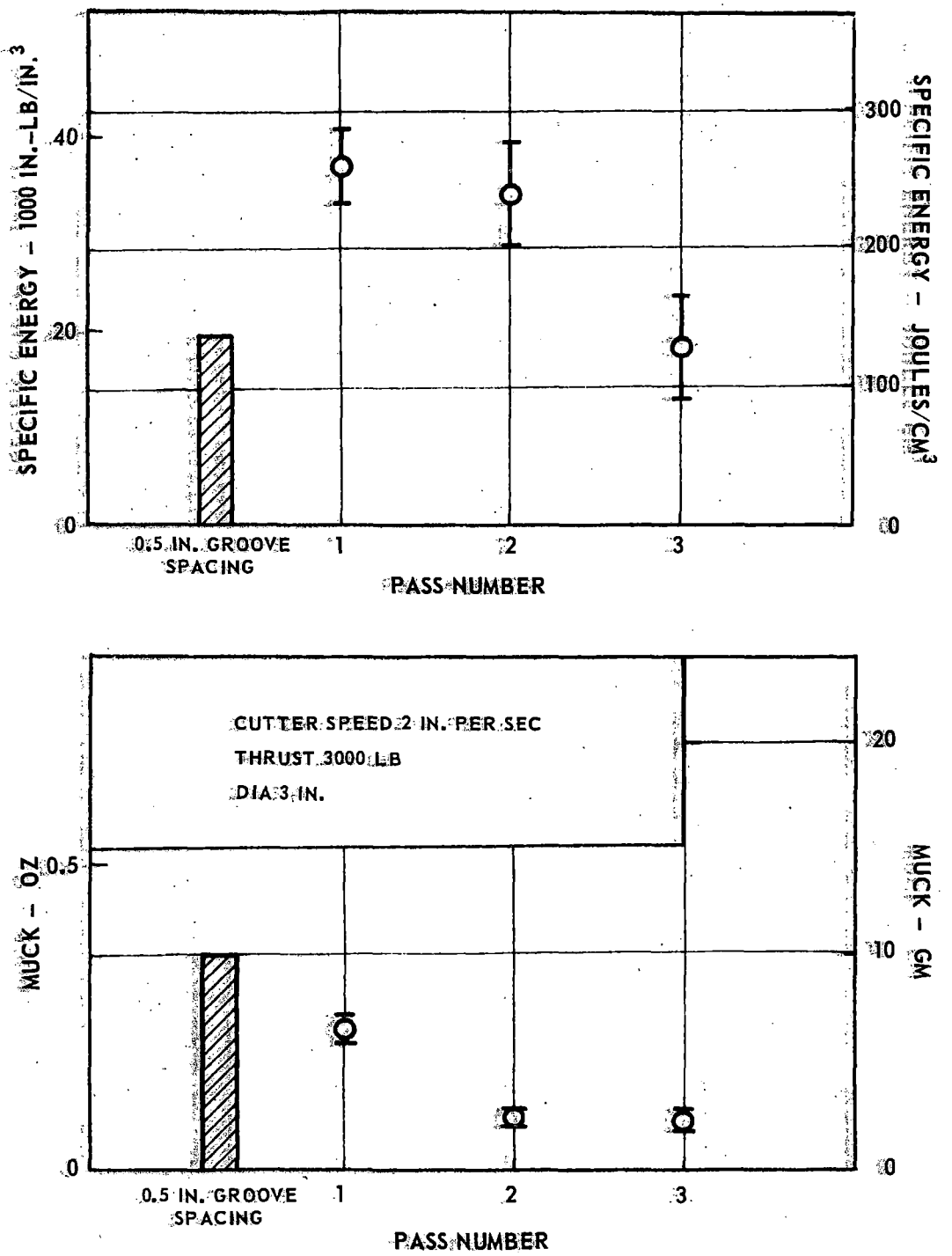

FIGURE 16. EFFECT OF MULTIPLICITY OF INDEPENDENT CUTS ON SPECIFIC ENERGY AND MUCK

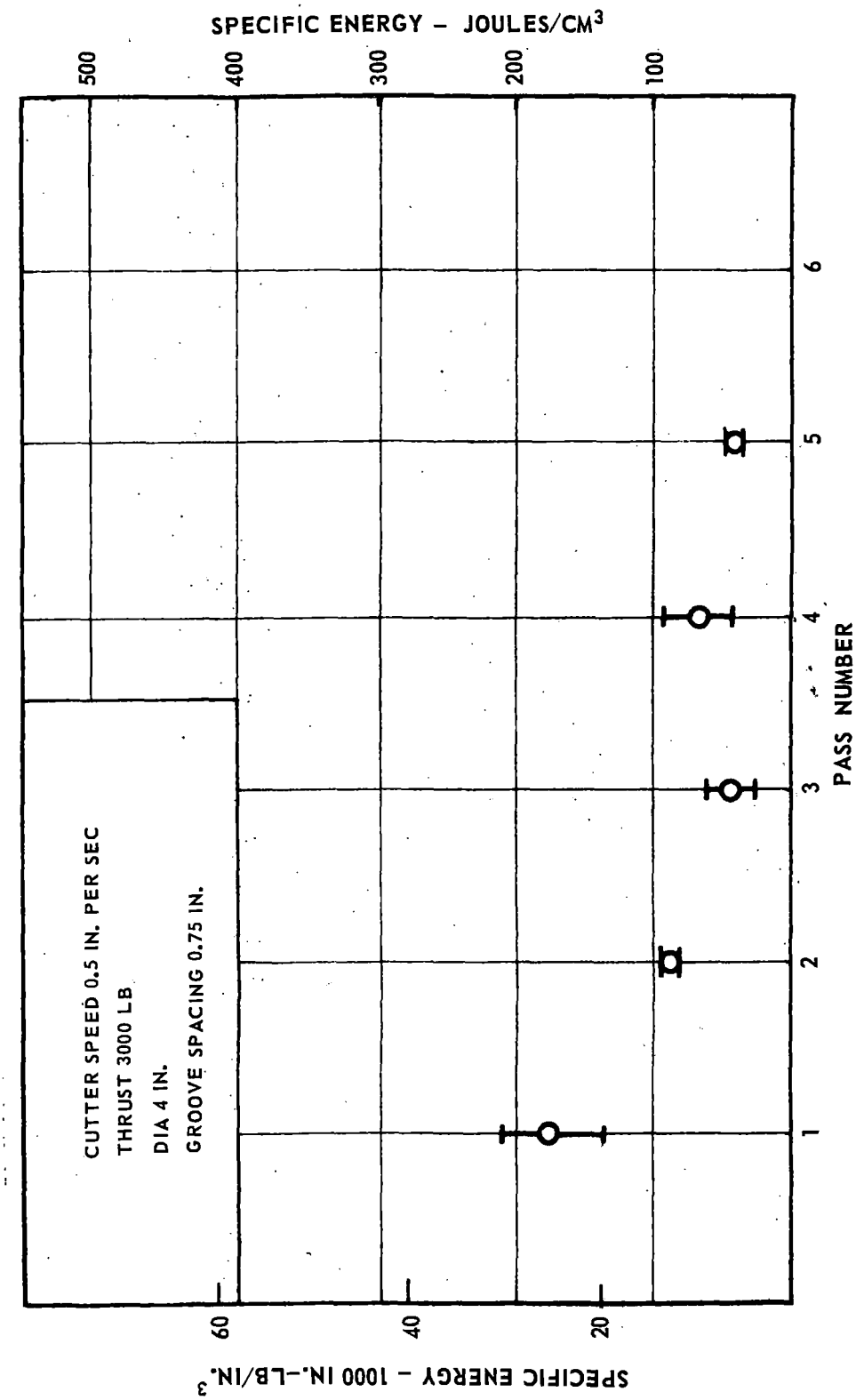

FIGURE 17. EFFECT OF MULTIPLICITY OF INTERACTING PASSES ON SPECIFIC ENERGY

cutting along the same grooves. The values of specific energy decrease in the second and the third passes and appear to reach a steady state after the third pass. The muck values are shown in Fig. 18; these values reach a steady state also. The grooves apparently behave independently for the first and second passes. When the third pass is made, the depth of the grooves is such that lateral forces are created which chip out fragments between two neighboring grooves. Since not all the material is so removed in the third pass, more would be removed in the fourth and fifth ones. In places where chips are removed, the grooves are deepened, and more material can be removed in the following passes. Therefore, the variation of results between successive passes in the steady-state conditions depends on groove spacing.

Optimum Cut Spacing for Multiple Cuts

For the single-pass cuts, the optimum spacing is such that the stresses developed in the first pass should be high enough to form chips between neighboring grooves. If passes are repeated in the same groove, the optimum spacing will be larger because deeper grooves allow more cutter penetration and set up stresses sufficient to remove larger chips. Figures 19 and 20 show averaged results obtained from the third, fourth, and fifth passes, with various groove spacings. These results indicate that, for untreated specimens, the optimum groove spacing is $\frac{3}{4}$ in.

Multiple Cuts at Low Thrust

At the standard condition of 3000 lb thrust on a four-inch cutter, it was seldom possible to obtain results beyond the fifth or sixth pass on any single block because of the likelihood of splitting. For this reason one test was run at a thrust of 1500 lb and a groove spacing of 3/8 inch; these conditions permitted at least a dozen passes. The results are shown in Figs. 21 and 22. It is quite obvious that a steady state has been reached for these test conditions after the fifth pass.

Effect of Cutter Speed for Multiple Cuts

The rate sensitivity of granite breakage causes an increase in the value of specific energy and a decrease in the amount of muck produced as the cutter speed is increased. These effects are not as pronounced for multiple passes as for single ones on a smooth surface. Figures 23 and 24 show the effect of cutter speed on the steady-state results for untreated specimens. As was found with single passes, the ratio of chips to fine material is high at lower speeds, helping to account for the trend in specific energy shown.

Although the amount of muck removed per unit length of groove is smaller if the cutting is done at higher speeds, the pass takes less time so the amount of material removed per unit time may be higher. Figure 25 shows that this is the case, within

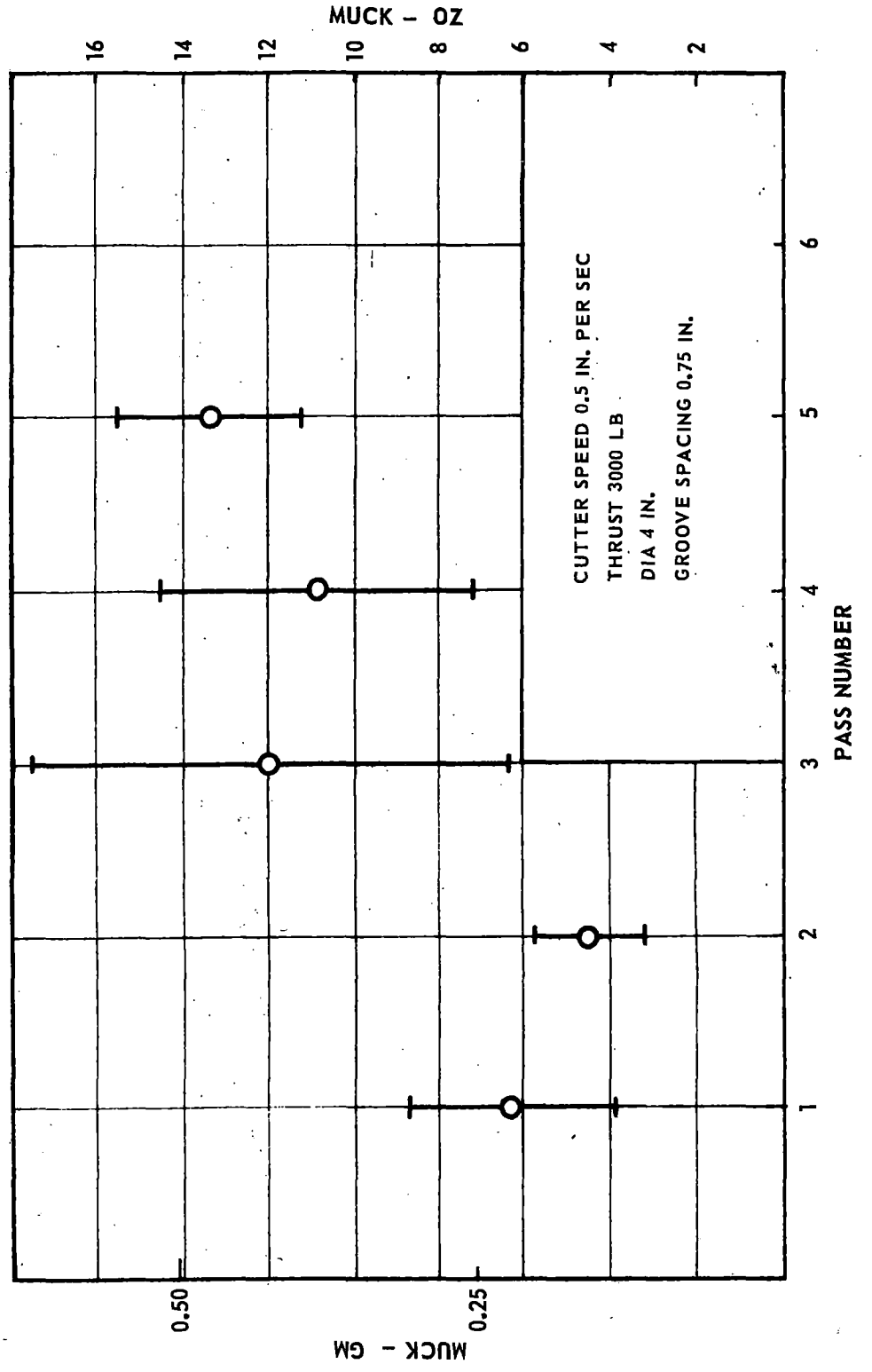

FIGURE 18. EFFECT OF MULTIPLICITY OF INTERACTING PASSES ON MUCK

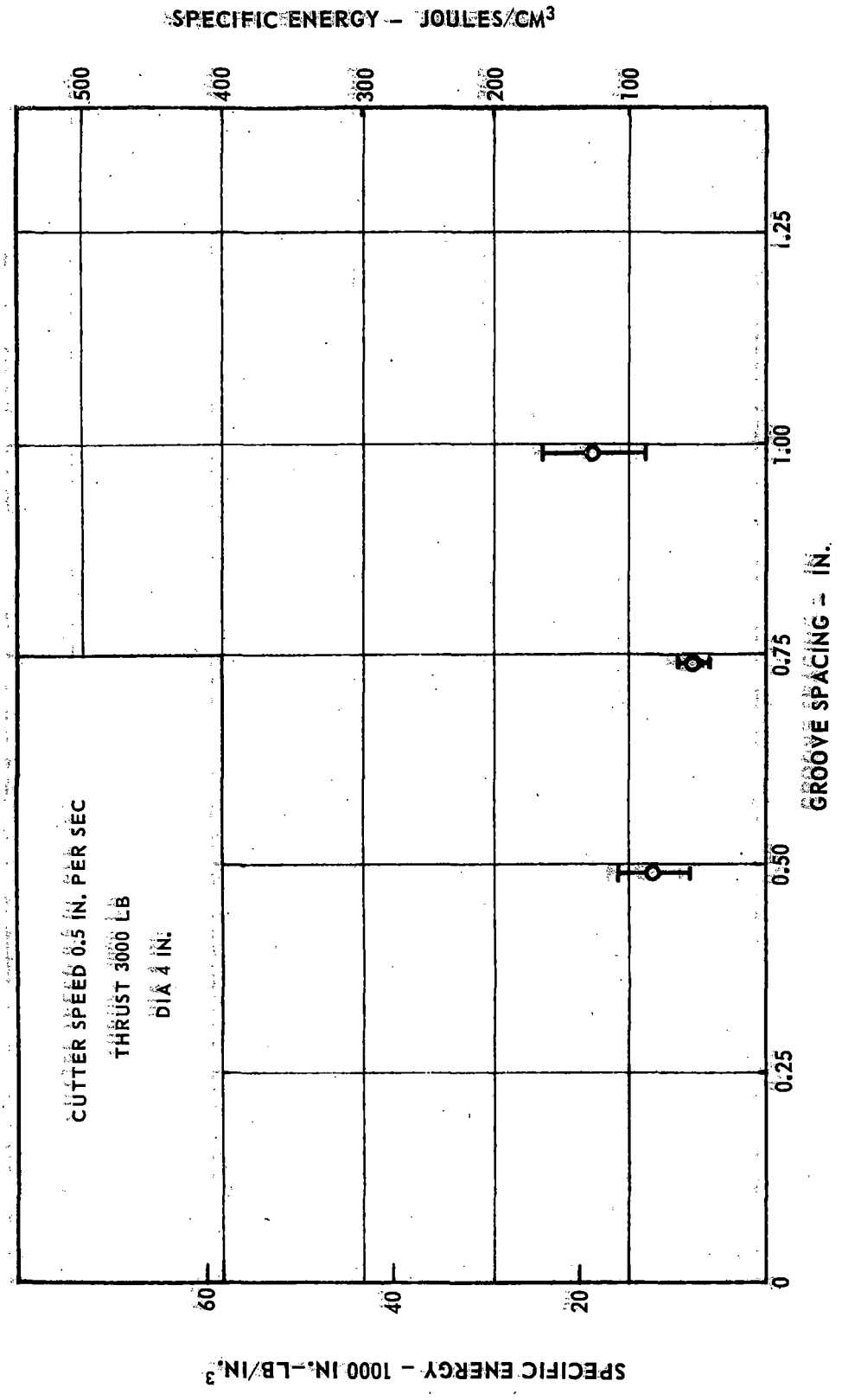

FIGURE 19. EFFECT OF GROOVE SPACING OF INTERACTING CUTS ON SPECIFIC ENERGY

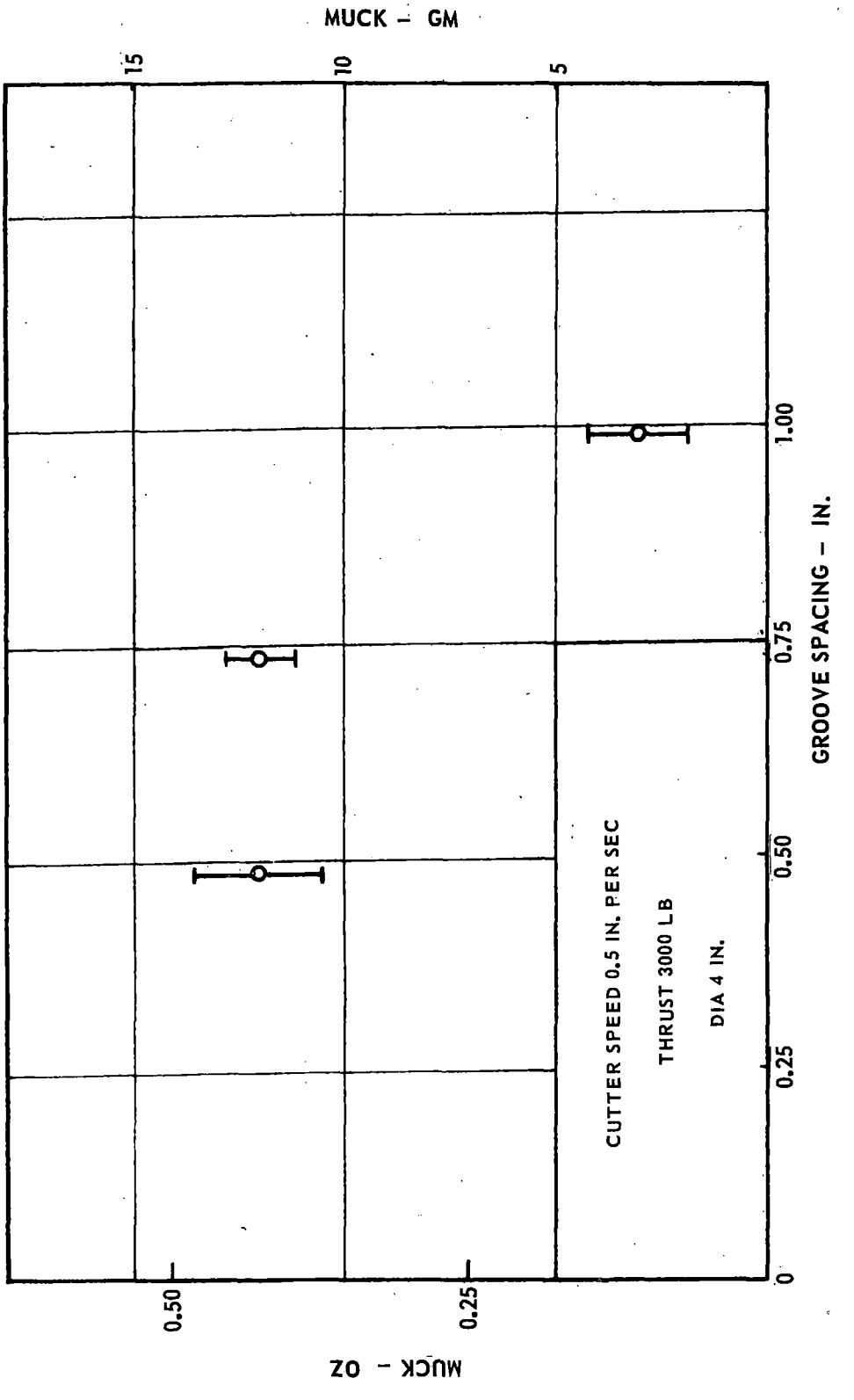

FIGURE 20. EFFECT OF GROOVE SPACING OF INTERACTING CUTS ON MUCK

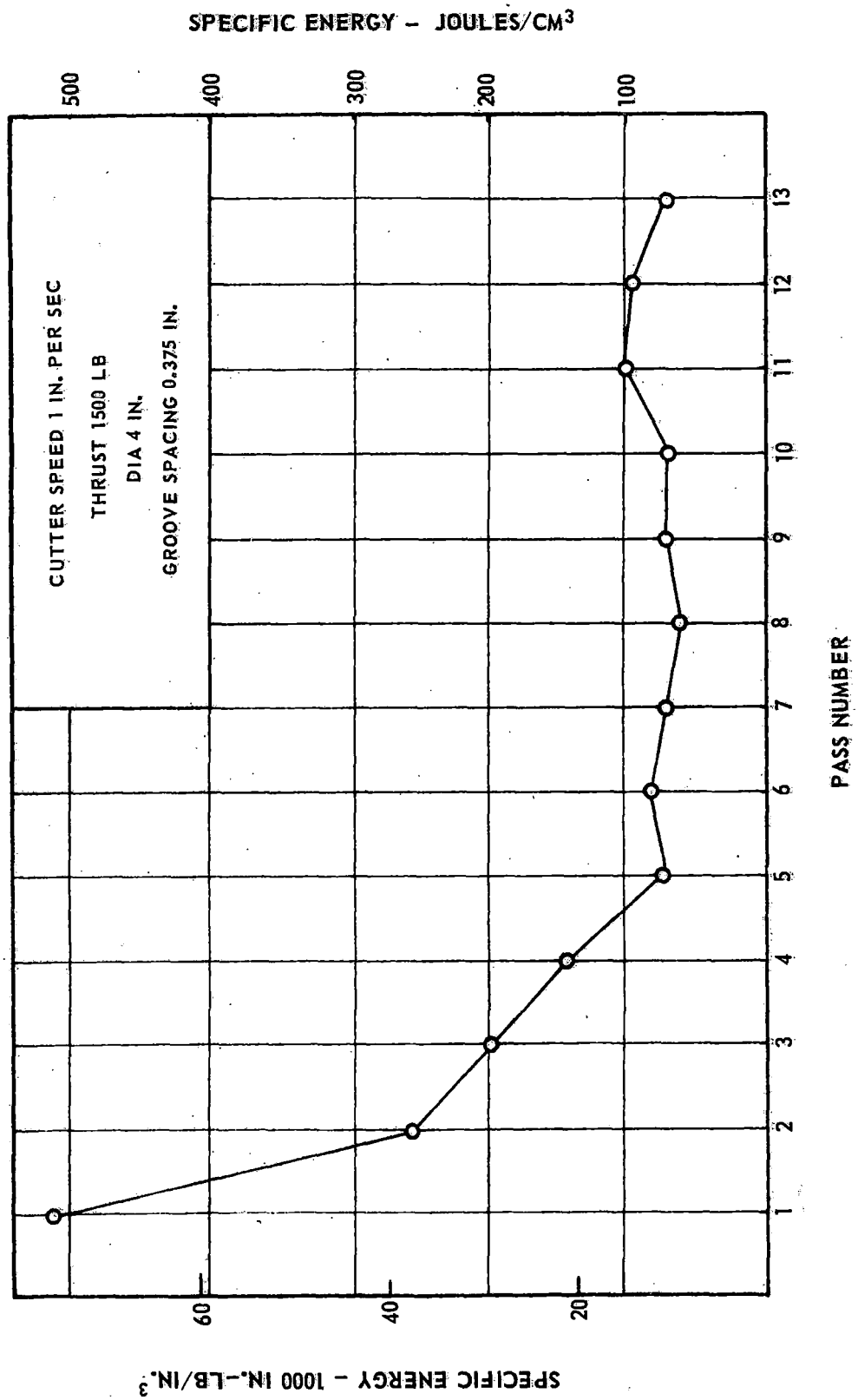

FIGURE 21. EFFECT OF NUMBER OF PASSES ON SPECIFIC ENERGY FOR INTERACTING CUTS

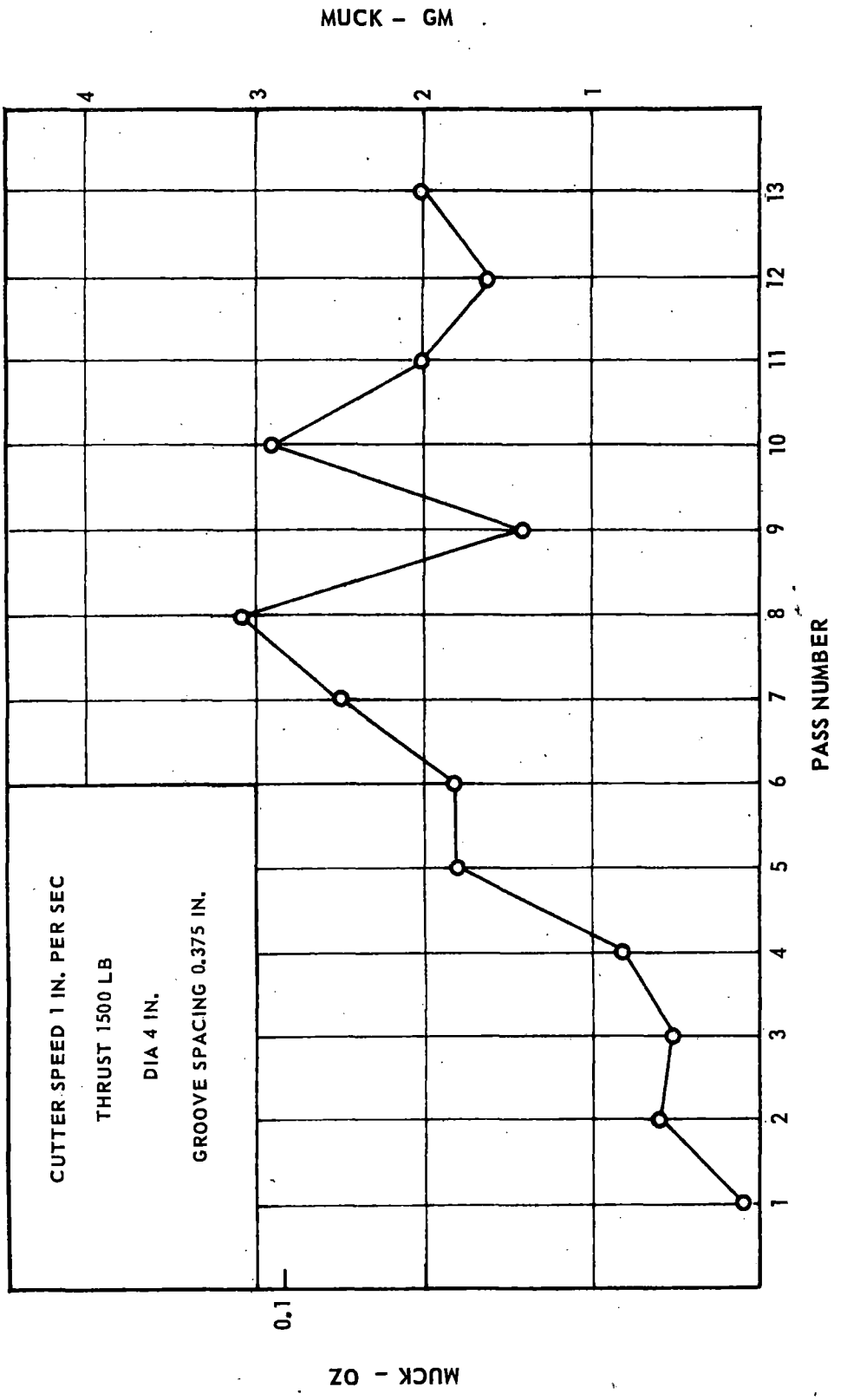

FIGURE 22. EFFECT OF LOW THRUST ON MUCK FROM INTERACTING CUTS

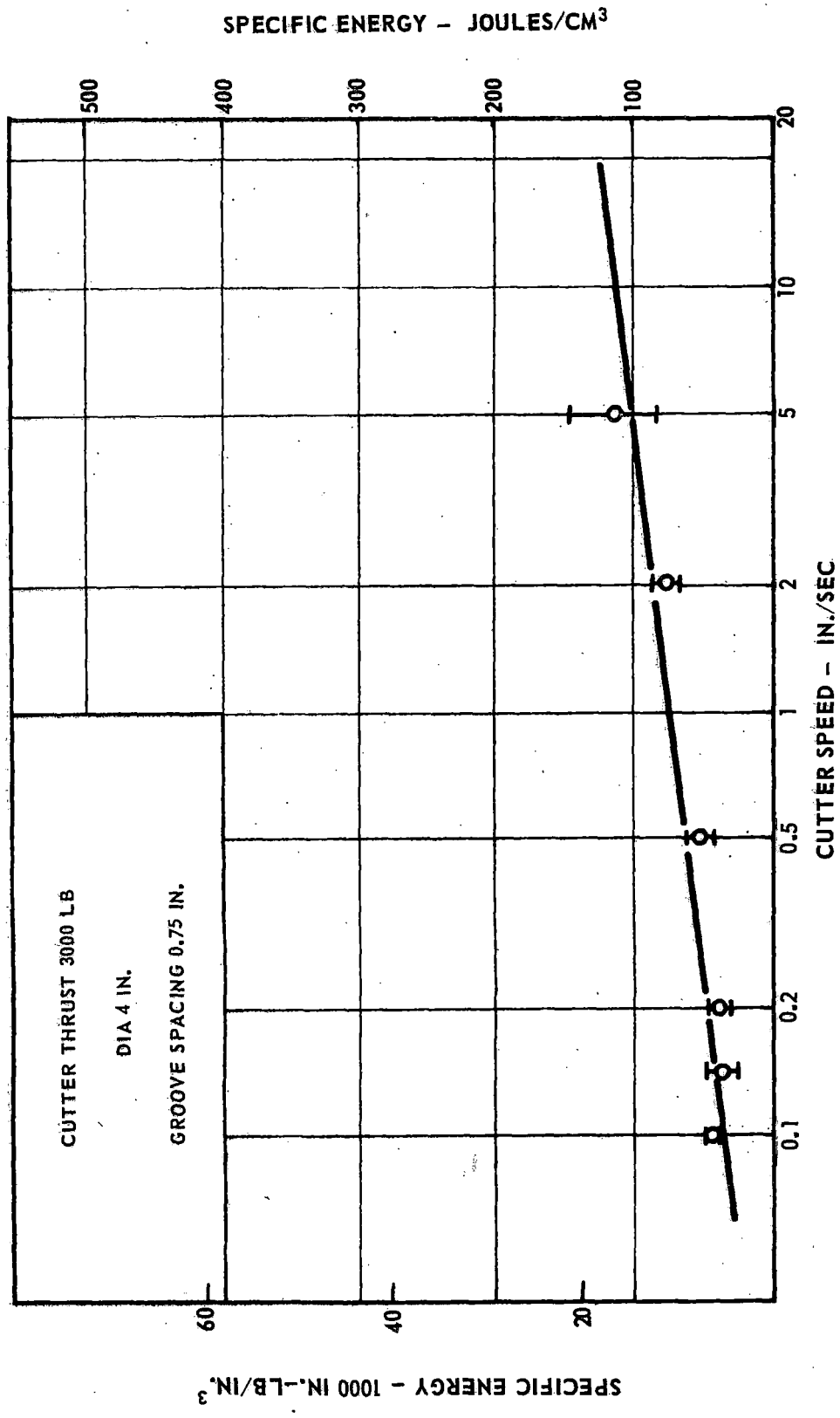

FIGURE 23. EFFECT OF CUTTER SPEED ON SPECIFIC ENERGY FOR INTERACTING CUTS

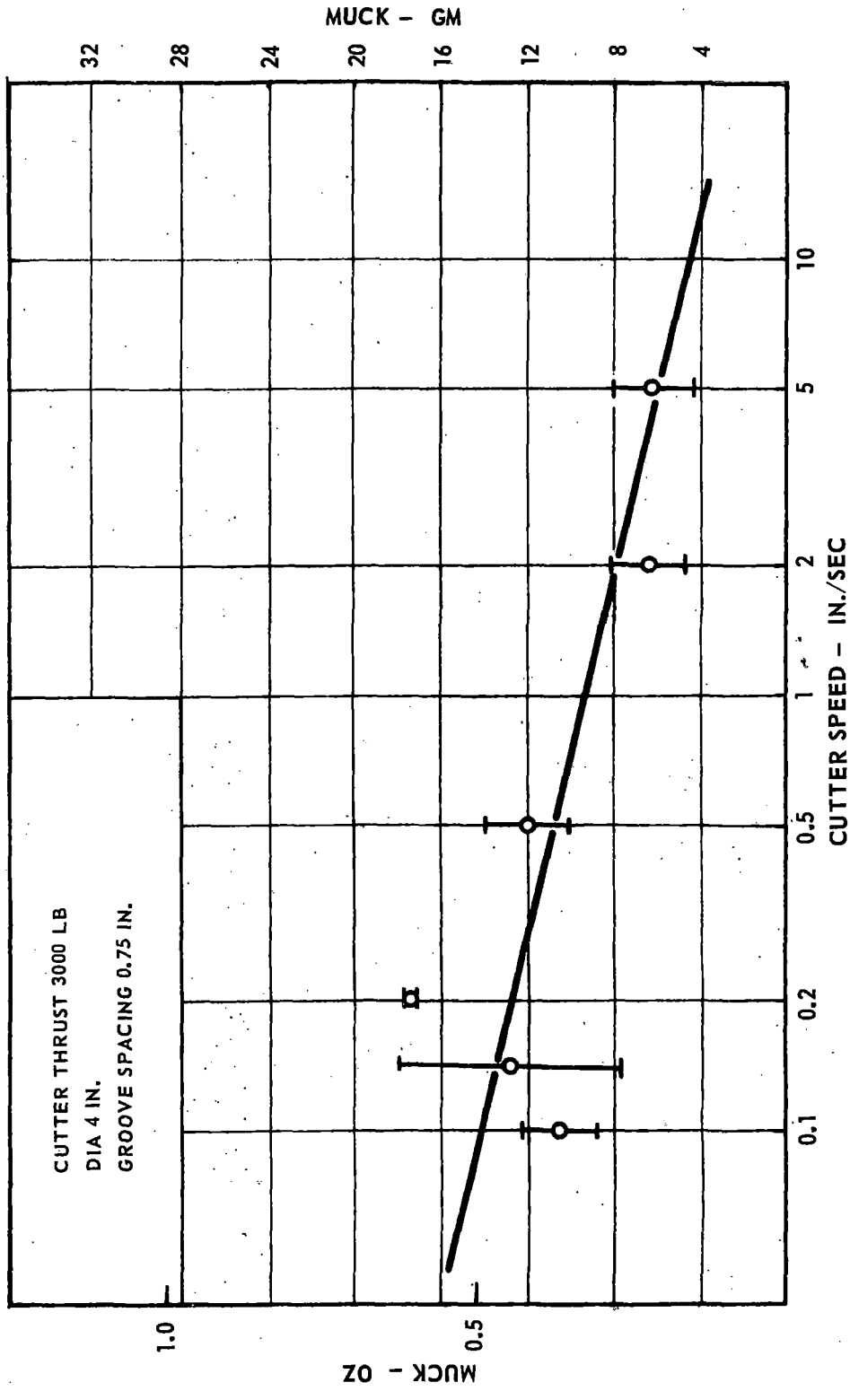

FIGURE 24. MUCK FROM INTERACTING CUTS VERSUS CUTTER SPEED

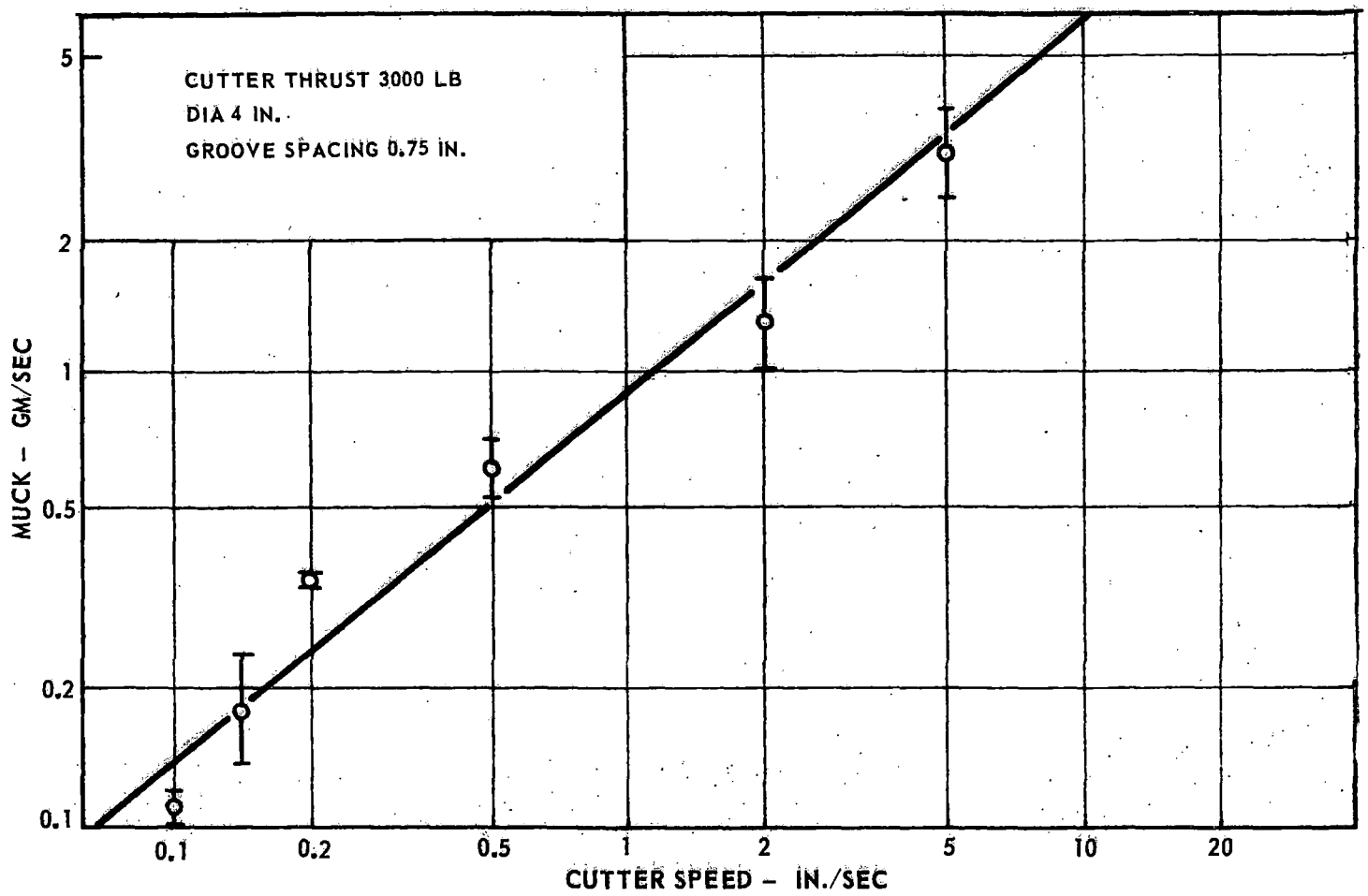

FIGURE 25. MUCK REMOVAL RATE FOR 4-INCH CUTTER

the range of speeds tested. Slow cutting, therefore, favors economy on a specific energy basis, while higher speeds favor increased advance rate, which is of at least equal importance in a practical situation.

TEST RESULTS - LASER TREATED ROCK

Single Cuts on a Smooth Surface

Local heating of the rock by lasing weakens it by creating intergranular and transgranular cracks as well as other types of permanent damage, and by creating thermal stresses which augment the mechanical stresses from the cutter. The extent of the laser damage to a specific rock type depends on laser beam power, beam size, beam traverse speed, patterns of heating, and whether or not the rock is allowed to cool before cutting.

Unfocused Laser - Rock Allowed to Cool

The extent of residual damage can be determined by exposing the rock to lasing and testing it when the rock has cooled to room temperature. Previous heat-weakening tests, summarized in Fig. 1, also allowed for rock cooling prior to mechanical testing. The residual damage occurs throughout the entire period of cooling. Figure 26 shows the variation of the fracture specific energy required with various heat dosages. Each block was passed under the reflected, unfocused 650-watt laser beam at a specified table speed. Repeating this procedure after moving the block laterally produced parallel, lased paths at equally spaced intervals. The energy input of the beam per linear inch of travel was therefore inversely proportional to the table speed. Cutting was done 24 hours later at the same table speeds at which the rock was lased. The specific energy values for the lased specimens are less than those for the untreated ones only when heat inputs of more than about 1000 joules per inch were used. The idea of a threshold amount of heating required to induce a noticeable rock weakness is consistent with the previous test results, as shown in Fig. 1. In both cases, the required threshold heat energy is on the order of 1000 to 2000 joules per square inch.

Figure 27 shows the amount of muck removed for these specimens. An increase in muck removal seems indicated for heat inputs higher than about 4500 joules per inch, although this increase may not be significant in view of the amount of scatter observed in these tests. A slight change of color was observed in the areas exposed to lasing, indicating some loss of moisture or other minor physical changes. These changes might be responsible for the lack, or even reversal, of the residual damage effect which occurs for lower heat input values.

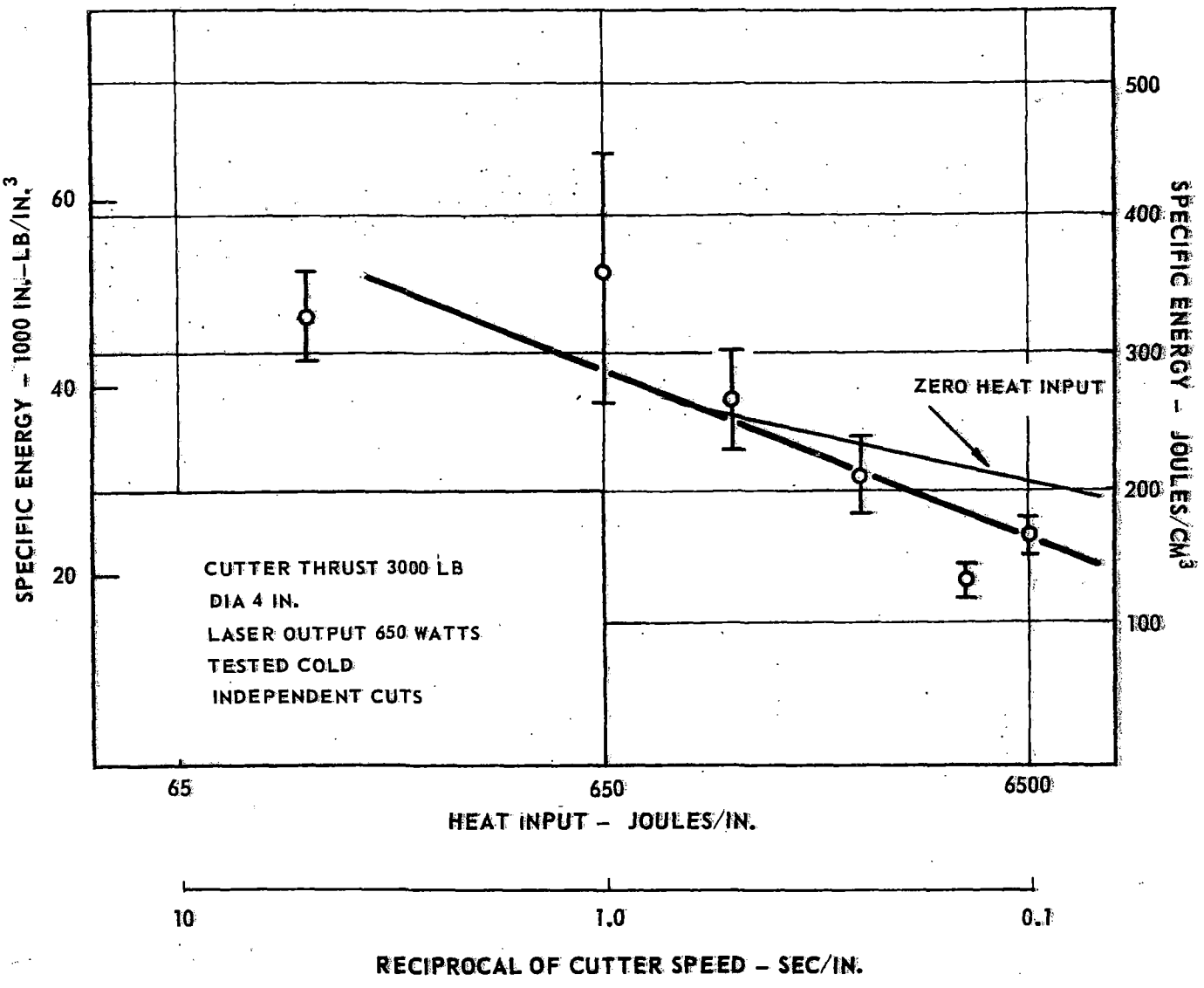

FIGURE 26. EFFECT OF RESIDUAL LASER DAMAGE ON SPECIFIC ENERGY

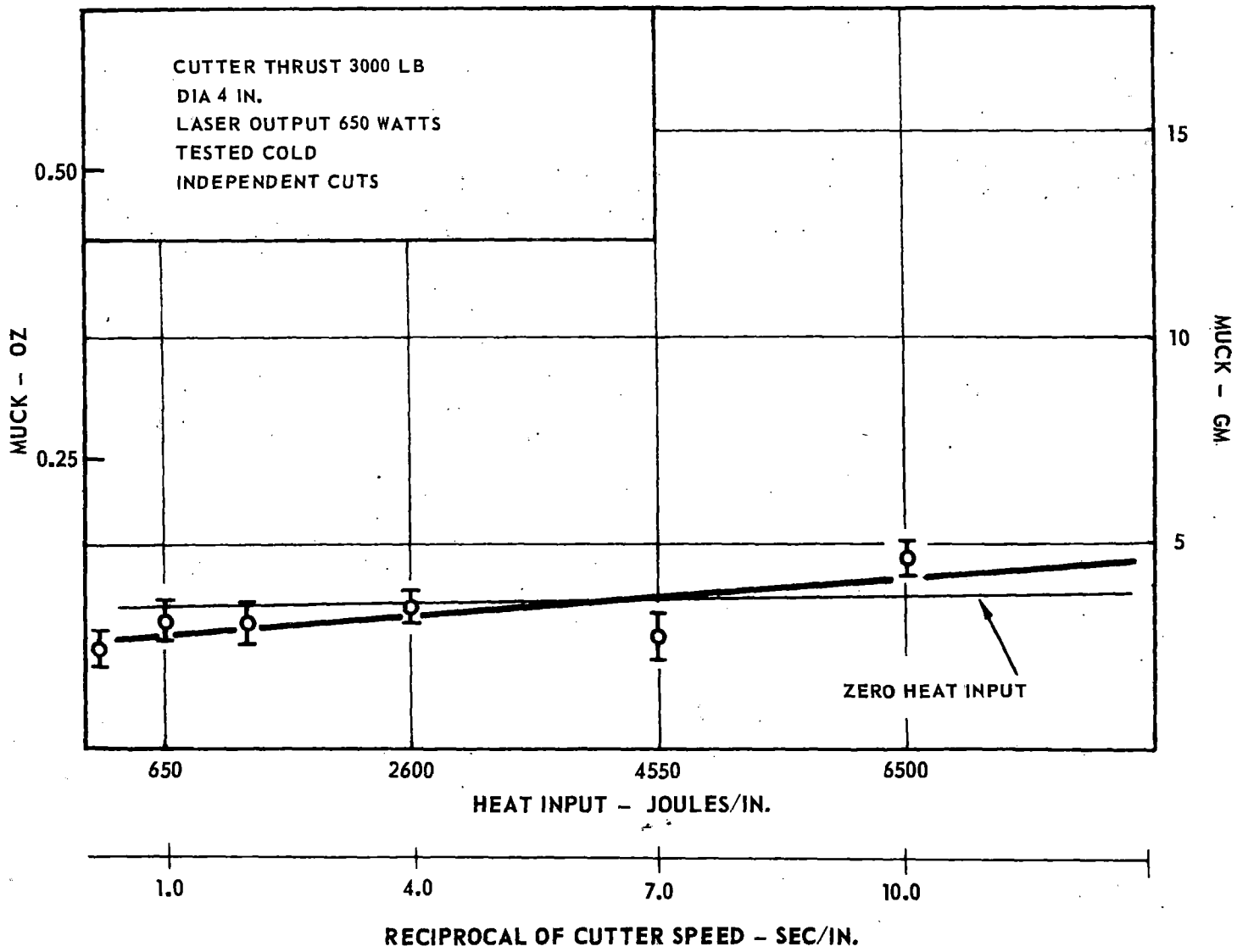

FIGURE 27. EFFECT OF RESIDUAL LASER DAMAGE ON MUCK

The results of these tests show that the permanent damage induced by the laser will not alter the muck removal pattern significantly but will decrease the value of specific energy if the heat input is higher than roughly 2000 joules/in. At an input of 4500 joules/in., the specific energy is reduced by about 15%.

Unfocused Laser - Rock Tested Hot

In addition to the permanent damage, the laser radiation produces a transient thermal stress in the rock. This stress aids the formation of larger chips from mechanical cutting, giving lower values of specific energy. Figure 28 shows the variation of specific energy with heat input in tests where the rock was cut while still hot. The 650-watt unfocused beam was aimed 5 inches ahead of the cutter, on the path the cutter followed. The total heat input was varied by changing the cutter speed; since there was a fixed separation between the cutter and the beam, this also changed the time between heating and cutting for each level of heat input. The values of specific energy are slightly less at each level of heat input than those obtained with the cooled specimens, and the regression lines indicate that desirable effects are produced for heat inputs greater than about 500 joules/in. Figure 29 shows the amount of muck removed from these specimens. The muck values for all heat inputs are higher than those from the cool specimens, and for the higher heat inputs they are significantly higher than those for the unlased specimens. For a heat input of 3000 joules/in., there is a 10% increase in the muck, compared to the untreated specimens.

Figure 30 shows the variation of specific energy for specimens treated in the same manner, but with a 325-watt beam. The desirable effects again occur only for heat inputs greater than 1000 joules/in., although for the range of speeds and heat inputs studied, the improvements are marginal. Figure 31 shows the muck removal values for these specimens; the regression line indicates muck removal has decreased for all the heat input values used. For an input of 3000 joules per inch, the specific energy is reduced by less than 10%, and there is a 15% decrease in the amount of muck. As before, these indications may be within the scatter of the experimental data.

Figure 32 shows results of a test with an unfocused laser beam, using a cutter thrust of 5000 lb and a cutter diameter of 4 in. These tests are compared, in Fig. 32, to the unheated rock results at 5000 lb thrust, shown in Fig. 13.

Based on the three types of tests discussed so far, there is apparently a threshold heat input value which must be exceeded for any improvement in cutting efficiency to be gained. This threshold effect had been observed in previous tests (Fig. 1). For the present case, if the heat input is less than this critical amount, the muck removal may be even more difficult and less efficient than in the case of unlased rock.

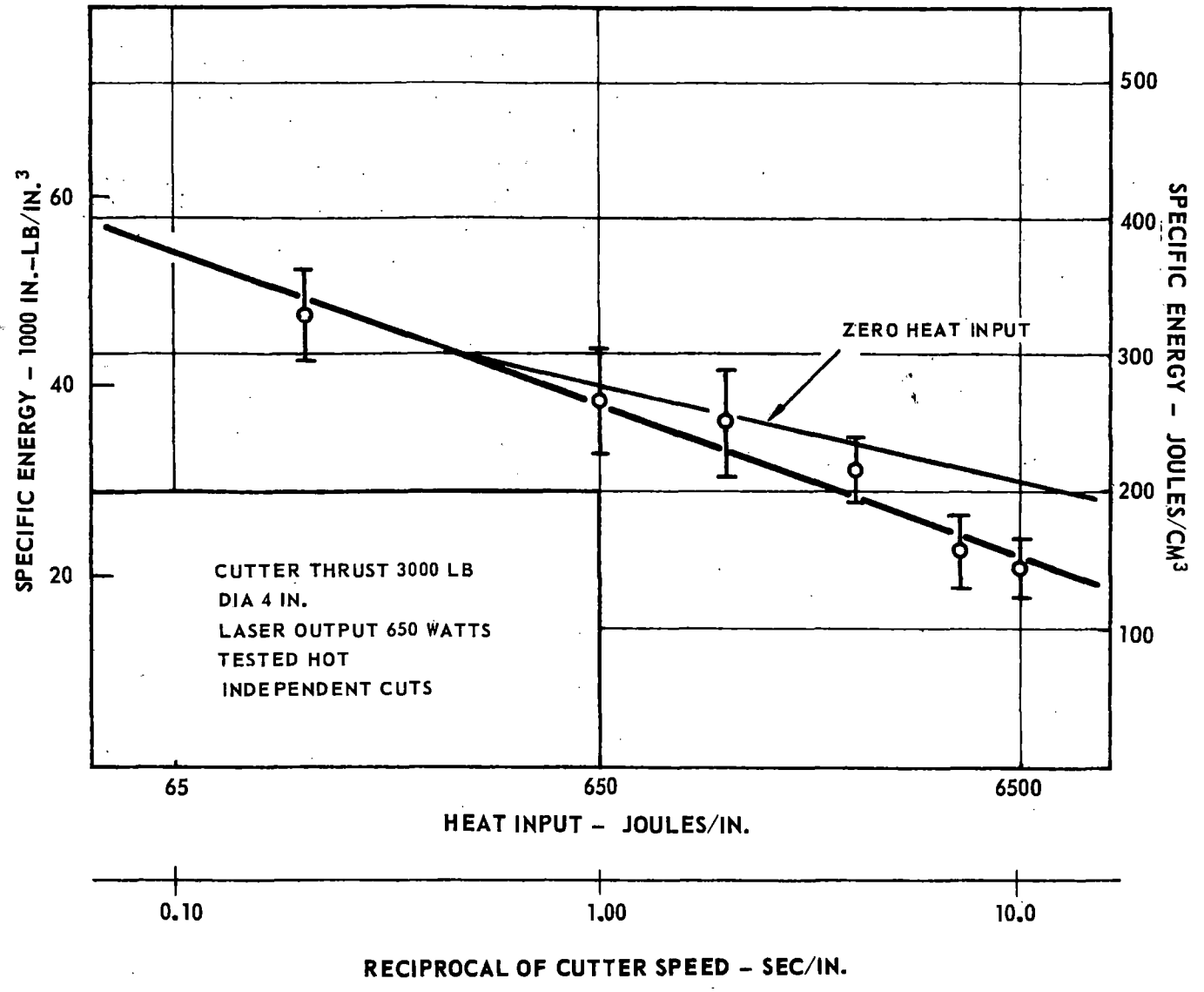

FIGURE 28. EFFECT OF LASER WEAKENING ON SPECIFIC ENERGY

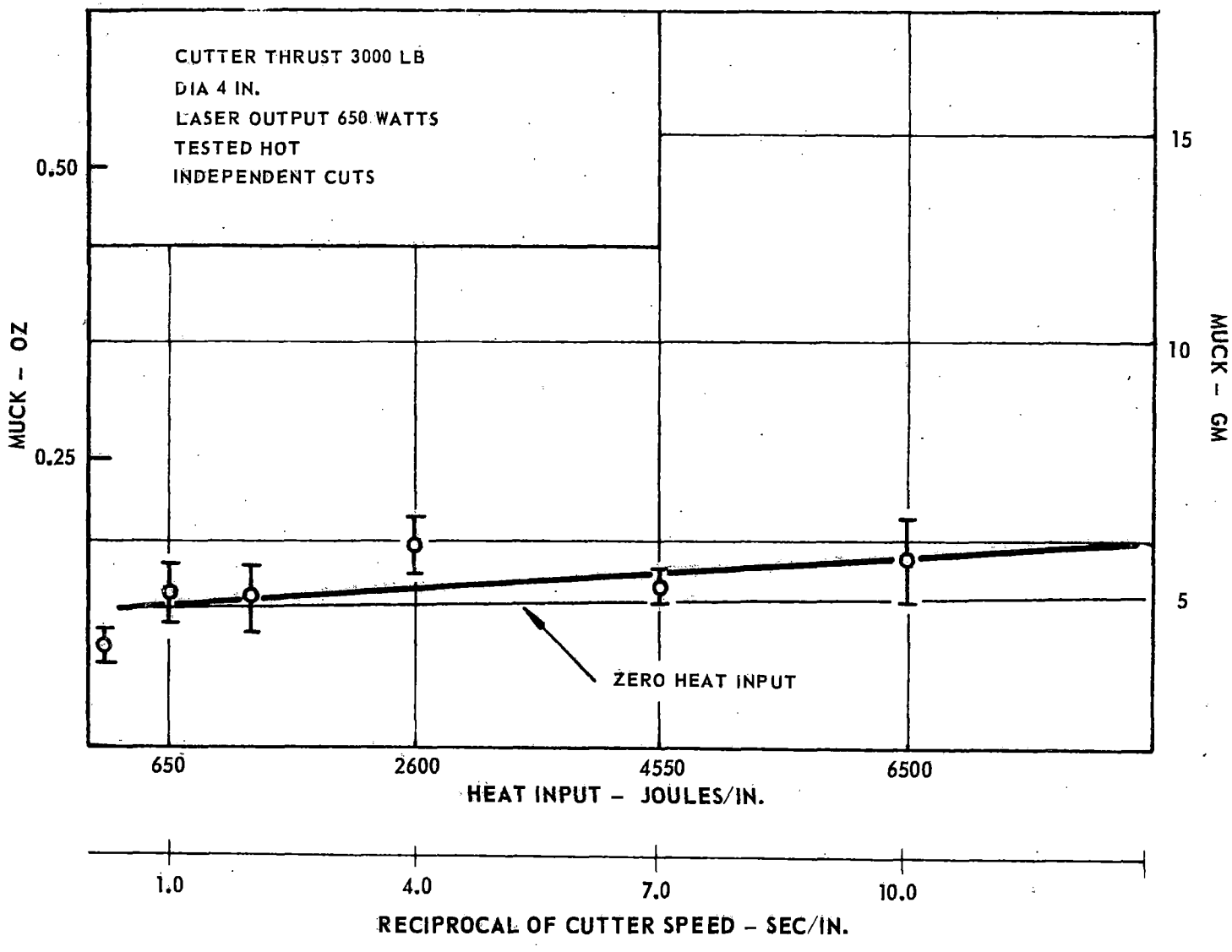

FIGURE 29. EFFECT OF LASER WEAKENING ON MUCK

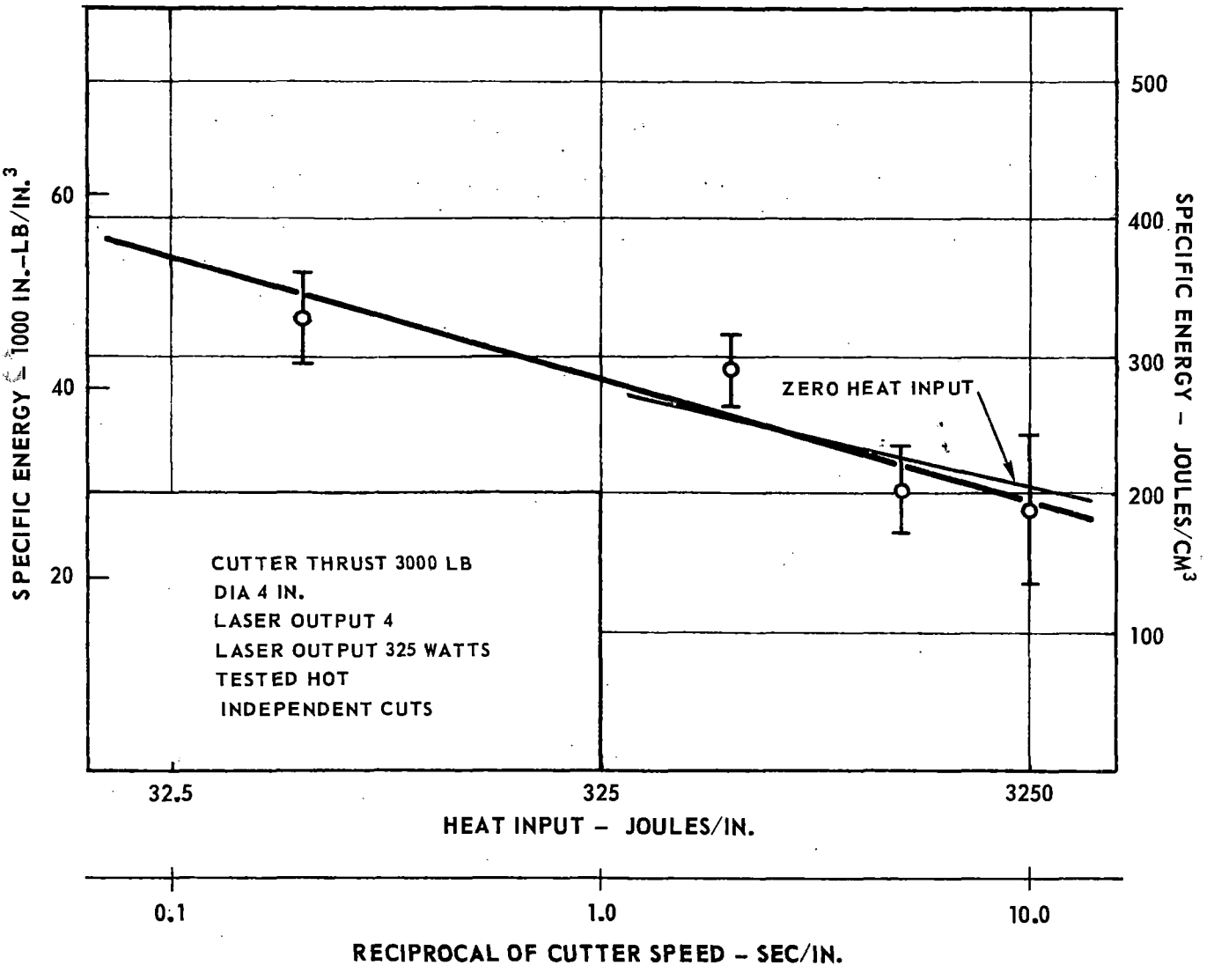

FIGURE 30. EFFECT OF LOW-OUTPUT BEAM ON SPECIFIC ENERGY

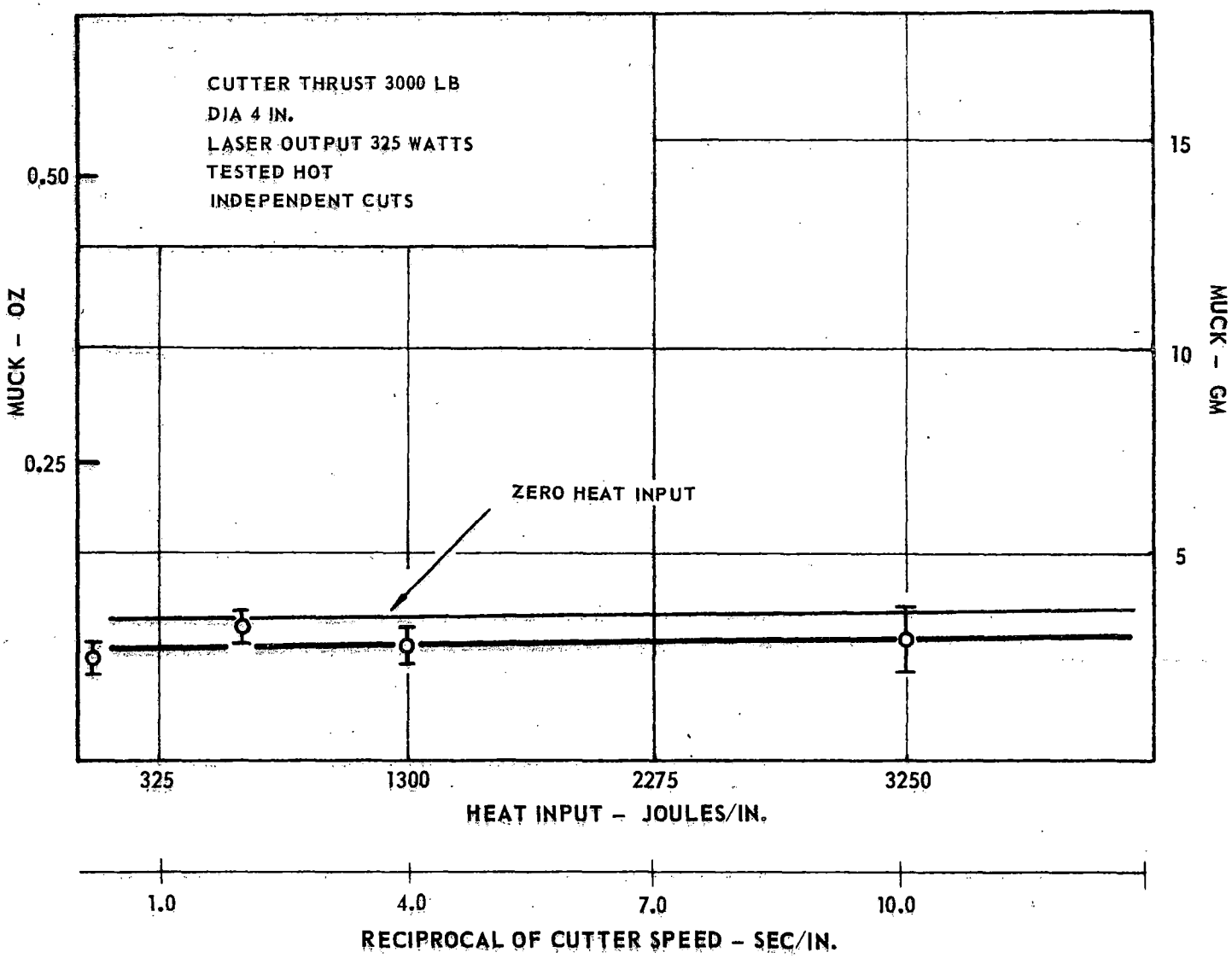

FIGURE 31. EFFECT OF LOW-OUTPUT BEAM ON MUCK

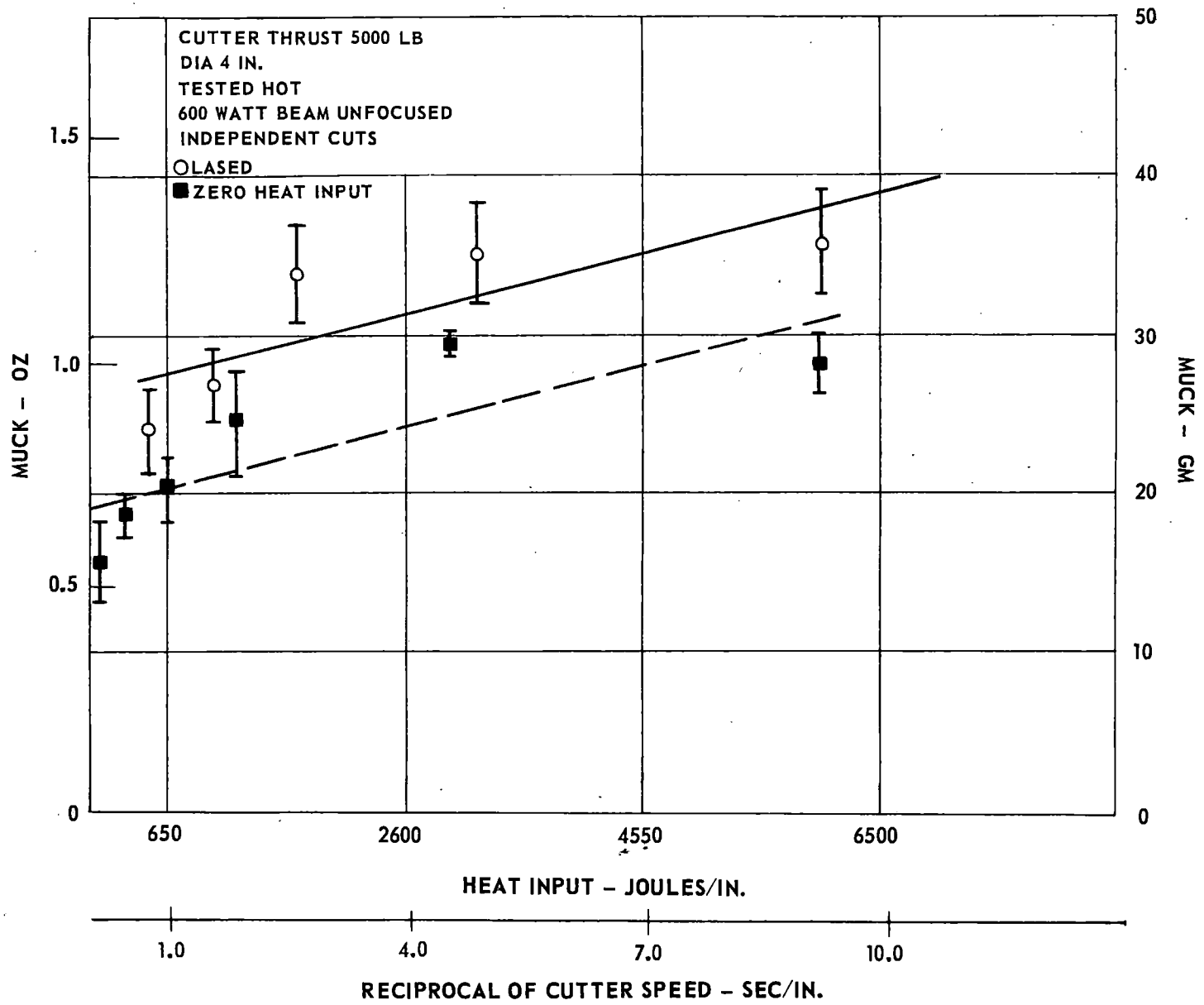

FIGURE 32. MUCK REMOVAL FOR 600-WATT BEAM

Focused Laser - Rock Tested Hot

The magnitude of the thermal stress depends on the temperature of the heated surface; this temperature can be increased by focusing the beam with a concave mirror. Figure 33 shows the variation of specific energy for specimens which were heated with a 650-watt focused beam prior to cutting. The radiation spot, about 3/8 in. in diameter, was aimed 5 in. ahead of the cutter on the same travel path. At very high energy input values, partial melting and beading of the heated area occurred. Figure 34 shows the amount of muck removed from these specimens. In comparison with the specimens which were treated identically, but with an unfocused laser beam, there is an almost fourfold increase in muck removal. A comparison of specific energy for these two cases shows that a focused beam is twice as effective as the unfocused one. Compared to the untreated specimens, there is a 35% increase in the amount of muck and a 65% decrease in the value of specific energy for an input of 3000 joules per inch.

Focused Laser - Rock Tested Hot - Laser Beam Offset from Cutter Path

Stress analysis studies have shown that both tensile and compressive stresses are developed by local heating of the rock samples. These studies suggest that the cutter path should be located adjacent to, rather than directly on, the heated path, to better initiate fractures which then may be propagated through the heated region by the compressive stresses occurring on the surface. The variation of specific energy with offset distance is shown in Fig. 35; the energy shows a minimum at about $\frac{1}{2}$ in. offset. Figure 36 shows the variation of muck for these specimens; with increasing offset, the amount of muck removed also shows a maximum but at about $\frac{1}{4}$ in. The optimum offset varies slightly with cutter speed and total heat input; since the values of these parameters were approximately midrange, one-half-inch offset was used for the heat inputs shown in Figs. 37 through 40. Figure 37 shows the variation of specific energy with cutter speed (and hence energy deposited per inch of cutter path) when the focused laser beam is aimed 5 in. ahead of the cutter and offset $\frac{1}{2}$ in. from its path. Figure 38 shows the muck removal for these specimens. These results display the best improvements in the values of specific energy and muck removal of all cases so far considered. For 3000 joules/inch heat input, there is a 70% decrease in the specific energy and a 120% increase in the amount of muck, compared to untreated specimens cut in the same manner.

Figure 39 shows the variation of specific energy for specimens which were treated with a 325-watt laser, offset $\frac{1}{2}$ in. from the cutter path. A significant reduction of energy is observed for all heat input values. Comparing the muck values shown in Fig. 40 with those for the 325-watt unfocused beam tests in Fig. 31 indicates that the timing and geometry of heat application can be as important in increasing removal efficiency as the heat input magnitude. For a heat input of 3000 joules/inch, a 90% increase in muck and a 45% decrease in specific energy are obtained due to these geometry and focusing effects alone.

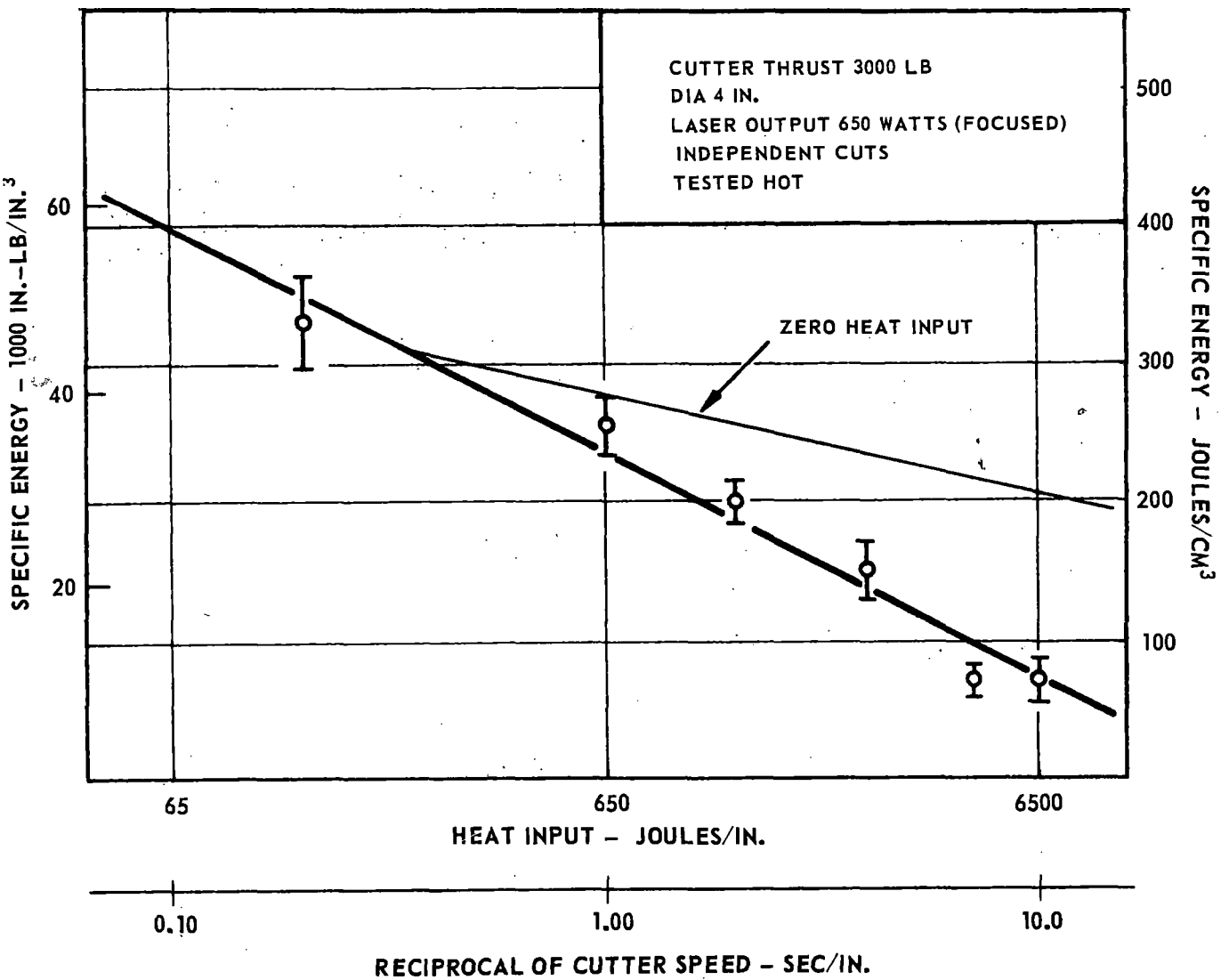

FIGURE 33. EFFECT OF FOCUSED LASER ON SPECIFIC ENERGY

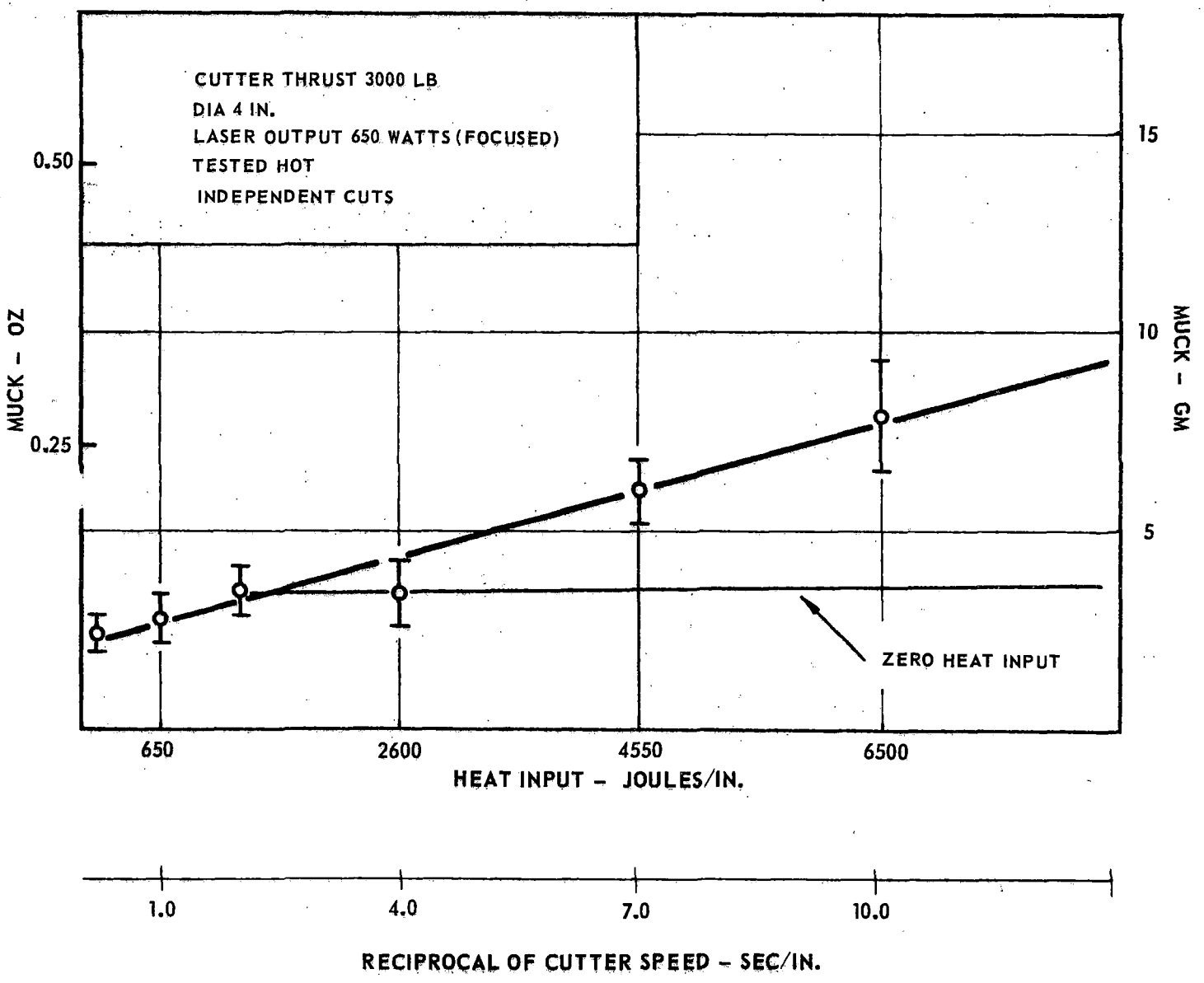

FIGURE 34. EFFECT OF FOCUSED LASER ON MUCK

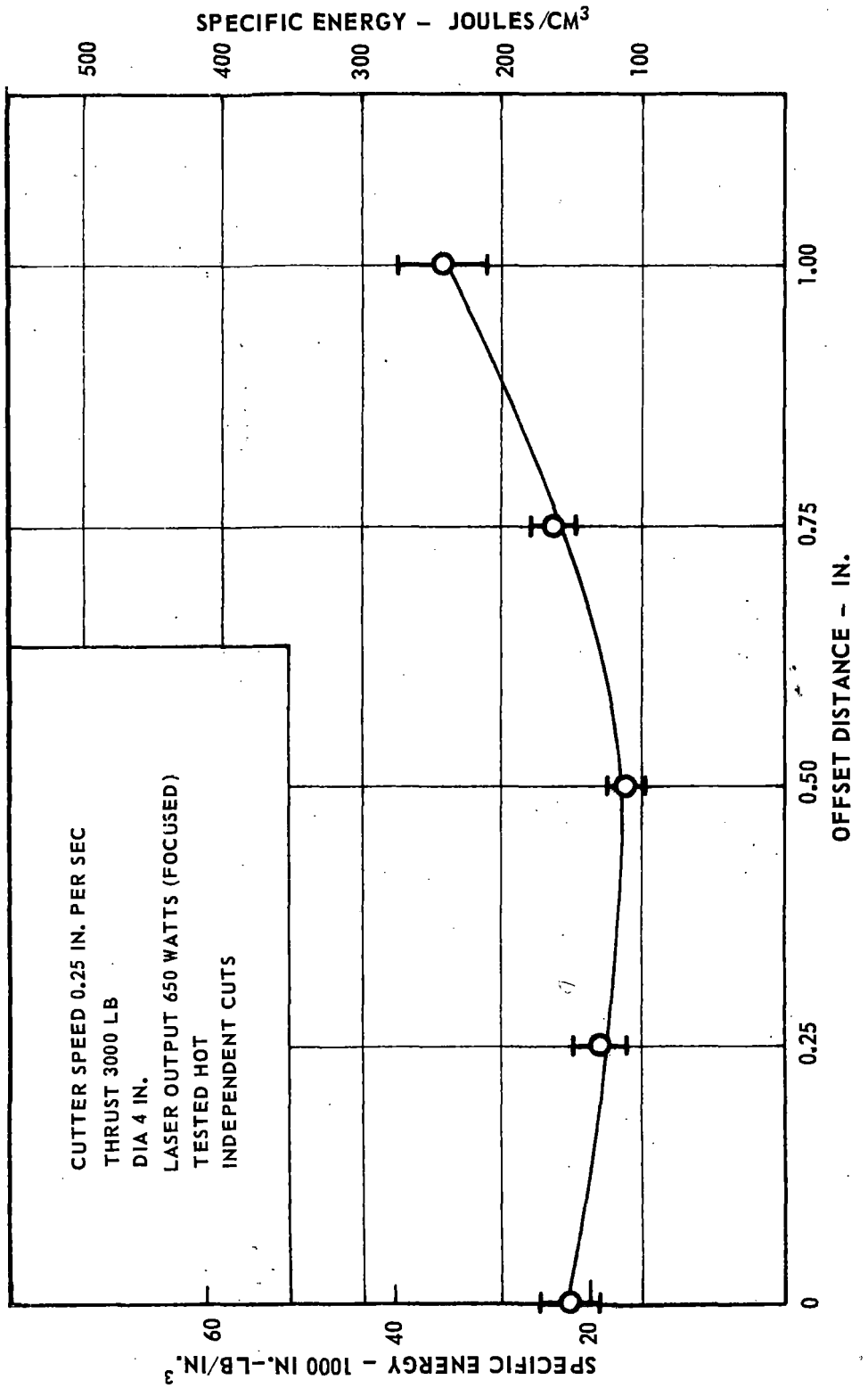

FIGURE 35. EFFECT OF BEAM OFFSET ON SPECIFIC ENERGY

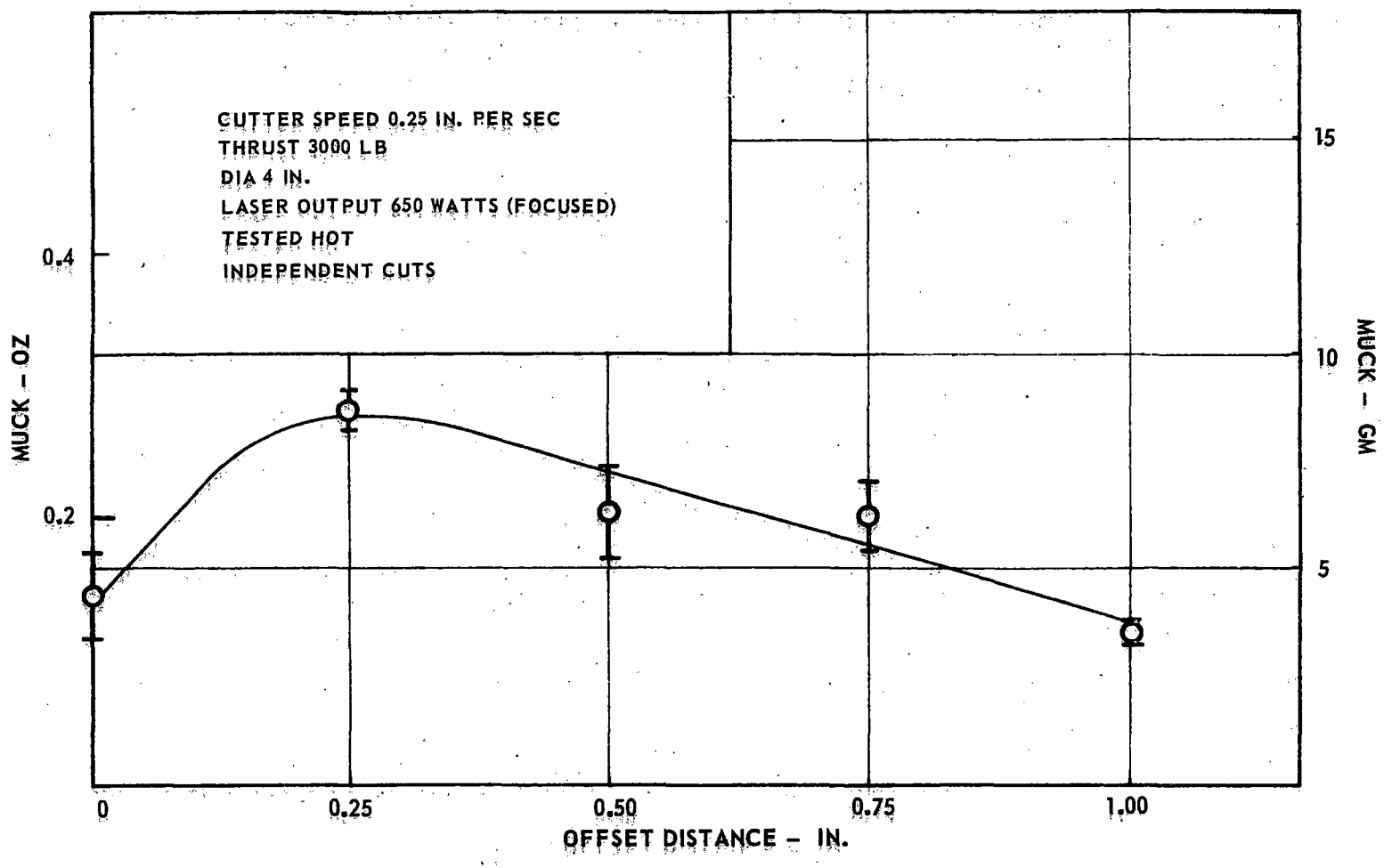

FIGURE 36. EFFECT OF BEAM OFFSET ON MUCK

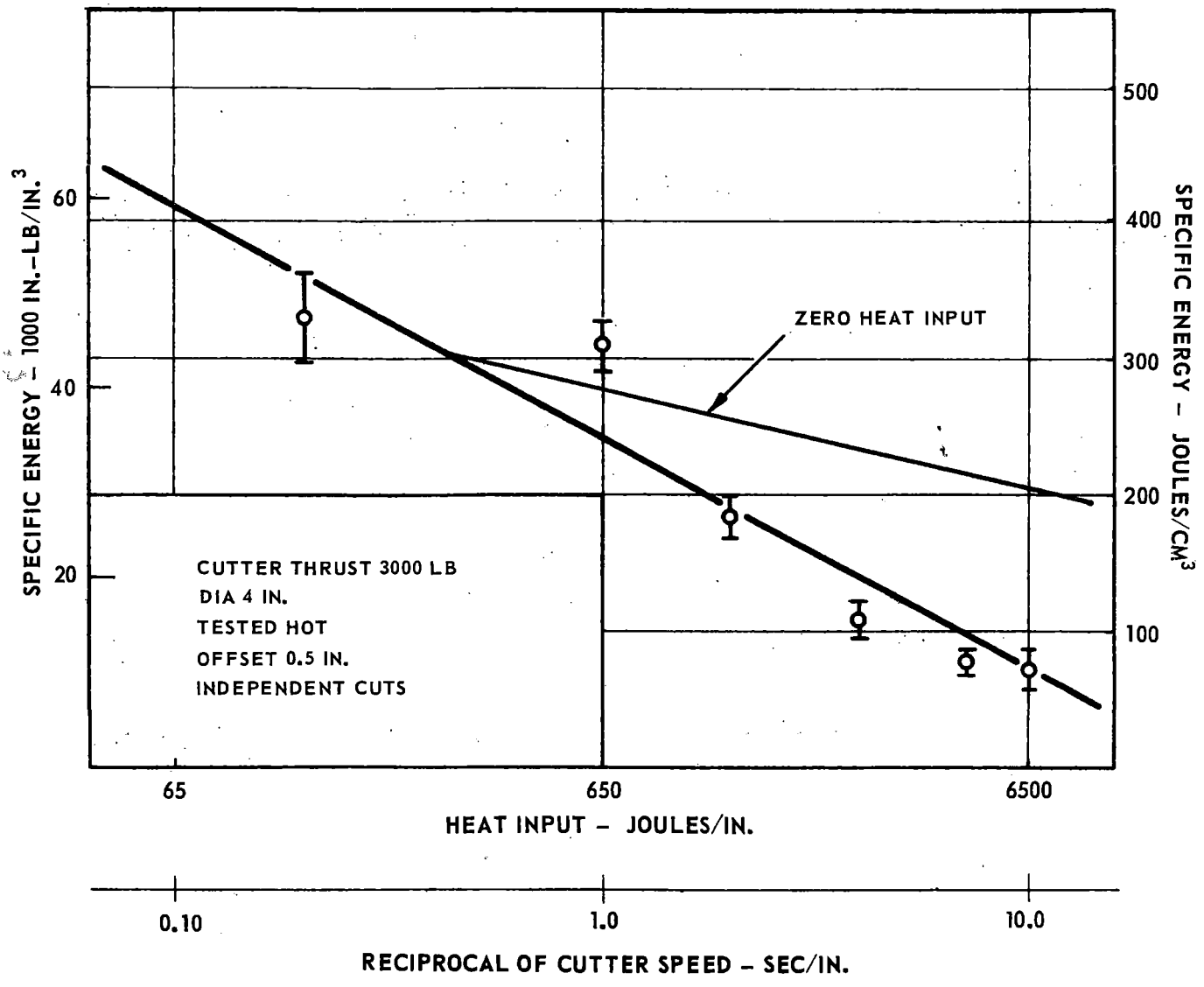

FIGURE 37. SPECIFIC ENERGY FOR 650-WATT FOCUSED BEAM

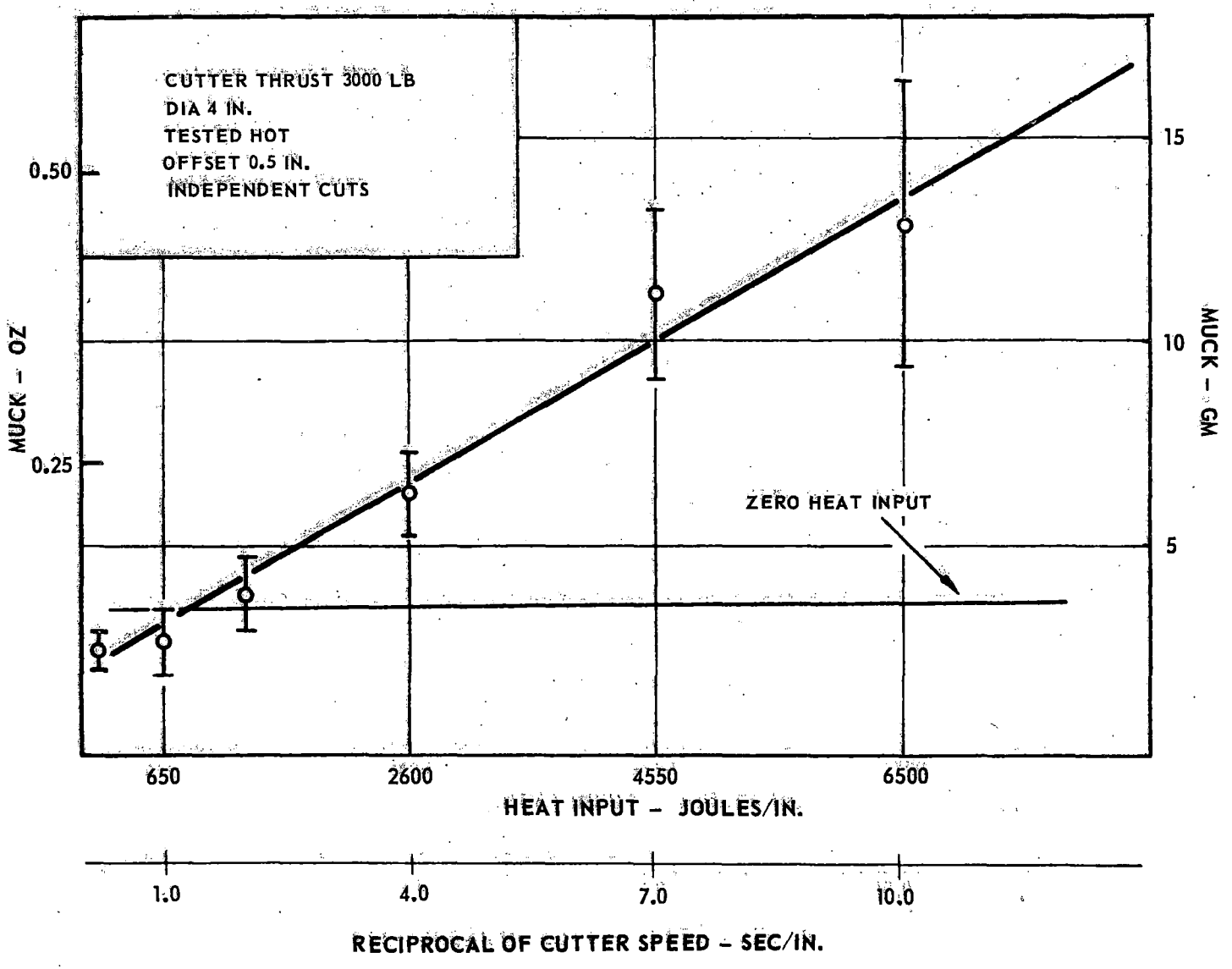

FIGURE 38. MUCK FOR 650-WATT FOCUSED BEAM

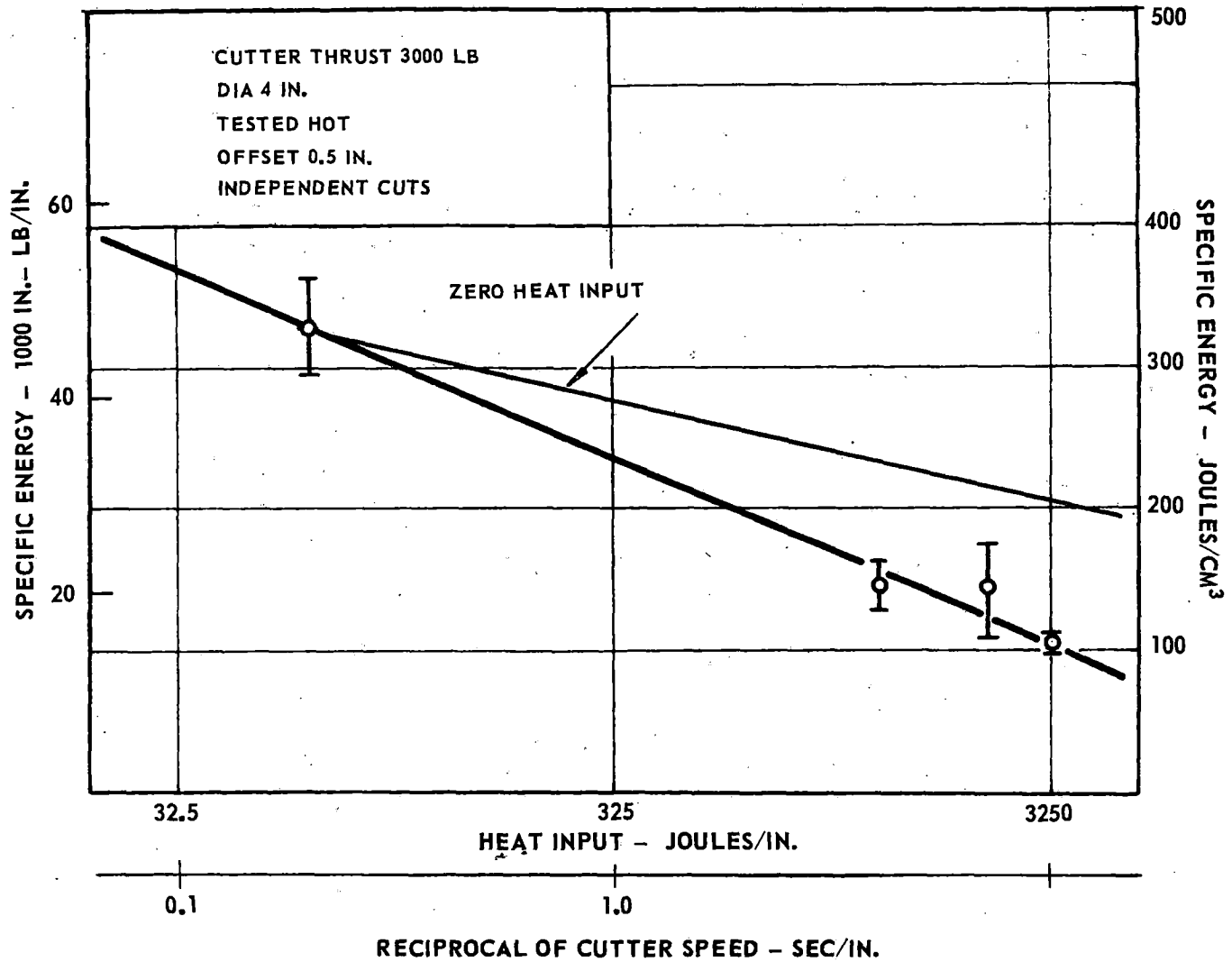

FIGURE 39 SPECIFIC ENERGY FOR 325 WATT FOCUSED BEAM

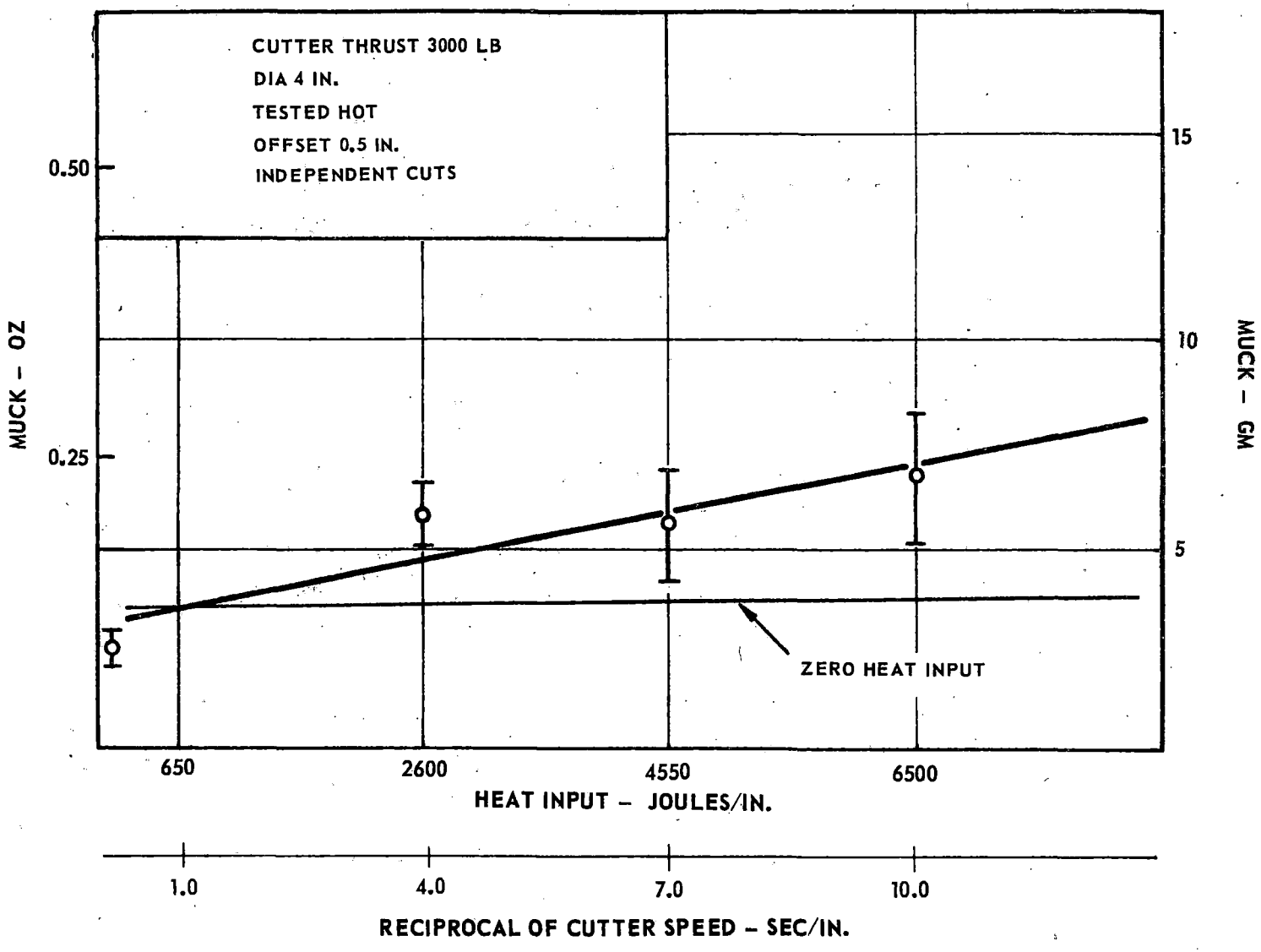

FIGURE 40. MUCK FOR 325-WATT FOCUSED BEAM

To better simulate removal conditions in a full-scale boring machine, a series of tests was run with a cutter thrust of 5000 lb. Figures 41 and 42 show the effect of heat input on rock removal for cutter diameters of 4 and 6 in., respectively, at a cutter thrust of 5000 lb.

Multiplicity of Cuts

Groove Spacing for Multiple Cuts with Heating

In the previous section, results were presented for multiple cuts with a 4-in. cutter operating with a thrust of 3000 lb. As shown in Figs. 19 and 20, these results indicated an optimum groove spacing of about 0.75 in. To investigate the effects of heat weakening at these spacings, the previous test series was repeated with a focused, 600-watt laser beam aimed midway between the groove being cut and the one to be cut next. The beam was aimed 2.5 inches ahead of the cutter. The results are shown, along with the results from the unheated tests, in Figs. 43 and 44. The heating, at a constant energy input of 1200 joules per inch (cutter and laser beam speed of 0.5 in./sec), evidently improved the cutting at all spacings. In addition, the optimum spacing remained unchanged, although the performance penalties in going to a 1.0-inch spacing are substantially less with the heat weakening.

Effect of Heat Energy on Rock Removal

To determine the effect of heat weakening in a manner similar to the tests done for single cuts on a smooth surface, a series of tests was run with various cutter (and therefore laser beam) speeds, making multiple heating and cutting passes. These tests employed a focused beam on a path halfway between cutter paths. A groove spacing of $\frac{3}{4}$ in. was used since this spacing gave good results for the heated tests run at 0.5 in./sec (1200 joules/inch), although the best groove spacing might be a function of the amount (i.e., the joules per inch) of heat weakening employed. Figures 45 and 46 show the results, in terms of specific energy requirements and muck removed, relative to the unheated case. Desirable effects are induced in both specific energy and muck removed, although the benefits are not as large as in the case of independent cuts on a smooth surface.

Analysis of the power required for the tests shown in Figs. 45 and 46 indicates that the mechanical power absorbed by the cutter is essentially unaffected by the application of the heat energy. This implies that the reduction in specific energy requirements is directly related to the increased rate of muck removal when heat is applied. Therefore, the effect of heat weakening in this case may be considered in terms of an increase in muck removal, at a constant mechanical power input.

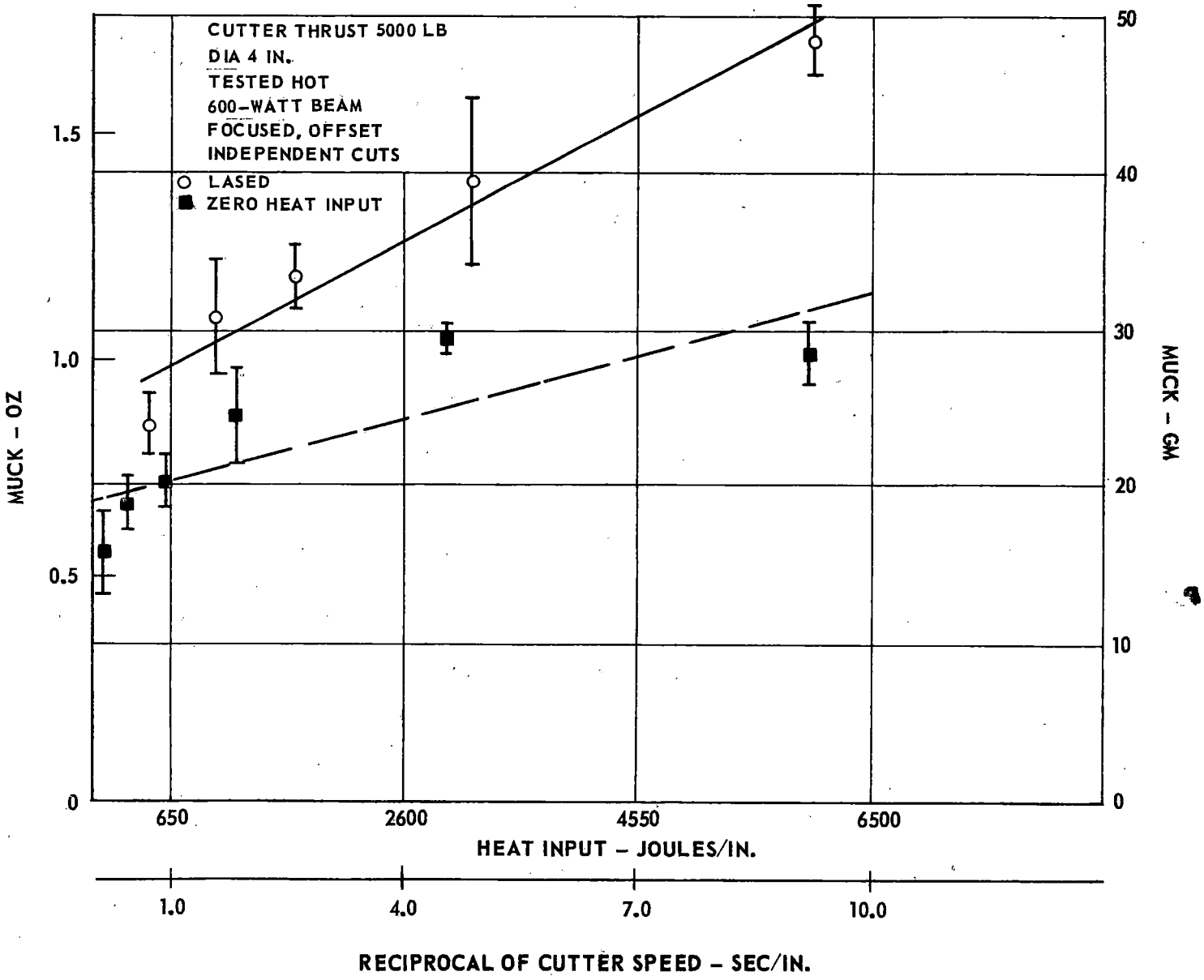

FIGURE 41. MUCK REMOVAL FOR 600-WATT BEAM

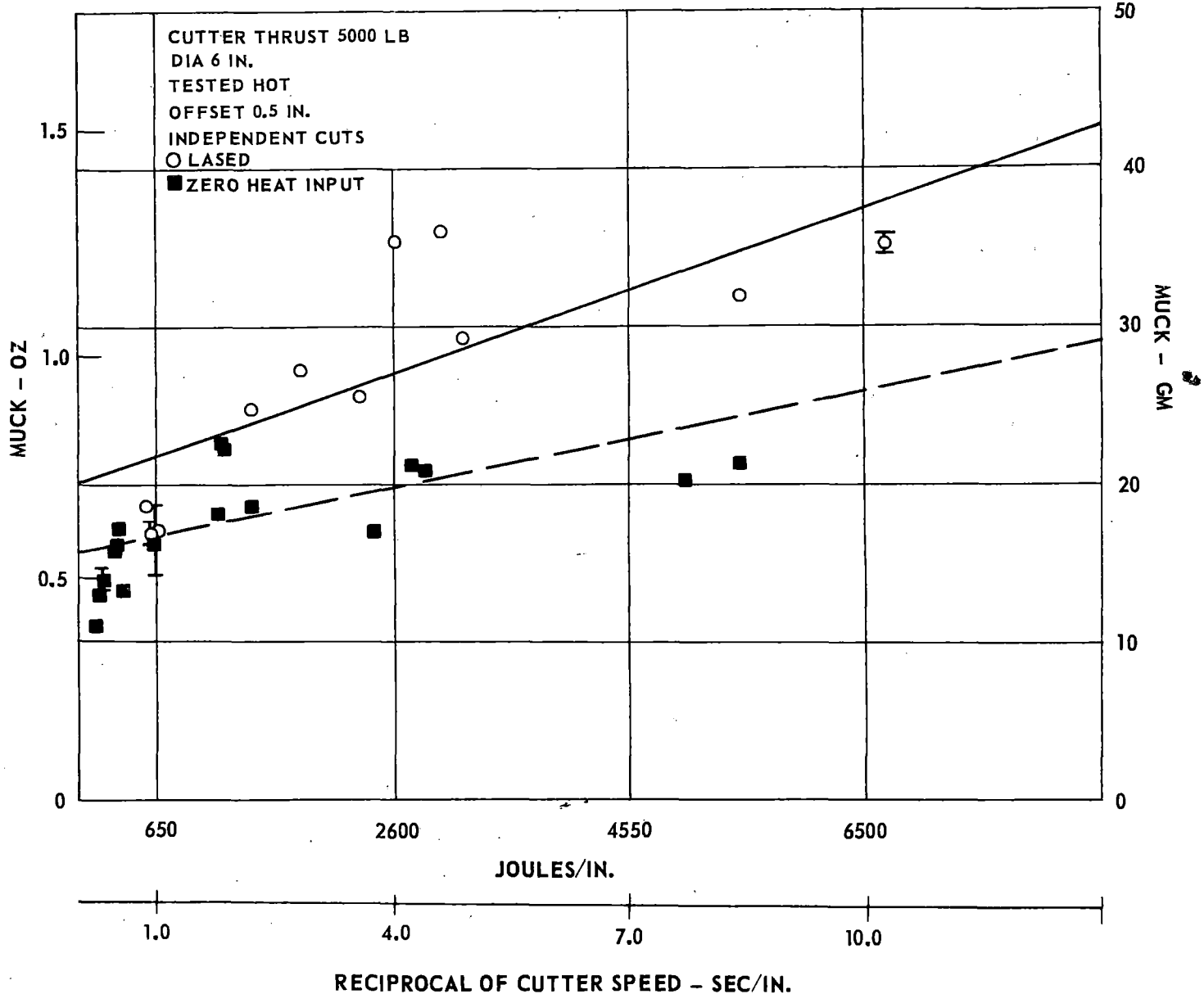

FIGURE 42. MUCK REMOVAL FOR A 600-WATT FOCUSED BEAM

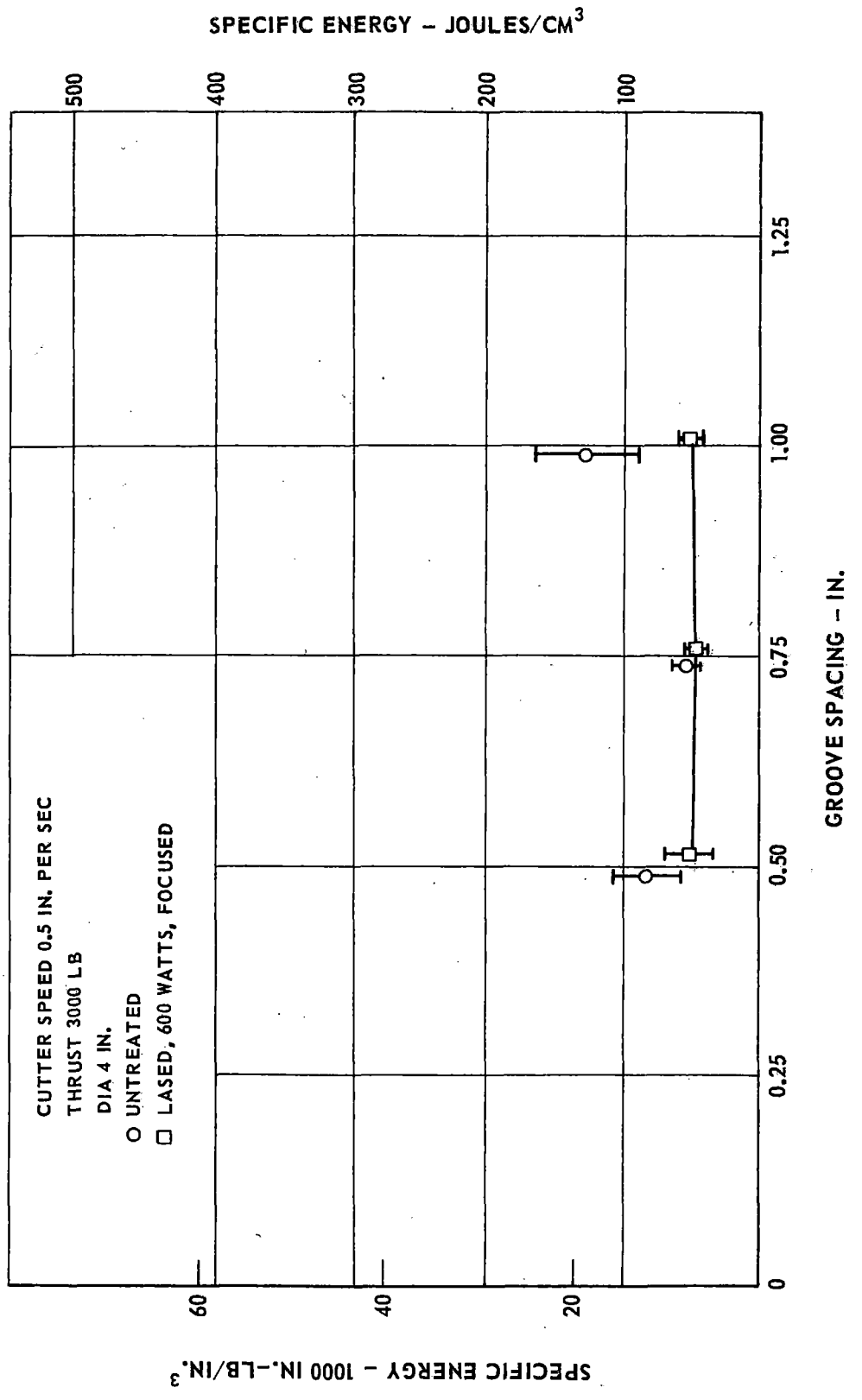

FIGURE 43. EFFECTS OF LASER HEAT INPUT AND GROOVE SPACING OF INTERACTING CUTS ON SPECIFIC ENERGY

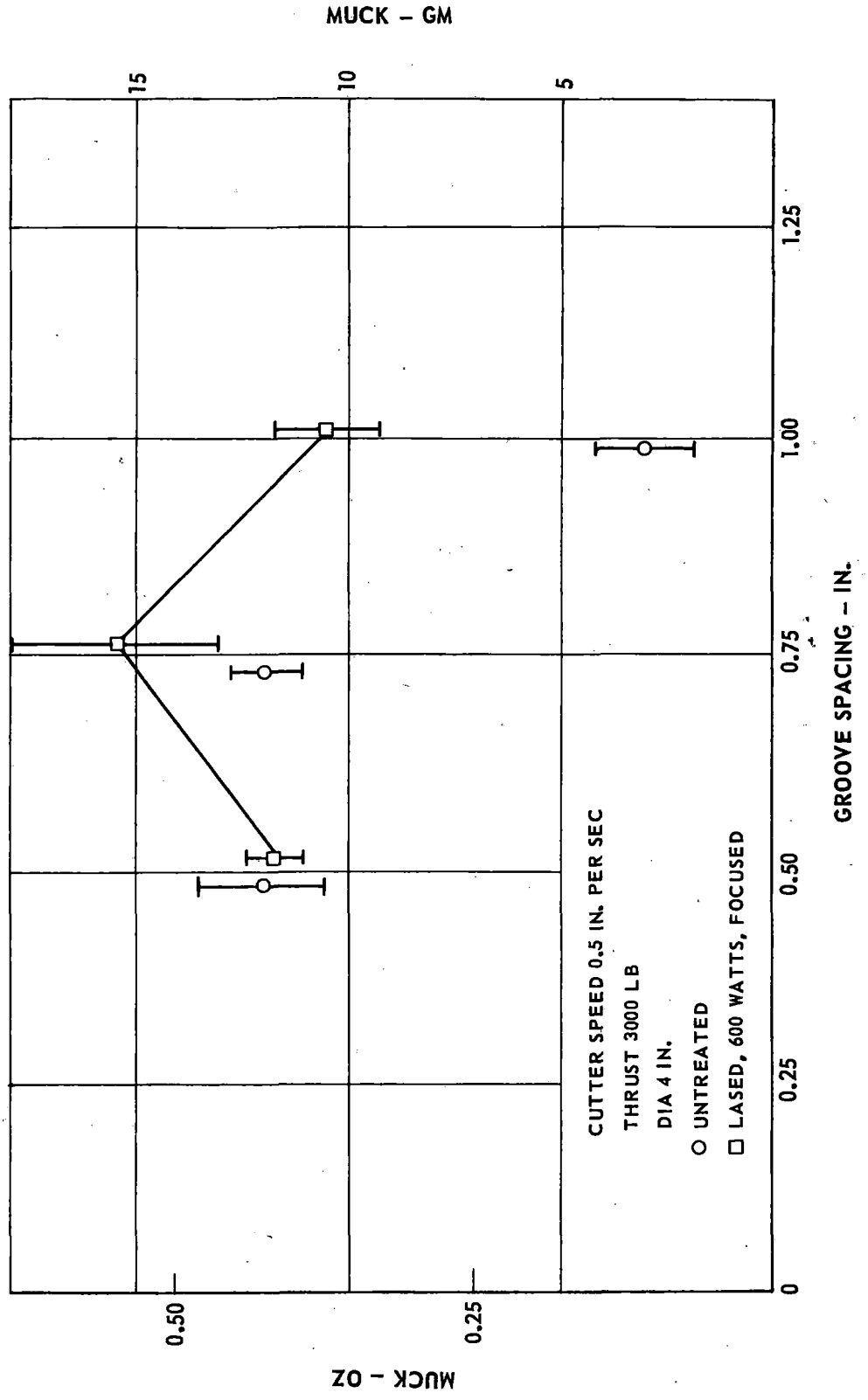

FIGURE 44. EFFECTS OF LASER HEAT INPUT AND GROOVE SPACING OF INTERACTING CUTS ON MUCK

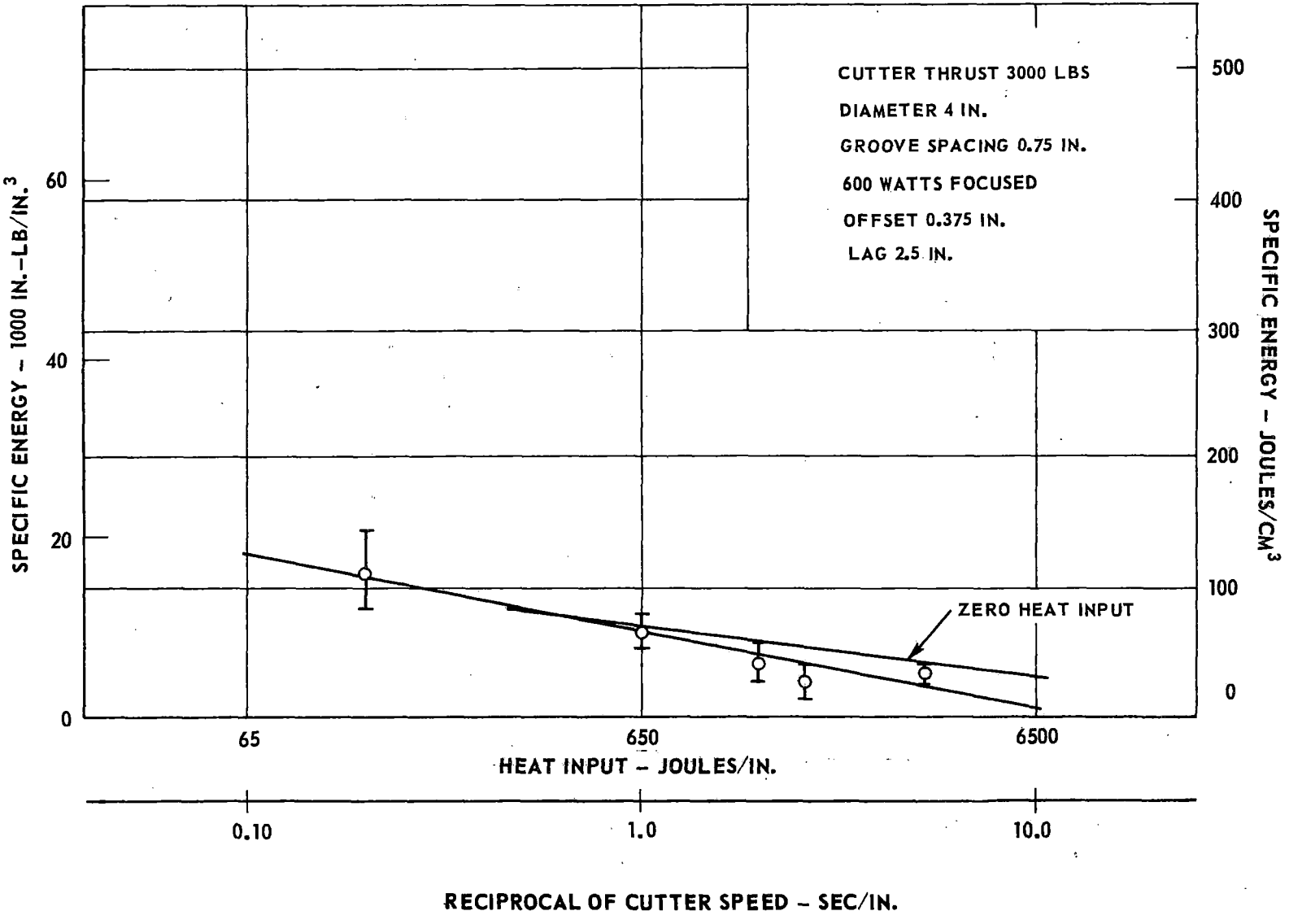

FIGURE 45. SPECIFIC ENERGY VERSUS HEAT INPUT

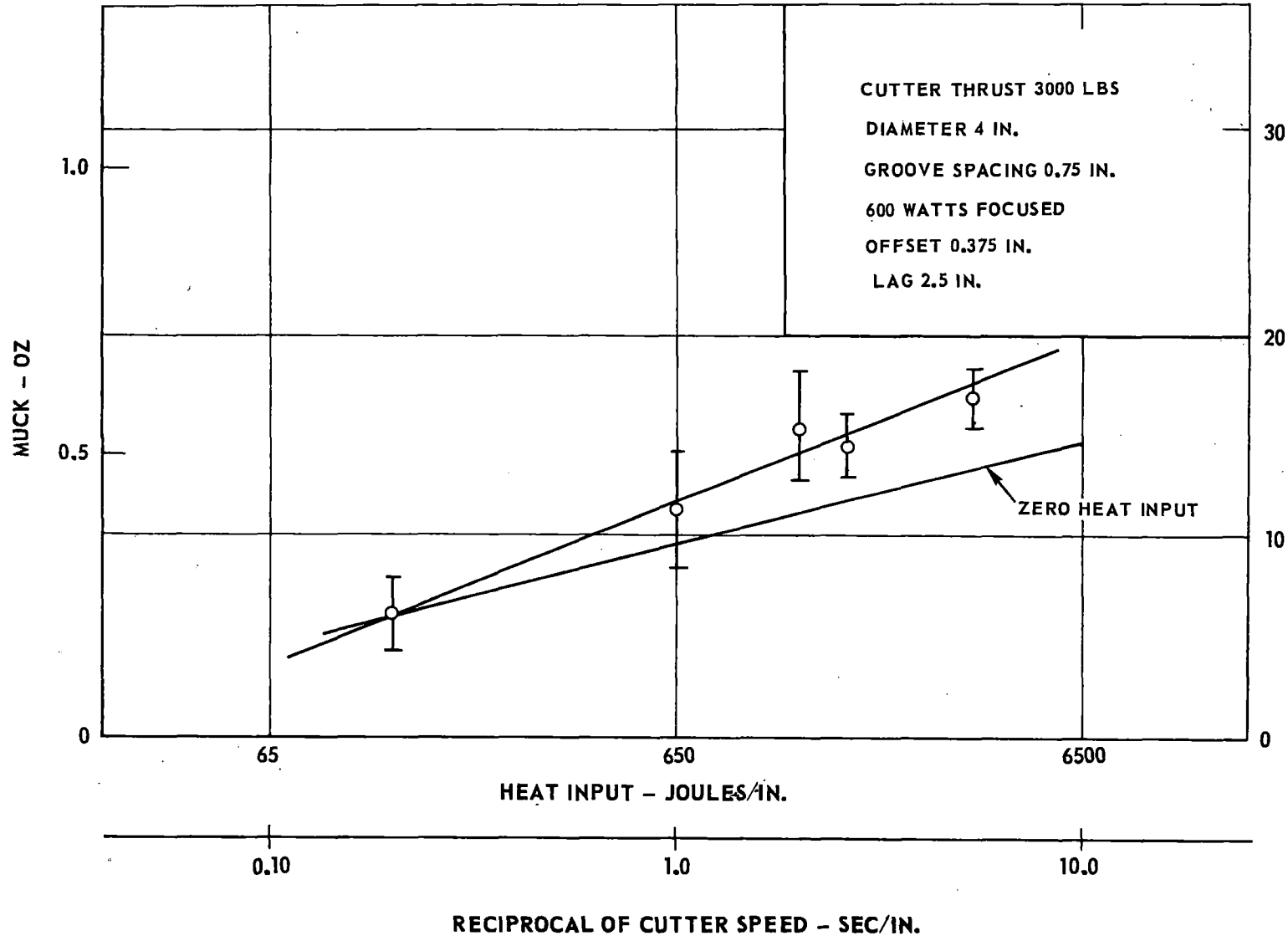

FIGURE 46. MUCK VERSUS HEAT INPUT

SUMMARY OF TEST RESULTS

The primary purpose of the test program was to generate data to be used in the evaluation of a full-scale application of heat weakening to hard rock tunneling. In this section the results of the test program are reviewed in this light, and representative data are selected for economic evaluation.

Selection of Representative Tests

The four specific test cases selected for analysis in the economic evaluation are listed and compared to estimated full-scale cutting parameters in Table 2. The reasons for selecting these tests for analysis are discussed below.

The first test series, employing a cutter thrust of 3000 lb and a cutter diameter of 4 in. with focused, offset laser radiation and single, independent cuts on an initially smooth block, is of interest primarily because there appeared to be a large effect due to the heating. The series of tests leading to these data established the beneficial effects of focusing the beam and heating along a path offset from the cutter path.

The second test series indicates, when the results are compared to the first, the effect of multiple cuts (i.e., repeated heating and then cutting in the same path, rather than just one cutter pass on a smooth surface) which is much more representative of a tunneling situation than the independent, single-cut situation. This test series was the only series of data taken showing the effect of various heat input levels on the multiple-cut situation.

Besides simulating the multiple-cut situation, the other major test parameter that was substantially different from the full-scale situation (and yet was under the control of the investigators, as the cutting speed was not) was cutter thrust. To improve this situation, two test series were run at a thrust level of 5000 lb with the 4-in.-diameter cutter, and are referred to in Table 2 as tests 3 and 4. These tests are substantially closer to the thrust loadings (in terms of cutter thrust per inch of cutter diameter) expected with a full-scale machine than the 3000 lb tests. Both focused and unfocused test results are included, since some heat sources (e.g., radiant heaters) do not enjoy the same focusing capability as the laser, so it is of interest to demonstrate the magnitude of the resultant performance decrement, due to lack of focusing, at the high thrust level. For these tests, the unfocused beam was not offset from the cutter path, and thus the performance degradation resulting from the use of an unfocused beam may be exaggerated in this case.

TABLE 2

ROCK CUTTING CONDITIONS

Test Conditions	Test 1	Test 2	Test 3	Test 4	Full-Scale
Mechanical					
Cutter Thrust, lb	3000	3000	5000	5000	~20,000
Cutter Diameter, in.	4	4	4	4	11
Cutter Speed, in./sec	0.1-2.0	0.1-2.0	0.1-2.0	0.1-2.0	~ 40-50
Cutter Path Spacing, in.	1.0(1)	0.75	0.625	0.625	3.0
Multiple (M) or Single (S) Cuts(2)	S	M	S	S	M
Thermal					
Beam Focused (F) or Unfocused (U)	F	F	U	F	-
Beam Power, watts	650	650	600	600	-
Heated Path Location(3)	offset	offset	on cutter path	offset	-

(1) Spacing set so that cuts are independent

(2) Single cuts are on initially smooth surface, multiple cuts are against rough surface

(3) Heated path location relative to cutter path is indicated

To summarize, the four particular test series were chosen as being most representative of the effects of heat weakening on tunnel boring due to their optimized heat input conditions, high thrust loadings, variations in beam focusability, and demonstration of heating effects of multiple vs single cuts.

Method of Presenting Data

Data from these four test series were analyzed based on muck removal only. For the first two series of tests, this approach was validated, since the decrease in specific energy was evidently due precisely to the increase in muck removal rate (i.e., the power absorbed by the cutter was the same for the unheated and the heated tests). For tests 3 and 4, at a thrust of 5000 lb, muck removal data is all that is available, since absorbed cutter power was not measured. It is implicitly assumed, therefore, that the relationship between muck removal and specific energy is similar to that demonstrated at the 3000-lb thrust level.

As mentioned in the previous discussions of the results of the tests, the only way to vary the heat input was to vary the speed of the heat source and also, therefore, the speed of the cutting tool. Cutting speed has an effect on the muck removed, independent of the amount of heat added, which complicates the correlation of muck removed with increasing heat input. To simplify the presentation of the test data for the cases of interest, data points were sought where unheated and heated tests were made at the same cutting speed. The ratio of the muck removed under the two test conditions at these speeds is then plotted. This approach avoids using the ratio of the curves fitted to the test data, which can give incorrect results in certain instances. Some pairs of data points were used in which the cutting speed varied only slightly. In these cases the slope of the data curve was assumed to pass through one of the points, and the resulting value at the appropriate cutter speed was read.

The ratios of muck removed with and without heating, which were generated in the manner described above, are presented in Fig. 47 for the tests listed in Table 2. For most of the test conditions, the interpretation of the data points is straightforward. However, for the multiple-cut case, with 3000 lb of cutter thrust, there were only two data points taken at the same speed. The third data point was generated by comparing the 3500 joule/inch data point with a neighboring, unheated case, as shown in Fig. 48. There are several unheated test points in the vicinity of the heated treated data point; the indicated point was chosen because it appears to be closest to the trend line for the unheated test results.

Discussion of Selected Test Results

The individual data points, shown in Fig. 47, calculated, as discussed above, by ratioing muck removal results at specific cutter speeds, are connected by straight lines to help delineate the different test conditions.

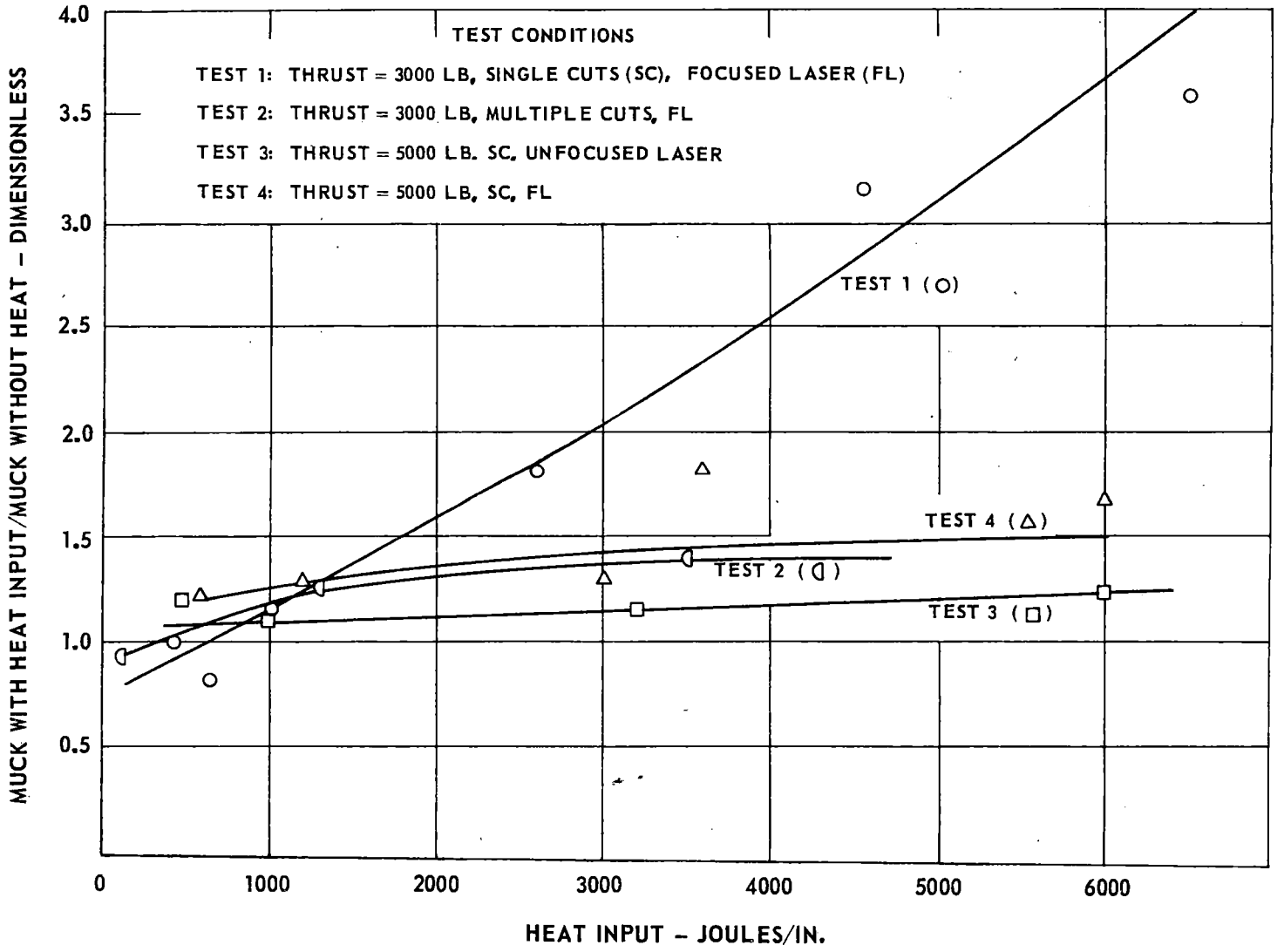

FIGURE 47. SUMMARY OF TEST RESULTS

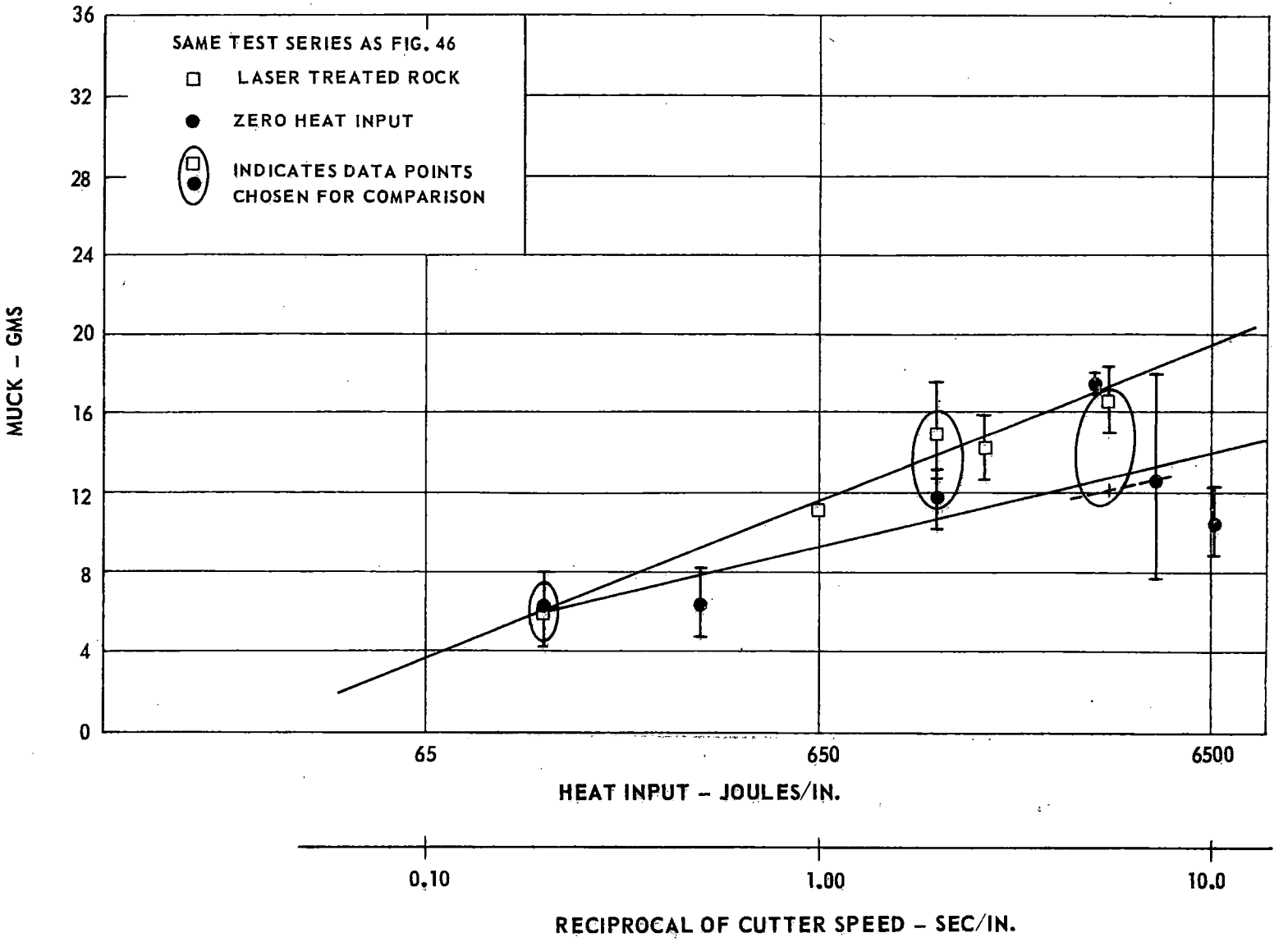

FIGURE 48. SELECTION OF SPECIFIC TEST POINTS USED TO DETERMINE MUCK REMOVAL RATIO

The greatest effects of heat weakening were observed for single cuts with 3000 lb of cutter thrust. For very high heat energy inputs, the amount of muck removed was increased by more than a factor of three. However, at least 1000 joules per inch were required to show any significant increase in muck removal rate.

For the multiple-cut situation, the increase in muck removal ratio was substantially less, showing a maximum increase of 40% at the highest energy input tested for this case (3500 joules/inch). This is due at least somewhat to the more-efficient cutting without heat in the multiple cut situation. Since cutting against the roughened, damaged face is more efficient to begin with, one would expect any specific amount of heating to have a smaller effect on the muck removal rate. Cutting against a roughened face is, of course, much more representative of the true tunneling situation, so this case is more representative of full-scale conditions than the first case.

Increasing the cutter thrust also has a deleterious influence on the effect of heating, although the higher thrust again is more representative of full-scale conditions. As the cutter thrust is increased, the mechanically stressed zone increases, and the heat-stressed zone becomes smaller by comparison.

With the unfocused laser, the increase in muck removed is further reduced for the 5000-lb-thrust case (Test 3), as was observed previously with 3000 lb of thrust (compare Figs. 28 and 37).

Thus it appears that, for the cases of most interest, i.e., the multiple-cut cases and the high-thrust cases, which best represent full scale, the increase in muck removal rate (or increase in advance rate at constant mechanical power input) which can be ascribed to the effects of heating is limited to less than 50%. The economic implications of increases in muck removal rate of this magnitude are discussed in Chapter VI.

CHAPTER II

GENERAL ANALYSIS OF HEATER SYSTEM DESIGN

The purpose of this chapter is to discuss some of the fundamental engineering design problems associated with heat-assisted tunnel boring machines, prior to the detailed analysis and design of some specific systems. The chapter begins with an analysis of tunneler heater power requirements as a function of machine size and rpm, and heating energy requirements. Present-day tunnel boring machine design is used as a point of departure for this analysis. Heat transfer efficiency from a heater to a rock face either by conduction (from a gas jet) or radiation is then considered. A fundamental treatment of the environmental control problem is also presented, along with the design of systems to alleviate the expected increase in tunnel ambient temperature. Finally, based on all of the above, some general considerations relative to a range of possible rock heating systems are presented, and reasons are given for the selection of three system types for more detailed analysis.

The analyses in this chapter form a necessary prelude to the detailed heater system design work discussed in Chapter III, as well as to the development of basic system relationships (e.g., heat transfer efficiency) used in the analysis of the economics of heat-assisted boring machines given in Chapter VI.

HEAT INPUT ANALYSIS

The test results presented in Chapter I usually present the effect of heat damage (weakening) done to the rock in terms of some net energy input per unit area of rock. This often is given in terms of joules per linear inch of heater pattern travel. Knowing the width of the heating beam, this readily can be converted into joules per square centimeter of heated rock. The purpose of this section is to show the implication of a given energy input per unit area on the total tunneler heating power required. Also, the effect of mechanical design (rpm) on heater power and the limitations on heating rate (power density) due to rock melting are considered.

Heating power in this section is considered to be the rate of heat actually flowing into the rock. Relating this rate to an actual heater output depends on the heater type under consideration; this subject is discussed in the next section. In general, the power going into the rock is only slightly less than the power output for radiant type heaters, but is substantially less than the total output for gas jet type heaters.

Power Required

For convenience, consider a circular tunnel. (Actually, all successful rock boring machines in this country have been circular, to allow efficient power transmission to the rock by pressing the entire rotating head into the rock face.) The geometry of the heating system power output relative to the cutters, as developed in the test program and design studies, is show schematically in Fig. 49. The heating power is assumed to emanate from a series of sectors which have a total central angle α. Within each sector, the heat may be concentrated in a band with width h, spaced (H-h) apart, as shown in Fig. 49.

Now, assuming for the moment that h = H (i.e., that the rock is heated equally at all radii), the amount of time that a particular piece of rock exposed to the tunneler will be heated during one revolution of the tunneler is, by inspection,

$$T = \frac{\alpha}{360} \frac{60}{rpm}, \tag{1}$$

where T = time of exposure of any given area of rock face to the heater system, seconds,
rpm = tunnel borer rate of rotation, and
α = total central angle of heater output, degrees

It is assumed that there is only one mechanical cutter at each radial location or cutter path. Thus, the rock is exposed, after cutting, for one full tunneler head revolution before being cut again. If a certain energy density, J_o, in joules/cm^2, is required prior to cutting the rock, then the power density flowing into the rock, P_o, in watts/cm^2, required to give that energy density is

$$P_o = \frac{J_o}{T} = 6\, J_o \frac{rpm}{\alpha} \tag{2}$$

where P_o = power density of heat input in $\frac{watts}{cm^2}$, and

J_o = energy density of heat input in $\frac{joules}{cm^2}$.

The total amount of heating system output (assuming 100% absorption by the rock) is the product of the heater area times the power density, or

$$P_T = P_o \frac{\alpha}{360} A_{FACE} = J_o \frac{rpm}{60} \frac{\pi D^2}{4}. \tag{3}$$

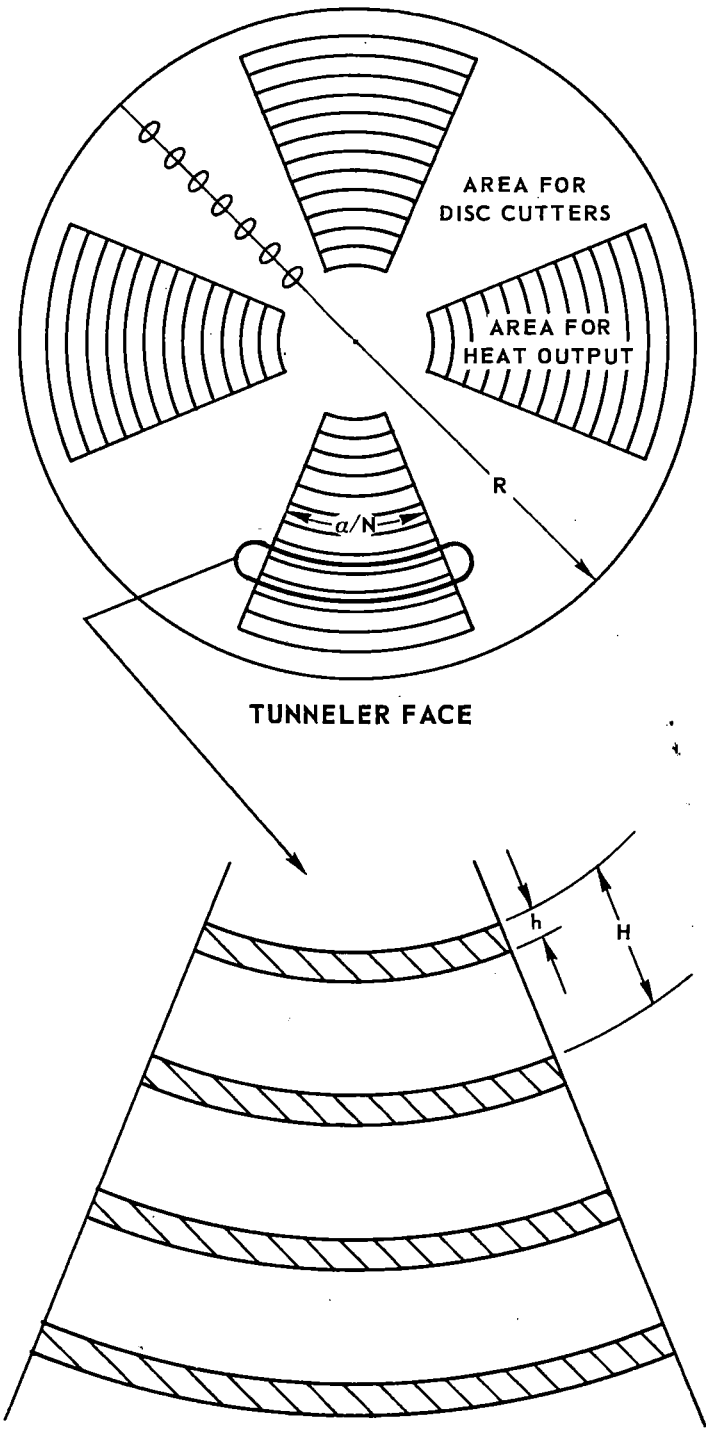

α = TOTAL CENTRAL ANGLE OF HEATER ARRAY
N = NUMBER OF HEATER SECTORS

FIGURE 49 GEOMETRY OF HEAT-ASSISTED TUNNELER FACE

Thus, the total power level of heat input to the rock face depends only on the energy density required into the rock face, the machine rpm, and tunnel diameter. The total heater system power output can now be defined as

$$P_{HS} = \frac{P_T}{\eta_D} = \frac{J_0}{\eta_D} \frac{rpm}{60} \frac{\pi D^2}{4} , \tag{4}$$

where η_D = efficiency of heat transfer from the heater to the rock.

Figure 50 shows total heating power level, P_T, for 10- and 20-ft-dia tunnels as a function of J_0 and rpm.

As can be seen from the above equations, the heater system power level, P_{HS}, is not a direct function of the heater power density. However, one of the limits on total heating power has to do with power density effects (rock melting) as is discussed below. It is therefore useful to express the power density explicitly for the configuration shown in Fig. 49, in order to relate limitations in power density to other system parameters.

If P_0 is the power density based on the entire face area, then this power density may be related to the power density based on the heated strip areas alone (i.e., the actual power density), by relating the heated area to the total face area. The ratio of heated area relative to the total face area is a function of the number of cutter paths on the face and the ratio h/H, as shown in Fig. 51. For values of R/H (R = tunnel radius) greater than 20, Fig. 51 indicates that h/H is an accurate value for the area ratio sought. Since cutter spacing (H) is usually no more than 3 in., and the smallest diameter to be considered is 10 ft (R = 60 in.), R/H will indeed have a value of at least 20. Therefore, the heat input power density for this case can now be written as

$$P_0 = \frac{P_0}{Ah/Af} = \frac{6\, J_0\, rpm}{\alpha(h/H)} . \tag{5}$$

Limits on Power Required

Total heater power obviously is a key parameter in determining the feasibility of heat-assisted tunneling. As discussed above, the requirements for weakening rock are expressed in terms of an energy density, J_0. Equation (4) indicates that the installed power (ignoring system inefficiencies) is directly proportional to this energy density, as well as to machine rpm, and diameter squared. Thus, to minimize the installed heating power required for a given energy deposition in the rock per revolution, the tunnel boring machine rpm should be as low as possible. A second limiting parameter on the amount of heat installed is the heater power density. Power density and rock exposure time must be set to avoid rock melting.

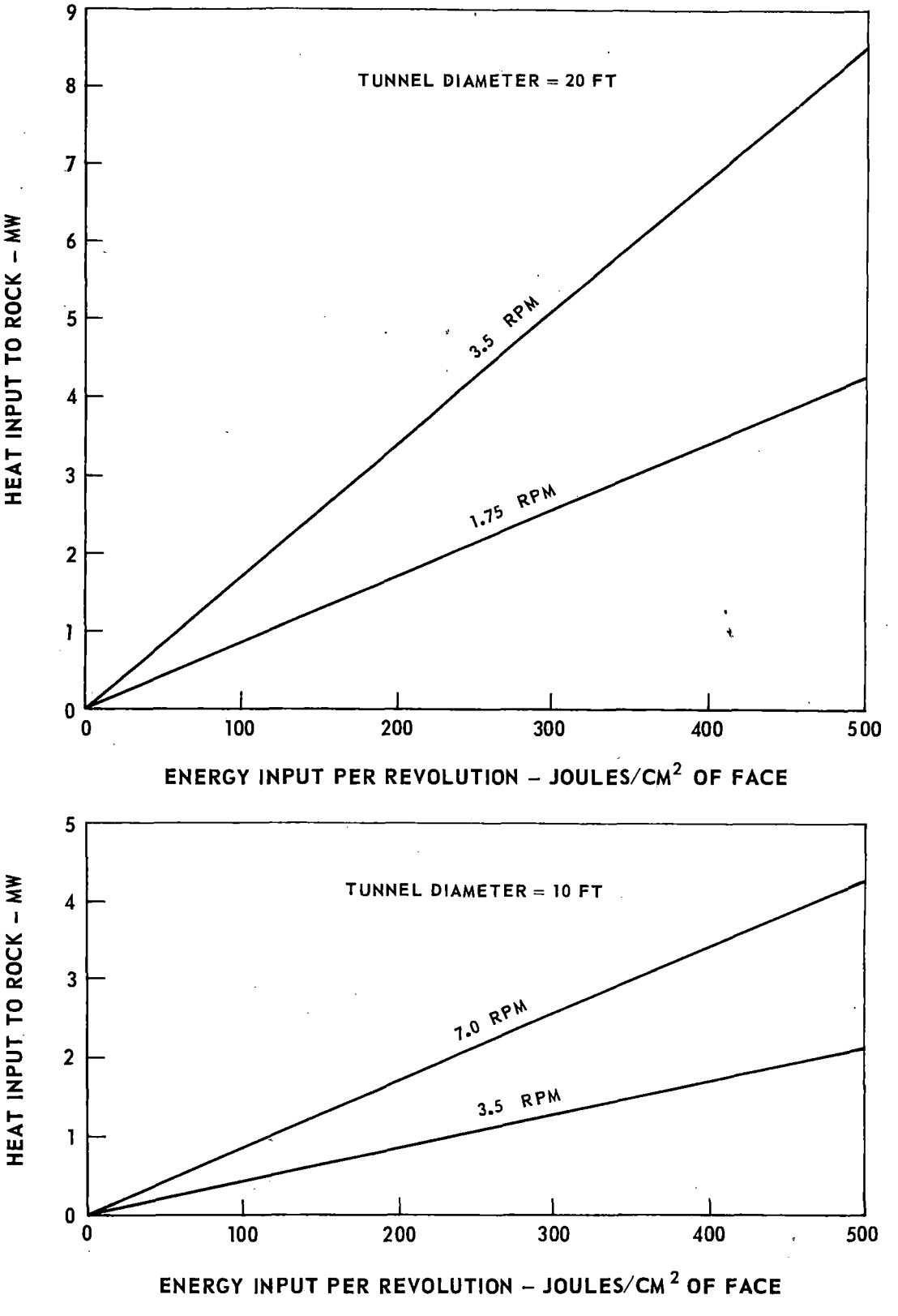

FIGURE 50 HEATER POWER REQUIREMENTS FOR HEAT-ASSISTED TUNNELING

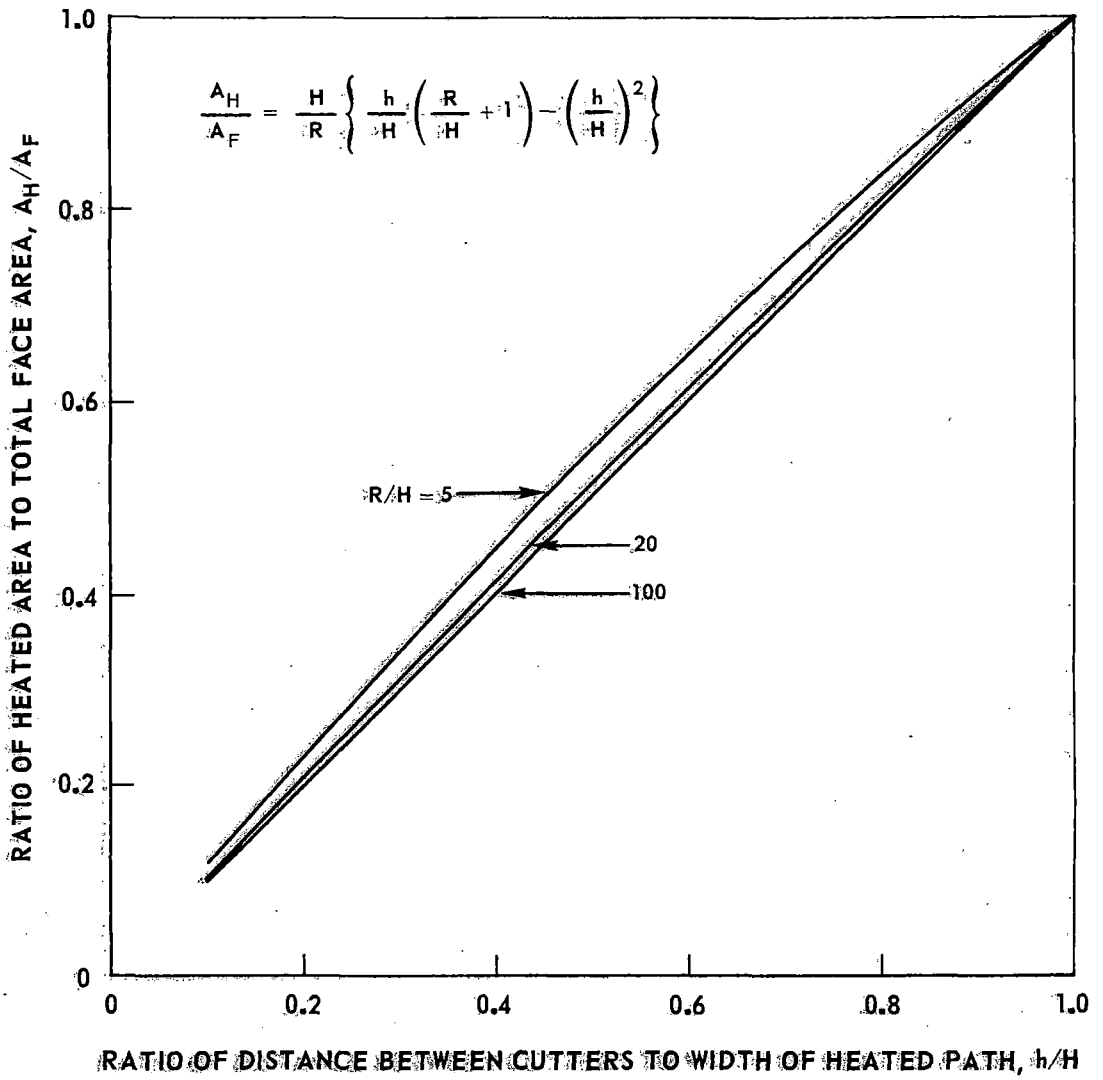

(SEE TEXT FOR NOMENCLATURE)

R/H = TUNNEL RADIUS/DISTANCE BETWEEN CUTTER PATHS

FIGURE 51 DETERMINATION OF HEATED FACE AREA

Rock melting will incur a higher power input per unit of heat delivered to the rock because of the energy lost in the phase change of the rock mass and the possible deleterious effects on rock thermal properties (e.g., absorption). These two factors, machine rpm and rock melting, are discussed below.

Machine RPM

Although heat is being used to effectively weaken the rock, the basic mode of actual rock removal is mechanical cutting, in a manner completely similar to the operation of present-day tunnel boring machines. Thus, the thrust and rpm of these machines must be adhered to, at least as a point of departure.

Penetration of rock by a boring machine depends on delivering mechanical power to the rock. Power delivered is proportional to the product of machine thrust against the face (which determines torque force required) and rpm. In general, one then might assume that rpm could be decreased and thrust could be increased to keep mechanical power, and therefore penetration rate, constant. However, cutter bearing life is affected much more by the thrust force than by rpm, so cutter costs would increase with increasing thrust and decreasing rpm. Thrust and rpm are, of course, also related to basic machine design and cutter type in other more subtle ways.

Rather than attempt a complete, or even a partial, basic analysis of mechanical machine design, examination was made of existing rpm trends with present-day machines. Figure 52 shows rpm as a function of tunnel diameter for several hard-rock tunneling machines. The lower rpm values for given machine types tend to follow lines of constant (rpm x diameter). A value of 80 for this product has been estimated by T. N. Williamson (Ref. 10), and various machine and bit manufacturers use different values. A value for (rpm x diameter) of 70 appears to be representative as a lower bound of the data and was used to determine conventional (nonheat-assisted) boring machine rpm for this study.

Rock Melting

Melting of the rock surface can be achieved with a range of combinations of heat input power density and rock surface exposure times. A one-dimensional analysis of heat flow into a semi-infinite solid, which had previously been developed at the United Aircraft Research Laboratories (Ref. 11), was used to describe the surface temperature and temperature profile under a heated spot.

The faster a given amount of heat energy is supplied to a unit area of rock surface by radiation, the higher will be the resulting surface temperature, and the steeper the resulting thermal gradient. This effect is shown quantitatively in Fig. 53. The rock properties assumed for this figure correspond roughly to Barre granite as given in Ref. 12. Examination of Fig. 53 indicates that there will be some exposure time for a given amount of heat energy at which the rock

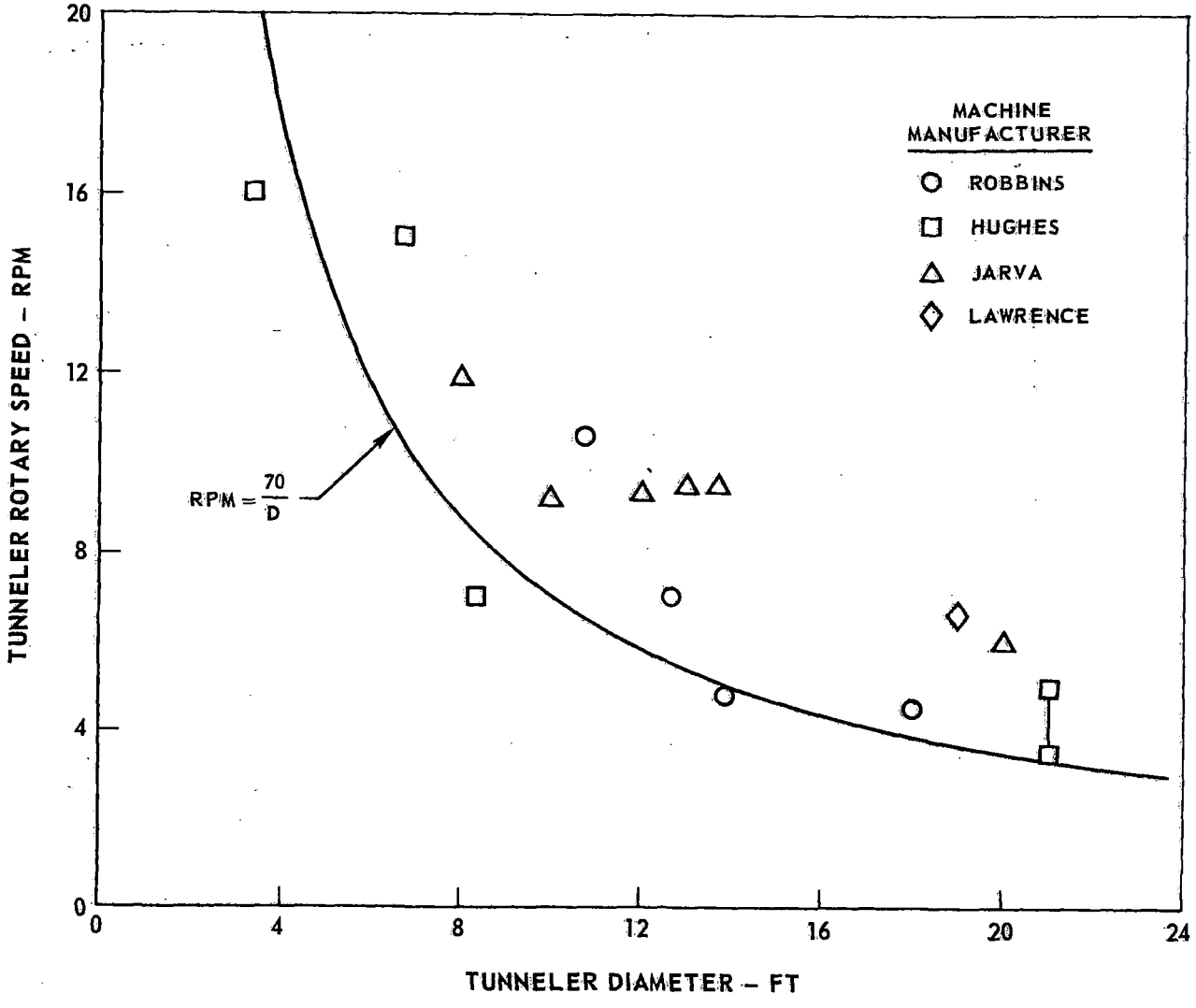

FIGURE 52 PRESENT-DAY TUNNELER RPM

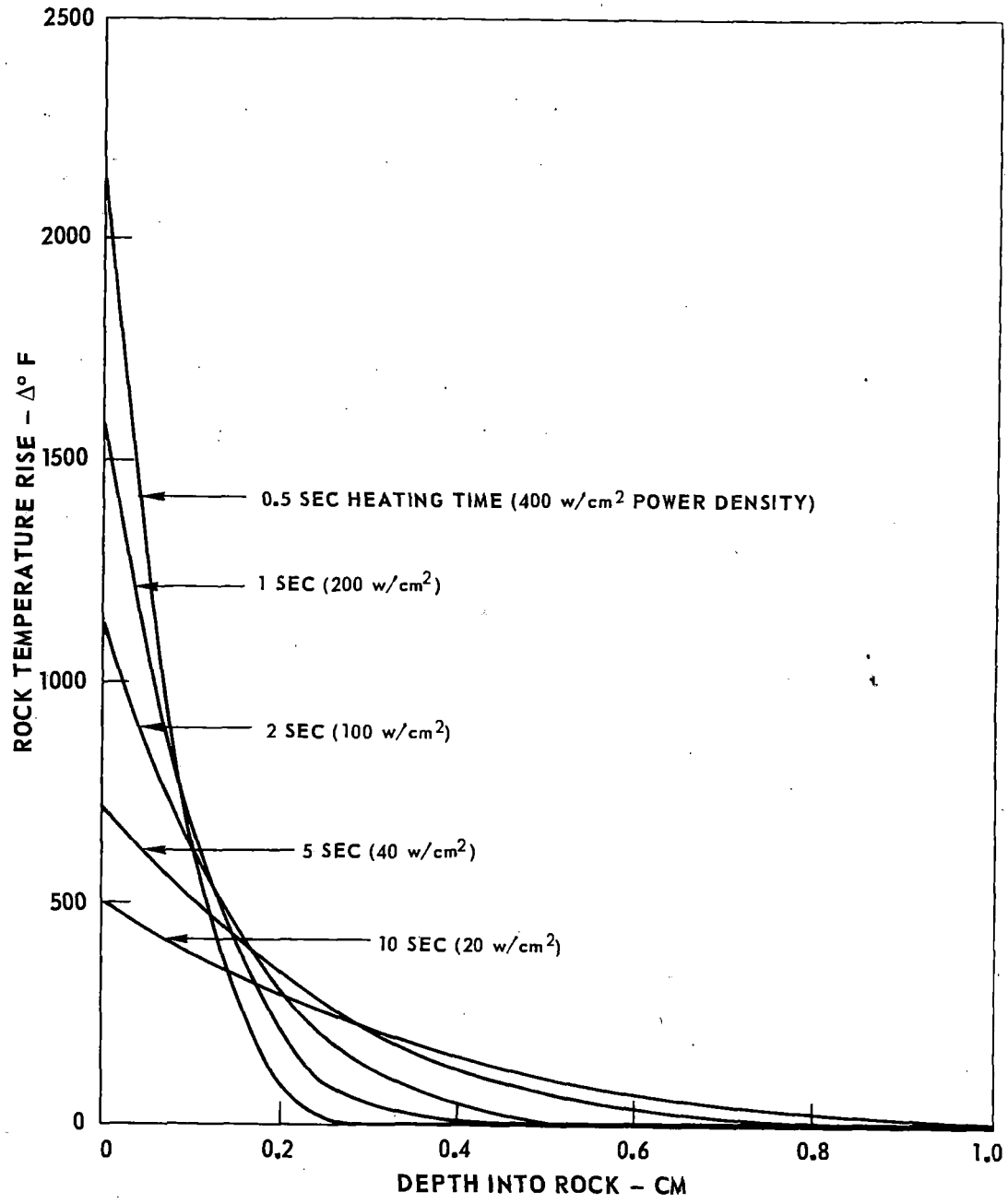

ENERGY ABSORBED = 200 JOULES/CM^2

FIGURE 53 TEMPERATURE GRADIENT IN HEATED ROCK

surface temperature will be sufficiently high to induce rock melting. Rock melting temperatures are on the order of 960 to 1160 deg C (1760 to 2120 deg F), as shown in Table 3.

In general, rock melting is to be avoided when attempting to heat-weaken rock. For one thing, the amount of heat energy lost in changing phase of the rock is wasted in terms of propagating a temperature profile into the rock. Also, molten rock may alter the rock surface absorptivity of radiation deleteriously, whereas this absorptivity is known to be relatively high for nonmolten rock, as discussed below.

These two limits (i.e., heating time [rpm], and rock melting) on the relationship between heat energy absorbed and heating power density are shown by the shaded areas in Fig. 54, which is a plot of energy density deposited in the rock vs power density flowing into the rock. The lines of constant exposure times express simply that energy = power x time. As discussed above, the heating time is a function of machine rpm and heater coverage of the face, α, as defined in Fig. 49. Assuming a heat-assisted boring machine rpm of between 2 and 4, and an α of between 90 and 180 degrees, the heating time is in the range of 4 to 15 sec. Limitations on α and rpm prevent the heating time from being significantly higher. The lines from the upper left to the lower right are the resulting surface temperature rise at the given heating conditions, as determined from calculations such as those in Fig. 53. A band is shown at around 2000 F to show the onset of melting. Also, lower temperatures are shown to allow estimation of rock surface temperature increase for specific design cases.

The result of these limitations, as shown in Fig. 54, is that the heater power density (assuming 100% efficiency of transfer of heat from heater to rock) should be in the range of 60 to 120 watts/cm^2 to allow the maximum amount of heat energy to be deposited on the surface without large amounts of melting. Also, the maximum amount of heat energy that can be pumped into the rock, observing these limits, is between 500 and 1000 joules/cm^2.

Alternate Configurations

At this point, it is well to review a basic assumption made implicitly by the selection of a rotating head machine design as shown in Fig. 49. Since time is such an important factor in determining the total heater power and rock face energy absorption, it is of interest to examine tunneling machine designs wherein the process of adding heat and the process of cutting are uncoupled (they are coupled in the present case through machine rpm).

One way in which greater heating depths could be obtained is in a machine incorporating two completely different heads, a cutting head and a heater, or bank of heaters, which would be controlled independently. An existing mechanical

TABLE 3

MELTING POINTS OF VARIOUS MINERALS

Mineral	Temperature - °C
Anorthite, natural	1165 - 1520
Anorthite, artificial	1544 - 1562
An_5AB_1, artificial	1516
An_2Ab_1, artificial	1477
Labradorite	1040 - 1370
Andesine	1155 - 1280
An_1Ab_1, artificial	1430
An_1Ab_2, artificial	1375
An_1Ab_3, artificial	1340
Oligoclase	1135 - 1260
Albite	1115 - 1259
Arthoclase	1185 - 1220
Leucite	1275 - 1430
Nepheline, artificial	1059 - 1526
Enstatite	1375 - 1400
$MgSiO_3$, artificial	1557
Wollastonite	1203 - 1366
$CaSiO_3$, artificial	1515 - 1540
Diopside, natural	1135 - 1270
Diopside, artificial	1391
Augite	1085 - 1230
Tremolite	1200 - 1270
Hornblende	1060 - 1200
Olivine	1265 - 1750
Quartz	1425 - 1780
Magnetite	1190 - 1225
Hematite	1300 - 1400
Fluorite	1270 - 1387
Sillimanite	1816

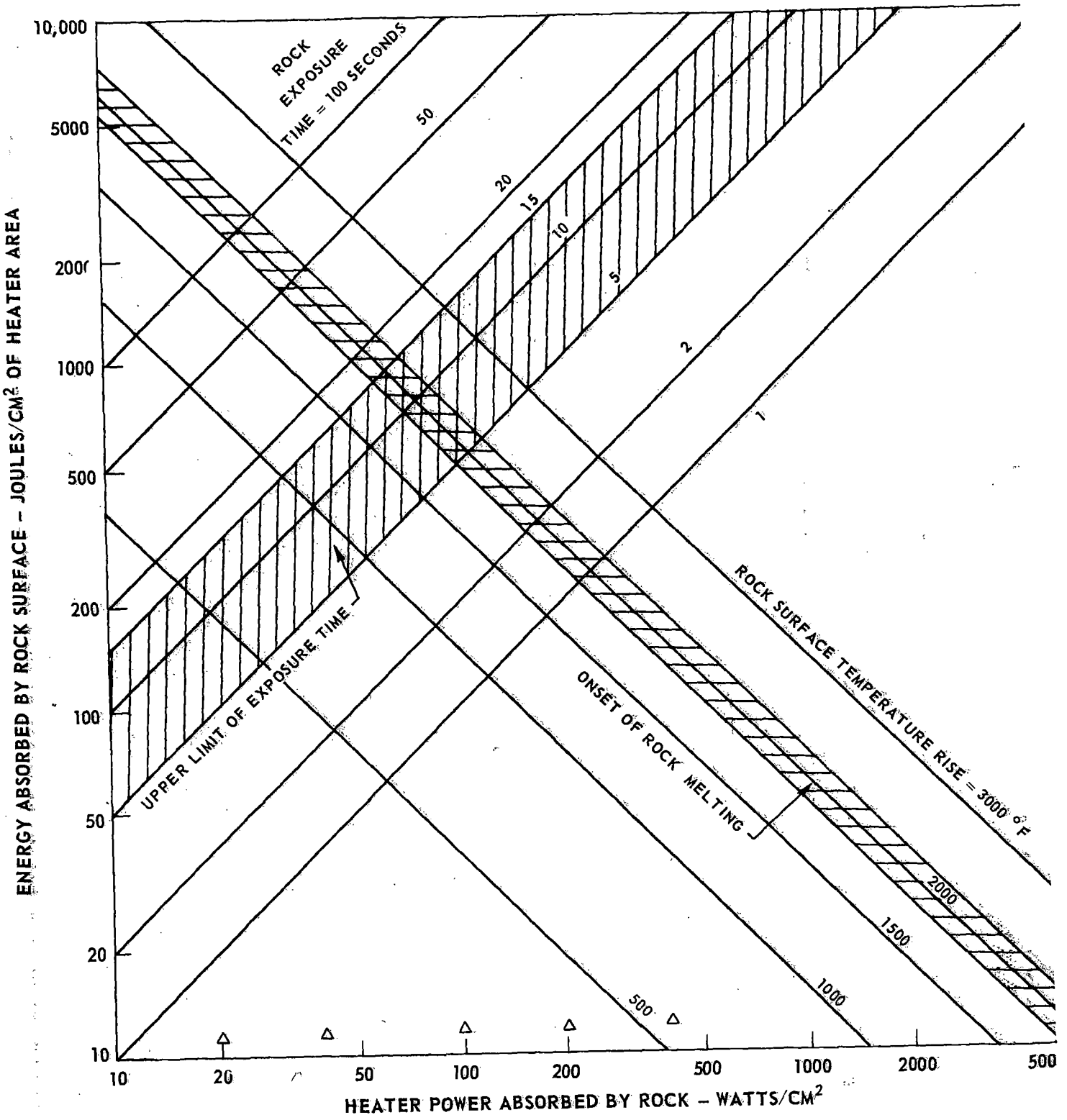

THERMAL CONDUCTIVITY = 1.68 BTU/HR FT °F

THERMAL DIFFUSIVITY = 0.0522 FT ^{2}/HR

FIGURE 54 ROCK HEATING RELATIONSHIPS

tunneler which could be adapted to this type of an operation is the Greenside-McAlpin (GM) tunneling machine shown in Fig. 55. This unit employs a rotating head with a diameter which is less than half the tunnel diameter, which indexes around the tunnel face cutting several inches deep at a single pass. Thus, a heating unit could be employed on a larger area of the face than the cutting unit, and the ratio of heating time to cutting time could be controlled.

This concept was not investigated in detail, since the advance rate with the GM type of machine is much less in borable rock than that of a full-face boring machine, due to the small area of rock attacked at a given time. Also, the basic concept of the present study involves adaptation of present-day boring machines to hard rock boring by the addition of a heater system. All successful mechanical rock tunneling machines in this country are of the full-face, rotary type, and therefore that type is considered in this study.

A more basic reason why combinations of mechanical and heating systems which allow very long heating times prior to rock removal may not be desirable is the slow rate of heat penetration in rock. For very long times between mechanical removals, the heat would penetrate to a depth less than the depth required for a given rate of mechanical penetration.

This idea is illustrated by the curves in Fig. 56. The dotted curves indicate the depth into the rock at which the rock temperature reaches 100 F for the heat input intensities shown on the dotted lines, and for the heating times indicated on the horizontal axis (notice that only those heat input conditions below the hatched limit line are of interest, since conditions above this line would theoretically induce rock melting at the surface). The solid lines on Fig. 56 indicate the amount of rock that would have to be removed corresponding to the heating times shown if certain advance rates were to be maintained and the rock were to be cut regularly at the time intervals given by the heating times shown. If, for example, a full-face rotary boring machine is assumed, the heating time is equal to the time between cutter passes which, if there is only one cutter located at each radius, is given by 60/rpm. By looking at the results shown in Fig. 56 it can be seen that the depth to which the heat penetrates will more closely approach the depth of penetration required per rotation of the tunneling head to maintain a reasonably high advance rate when the rpm of the machine is kept high, thereby causing relatively low heating times (less than 20 to 30 sec). It is apparent that, for very long heating times (e.g., heating times greater than 30 sec), the depth of heat penetration will be substantially less than the depth of penetration per rotation as required, for instance, for an advance rate of 10 ft/hr. This argument is at best qualitative, since it is not clear that the extent of the heat weakening phenomenon exists only to the depth at which a sensible increase in rock temperature occurs. Undoubtedly, some of the weakening effect is due to the thermal stresses induced in the rock which obviously can penetrate to depths below those depths at which the rock is noticeably heated.

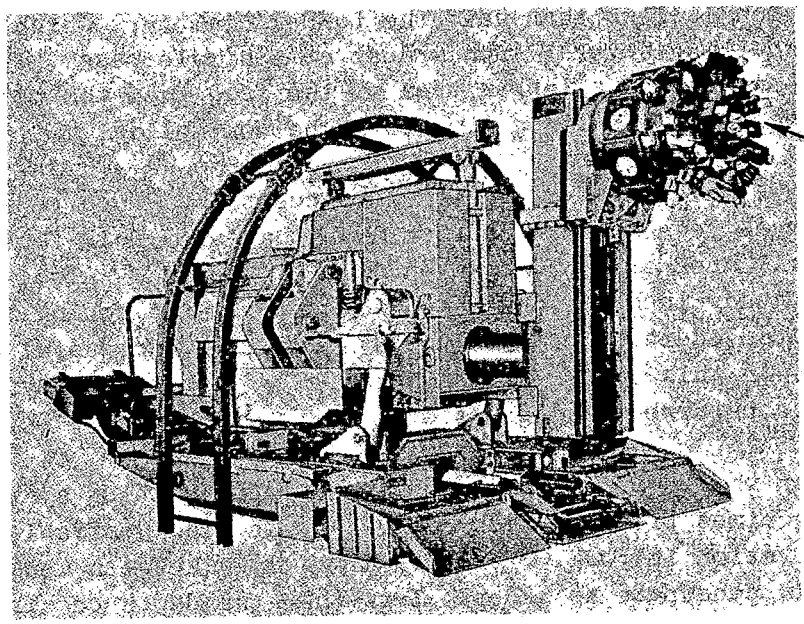

GENERAL VIEW

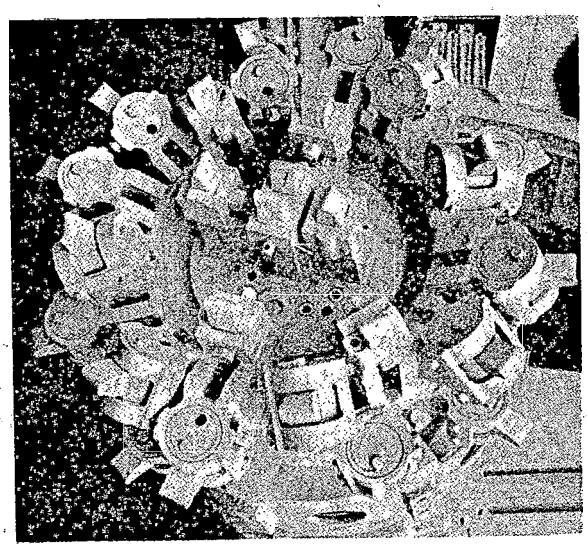

CLOSE-UP OF BORING HEAD

FROM MANUFACTURER'S BROCHURE

FIGURE 55 GREENSIDE–McALPINE TUNNELING MACHINE

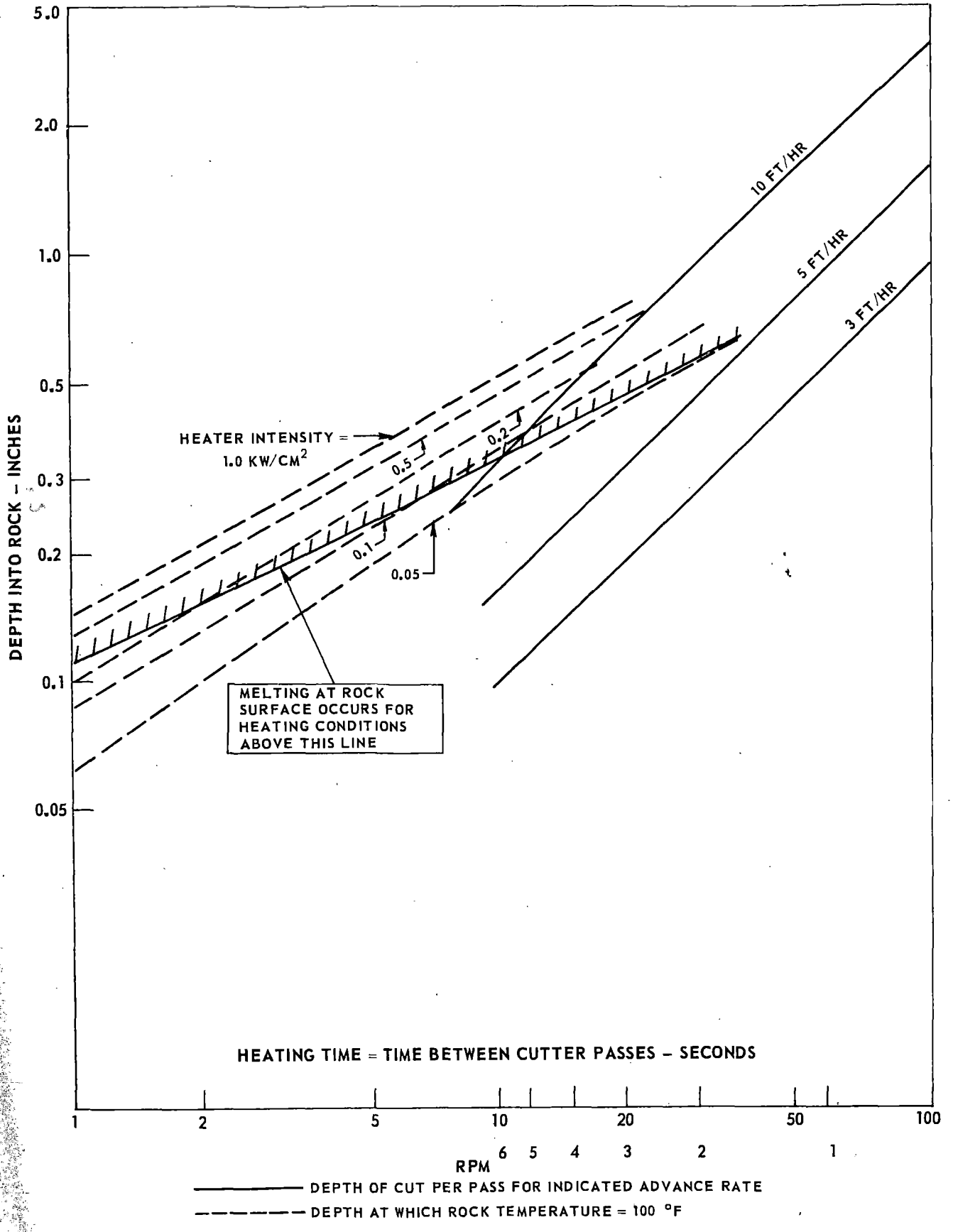

FIGURE 56 PENETRATION REQUIREMENTS FOR HEAT–ASSISTED TUNNELER

However, the general trends indicated by Fig. 56 -- namely, that the heat penetration and mechanical penetration are more likely to match each other for low heating times (rpm greater than one) -- is still valid.

HEAT TRANSFER ANALYSIS

Having established the factors that influence the rate of heat flow into the rock, it is of interest now to determine the heater power output necessary to realize the desired heat flow. Table 4 lists the basic heater system types investigated. Three of these are basically gas jet systems, in which the heat is transferred from a gas stream impinging on the rock tunnel face to the rock. Another type of heater transfers heat to the rock by radiation, which would include a radiant (electric) heater and a laser beam. Heat transfer from an electron beam to rock is considered separately.

Determination of this heat transfer efficiency from the device to the rock is crucial for two main reasons. First, a low efficiency will imply problems with control of tunnel temperature, as is discussed in detail in the next section. Second, some of the systems considered (e.g., the laser) have high capital costs, so any increase in the size of the heater due to heat losses can seriously affect the economy of the system. Of course, reduced heat transfer efficiencies also mean a higher power cost. However, the power cost can be small relative to the other factors mentioned in many cases of interest.

Heating Efficiency of Gas Jet Devices

Gas jet heaters depend on convection to transfer heat from the gas to the rock. For any particular area and rock temperature gradient, this convective heat transfer depends directly on the magnitude of the heat transfer coefficient immediately adjacent to the rock surface. Except for certain ablative missile investigations in which re-entry heat transfer characteristics are considered, few empirical efforts have been directed toward investigating heat transfer between a heated stream directed normal to a cold surface and the surface itself. Fortunately, this particular topic was the subject of an investigation conducted at Stanford University in 1962 (Ref. 13). Although the sizes of jets considered in Ref. 13 are smaller than those expected to be used in an actual tunnel operation, it appears that the results of that study can be applied, with little loss of accuracy, to larger jet-type devices.

The derivation of the heat transfer equations which were developed to analyze jet-type heat flow in a heat-assisted tunneling operation are discussed below.

TABLE 4

HEATER SYSTEMS CONSIDERED

1. Laser
2. Electron beam
3. Radiant Heater
4. Plasma Jet
5. Flame Jet
6. Steam Jet

In addition, the computer program which was developed for this analysis is described along with sample results which illustrate the efficiency of heat transfer between a gas jet and a rock surface.

System Description

A schematic diagram of the model established to determine the heat transferred from the jet exhaust to the rock wall is presented in Fig. 57. A flame jet or a plasma jet is located a distance, L, (nominally 6 to 15 in.) from the rock surface, and the jet exhaust is directed normal to the rock wall. It is assumed that the jet is attached to a large cutter arm and is moving in a direction parallel to the rock wall at a transverse velocity, v.

Since the exposure time for any small element of rock extending from the rock surface into the semi-infinite surface is small (because of the relatively large transverse velocity of the jet), it is possible to make the assumption that only one-dimensional heat transfer occurs. Corollary to this is the assumption that the heat intensity profile normal to the jet axis at the wall is uniform. The fundamental results of this model indicate that every element within the path of the traversing jet heater will have an identical temperature profile. Therefore it becomes necessary to concentrate attention only on one single, small, rock element, coaxial with the jet, which is exposed only for that time it takes for the jet to traverse an effective (stationary) target heat transfer area on the rock wall surface.

Method of Analysis

Hot gases of known composition are expanded through the nozzle of the jet-type heater from combustion pressure to ambient pressure at the rock face. These gases expand in a cone-shaped fashion, strike a target area on the wall, and then pass radially outward and away from the target. The area of the target is assumed to be circular and is geometrically determined from the exit diameter of the nozzle, the nozzle-to-wall distance, and a jet spreading angle of 6 deg. The heat transfer coefficient adjacent to the wall surface is derived from a relationship among the Stanton, Reynolds, and Prandtl numbers, described in Appendix A and based on information from Ref. 13. Once the film coefficient and gas temperature are established, an expression for the temperature variation with time for any axial location within the rock can be developed, based on the assumptions given in the description of the system model, and assuming rock properties invariant with temperature changes. Such an analysis is given in many standard reference works, such as Ref. 14, and is entirely similar to the analysis leading to the results shown in Fig. 53. Finally, it becomes necessary only to determine the maximum time of exposure for any element of area on the rock surface, which is equal to the target diameter divided by the linear velocity of the jet device.

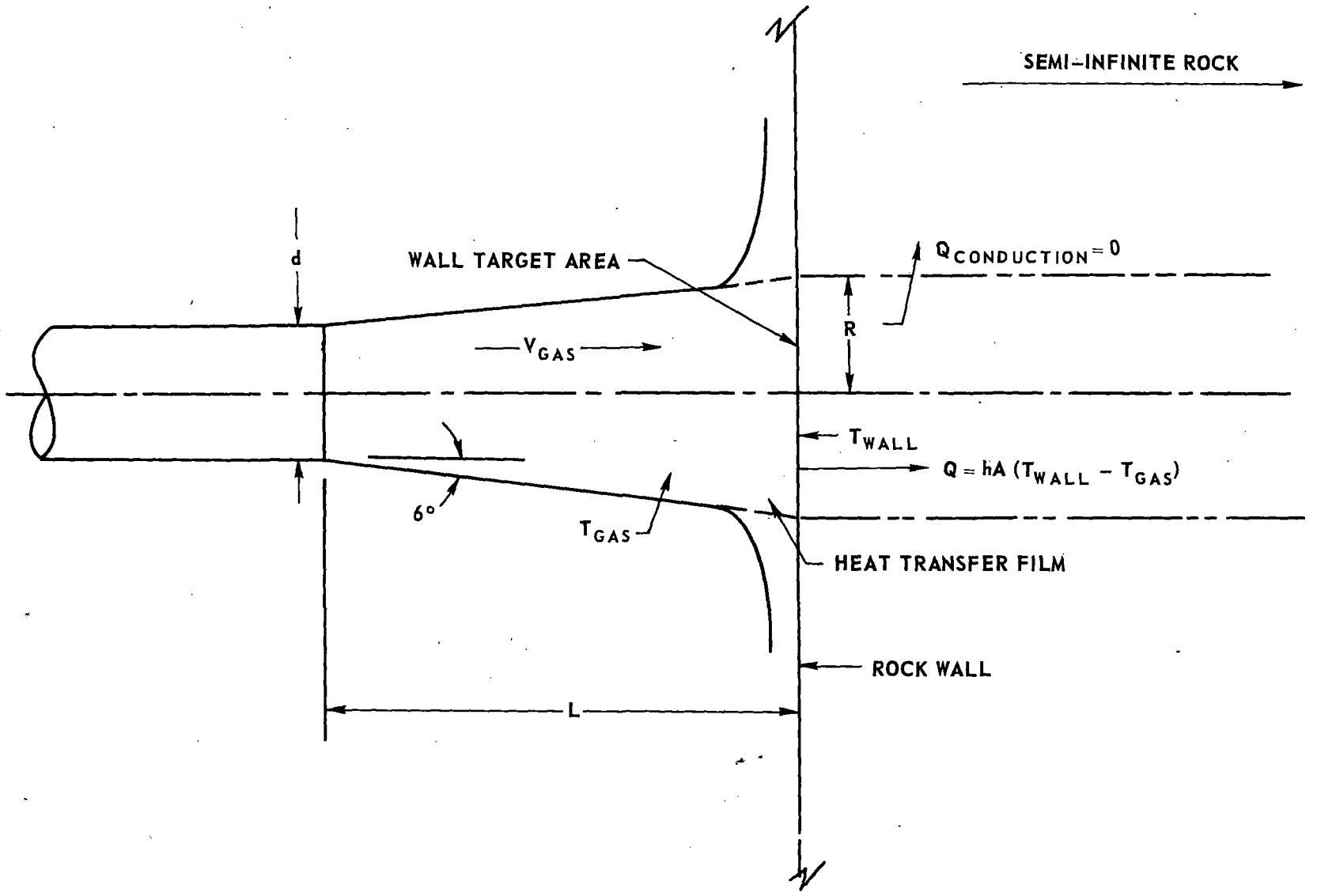

FIGURE 57 SCHEMATIC DIAGRAM OF HEAT COUPLING BETWEEN GAS JET AND ROCK WALL

This procedure readily lends itself to computer programming; a copy of the program used for the flame jet analyses is presented in Appendix B. Unfortunately, it is impossible to describe precisely the temperature history of a single point exposed to a number of spaced jet heaters using the analysis described herein, since the rock must be at a uniform temperature prior to heat application. The spaced jet heating situation may be described more accurately with a finite element technique. However, the method described herein is applicable to circumstances in which a given rock element area is continuously heated by a series of jet heaters.

Discussion of Results

Sample results presented in Fig. 58 indicate the temperature profiles which are expected to exist in granite for plasma, flame, or steam jet systems operating at 10 kw of equivalent jet power and at a traverse velocity of 5 in./sec. Even at this relatively low traverse velocity, it can be seen that the depth of heat penetration into the rock is quite shallow, reaching inward only to 0.10 in. This illustrative case could correspond to that of a single jet heater located near the center of rotation of a large mechanical cutter, or it could correspond approximately to a series of six consecutive jets located far out on the radius arm of a cutter where the transverse velocity is 30 in./sec.

The surface temperature variation of granite rock exposed to a flame jet-type heating device is shown as a function of cutter (or jet device) transverse speed in Fig. 59. For most single-jet heaters, it should be noted that the temperature produced in the rock surface layer is not sufficient to induce significant thermal weakening. Heat transfer results also shown in Fig. indicate that, except for extremely low transverse velocities, the energy input is never above about 300 watt-sec (joules) per square inch, which is inadequate for producing significant damage. Consequently, the results suggest an interesting conclusion: single flame (and steam) jet heater systems are insufficient to cause major heat weakening of most igneous rocks -- multiple jet systems are necessary. However, even when multiple jet systems are employed (i.e., several jet devices located ahead of a cutter at each radius), there may be a practical limitation as to the number of devices which can be located on a boring machine. This situation also is evident with plasma jet systems although to a lesser degree.

It is of interest to determine the extent to which these results can be altered by changing the jet characteristics. Upon examining Eq. (24) in Appendix A, it can be seen that the only parameters which can be controlled for a particular device are the exhaust velocity, V, and the target radius, R. Since the exhaust cone diverges only slightly in traversing the space between the jet nozzle exit plane and the wall surface, the exhaust velocity is expected to vary little. Once the exhaust strikes the wall, it will turn radially outward, and its velocity will vary approximately inversely as the spreading jet radius. If the radius of the target were increased (i.e., a larger divergence angle), the heat transfer coeffi-

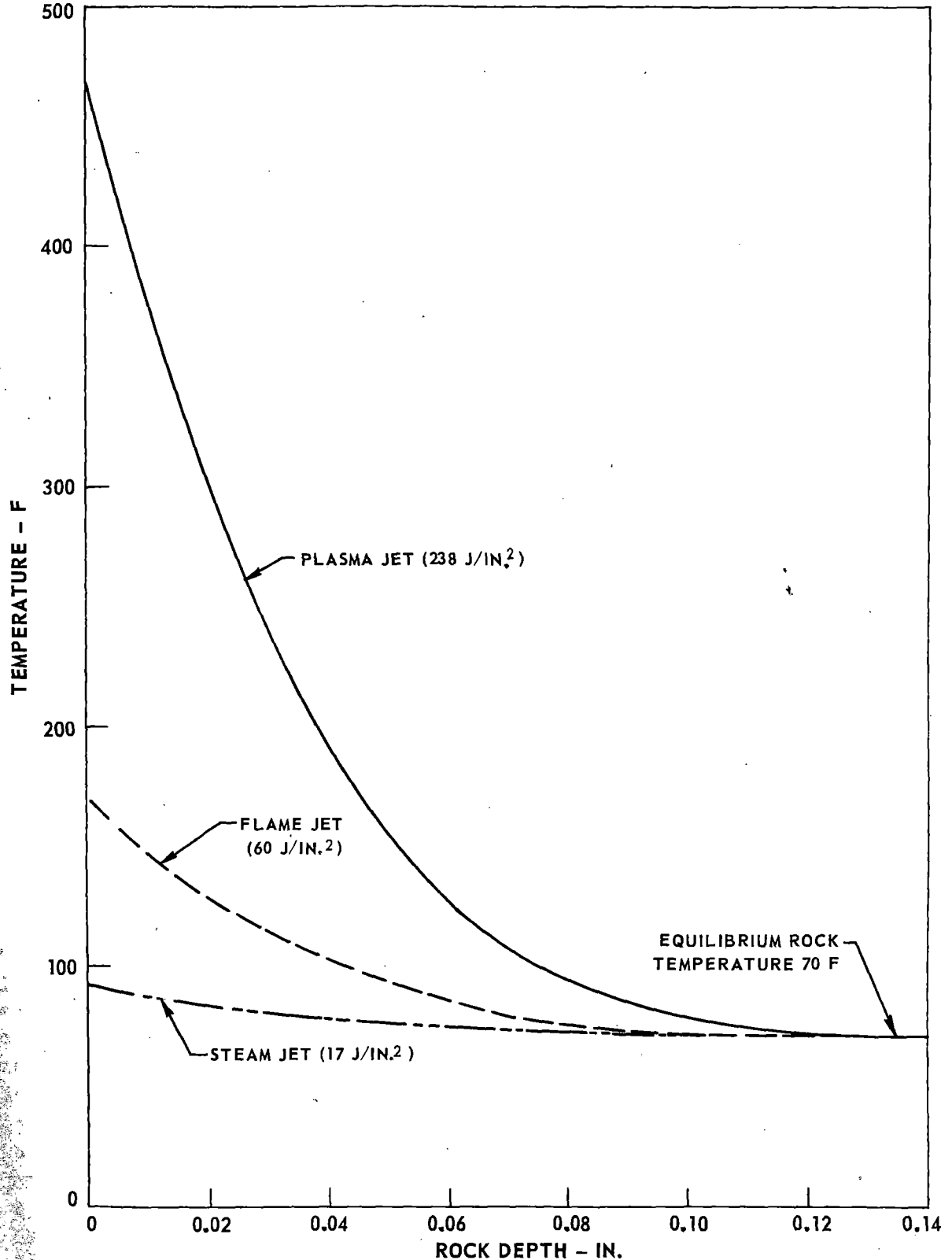

CUTTER SPEED – 5 IN./SEC

POWER IN JET – 10 KW

TOTAL PRESSURE – 21 PSIA

FIGURE 58 TEMPERATURE PROFILE WITHIN GRANITE ROCK SUBJECTED TO JET-TYPE HEATERS

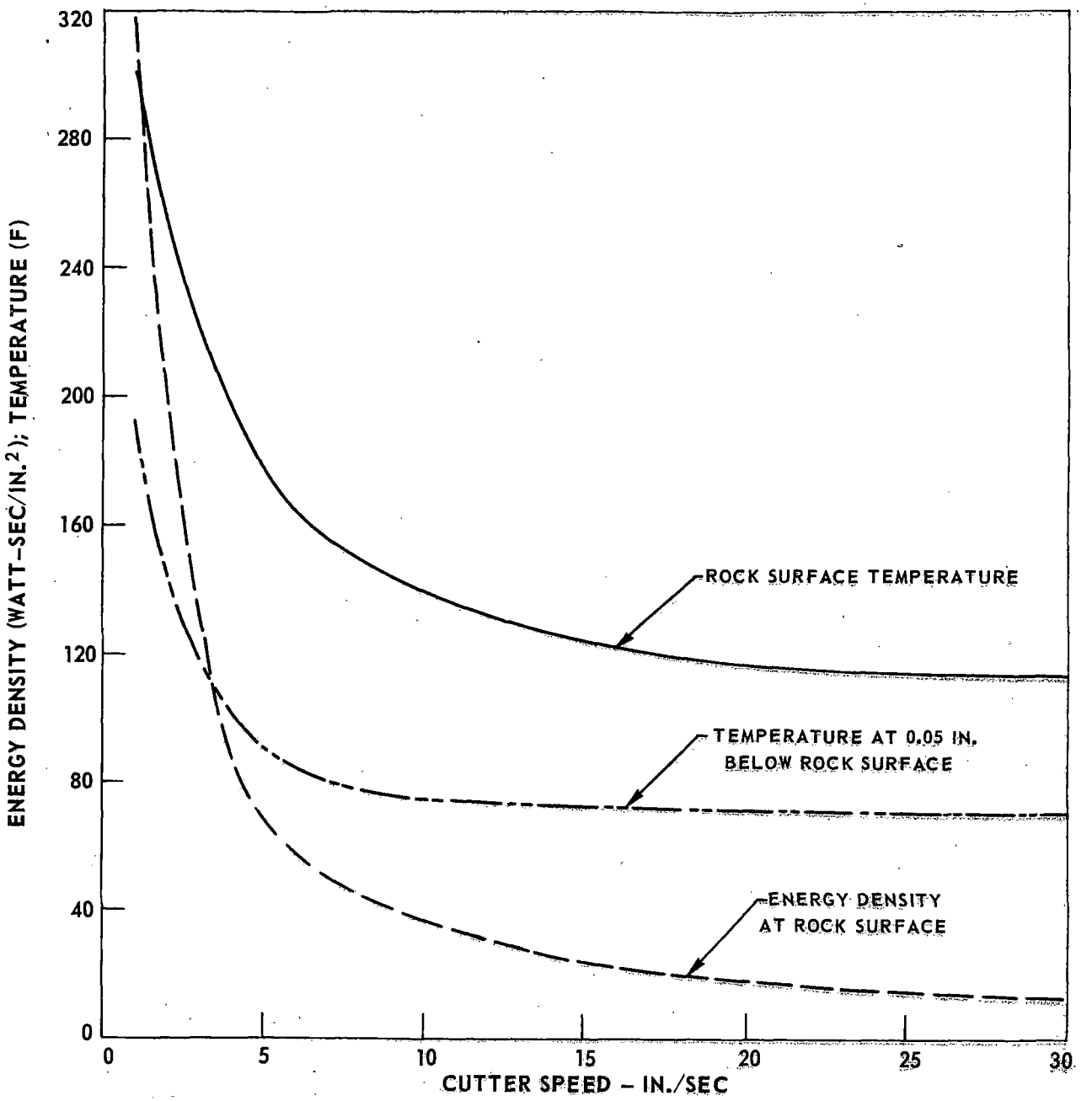

ROCK TYPE – GRANITE
POWER IN JET – 10 KW
JET FLOW – 6.12 SCFM
P_O JET – 25 PSIA
T_O JET – 4000 R
ROCK THERMAL CONDUCTIVITY – 1.68 BTU/HR-FT-F
$T_{EQUILIBRIUM-ROCK}$ – 70 F

FIGURE 59 ROCK SURFACE CHARACTERISTICS WHEN EXPOSED TO A FLAME-JET HEATER

cient would decrease with increasing target radius. However, the combined effect of velocity and radius seems to indicate that heat transfer coefficient is nearly insensitive to target radius. This means that the heat absorbed by the rock is primarily dependent upon exhaust gas temperature and velocity (i.e., pressure ratio).

Sample parametric calculations presented in Fig.60 indicate that the power density for a flame-jet heater peaks at a chamber pressure of approximately 50 psia (an expansion ratio of approximately 3.33). Above this pressure the Reynolds number appears to increase rapidly with pressure ratio, and therefore the heat transfer coefficient (which is inversely proportional to Reynolds number; see Appendix A, Eq. (24)) decreases. Below this pressure the gas velocity appears to be too low (i.e., a low expansion ratio) to promote good turbulent heat transfer. Similar flow characteristics, heat transfer coefficients, and power densities are noted in Figs. 61 and 62 for steam jet and plasma jet heaters, respectively.

There appears to be little that can be done to improve the heat input and temperature gradients at the rock surface for a given type of heater system. A second question then arises: Is the target selected for the thermodynamic model representative of the true operational situation? An increase in target radius only means that more heat from a single burner will enter the rock.. It does not imply a higher gradient, only a larger area. As a result it is believed that the target area selected may be slightly conservative. However, in the actual operation of jet-type heaters, the exhaust gas will flow in the radial direction, scrubbing the wall as it passes, but only for a short distance before it turns to flow away from the rock face. This is due to a combination of circumstances, the primary of which are the collision of the exhaust gas with that from adjacent burners, and the introduction of cooling air in the vicinity of the rock face. An increase in effective target radius likely will be small and will affect only the total number of jet devices required, not the heat flow per unit area.

Having described the heat transfer characteristics of gas jet-type heating devices, it is worthwhile to consider the percentage of heat in the jet actually absorbed by the rock. Several illustrative cases are presented in Table 5 for all three types of heaters and varying (linear) traverse velocities. It can be observed from these results that the heat transferred to the rock surface is proportional to the temperature of the gas in the jet heater (or, in other words, the temperature difference between the gas and the rock). As a result, it is possible to obtain nearly a 30% coupling (heat absorbed in the rock divided by the energy in the jet stream) with a 10-kw plasma jet, but only 3% and 8% coupling, respectively, with a steam jet and a flame jet. It also can be seen that for a given energy in the gas jet, the coupling increases with increasing traverse speed, a fact which can be explained quite simply. The rock surface temperature increases with increased time of exposure to the hot gas jet (i.e., decreased traverse velocities), and therefore the temperature difference between the (constant temperature) gas jet and the rock surface decreases. An integrated curve of temperature difference

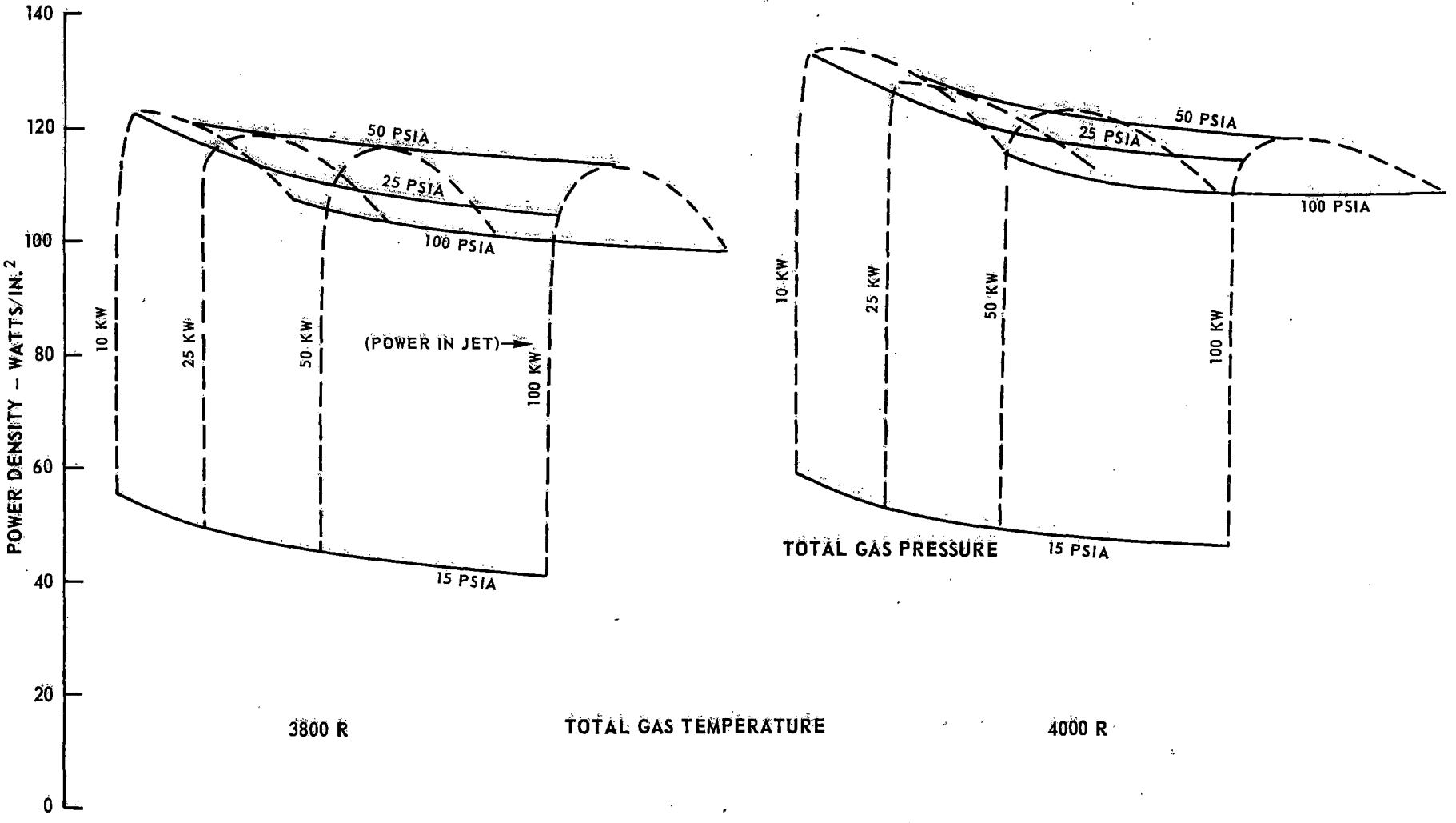

FIGURE 60 POWER DENSITY FOR FLAME JET ROCK HEATER SYSTEMS

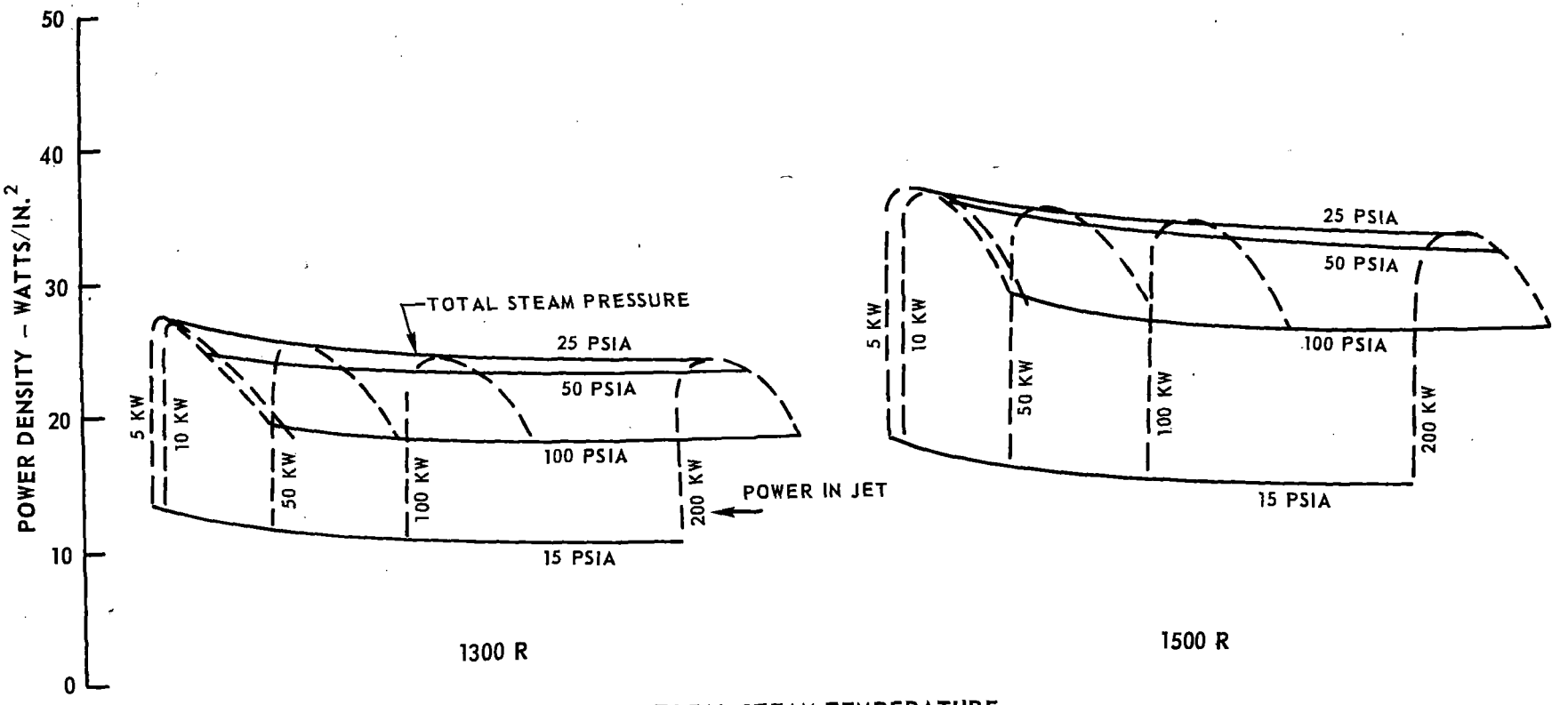

FIGURE 61 POWER DENSITIES FOR STEAM JET HEATER SYSTEMS

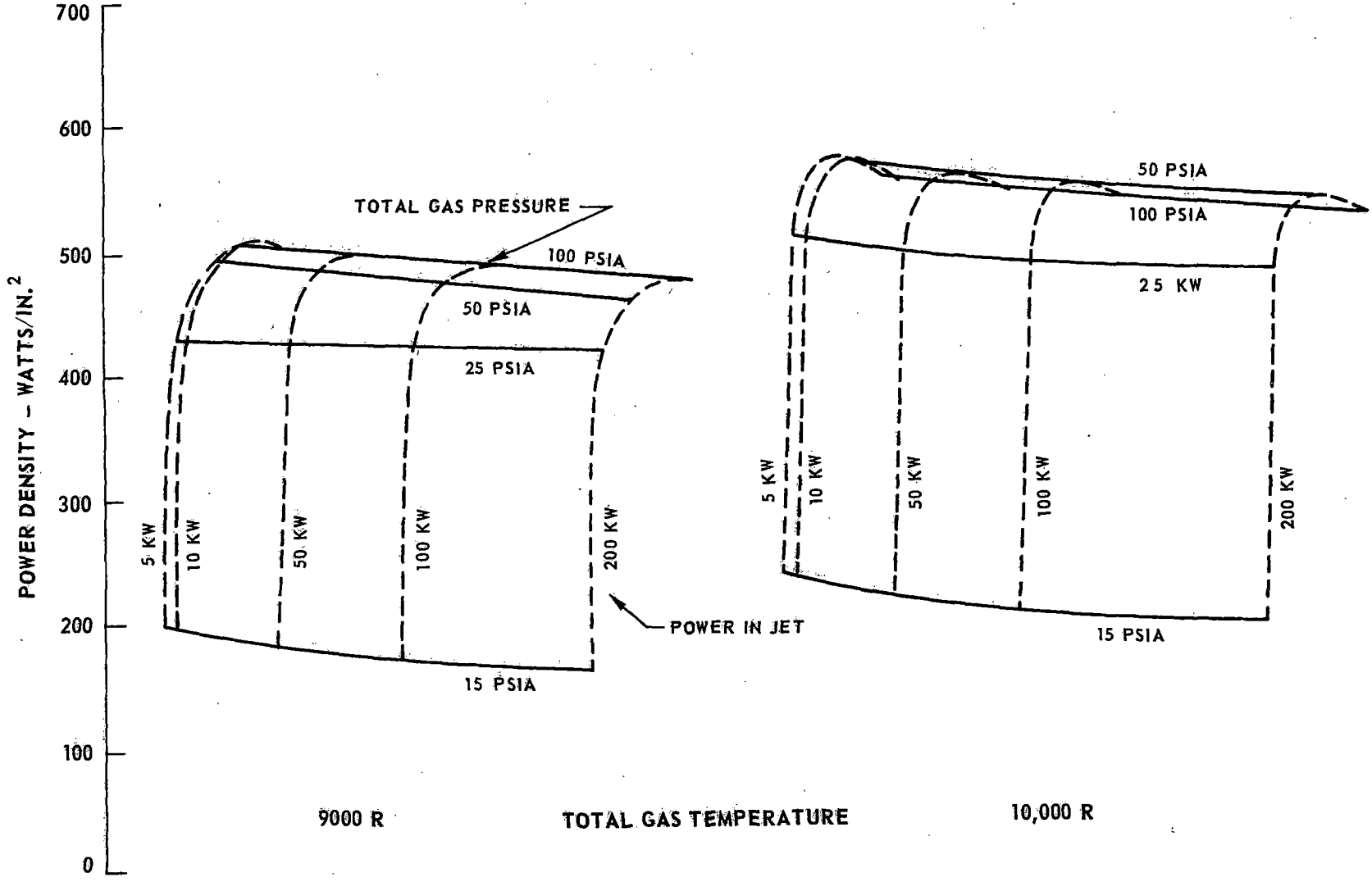

FIGURE 62 POWER DENSITIES FOR PLASMA JET HEATER SYSTEMS

TABLE 5

HEAT COUPLING BETWEEN JET-TYPE HEATERS AND HEATED ROCK SURFACE

Initial Rock Equilibrium Temperature - 70 F

Heater Type	Energy in Jet (kw)	Heater Traverse Velocity (in./sec)	Spot Exposure Time (sec)	Heat into Rock (Btu)	Rock Coupling (Heat Absorbed in Rock to Heat in Jet) (%)
Flame Jet	10	5	0.55	0.363	7.0
	10	10	0.30	0.222	7.8
	10	30	0.09	0.071	8.3
	50	30	0.11	0.099	9.5
	100	30	0.12	0.122	10.7
Steam Jet	10	5	0.09	0.168	3.2
	10	30	0.55	0.032	3.7
Plasma Jet	10	0.5	5.3	12.0	23.7
	10	5	0.53	1.32	26.3
	10	10	0.27	0.68	26.5
	10	20	0.13	0.37	29.0
	10	30	0.09	0.25	29.5
	40	30	0.09	0.29	34.2

vs exposure time then would reveal that the net average heat flow rate (proportiona to the temperature difference) is less, the longer a jet of a given power is expose to the rock. Since total heat flow is proportional to the heat flow rate and the exposure time, a greater fraction of the heat in the jet will pass into a given rock element exposed to the jet travelling at high traverse velocities than will flow into the rock at low velocities. It appears that little can be done to increase the coupling efficiency of jet-type heater devices over that shown in Table 5.

Heating Efficiency of Radiant Devices

Two of the proposed heating system types depend on the absorption of radiant heat energy by the rock. These systems are the laser, which produces light at a single frequency, and a radiant heater, which,like a black body, radiates over a range of wavelengths. Radiant energy falling on the rock is either absorbed, reflected, or transmitted. Since the rock face is essentially a semi-infinite mass the transmitted energy can be assumed equal to be zero. Therefore, absorptivity is defined as one minus the reflectivity. Data on both of these quantities can be found in the literature.

The principal source of radiation data of this nature was found in the area of astronomy. The spectral radiation characteristics of a number of naturally occurring materials were determined at the Goddard Space Flight Center to aid in identifying the surface composition of celestial bodies. Such an investigation int the infrared reflectance of igneous rocks is reported in Ref. 15. The reflectance spectra in Ref. 15 were reduced to straight-line segments for calculation purposes and are shown in Fig. 63.

Absorptivity of Laser Radiation

It is interesting to note that in Fig. 63 there is a local peak in the reflectivity at a wavelength of approximately 10 microns for all the materials investigated. This region also coincides with the wavelength of the energy emitted from the CO_2 molecular lasers (i.e., 10.6 microns) assumed in the laser-assisted system. This peak represents a significant reduction in the absorptivity. Based on the data in Fig. 63, an absorptivity of CO_2 laser radiation by rocks of 85% appears to be a valid assumption.

Absorptivity of Noncoherent Radiation

A mean absorptivity of black body thermal radiation by rock can be obtained by averaging the absorptivity shown in Fig. 63 over all wavelengths with Planck's distributive law (which gives radiant energy as a function of wavelength for given black body radiating temperatures) as a weighting function. An approximation to

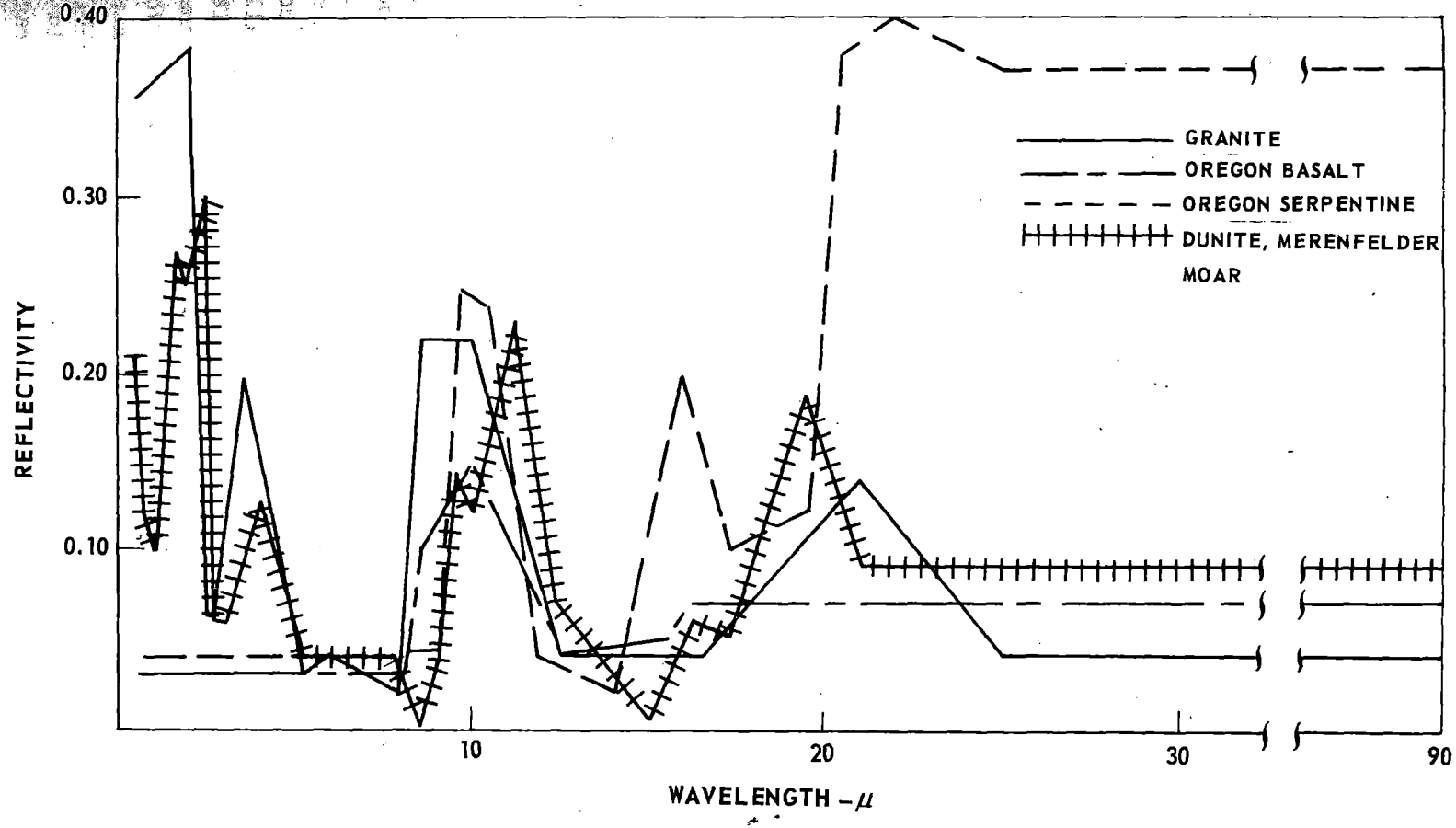

FIGURE 63 APPROXIMATE INFARED REFLECTANCE SPECTRA OF IGNEOUS ROCKS

such an average may be obtained by a step-wise numerical integration of the radiant energy spectrum between the wavelengths of 0.5 and 90 microns. The straight-line approximations to the reflectivity data shown in Fig. 63 were made for this purpose. In addition, these data were extrapolated as shown to provide reflectivity data between 22 and 90 microns. It is known that the amount of energy radiated at those wavelengths is sufficiently small so that the errors introduced by such an extrapolation should not have an appreciable effect on the calculated average absorptivity. A possible exception would be the Oregon Serpentine. This linear extrapolation at the high wavelengths is equivalent to assuming an asymptotic value of the reflectivity (i.e., asymptotic to the value shown at the higher wavelengths) at low radiating temperatures.

The calculated average absorptivities of four igneous rocks are shown in Fig. 64. In general, these absorptivities are all near 0.90, with an extreme range of 0.966 to 0.833. An average absorptivity of about 0.85 appears justified in the temperature range of interest (1600 to 2000 R) for the Dunite and granite; for the other rocks this value would be 0.95. Thus, the absorptivity in black-body radiation of the rocks tested appears to be as high as or higher than the absorptivity of these rocks in the 10.6-micron radiation of a CO_2 laser.

Heating Efficiency of Electron Beams

Commercial electron beam equipment has been produced for many years and has been used successfully in such varied applications as radiation studies, welding, and metal cutting. A full discussion of the problems of adapting electron beam technology to tunneling equipment is presented in Chapter III. Therefore, the present discussion is concerned only with the efficiency of transferring a beam of electrons from the electron beam machine outlet orifice through air to the rock surface.

Collisions between electrons from the electron beam machine and electrons in the atmosphere are of prime importance because of the resultant loss of energy associated with each collision. Collisions (really deflections) between electrons in the beam and the gas molecules may cause a slight scattering of the beam electrons but not significant loss of energy. As a result, these latter collisions are of minor importance. Because of these reasons, electron beams generally are used in a vacuum, where the probabilities of collisions are considerably lessened. Some success has been achieved in recent years with machines emitting beams of electrons out of vacuum, primarily into lightweight gases (e.g., helium) where collisions do not disperse the beam as much as in air. However, in a tunneling application, ensuring that electron collisions will not occur is nearly impossible, and the use of helium or a similar lighter-than-air gas molecule to shield the beam may be expensive. Consequently, it is of interest to examine the transfer of electron beam energy through air to a rock face.

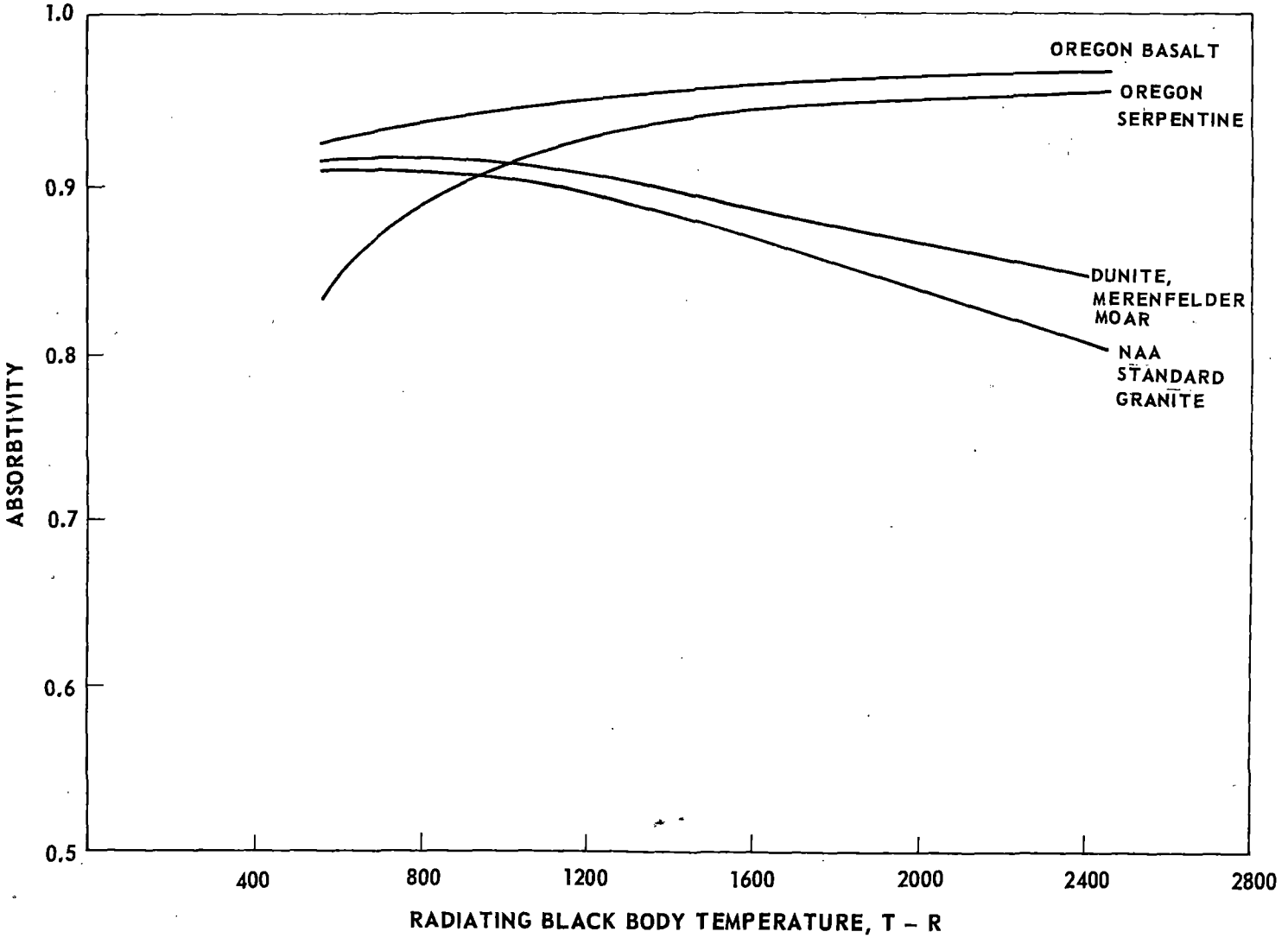

FIGURE 64 THERMAL ABSORBTIVITY OF IGNEOUS ROCKS

Information presented in Ref. 16 indicates that the practical range of an electron is related to the initial electron voltage by the equation:

$$S = \frac{0.00457}{\rho} E_0^{1.75}, \qquad (6)$$

for $(5 < E_0 < 120$ kv),
where S = practical range (cm),
E_0 = initial charge voltage (kv), and
ρ = density of gas into which electron passes (gm/cm^3)
$(= 0.001178\ gm/cm^3$ for air).

Information presented in Ref. 16 indicates that the normalized fraction of energy which can be transmitted beyond a certain depth in air as a function of a depth-to-range parameter is virtually independent of initial beam voltage up to a level of approximately 100 kv. As a result it is possible to investigate the machine-to-rock coupling efficiency for several voltage levels using the same normalized information. Energy transmission results for selected charge levels of 60, 90, and 120 kv are presented in Fig. 65 and in Table 6 to depict the penetration of electrons into air. Extending the use of the basic graphic relationships in Ref. 16 to 120 kv may introduce some error, but it is believed this will be small when compared with the total losses shown here. It can be seen that the beam intensity drops to 20% of its initial intensity within 4 cm with an initial charge of 60 kv. On the other hand, beam intensity drops to the same level after a distance of approximately 14 cm when the initial voltage is increased to 120 kv. These results also suggest that in order to achieve a given electron intensity on the surface of rock to be heated, either the exit plane of the machine must be very close to the surface or the initial voltage of the electrons must be high. Locating the machine close to the work surface has been found unsatisfactory both in experiments and from a practical design standpoint, and consequently, the initial electron voltage must be increased as standoff distance is increased.

TUNNEL ENVIRONMENTAL TEMPERATURE CONTROL

A major problem expected with the use of heat-weakening systems for hard-rock tunneling is the control of the ambient temperature in the tunnel. Past studies have shown that excess heat in a tunnel is difficult to handle and expensive to eliminate. However, it was believed that this problem would be less with the heat-weakening mode than with other modes of thermal rock fracture due to the lower total heat flow rate per unit of affected face area than with more intense heating modes, such as melting.

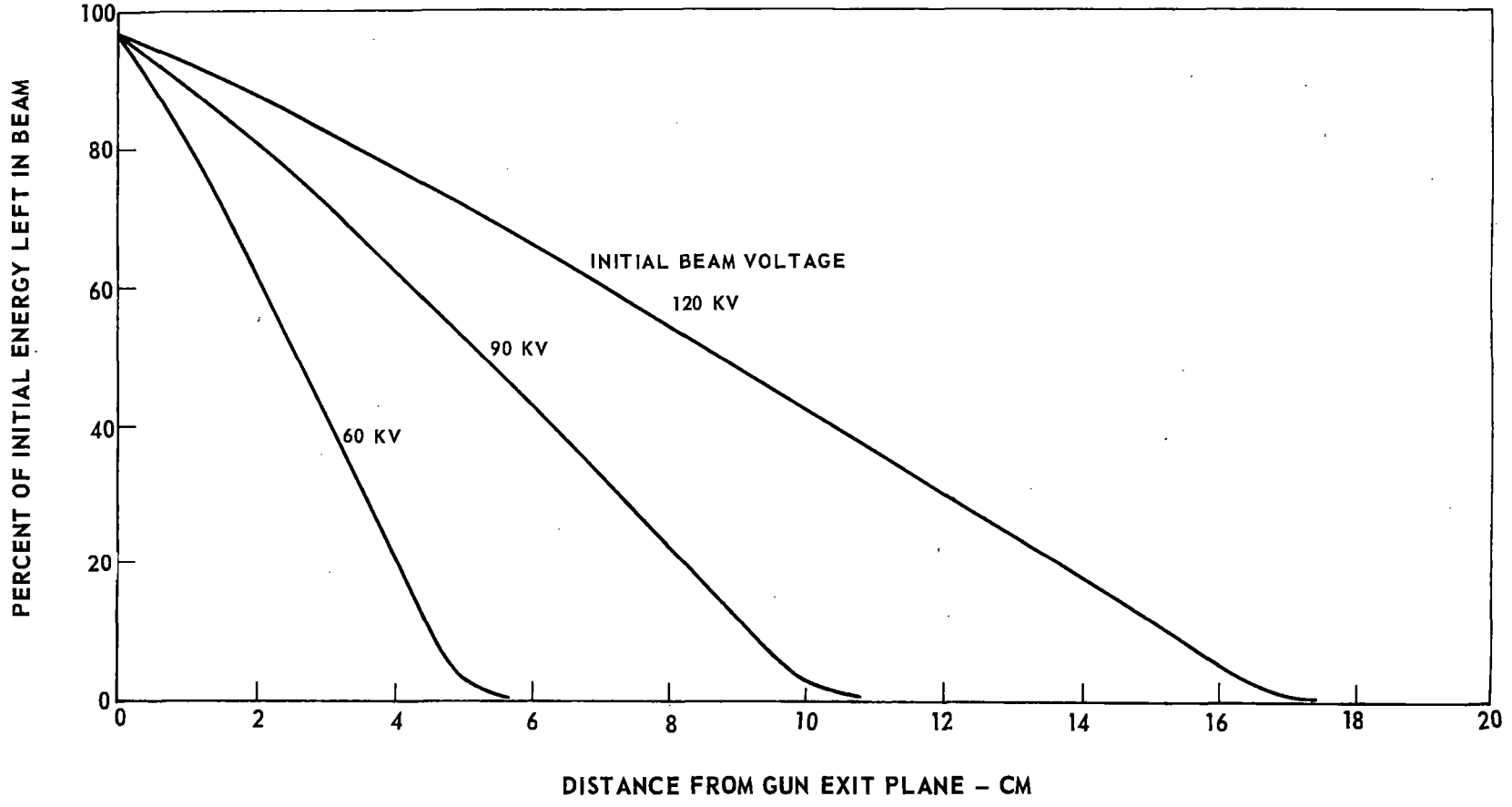

FIGURE 65 ENERGY LOSS IN A BEAM OF ELECTRONS DISCHARGED INTO AIR

TABLE 6

DEVICE-ROCK COUPLING EFFICIENCY FOR ELECTRON BEAM MACHINES IN AIR

Initial Voltage (kv)	Distance into Air (cm)	Coupling Efficiency (%)
60	1	81
	3	42
	5.01*	~ 0
90	1	89
	3	72
	5	53
	7	33
	9	12
	10.2*	~ 0
120	1	93
	3	83
	5	72
	7	61
	9	49
	11	37
	13	25
	15	12
	16.88*	~ 0

* Denotes Maximum Practical Range

Results presented in Fig. 66 show the relationship between the total heat released near the tunnel face and the heat energy intensity which actually impinges upon the rock surface in a 20-ft-diameter tunnel. For reference, if a three-inch cutter spacing is assumed, then a value of 1000 joules/inch of heater path (which is usually about the minimum required to show any significant rock-weakening effect, as discussed in Chapter I) corresponds to an overall heat input of about 52 j/cm^2 in Fig. 66. The flame jet (or fuel oil and compressed air burner) is a simple, but inefficient, device for this application since only approximately 8% of its heat energy actually is absorbed by the rock (Table 5). This is due primarily to the poor heat transfer coefficients at the rock surface and the high gas velocities. As a result, most of the heat in a flame jet gas stream passes into the air around the work surface. Therefore, to achieve a particular surface heat intensity, the total heat released in the face area is prohibitively high.

Objections to a plasma jet heater closely parallel those for flame jets, even though the rock coupling efficiency of the plasma jet approaches 30%. This higher efficiency is due primarily to the jet temperature which may approach 10,000 F for many operating conditions. Regardless of this fact, the coupling efficiency of and total heat release into the tunnel from the plasma jet are still poor relative to the laser and not significantly different from those of the flame jet. The heat released to the tunnel by a steam jet heater is greater than even that of a flame jet, and therefore its performance was not even included in Fig. 66.

The rock coupling efficiency of both the laser and radiant heater devices has been estimated to be approximately 85%, indicating that nearly all of the energy emitted by these devices is absorbed by the rock at the tunnel face. Consequently, only a small amount of heat is deposited in the air adjacent to the work surface, and control of the temperature in the vicinity of the tunneling machine becomes a relatively simple process. For comparative purposes, the heat released by a 1000-hp conventional mechanical tunneler also is shown in Fig. 66. In general, few environmental controls other than those necessary to supply sufficient air to the workmen and to remove dust are needed in conventionally bored tunnels. However, results presented in this figure indicate that some additional type of environmental controls will be required even in the most efficient heat-assisted systems to ensure that a workable atmosphere will be provided for the tunnel crew members. Graphic presentations of the heat release for the same types of heaters in 10- and 15-ft-diameter tunnels would show that for any surface heat intensity, the total heat released would be one-half and three-quarters of the values shown in Fig. 66, respectively.

Estimates of the average temperature of the rock chips cut from the work surface of a tunnel which has been heat weakened are shown in Figs. 67 and 68 for tunnel diameters of 10 and 20 ft, respectively. As would be expected, the average rock chip temperatures decrease with an increase in advance rate at a constant power output (to the rock). This occurs because, at a fixed power input level, a given volume of rock removed will absorb less energy per unit time as advance rate

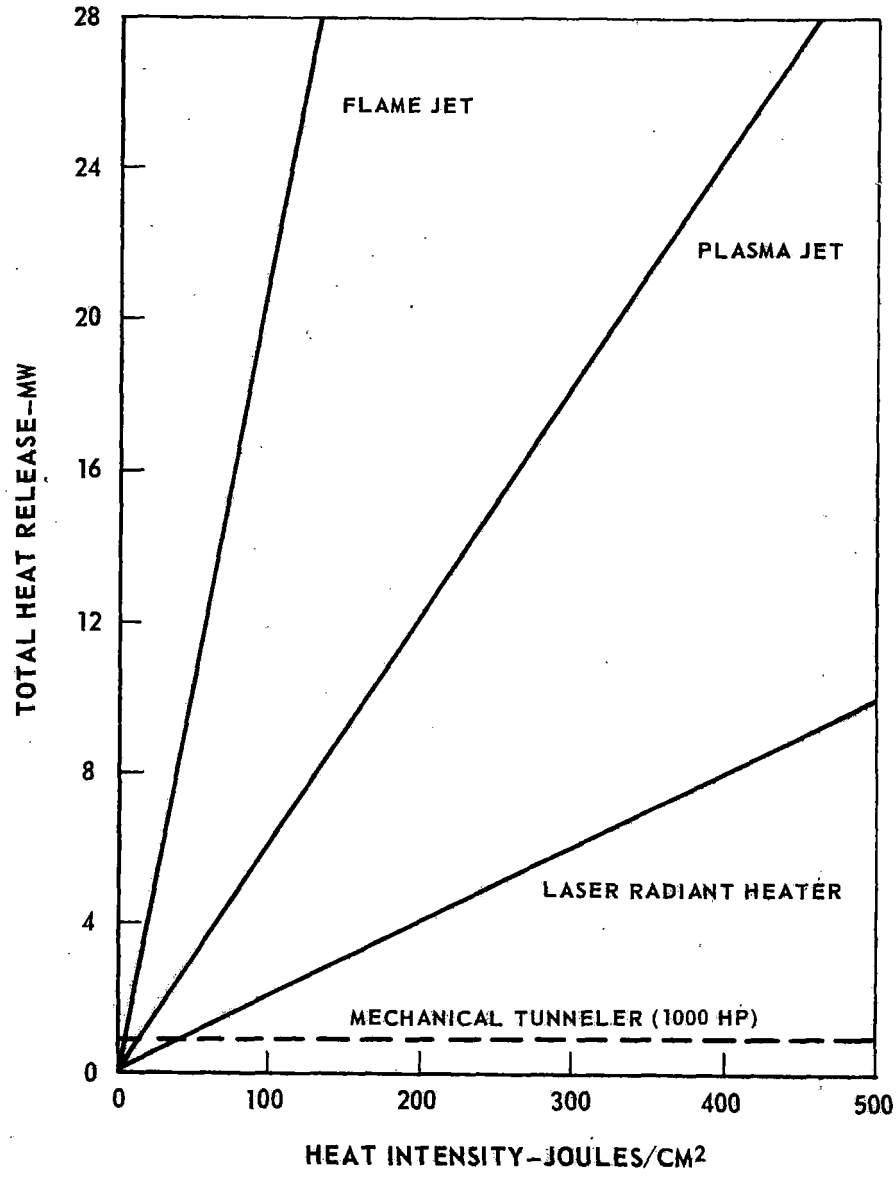

TUNNEL DIAMETER-20 FT

CUTTER HEAD SPEED-3.5 RPM

FIGURE 66 TOTAL POWER RELEASED BY VARIOUS TUNNEL HEATER DEVICES

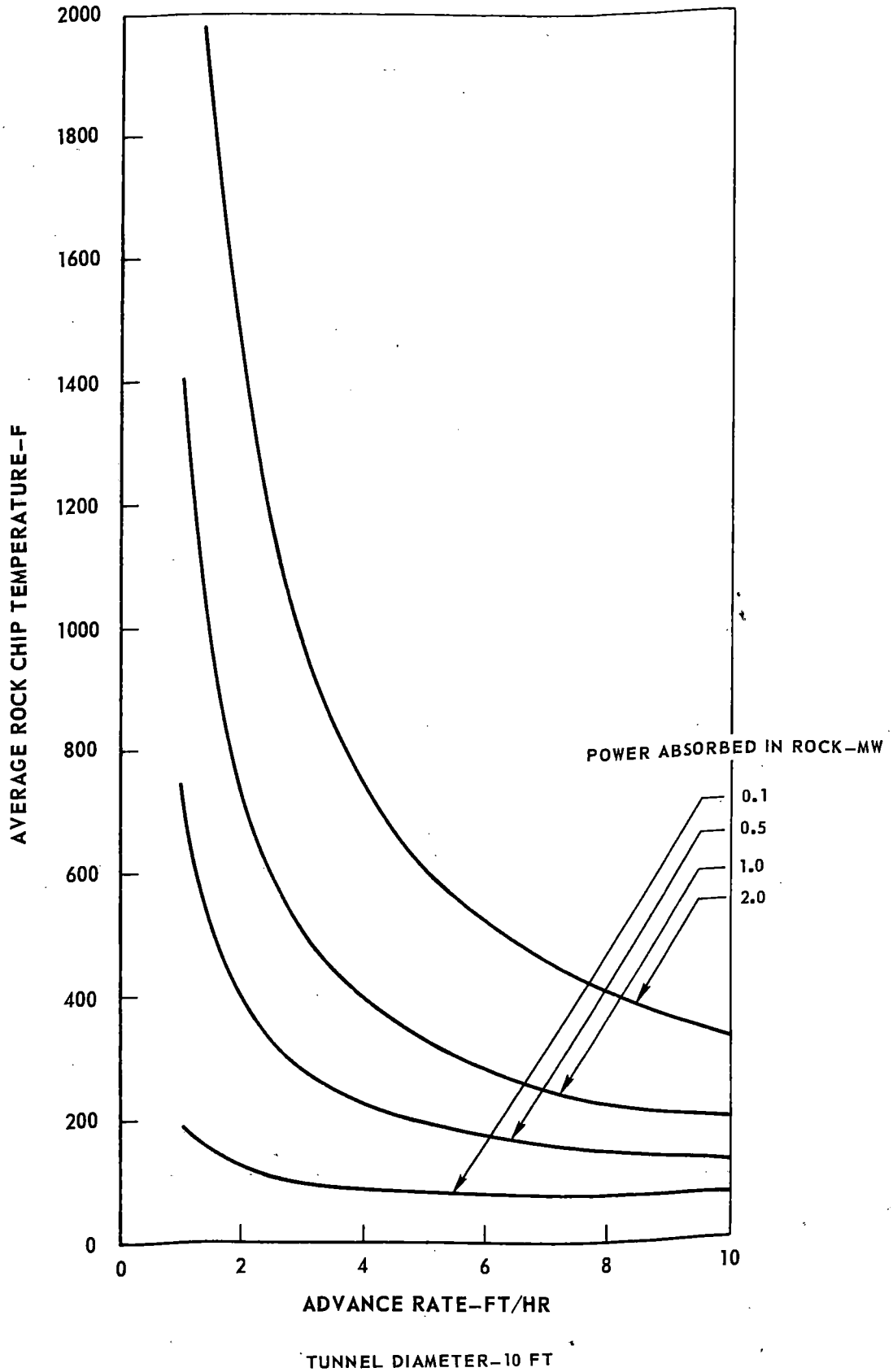

FIGURE 67 ROCK CHIP TEMPERATURES FOR LASER HEAT ASSISTED TUNNELING CONCEPT

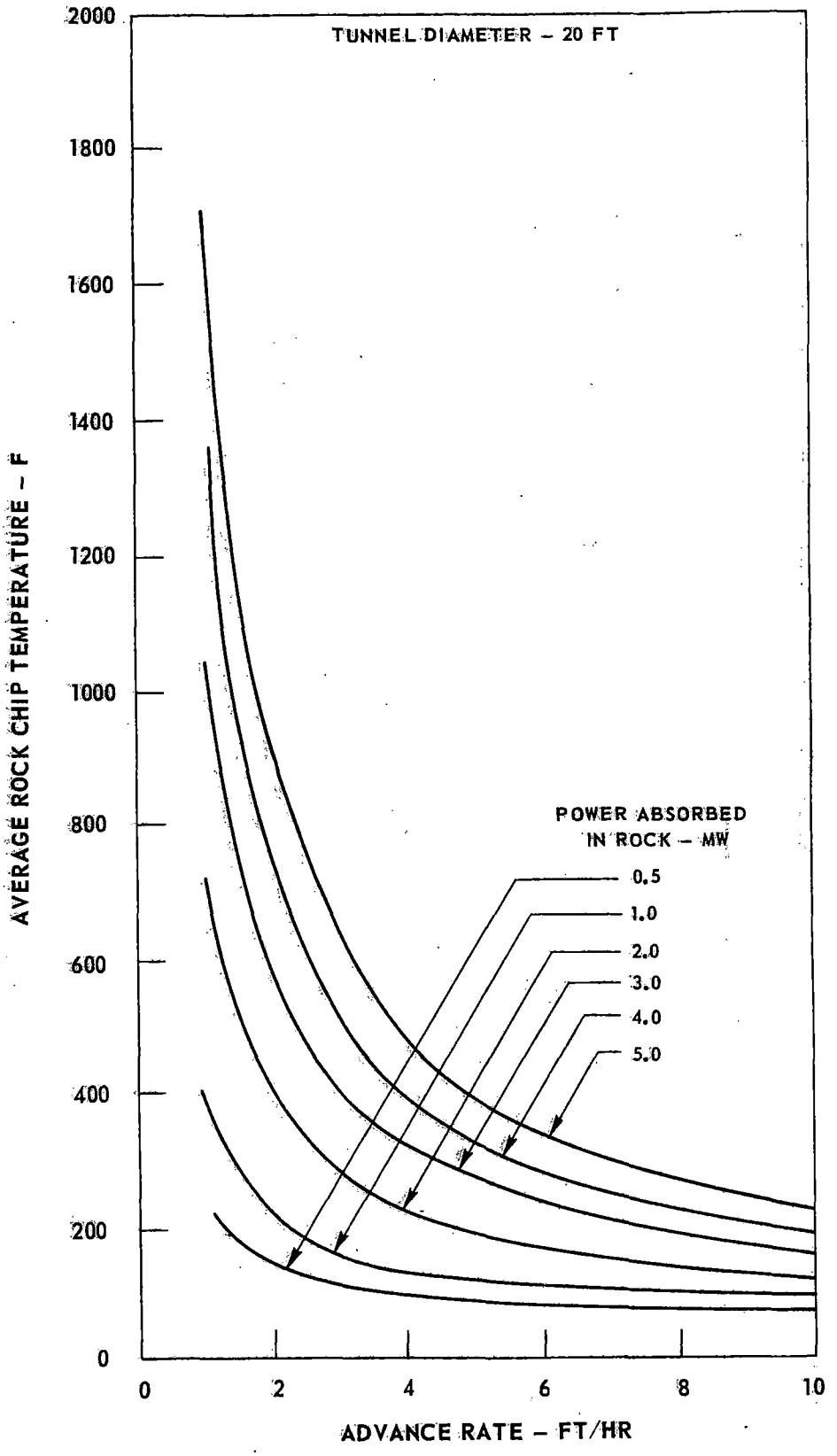

FIGURE 68 ROCK CHIP TEMPERATURES FOR LASER HEAT ASSISTED TUNNELING CONCEPT

increases. It is also true that of a given power input level and advance rate, a unit volume of rock will absorb more energy per unit time in smaller tunnels. As a result, the average rock chip temperatures in a 10-ft tunnel will be higher for a given set of operating conditions than chip temperatures for the same conditions in a larger tunnel. The trends shown both in Fig. 67 and in Fig. 68 are not in themselves startling, but the magnitude of the temperatures may be cause for some concern, particularly when low values of advance rate are encountered. Even higher local values of muck temperature than those noted here may be encountered if heating in small discrete circumferential paths, rather than over the entire face as assumed in these figures, is employed for greater cutting efficiency. Regardless of the heating method selected, these results emphasize a potentially difficult muck-handling problem which may be encountered in the absence of special precautions (such as muck cooling) prior to removing the muck from the work area.

High rock muck temperatures coupled with the heat released into the air adjacent to the work face dictate that special precautions be taken to protect the crew members, not only from hot muck but also from a potentially fatiguing work environment. It therefore is necessary to provide a basic environmental control system for the heat-assisted tunneling system. It is assumed for this work that the heating system will not be a gas jet type. Because of the lower heat intensities and the anticipated lack of toxic gases with either the laser of the radiant heater, it is believed this environmental control system can be simplified considerably relative to that system described for the flame jet tunneler in Ref. 2.

Environmental Control System Model

A simplified schematic diagram of the ventilation/cooling system selected for environmental control in a heat-assisted tunnel system is shown in Fig. 69. In this system, air from a transportable, gas-turbine-driven compressor is blown through an air duct extending from the surface, down the shaft, and along the ceiling of the tunnel. This air serves not only to absorb heat from the tunnel work area but also to replenish the breathing supply for the work crew. Stale, heated air is exhausted naturally down the tunnel and out the access shaft. Cooling water is brought by a separate pipe down the same access shaft and then to the tunnel work face where it is sprayed onto the muck. Water which is not vaporized from the muck surface is collected in a sump beneath the tunneler and directed back to the surface in a second pipe (not shown in this figure). The return water is either discarded, or if a sufficient supply of make-up water is not available, it is filtered and then cooled in cooling towers prior to returning it to the tunnel.

A schematic diagram of the model which was used to describe the thermodynamic and heat transfer processes occurring adjacent to the tunnel work face is shown in greater detail in Fig. 70. For the thermodynamic analysis, this model is divided into three distinct zones, although in actuality all mixing and heat transfer

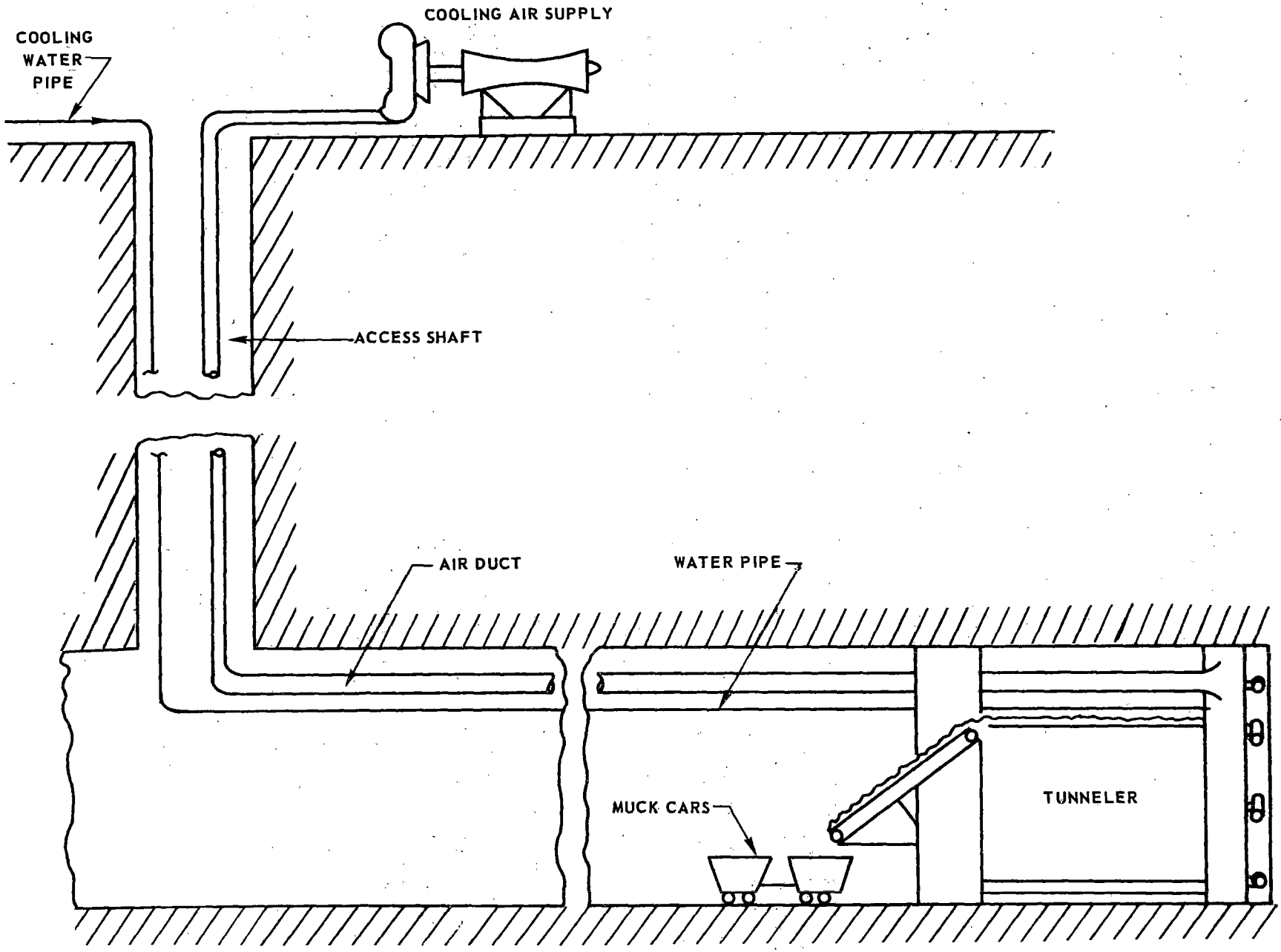

SCHEMATIC DIAGRAM OF VENTILATION–COOLING SYSTEM FOR HEAT–ASSISTED TUNNELING CONCEPT

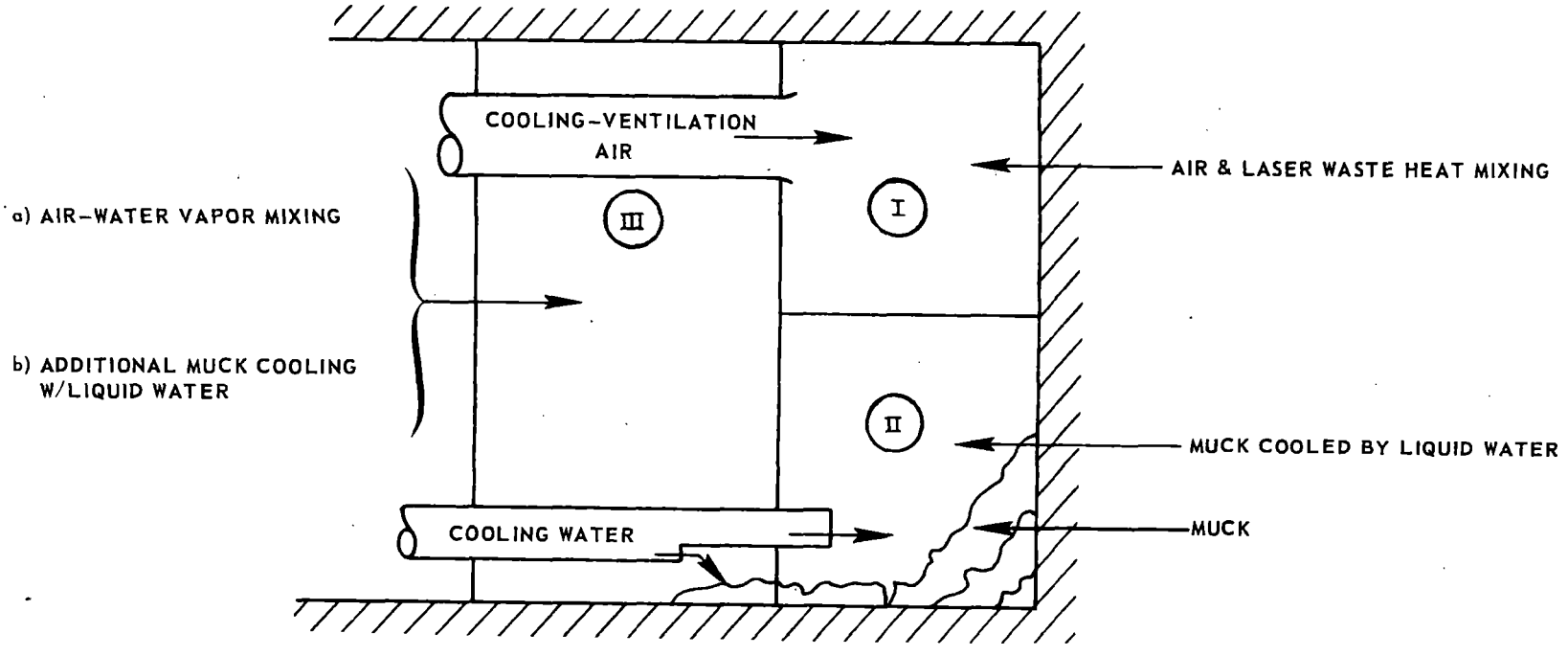

FIGURE 70 SCHEMATIC DIAGRAM OF THERMAL COOLING-VENTILATION MODEL

processes would take place simultaneously through the entire work area. In Zone I cooling air enters the work area to absorb the heat which does not pass directly into the rock from the heaters, and an energy balance equation adequately describes this process for any amount of air brought into the zone. Reradiation of heat from the rock working face was ignored in the analysis since the rock will be heated to a high temperature for only a short time before it is cut, and further, all of the heat energy absorbed by the rock is taken into account in Zone II.

In Zone II it is assumed that sufficient quantities of water are pumped into the work zone to cool the muck to some desired temperature. It is also assumed that this water will be sprayed onto the muck both as it falls to the tunnel floor and as it is transferred from scoops on the cutter head to the conveyor. Such an arrangement ensures thorough mixing between the water spray and the rock chips. As the liquid water cools the rock, a portion of this water spray will vaporize and mix with the heated cooling air. The amount of vaporization which occurs is dependent upon the volume flow of air and the temperature of the air after absorbing the excess heater energy. When the desired final exhaust air temperature and cooled muck temperature are prescribed, the energy equation, combined with equations defining relative humidity, can be used to determine the exact amount of water which vaporizes. These equations then define the processes which are assumed to occur in Zone III of the model.

Temperature equilibrium is assumed to exist in each zone at all times. Although this is a conservative assumption, it is reasonably realistic considering the actual volume in which each of the processes occurs, the turbulence created by the cutter head rotation, and the further turbulence created by the air exiting from the air pipe. Homogeneous, moisture-laden air is assumed to exit from Zone III and then pass over and around the muck cars as it flows out of the tunnel. Depending upon the local relative humidity, water also will be drawn from this zone via a sump and pipe located on the tunnel floor. For any advance rate, net heat input to the rock, and heat-coupling efficiency (a characteristic of each heater device), several combinations of airflow rate and water flow rate can be selected to maintain the temperature of the existing exhaust air and muck at their prescribed levels. For example, air and water flow rates for an environmental control system in a typical heat-assisted tunnel are presented in Fig. 71 for an advance rate of 5 ft/hr and a 3-Mw heat input to the rock. These results present a clear picture of the trade-off between airflow and water flow which also are representative for other operating conditions when muck and tunnel face air temperature are held constant. It should be noted, however, that for certain combinations of rock power input, advance rate, and airflow rate, there may be no water flow required since the heat absorbed by the rock may be insufficient even to increase temperature of the muck to the prescribed level.

The criteria that determine the proper combination of water and airflow rates are: (1) that airflow rate necessary to supply fresh oxygen to the workmen in the tunnel; and (2) that system with the lowest net environmental control system

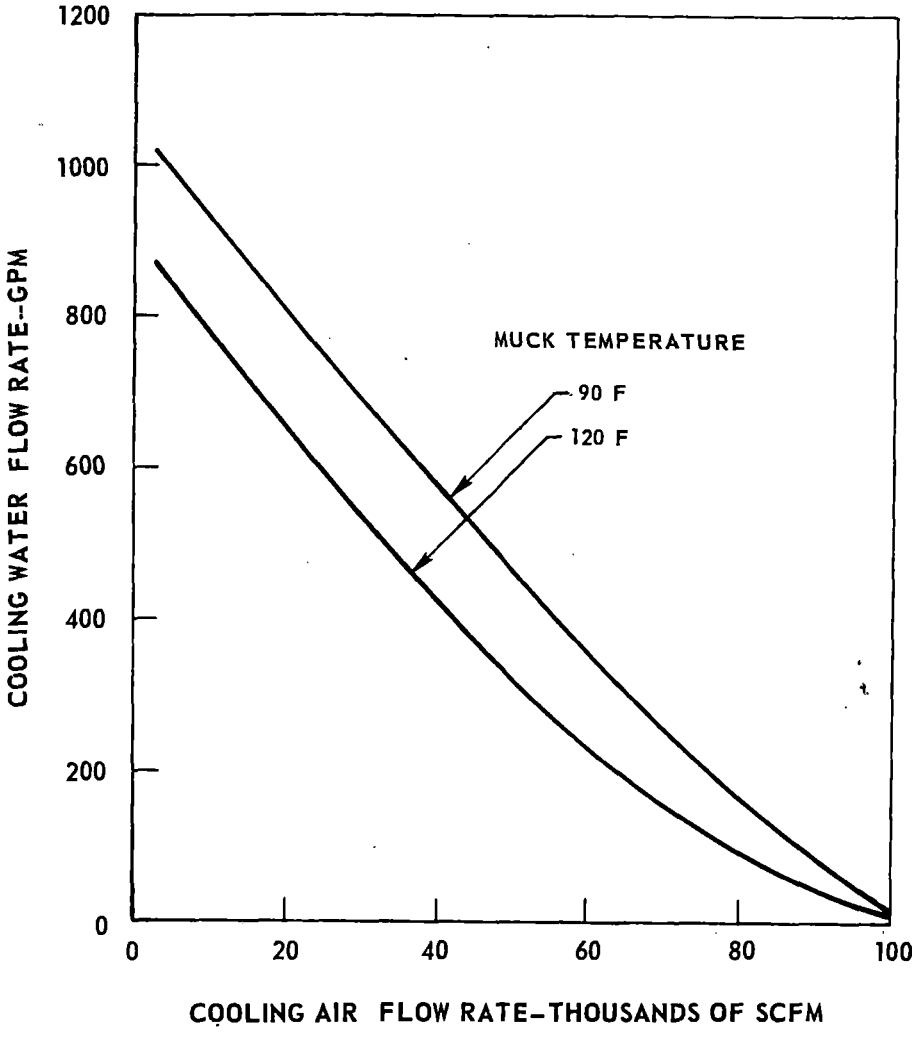

LASER HEAT SYSTEM

POWER INTO ROCK-3MW

TUNNEL DIAMETER-20 FT

TUNNEL FACE AIR TEMPERATURE 80 F

FIGURE 71 AIR AND WATER FLOW RATES REQUIRED TO MAINTAIN CONSTANT TEMPERATURES IN THE VICINITY OF THE TUNNEL WORKFACE

cost. That system which satisfies the first criterion at minimum cost obviously is the best selection. The system of computer equations which were used to determine the exhaust temperature, rock mixing, and water flow rates is presented in Fig. 72 prior to step 39.

Effect of Mucking System Conditions on Tunnel Temperature

As the water-air exhaust gas mixture passes from the work zone, it flows over the muck train which is being filled with the cut rock from the working face. Depending on the cooled muck temperature as it comes from the work zone, heat will be transferred from the muck to the exhaust gas mixture. Simultaneously, a portion of this heat energy will be transferred from the exhaust gas mixture to the tunnel walls and into the rock beyond. Standard convective heat transfer equations adequately describe both of these heat exchange processes, while heat transfer coefficients for the muck-to-exhaust gas energy exchange process and for the exhaust gas-to-tunnel wall can be found in Refs. 2 and 17, respectively. One factor which complicates the definition of this heat exchange process is that the exhaust gases pass over a progressively greater number of filled muck cars with the passage of time. The heat lost to the exhaust gas from the first car as it is filled will be reflected in a net decrease in the temperature of the muck in that car, so when the second car is being filled the muck in the first car will be slightly cooler. As a result, each progressively filled car behind the tunnel machine contains muck at a slightly higher temperature as the exhaust gas absorbs heat and carries it out of the tunnel. The equations describing the analytical procedure which calculates the exhaust gas temperature at the end of the last filled car in the muck train are presented in Fig. 72 beyond step 39.

Use of the digital computer program shown in Fig. 72 makes it possible to determine for any prescribed airflow rate, heat absorbed in the rock, and exhaust gas temperature: (1) the water flow rate necessary to attain a given muck temperature; (2) the realtive humidity of the exhaust gas in the vicinity of the tunneling machine; (3) the temperature of the exhaust gas leaving the rear of the tunneling machine; and (4) the temperature of the exhaust gas leaving the location of the last muck car. Muck car volume (and therefore fill-time for a given advance rate) and muck train length can be varied for any set of tunnel operating parameters.

Illustrative exhaust gas temperatures leaving the vicinity of the muck train are shown in Fig. 73 as a function of the cooled muck temperature leaving the tunnel face area. These data are for an advance rate of 5 ft/hr and a rock heat input of 3 Mw using a laser heater. The results show the large effect on tunnel temperature of increases in muck train length and/or muck temperature. If for some reason high muck temperatures cannot be avoided (e.g., possible restriction in water flow rate), some additional covering over the muck cars may be necessary to protect the work crew. A possible alternative solution would be to pump additional cooling air into the tunnel and to direct this air into the exhaust gas flow at a

```
      DIMENSION TITLE(12),EMAI(7),X(7),TTAO(10),TM(10),NN(10),IJK(8)
      DATA NN/1,2,3,4,5,6,7,8,9,10/
      NAMELIST/INPUT/RHOR,D,CSI,TRI,TAI,TWI,CPR,PT,TMIX,
     1   TROCK,VC,AR,NCARS,IPRIN
      READ(5,104) NX,(X(I),I=1,NX)
      READ(5,104) NMA,(EMAI(I),I=1,NMA)
3     READ(5,INPUT)
      READ(5,100) (TITLE(I),I=1,12)
      READ(5,104) K
C  K=0, MORE CASES FOLLOW   K>0, LAST CASE
C  IPRIN=1, DETAILED PRINTOUT    IPRIN=2, SHORT PRINTOUT
      PI=3.14159
      TAII=TAI
      TROCKI=TROCK
      WRITE(6,101) (TITLE(I),I=1,12)
      WRITE(6,102) RHOR,D,AR,CSI,TRI,TAI,TWI,CPR,PT,TMIX,
     1  TROCK,VC
      DO 50 J=1,NX
      IJK(J)=0
      IF(IPRIN.EQ.2)  WRITE(6,106) X(J)
      IF(IPRIN.EQ.2)  GO TO 2
      IF(J.EQ.1)  WRITE(6,106) X(J)
      IF((J.GT.1).AND.(IJK(J).LT.IJK(J-1)))  WRITE(6,106) X(J)
2     DO 50 L=1,NMA
      KON=0
      TRI=TRI+460.
      TAI=TAI+460.
      TMIX=TMIX+460.
      TWI=TWI+460.
      EMA=EMAI(L)/13.1
      EMR=(PI*RHOR*D*D*AR)/240.
      TEXH=TAI+((1.-CSI)*X(J)*56920.)/(.24*CSI*EMA)
      TC=(56920.*X(J))/(EMR*CPR)+TRI
      PP1=PP(TMIX)
      EL1=ELMDA(TMIX)
      EMWEV=(.622*PP1*EMA)/(PT-PP1)
      TROCK=TROCK+460.
      IF(TROCK-TC) 8,7,7
7     TROCK=TC
      KON=1
      IJK(J)=1
8     EMWL=(EMR*CPR*(TC-TROCK)+.24*EMA*(TEXH-TMIX)-EMWEV*EL1)
     1   /(TMIX-TWI)
      RH=100.
      IF(EMWL-EMWEV)  10,12,12
10    EMWL=(EMR*CPR*(TC-TROCK)+EMA*.24*(TEXH-TMIX))
     1   /(TMIX+EL1-TWI)
      RH=(EMWL*(PT-PP1)*100.)/(.622*PP1*EMA)
```

FIGURE 72a COMPUTER PROGRAM TO DETERMINE TUNNEL ENVIRONMENTAL CONDITIONS

```
12     WTR=(EMWL*7.48)/62.4
       IF(IJK(J).EQ.1)  GO TO 39
       IF(IJK(J).LT.IJK(J-1))  GO TO 39
       IF(IPRIN.EQ.2)  GO TO 39
       GO TO 66
39     DO 38 I=1,NCARS
38     TM(I)=TROCK
       TAI=TMIX
       TAO=TMIX+10.
       EMA=EMA+EMWEV
       HW=(.109/D)*(EMA/D)**0.8
       VEXH=.288*(EMA/(0.25*D**2))
       HM=(.535/30.)*(ABS(8.-VEXH))**0.8
       DLOG=ALOG((D+2.)/D)
       DENOM=60.*EMA*.24 + .5*HW*PI*D*30. +
      1       .5*HM*45.
       TERM=TAI*(60.*EMA*.24 - (30.*D*HW*PI)/2. -
      1    (30.*HM*1.5)/2.) + HM*45.*TROCK
       N1=0
25     TW=(HW*D*DLOG*(TAI+TAO)+33.7)/(2.*HW*D*DLOG+.065)
       TAOM=(TERM+HW*30.*D*TW*PI)/DENOM
       IF(ABS((TAO-TAOM)/TAO).LE.0.01)  GO TO 29
       TAO=TAOM
       N1=N1+1
       IF(N1.GT.200)  GO TO 201
       GO TO 25
29     VEXH=(.288*EMA)/(.75*D**2)
       HM=(.535/20.)*(ABS(8.-VEXH))**0.8
       TAI=TAOM
       TAO=TAI+5.
       DENOM=14.4*EMA + 10.*HW*D*PI + 15.*HM
       TERM=TAI*(14.4*EMA-10.*D*PI*HW-15.*HM) +
      1     30.*HM*TROCK
       N2=0
33     TW=(HW*D*DLOG*(TAI+TAO)+33.7)/(2.*HW*D*DLOG+.065)
       TAOS=(TERM+20.*D*PI*TW*HW)/DENOM
       IF(ABS((TAO-TAOS)/TAO).LE.0.01)  GO TO 37
       TAO=TAOS
       N2=N2+1
       IF(N2.GT.200)  GO TO 203
       GO TO 33
37     Z=(VC/2.)**.333333
       Z2=Z**2
       AW=PI*D*(2.*Z+2.)
       DO 80 M=1,NCARS
       DO 80 N=1,M
       IF(N.GT.1)  TAI=TTAO(N-1)
       IF(N.EQ.1)  TAI=TAOS
```

FIGURE 72b ENVIRONMENDAL COMPUTER PROGRAM (Cont.)

```
      TAO=TAI+5.
      N3=0
41    HT=.35*((TM(N)-(TAI+TAO)/2.)/(2.*Z))**.25
      HS=.13*((TM(N)-(TAI+TAO)/2.)/(2.*Z))**.333333
      TW=(HW*D*DLOG*(TAI+TAO)+33.7)/(2.*HW*D*DLOG+.065)
      DENOM=.24*EMA + .5*AW*HW + HT*Z2 + 2.*Z2*HS
      T1=TAI*(EMA*.24-2.*Z2*HS-Z2*HT-.5*HW*AW)
      T2=2.*Z2*TM(N)*(2.*HS+HT) + HW*AW*TW
      TTAO(N)=(T1+T2)/DENOM
      IF(ABS((TAO-TTAO(N))/TAO).LE.0.01)  GO TO 42
      TAO=TTAO(N)
      N3=N3+1
      IF(N3.GT.200)  GO TO 205
      GO TO 41
42    TIMEPC=VC/(1.0439*D**2*AR)
      OMUCK=2.*Z2*(TM(N)-(TTAO(N)+TAI)/2.)*(2.*HS+HT)*TIMEPC
      TM(N)=TM(N)-OMUCK/(VC*.75*RHOR*CPR)
80    CONTINUE
      DO 81 I=1,NCARS
81    TTAO(I)=TTAO(I)-460.
      WRITE(6,107) EMAI(L)
      IF(KON.EQ.1)  WRITE(6,105)
      GO TO (82,83), IPRIN
82    WRITE(6,111)
      WRITE(6,108) NN(1),TTAO(1),TAOS,WTR
      WRITE(6,109) NN(2),TTAO(2),TAOM,RH
      WRITE(6,110) (NN(I),TTAO(I),I=3,NCARS)
      GO TO 14
83    WRITE(6,120) TROCKI,WTR,RH,NN(NCARS),TAOS,TAOM,TTAO(NCARS)
      GO TO 14
201   WRITE(6,202) X(J),EMAI(L),TW,TAO,TAOM
      GO TO 14
203   WRITE(6,204) X(J),EMAI(L),TW,TAO,TAOS
      GO TO 14
205   WRITE(6,206) X(J),EMAI(L),TW,TAO,TTAO(N),N,M
      GO TO 14
66    IF(L.EQ.1)  WRITE(6,112)
      IF(L.GT.1)  GO TO 67
      IF(KON.EQ.1)  WRITE(6,105)
      WRITE(6,113) X(J),EMAI(L),WTR,RH
      GO TO 14
67    IF(KON.EQ.1)  WRITE(6,105)
      WRITE(6,114) EMAI(L),WTR,RH
14    TRI=TRI-460.
      TAI=TAII
      TMIX=TMIX-460.
      TWI=TWI-460.
      TROCK=TROCKI
```

FIGURE 72c ENVIRONMENTAL COMPUTER PROGRAM (Cont.)

```
50     CONTINUE
       IF(K.EQ.0)  GO TO 3
100    FORMAT(2X,12A3)
101    FORMAT(//2X,12A3/)
102    FORMAT(2X,12HROCK DENSITY,26X,F6.2,9H LB/FT**3/
      1 2X,15HTUNNEL DIAMETER,24X,F5.2,3H FT/
      2 2X,12HADVANCE RATE,27X,F5.2,6H FT/HR/
      3 2X,39HFRACTION OF TOTAL HEAT ABSORBED BY ROCK,1X,F4.2/
      4 2X,24HINITIAL ROCK TEMPERATURE,13X,F7.2,2H F/
      5 2X,23HINITIAL AIR TEMPERATURE,14X,F7.2,2H F/
      6 2X,25HINITIAL WATER TEMPERATURE,12X,F7.2,2H F/
      7 2X,21HSPECIFIC HEAT OF ROCK,19X,F4.2,9H BTU/LB-R/
      8 2X,15HTUNNEL PRESSURE,23X,F6.2,5H PSIA/
      9 2X,33HDESIRED FINAL MIXTURE TEMPERATURE,4X,F7.2,2H F/
      1 2X,16HROCK TEMPERATURE,21X,F7.2,2H F/
      2 2X,21HVOLUME OF MUCK CAR(S),17X,F6.2,8H CU. FT.)
104    FORMAT(I4,7F10.0)
105    FORMAT(4X,46HROCK TEMPERATURE SET EQUAL TO CHIP TEMPERATURE/)
106    FORMAT(//2X,26HHEAT ABSORBED BY ROCK (MW),3X,F5.2)
107    FORMAT(/4X,18HAIRFLOW RATE (CFM),2X,F8.1)
108    FORMAT(8X,I2,E15.5,5X,4HTAOS,E12.5,5X,3HWTR,E12.5)
109    FORMAT(8X,I2,E15.5,5X,4HTAOM,E12.5,6X,2HRH,E12.5)
110    FORMAT(8X,I2,E15.5)
111    FORMAT(/6X,7HCAR NO.,6X,3HTAO)
112    FORMAT(//4X,13HHEAT ABSORBED,5X,7HAIRFLOW,4X,
      1 14HREQ WATER FLOW,5X,8HRELATIVE/
      2 4X,13HBY ROCK  (MW),4X,10HRATE (CFM),4X,
      3 10HRATE (GPM),5X,12HHUMIDITY (%))
113    FORMAT(/8X,F4.1,9X,F8.1,2E16.5)
114    FORMAT(21X,F8.1,2E16.5)
120    FORMAT(4X,24HMAXIMUM MUCK TEMPERATURE,2X,F6.1,2H F//
      1 7X,3HWTR,E13.5,6X,2HRH,E13.5,4X,7HCAR NO.,2X,I2/
      2 6X,4HTAOS,E13.5,4X,4HTAOM E13.5,8X,3HTAO,E13.5/)
202    FORMAT(//2X,23HN1 ITR., NO CONVERGENCE/
      1 6H      X,E12.5,4X,6H   EMA,E12.5,4X,6H    TW,E12.5/
      2 6H   TAO,E12.5,4X,6H  TAOM,E12.5//)
204    FORMAT(//2X,23HN2 ITR., NO CONVERGENCE/
      1 6H      X,E12.5,4X,6H   EMA E12.5,4X,6H    TW,E12.5/
      2 6H   TAO,E12.5,4X,6H  TAOS,E12.5//)
206    FORMAT(//2X,23HN3 ITR., NO CONVERGENCE/
      1 6H      X,E12.5,4X,6H   EMA,E12.5,4X,6H    TW,E12.5/
      2 6H   TAO,E12.5,4X,6HTAO(N),E12.5,4X,2HN=I2,4X,2HM=I2//)
       END
       FUNCTION PP(X)
       Y=X-460.
       IF(Y-100.) 1,2,2
1      PP= -.067655084 + .007029444*Y - .00011534928*Y**2
      1   + .0000014661674*Y**3
```

FIGURE 72d ENVIRONMENTAL COMPUTER PROGRAM (Cont.)

```
      RETURN
2     PP= 2.1787062 - .06943429*Y + .00092135193*Y**2
     1   - .000005201841S*Y**3 + .00000017945991*Y**4
      RETURN
      END
      FUNCTION ELMDA(X)
      Y=X-460.
      IF(Y-100.) 1,2,2
1     ELMDA= 1093.9123 - .56642204*Y
      RETURN
2     ELMDA= 1090.3757 - .50184968*Y - .00030341856*Y**2
      RETURN
      END
```

FIGURE 72e ENVIRONMENTAL COMPUTER PROGRAM (Cont.)

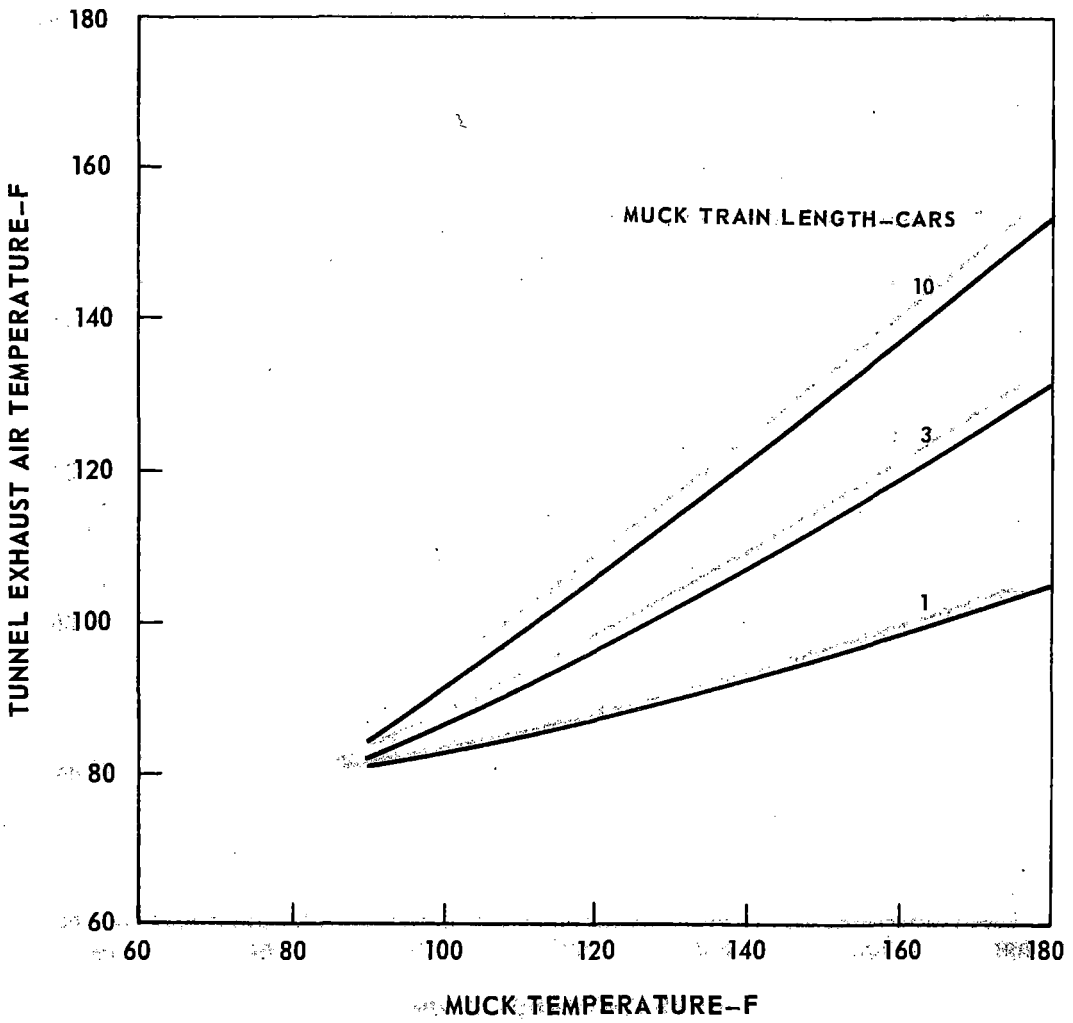

AIR TEMPERATURE LEAVING WORKING FACE–80 F

LASER HEATER SYSTEM

MUCK CAR VOLUME–10 YD^3

TUNNEL DIAMETER–20 FT

VOLUME FLOW OF COOLING AIR–10,000 SCFM

FIGURE 73 EFFECT OF MUCK TRAIN LENGTH ON TEMPERATURE OF EXHAUST AIR IN TUNNEL

point just ahead of the first muck car. The resulting mixture temperature then could be lowered at the expense of an increased air system cost, a situation which may outweigh the increase in cost of a water system capable of accomplishing the same effect.

Several points should be mentioned relative to the data shown in Fig. 73. First, these temperatures are the maximum values which the exhaust gases would be expected to reach in the tunnel. At many operating conditions (i.e., lower heat input to the rock and/or higher advance rates) the muck temperature will never reach the highest values shown in this figure, and therefore, the exhaust gas temperature will be less than that shown. However, input heating power levels of interest seldom are expected to exceed.3 Mw. Second, the exhaust gas temperatures shown are those which are attained after the last car is filled. The exhaust gas temperatures adjacent to the cars preceding the tenth car at the same point in time, or the temperatures opposite these cars at earlier points in time will be less than the maximum values noted in this figure. The exhaust gas temperature opposite the first and third cars of a ten-car train should be slightly less than those shown in this figure for a one- or three-car total train length, at any muck temperature. Similar temperature profiles exist for other airflow rates although the absolute magnitude of the exhaust gas temperature will be different. As airflow increases at a fixed muck temperature, the exhaust gas temperature will decrease slightly because more heat is being absorbed per unit time by the exhaust gases (due to a greater air mass flow and heat transfer coefficient). Similarly, an opposite trend occurs at lower cooling airflow rates. Again, the final selection of the system configuration will depend upon many factors, the primary of which will be the overall environmental control system cost. It appears desirable, however, that an attempt should be made to attain a muck temperature as low as practicable in order to reduce the necessity of providing the workers with additional protection (e.g., shields or muck car insulation) from the muck car heat.

Environmental Control System Cost

The cost of the entire environmental control system comprises four major subsystem capital costs and an operating cost. The capital costs are for the shafts, the air ducts, the gas turbine-air compressor package, and the water system, while the operating cost is for the gas turbine engine fuel and maintenance allowance. In this program, unit costs were allocated to the tunnel in a manner similar to that described in Ref. 2. A breakdown of the air ventilation system for a typical 20-ft-diameter tunnel with a 1.8-ft-diameter air duct, a 10,000-scfm airflow rate, a 2-mi shaft spacing, a 1000-ft shaft depth, and a 5-ft/hr advance rate is shown in Fig. 74. It can be seen that for the selected shaft spacing, the shaft costs constitute by far the largest portion of the cost. As shaft spacing increases, the shaft drilling cost is allocated over a greater distance, and therefore the portion of the air ventilation cost attributable to this component decreases significantly. However, investigations (Ref. 2) have revealed that a 2-mi shaft spacing

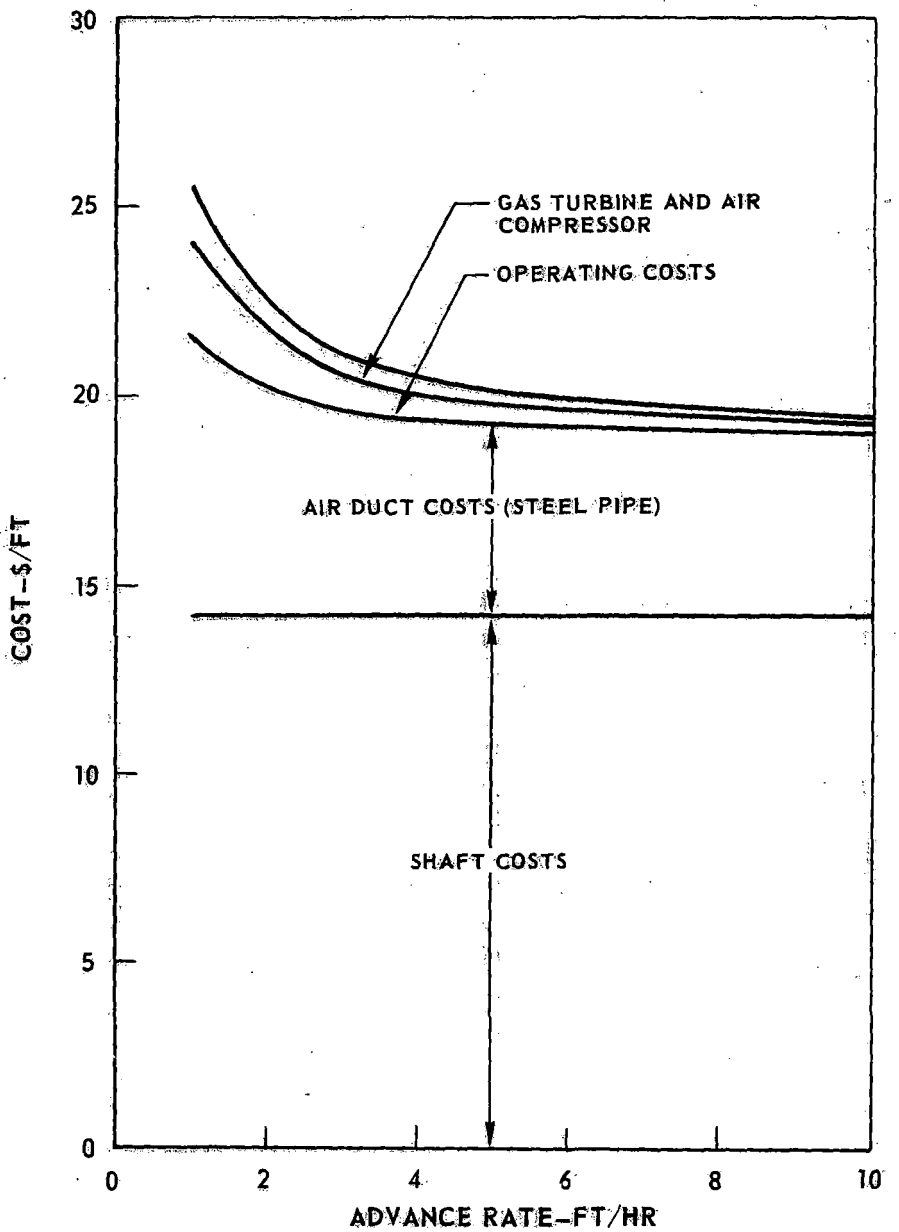

2–MILE SHAFT SPACING
DUCT DIAMETER–1.8 FT
VENTILATION AIRFLOW 10,000 SCFM
ADVANCE RATE–5 FT/HR
TUNNEL DIAMETER–20 FT

FIGURE 74 BREAKDOWN OF COMPONENT COSTS FOR AIR VENTILATION SYSTEM IN HEAT–ASSISTED TUNNELING CONCEPT

is highly desirable from the standpoint of ventilation, and therefore, the cost allocation shown in this figure is typical of what would be expected in a real situation. The other air ventilation system costs are not dependent on shaft spacing and will remain approximately the same for all shaft spacings. However, these remaining system costs are quite dependent upon the advance rate which can be achieved with heat assistance. The results indicate that a decrease of 50% in the air system costs (exclusive of shaft costs) is quite typical of that which can be attained as advance rate is increased from 1 ft/hr to 10 ft/hr.

Curves of the total environmental control system costs for a typical heat-assisted tunnel arepresented in Fig. 75 for an advance rate of 5 ft/hr and a 3-Mw heat input to the rock. These results show that the lowest-cost system is the one which requires the lowest possible airflow rate. This phenomenon occurs because the cost contribution of the water flow system to the overall system cost is so small that the air system cost predominates.

A composite plot of total air ventilation system cost for two typical advance rates, differing air duct diameters, and airflow rates from 2500 cfm to 100,000 cfm in a tunnel with a 2-mi shaft spacing is presented in Fig. 76. These curves, which include all of the cost components shown in Fig. 74, were used as working data in the selection of the optimum (lowest cost) air ventilation system for any airflow rate. It can be seen that the system cost for any particular airflow rate varies considerably with air duct diameter. This variation is caused by the combined effect of air duct (capital) cost and duct wall friction (which, in turn, affects the pumping power and therefore operating cost). For each airflow rate there is a particular duct size which minimizes the net system cost. Similar working curves were prepared for the analysis of other advance rates and shaft spacings.

The costs for the water system required in the tunnel also are based on data presented in Ref. 2. These data are presented for reference in Fig. 77 to show the relationship between the pipe cost and the cost of peripheral equipment (which includes a cooling tower and appropriate pumps on the surface). A limit of 2000 gpm was imposed primarily because higher water flow rates would be rather difficult to handle adequately in the tunnel. In nearly every case examined, however, it was unnecessary to specify a water flow rate above 2000 gpm, primarily because the larger water systems forced the total environmental system cost beyond their minimum values.

Detailed analyses of the tunnel environmental temperature indicate that an airflow rate of 5000 cfm may be adequate to cool the tunnel work face while providing a sufficient oxygen supply to the crew in the tunnel. However, results similar to those presented in Fig. 73 indicate that the air temperature in the vicinity of the muck cars may reach uncomfortable levels at an airflow rate of 5000 cfm. Therefore, a comparison of total ventilation system cost for airflow rates of 5000 and 10,000 cfm was made, and this comparison is presented in

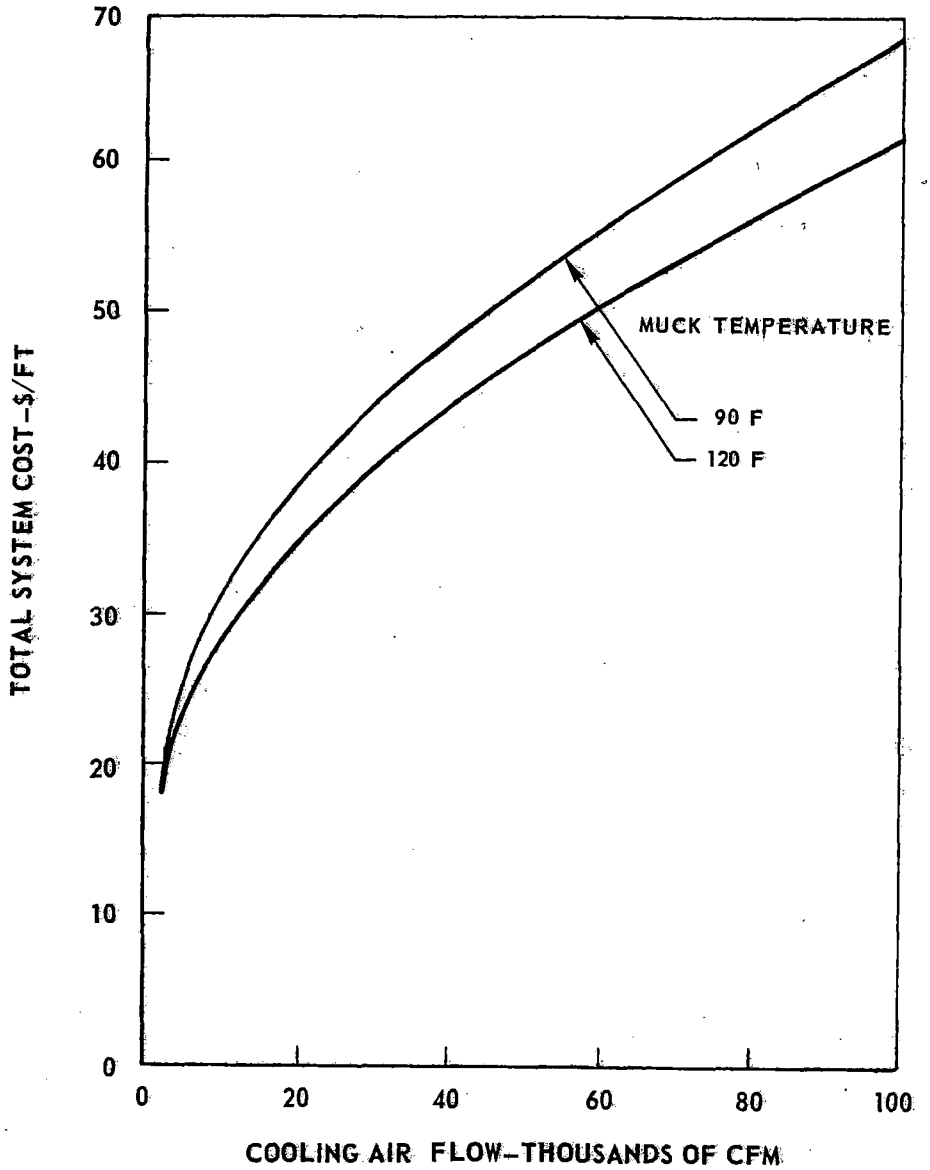

POWER INTO ROCK–3 MW

ADVANCE RATE–5 FT/HR

TUNNEL DIAMETER 20 FT

TUNNEL FACE AIR TEMPERATURE 80 F

FIGURE 75 TOTAL COST FOR ENVIRONMENTAL CONTROL SYSTEM FOR TYPICAL HEAT–ASSISTED TUNNEL SYSTEM

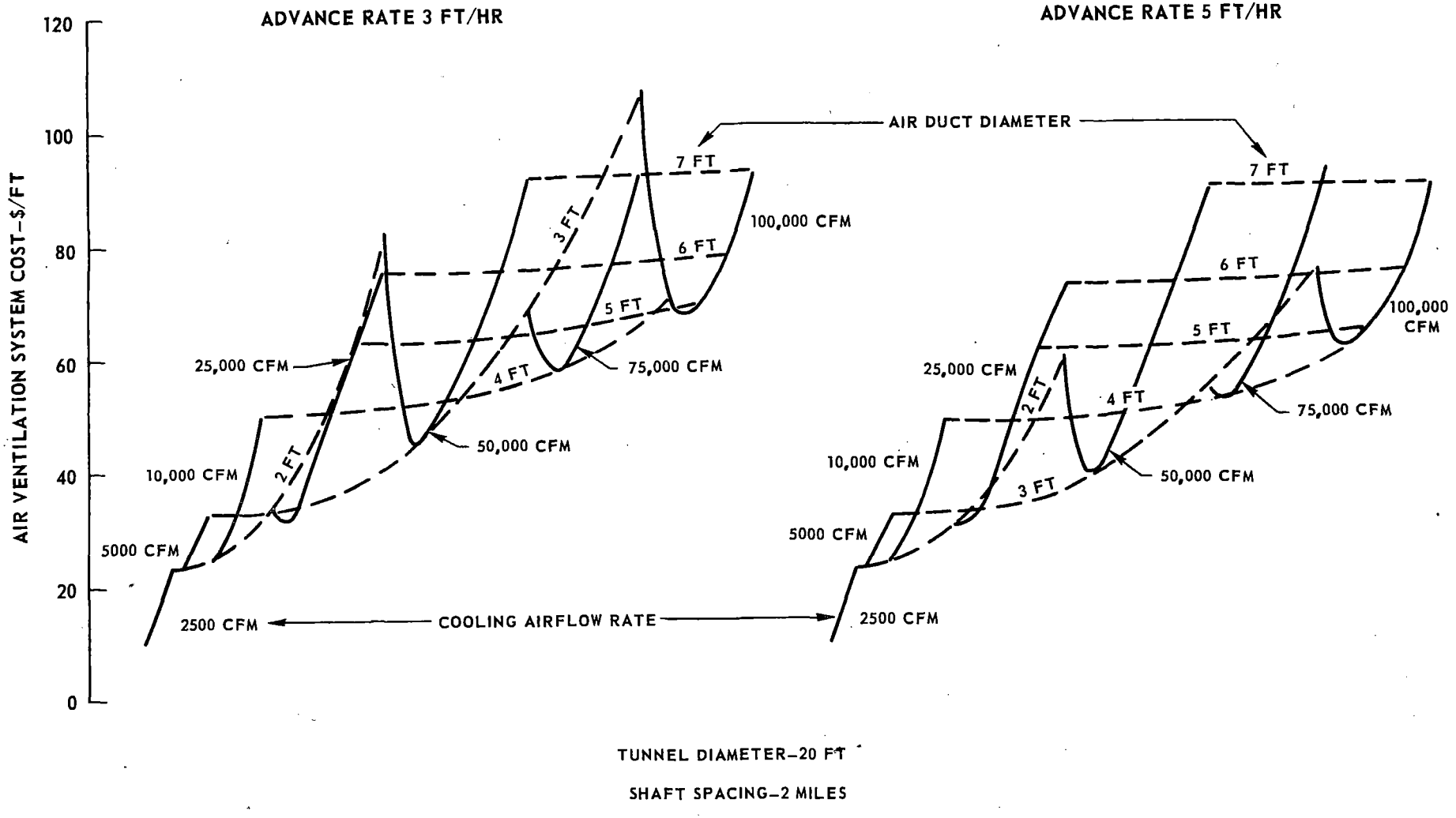

FIGURE 76 TUNNEL AIR VENTILATION SYSTEM COST

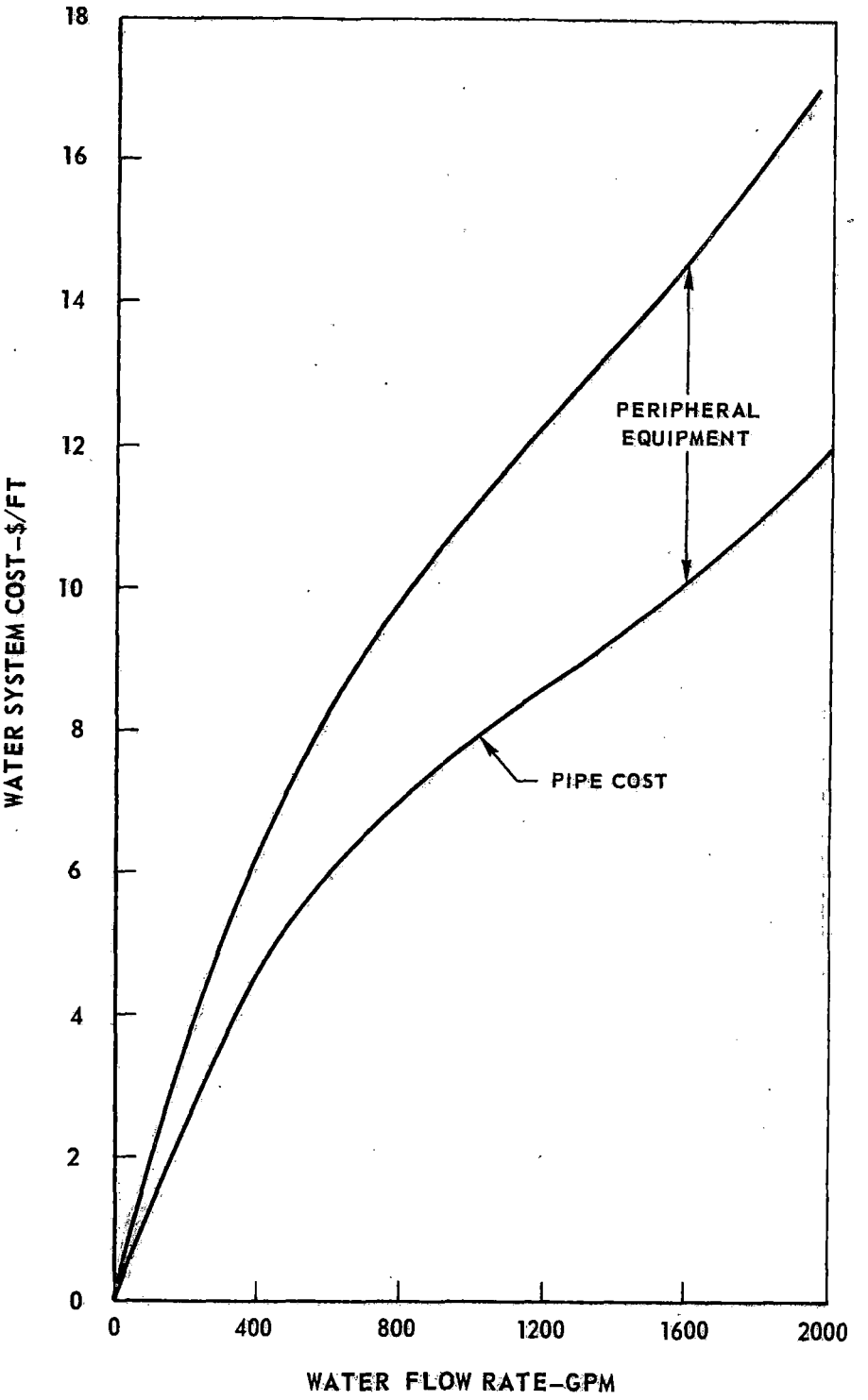

FIGURE 77 WATER SYSTEM COST FOR ENVIRONMENTAL CONTROL SYSTEM IN HEAT-ASSISTED TUNNELING CONCEPT

Fig. 78. These results indicate that the minimum total environmental control system cost (for any set of operating heat input and advance rate) increases only slightly with the selection of the higher airflow rate. From these results, it was concluded that selection of a 10,000 cfm cooling airflow rate for all subsequent analyses would ensure adequate work face cooling and ventilation and maintain a reasonable temperature in the vicinity of the muck cars without severely penalizing the cost of the overall operation.

A comparison of the minimum environmental control system costs for tunnels with various diameters, advance rates, and heat power absorbed by the rock is presented in Fig. 79. It can be seen that there is a slight decrease in total system cost with an increase in tunnel diameter for any advance rate and power level. This decrease occurs because less water is required to cool the lower-temperature rock chips in large tunnels at a fixed power rate and advance rate. In other words, as muck flow increases, the average temperature rise per unit mass removed decreases, and less heat is absorbed by the cooling water. The overall trend (of design points) shown in this figure must not be confused with the costs for a particular tunneling operation, however. Based on the results shown in Fig. 79, it seems reasonable to conclude that for purposes of estimating system costs, the variation in total environmental system costs with tunnel diameter is insignificant in the diameter range of interest.

Results presented in Fig. 80 show the variation in total environmental control system cost with an increase in muck temperature at an airflow rate of 10,000 scfm. The slight decrease in total system cost with an increase in muck temperature is an indication of the efficient cooling characteristics of the water which is sprayed onto the muck. This indicates that as the final muck temperature decreases, only a slight increase in water flow rate is required to attain the desired final muck temperature. This water flow rate increase is interpreted as an increase in water system cost, but because the water flow system constitutes a very small portion of the total environmental control system cost, the overall effect of muck temperature on cost is essentially negligible as is indicated in this figure.

It should be noted that for certain combinations of low power absorbed by the rock, and/or high advance rates, the average muck temperature leaving the work surface may never reach temperature levels in the range of 150 to 180 F (see Figs. 67 and 68). As a result, less water will be required to cool the muck to the 90 to 120 F levels, and no water will be required to cool the muck to higher levels (also see Fig. 71). However, as noted in the previous paragraph, the water system cost is such a small portion of the total environmental control system cost that the overall system costs will not vary significantly from those costs already presented.

Upon review of the combined effects on overall system cost of variations in tunnel diameter, heat absorbed by the rock, advance rate, final muck temperature, and cooling airflow rate, it can be seen that for a fixed airflow rate, only advance

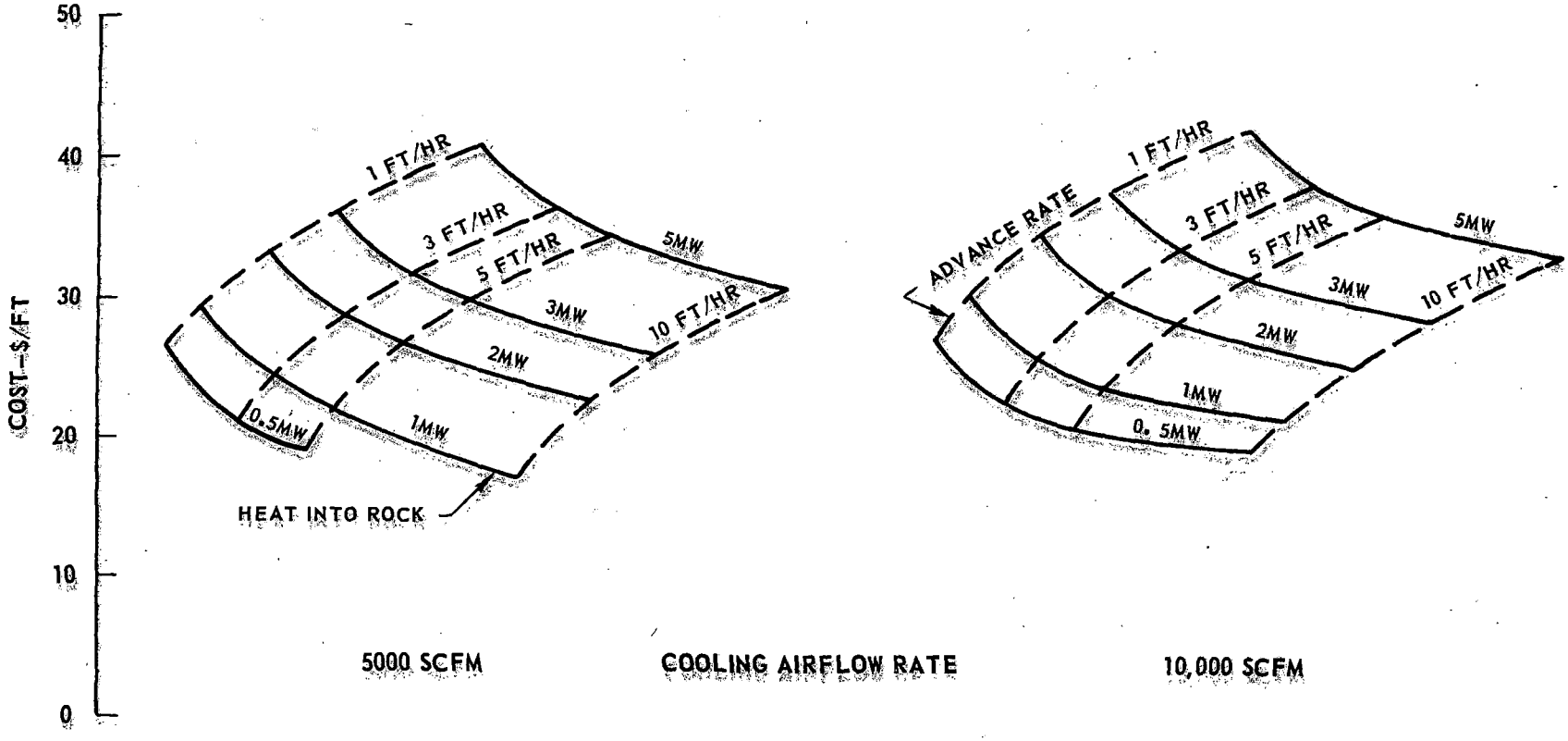

TUNNEL DIAMETER–20 FT

MUCK TEMPERATURE–90 F

TUNNEL EXHAUST TEMPERATURE–80 F

LASER HEATER SYSTEM

FIGURE 78 EFFECT OF COOLING AIRFLOW RATE ON THE COST OF THE ENVIRONMENTAL CONTROL SYSTEM IN THE HEAT ASSISTED TUNNELING CONCEPT

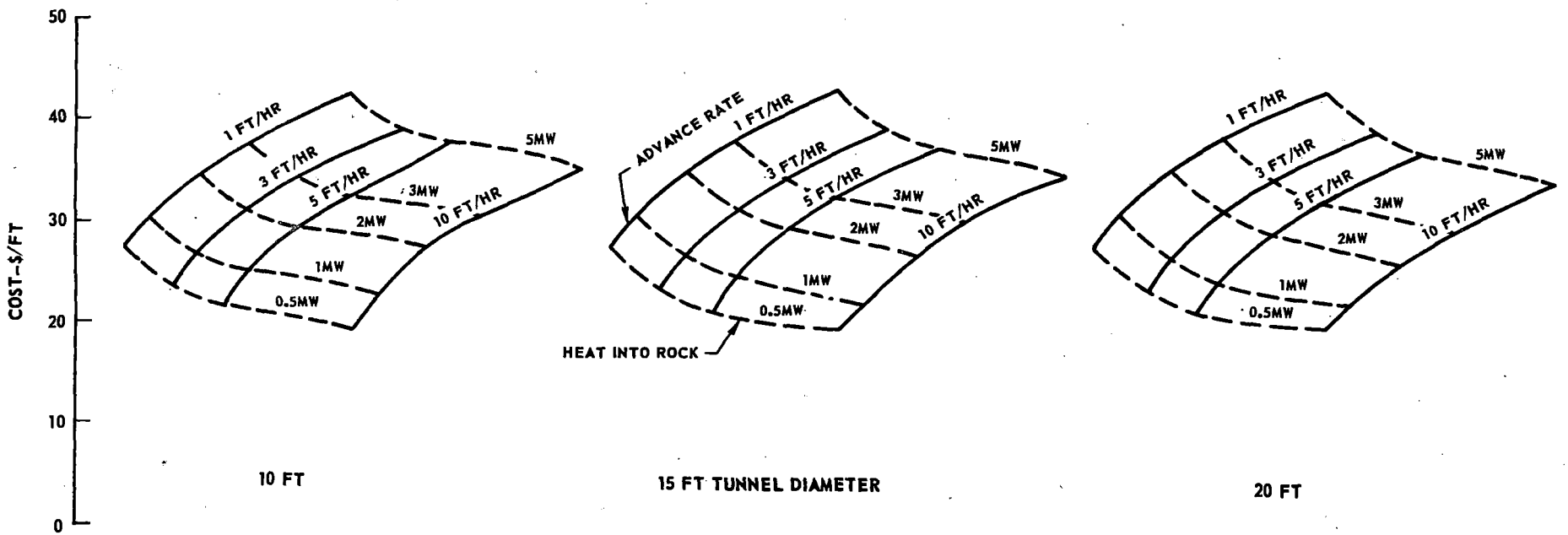

MUCK TEMPERATURE–90 F

COOLING AIRFLOW RATE–10,000 SCFM

TUNNEL EXHAUST TEMPERATURE–80 F

LASER HEATER SYSTEM

FIGURE 79 TOTAL ENVIRONMENTAL CONTROL SYSTEM COST FOR HEAT ASSISTED TUNNELING CONCEPT

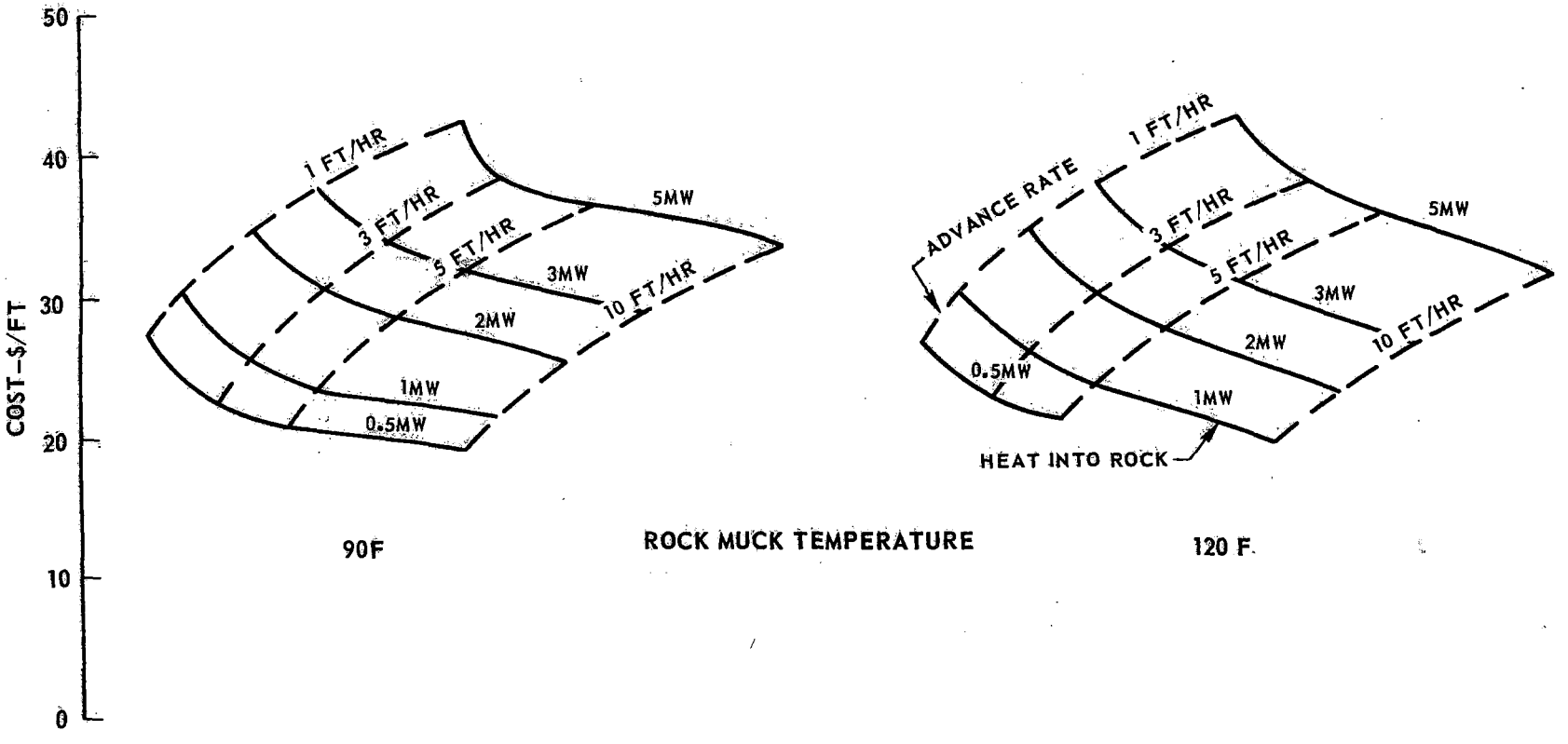

TUNNEL DIAMETER-20 FT
COOLING AIRFLOW RATE-10,000 SCFM
TUNNEL EXHAUST TEMPERATURE-80 F
LASER-HEATER SYSTEM

FIGURE 80 EFFECT OF ROCK MUCK TEMPERATURE ON THE COST OF THE ENVIRONMENTAL CONTROL SYSTEM IN THE HEAT-ASSISTED TUNNELING CONCEPT

rate and heat absorbed by the rock significantly affect the total environmental control system costs for all tunnel systems being considered. Therefore, a general set of curves, shown in Fig. 81, can be established to provide reasonable estimates of the minimum overall environmental control system costs for the heater systems considered in detail for this tunneling concept (i.e., the laser and radiant heater).

Temperature at the Face with No Cooling Water

In studies of water absorption by laser radiation, which are discussed in Chapter III, it was found that excess water between the beam and the rock (which would mean anything worse than a "wet rock" situation where the water film is stationary) must be avoided at all costs. It may therefore be desirable to add the cooling water to the muck stream once the muck has been scooped out of the face area proper, and to prevent water build-up on the face (from naturally present water) by injecting the cooling air as concentrated jets spread over the tunneler face. In this case, the waste heat from the heater system would be handled only by the cooling air, in the immediate vicinity of the face and the cutters. It is of interest to determine the resulting ambient air temperature in which the cutters are working.

Figure 82 shows the air temperature for this "dry" case. For the efficiency range of interest for laser and radiant heater systems (70 to 85% of heater output absorbed in the rock) the temperature will be in the range of 100 to 500 F for power levels absorbed by the rock of up to 3 Mw. The results shown here neglect heat transfer from the hot rock to the air, which probably does not incur great inaccuracies, since fresh (cold) rock is continually being exposed, and the residence time of the hot rock in the face area is small. Also, playing the cooling air jets directly on critical areas may be sufficient to prevent local overheating. However, for heating power levels greater than one or two megawatts, consideration may have to be given to special cooling systems for the cutter bearings.

PRELIMINARY CONSIDERATIONS OF HEATER TYPES

Based on the information presented above on heating power requirements and limitations, heat transfer efficiency, and environmental temperature control, some preliminary comparisons among the various types of heaters considered (Table 4) can be drawn. These comparisons are a prelude to the more detailed analysis of radiant heater systems presented in the next chapter. This section contains a discussion of the factors which were evaluated in the preliminary comparisons and summarizes the reasons for the selection of certain systems for more detailed analysis. A chart presenting the overall results of the comparison is shown in Table 7.

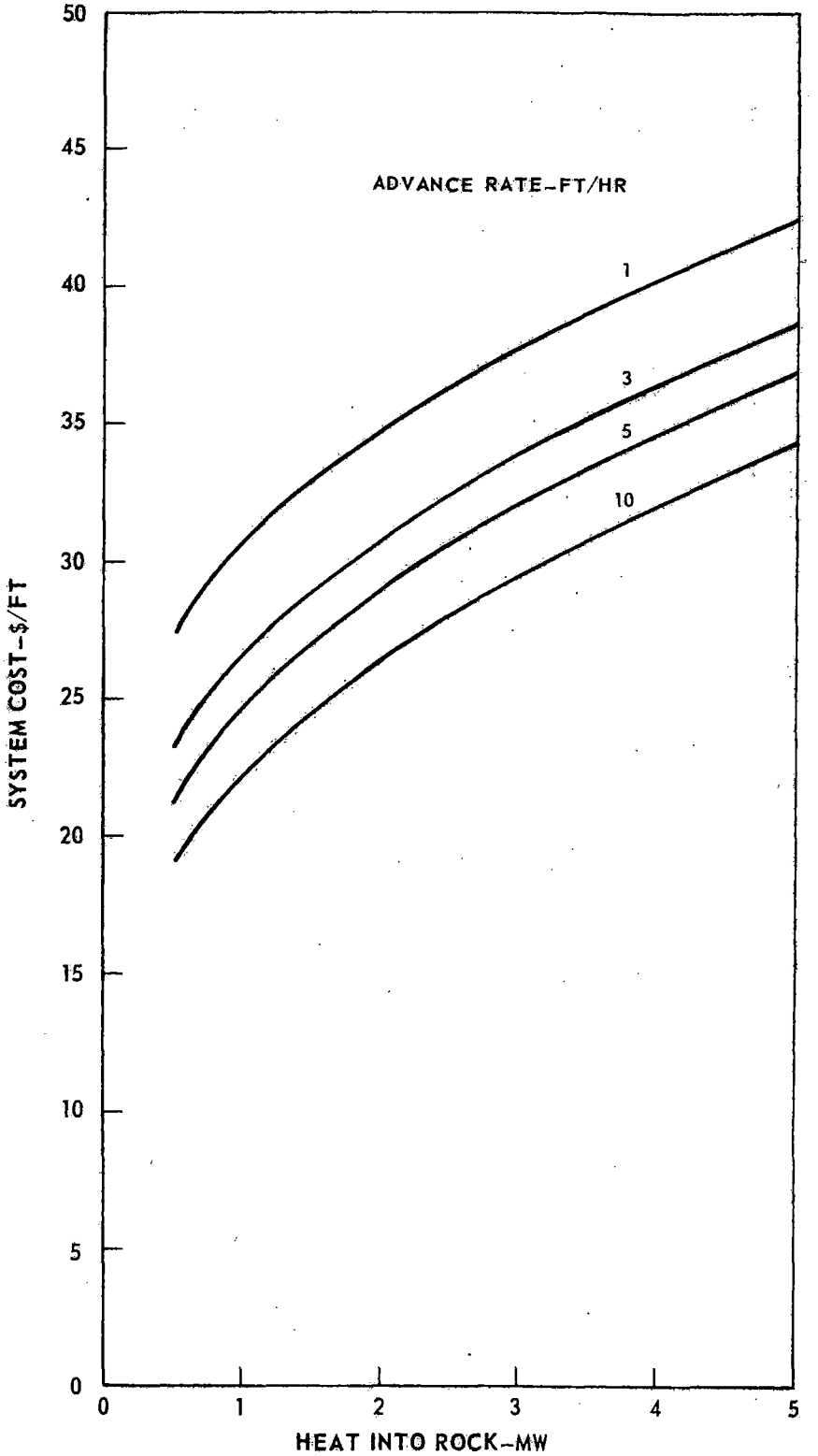

COOLING AIRFLOW-10,000 SCFM
MUCK TEMPERATURE-90 F
TUNNEL DIAMETERS-10,15,20 FT
TUNNEL EXHAUST TEMPERATURE-80 F

FIGURE 81 TOTAL COST FOR ENVIRONMENTAL CONTROL SYSTEM

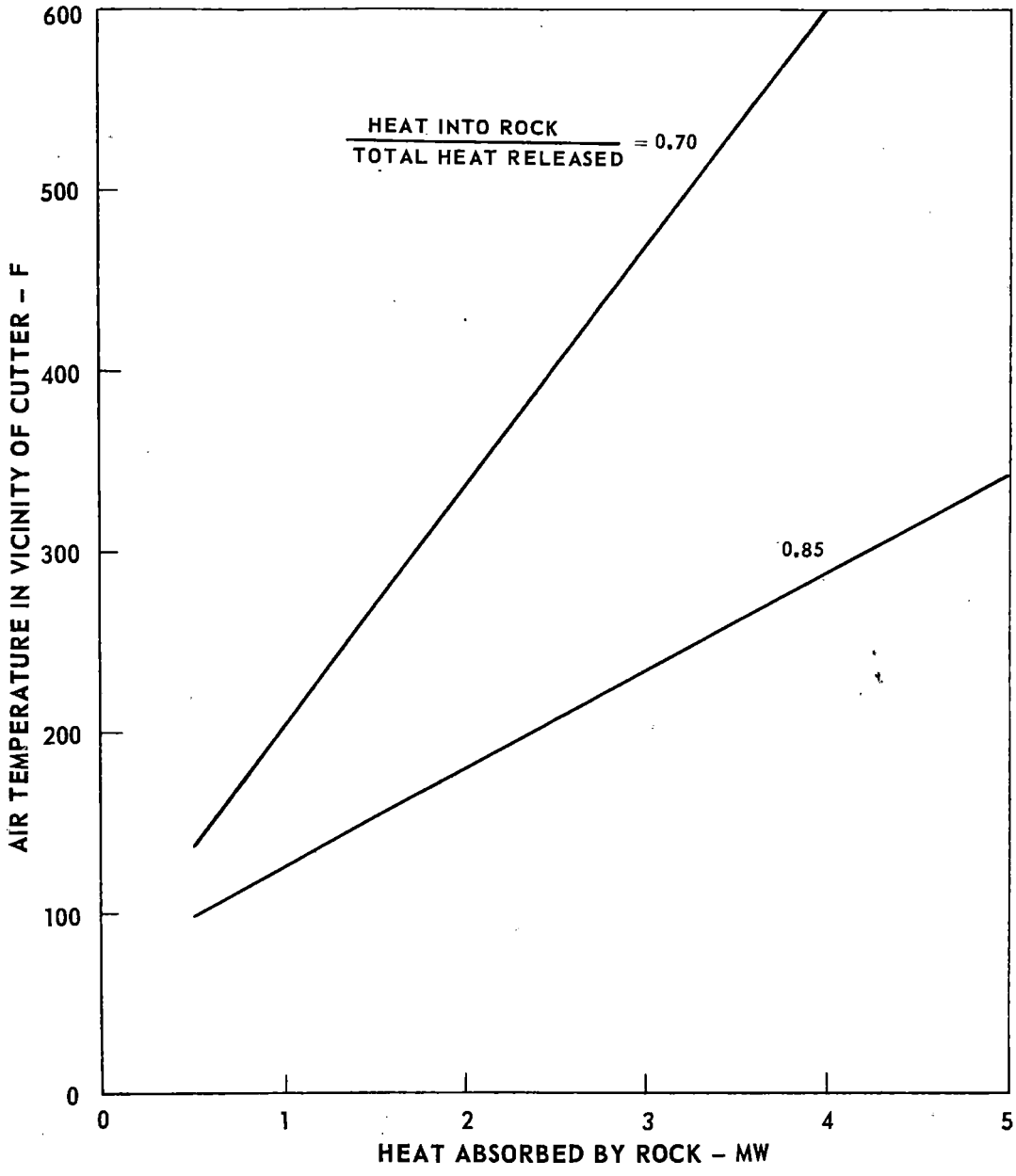

COOLING AIR FLOW RATE = 10,000 CFM

COOLING AIR TEMPERATURE = 80 °F

FIGURE 82 AIR TEMPERATURE IN AREA OF CUTTER AFTER ABSORBING HEATER WASTE HEAT

TABLE 7

HEATER SYSTEM COMPARISONS

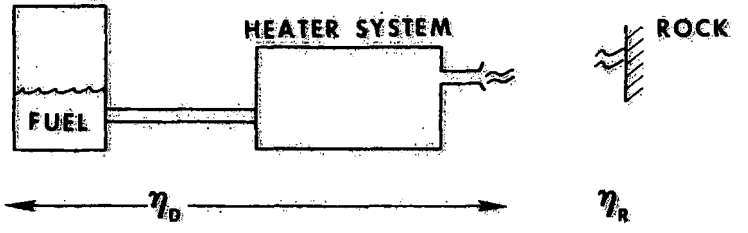

$\eta_{OVERALL}$ (FUEL TO HEAT IN ROCK) = $\eta_D \cdot \eta_R = \eta_O$

SYSTEM	DEVICE EFFICIENCY $-\eta_D$%	ROCK HEATING EFFICIENCY $-\eta_R$%	OVERALL EFFICIENCY $= \eta_D \cdot \eta_R$	CAPITAL COST $/KW	ENVIRON-MENTAL PROBLEMS	MAXIMUM POWER DENSITY INTO ROCK[3] - WATTS/CM^2	FOCUSABILITY OF SYSTEM[4]
LASER	3-6[1]	85	3-6	10^4	PROTECTION FROM LASER BEAM	$>10^3$	GOOD
ELECTRON BEAM	25-30[1]	10-20[2]	3-6	$6 \cdot 10^3$	X-RAYS, HIGH VOLTAGE	$>10^3$	SOME
RADIANT HEATER	25[1]	85	20	10^2	—	~20	SOME
FLAME JET	95	8	8	10-20	HEAT, NOISE, TOXIC GAS	~20	POOR
PLASMA JET	20[1]	28	6	$2 \cdot 10^2$	HEAT, NOISE, TOXIC GAS	~100	POOR
STEAM JET	—	4	—	—	HEAT	~5	POOR

(1) INCLUDES EFFICIENCY OF CONVERTING FUEL TO ELECTRICITY, TAKEN AS 30%
(2) FOR STAND-OFF DISTANCE ~ 0.5 FT. FOR CLOSER DISTANCES AND VERY HIGH VOLTAGE, CAN BE 90%
(3) MOST DESIRABLE POWER DENSITY FOR HEAT WEAKENING = 60-120 W/CM^2
(4) FOCUSING DESIRABLE FOR EFFICIENT USE OF HEAT

Overall Heating Efficiency

The overall heating efficiency, as shown in Table 7, is the product of the efficiency of the heating device and the efficiency of heat transfer into the rock. Energy is assumed to be supplied in the form of fuel, and the overall efficiency indicates what fraction of the energy in that fuel will actually be deposited as heat in the rock face.

Device efficiencies are shown in the first column of Table 7. For the laser, electron beam, radiant heater, and plasma jet, these efficiencies all include the efficiency of converting fuel into electrical energy, and the respective device efficiencies are thus bounded below a maximum of 30%. The laser has the lowest efficiency in converting electrical energy into output, which is assumed here to be 10 to 20%, giving a device efficiency of only 3 to 6%. The other heater sources requiring electrical energy all have reasonably high electrical input to heat output efficiencies. The flame jet, which is assumed to be a compressed air-fuel oil burner, has a high device efficiency, since the fuel is burned directly to produce a hot jet.

The rock heating efficiency of each mode of heat output, as listed in the second column, is of particular significance since the heat from the heater which does not go into the rock acts to increase the tunnel temperature. This is not true of the device wasted heat, since much of this can be generated, and therefore can be dissipated easily, outside of the tunnel (e.g., electricity generation). The absorption of the radiation by the rock of both laser and noncoherent radiation is indicated to be quite high. This indicates a minimum of environmental temperature problems with these two heater types.

Heating efficiency with an electron beam machine is low due to spreading and dissipation of the beam in air. As discussed in a previous section, the amount of energy so lost is a function of the distance between the beam outlet and the rock and of the beam accelerating voltage. While this loss can be overcome somewhat by flooding the face area with helium to reduce beam scattering, it probably always will represent a significant power drop due to the relatively large standoff distances required. Due to the expected surface irregularities of the rock face and the rock chips flying about, the distance between beam outlet and rock probably will be a minimum of several inches. Thus, a relatively low efficiency is assumed here for comparison purposes.

Heating efficiencies with gas jets are generally low, as discussed in detail earlier in this chapter. These are greatly affected by the temperature of the jet. The 28% efficiency of the plasma jet is therefore the highest of all the gas jet systems, while the chemically heated flame jet has only an 8% efficiency. At an efficiency of 28%, roughly 2.5 kilowatts of heat are released directly into the tunnel for every kilowatt deposited in the tunnel face. This low efficiency renders gas jet heaters unattractive; the problem of dissipating the heat generated

in the tunnel by a flame-jet system has already been shown to be formidable (see Ref. 2). The indicated efficiency of a steam jet of only 4% is low enough to eliminate any further consideration of that type of system.

Overall efficiency of heating (shown in column three) is of interest both as a general efficiency parameter and as an indication of expected power costs and heater system costs with the various heater types. Although installed power costs and energy use charges are not large components on present-day boring machines, this situation cannot be assumed for heat-assisted tunnel boring machines, since the net power requirements for the latter systems may be significantly greater. Except for the radiant heater system, this overall efficiency is under 10% for all heater types. The radiant heater system appears to be capable of overall efficiencies in the region of 20%, which distinguish this heater type for further analysis.

Capital Cost

The capital costs of the heater systems vary over a tremendous range from the $10,000/kw estimated for large laser systems to the $20/kw expected for a flame-jet. This factor alone indicates that the capital cost of the device likely will be a significant criterion.

The $10,000/kw laser cost is based on a 10% laser efficiency in converting electricity into laser energy. Although a detailed discussion of present-day laser costs is presented in Chapter III, future laser costs are expected to decrease, perhaps as much as an order of magnitude.

Although production experience has been factored into the $6000/kw estimate of present-day electron beam equipment, this cost is not significantly less than that for laser systems. Adaptation of electron beams for use in tunneling would require some new developments, as discussed in Chapter III, and the effects of these on costs is unknown.

Even with the uncertainties surrounding the costs of these two heater types (lasers and electron beams), it is clear that they are both much more expensive than plasma jets and radiant heaters. Experience at the United Aircraft Research Laboratories indicates that the power conditioning, air supply, and jet equipment for a plasma jet in the several hundred kilowatt size will run about $80/kw. Allowing $120/kw for power generation, a total cost of $200/kw was developed. Radiant heaters, on the other hand, are very inexpensive; the heating element itself costs less than $30/kw. It was assumed, therefore, that the cost of generating electricity would dominate the cost of a radiant heater system, and the total cost was assumed at $150/kw.

The gap in the cost per kilowatt between the plasma jet and radiant heater systems, on the one hand, and flame jet heaters, on the other hand, is again larger than the uncertainties in the costs of the individual systems. The flame jet system consists of a burner, fuel pump, air compressor system, and the necessary plumbing and controls. Based on system cost data presented in Ref. 2, the largest part of the system cost is the air compressor, and the entire system cost will vary from about \$10/kw for a very large system to \$20/kw for smaller systems (< 15,000 kw). These numbers reflect primarily the cost variations in the required compressor. For any reasonable size, the flame jet system will be the lowest-price complete system of any heater units considered. (If, however, there is no need to purchase electric power generating equipment, then the price of the radiant heater system may be the lowest.)

Environmental Problems

A general environmental problem with heat-assisted boring machines is the resultant tunnel ambient temperature. This problem was discussed at length in a preceding section of this chapter. One other general problem which will exist for any kind of heat-assisted boring operation is the ignition of methane gas. Other environmental problems are mentioned below for each heater type.

Methane Flammability

A serious factor in the evaluation of heat-assisted boring machine concepts is the possibility of leakage of underground methane or natural gas into the tunnel cavity and an explosion resulting from the exposure of a gas-air mixture to a high-temperature rock face or open flame. In order to define the conditions under which such a series of events may occur, a brief survey was made of methane flammability and ignition temperature data.

A plot of the flammability limits and the ignition temperature for methane as a function of temperature is shown in Fig. 83. Ignition temperatures of a typical natural gas in air are also shown in this figure. These data should be construed as a general indication of the dangerous temperature and concentration regimes since the precision of these values is somewhat questionable.

The flammability limits of a fuel gas or vapor are those concentrations of the fuel below which, once ignited, a flame will not proceed without the continual addition of energy. For instance, with reference to Fig. 83, at 70 F a flame will not propagate through a CH_4-air mixture which contains 6% CH_4 by volume, but will propagate through such a mixture if the methane concentration is increased to 6.5%. Either mixture will be dangerous if the temperature is raised to 200 F.

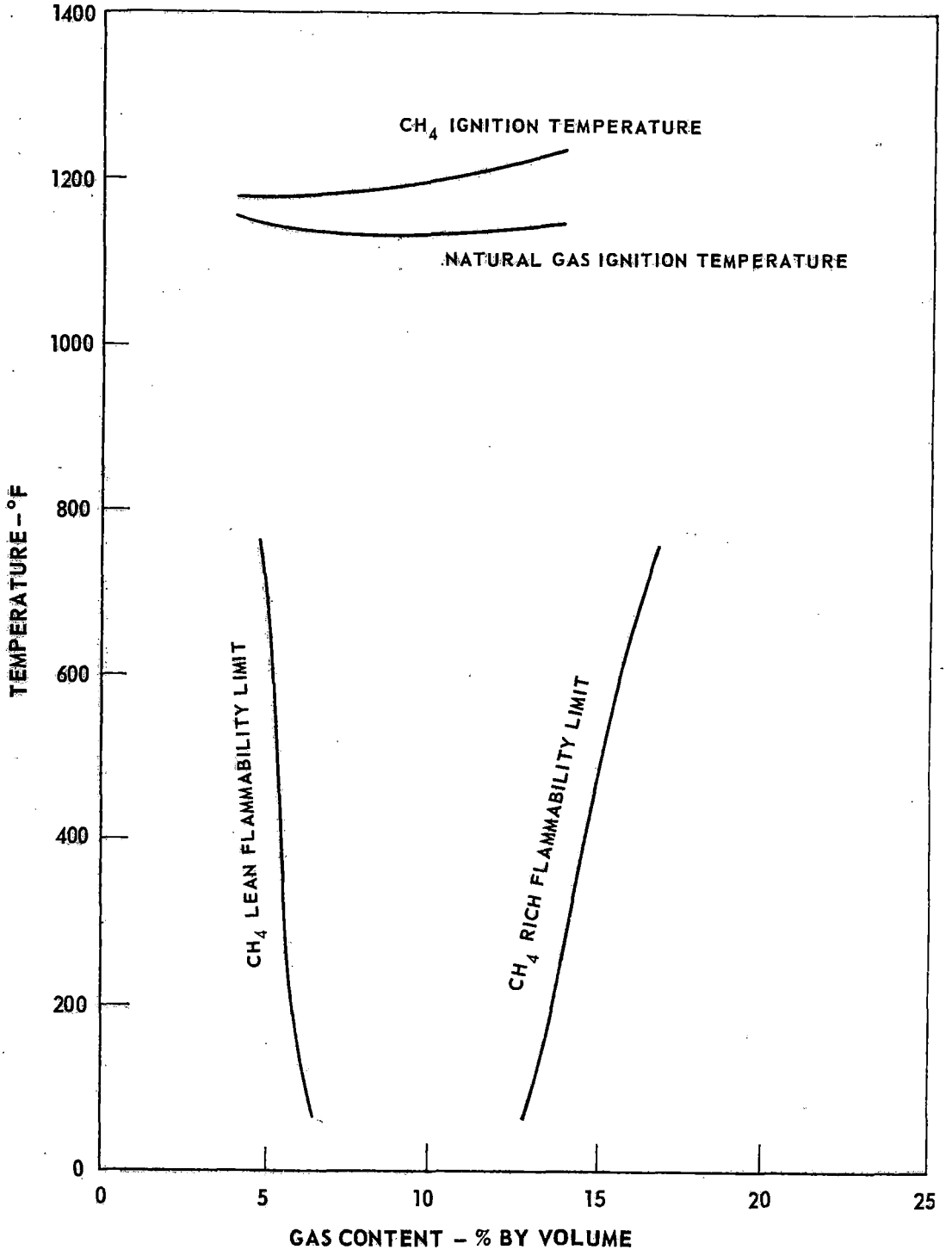

FIGURE 83 METHANE AND NATURAL GAS FLAMMABILITY DATA

The ignition temperature is that temperature at which spontaneous ignition of a quiescent mixture is possible. Thus, any surface at a temperature greater than the 1100 to 1200 deg F shown in Fig. 83 will cause ignition of gas-air mixtures within the limits shown.

Since rock surface temperatures of this order or greater are required for the use of the heat-weakening technique, it appears that methane explosions at the tunneling face are a possibility with any form of heating system. Of course, an open flame will, in general, provide a greater chance of detonation than, say, a laser system (wherein no component of the laser mirror system is at a higher temperature than the rock face), but if the rock temperature goes over 1100 F, an explosion can occur in either case.

Although this problem deserves careful consideration, it is not likely that it will prevent (by itself) the general application of heating systems to boring machines. For one thing, the real danger lies in ignition of a large reservoir of a suitable gas-air mixture. It is assumed that gas detection systems operating near the face and further back in the tunnel will prevent the buildup of large quantities of explosive gas in the tunnel. Also, many hard-rock formations are not expected to yield natural gas or methane in significant amounts. For example, on some hard-rock boring jobs now, it is common practice to use welding torches, or for miners to smoke, without excessive precautions in determining the air quality. For tunneling jobs which are expected to encounter large pockets of methane gas, however, it is unlikely that rock heating systems, as discussed here, will be utilized.

Other Environmental Problems

Other problems caused in the tunnel environment are listed for each type of heater in Table 7. A major problem with the laser heating system is the delivery of the laser energy to the tunneler. As discussed in Chapter III, the safety aspects of preventing beam impingement on the tunnel personnel will involve enclosing the beam in a special tube. Safety hazards with the electron beam device are also treated in detail in Chapter III.

A primary problem of all gas jet heaters is their exhaust heat, noise, and (for flame and plasma jets) fumes. The heat problem is considered at length in the previous section and is sufficient to eliminate the steam jet from further consideration. The noise levels to be expected with flame jets are also critical, as detailed in Ref. 2, although hearing protection and proper shielding should solve that problem. Ultimately, the most difficult problem associated with the flame jet is the emission of toxic gases, which are in too great quantities to be treated by dilution, and will require a very-high-capacity, totally effective exhaust system. Due to the formation of oxides of nitrogen in a heated air stream, this problem will also exist with a plasma jet.

In the plasma jet, the heating rate of the air as it passes the electric discharge arc is almost instantaneous. Since this rate far exceeds that which corresponds to the equilibrium formation rate of nitrogen oxides, their formation will be different from the amounts formed according to equilibrium calculations. However, the high jet temperature, both during heating and subsequently during the jet expansion process, coupled with a relatively long gas residence time at these elevated temperatures, eventually will force the production of increasingly larger amounts of nitrogen oxides. That gas temperature at which the equilibrium production rate equals the jet stream temperature determines the maximum amount of oxides produced in a particular reaction. Depending on the physical changes in the flow stream, this equilibrium point may occur during the expansion (cooling) process for plasma jet devices.

Empirical data reported in Ref. 17 and replotted in Fig. 84 indicate the amount of nitrous oxide (NO) which is formed in the exhaust of plasma jets at various temperatures. These results appear to be relatively insensitive to flow rate, jet power input, and the size of the probe used to sample the flow stream. In a tunneling operation it is anticipated that the static temperature of the flow stream exiting from the jet device will at least be above 3000 K (approximately 5000 F) indicating that the NO production may comprise approximately 2% (or 20,000 ppm) of the jet flow stream. Since NO dissociation is a slow process, it is expected that this equilibrium concentration would exist at lower tunnel temperatures until removed in a suction system or significantly diluted with additional cooling air. Information presented in Ref. 18 indicates that the maximum total tolerable 8-hr NO-compound concentration in industrial shops should not exceed 5 ppm. The production of NO by a plasma jet heater system far exceeds this limit.

Air dilution cannot solve this problem since the supplemental airflows required to reduce the NO-compound concentration to tolerable levels are excessive. The addition of a suction system to the tunnel, as developed in Ref. 2 , would roughly double air handling costs and still would not guarantee complete elimination of all traces of these NO-compounds. Consequently, the toxic gas handling problem, in addition to the heat and noise, seriously handicaps the desirability of a plasma jet system.

Power Density and Focusability

Two other criteria listed in Table 7 are heater output power density and focusability of the power output. Heater output power density affects the total amount of heating that can be accomplished by any given heater type, among other things. Power density is a limiting factor on the effectiveness of radiant heater or flame-jet systems and should offer no trouble for a laser system. For an electron beam, the beam power density is less important than the device size, as is shown in Chapter III.

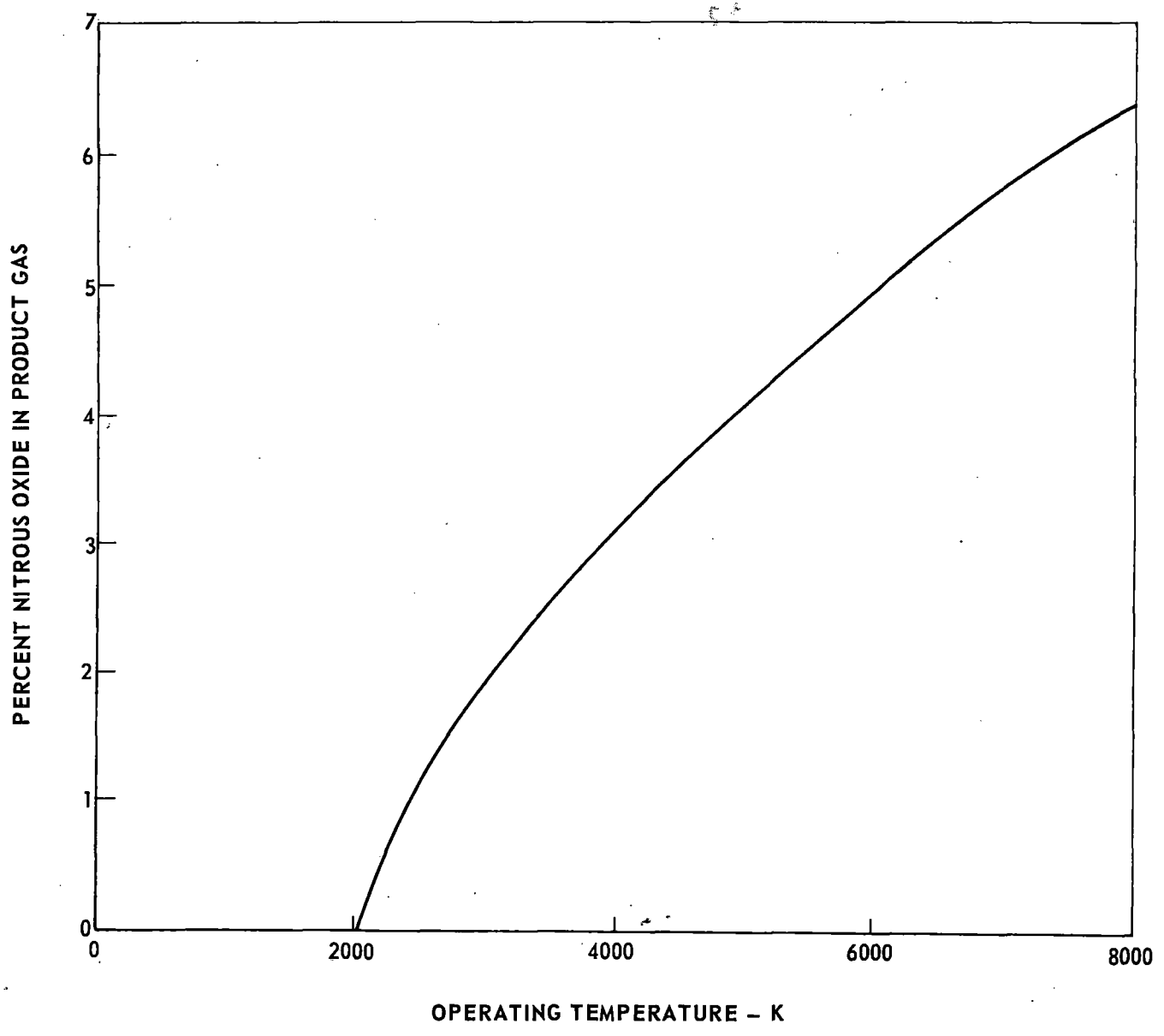

FIGURE 84 CONCENTRATION OF NITROUS OXIDE IN THE EXHAUST GAS OF AN ELECTRIC ARC DISCHARGE PLASMA JET OPERATING AT VARIOUS TEMPERATURES

Heater beam focusability is also desirable, as shown by the test results reported in Chapter I. As indicated on Table 7, some focusability is available with an electron beam machine (by increasing or decreasing stand-off distance, or rapid scanning) and with a radiant heater (by the use of suitably shaped reflectors). The nature of gas jet systems renders precise focusing difficult, although some kind of a focusing effect (within the dimensions of interest) could be achieved with plasma jets by suitably arranging many small ones rather than fewer large ones. The potential of laser energy for focusing, by the use of suitably designed mirrors, is high.

Selection of Candidates for Further Analysis

Based on the information presented above, the gas jet systems were eliminated from further consideration. This decision is based primarily on the environmental side effects of using such devices in a closed tunnel. In addition to the heat and the noise, elimination of the toxic gases would be difficult in the case of the flame jet or plasma jet. Elimination of toxic gases is felt to be basically feasible, by the suitable arrangement of aerodynamically controlled exhaust systems, as developed in Ref. 2. However, the added complication of developing such a system caused attention to be directed toward the less obnoxious radiant and electron beam heating systems.

CHAPTER III - DESIGN AND ANALYSIS OF HEATER SYSTEMS

This chapter contains information developed on specific heater types relative to their incorporation in a heat-assisted tunnel boring machine. The chapter sections are concerned with laser systems, radiant heaters, and electron beam systems.

The nominal heater configuration employed for design purposes assumed a heater power output of 450 kw in a 18-ft-dia tunneler. The heating is assumed distributed between cutter paths separated by 3 inches (see Fig. 85). The resultant power density corresponds to a heat input of roughly 600 joules per inch of heated path, which is near the minimum needed to induce a significant weakening effect on the rock.

The third section, on electron beams, does not include a design for the desired tunneler configuration, because these design conditions cannot be met with electron beams. Some feasible design arrangements are shown, but the emphasis in the electron beam section is on the design of the device itself.

CONCEPTUAL DESIGN AND ANALYSIS OF LASER SYSTEM

In order to provide a basis for a technical and economic evaluation of a laser-assisted tunneling machine, it is necessary to establish the characteristics of the associated laser energy transmitting equipment. Almost none of the vital components of the laser system are presently available as standard equipment, and even their desired characteristics cannot be established until a conceptual design has been completed. Therefore, a design study of the laser system was undertaken to provide some indication of technical feasibility, probable performance level, and preliminary cost estimates. This study was based on the heat output configuration and total energy design point discussed above and shown in Fig. 85. The following discussion covers the system configuration, performance (i.e., power losses), and cost.

System Components

Laser System

A complete design of an actual laser and its associated equipment is beyond the scope of this study. However, to make a meaningful cost estimate, it is necessary to establish certain features of the laser system to allow definition of the characteristics of the emitted radiation. There are many different lasers under current development varying in basic type (e.g., solid state, glass, and gas or molecular lasers), output wavelength, means of excitation, and practical output power ranges.

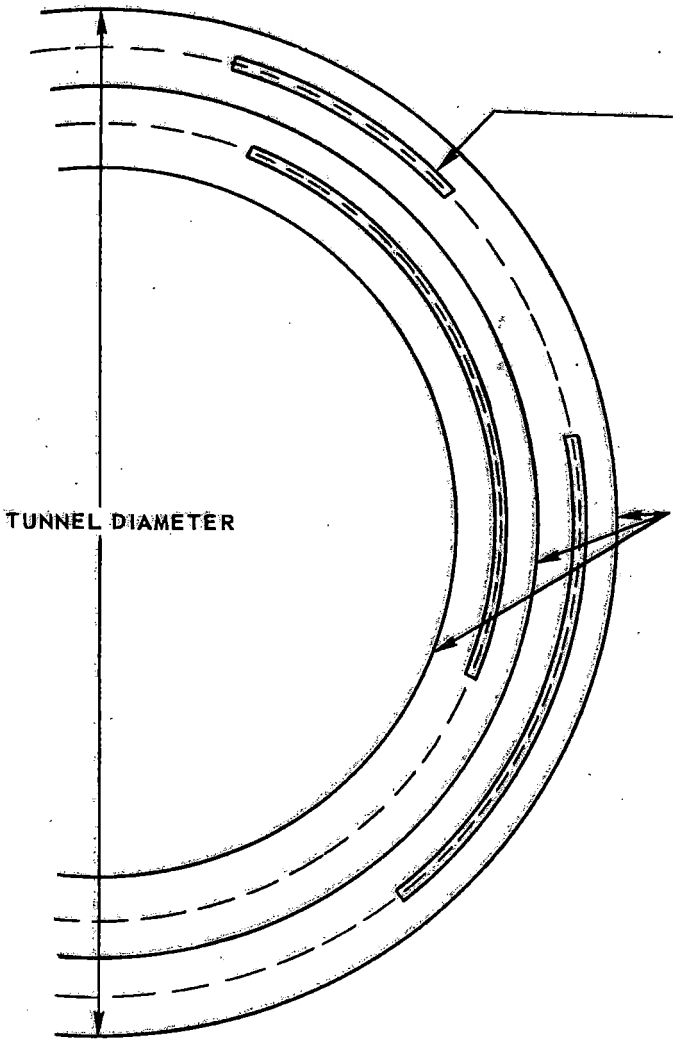

TUNNEL DIAMETER = 18 FT

TOTAL LASER POWER OUTPUT = 450 KW

FIGURE 85 LASER BEAM OUTPUT CONFIGURATION

The total laser energy required at the tunnel face by the reference design is 450 kw. When allowance for losses at mirrors and in transmission is included, a total laser output close to a megawatt may be required. The only laser type which appears to have a significant probability of achieving a power output of this order is the CO_2-N_2 molecular laser whose output is at a wavelength of 10.6 μ. Other lasers may eventually prove capable of the same or of a greater power level, but they are likely to be molecular lasers whose output is a vibrational quantum, and they are therefore likely to have similar output wavelengths. Consequently, it appears that the CO_2-N_2 molecular laser can be taken as representative of lasers which might be used for this type of application.

A schematic diagram of a standard low-flow electric discharge CO_2-N_2 laser is shown in Fig. 86. A mixture of CO_2, N_2, and various diluent gases is supplied to a long discharge tube at a pressure on the order of 0.01 atm. The vibrational states of nitrogen are excited selectively by certain nonequilibrium phenomena in the glow discharge to produce a population inversion, i.e., more molecules in an upper vibrational state than in the lower state. This population inversion is drained preferentially through the CO_2 molecules because of marked differences in the reaction times of all the other available modes of relaxation. A population inversion is thus created in the CO_2 molecules which is released by stimulated emission of a quantum of energy having a wavelength of 10.6 microns. This radiation is returned through the cavity by the mirrors, thereby stimulating further emission.

Depleted gas is withdrawn by a vacuum pump, and the cavity tube is cooled by a water cooling system. The electrical energy is supplied at voltages on the order of tens of kilovolts, and the electrical-to-radiated energy conversion efficiency is typically on the order of 10% (although efficiencies of over 20% have been reported for some units). Output power levels of 50 to 100 watts/meter of cavity length, regardless of cavity diameter, appear to represent some type of maximum value for low-flow devices of this nature.

There are other molecular lasers which have different operating characteristics. For instance, several high-flow CO_2-N_2 lasers have been reported which operate at higher pressures and at greater flow rates. These lasers are basically conventional glow discharge lasers with modified cavities. Outputs as high as 4 w/cm^3 of cavity volume have been quoted (Ref. 19) for these lasers. Very high specific power outputs have also been calculated for chemical lasers, in which the excitation is provided by combustion. Excitation by combustion, however, is not selective as is excitation by glow discharge, and significantly lower energy conversion efficiencies result. In general, the conventional glow discharge CO_2-N_2 laser appears to represent the most practical laser configuration likely to be available for tunneling applications in the reasonably near future in all respects, except for the specific power output.

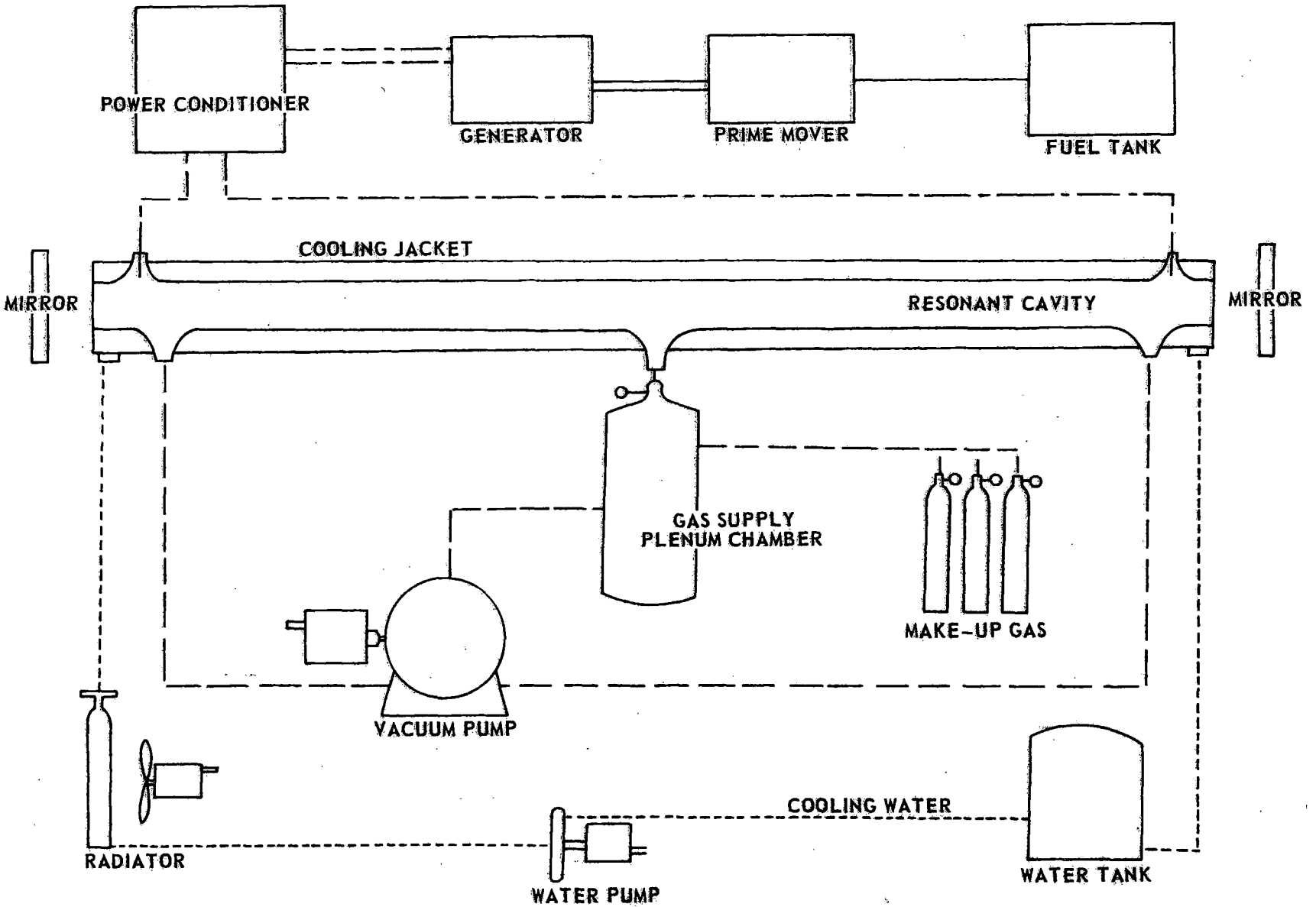

FIGURE 86 CONVENTIONAL ELECTRIC DISCHARGE LASER SYSTEM

A specific power output on the order of 4 w/cm^3 appears to be reasonable to assume, in view of the number of high-flow lasers under development.

Boring Machine Head

A major problem in adapting a laser rock-heating system to a tunnel boring machine is providing a passage for the laser energy through the machine head. Typical boring machine heads are solid over their entire face except for small passages to allow men to pass for maintenance of the cutters. The heads are made of heavy (up to 4 in. thick) steel plate. A typical boring machine head is shown in Fig. 87 in which a disk cutter distribution typical of a Robbins machine is shown. The cutters on this head have been rearranged slightly, to lie along radial lines. This was done in anticipation of the need for providing slots in the tunneler head to allow passage of the laser energy. The head is welded to supporting webs which tie into the main bearing support immedicately aft of the head. The cutter mountings are welded or bolted onto the head.

Muck buckets, or scoops, are mounted around the periphery of the head (these are not shown in Fig. 87. These buckets scoop the muck from the bottom of the tunnel, and the muck falls down behind the head from each scoop as the machine rotation brings each bucket to the top of the head. This falling muck is collected in a hopper, from which it is carried away by a conveyor system.

According to the desired rock heating configuration established by the test program discussed in Chapter I, and specified in Fig. 85, heating of the face is to be along circular paths located between the cutter paths (i.e., every 3 inches). Also, to avoid rock melting, the heating should be at as low a power density as possible, as discussed in Chapter II. Therefore, an effort was made to determine the maximum length of the heating output along each path. The results are shown in Fig. 88.

As in Fig. 87, the cutters are arranged along ordered radial lines to allow for sectors of slots in the head for the laser beams. The central angle of each of these sectors is roughly 11 degrees. This angle is limited at the center of the machine by the space requirements for cutters (note the smaller size cutters required near the center to allow the 11-degree slot sectors). A limitation is also encountered at the outer edge of the face due to the space required for the gage cutters and the muck buckets. (Note that Fig. 88 is a projected plan view, so that the outside gage cutters are seen "edge-on", whereas due to the dished shape of the tunneler head, they should be seen at an angle, as shown in Fig. 87. The total effective central angle of the heating system, then, is 8 x 11 = 88 degrees, with 35 slots in each of the 8 sectors.

Directly behind the rotating head there is usually a crowded area which complicates the problem of bringing laser energy from the rear of the machine to the

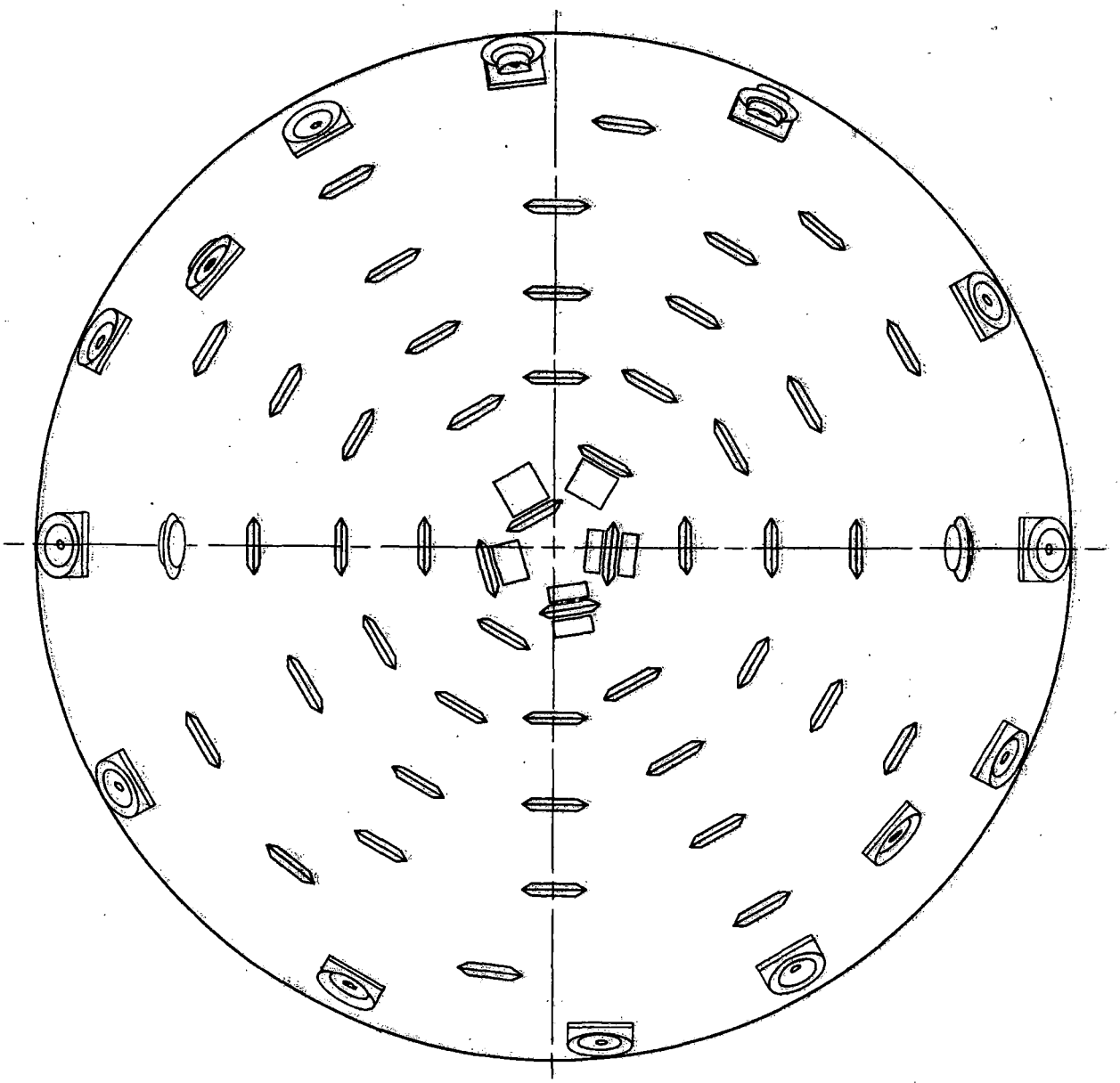

NOTE: MOST CUTTERS ARE SHOWN EDGE-ON FOR SIMPLICITY

FIGURE 87 FACE VIEW OF TYPICAL BORING MACHINE HEAD

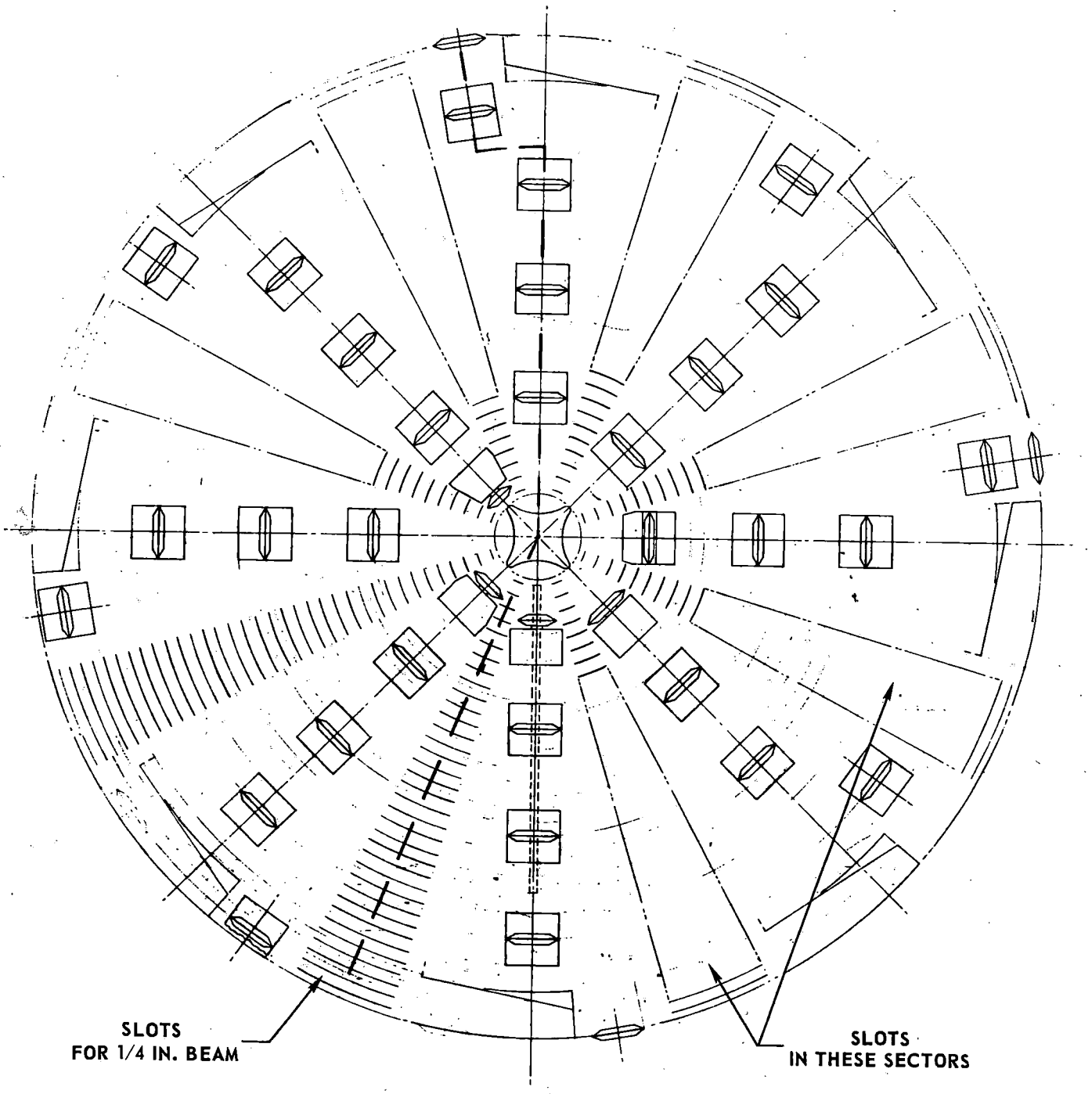

FIGURE 88 FACE VIEW OF TYPICAL BORING MACHINE HEAD WITH SLOTS FOR LASER BEAMS

tunneler head. Immediately aft of the head there is often a large shield which is used as a pressure bulkhead to allow a slightly negative pressure to be maintained at the face for dust control. Other equipment, including structural supports, muck hopper and conveyor, the main bearing, and the operator's control station, is also in the area behind the rotating head.

There is insufficient volume to install the laser cavity itself behind the rotating head, and therefore some means must be devised for transmitting a concentrate beam of laser energy into the machine head, and then dispersing this beam to the 35 slots in each of the eight sectors. Dispersing systems of this nature can be divided into two categories: those in which the central shaft of the boring machine can be used for passage of the laser beam, and those in which the central shaft is solid.

Hollow-Shaft Machines

For machines with hollow shafts, the laser beam can be transmitted through the shaft to a multifaceted mirror which is attached to the rotating head, as shown in Fig. 89; this design is based on an 18-ft-dia Robbins-type machine. The central multifaceted mirror divides the incoming laser beam into eight separate beams, each with a triangular cross-section, and each at a fixed position inside the rotating head. Each radial beam is, in turn, divided into 35 beams which pass through the 35 slots shown in Fig. 88. Only eleven of these mirrors are shown on Fig. 90, where every third mirror in one sector is shown; the centerlines of the beam paths reflecting off each mirror are also shown.

Figure 90 also shows the major modifications required of a standard tunnel boring machine of this type to convert it into a laser-assisted machine. These include (a) the slots in the head for the laser energy passage, (b) alignment of the cutters along radii which are located directly over thick head-supporting webs (Section A-A in Fig. 90), (c) placement of the head roughly 1 ft further forward from the main bearing than usual to make room for the mirrors and laser beam paths, and (d) the placement and design of the mirrors themselves. The slots in the machine head for the individual heating beams are a maximum of $\frac{1}{2}$ in. wide, so that for the 18-ft-dia machine shown, the slot area represents only about 15% of the head area in the slotted regions. With the cutters moved to positions directly in front of the supporting webs, the slots should not significantly reduce the stiffness of the head. It was further assumed that the ordered repositioning of the cutters would not create any vibrational problems.

The most important new components are, of course, the mirrors. As mentioned, there is a large eight-faceted mirror in the center of the rotating head, and a total of 280 smaller mirrors distributed 35 to each of the eight sectors. Greater detail of the placement of these mirrors is given in Fig. 91 (a section of one sector near the center of the machine) and Fig. 92 (an elevation view showing some typical ray-paths perpendicular to the tunneler centerline).

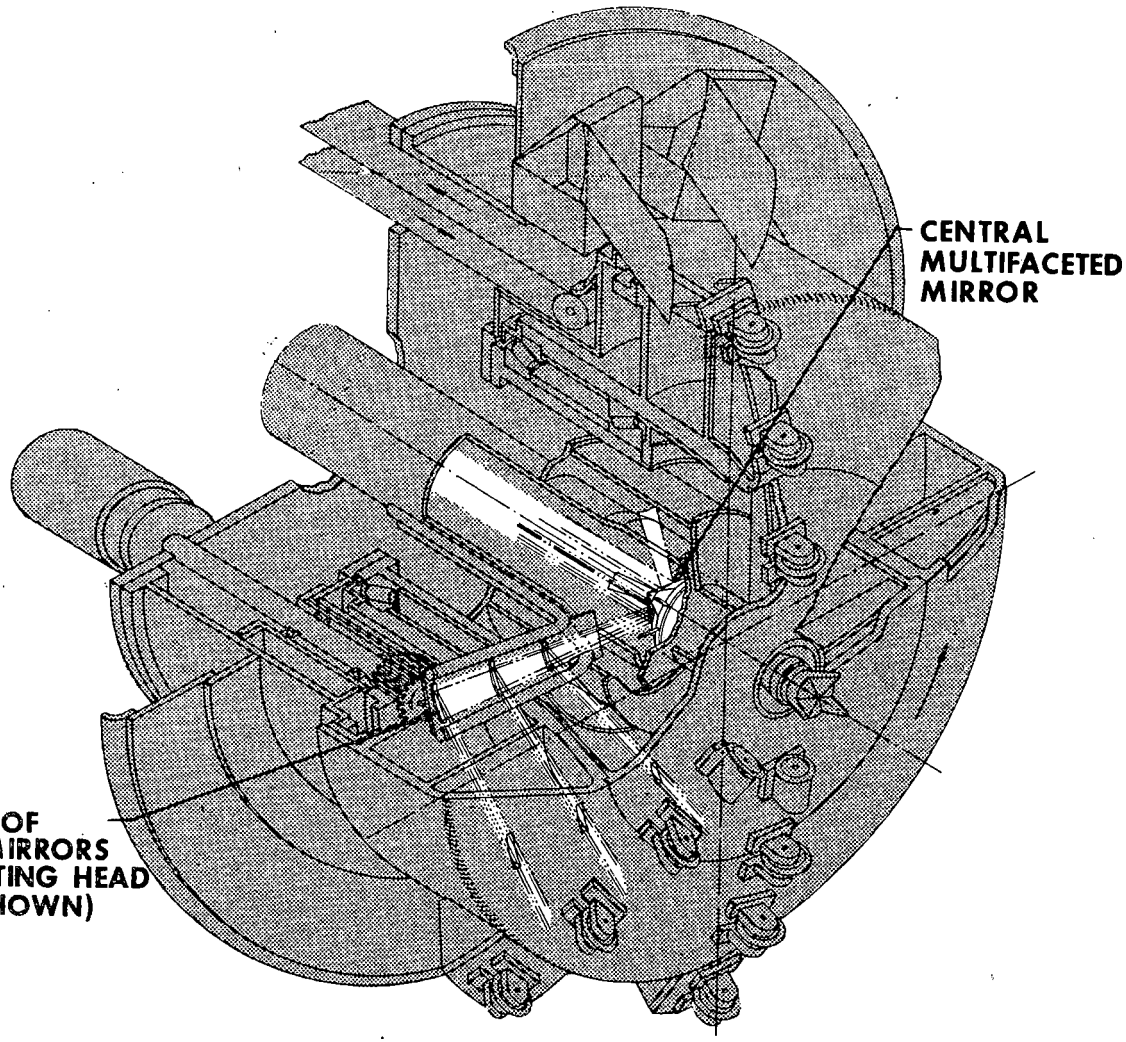

FIGURE 89 **18 FT DIA LASER-ASSISTED TUNNELING MACHINE**

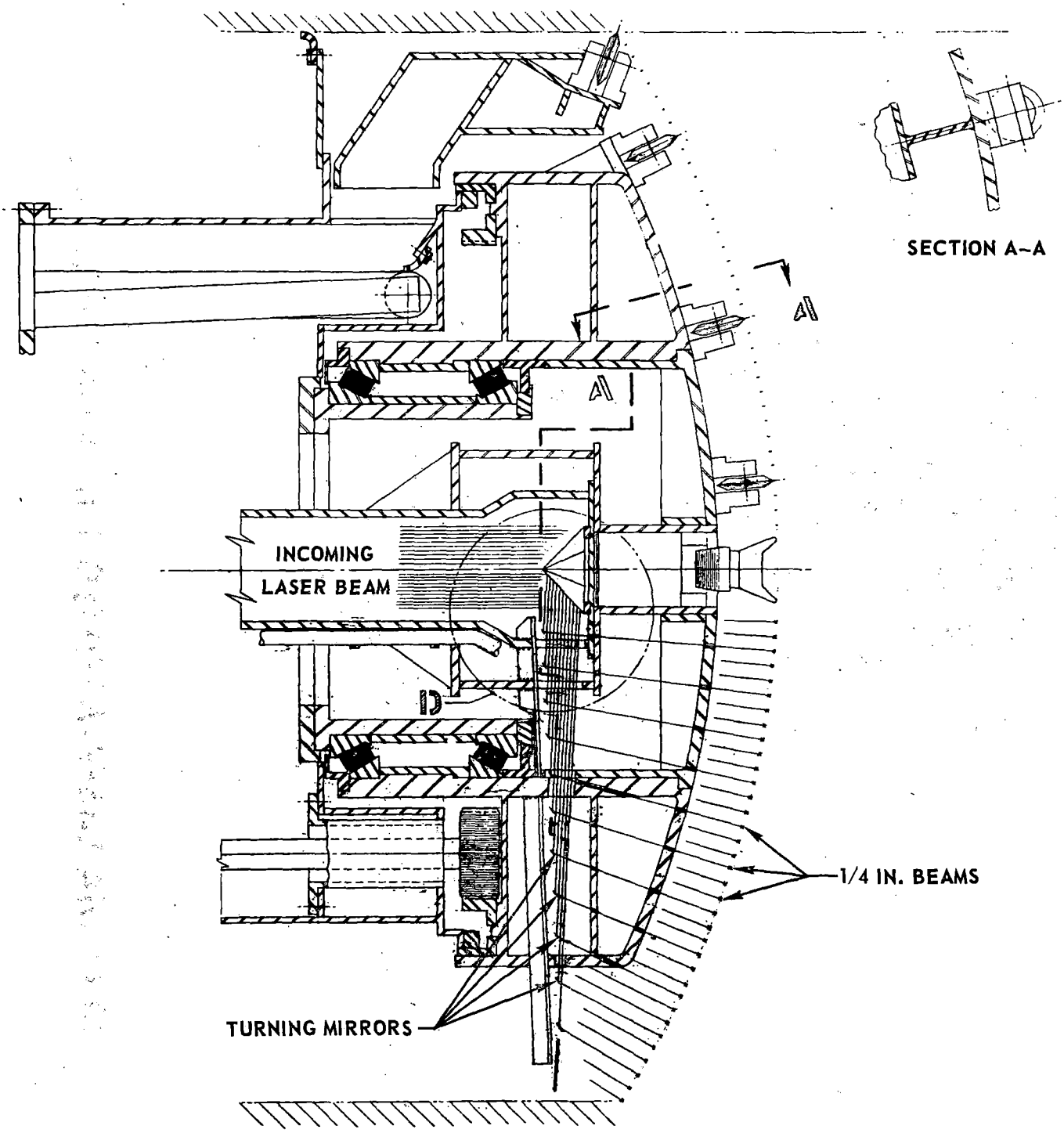

FIGURE 90 DISPERSAL SYSTEM IN THE HEAD OF A TUNNELER WITH A HOLLOW CENTRAL SHAFT

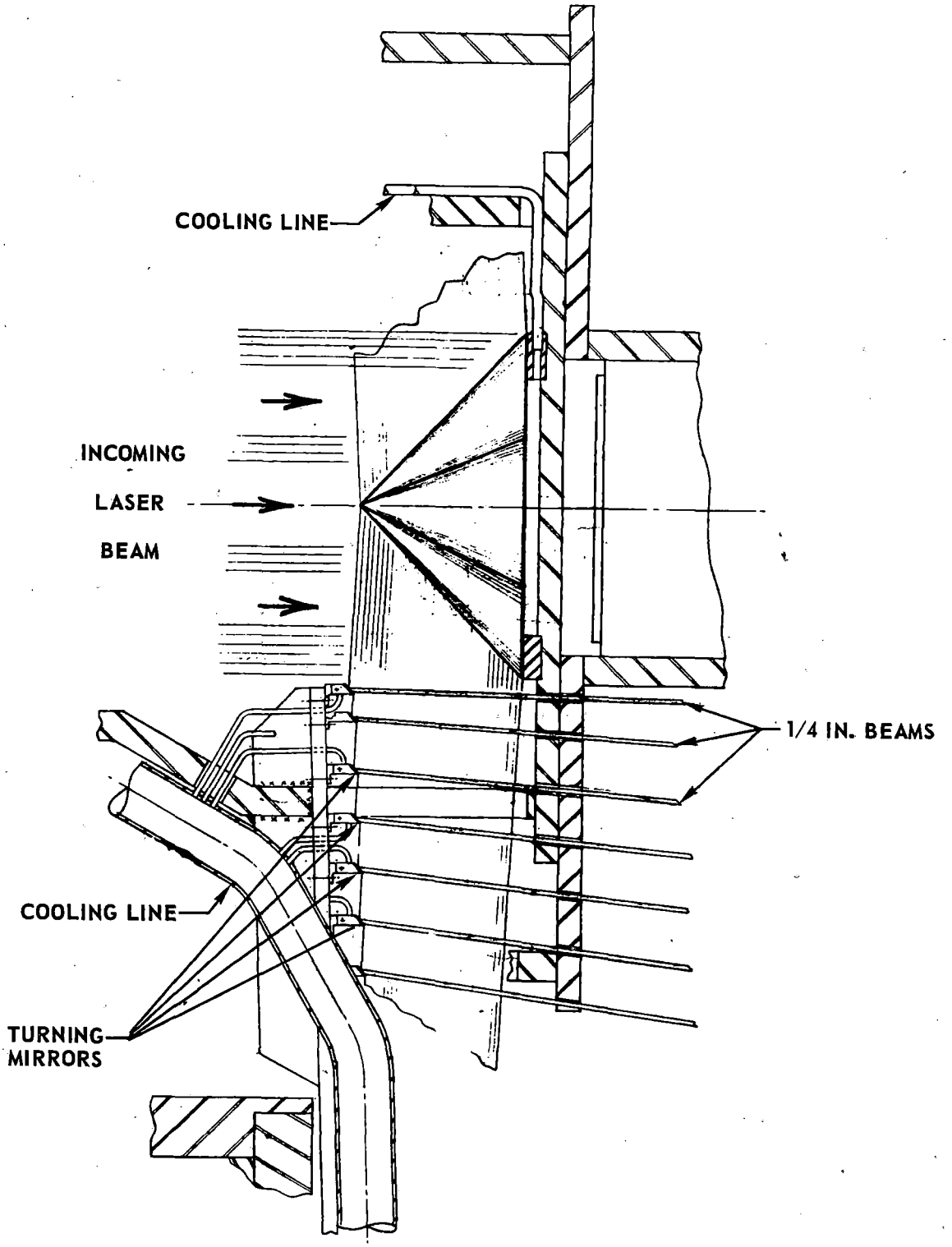

FIGURE 91 ENLARGED VIEW OF CENTRAL MIRROR

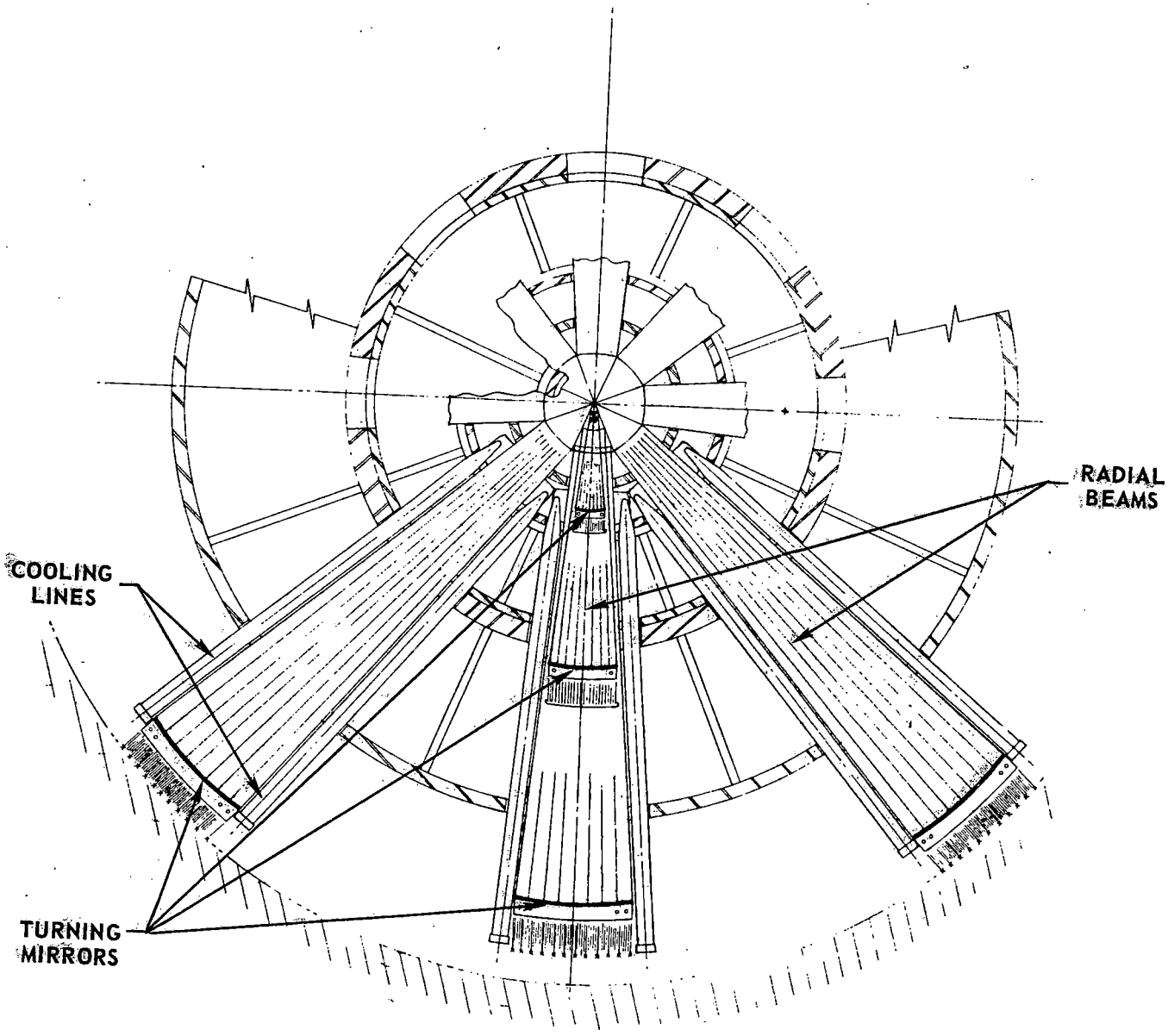

FIGURE 92 SECTIONAL END VIEW OF BORING MACHINE HEAD

The central mirror is divided into eight equal facets, giving each facet a central angle (in a plan view projected into a plane perpendicular to the boring machine longitudinal axis) of 45 degrees. The reflected energy from each of these eight facets is directed into beams which intersect the turning mirrors, which mirrors are designed to fit into sectors with a central angle of 11 degrees. The geometry of this situation is shown for a single turning mirror in Fig. 93.

This figure illustrates the beam spreading effect which reduces the power density impinging on the tunnel face to about 33% of that in the incoming beam. The power density in the incoming beam is 290 watts/cm^2, and thus is about 87 watts/cm^2 on the rock. This is a good value to allow a high total energy input without rock melting (see Fig. 54). To keep the power density a constant (which it should be for equal energy deposited per foot of heated path at any radius on the face), the ratio of $R_i R_o$, defined in Fig. 93, should also be kept constant. Thus the energy from the center of the incoming beam goes to the center part of the tunneler, and the energy from the outer edge of the incoming beam goes to the outermost diameter.

Substantial economies in mirror costs can be achieved by accpeting less than a high-quality optical finish on these mirrors (both the central and circumferential turning mirrors). Mirrors of high optical quality have a surface roughness on the order of a single wavelength, and reflectances on the order of 99% (Ref. 20). Normally such surfaces are highly polished to a tolerance which is checked by counting the interference fringes when compared to a standard surface. For a CO_2-N_2 laser, however, the reference standard for surface roughness (i.e., the wavelength) is an order of magnitude larger than for the visible spectrum. At a distance of 2 ft (typical distance from turning mirrors to the face), if a $\frac{1}{4}$-in. beam were scattered over an angle 10 times greater than that associated with a surface roughness of one quarter of a wavelength, 90% of the (initially uniform) beam would still fall within the $\frac{1}{4}$-in. targer width. Since commercial aluminum can be supplied with a surface roughness of 1/5 the wavelength of CO_2-N_2 laser radiation (Ref. 20), it appears reasonable to assume that simple carefully machined aluminum blanks would serve adequately for the 280 directing mirrors, and for the central mirror. Mirrors so constructed would then be easy to maintain, since water sprays and the abrasive action of a wiper (for periodic cleaning) would probably not be harmful.

Solid-Shaft Machines

The simplicity of the previous design depended on delivering the laser energy through a hollow central shaft. In some types of tunneling machines, such a design is impossible, since the center of the machine is necessarily filled with other systems. These machines then require a basically new approach to delivering the laser power to the rotating head. Dispersal of the laser beam can be accomplished in a similar manner to the above design once the beam has penetrated the head and

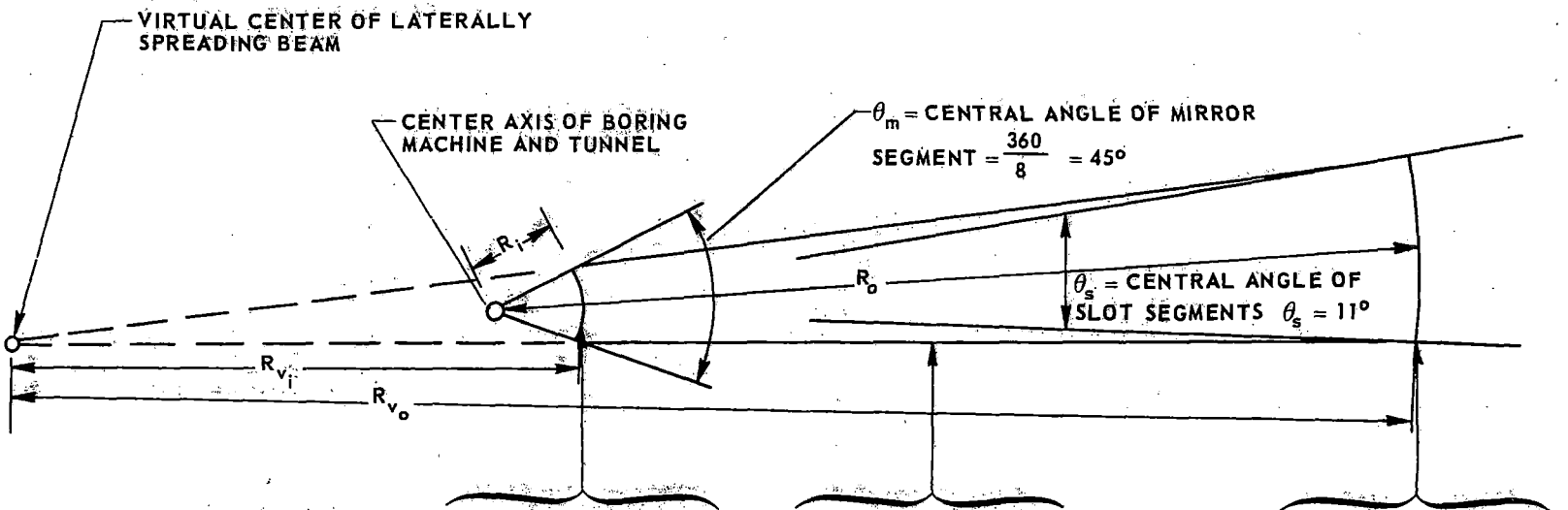

INCOMING CIRCUMFERENTIAL STRIP OF LASER BEAM IS =

a) INTERCEPTED BY CENTRAL MULTI-FACETED MIRROR AT THIS RADIUS, AND TURNED 90°,

b) DECREASES IN POWER DENSITY AS IT TRAVELS OUTWARD PER-PENDICULAR TO TUNNEL CENTRAL AXIS, AND

c) IS INTERCEPTED AT THIS RADIUS AND TURNED TO IMPINGE ON FACE AT A RIGHT ANGLE.

DECREASE IN POWER DENSITY DUE TO BEAM SPREADING FROM R_i TO R_o [ASSUMING CONSTANT BEAM WIDTH (DIMENSION PARALLEL TO TUNNELER CENTRAL AXIS) DURING LATERAL EXPANSION] IS GIVEN EXACTLY BY R_{v_i} / R_{v_o}

IGNORING DETAILED CURVATURE EFFECTS;

$$\frac{\text{POWER DENSITY AT } R_o}{\text{POWER DENSITY AT } R_i} = \frac{R_{v_i}}{R_{v_o}} \approx \frac{R_i\,\theta_m}{R_o\,\theta_m} = \frac{0.73^*(45)}{9.0^*(11)} = 0.332$$

* MAXIMUM VALUES OF R_i AND R_o FROM REFERENCE DESIGN

FIGURE 93 DISPERSAL OF LASER BEAM TO 11° SEGMENTS

is stationary with respect to the rotating frame of reference of the head. The eight radial sectors of laser output from the head can theoretically originate anywhere along the radius, leaving the central multifaced mirror with a large blank center. In the extreme, the eight beams could originate on the dircumference and be directed radially inward in a design inverse to that developed above.

The difficult problem associated with the use of a boring machine with a solid central shaft, then, is the problem of getting the beam through the back of the boring machine head, and into the rotating frame of reference. All schemes to achieve this can be put in two categories: (a) those schemes employing a passive aiming system, i.e., one in which the appropriate laser beam paths are achieved without mirror movement, and (b) those schemes employing an active aiming system, i.e., one in which the proper beam direction is achieved by a constant controlled aiming or movement of some or all of the mirrors. An active system has been devised and is described here to illustrate both the feasibility of an energy-dispersal system in a solid-shaft boring machine, and the use of an active system in general. No passive dispersal system for a machine with a solid shaft was determined. Such a system would require a very clever design, if it is feasible at all.

A drawing of a tunnel boring machine incorporating an active, noncentral beam dispersal system is shown in Fig. 94. The basic machine configuration is that of an Alkirk tunneler, built by the Lawrence Manufacturing Company. This machine has a long central drill shaft, which bores ahead of the rotating face, and then is swallowed by the face as it follows, thus obviating alternative uses of the volume along the machine longitudinal axis near the rotating head.

An enlarged view of an area near the head is shown in Fig. 95. The incoming laser beam is split into two separate beams at the rear of the boring machine. These beams can be located in any convenient circumferential position, 180 deg apart, as available space dictates. For the preliminary design considered here, the beams were located opposite each other and 45 deg from the vertical, but they are drawn in a rotated (vertical) position in Figs. 94 and 95 for clarity.

The two separate beams are directed past the main body of the tunnel boring machine to a pair of dispersing mirrors which divide each beam into four separate beams, as shown in Fig. 96. These four beams are aimed at turning mirrors which are equally spaced around the boring machine and which direct the eight separate beams toward the boring machine head. The two dispersing mirrors and the eight turning mirrors are mounted on a nonrotating mirror mounting plate, as shown in Fig. 96.

The eight beams from the turning mirrors are directed at an annular mirror formed in a conical section and mounted on the back of the rotating head (see Fig. 95).

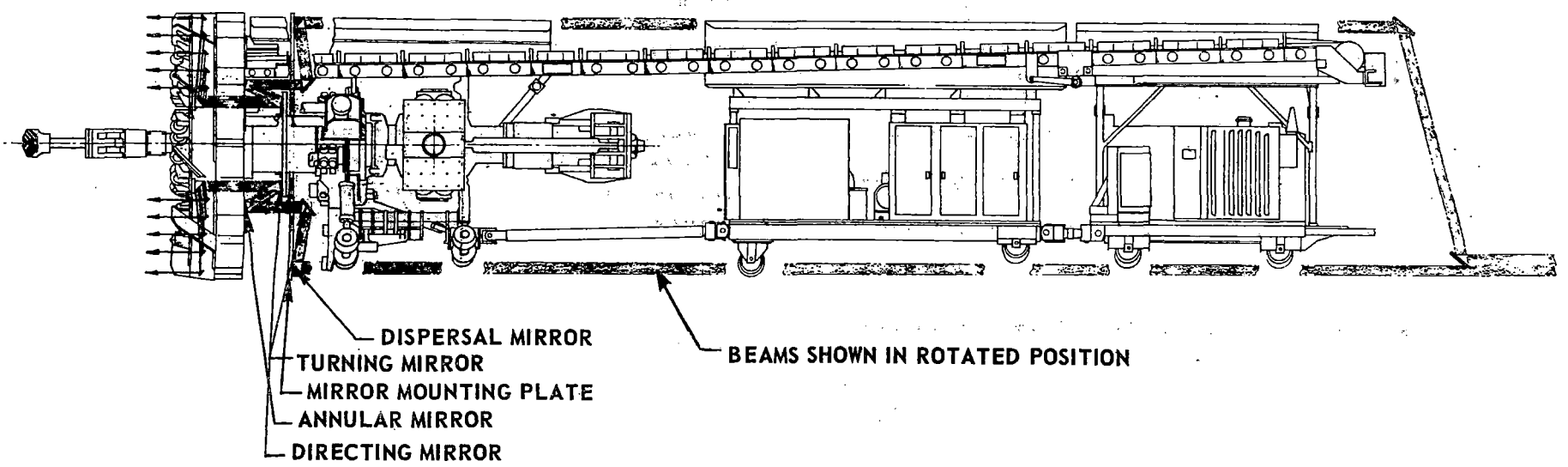

FIGURE 94 DISPERSAL SYSTEM APPLIED TO TUNNELER WITH SOLID CENTRAL SHAFT

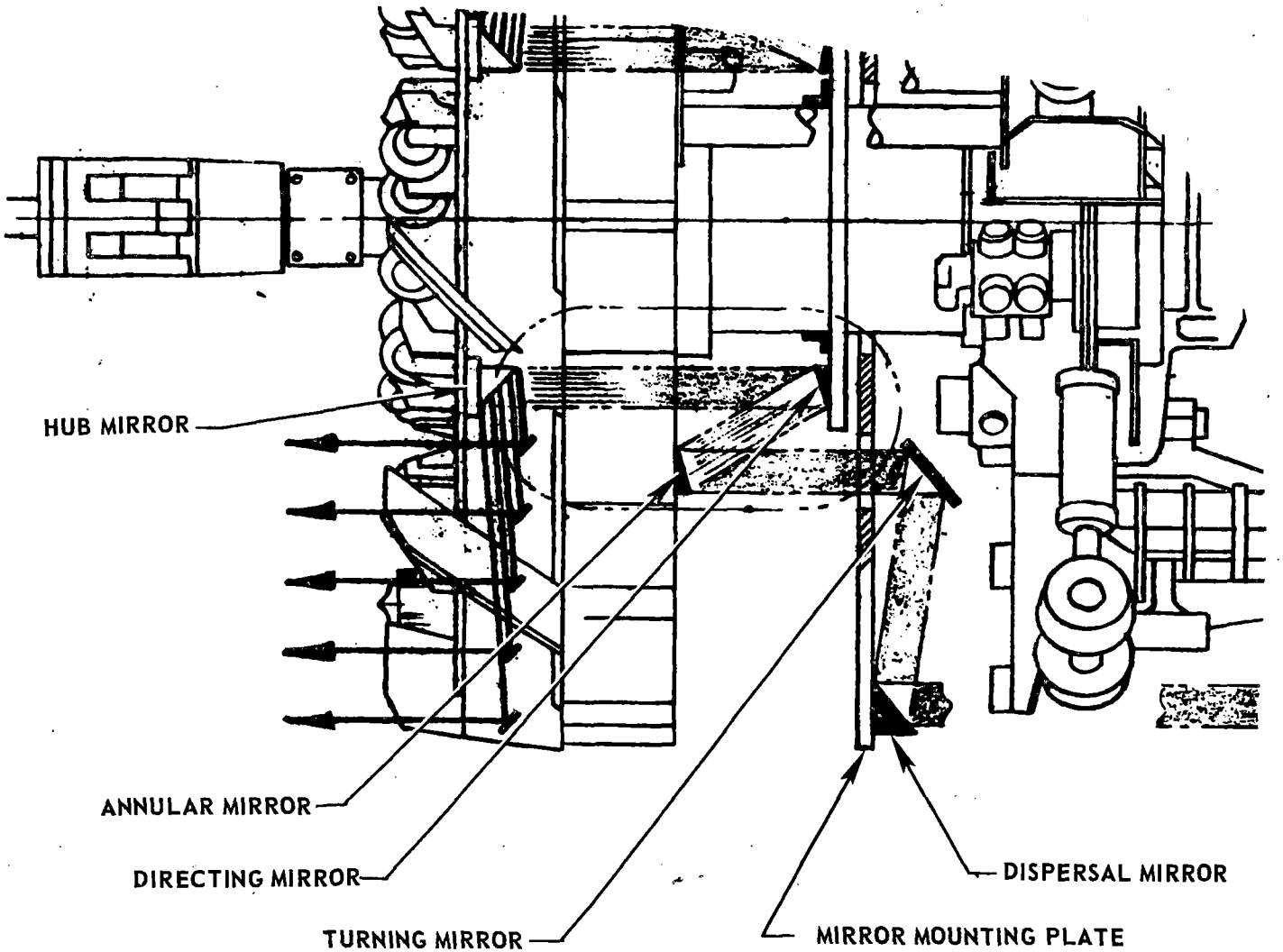

FIGURE 95 ENLARGED VIEW OF DISPERSAL AND TURNING MIRROR AREA

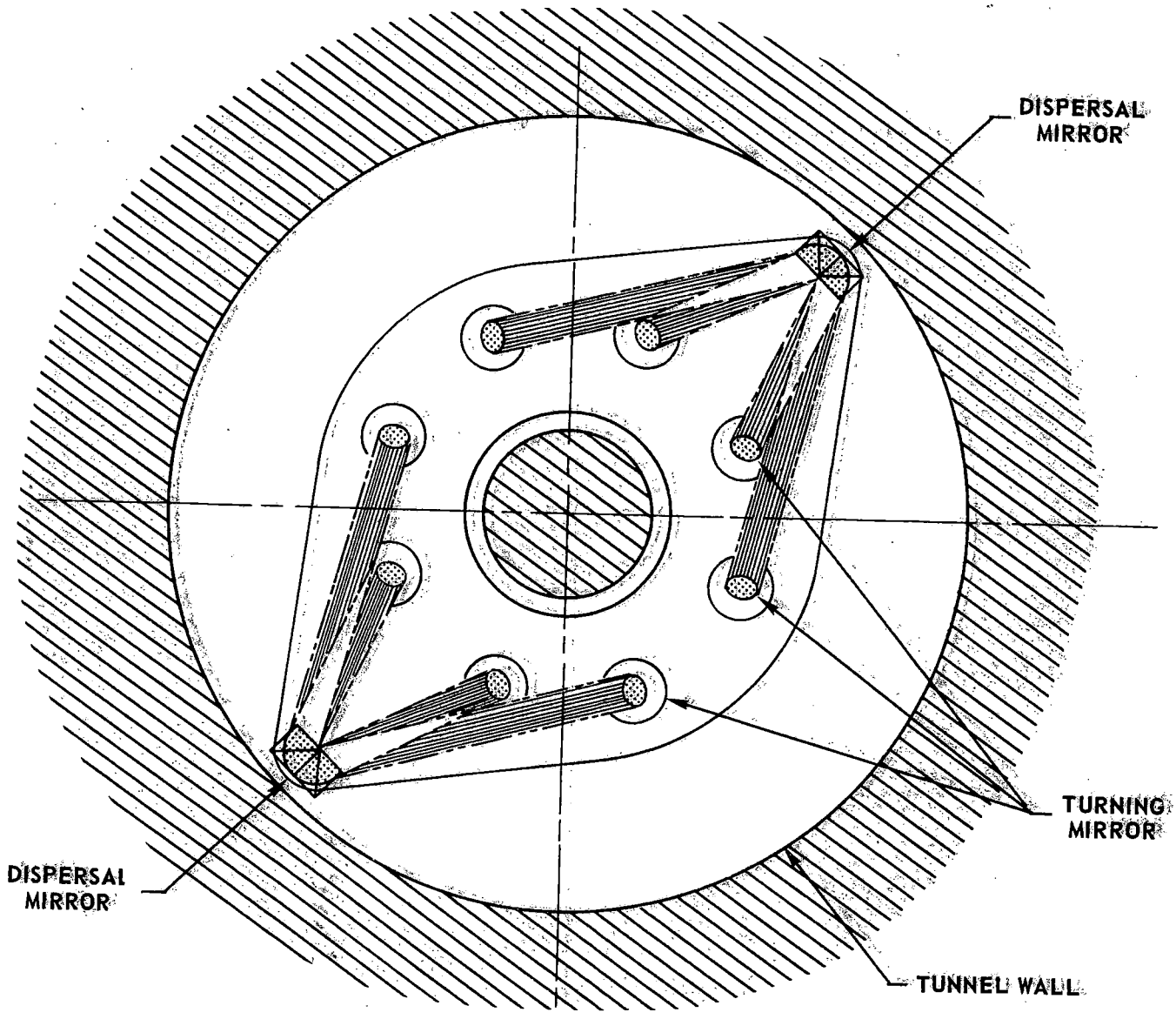

FIGURE 96 END VIEW OF MIRROR MOUNTING PLATE

The eight beams are fixed in their radial position, so the rotating annular mirror will always direct these beams toward a series of directing mirrors (see Fig. 95) from the same position. (If the location of other equipment on the boring machine would permit, it is conceivable that the dispersal mirrors could be mounted in such a way as to aim the eight beams directly toward the series of directing mirrors, without the intervening turning and annular mirrors.)

The directing mirrors are a series of movable plane mirror sections mounted on a rotating plate just in front of the nonrotating mirror mounting plate. These mirror sections are mounted in such a way that when driven by a follower sliding on a cam on the face of the mirror mounting plate, they will aim the eight nonrotating laser beams toward eight rotating target apertures in the rotating boring machine head. The beams then fall on dispersing hub mirrors, which are fixed to the rotating head, as shown in Fig. 95. A sequential diagram of some of these directing morror segments in five different positions is shown in Fig. 97. Although this diagram contains a number of simplifications, it appears that the complex aiming pattern required of these mirrors can be accomplished with 16 simply pivoted segments.

Once the boring machine head is penetrated by eight separate beams, whose positions are fixed with respect to the rotating frame of reference in the head, the dispersal of these beams can be accomplished in a manner similar to that employed in the boring machine with a hollow central shaft. The fact that the eight beams are coming from changing directions can be handled by carefully shaping the main dispersal mirrors within the head so as to properly average out the laser power supplied to each of the final turning mirrors.

Transmission System

Compared to nearly any other source of heat applicable to heat-assisted tunnel boring, laser systems are very large, cumbersome collections of equipment. The size of a 10-kw laser system, based on the only laser capable of such powers as recently as September 1968 (Ref. 21), is shown in Fig. 98. Significant improvements in laser size have been made since that time, and significant improvements in large sizes are predicted for the near future. Nevertheless, it is apparent that the size of a complete laser system producing more than 450 kw of optical energy may prove too large to include in the tunnel with the boring machine, and some means must be devised for transmitting the laser energy to the boring machine.

Three basic configurations of laser systems for heat-assisted tunnel boring may be identified. These categories, which are illustrated in Fig. 99, are an in-situ laser system, in which all of the laser system is in the tunnel; a split laser system, in which a component of the laser system, such as the cavity, is in the tunnel; and a remote laser system, in which all of the laser system is on the surface. Although

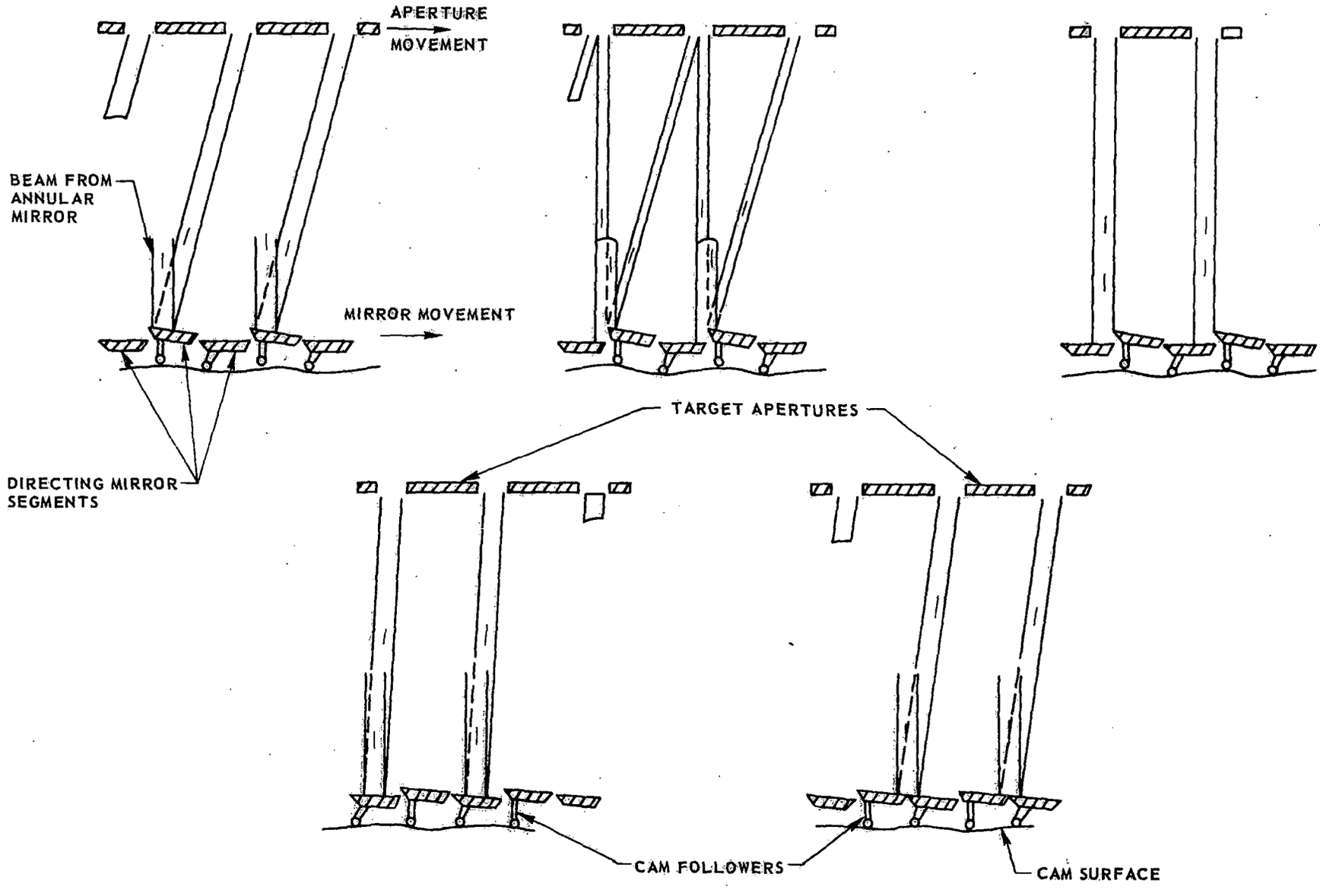

FIGURE 97 SEQUENTIAL DIAGRAM OF THE POSITIONS OF THE SEGMENTING DIRECTING MIRRORS

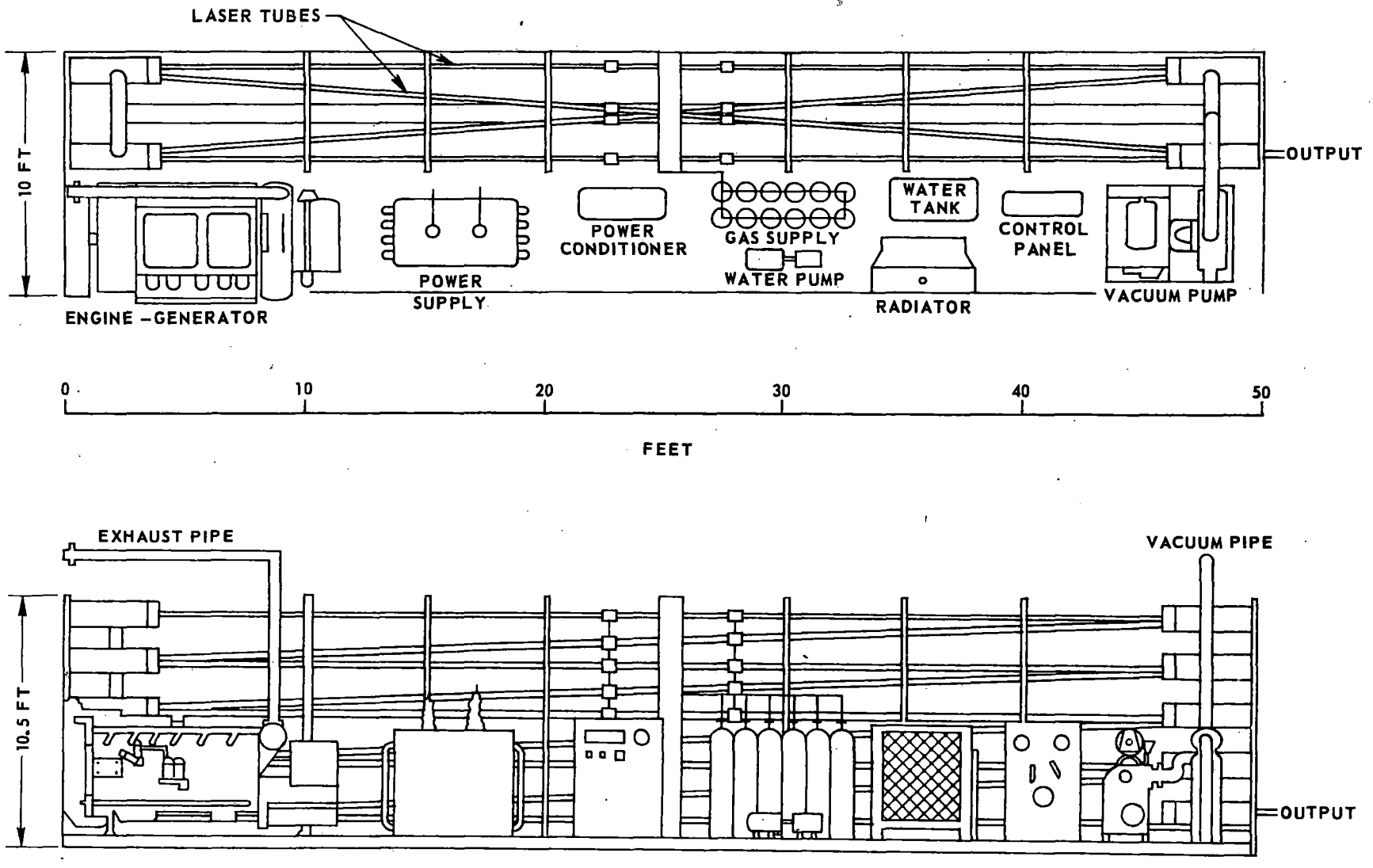

FIGURE 98 10 kw FOLDED LASER SYSTEM

IN-TUNNEL LASER SYSTEM

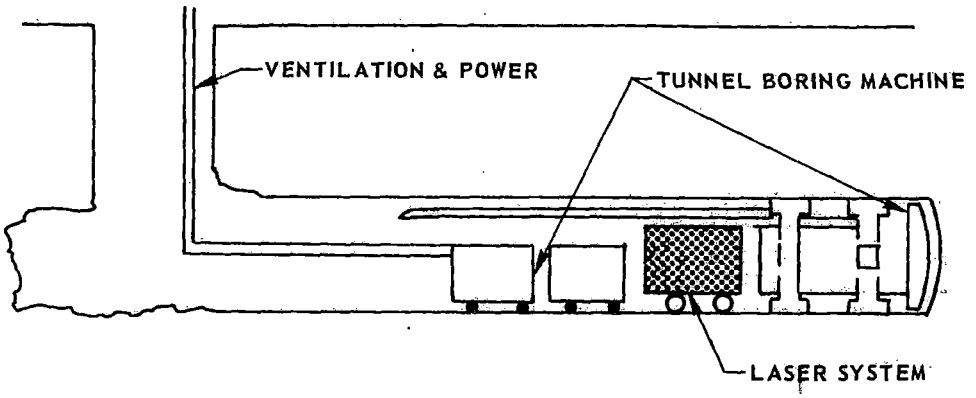

SPLIT LASER SYSTEM

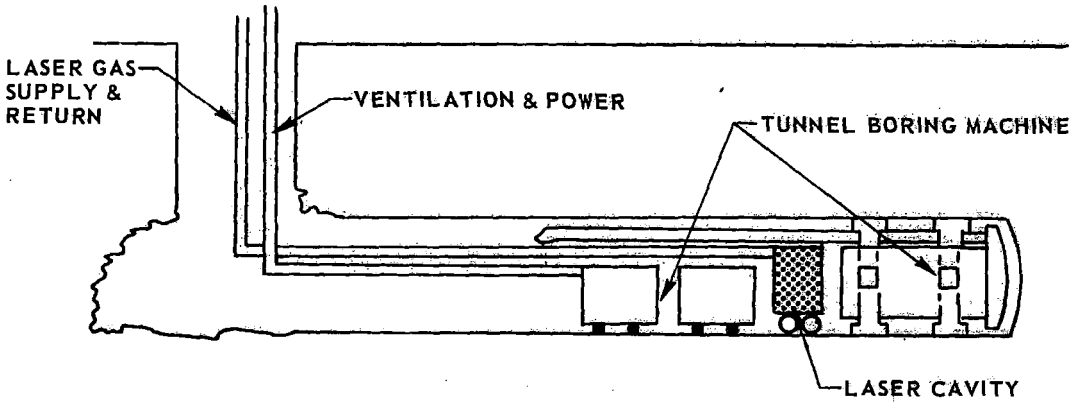

REMOTE LASER SYSTEM

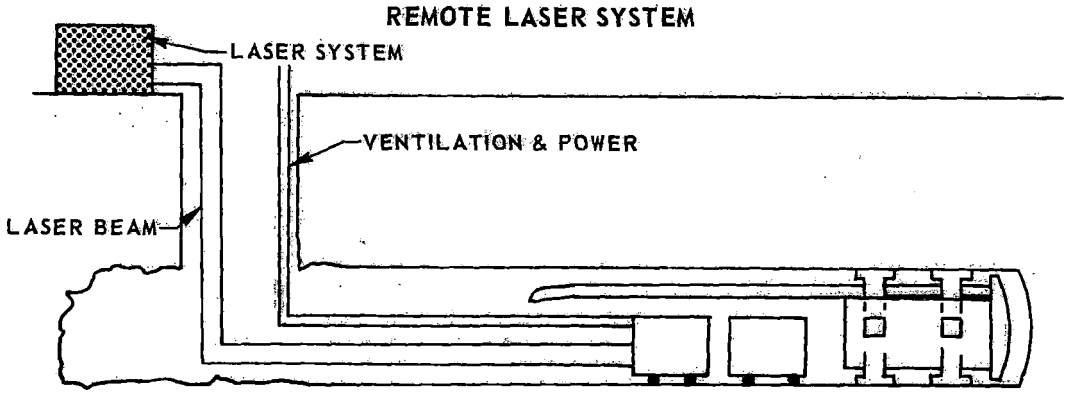

FIGURE 99 BASIC LASER ENERGY TRANSMISSION SYSTEM

the split laser system might be attractive if the cavity could be made small enough, only the remote laser system has been considered in depth. The remote system is the only system requiring detailed specification of a long optical transmission system, and also is the only presently practical system.

Protective Tube

The transmission of a laser beam through a tunnel will have to be in some protected duct or tube because of the presence of a damp atmosphere within the tunnel and the presence of unprotected workmen within the tunnel. The laser beam power losses in air at atmospheric pressure are shown as a function of humidity in Fig. 100, which is based on the calculated and experimental data in Ref. 22. As these data show, an increase in relative humidity from 10% to 80% causes a tripling of the energy absorbed. Transmission through a three-mile tunnel at 10% humidity would result in the loss of approximately 30% of the initial energy, but the same transmission could be essentially impossible at 100% humidity. Therefore, a transmission tube, constantly replenished with dry air, is imperative.

A protective tube for the laser beam is also required in the interest of safety. The maximum permissible exposure level of continuous, far infrared radiation recommended by the AEC, for either the skin or the eye, is 1 w/cm^2 (Appendix C). In order to reduce the beam intensity in the tunnel to 1 w/cm^2, a beam 22 ft square would be required. Therefore, it is necessary to enclose the beam and prevent any exposure.

The inclusion of the laser beam in an air-confining duct introduces a new complication, the "thermal blooming" effect (Ref. 23). If an optical beam is transmitted through a slightly absorbing medium such as air, there will be a slight temperature rise in the medium. In a fluid medium, this temperature rise will lead to convective currents. These currents will cause a net velocity of the medium across the beam which will, in turn, produce a temperature gradient across the beam. Since the index of refraction in a medium is a function of the temperature, a temperature gradient causes a gradient in the index of refraction which will have an optical effect on the beam similar to that of a lens. The net result will be a deflection and defocusing of the laser beam. Figure 101 contains tracings of the burn spots produced at different convective wind velocities in an experimental study of thermal blooming (Ref. 23). The original burn spot for each of these figures, in the absence of any thermal blooming, would have been a circle centered on the cross. It is clear that beam deflections into the wind on the order of the spot are possible, and that the deflections decrease as the convective velocity is increased. The effect of increased wind velocity is one of heat removal; the absorbed energy is removed before a significant temperature gradient can be established. It is also clear that such blooming could cause considerable problems in the design of

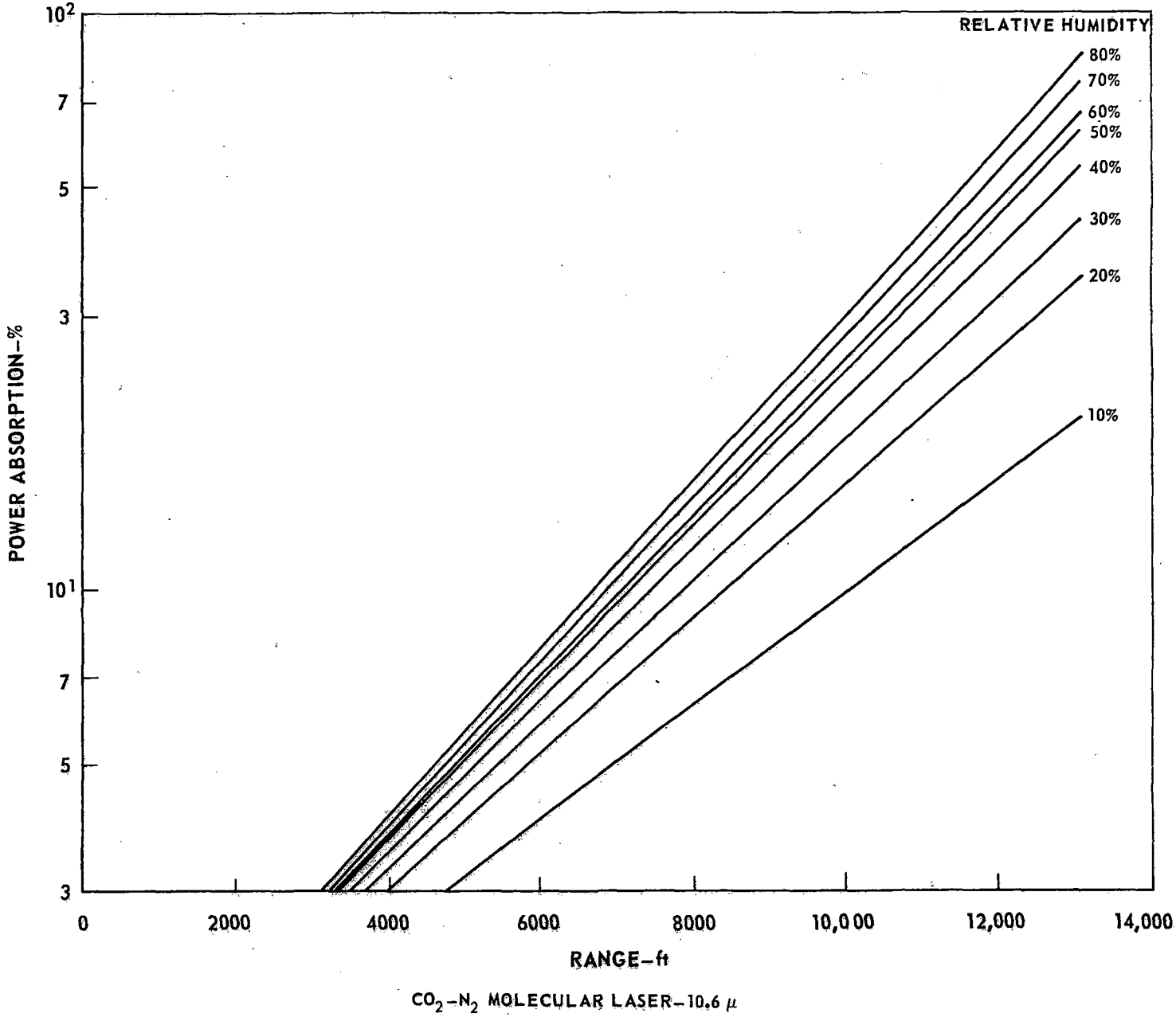

FIGURE 100 LASER BEAM LOSSES IN AIR

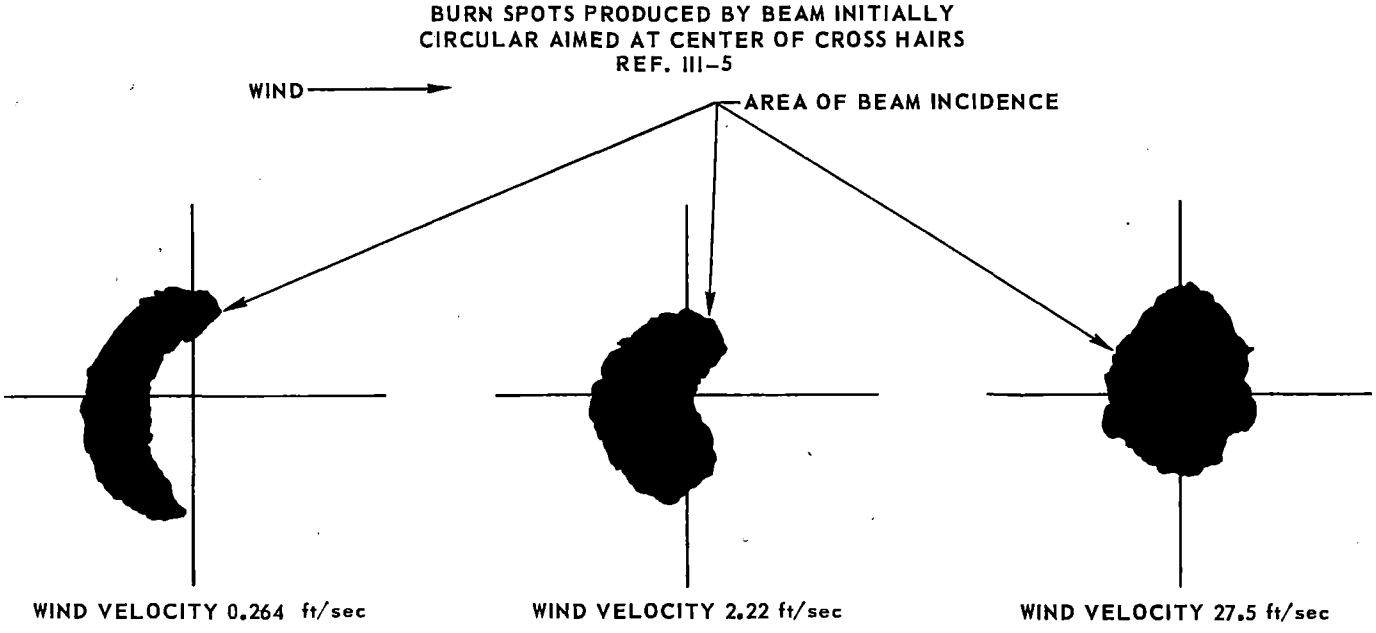

FIGURE 101 THERMAL BLOOMING EFFECTS

the laser transmission duct if preventive measures are not taken. However, it has been assumed for this study that the creation of turbulent airflow in the protective duct will be sufficient to prevent the formation of a temperature gradient.

Turning Stations

Since not all tunnels will be straight, it is necessary to provide a means of transmitting the laser beam around a bend. Such turning can be accomplished with a set of mirrors placed in a protective junction box. A schematic diagram of such a turning station is shown in Fig. 102 . The junction box would be constructed with special fittings to couple with the protective laser beam tube. These fittings would be free to turn through small angles so that the box could be used in different installations and at different attitudes. The aiming of the mirrors could be coupled to the fittings to provide for automatic alignments. The turning mirrors are mounted at different elevations to prevent internal obscuration when used for small turning angles.

The mirrors used in the turning stations will require water cooling if the laser beam has a power density significantly greater than 100 w/cm^2. Water-cooled mirrors in many different configurations have been built and tested as part of the various laser research efforts under way throughout the country. A drawing of a mirror typical of this technology is shown in Fig. 103. This mirror has been built in sizes of nearly 3 ft in diameter, and no unusual problems in either construction or use have been encountered.

Refocusing Stations

No allowance has been made for losses due to diffraction, and no effort has been made to analyze the diffraction associated with all of the mirrors and guidance apertures in the transmission system. However, without careful design, diffraction losses can be very serious in systems of this nature. Losses as high as 70% due to diffraction, and associated problems, have been encountered in some experimental systems. Therefore, some provision must be made to minimize the losses due to diffraction.

The technique for minimizing diffraction losses in the transmission system conceived for this study involves focusing. The maximum mirror size assumed to be practical for this study and the maximum protective tube diameter assumed to be feasible in the tunnel are both 30 in. The theoretical minimum spot size for a 10.6 μ beam focused from a 30-in. aperture on a target 1000 ft away is on the order of one centimeter. It is reasonable to assume that the energy outside of the target centimeter, either from diffraction or misalignment, would be retained within the 30-in. duct.

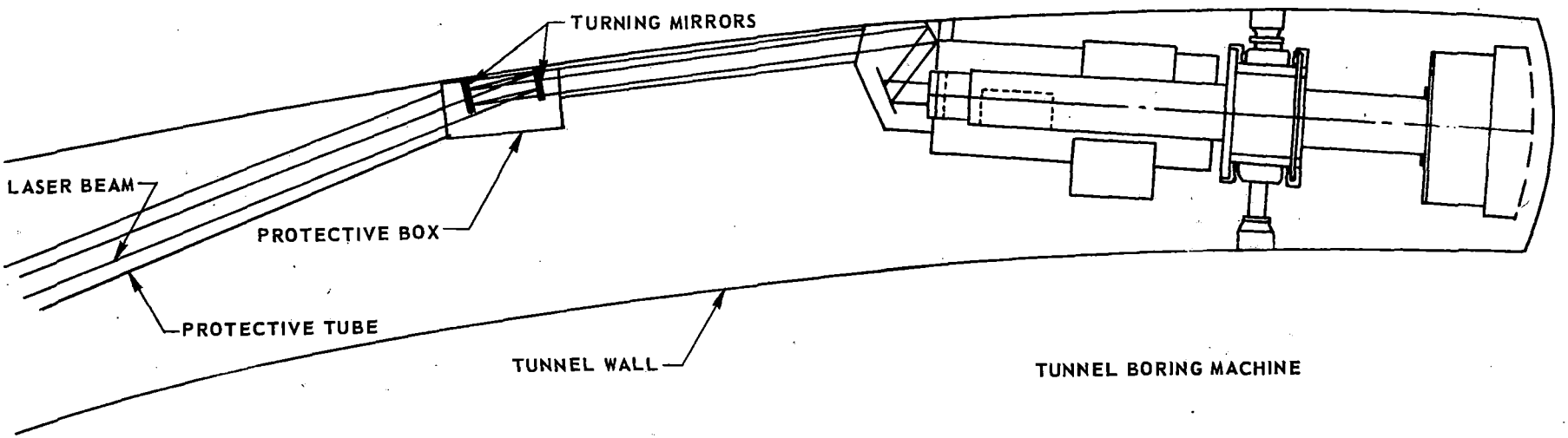

FIGURE 102 LASER BEAM TURNING STATION

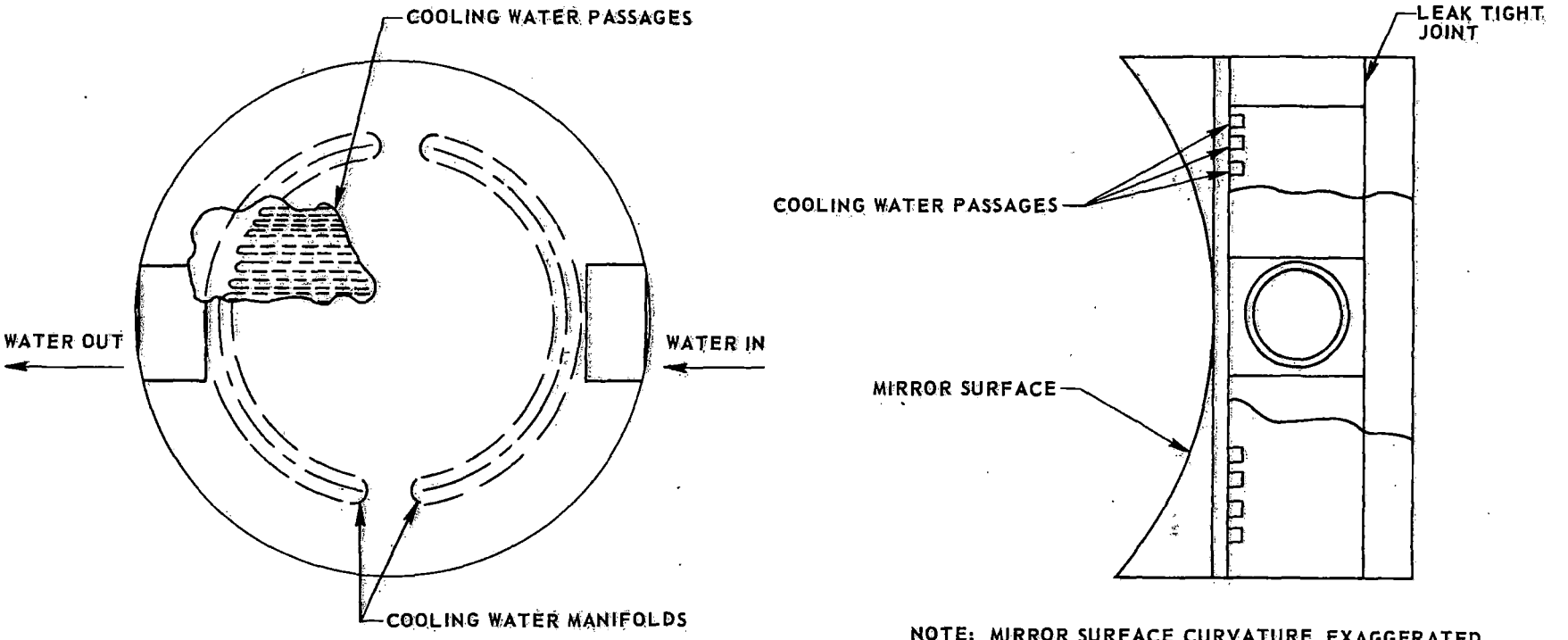

FIGURE 103 TYPICAL WATER-COOLED MIRROR

Simple spherical mirrors cannot easily be ground to radii significantly greater than 200 m. Therefore, focal lengths greater than 100 m are not practical for simple refocusing stations, and many stations would have to be used for tunnels whose lengths are frequently measured in miles. Multiple mirror stations are impractical because of the cost and absorption losses encountered. However, refocusing stations with long effective focal length can be constructed with mirrors of short radius, through the use of a Cassegrain mirror system. This system is simply a reversed Cassegrain telescope. A schematic diagram of such a system is shown in Fig. 104. Both a collecting telescope and a focusing Cassegrain mirror system are shown, but the collecting telescope could be eliminated if the incoming beam were focused to a small enough spot .

The main problem associated with a Cassegrain mirror system is the obscuration loss associated with the blind central spot. For normal laser operation this spot would be in the position of greatest energy density, at least in the first station. However, the dimensions of the laser cavity are so large compared to the wavelength that many modes of resonance are possible. One mode which is easy to induce in a laser is the TEM^*_{01} mode in which the peak energy intensity is distributed in a torus with a blank spot in the center. A plot of the power density profile of a laser in the TEM^*_{01} and the more basic TEM_{00} mode is shown in Fig. 105. If a laser operating in the TEM^*_{01} mode is assumed, the obscuration losses should be minimized.

Beam Profile

One problem which has not been considered in the discussion of the transmission system or the boring machine head is that of the beam power density profile. Electromagnetic waves are not generally propagated as uniform plane waves, but have a profile which is determined by the distance from the last aperture and the illumination function of that aperture, i.e., essentially the profile of the beam incident on that aperture. The typical profile encountered is gaussian, but other profiles are also common. In general, the presence of nonuniform beams will not have a great effect on any of the previous discussion, as long as the beam is not widely dispersed. However, some method of forming and measuring a uniform beam will be required ahead of the beam dispersal system in the boring machine head.

System Performance

A complete system, capable of transmitting far infrared radiation from a remote surface laser system to a tunnel boring machine, penetrating the boring machine head, and dispersing the radiation over the tunnel face has been described. Clearly some degradation of the initial laser beam in terms of total beam power and beam profile will be encountered in such a system. The degradation of the

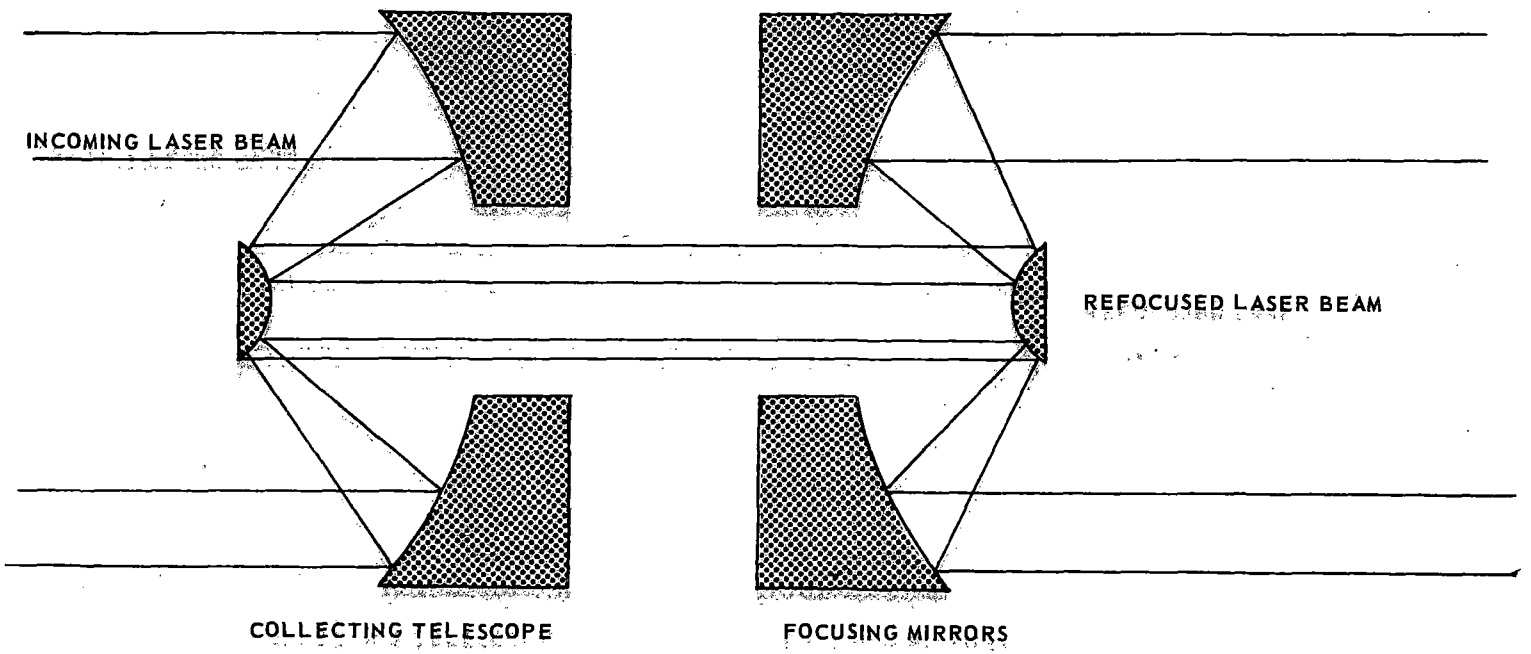

FIGURE 104 CASSEGRAIN MIRROR REFOCUSING STATION

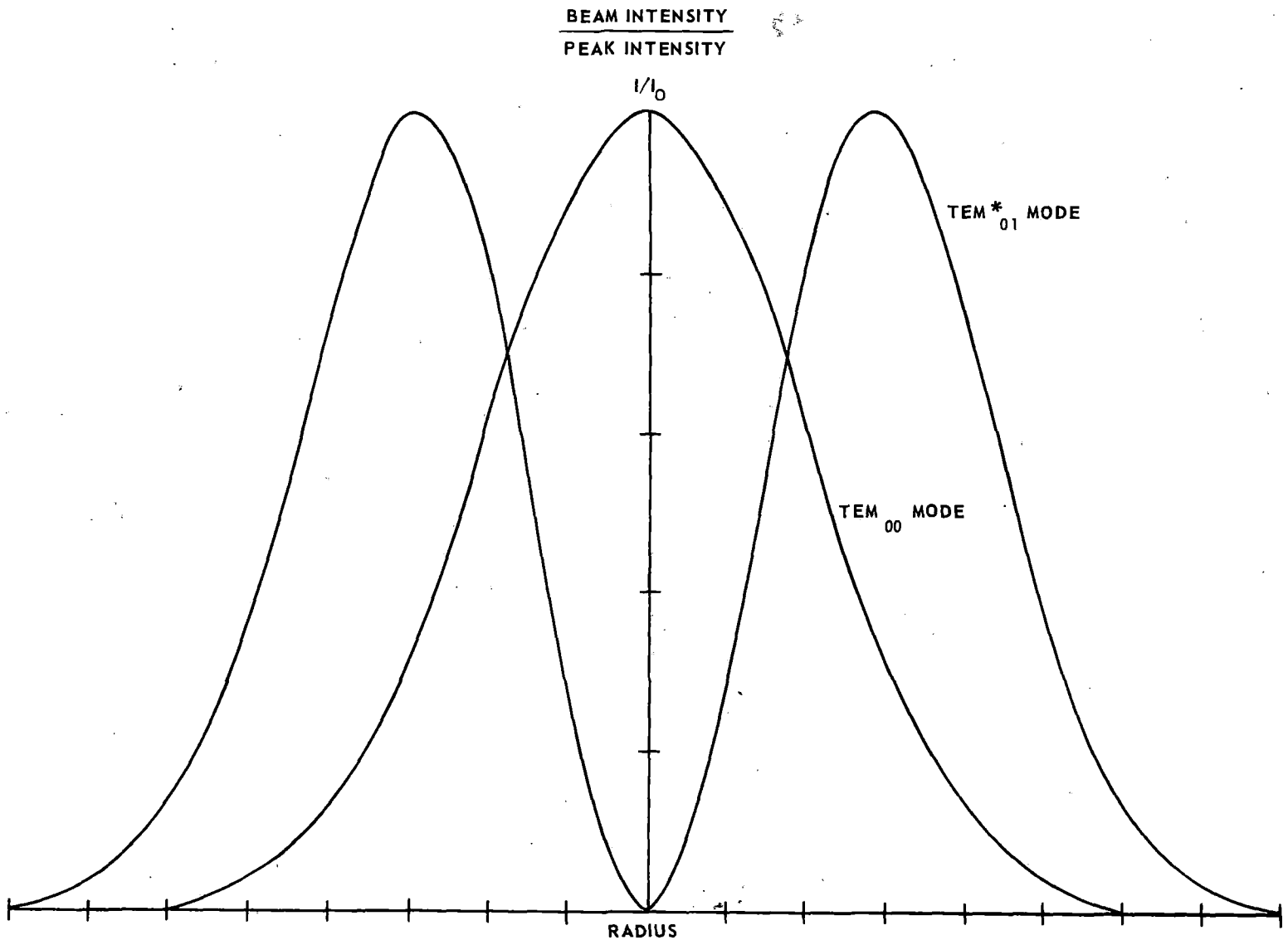

FIGURE 105 BEAM PROFILES OF TWO CAVITY RESONANT MODES

initial beam profile has been discussed above in as much detail as considered within the scope of this study, but the energy losses have not been discussed and could be a serious deterrent to the whole concept. These losses include extinction due to dust or water in the space between the machine head and the tunnel face, mirror losses in the machine head, mirror losses in the transmission system, and atmospheric absorption in the transmission system.

Beam Losses at the Face

Dust

The space between the boring machine head and the tunnel face is filled with a significant amount of dust and rock fragments. A quick view into an opening in an operating boring machine, boring in hard limestone, gave the impression that the dust was opaque to the visible spectrum within a few inches, but that large rock fragments were sufficiently infrequent to be ignored (Ref. 24). Standard texts such as Refs. 25 and 26 indicate that the dust generated in similar environments runs between 30 and 70 mppcf (million particles per cubic foot) and that the particle diameters range between 0.5 and 3.0 μ. This range of dust size and density occurs in rock drilling in the open air, and is equivalent to what would be an explosive mixture of coal dust. For comparison, the concentrations in a dust storm cover nearly the same range.

The extinction coefficient (see Fig. 106 for definition) of a dust whose particles are of the same order or smaller than the wavelength is described by the Mie scattering theory (Ref. 27). This theory is based on an assumption of uniform spherical particles. The theory has been reduced to a computational program (Refs. 28 and 29) and was available for this study, but a complex index of refraction, including a coefficient of refraction and absorption, is required as input. Reasonable experimental methods of determining the complex index have been developed only recently, e.g., Ref. 30, and values are not available for igneous minerals other than quartz and cristobalite. Therefore, extinction coefficients for quartz and cristobalite were determined at various concentrations, and assumed to be representative of all hard rock dusts. The results of these calculations are shown in Fig. 106, where the total extinction is shown as a function of the distance between the boring machine head and the tunnel face, for various dust compositions. It appears that, although the dust is opaque to the visible spectrum, no energy loss more serious than 6% will result in the far infrared.

The importance of differences in the dust particle size (or, conversely, in the wavelength of the radiation) is clearly demonstrated in Fig. 107. This figure contains the results of extinction calculations for dusts of various particle sizes. As the particle size approaches the wavelength, scattering becomes more important than absorption, and dusts which were relatively clear at 3.0 μ become completely

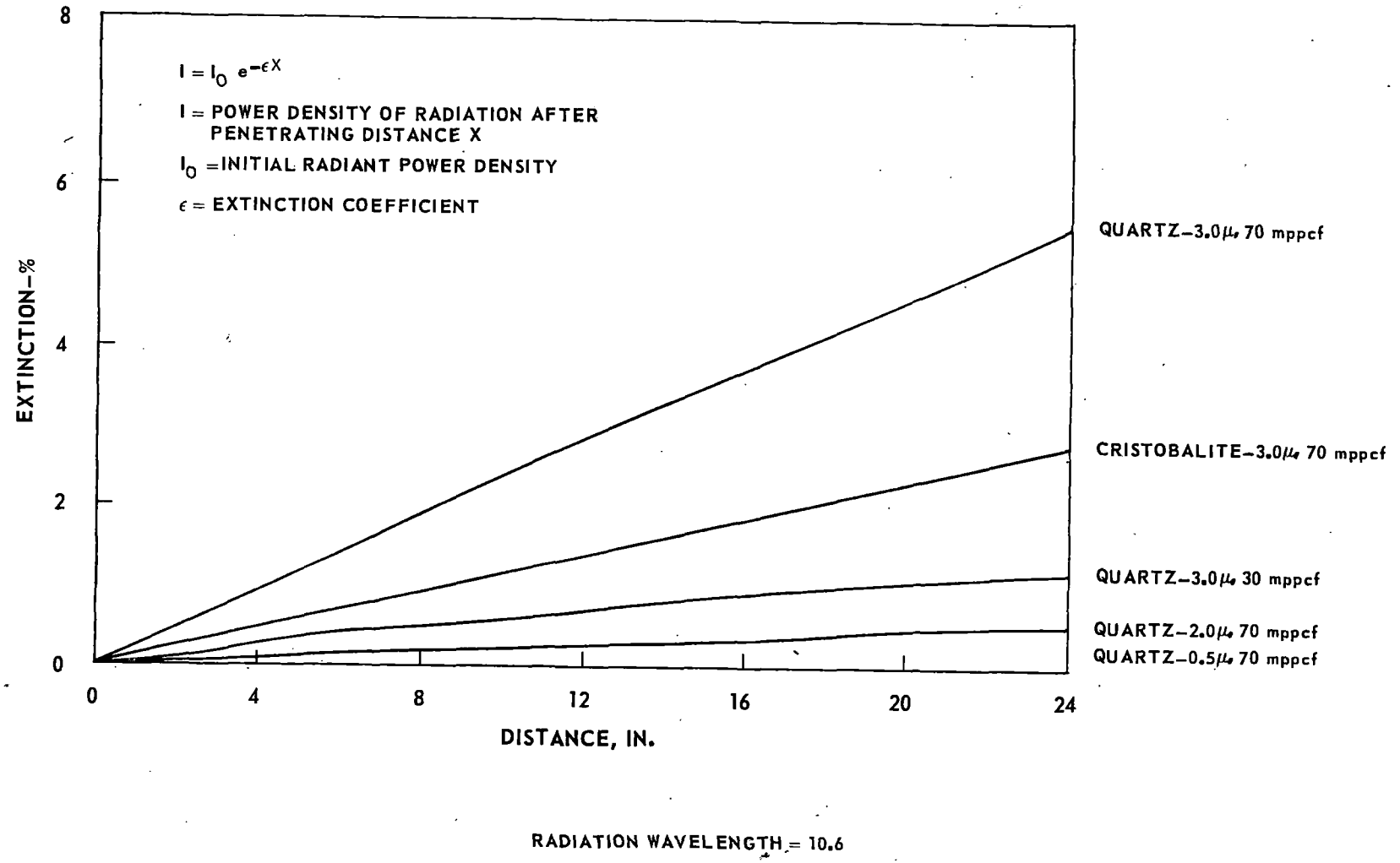

FIGURE 106 ENERGY LOSSES DUE TO DUST BETWEEN TUNNELER HEAD AND TUNNEL FACE

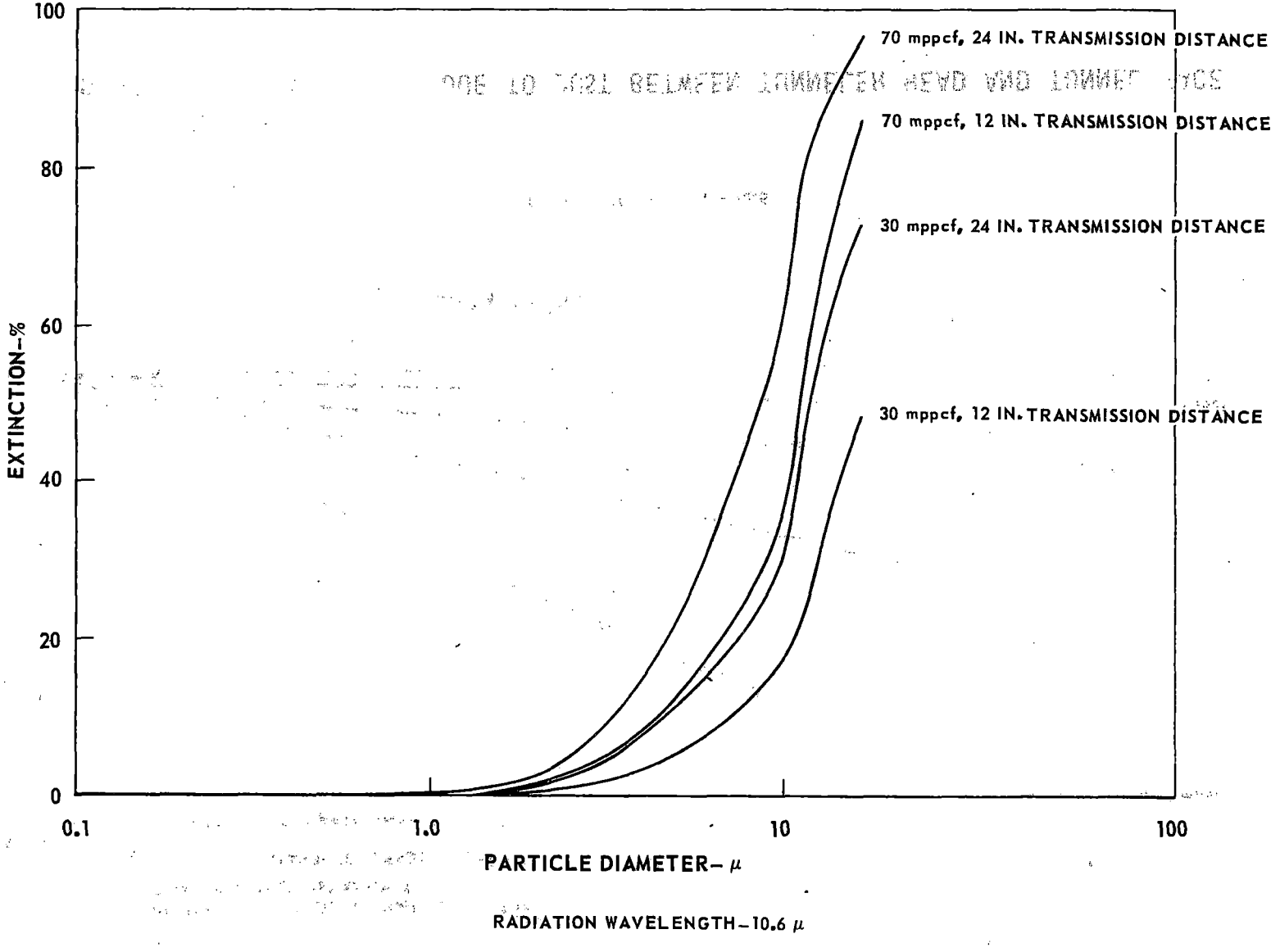

FIGURE 107 IMPORTANCE OF DUST PARTICLE SIZE

opaque by 20 μ. The accuracy of the reported range of dust particle size is therefore very important, and should probably be confirmed experimentally.

Water on the Tunnel Face

Water has a high absorptivity for 10.6-μ radiation. In the liquid state, the absorption coefficient for use in the Lambert law is 0.107 μ^{-1} (Ref. 20). That is, a 10-micron layer of water would be capable of absorbing 63% of the impinging radiation. Therefore, the possibility of water on the tunnel face must be considered, and an estimate of the losses due to this water must be made.

A convenient model for estimating the effects of water on the tunnel face is that of a falling film. An analytical model of a film of water flowing down a smooth surface under the influence of gravity is fairly common and shows a dependence on the viscosity and the flow capacity of the source. The velocity and film thickness predicted by this model for 100 F water are shown in Fig. 108. This model is probably not accurate at flow rates of more than 50 lb/ft-sec (i.e., 50 lb/sec of water flowing down past a one-foot-long horizontal boundary or wall), which results in an average flow velocity of 100 ft/sec and a film thickness of 0.1 in. Higher flow rates would probably not contain the fully developed laminar boundary layer which is required for the model. However, a higher rate of water flow than 50 lb/ft-sec would not be considered since this much water would probably create sufficient problems in the tunnel to cause temporary shutdown of the boring machine. The falling film model is also not accurate at very low flow rates, assumed to be less than 0.05 lb/ft-sec in this study, because at very small film thicknesses surface tension effects become significant. Lower flow rates may be considered equivalent to a wet rock.

The absorption of a 10.6-μ beam with an energy density of 100 w/cm^2 by a film of water with the thickness of the theoretical falling film is shown in Fig. 109. The fraction of the incident energy absorbed is essentially 100% for all films over 0.001 in. thick, i.e., for all films with a flow rate greater than 5 x 5 10^{-5} lb/ft-sec. This can be interpreted to mean that any reasonably sized film including the stationary film on a wet rock is capable of absorbing all of the incident energy as long as the film remains. However, an energy flux of 100 w/cm^2 is sufficient to evaporate very thin films. The length a falling film would flow at its natural velocity before it is evaporated is also shown in Fig. 109. It appears that a film thin enough to be considered essentailly stationary, i.e., that on a wet rock, could rapidly be boiled away, but as flow rate and, consequently, film thickness increase the impinging energy will be totally absorbed in the water. In summary, the stationary film on a wet surface seems tolerable, but a flowing film on the tunnel face is catastrophic without some alternate drying technique.

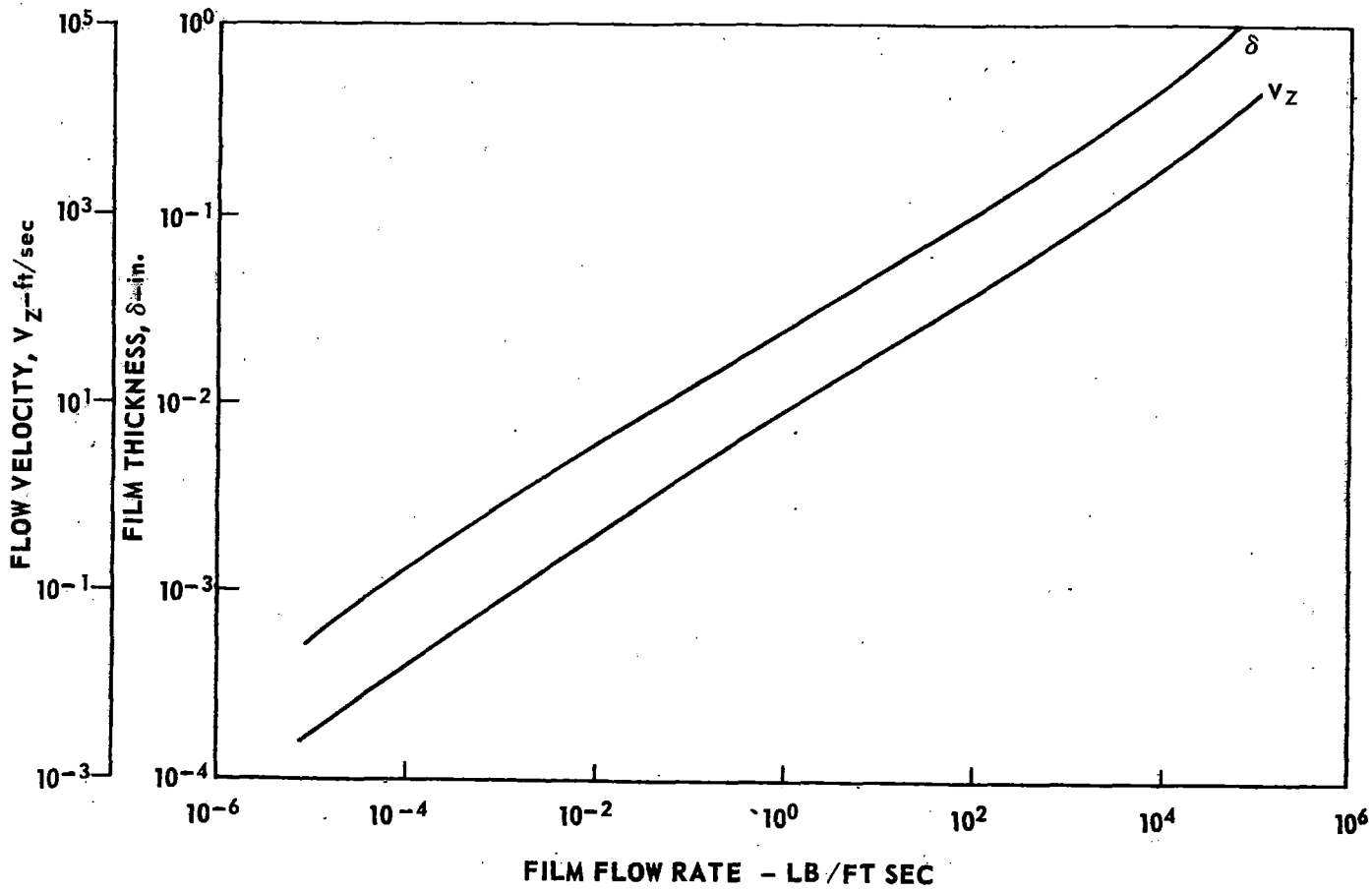

FIGURE 108 THEORETICAL FALLING FILM CHARACTERISTICS

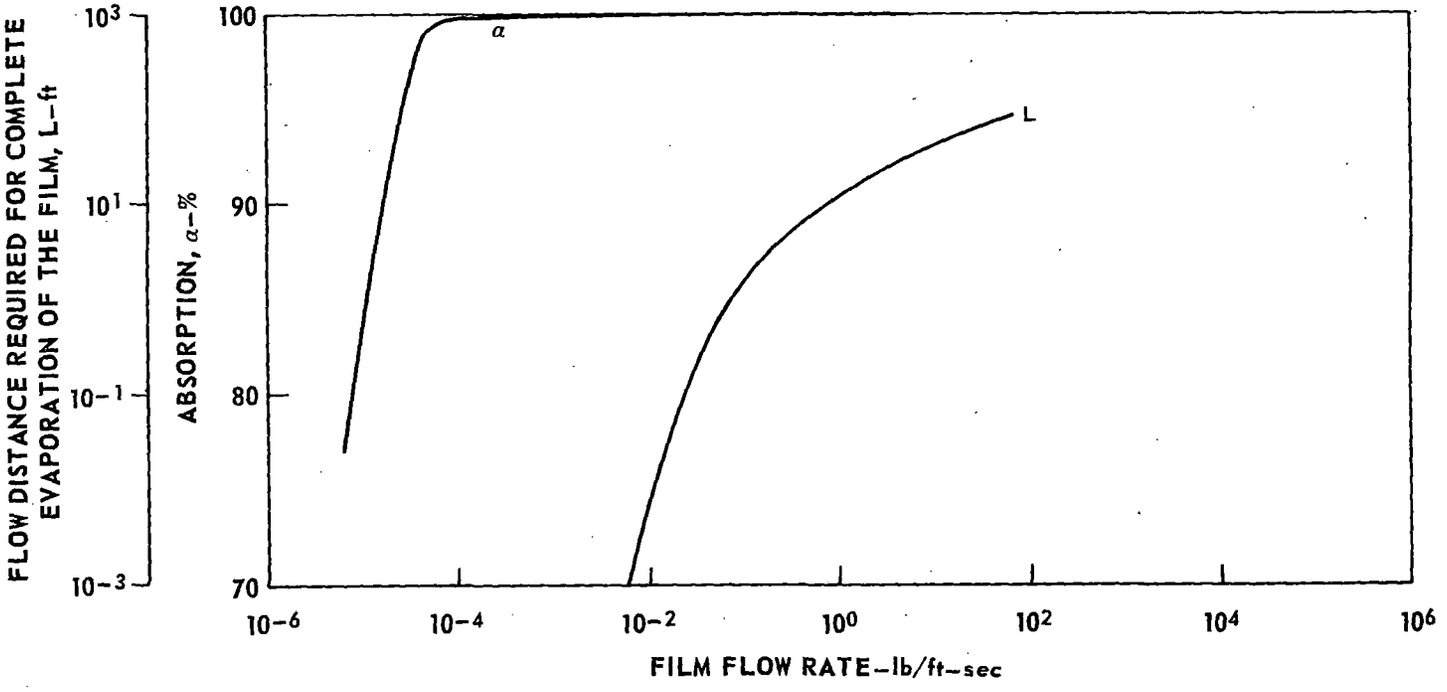

FIGURE 109 EFFECT OF WATER FILM ON LASER BEAM TRANSMISSION

Mirror Losses

Within reasonable angles of incidence, extremely efficient mirrors can be obtained for 10.6-μ radiation. Figure 110 (from Ref. 31) contains both experimen and theoretical values of reflectance for a good coated mirror. Values of nearly 99% are shown for angles of incidence up to 45 deg. Certain copper-based mirrors have shown small-angle reflectance of more than 99.26% (Ref. 31). Therefore, it appears reasonable to assume that mirrors with 98% reflectance can be obtained for the transmission system.

The mirrors in the dispersal system within the boring machine head will not have the same high reflectances. These mirrors have been assumed to be machined surfaces on a simple material such as aluminum or stainless steel. Such mirrors will be considerably cheaper, and adequate in terms of accuracy, but the reflectar will decrease. A reflectance of 90% for each mirror in the head has been assumed for this study.

Overall Transmission Losses

The overall transmission losses will consist of absorption by the atmosphere the losses in the mirrors of the refocusing and turning stations, and the mirror losses in the dispersal systems. The atmospheric absorption losses have already been shown, Fig. 100, and the various mirror losses are described above. Extinct can probably be ignored since it is one percent or less for all but the heaviest dusts. Water absorption losses are either nonexistent or catastrophic, so some means will have to be provided to ensure that they are nonexistent. The resultin overall transmission efficiency is shown in Fig. 111 as a function of mirror spac and tunnel length. The mirror stations were assumed to be two-mirror rather than four-mirror stations.

The separate effect of each of the component losses is shown in Fig. 111. first 19% loss is caused by the two inefficient mirrors in the head (the calculat were made for a hollow-central-shaft machine). All of the subsequent losses out 10,000-ft tunnel length shown on the curve for 10,000-ft mirror spacing are due t atmospheric absorption in the laser duct. The effects of multiple mirror station are shown on the remaining curves. In general, overall transmission efficiencies of 60 to 80% appear to be feasible, but the number of turning and refocusing stat should be kept to a minimum.

Cost Estimates

A principal reason for the conceptural design studies described above is to provide a basis for equipment cost estimates. Despite the preliminary nature of

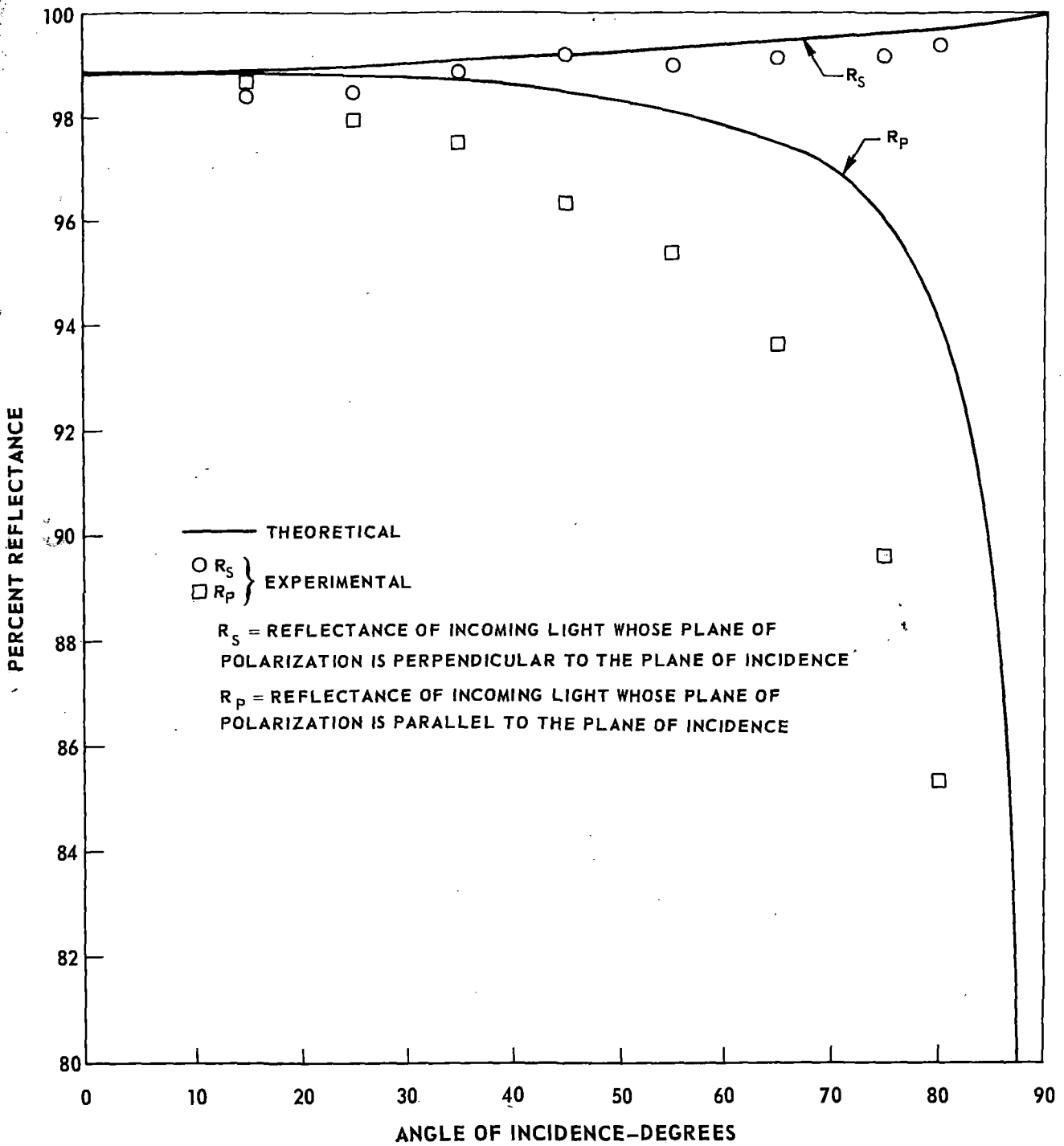

REF. 31

FIGURE 110 REFLECTION OF PLANE POLARIZED 10.6μ RADIATION FROM CHROMIUM–GOLD WITH MAGNESIUM FLUORIDE OVERCOAT

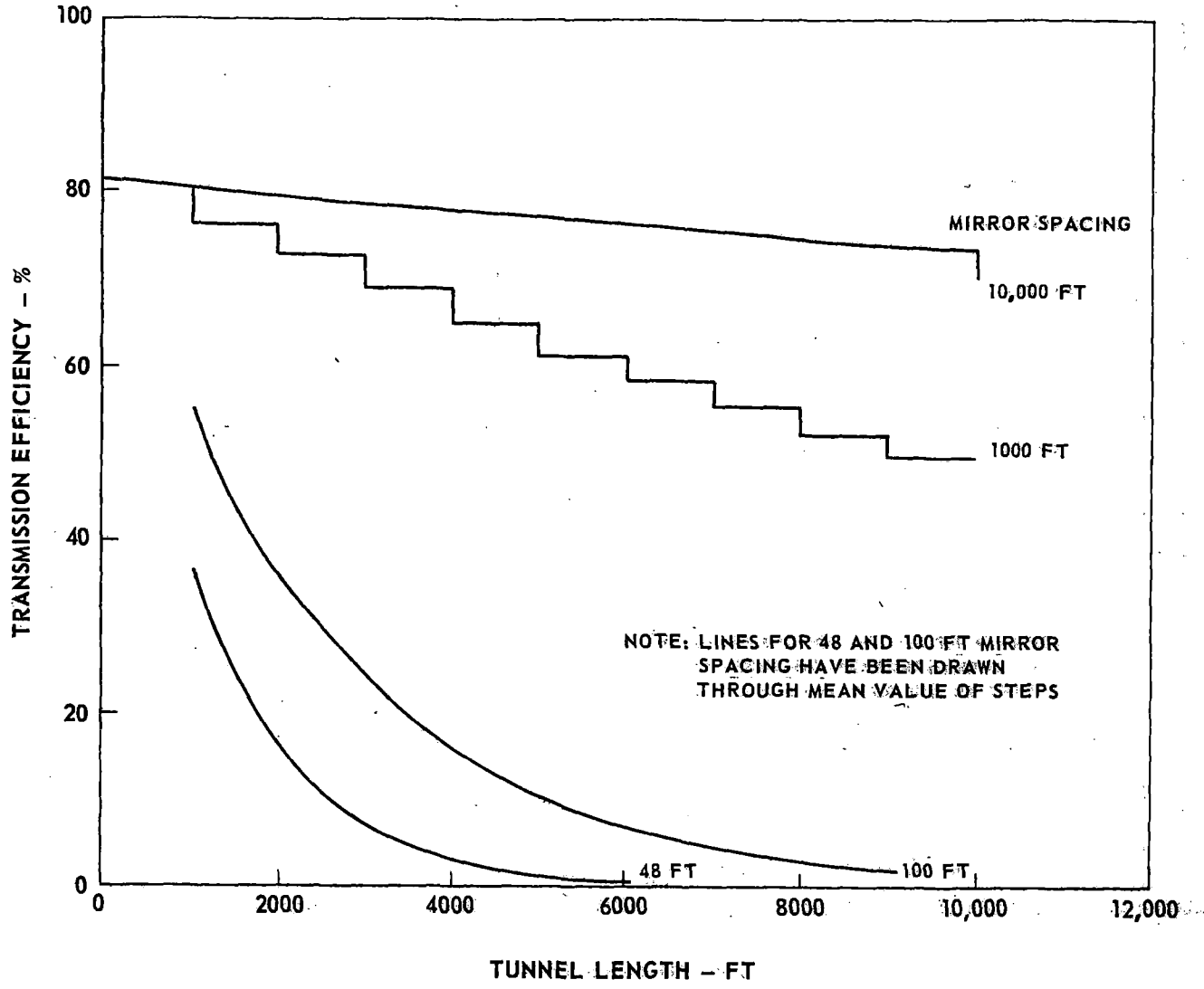

FIGURE 111 ATMOSPHERIC AND MIRROR ABSORPTION OF LASER BEAM

conceptual designs, cost estimates sufficiently accurate for a preliminary economic evaluation of the various heat-assist concepts being considered can be made. The major areas of cost analysis considered in this phase of the study are the laser cost, the mirror costs, the cost of peripheral equipment such as the blower and dehumidifiers, and the combined system costs. Also, the system cost sensitivity to key parameters was determined.

Laser Cost

Estimates of conventional CO_2-N_2-He electric-discharge lasers have been made at UARL for a variety of power output levels. The cost trend indicated from these estimates is shown in Fig. 112, along with advertised costs of some commercial units for comparison. The curve indicates that laser output has relatively little effect on specific cost ($/kw) above a size of about 10 kw, and for larger systems the specific cost remains close to $10,000/kw.

A component breakdown of these costs is shown in Table 8. The laser for which this cost estimate was made has a design power level that has never actually been achieved by an electric discharge laser. The estimate therefore includes a substantial amount of conjecture, as it is based on an extrapolation of present-day laser technology. However, the estimate agrees well with exploratory cost estimates of other electric discharge laser systems being explored at UARL, and also fits in with the trend indicated by the commercial units in Fig. 112. One reason for this apparent consensus is that the power supply represents such a large fraction (~50%) of the overall system cost.

However, there is hope for reducing the cost levels indicated here. Many of the systems whose cost is reflected in Fig. 112 have lightweight or low volume restrictions on the powerplant. In a tunneling application, these restrictions could be relaxed somewhat. Also, there is some hope of achieving operating efficiencies (laser power output to electric power) in the neighborhood of 20%. A recent UARL cost estimate for a 100-kw output electric-discharge CO_2 laser design, based on a somewhat more advanced design than many of those indicated in Fig. 112, and assuming a 15% laser efficiency, was roughly $8000/kw. With further increases in laser efficiency and attention to inexpensive subsystems, cost of $5000/kw may be achieved for large industrial-type laser systems.

Mirror Costs

Estimates have been obtained for the costs of the mirrors required in the boring machine head and in the transmission system. The cost of the simple machined mirrors in the boring machine head have been estimated to be so small, on the order of $40 per mirror, compared to the cost of other equipment in the overall system that detailed accurate cost estimates were not deemed necessary. The costs of a mirror typical of the transmission mirrors has been estimated to be $3550 on the basis of the specifications shown in Table 9.

Peripheral Equipment Costs

The cost of the peripheral equipment, such as the piping for the duct (assumed to be similar to aliminum irrigation pipe), the blower, the dehumidifier, the mirror

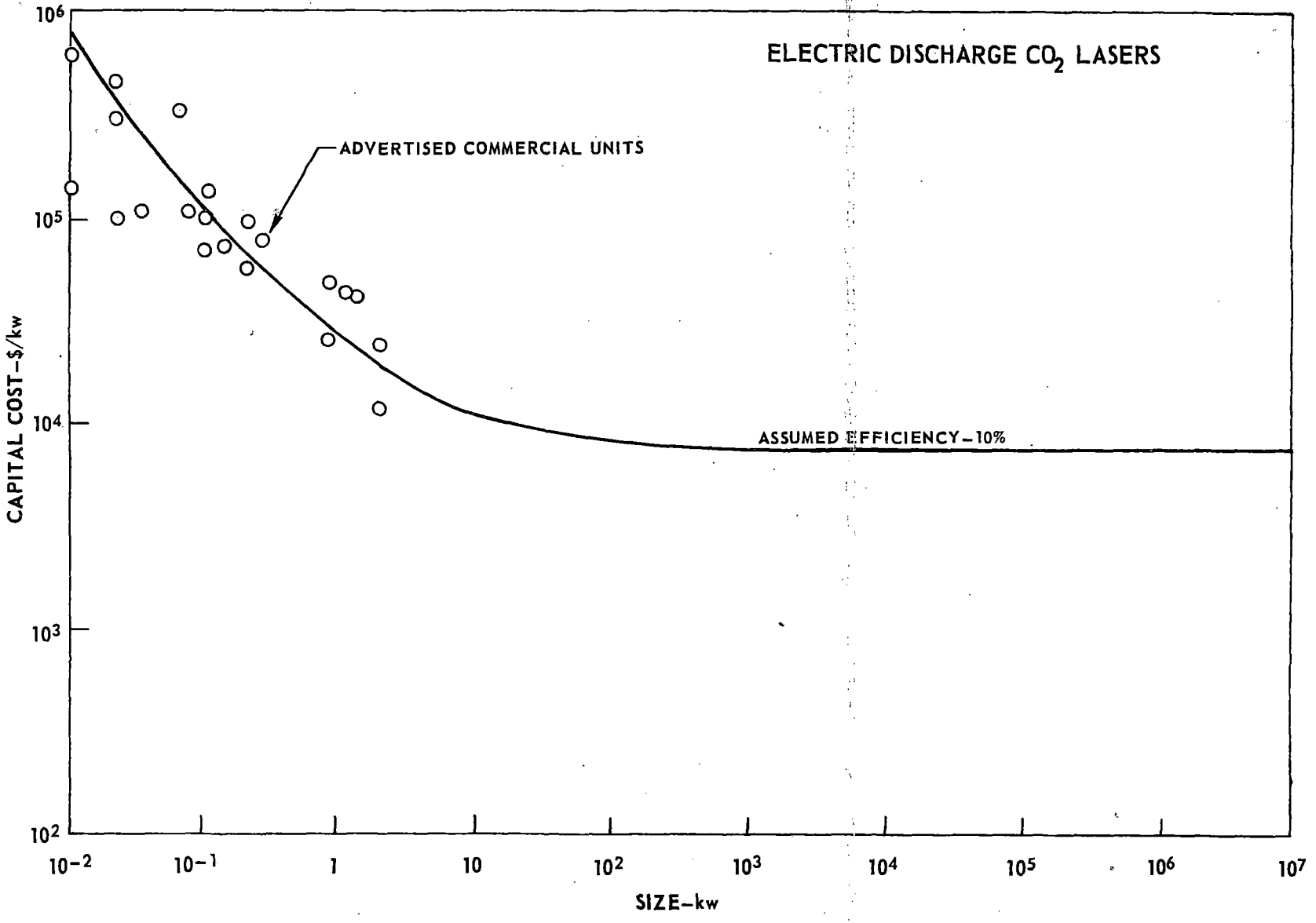

FIGURE 112 ESTIMATED LASER SYSTEM COST

TABLE 8

ESTIMATED LASER SYSTEM COST FOR LARGE SYSTEMS

Assumes 10% laser efficiency

$$\left(\frac{\text{optical power output}}{\text{electric power input}}\right)$$

		10^3 \$/kw
Cavity and Associated Equipment		1.75
Mirrors and Mirror Mounts		0.14
Power Supply System		
Conditioner	1.50	
Generation System	0.89	2.39
Vacuum System		0.70
Cooling System		0.11
Miscellaneous		0.03
Direct Material Cost		5.12
Assembly, Overhead, etc.		5.12
TOTAL		10.24

TABLE 9

POWER TRANSMITTING MIRROR

DESCRIPTION:	20-inch-diameter, thin-skin, cooled mirror
FIGURE:	flat 1/10 λ @ 10.6 microns over any six-inch aperture
OPTICAL APERTURE:	figure to be maintained over 18-inch central diameter
SUBSTRATE:	OFHC copper, 2 inch thick ≈ 200 lb
COOLING:	thin-skin technique
COST ESTIMATE:	(based on a minimum of 12 units)

Machining (150 hours)	1400
Brazing	200
Materials	350
Optical polishing	1400
Optical coating	200
TOTAL	3550

station boxes, and cooling equipment has been estimated on the basis of standard cost-estimating texts such as Refs. 32 and 33. In all of this equipment, the only item whose cost was not well established was the dehumidifier. An air dehumidifier nearly ten times larger than any quoted in the reference material will be required, but there are indications that there will be considerable economies of scale. Therefore, a unit price of one-half the unit price of the largest dehumidifier quoted was used.

Combined System Cost

The combined incremental laser system cost, i.e., the estimated cost of all of the items added to the tunnel machine to accomplish the laser assist, is shown as a function of tunnel length and mirror spacing in Fig. 113. Some component breakdowns of these costs are shown in Table 10. The most obvious conclusion to be made on the basis of the figure and table is that the minimum number of mirror stations must be used. Not only are the mirrors expensive, but their effect on the transmission efficiency is such that a larger laser must be used, which causes a great increase in overall system cost. A more thorough and detailed long-range refocusing station design effort should probably be included in any future studies.

Cost Sensitivity

As shown in Table 10, the major cost component of the incremental laser system cost is the laser itself, regardless of what tunnel length or mirror spacing is considered. As already discussed, there is at least one area of technical improvement which could lead to major laser cost reductions, i.e., an increase in the efficiency. Therefore, additional cost estimates were made at different laser unit costs to demonstrate the system cost sensitivity to the laser cost.

The incremental laser system costs shown in Fig. 113 were based on a laser unit cost of $10,000/kw, as discussed in the laser cost section. Incremental laser system costs for laser unit costs of $1000/kw, $3000/kw, and $6000/kw are shown in Figs. 113 114 and 115, respectively. The effects of varying laser unit costs on incremental laser system cost of a 5000-ft tunnel installation are further illustrated in Fig. 116. The conclusion which can be made from these figures is perhaps elementary, but sufficiently significant to bear repeating. The laser unit cost is the primary factor in the total laser system cost. Doubling the laser unit cost nearly doubles the overall system cost. Therefore, any future development which invalidates the laser unit cost estimate can have a major effect on the economics of a laser-assisted tunnel boring machine.

RADIANT HEATERS

In contrast to a laser or electron beam heating system, the electrically powered

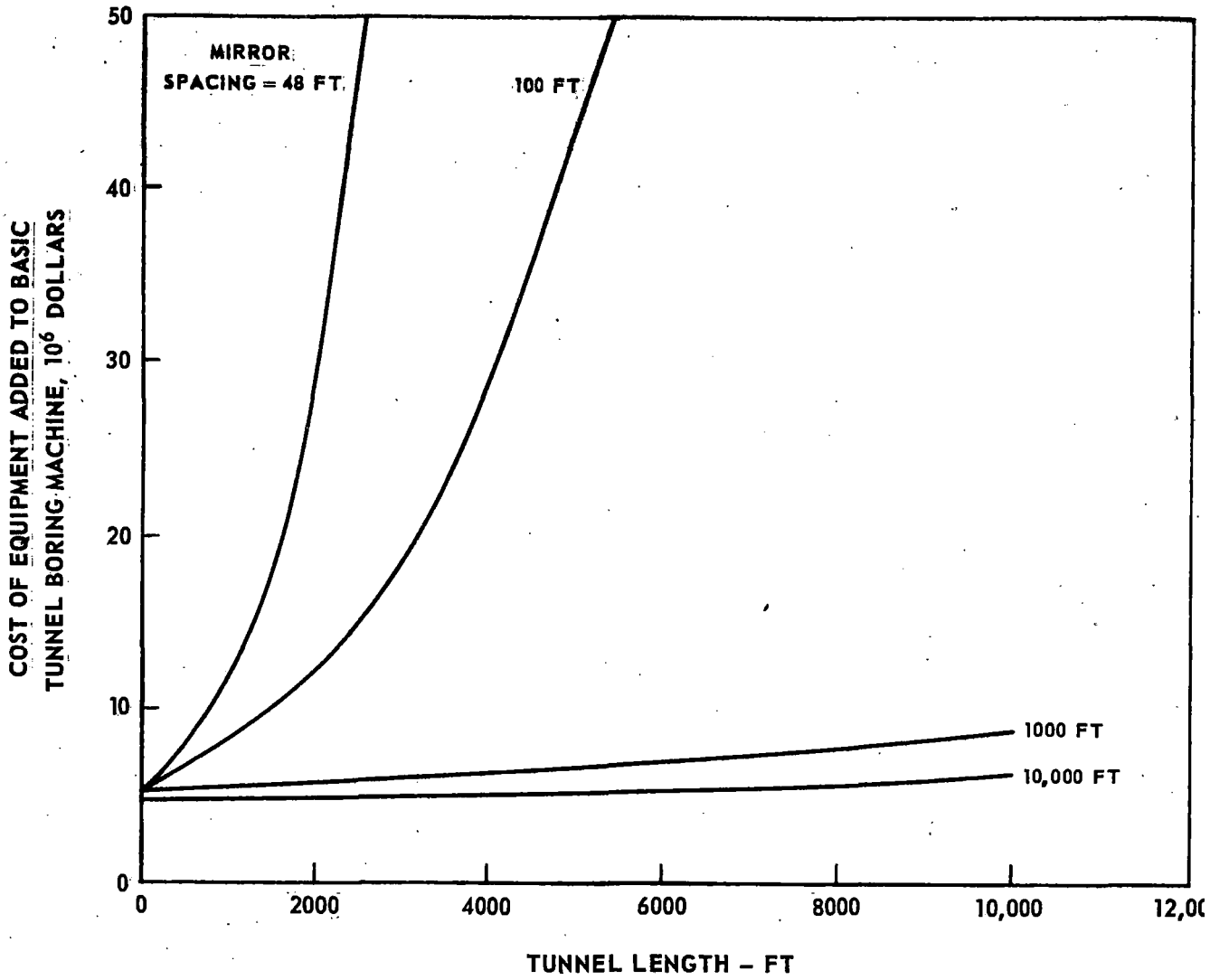

LASER UNIT COST – $\$10^4$/KW

POWER = 450 KW

FIGURE 113 INCREMENTAL LASER SYSTEM COST

TABLE 10

INCREMENTAL LASER SYSTEM COST

Tunnel Length 5000 ft

Mirror Spacing	48 ft	100 ft	1000 ft	No Mirrors
Pipe Cost	$135,400	$119,600	$106,500	$105,100
Mirror Cost	738,400	355,000	35,500	3,550
Laser Cost	8820×10^6	1920×10^6	7.91×10^6	6.876×10^6
Blower Cost	20,000	20,000	20,000	20,000
Dehumidifier Cost	50,000	50,000	50,000	50,000
Miscellaneous Cost	3,000	3,000	3,000	3,000

Tunnel Length 500 ft

Mirror Spacing	48 ft	100 ft	No Mirrors
Pipe Cost	$ 13,500	$ 12,000	$ 10,500
Mirror Cost	73,840	35,500	355
Laser Cost	9.39×10^6	7.15×10^6	5.6×10^6
Blower Cost	20,000	20,000	20,000
Dehumidifier	50,000	50,000	50,000
Miscellaneous Cost	3,000	3,000	3,000

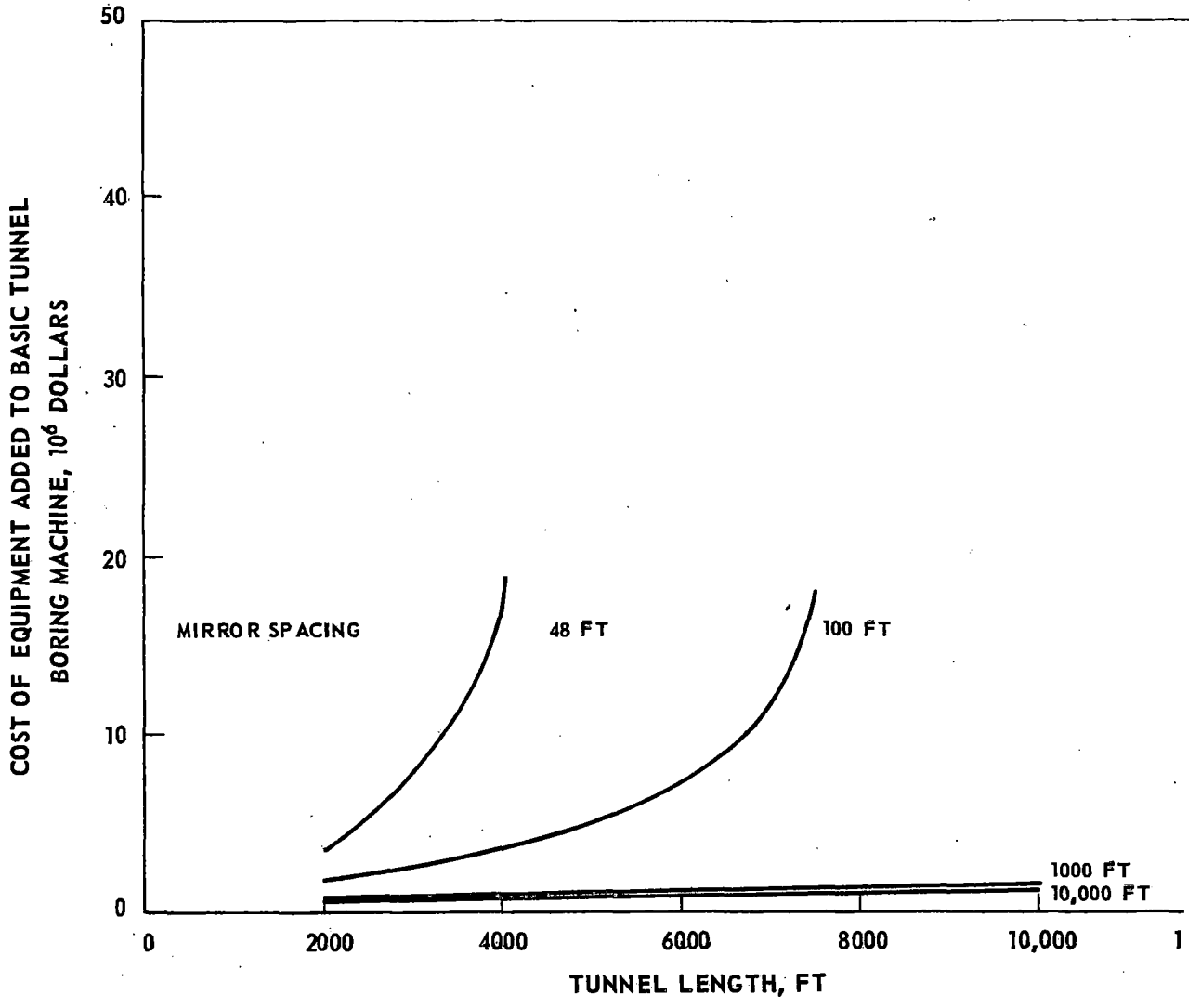

LASER UNIT COST – $\$10^3$/KW

POWER = 450 KW

FIGURE 113 INCREMENTAL LASER SYSTEM COST

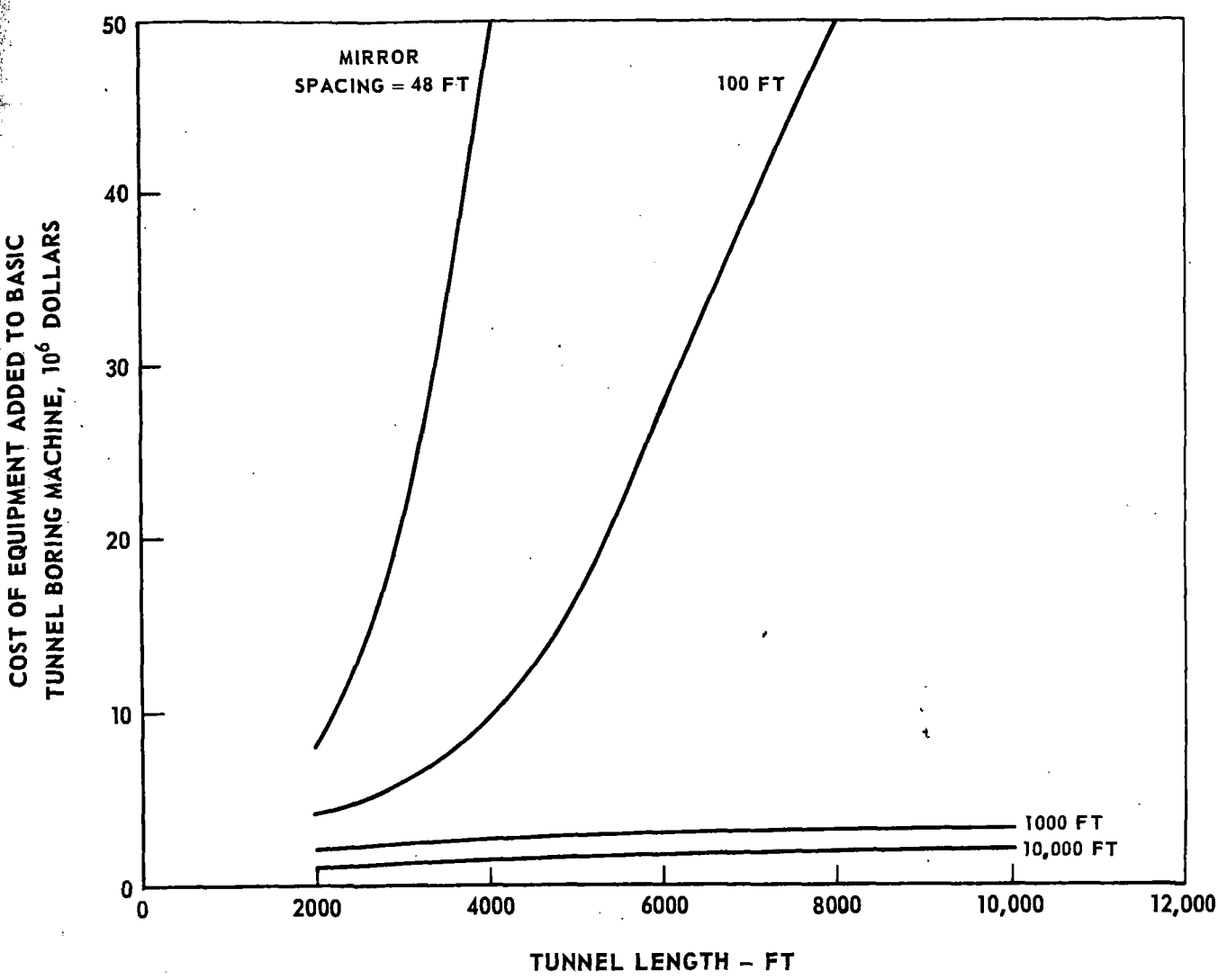

LASER UNIT COST – \$3 X 10^3/KW

POWER = 450 KW

FIGURE 114. INCREMENTAL LASER SYSTEM COST

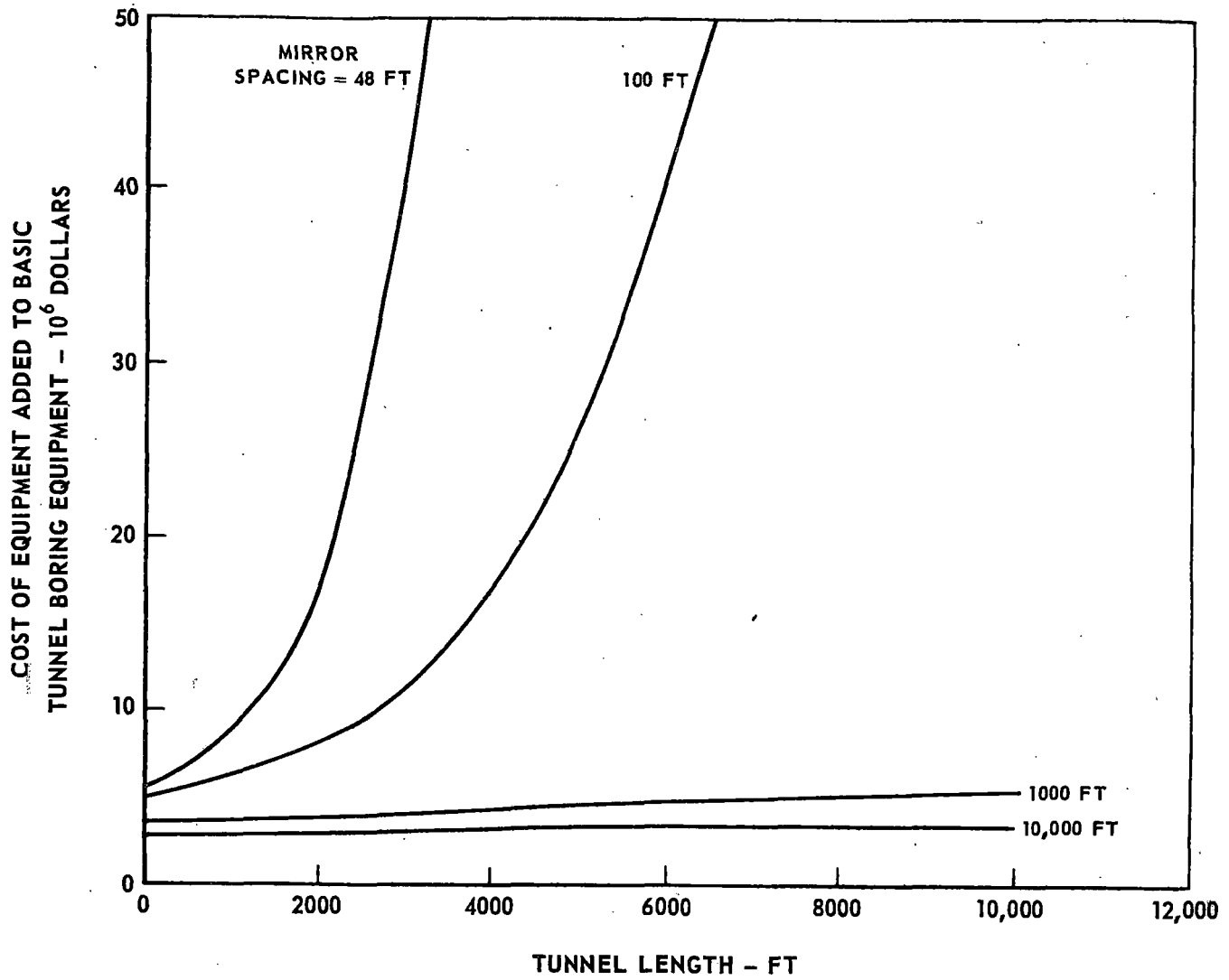

LASER UNIT COST \$6 X 10^3/KW

POWER = 450 KW

FIGURE 115 INCREMENTAL LASER SYSTEM COST

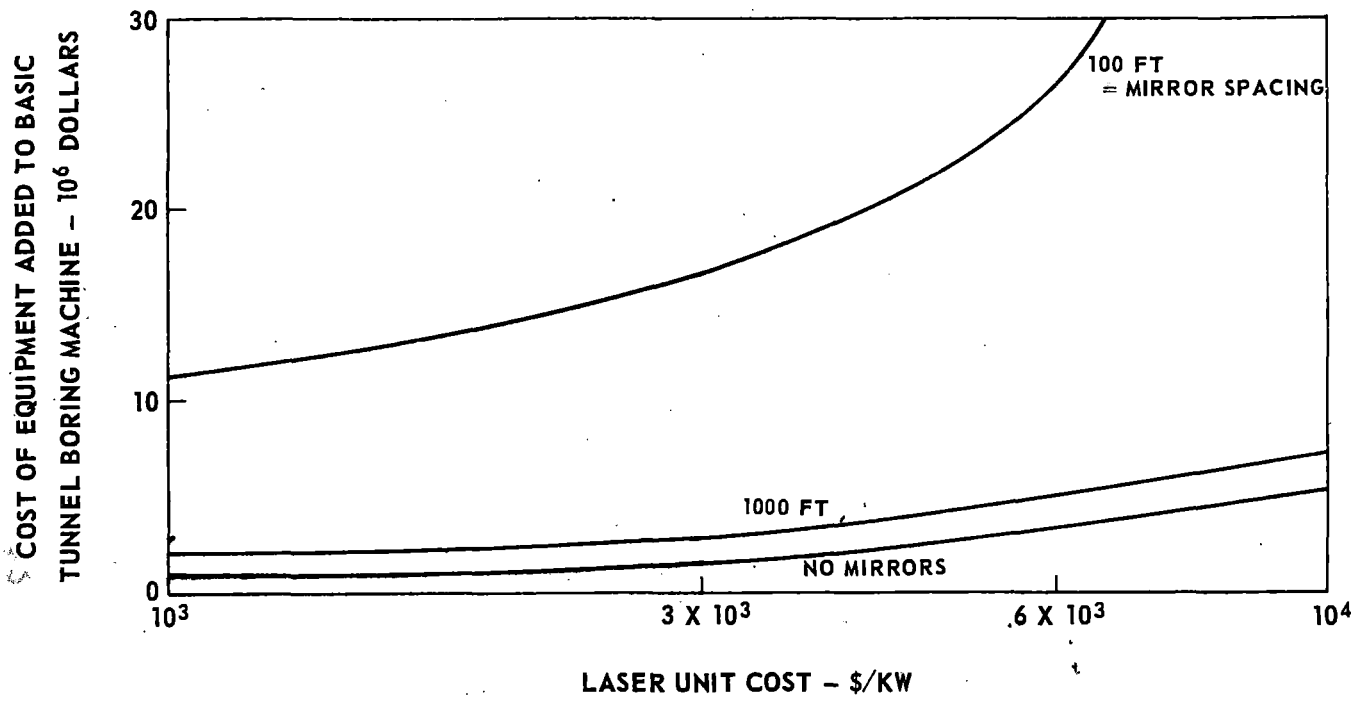

5000 FT TUNNEL

FIGURE 116 LASER SYSTEM COST SENSITIVITY

radiant infrared heater is basically a simple device, requiring no more complicated support than a low-voltage electric power supply.

The radiant heaters considered here are basically resistance elements whose temperature is allowed to increase until the thermal radiation is nearly equivalent to the electrical energy input. The major technical problem is to design an element which will have a long life in the open air at the elevated temperature required. There are three basic types of elements in common use today: the metal-sheathed resistor whose surface temperature is on the order of 1500 deg F, the quartz tubular heater with surface temperatures on the order of 1800 deg F, and the quartz lamp whose filament temperature is typically 4000 deg F. According to manufacturer representatives and catalogs, the only type of heater capable of withstanding the heavy vibrational environment of a tunnel boring machine is the metal-sheathed resistor. Such units should have lives of 1000 to 2000 hr under the conditions expected (e.g., Ref. 34).

The heating elements proposed for this application are nearly $\frac{1}{2}$-in. in diameter and are rated at 70 watts of radiant heat output per linear inch of heater. As indicated by the test program, it will be desirable to concentrate this heat over as narrow an area as possible. Therefore, each heater element should be backed by a carefully contoured reflector and placed as close to the face as possible. Even with a contoured reflector, the heated path image on the rock face will be larger than the heating element and the image size will increase as the reflector to tunnel face distance increases. If a minimum clearance of $1\frac{1}{2}$ in. and a reflector diameter of 3 in. are assumed, the heater element image on the rock face will be nearly an inch wide. Therefore, very close spacing between the reflector and the tunnel face will be required. It should be pointed out that the concentrated energy on the face represents only part of the total heat radiated from the heater rod. The test data, in conjunction with which the radiant heater will be evaluated, will be the "unfocused" data, which assumes a heated path of roughly $1\frac{1}{4}$ in.

A schematic diagram of such a heater installation is shown in Fig. 117. Preliminary design layouts indicate that it should be possible to install the total power capacity contemplated for an 18-ft boring machine, i.e., 450 kw, with units rated as low as 61 w/in. in this configuration. Alternatively, at 70 watts/in., the total heater power installed would be 516 kw. Based on this design point, maximum installed radiant powers of 650, 358, and 160 kw could be installed on 20-, 15-, and 10-ft-diameter boring machines, respectively.

A diagram of a metal-sheathed radiant heating element is shown in Fig. 118. The heat is generated in the nickel-chromium resistance wire and must be conducted to the surface through the protective metal sheath and dielectric. There is a maximum temperature limit on each of these materials, but in practice it is the

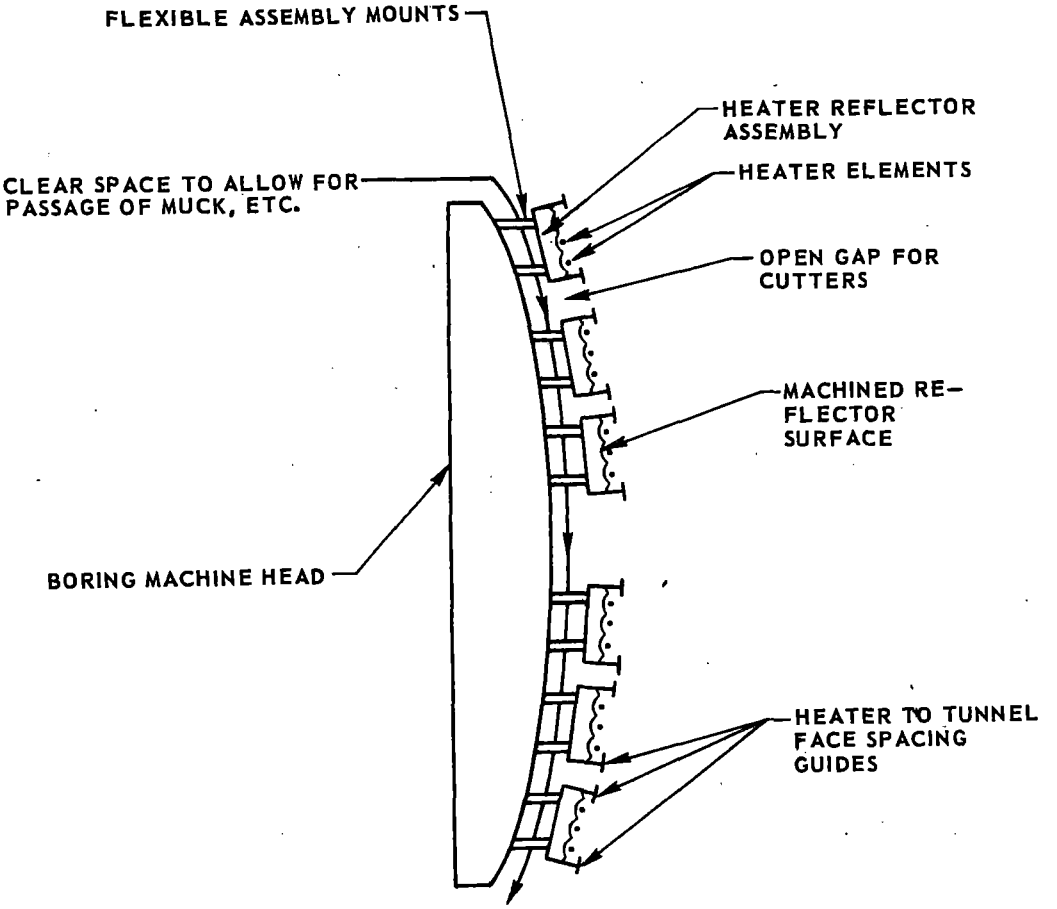

FIGURE 117 ADAPTATION OF RADIANT HEATERS TO BORING MACHINE

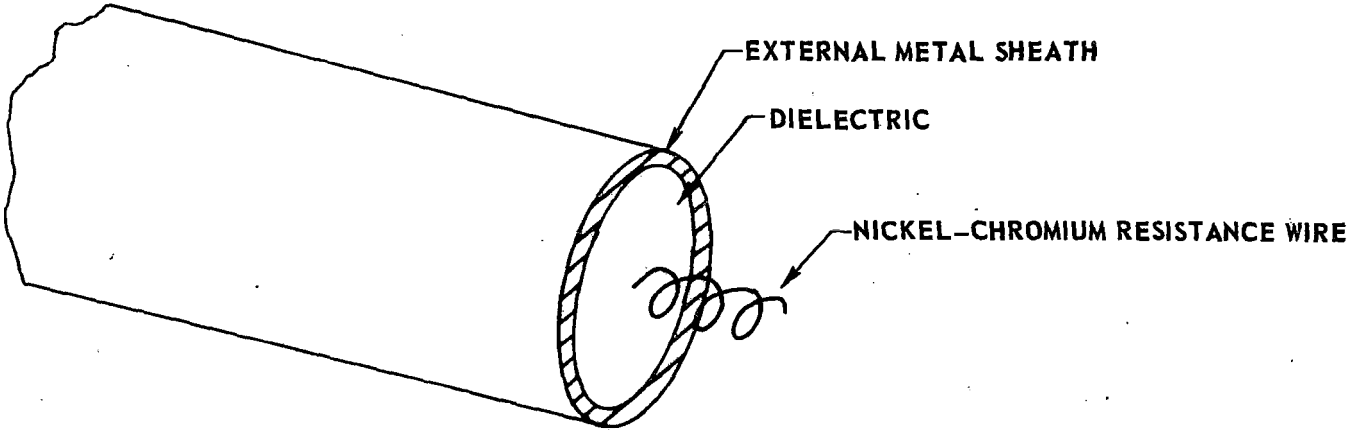

FIGURE 118 TYPICAL RADIANT HEATER ELEMENT

temperature of the metal sheath that is critical. For this reason, the heat lost through nonradiant transfer mechanisms is not included in the rating. When free standing in open air, an element radiating 40 w/in.^{2} can lose as much as an additional 40 w/in.^{2} to convection. If the convection is decreased, the current flow in the heater must be decreased so that the sheath temperature remains constant, and the radiant flux is still 40 w/in.^{2}. Therefore, the convective losses are of importance in determining heater efficiency. Because of the cramped spaces contemplated (see Fig. 117), it appears reasonable to assume that the convective losses in the boring machine installation will be less than 50%. Since the convective losses associated with the configuration shown in Fig. 117 are not amenable to simple analysis, a loss of 15% was assumed. Considering also the radiant heat energy which will be absorbed by the reflectors, an overall radiator efficiency of 70% was assumed.

Preliminary layouts of radiant heater systems on tunnel boring machine heads have indicated that roughly 60% of the face area would be covered by heater elements, the rest of the area being occupies by cutters and cutter mounts. With the required power spread over this much of the tunnel face, and assuming at least half the radiant energy concentrated in a one-inch strip between cutters, the maximum rock face temperature will be on the order of 500 deg (see Fig. 54). Since the heating element is partly focused on the rock face, the hot strip of rock is conversely focused on the heating element. The heating element will then see the radiant energy from a 500 deg F target, and the net radiation from the element to the target will be reduced accordingly. An estimate of the magnitude of this effect is illustrated in Fig. 119, where the degradation in net radiated power is shown as a function of rock face temperature for the three basic types of radiant heating elements. If the rock face temperature were as high as 650 deg F, and were focused perfectly back on the heater element, the metal sheath radiant element would be capable of radiating only 90% of its normal rated power. The maximum radiating power that can be installed in a tunneler would be reduced correspondingly.

Although the reradiation from the hot tunnel face does not have any direct effect on the efficiency of the radiant heater, there is a secondary efficiency effect which should be noted. As mentioned above, the principal loss mechanism in a radiant heater is that of convective losses to the air. These losses are a function of the geometry of the air-flow passage and the temperature of the heating element. Since neither of these variables change as the rock face temperature increases, the convective losses also remain the same. However, the radiated power decreases as the rock face temperature increases, and the convective losses therefore represent a higher percentage loss. Therefore, the assumed heater power loss of 15% in convective heating of air could be somewhat higher, depending on the exact rating of the heater elements. A graphical summary of the efficiency of the radiant heaters is shown in Fig. 120.

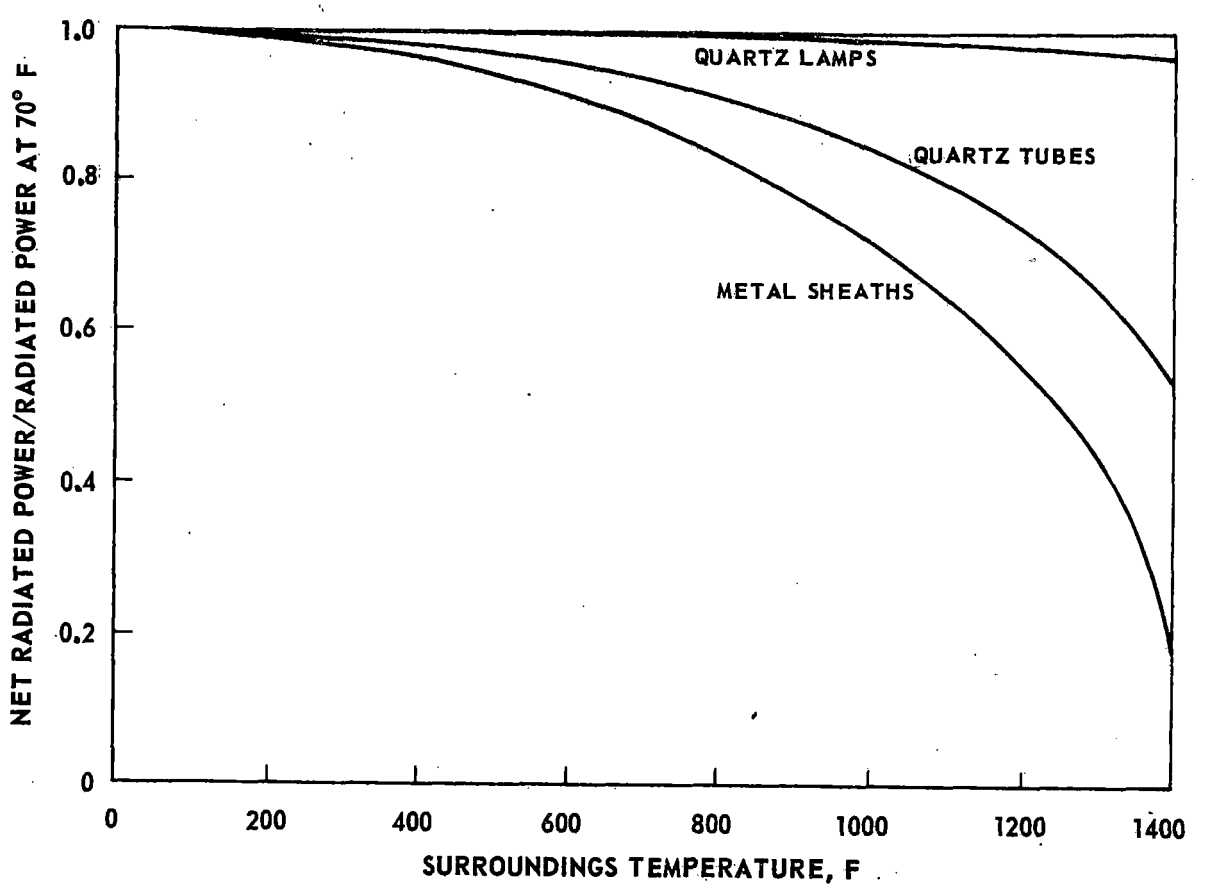

FIGURE 119 EFFECT OF INCREASED AMBIENT TEMPERATURES ON THREE TYPES OF RADIANT HEATERS

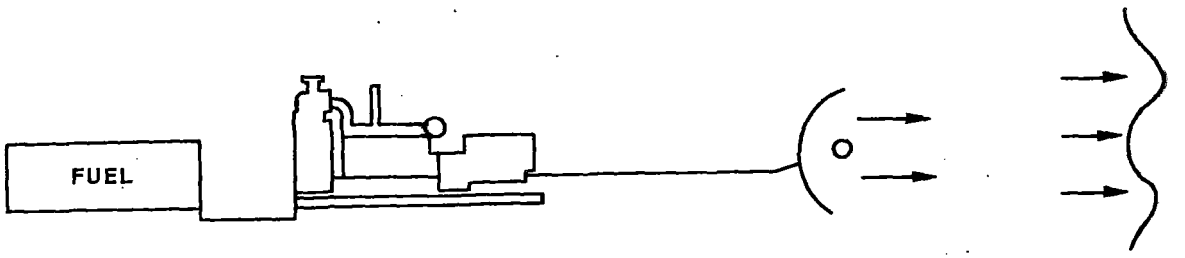

	CHEMICAL ENERGY IN FUEL	FUEL TO ELECTRIC POWER	ELECTRIC POWER TO RADIANT ENERGY	RADIANT ENERGY INTO WALL (ie ABSORPTION LOSS IN REFLECTION)
EFFICIENCY	100%	30%	85%	90%
OVERALL EFFICIENCY	100	30	25.5	23

FIGURE 120 COMPONENT EFFICIENCIES OF RADIANT HEATER SYSTEM

The cost of the radiant heating elements alone is quite low, i.e., just $3.50/ft, or about $4/kw. The cost of the heaters including reflectors similar to those required in this application, however, is on the order of $30/kw. When the power generation system is included, the radiant heater system can be expected to approach $150/kw or $675,000 for a 450-kw installation.

CONCEPTUAL DESIGN OF ELECTRON BEAM UNIT

The electron beam cutting process involves bombardment of the rock with a dense stream of high-velocity electrons, with virtually all the kinetic energy of the electrons being transformed into heat upon impact. Electron beam machines depend on a high vacuum for generating the electron stream, and the range of the electrons in air is very short, usually being measured in inches. Therefore, the electron beam generating unit must be incorporated directly with the other equipment operating in the face area.

This section comprises a review of current electron beam technology, a discussion of the limits in applying electron beam machines to heat-assisted tunneling, and a revie of a 150-kw electron beam machine design concept for tunneling operations. Some information on X-ray generation with electron beams is also included. A discussion of the basic design considerations of electron beam units is presented in Appendix D.

Review of Pertinent Electron Beam Technology

Commercial electron beam equipment being marketed today consists of either vacuum, partial vacuum, or what is commonly referred to as nonvacuum type of equipment. The vacuum equipment requires a vacuum of 10^{-4} torr in the electron optics column as well as in the adjoining work chamber. For partial vacuum equipment, only the upper column is maintained at 10^{-4} torr, whereas the work chamber is maintained at a pressure of 50 to 300 microns. In nonvacuum equipment, the electrons are projected from a high-vacuum electron optical column directly into atmospheric pressure. A typical nonvacuum electron beam welding unit is shown in Fig. 121 . Transmission of the electrons to the workpiece is accomplished by the use of multiple staging orifices located at the bottom or extreme end of the electron optical column.

The out-of-vacuum system is best suited for consideration in the cutting of rock. Some degree of mobility and versatility with a nonvacuum electron beam gun can be achieved for proposed mining or heat-assist operations.

Some of the limitations with the present electron beam equipment for this proposed application are: lack of rugged design, filament lifetime, debris ingestion, and overall size. However, it should be noted that for applications

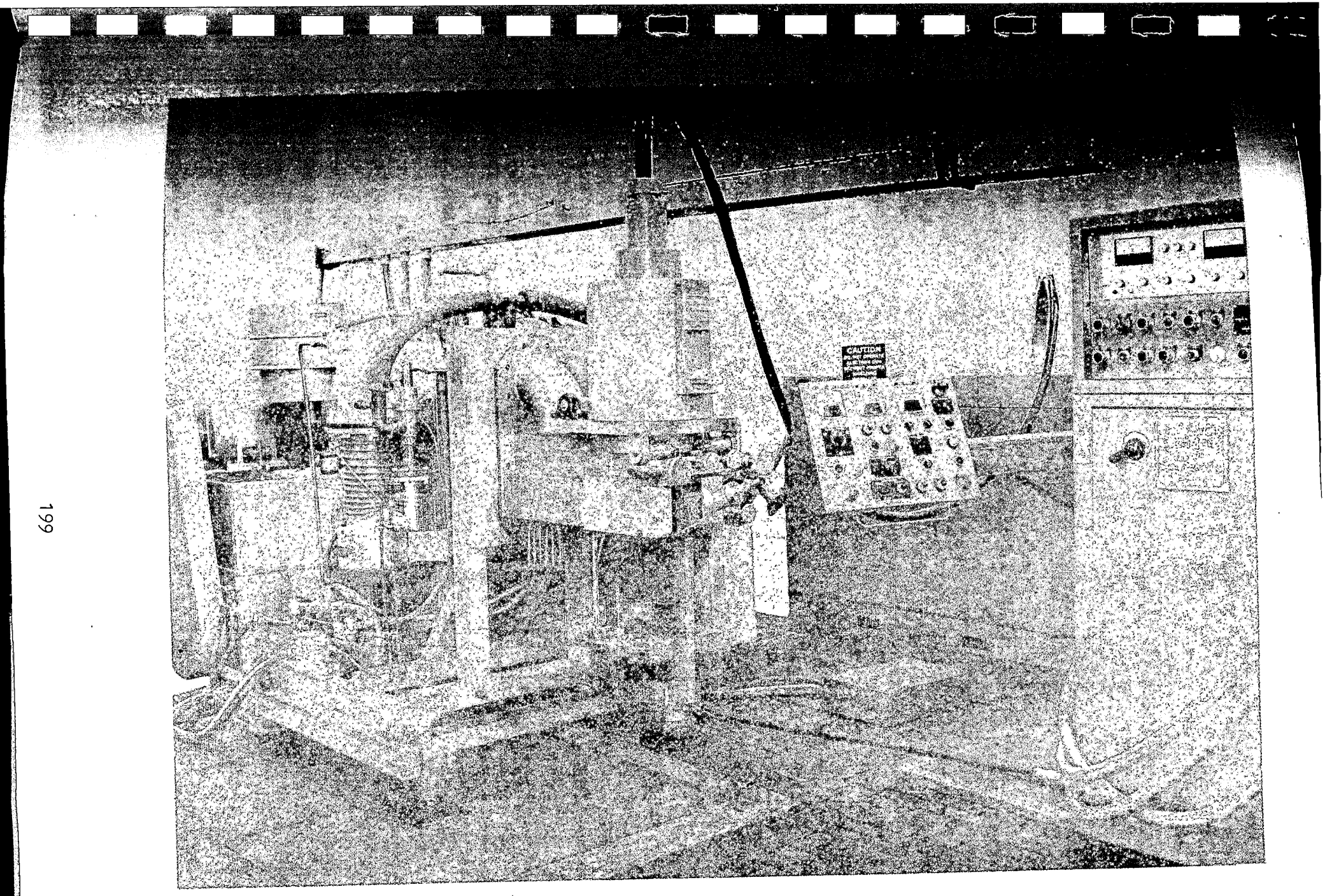

FIGURE 121 12.0 KW NONVACUUM WELDER

requiring or permitting a static installation, the equipment design is more than adequate. Exhaustive tests with the present equipment for the last eight years hav shown that a high degree of reliability can be achieved for commercial applications if the system parameters have been adequately specified. The present systems, in general, are limited to shock loads of approximately 4 g's. These shock limitation: are primarily concerned with the power supply and the appropriate control panels. In addition, filament lifetime for most gun systems now permits operation between 15 and 20 hours. After this period, the filament, which is constructed of tungsten material, must be replaced. The replacement cost is nominal (approximately $15), and the time required for filament replacement is 10 minutes or less. For some of the nonvacuum systems, particularly when operating at high power (e.g., 25 kw), care must be exercised to prevent ingestion of debris into the orifice assembly and/or build-up of debris in and on the orifice stage closest to the workpiece. An excess accumulation of debris can cause loss of efficiency in electron transmission and/or a degeneration of the energy distribution within the electron beam itself.

Recent developmental work has been aimed at the correction of some of the aforementioned problems and limitations during extended operation. Specifically, more rugged filament designs now are being investigated to permit increased lifetimes as well as operation at higher powers. Indirectly heated types of cathodes are also being investigated to provide high electron emission at tolerable gun head temperature limits. Another cathode design being considered is the cold cathode type of emitter.

Two specific improvements for increasing the ruggedness and reliability of the power supply and control components of an electron beam system have recently been incorporated in existing equipment. These are the use of shock-mounted insulators between the cabinet and mounting frame assembly and the upgrading of the interna power supply components to withstand shock loads of 10 g's. Such equipment has been manufactured to provide a service life of at least ten years or 25,000 hours. This type of equipment is intended for use on gas pipeline rights-of-way for joining large-diameter pipes. In addition, the power supply has been designed to meet NEMA 4 specifications (all-weather protection) and to operate on a 20% grade.

During extended periods of welding (or cutting), any significant debris build-up or ingestion into the gun structure is not desirable. This problem has been resolved to a large extent by the use of special external blowers as well as operating the various stages at higher vacuum. Operations in excess of eight hours without maintenance with these incorporated improvements have been realized. It should be noted that for rock cutting applications, further improvement of operation can be expected relative to debris build-up. For metal working operations, the molten material in the form of liquid droplets or vapor deposition has a tendency to coalesce and deposit on a cold surface. However, for rock cutting operations, a

considerable section of the cut portion will remain in its parent state, i.e., sandlike composition. These fine sand particles are not as adherent as molten metal and, in fact, may assist in maintaining a clean exit orifice assembly as a result of the natural sand-blast process that will occur during cutting.

Limitations on the Application of Electron Beam to Heat-Assisted Tunneling Operations

Current electron beam machines, and those envisioned for heat-assist in tunneling, will require both high voltage and vacuum supply lines. Since no method has been envisioned for providing these utilities to a machine rotating about a solid shaft, the integration of electron beam devices with a tunnel boring machine head (in the manner envisioned for laser or radiant heater systems) is felt to be unworkable.

Even if such an integration could be arranged from the point of view of machine support, the bulk density of the electron beam generating units themselves is too low to allow sufficient packing of devices to achieve rock heating power outlets every 3 in. along a radius, as is suggested in Fig. 85. A sketch illustrating the problems of incorporating present-day 10-kw electron beam machines in the head of a large tunneling machine is shown in Fig. 122. This shows that only six such devices could be installed with a minimum radial distance between points of electron beam output of 9 in., in a typical 20-ft tunneler. As device power output increases, size is not increased proportionately, and a similar sketch indicates that three 150-kw electron beams could be fitted into the basic tunneling head shown in Fig. 123. However, rock-heating could then be performed only at three discrete radii. In any event, the power and vacuum supply problems of electron beam equipment preclude the possibility of packing a boring machine head as shown in Fig. 123.

To develop information on potential high-power electron beams for use in evaluating heat-assisted tunneling by other means than heat-weakening (e.g., possibly some kerfing mode), information was developed on a device which would work independently of a mechanical cutter. To take advantage of the size-power relationship for electron beam machines, a power level of 150 kw was assumed. Development of this concept is discussed below.

150-kw Design Concept

The heart of this design concept, developed specifically to provide the ruggedness necessary in a tunneling environment, involves the use of a semisealed indirectly heated cathode. The design of this device, shown schematically in Fig. 124, will provide 150 kw of beam power at an accelerating potential of 200 kv.

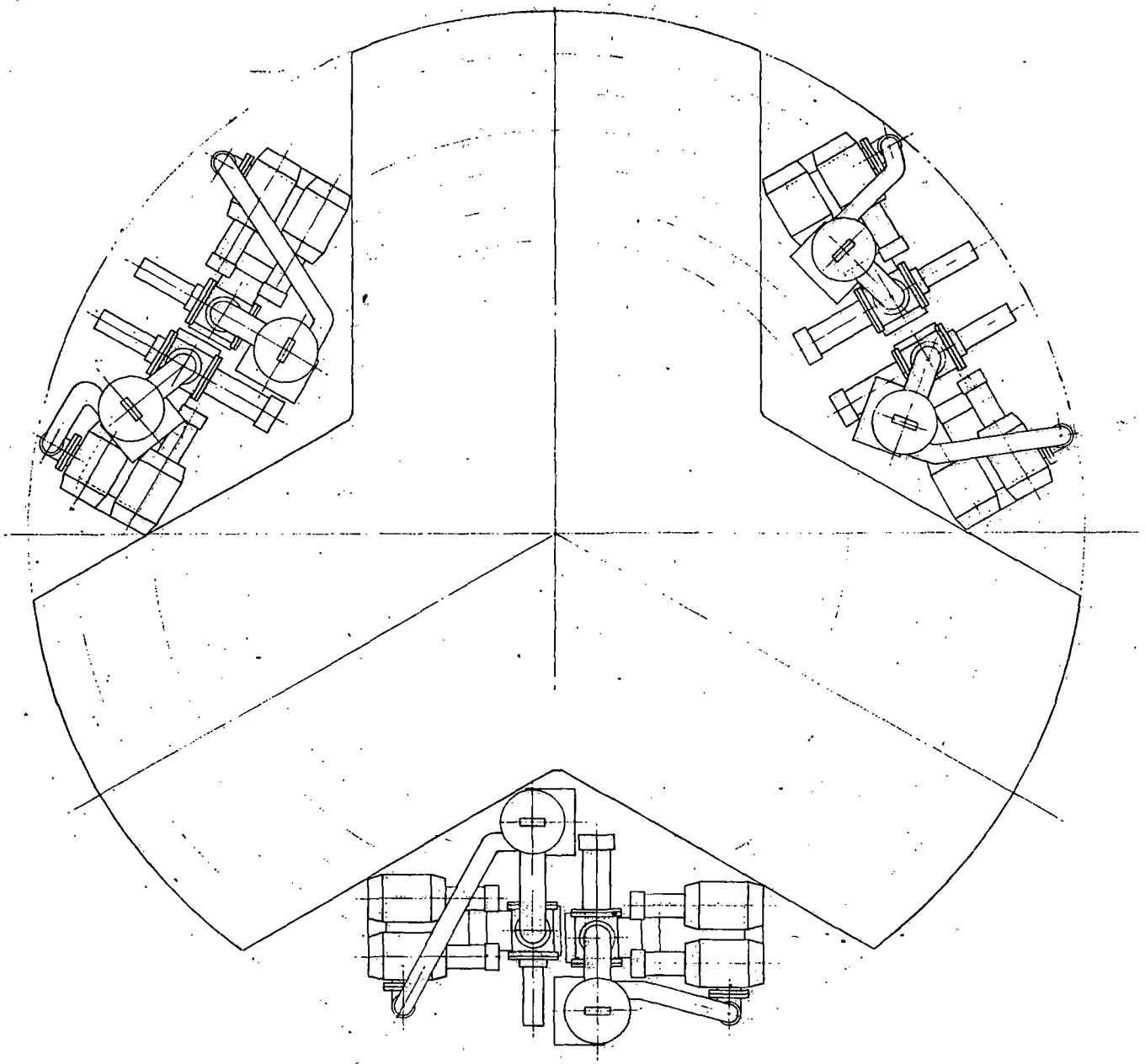

VIEW LOOKING TOWARD THE FRONT OF MACHINE

SKETCH SHOWING PLACEMENT OF SIX 10-KW ELECTRON BEAM UNITS ON 20 FT DIAMETER TUNNELER

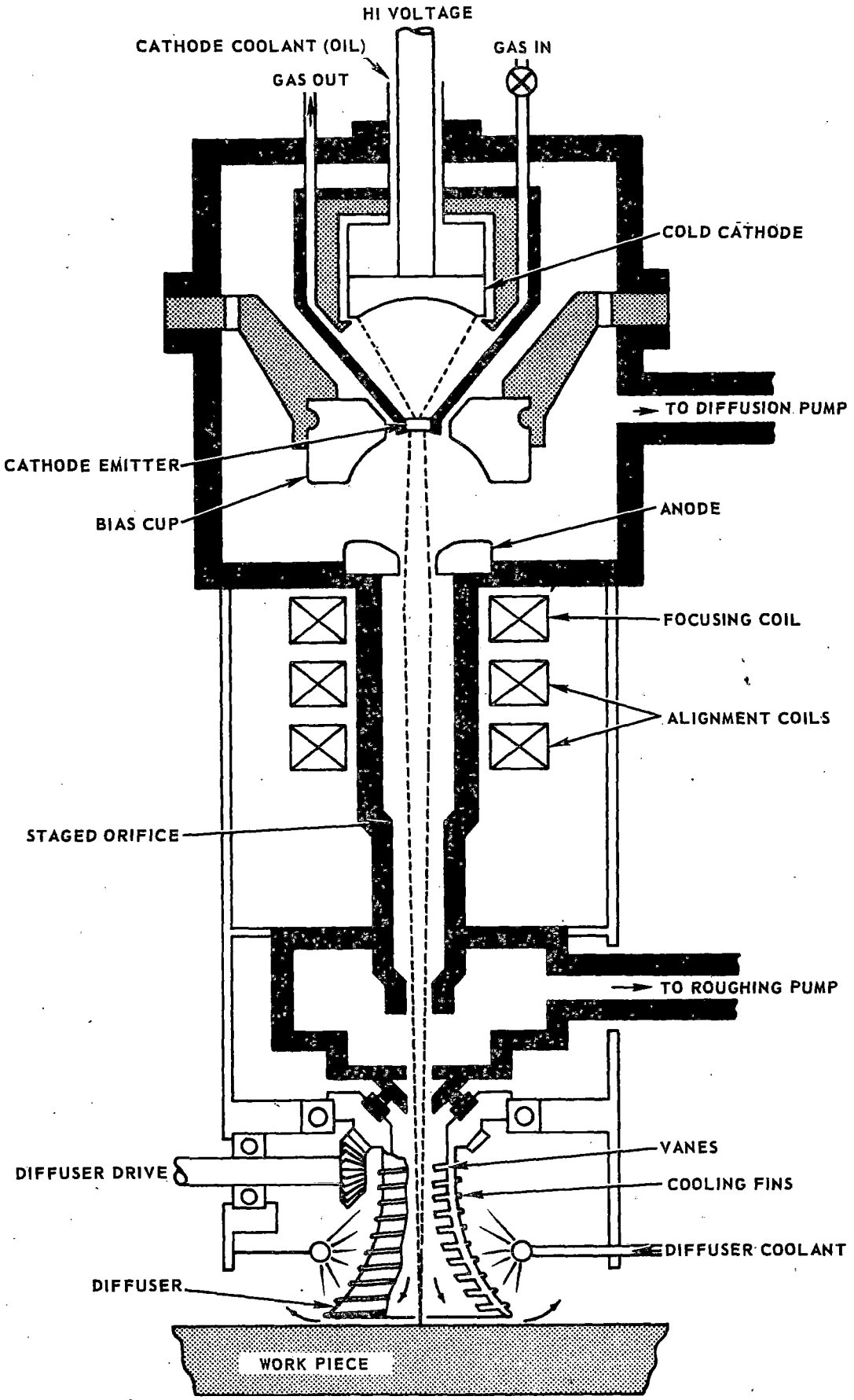

FIGURE 123 NONVACUUM HIGH-VOLTAGE COLD CATHODE SYSTEM

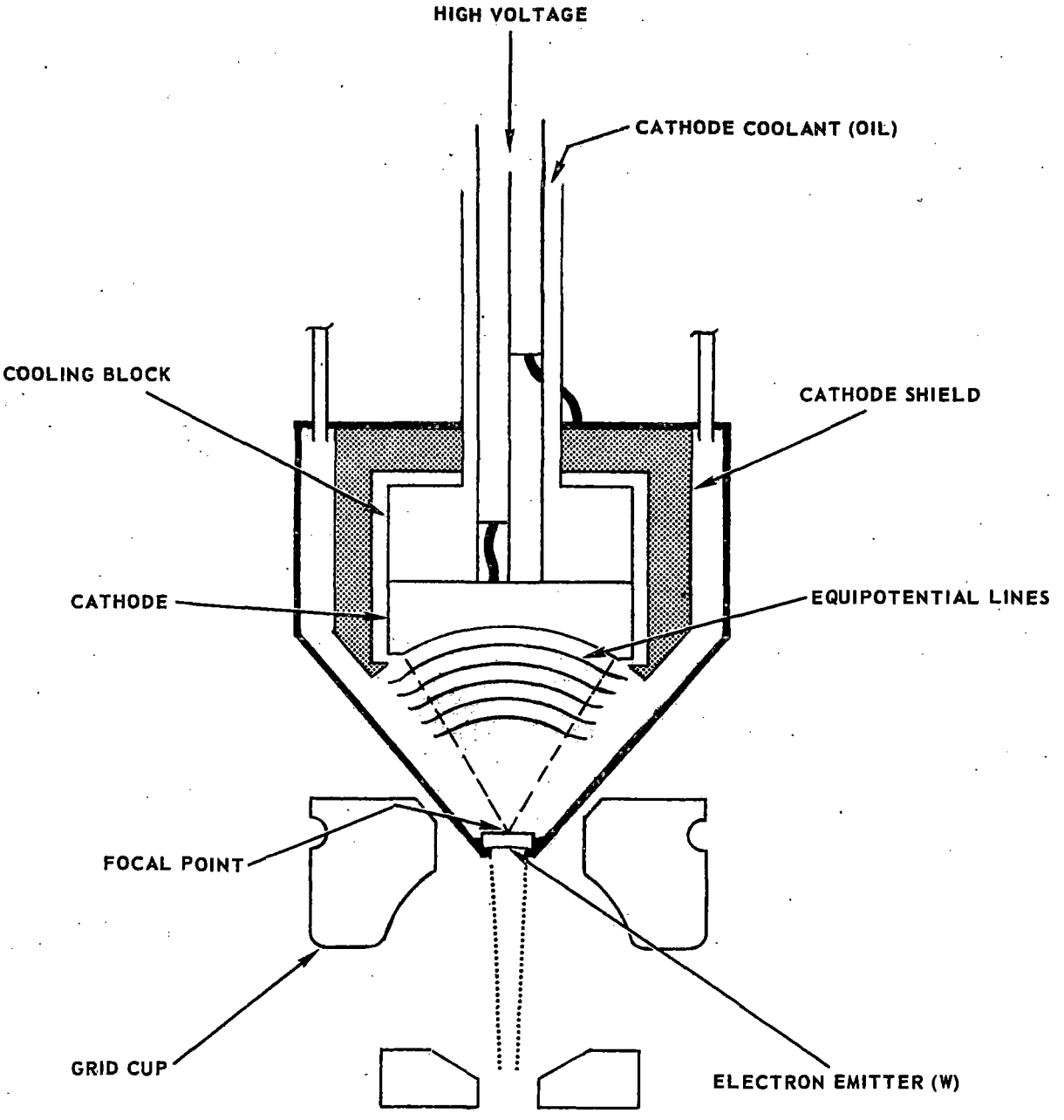

FIGURE 124 CONTOURED CATHODE FILAMENT STRUCTURE

As illustrated in Fig. 124, the heating of the primary cathode is accomplished by a contoured cold cathode. The environment or required operating pressure within the confines of the contoured cathode are indpendent of the vacuum pressures in the other portions of this out-of-vacuum gun. The conditions which must be met for operating at high beam power (i.e., > 100 kw) and for out-of-vacuum operation (see Appendix D) can still be fulfilled. This is achieved by accelerating the electrons from the primary cathode at high voltage and high vacuum, thus minimizing beam spread. To accomplish this, the electron optical column must be pumped to a vacuum of 10^{-4} torr or less to maintain an effective mean free path of approximately one meter. For this equivalent length, the electrons exhibit minimum beam dispersion as they then pass through the appropriate orifice assemblies.

The following sections describe the electron beam gun and cathode assembly, the system support equipment, equipment operation, and the estimated floor space requirements.

Electron Beam Gun

An axial-beam contoured cathode similar in principle to that shown in Fig. 124 is used for heating the primary electron beam emitter of Fig. 123. The contoured cathode functions as one of the primary elements for an indirectly heated electron beam gun. Data obtained from tests indicate that pressures of 100 to 1000 microns will provide an adequate cathode discharge current. A power of 250 watts/in.^{2} of cathode surface has been outlined for a cathode voltage of 6 to 12 kv and a pressure of 400 microns. For a primary beam density of 5 amps/cm^2 and a beam current of 750 ma, the primary cathode diameter is computed to be 0.25 inch. Accordingly, the beam obtained from the contoured cathode must be capable of being focused to this equivalent diameter or less. Beam spot sizes of this diameter have been realized from similar contoured cathodes.

The contoured cathode can be manufactured from nonmagnetic stainless steel. Water cooling of the contoured cathode will be provided since the total power output to the primary emitter is expected to be in the order of 500 watts. Material for the primary emitter will consist of tantalum or tungsten. Tantalum has a slightly lower work function than tungsten (4.11 vs 4.55 electron volts) which may be an advantage for operating the filament at a lower temperature. However, cathode resistance against ion erosion, particularly at high voltage, also must be taken into consideration for a high-power gun. Tests with both types of emitter materials can be conducted and the optimum then selected.

To provide a beam power of 150 kw, an accelerating potential of 200 kv as applied between the primary emitter and anode is recommended. The anode is at ground potential. Regulation of beam current is provided by control of the grid bias. For a condition of beam shut-off, the grid voltage is expected to be 3000 to 6000 volts.

Focus of the beam is accomplished by use of a magnetic lens located in close proximity to the anode. To provide for the option of aligning or fine trimming of the beam, two alignment coils are located adjacent to the focus coils.

Projection of the electron beam into ambient pressure is finally achieved by transmitting the high-velocity electrons from vacuum environment (i.e., 10^{-4} torr) through several orifice stages. A staged vacuum/partial vacuum technique coupled with appropriate vacuum diffusion and roughing pumps is used to accomplish the nonvacuum electron beam transfer process.

System Support Equipment

The support equipment required to provide an integrated system consists of a vacuum system, high-voltage power supply, control cabinet, operator's control station, motor-generator set, and associated cables and interconnections. An air supply at 75 to 110 psig, and 3.5 gpm of water at 45 to 90 psig and 77 deg F maximum will also be required. Electric power may be obtained from a 440- or 2300-volt, 3-phase, 60-cycle line.

A schematic of the 150-kw electron beam heat-assist tunneling system is shown in Fig. 125. A layout of this system is shown in Fig. 126. The following indicated values for system components are preliminary estimates of what could be expected for an operational tunneling machine:

- Power Supply - 150 kw
- Induction Voltage Regulator - 225 kva
- Vacuum System -

  a. Two 500 cfm blowers
  b. One 1300 cfm blower
  c. One 10-inch diffusion pump
  d. One 140 cfm roughing pump

Space Requirements

A floor plan for the 150-kw system is shown in Fig. 127. As indicated, the gun and vacuum modules require an estimated area of 5 by 7 feet. The control cabinet or operator's console is shown as a separate shaded section. The size of this enclosure is somewhat undefined depending on the desired degree of comfort and environmental isolation. The operator's console and enclosures conceivably would be mounted on a powered vehicle. This same vehicle would support the gun assembly and also provide gun motion during cutting or heat-assist operations.

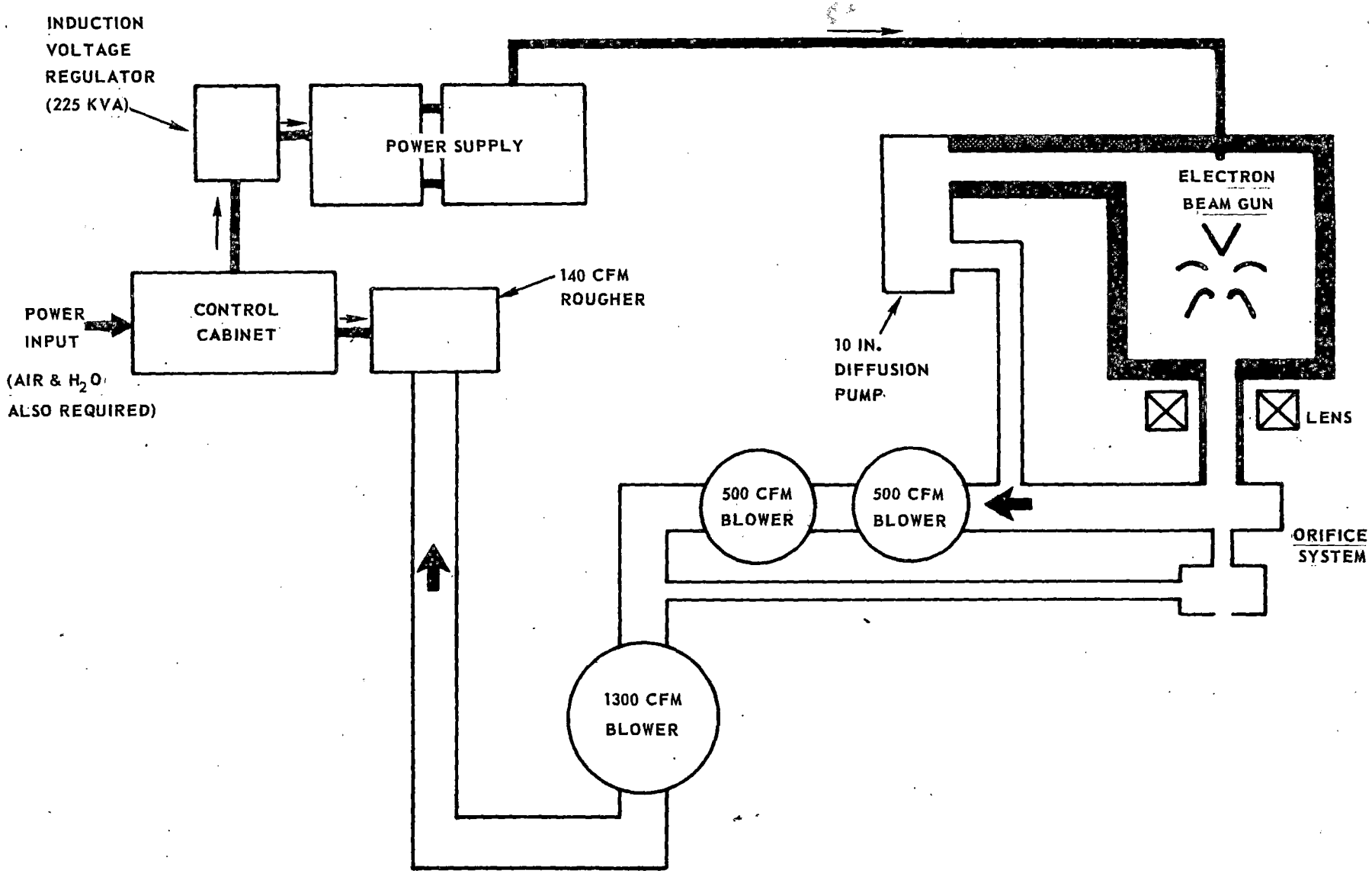

FIGURE 125 SCHEMATIC OF PROPOSED 150 KW ELECTRON BEAM CUTTING SYSTEM

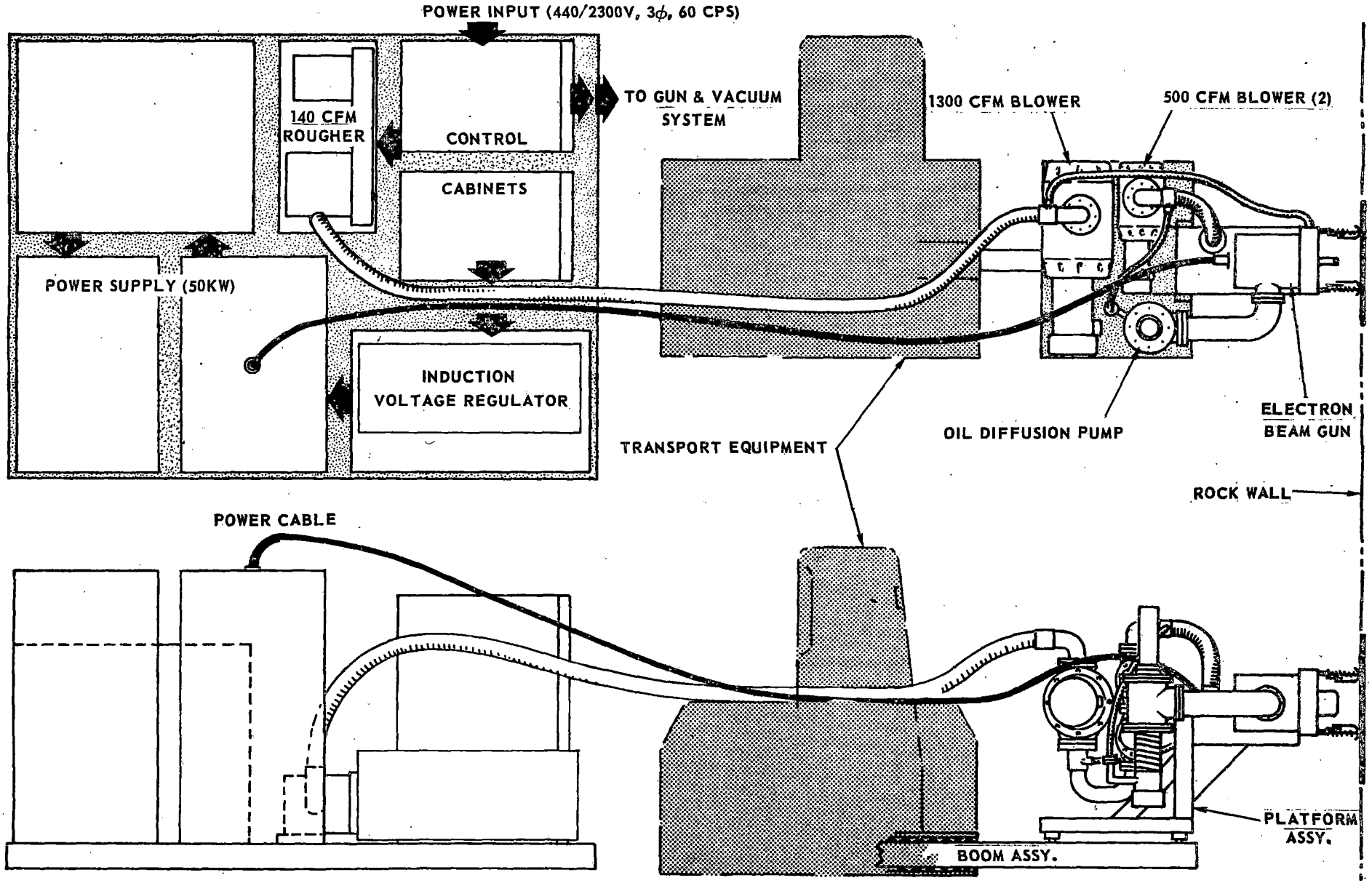

FIGURE 126 LAYOUT OF 150-KW ELECTRON BEAM CUTTING SYSTEM

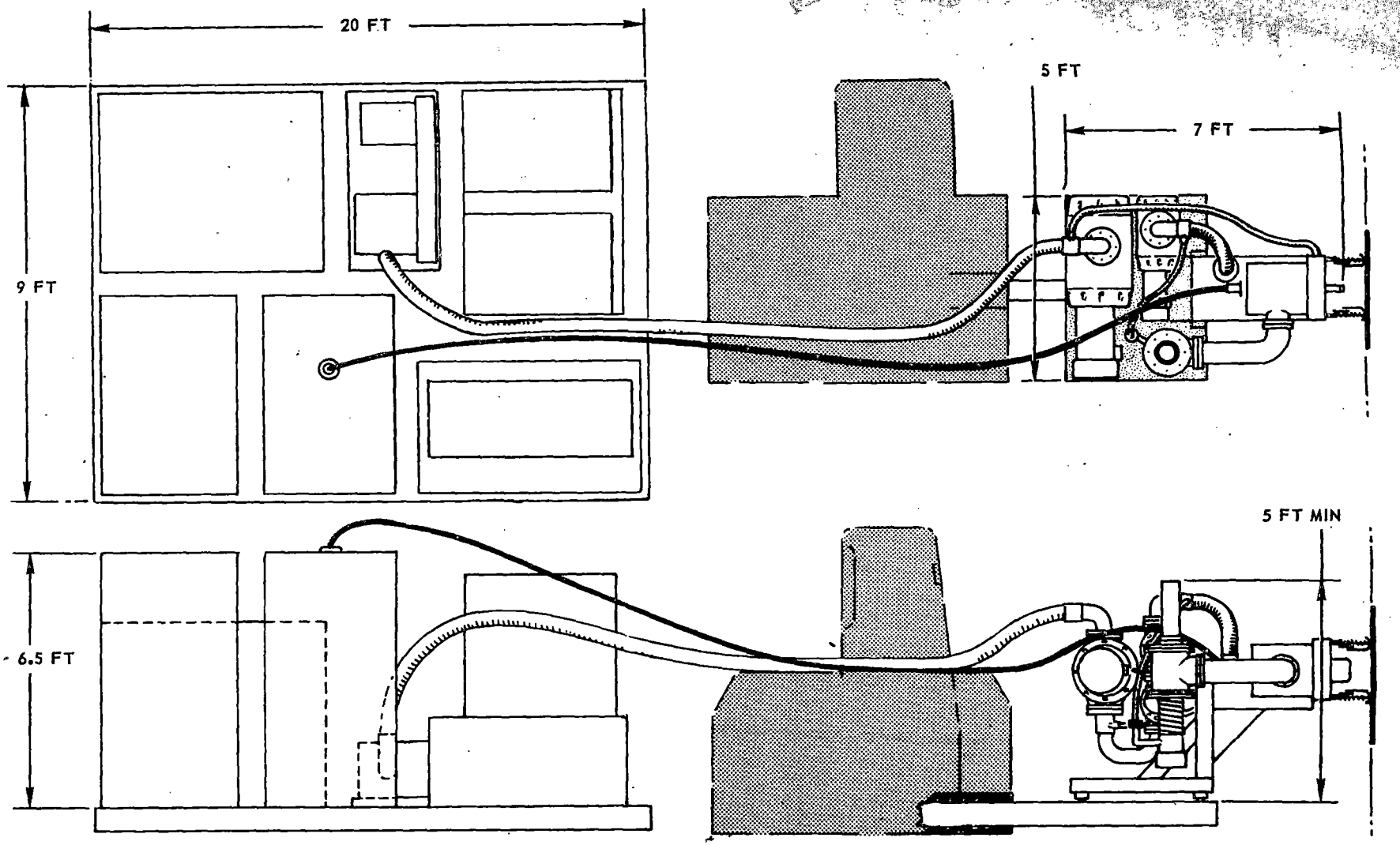

WEIGHT 4000 LB (EST)

GUN	250 LB	BLOWERS (500)	600
FRAME & PLATFORM	800	BLOWER (1300)	1000
DIFFUSION PUMP & VALVES	450	MISC	900

FIGURE 127 SPACE REQUIREMENT & ESTIMATED WEIGHT OF 150-KW ELECTRON BEAM CUTTING SYSTEM

The electron beam gun and blower assemblies would be mounted on a platform which in turn would be supported on an L-type frame assembly. The other equipment of the system such as the power supply, control cabinet, induction voltage regulator, and back-up blower would be mounted on a suitable transport vehicle.

Operator controls for the cutting machine would be mounted in the control cabinet. The cabinet is platform-mounted on shock isolators. Connection to other equipment is made by flexible conduits or cable assemblies.

Safety Considerations

In order to assure safe performance as well as optimum operations of a heat-assist tunneling machine, the following major items need to be considered:

- Use of In-Position Interlocks
- Use of Waterproof Couplings for all Electrical Connections
- Employment of Adequate X-Ray Shielding
- Explosion-Proof Consideration

Use of in-position interlocks is recommended to preclude inadvertent operation of the equipment which could present potential health hazards. Requirements for electrical and mechanical interlocks could be coupled with an appropriate audio signal prior to activating the electron beam.

Use of water-proof couplings for all electrical connections is recommended to permit operation in accordance with NEMA 4 codes.

Since a nonvacuum machine operates at high voltage (175 kv or greater), it is recommended that the operator be enclosed in a small booth-like structure, incorporating shielding against X-radiation. For 175-kv accelerating voltage, shielding of $\frac{1}{4}$-inch-thick lead or 1-inch-thick lead glass having equivalent attenuation is required for the operator compartment.

For operation at voltages greater than 175 kv and at powers in excess of 30 kv, the required lead thickness to attenuate X-radiation to a tolerable level (2 mR/hr) must be increased from $\frac{1}{4}$ in. to recommended values of 0.55 in. and 0.70 in. for an accelerating voltage of 250 kv and beam powers of 25 kw and 300 kw, respectively. To more carefully determine the amount of shielding required, some radiation tests were run, which are discussed below.

For out-of-vacuum operations, the high-voltage electron beam will produce some ozone. The ozone, in turn, can contribute to the acceleration of corrosion on unprotected metal components such as steel. Also, ozone contributes to the long-term degradation of oils, rubbers, and plastics that may be near the gun. Ventilation or protection of the technician and his compartment against prolonged ozone exposure likewise must be provided.

Finally, all components of the system assembly (i.e., pumps, motor-generator set, high-voltage supply electron column, and control cabinet) must be interconnected with grounding straps, and in turn connected to a ground via a master grounding strap. In addition, for mining operations, special explosion-proof electrical equipment will be needed, as a result of the environments which contain finely divided matter as dust particles, naturally appearing combustible gases as methane, or natural earth products which exhibit flammable decomposition.

Radiation Tests

In order to ascertain the approximate degree of X-radiation that will be produced by electron beam impingement on rock material, a series of granite exposure tests to electron beam radiation was conducted. In brief, sensitive X-ray film badges having various X-ray densities were used as the recording means. The badges were located at various distances from the granite target; the film was mounted so that the recording face of each film was in line with and perpendicular to the point of beam impingement. The electron beam gun was operated at 12 and 25 kw for periods ranging from 1 to 4 sec. Parameters recorded were beam power, time of exposure, and distance from the target to the badge.

Comparative tests of inclining granite and tungsten targets at 45 deg also were conducted; these tests indicate the approximate maximum X-radiation that can be expected for granite. The data for all tests are tabulated in Table 11. The radiation levels in roentgens per second versus beam power are illustrated graphically in Fig. 128.

The intensity of radiation at a given distance from a point source of monochromatic radiation with a shielding barrier between is given by:

$$I = \frac{(1 + \beta)\, I_o e^{-\mu t}}{x^2} \qquad (7)$$

where I_o = intensity of source at one foot in air

x = distance in feet between source and observer

TABLE 11

SUMMARY OF X-RADIATION DATA

KW	Time (sec.)	Distance (inches)	Intensity (Roentgens)	Target Material	Work Distance (inches)
12	1	50	2.5	Granite at 90°	2
12	1	88	1.2		
12	2	50	5.8		
12	2	76	2.0		
12	2	76	2.25		
12	2	88	1.7		
12	4	50	5.0		
12	4	76	3.8		
12	4	76	3.6		
12	4	88	2.25		
25	1	50	2.4		
25	1	88	1.6		
25	1	50	2.5		
25	1	88	1.2		
25	3	88	5.4		
25	3	50	5.25		
12	2	76	3.0	Granite at 45°	~ 4
12	4		7.5		
25	2		8.0		
25	4		11.0		
12	2		9.0	Tungsten at 45°	
12	4		13.5		
25	2		13.5		
25	4		21.0		

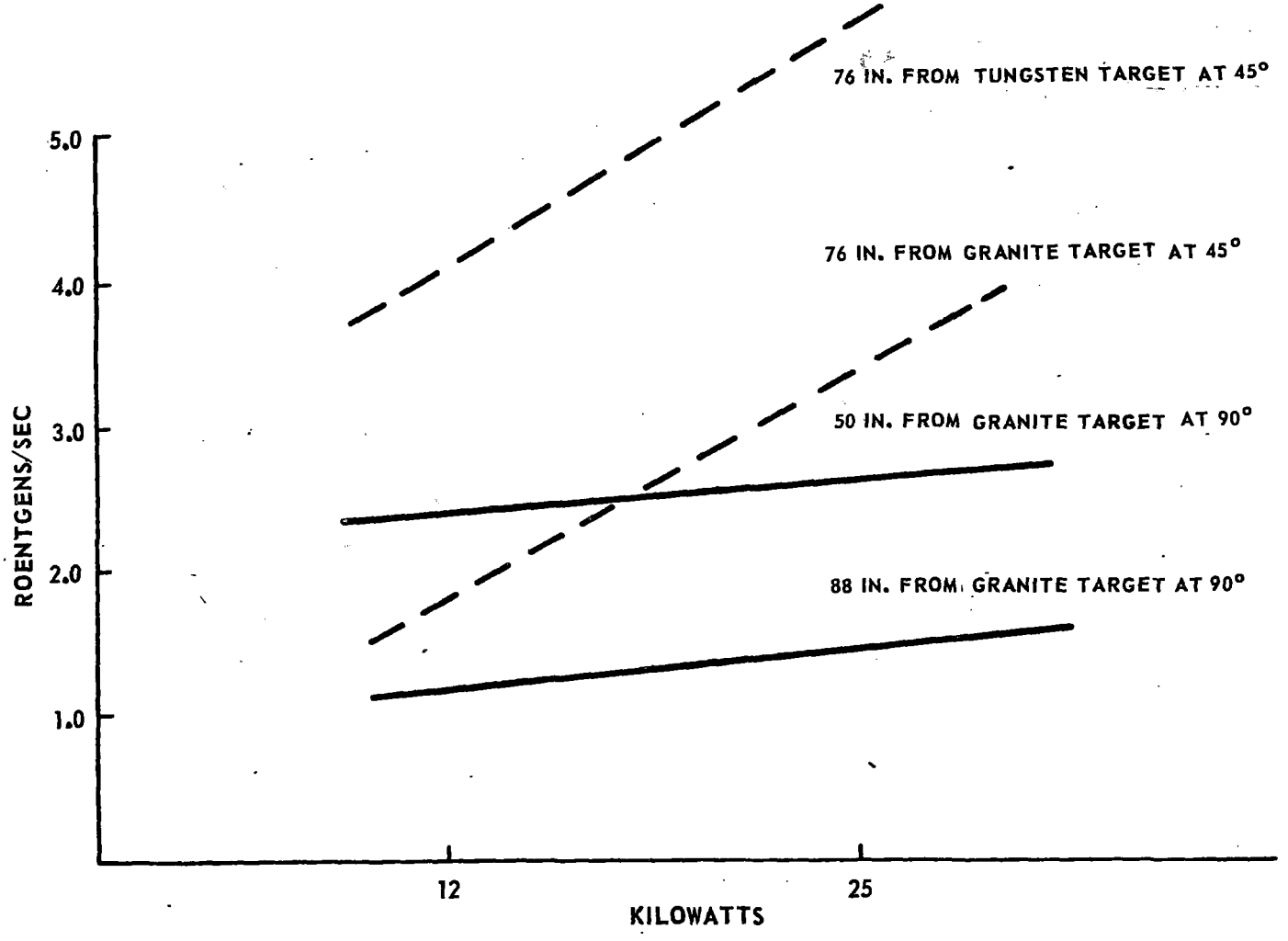

FIGURE 128 X-RADIATION VS BEAM POWER

t = thickness of barrier (inches]

μ = absorption coefficient of barrier material ($inch^{-1}$)

β = build-up factor which varies with barrier substance and thickness and also with source energy and intensity

The determination of the necessary thickness of a shielding barrier requires the solution of the above attenuation equation. Taking the natural logarithm of both sides,

$$\ln \left| \frac{1}{(1 + \beta)\, I_o} \right| = \mu t - \ln x^2. \qquad (8)$$

If it is assumed that either β is zero or that the build-up factor is compensated for by assuming an effective I_o' equal to $(1 + \beta)\, I_o$, then

$$\ln \left(\frac{I}{I_o'} \right) = - \mu t - \ln x^2, \qquad (9)$$

which states that for a given x, μt will vary linearly with $\ln I/I_o$.

No attempt is made in this report to define the final permissible radiation level. However, the Administrative Regulation for the Connecticut State Department of Health (Ref. 35), has defined the maximum permissible dose as 96 milliroentgens per week for total body exposure. This is equivalent to approximately 2.4 milliroentgens per hour for a 40-hour work week. Attentuation of X-radiation for Hamiltion Standard electron beam equipment is limited to a rate of 0.5 milliroentgens per hour in accordance with the latest Federal and Connecticut regulations.

For standard electron beam equipment, the radiation barriers are designed to attenuate radiation from impingement of the electron beam on a tungsten target which has an atomic number of 74. For rock-like materials which exhibit an abundance of silicon mixed with other elements, the equivalent atomic number is considerably less than tungsten. For Si the atomic number is 14. It therefore can be expected that the corresponding X-radiation from granite-like rock will be significantly less than that realized for tungsten (Reference Fig. 128). Thus, the values of lead thicknesses referenced above for various powers should be generous for all expected electron beam heat-assist or rock-cutting operations.

CHAPTER IV - PERFORMANCE AND ECONOMICS OF PRESENT-DAY TUNNEL BORING MACHINES

In order to evaluate the performance improvement and economics of heat-assisted tunnel boring machines, a base-line description of the performance and economics of present-day, nonheat-assisted tunnel boring machines is necessary. Such a description was developed and is presented in this Chapter. The purpose here is not to give a complete technical description of present-day rock tunneling equipment. Such descriptions have recently been given in the literature (e.g., Refs. 36 through 38). Rather, a consistent, quantitative estimate of tunnel boring machine performance and economics, as affected by rock type and strength, was sought.

TUNNEL BORING MACHINE PERFORMANCE

Information was compiled on a series of tunneling jobs, wherein both rock strength and penetration rate were recorded. These data are shown in Table 12 For each job recorded in Table 12, the machine installed horsepower was divided by the removal rate in cubic feet per hour, to yield an effective specific energy, or installed horsepower hours expended per cubic foot removed. As an actual indicator of the specific energy of rock removal this value is not very accurate. Variations in the actual removal rate during the course of a job and the operation of tunneling machines at power levels well below the installed horsepower capacity both combine to make the above indicator only roughly relate to the actual specific energy or rock removal. In any event, this parameter can be correlated with rock strength, as shown in Fig. 129.

Figure 129 incorporates a second simplification in attempting to relate rock removal power requirements only to rock hardness as measured by rock compressive strength. It is well known that rock compressive strength is an incomplete indicator of the borability of a rock type, and many correlations have been developed which depend upon parameters other than rock strength. However, most of these correlations and parameters are proprietary to the cutter bit or tunneling machine manufacturers who have developed them. Also, even if a good correlation were made based on some property other than rock compressive strength, information on such other properties is usually not available for a given job. Another problem with basing a penetration rate on any particular rock parmeter is the well-known fact that most rock masses are nonhomogeneous, and specific tests of rock properties at various points in a tunnel yield a variation in any given rock physical parameter. The use of rock compressive strength as a parameter to correlate borability of different tunneling jobs is therefore primarily a convenience. Compressive strength, while generally accepted as not being the sole indicator of borability, is at least recognized as a significant parameter by the hard rock tunneling equipment manufacturing industry.

TABLE 12

DATA ON ROCK BORING JOBS

	Diameter	Installed Power horsepower	Rock Compressive Strength psi	Penetration Rate ft/hr
A. Data from Tunneling Jobs	10'-9"	400	27,000	1.5
	10'-7"	300	5,000	18
	20'	1,000	6,000	4.0
	8'	330	15,500	4.3
	8'	330	15,500	5.0
	8'	330	15,500	3.4
	8'	330	15,500	4.2
	10'	440	22,500	1.6
	13'	540	10,000	5.0
	8'	330	13,000	5.7
	13'-8"	540	15,500	4.4
	7'	100	14,000	3.1
	12'	300	17,000	5.0
	9'-3"	100	4,000	9.0
	10'-7"	300	5,000	10.0
	18'	1,500	20,000	3.0
	12'	600	32,500	3.0
	13'-6"	600	20,000	5.0
	18'-3"	750	8,000	10.0
	11'	550	27,000	3.0
	12'	560	25,000	4.0
	11'	550	21,000	3.25
	13'	560	35,500	3.0
B. Data from Raise-Bored Shafts	4'	75	37,500	3.05
	6'	150	37,500	3.20
	5'	150	40,000	1.7
	4'-6"		38,000	2.6

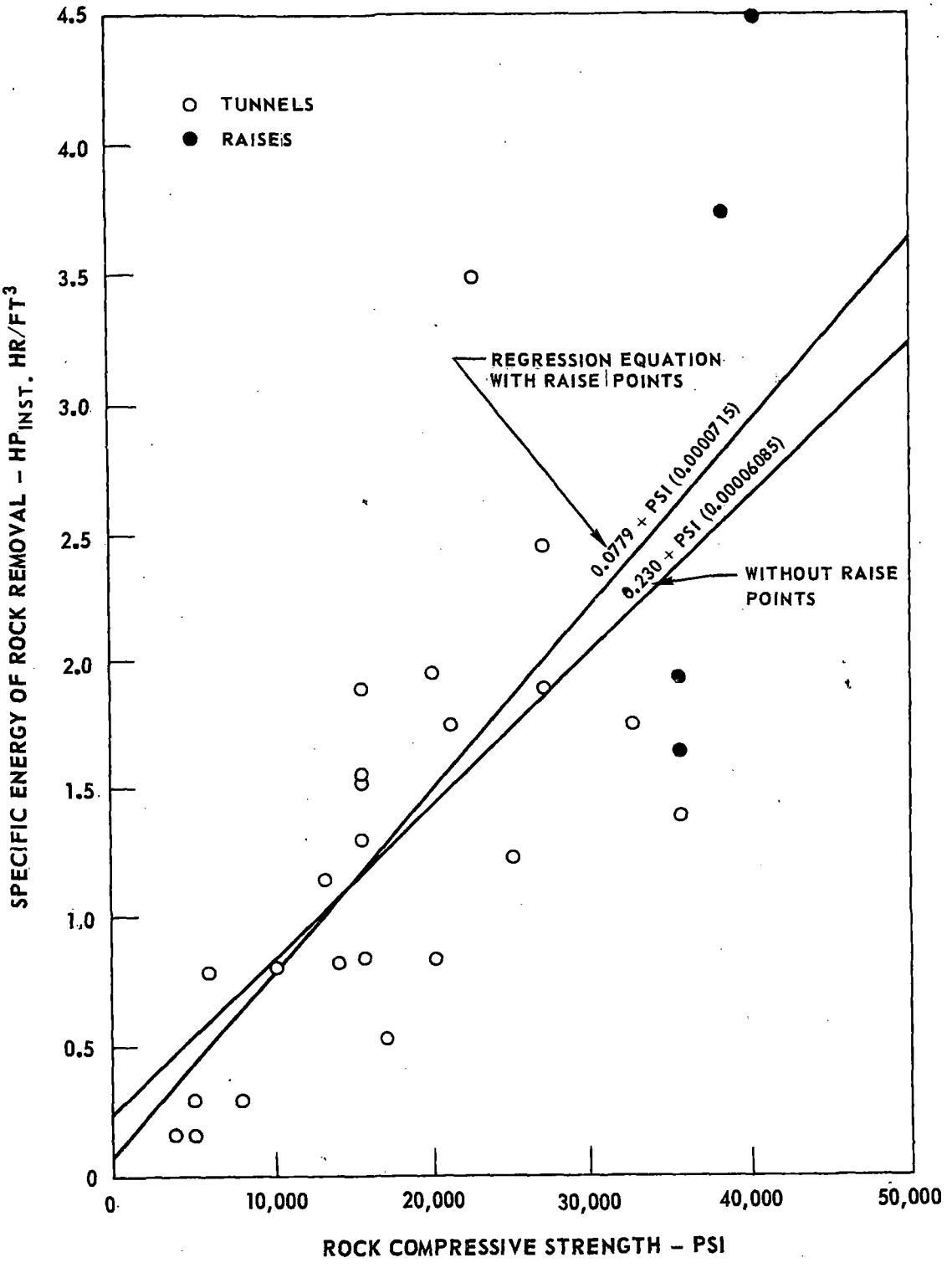

FROM DATA IN TABLE 12

FIGURE 129 EFFECT OF ROCK COMPRESSIVE STRENGTH ON REMOVAL EFFICIENCY

A regression analysis, assuming a linear relationship between installed horsepower hour per cubic foot and rock compressive strength, was performed, and the results are indicated in Fig. 129. With this relationship in hand it is merely necessary to estimate installed horsepower in order to estimate a penetration rate for a given rock strength and a given tunnel diameter. For a 10-ft-diameter tunnel, an installed power of 400 hp was assumed. As tunnel size increases the power loading per unit area of rock face is held constant, resulting in an assumed machine installed power of 1600 hp for a 20-ft-diameter tunneler. This assumption results in the penetration rate being a function solely of rock compressive strength, and not of tunnel diameter. The penetration rates derived from this analysis are shown in Fig. 130, along with a table indicating the installed tunneler power at various diameters. Although the penetration rate, as shown in Fig. 130, is not affected by the tunnel diameter, the volumetric removal rate would be affected by tunnel diameter since the speed of advance is assumed to be equivalent at any diameter for a specific rock strength. Figure 131 shows the derived volumetric removal rates as a function of rock strength.

Thus far the penetration rate only has been considered. Under the assumptions of this study, the penetration rate refers to the short-term penetration capability of a boring machine during, for instance, a single stroke of the machine, as opposed to a sustained advance rate over a 24-hr period. The latter rate takes into account machine down time due to advancing the mucking system, making cutter changes, and other routine maintenance. It is in this context that the two terms "penetration rate" and "daily advance rate" are used throughout this report.

Figure 132 gives an efficiency factor which may be used to convert penetration rate into a daily advance rate. The efficiency of a boring machine is plotted in Fig. 132 as a function of penetration rate in feet per hour. Efficiency is the total system efficiency as opposed to machine efficiency alone. It is the percentage of the time that the machine is actually working at its calculated penetration rate. Figure 132 was constructed using only three points. The rationale of this curve is simple. It implies that the faster a tunnel face is capable of being advanced, the greater the chance for a system breakdown or other delays which might contribute to a decreasing overall percentage of time spent in actual tunneling. The upper and lower limits of efficiency are more or less arbitrarily assumed to be 85% and 30%, respectively. These values were chosen because 85% efficiency appeared to be a reasonable upper limit and one which applies to a variety of successful construction operations. Thirty percent was chosen as a plausible lower limit simply because it is difficult to contemplate any tunneling or other construction operation with a lower efficiency. The third, and perhaps most important, point on which the curve is based comes from tunnel boring experience gleaned from the literature on bored tunnels, and coincidentally, the experience of Fenix & Scisson in boring the Navajo No. 1 tunnel in New Mexico with the 20-ft Betti-I tunnel boring machine. The coordinates of this point are 40% efficiency at a 4 ft/hr penetration rate.

ASSUMES SPECIFIC ENERGY REQUIREMENTS

SHOWN IN FIG. 129, AND HP/FACE AREA = $16/\pi$

TUNNEL DIAMETER	INSTALLED POWER
10 FT	400 HP
15 FT	900 HP
20 FT	1600 HP

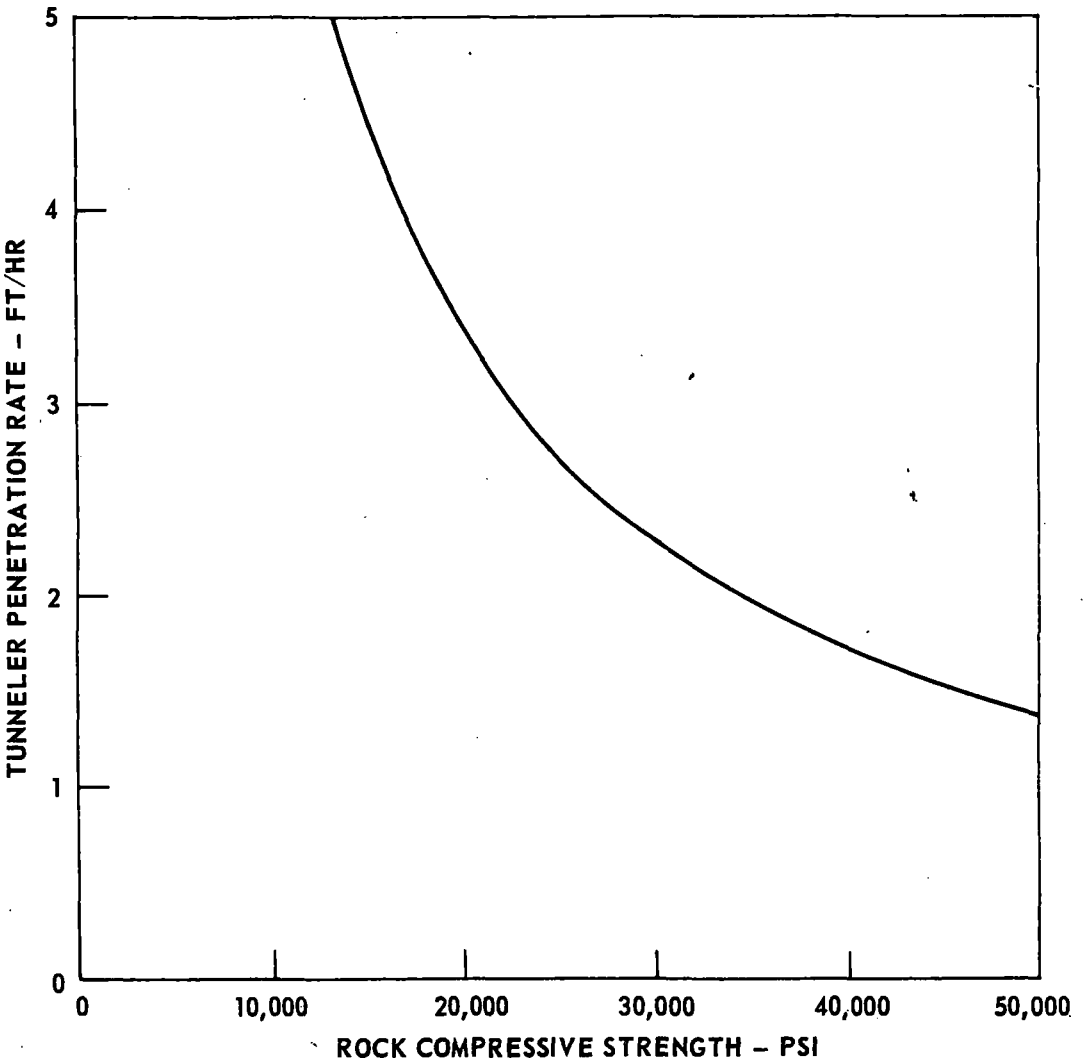

FIGURE 130 BORING MACHINE PENETRATION RATE IN HARD ROCK

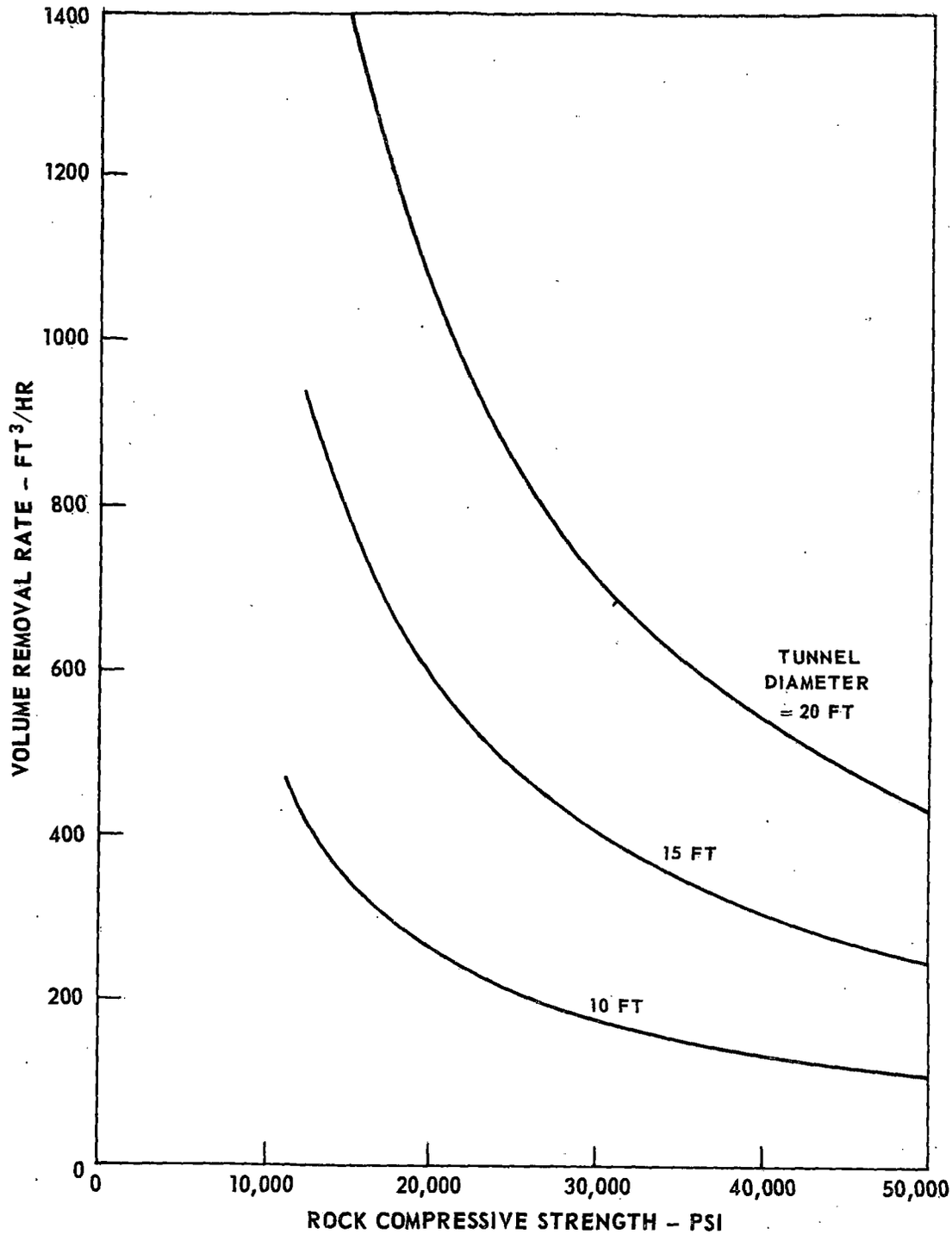

BASED ON PENETRATION RATE GIVEN IN FIG. 130

FIGURE 131 TUNNELING VOLUME REMOVAL RATE IN HARD ROCK

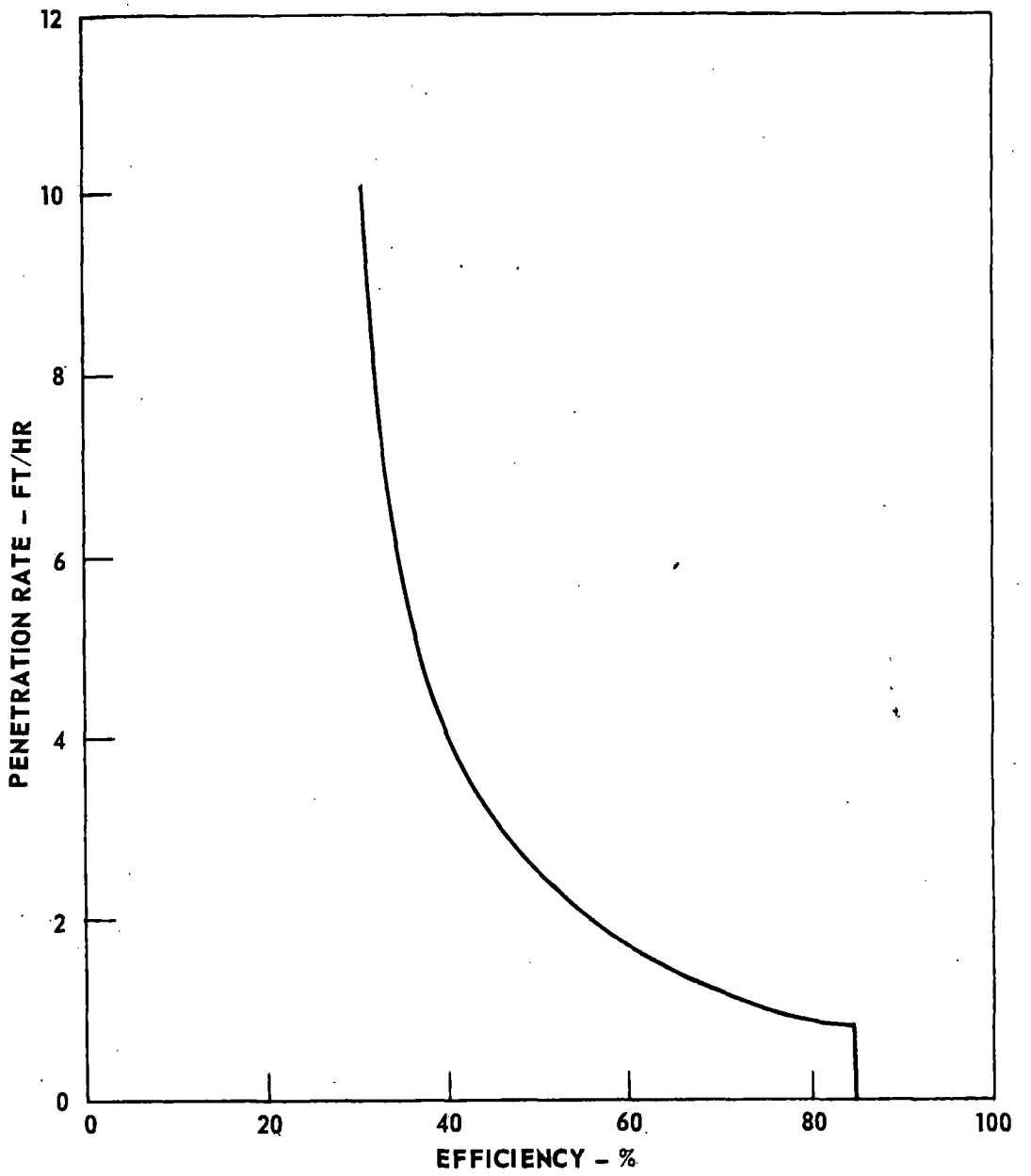

EFFICIENCY = PERCENT OF TIME SPENT BORING AT DESIGN PENETRATION RATE

FIGURE 132 TOTAL SYSTEM OPERATIONAL EFFICIENCY

By combining the efficiency indicated in Fig. 132 with the penetration in Fig. 130, a curve of expected daily advance rate as affected by the compressive strength of the rock being bored can be constructed; it is shown in Fig. 133. This curve represents the overall effect of rock strength on tunneling machine and overall excavation performance as is required in the following work on cost.

TUNNEL BORING MACHINE ECONOMIC ANALYSIS

Cost Categories

As mentioned above, the purpose of this economic analysis is to form a base-line reference with which the costs of heat-assisted tunnel boring can be compared. For this analysis the costs of machine tunneling were divided into three basic types: fixed costs, variable costs, and cutter costs.

Fixed costs are those costs which are (a) not affected by the machine rate of penetration, and (b) not cutter costs. A good example of a fixed cost is the cost of concrete lining. Strictly speaking, it is fallacious to consider this cost "fixed", since it changes with rock conditions and use of the tunnel, from one tunnel to another. However, since the expected benefits of heat-assisted boring are an increase in advance rate and/or a decrease in cutter costs, more detailed characterization of these fixed costs is unnecessary to permit evaluation of the heat-assisted boring concept.

Variable costs include all cost items whose associated total charges are direct functions of boring time. The best example (and largest single component) of this category is direct labor. If the time to excavate a tunnel with a fixed-size tunnel drew is halved, the corresponding total direct labor bill (or dollars/foot charged to labor) is also halved. All of these variable expenses are expected to be reduced by increasing machine advance rate, which can be one result of adding a heating system to a boring machine.

Cutter costs, which have been determined largely by data from cutter bit manufacturers, are considered to be a function of tunnel diameter, rock type, and rock strength. Cutter thrust is not considered specifically as a parameter; the cutter costs are assumed to be representative of present-day power loadings.

These three types of costs can be combined to estimate the total cost of a tunnel. The penetration analysis relates advance rate to rock strength (Fig. 133), so the total costs can be plotted against either of these two parameters.

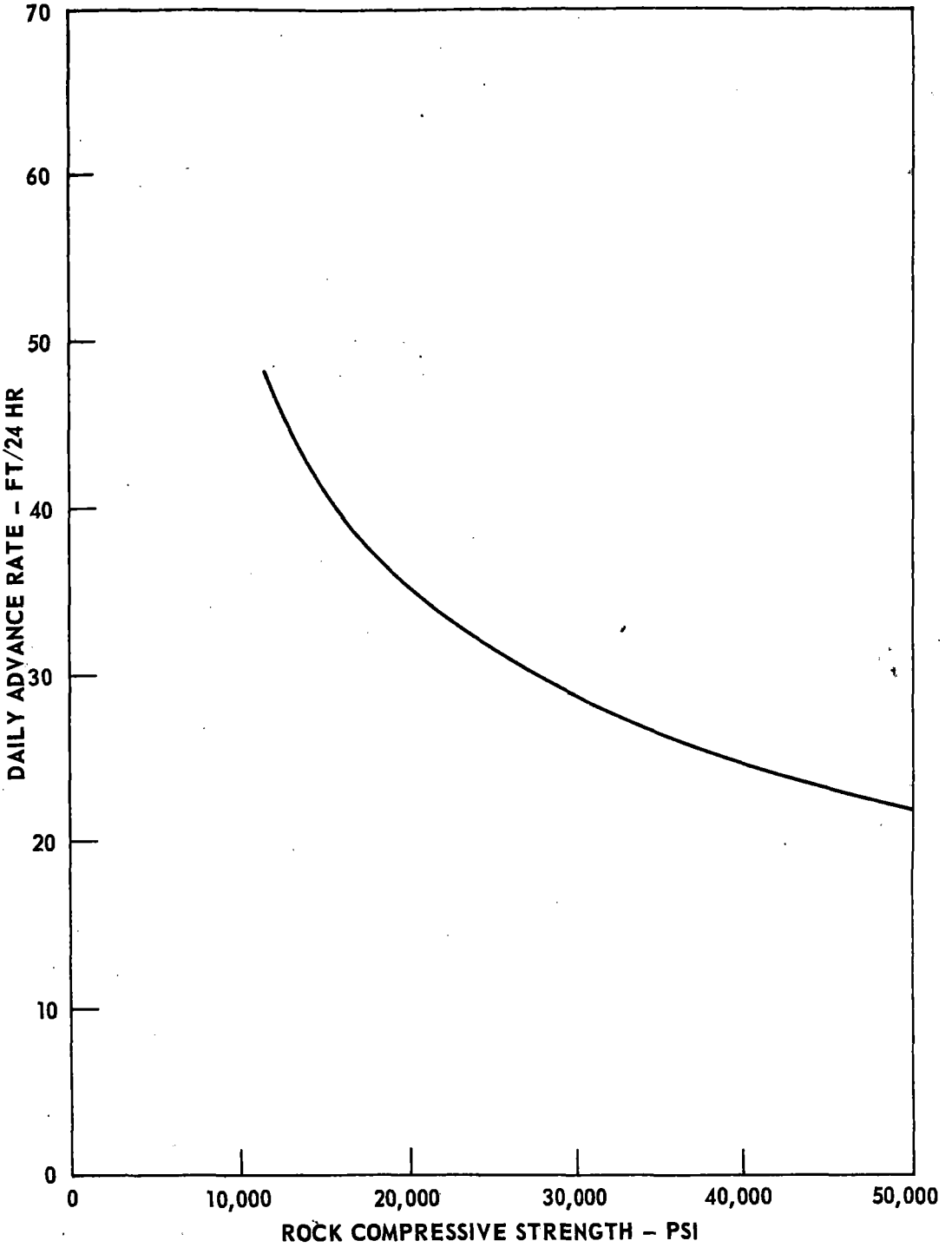

DAILY ADVANCE RATE = PENETRATION RATE (FIG. 130)
X EFFICIENCY (FIG. 132) X 24

FIGURE 133 DAILY ADVANCE RATE

Several of the assumptions made in determining and assigning the various cost components are as follows:

1. Tunnel length, and therefore contract duration, is assumed to be sufficiently long to allow complete amortization of all equipment.

2. Tunnel diameter or size is not, of itself, a specific consideration.

3. An effort is made to present the complete cost of tunneling, which involves estimation of certain items (for example, concrete) which are basically unrelated to the parameters or expected effects attributable to the introduction of heat-assisted tunnel boring.

4. Indirect costs (except for labor) and profit are variable only in a sense that they are a percentage of the total cost of all other cost components.

Initially, a complete list of the cost components of a tunneling operation was made, and the various elements were grouped according to fixed or variable costs relative to advance rate. The various cost elements were then combined as shown in Table 13, for the purpose of constructing a cost model. The establishment of the various cost categories listed in Table 13 is discussed below.

Fixed Cost Determination

Indirect Labor

Indirect labor consists of engineering, management, office employees, and similar salaried personnel required for an initial start-up period before boring begins, and for a close-out period upon completion of work. This cost item is assumed to be constant at $150,000.

Concrete

Concrete lining costs in dollars per linear foot of tunnel are shown as a function of tunnel diameter in Fig. 134. Data points upon which this curve are based were obtained from recent Bureau of Reclamation bids on 6 different machine-bored tunnels. The bid prices from the Bureau of Reclamation were escalated to September 1969 costs using Engineering News-Record cost index data. While there were few data points used to construct this curve, it is sufficiently accurate for the purpose of this study. As mentioned previously, this cost could vary with different rock conditions or ultimate tunnel use, but such variation is outside the scope of this study. Therefore the concrete cost is considered as a constant cost throughout, varying only with tunnel diameter. The values shown contain all labor, material, and equipment costs for emplacement of the concrete lining.

TABLE 13

GROUPING OF TUNNELING COST ITEMS

Fixed Cost Items	Variable Cost Items
Indirect labor	Direct labor
Concrete (includes labor, material, and equipment)	Indirect Labor
Utility lines	Haulage (includes track, equipment and operating supplies)
Other miscellaneous equipment (includes fuel, parts, and repair)	Ventilation (includes equipment, parts, and power)
	Boring machine power (includes equipment, supplies, and parts)
	Boring machine write-off
	Boring machine repair parts and operating supplies

Other Costs

Cutter Costs

All Other Indirect Costs

Profit

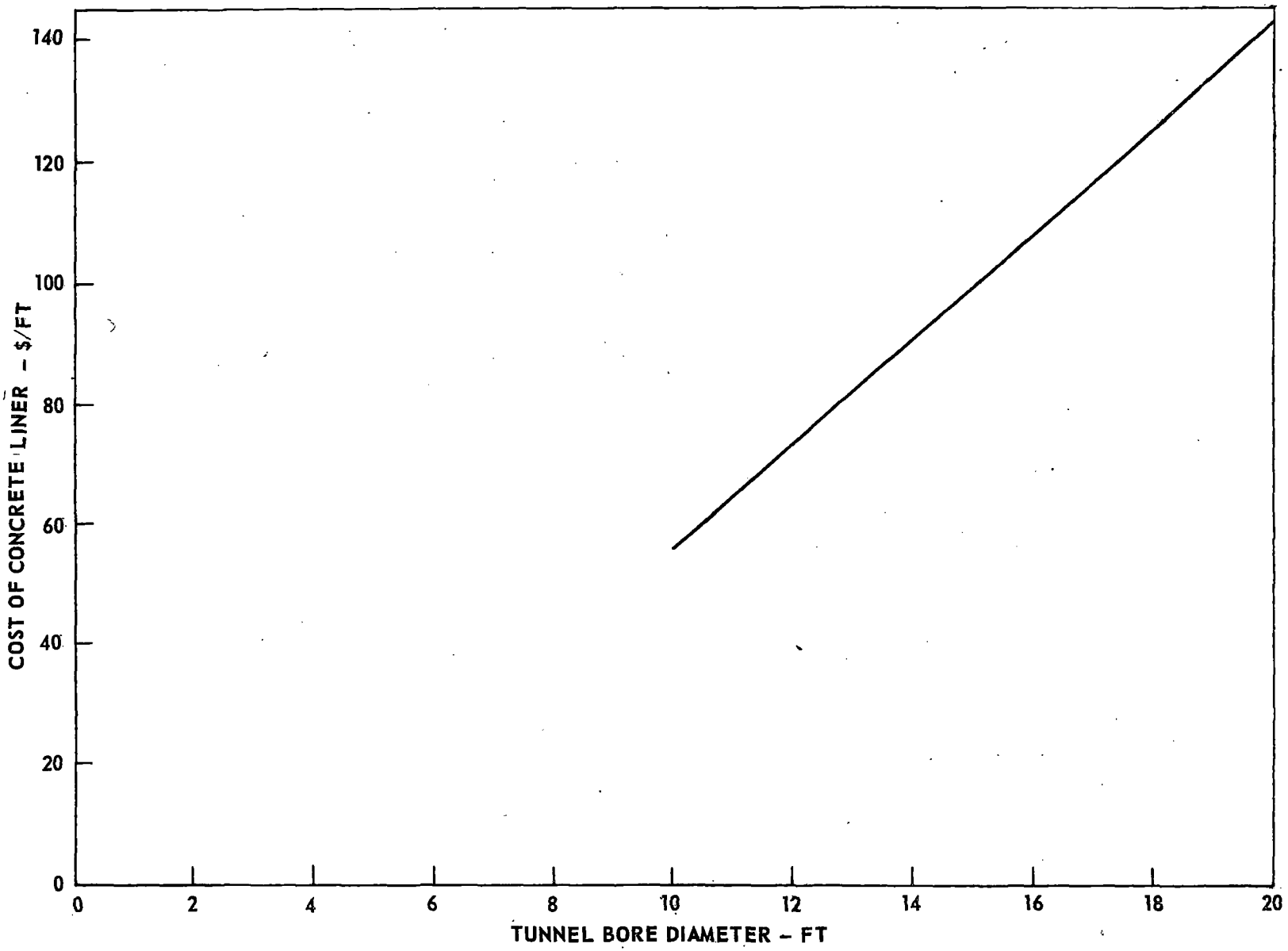

FIGURE 134 TUNNEL CONCRETE LINER COST

Utility Lines

A fixed cost item was allowed to cover all utility lines. The utilities that are covered and the values used are presented in Table 14.

Miscellaneous Equipment

Table 15 shows equipment items which are usually required in all tunnels. Muck-handling equipment and concrete equipment are not included. The average costs of miscellaneous equipment used for estimating purposes for the present study are indicated as a function of tunnel diameter on Table 15.

Boring Direct Labor

Boring labor costs are presented in Fig. 135. To construct these curves, crew requirements were determined and wage rates assigned. The figures thus developed were multiplied by 24 hr to yield a total labor cost per 24 hr. This cost was then divided by various assumed amounts of advance during a 24-hour period to produce the indicated cost per linear foot of tunnel for boring labor, as a function of the daily advance rate as shown in Fig. 135. A $6 per hour average base wage rate was used to compute the costs shown in Fig. 135. This data can therefore be converted to any other average wage rate desired by multiplying the values in Fig. 135 by the ratio of the base wage rate desired to $6.00. The wage rates discussed here include the entire labor burden, which is composed of insurance, taxes, and fringe benefits.

Boring Indirect Labor

Variable indirect labor costs (as distinguished from fixed indirect labor costs discussed earlier) are due to a complement of personnel including the project manager and all engineering, clerical, accounting, and administrative personnel. These people are all assigned a monthly salary, which is converted to a cost per foot depending upon advance rate in a manner similar to the direct boring labor. The total monthly charge for all indirect labor is $23,500 or $1066 per day. This item of cost is plotted as a function of advance rate in Fig. 136.

Haulage

It is evident that the muck haulage system must be designed for the maximum volume removal rate and not the average removal rate, since the tunnel heading may, in fact, advance for short-duration periods at very high rates, equal to the maximum penetration capability of the machine. The first step in computing a cost for the haulage system, therefore, is to determine a reference maximum rate of volume removal. Since the heat-assist method of tunnel boring is under

TABLE 14

TUNNEL UTILITY COSTS
(assuming 100% write-off)

Item Description	Cost Per Foot of Tunnel 10-ft dia	Cost Per Foot of Tunnel 15-ft dia	Cost Per Foot of Tunnel 20-ft dia
Air Lines - 6 inches	$ 1.50	$ 1.50	$ 1.50
Water Lines - 6 inches	1.50	1.50	1.50
Discharge Lines - 6 inches	1.50	1.50	1.50
Light and Communications	4.00	4.50	5.00
Misc. Electrical Items	2.50	3.00	3.50
TOTAL	$11.00	$ 12.00	$13.00

TABLE 15

TUNNEL PLANT AND EQUIPMENT
(No Muck Handling or Concrete Equipment Included)

	Description	Approx. Total Cost	Cost Per ft of Tunnel	Bases of Cost/ft (see below)	No. Req'd	Total Cost/Ft
Elect	900 cfm Air Compressor	23,000	0.58	(6)	2	$ 1.16
Diesel	600 cfm Air Compressor	27,000	0.68	(6)	1	0.68
Elect	365 cfm Air Compressor	11,000	0.28	(6)	1	0.28
	12.51 Hydracrane	35,000	1.17	(4)	1	1.17
	Pumps - Elect	2,500	0.10	(4)	10	1.00
	Pumps - Air	1,500	0.06	(4)	10	0.60
	Air Tools	1,000	0.07	(1)	25	1.75
	Weld. Machines	2,500	0.06	(8)	5	0.30
	Pickups	3,500	0.23	(1)	8	1.84
$2\frac{1}{2}$T	Flat Bed Trucks	6,000	0.24	(3)	2	0.48
	Ambulance	4,000	0.16	(3)	1	0.16
	Transformers (small)	2,000	0.04	(8)	10	0.40
	Transformers (large)	5,000	0.10	(8)	3	0.30
	Air Receivers	1,500	0.04	(6)	2	0.08
	Office Building	12,000	0.24	(8)	1	
	Warehouse Building	12,000	0.24	(8)	1	0.24
	Change Hse.	12,000	0.48	(3)	2	0.96
	Engineering Equipment	3,000	0.08	(6)	1	0.08
	Office Equipment	5,000	0.13	(6)	1	0.13
	Shop Equipment	10,000	0.33	(4)	1	0.33
						$12.18
	Fuel & Power 30%					3.65
	Repair Parts 50%					6.09
				TOTAL		$21.92/ft

Use $22/ft for 20-ft diameter
$20/ft for 15-ft diameter
$16/ft for 10-ft diameter

Basis of Cost Write-Off

No.	Tunnel Length (ft)	Useful Life (Years)*
1. 100% of cost over	15,000	3
2. 100% of cost over	20,000	4
3. 100% of cost over	25,000	5
4. 100% of cost over	30,000	6
5. 100% of cost over	35,000	7
6. 100% of cost over	40,000	8
7. 100% of cost over	45,000	9
8. 100% of cost over	50,000	10
9. 100% of cost over	55,000	11
10. 100% of cost over	60,000	12

*From: "Estimating Construction Cost," Peurifoy, 1st Edition.

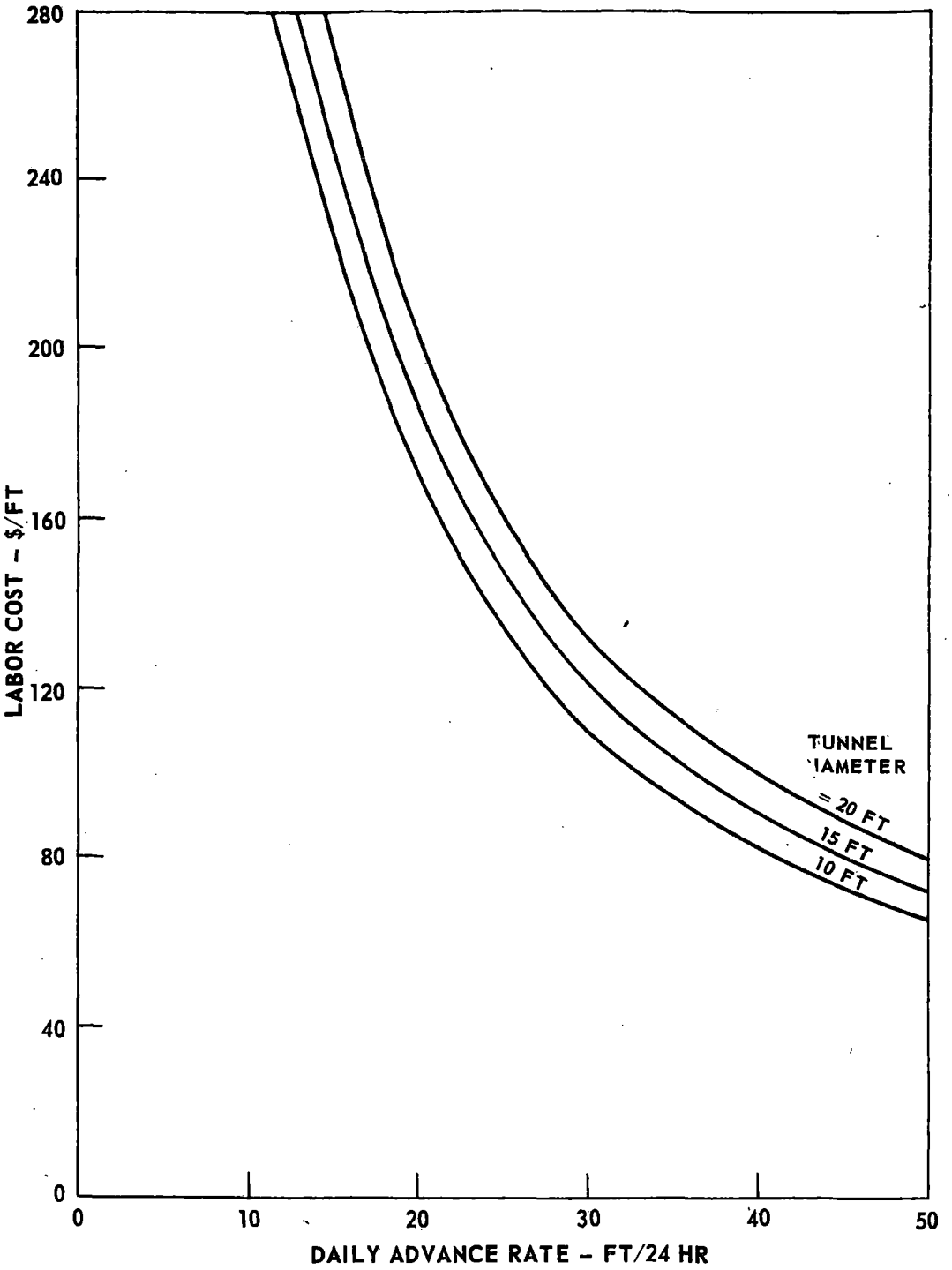

BASE WAGE RATE = $6/HR

FIGURE 135 EXCAVATION LABOR COST

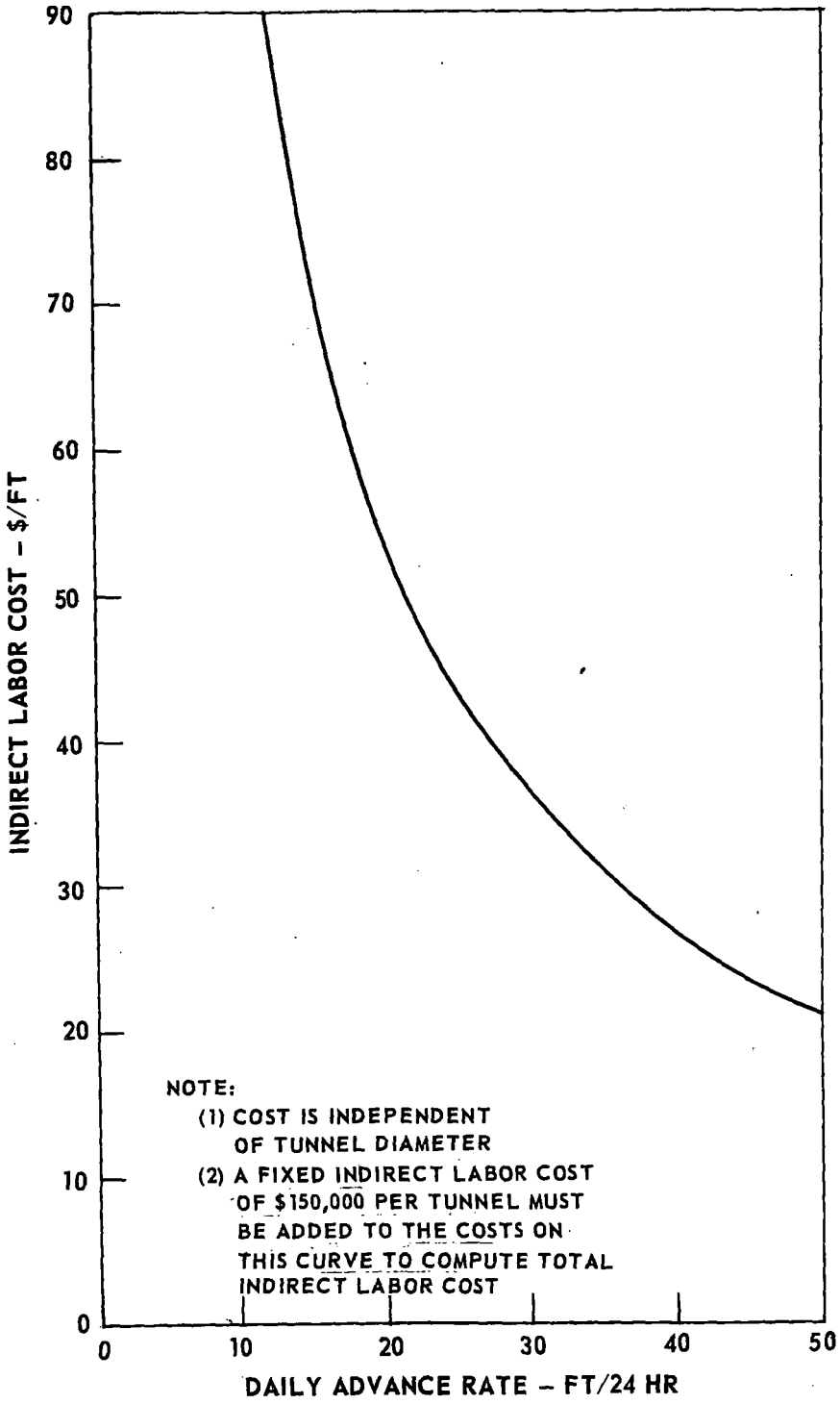

FIGURE 136 INDIRECT LABOR COST

consideration only for rocks of extreme hardness, a good basic data point would be to consider the maximum rate of penetration in a rock of 25,000 psi strength. From Fig. 131, for a 20-ft-diameter tunnel and a rock strength of 25,000 psi, the maximum volumetric removal rate would be of the order of 850 cubic feet per hour. Assuming a rock density of 168 lb/ft^3, this volumetric removal rate corresponds to roughly 144,000 lb/hr or 72 tons per hour. Therefore, a nominal haulage capacity of 70 tons of muck per hour was assumed for the 20-ft-diameter tunnel. This haulage capacity can easily be developed by three muck trains, each consisting of a 15-ton locomotive and seven 10-cubic-yard cars. For a 15-ft tunnel, the volume removal rate assumed would be 56% of that for a 20-ft diameter (see Fig. 131), so the required capacity would be approximately 39 tons per hour. This would require three trains each consisting of a 10-ton locomotive and five 7-cubic-yard cars. For the 10-ft-diameter tunnel, the maximum penetration rate would be one-quarter that of the 20-ft-diameter tunnel or 17½ tons per hour. This tunnel size would require three trains each with a 5-ton locomotive and four 5-cubic-yard cars.

Cost data developed in Ref. 2 indicate that the costs for diesel-powered and electrically powered rail haulage systems are, for all practical purposes, equal. The diesel system was chosen for the cost model. The costs developed for these three haulage systems, which are used in the parametric cost model, are given in Table 16.

Ventilation

The curves shown in Fig. 137 for ventilation costs were derived from the costs incurred on the Navajo No. 1 tunnel, which was a 20-ft-diameter bored tunnel. The ventilation system on that tunnel consisted of an exhaust system with a maximum flow rating of 35,000 cfm. The cost of this system is made up of (a) ventilation line and couplings, (b) fans and adaptors, (c) replacement blades and repair parts, and (d) power necessary for system operation. The cost of the first three items listed above is considered fixed and amounts to $13.50 per linear foot of tunnel. Power costs are considered to be variable depending upon advance rates, and are derived from a base cost of $144 per 24 hr. Costs for the 10- and 15-ft-diameter tunnels were computed from the 20-ft-diameter cost by applying a reduction factor proportional to the decrease in volume of the smaller tunnels.

Boring Machine Power

To compute the required cost for primary machine power, experience from the Navajo No. 1 water tunnel was again utilized. In addition to the energy and demand charges for power, which are variable with system advance rate, such items as mole cable, transformers, miscellaneous electrical starters, and switches are included.

TABLE 16

HAULAGE COST

	20' Diameter (70 TPH Cap.)				15' Diameter (35 TPH Cap.)				10' Diameter (17.5 TPH Cap.)			
			Cost ($K)				Cost ($K)				Cost ($K)	
	Size	No. Rqd.	Each	Total	Size	No. Rqd.	Each	Total	Size	No. Rqd.	Each	Total
Locomotive[1]	15 T	4	$37.5	$150	10 T	4	$28	$112	8 T	4	$24	$96
Side Dump Cars[1]	10cy	23	4	92	7 cy	18	2.8	50.4	5cy	15	2.5	37.5
Car Dumper[1]	--	2	2.7	5.4	--	2	2.3	4.6	--	2	2	4
Car Loader[2]	150'	1	39	39	120'	1	31.2	31.2	100'	1	26	26
Calif. Switch[3]	200'	2	16	32	180'	2	14.4	28.8	150'	2	12	24
Subtotal				$318,400				$227,000				$187,500
Dump Dozer and Miscellaneous				66,600				63,000				62,500
Total Capital Expenses				$385,000				$290,000				$250,000
Fuel and Repair Parts (50%)				190,000				145,000				125,000
Total System Variable Cost				$575,000				$435,000				$375,000
Total System Fixed Cost (50,000')				275,000				275,000				275,000
Total System Cost				$850,000				$710,000				$650,000
System Cost/Ft (50,000')	$17.00				$14.20				$13.00			
	Use $17.00/Foot				Use $14.00/Foot				Use $13.00/Foot			

(1) Cost from Figure 31 of Ref. IV-4

(2) Cost from Equipment Manufacturers' Quote ($260/ft)

(3) Cost from Equipment Manufacturers' Quote ($80/ft)

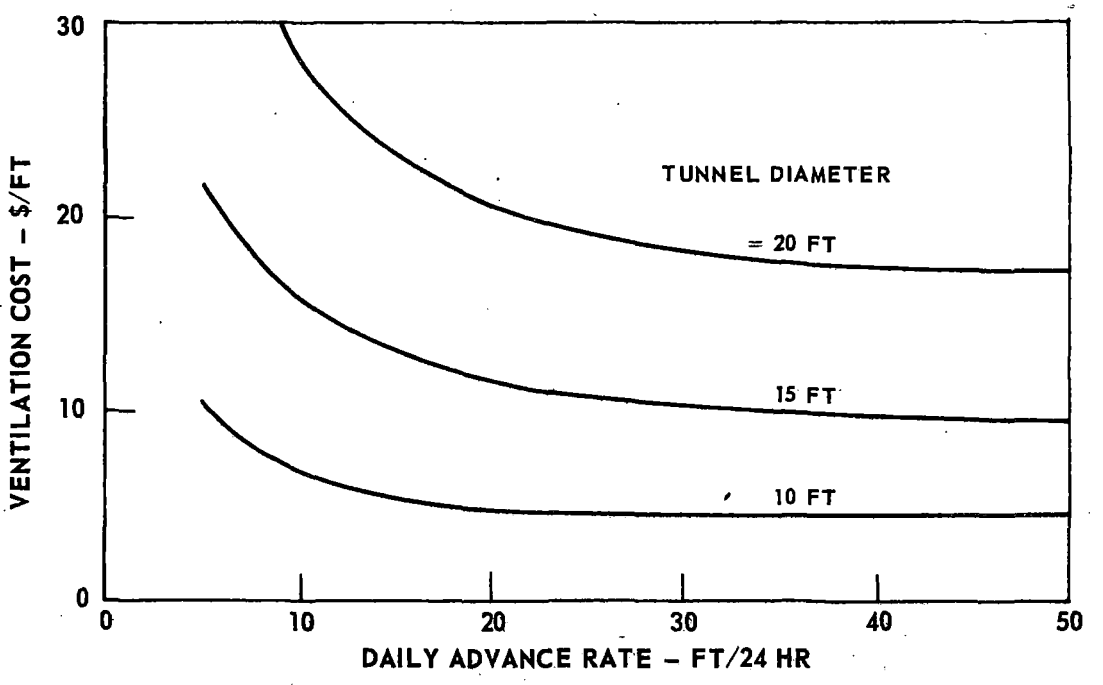

BASED ON 36,000 CFM FOR A 20 FT DIAMETER TUNNEL

FIGURE 137 VENTILATION COST

An allowance is also made for providing a vertical drilled power cable hole at intervals, and for moving and resetting substations to keep the transmission line to the machine at what is considered to be an optimum length. A fixed cost of $3.40 per foot was assigned to cover these items and was used in developing the curves shown in Fig. 138. For the determination of the energy and demand charges, installed machine power required was assumed to be 425 kw, 956 kw, and 1700 kw for 10-, 15-, and 20-ft-diameter tunnels, respectively. A basic energy cost of 2¢/kw hr is assumed. The curves shown in Fig. 138 are obtained by adding the $3.40/ft fixed cost to each of the three variable costs (for each diameter) after the variable power costs are computed for the various indicated rates of advance.

Boring Machine Write-Off

To make estimates of tunneling machine costs, a set of data on the cost of various tunneling machines was assembled and is given along with certain details concerning the machine and the job for which it was designed in Table 17. As a first attempt to correlate the machine cost to the various design parameters expected to affect the cost, a correlation analysis was done at the United Aircraft Research Laboratories. The results of this analysis indicate that machine weight is the most important single parameter influencing the cost of a tunneling machine, and that both rock strength and tunnel diameter correlate negatively with increases in machine cost. The final equation derived, using all of the assembled data in Table 17, is given in Table 18. This equation estimated all the machine costs given on Table 17 with an average error of only $38,550, as shown in Table 18.

After considering the results of this correlation analysis, a somewhat simpler approach was chosen for estimating boring machine costs for the present study. For the present study, arbitrary values of machine cost were chosen. Machine cost was set at $400,000, $600,000, and $800,000 for 10-, 15-, and 20-ft-diameter tunnels, respectively. These machine costs appear reasonable when compared to the tabulation shown in Table 17.

Using these machine costs an excavation cost due to the machine cost per linear foot of tunnel is determined by assuming a 10,000-hr operating life for the machine. Using this operating life the cost per linear foot can be approximated by the following formula:

$$\frac{\text{Machine Cost}}{[10{,}000\ \text{hr}] \times [\text{penetration rate}]} = \$/\text{ft attributable to machine cost}$$

From this formula, Fig. 139 was constructed to give machine write-off cost in $/linear ft for 10-, 15-, and 20-ft-diameter tunnels, for various daily advance rates.

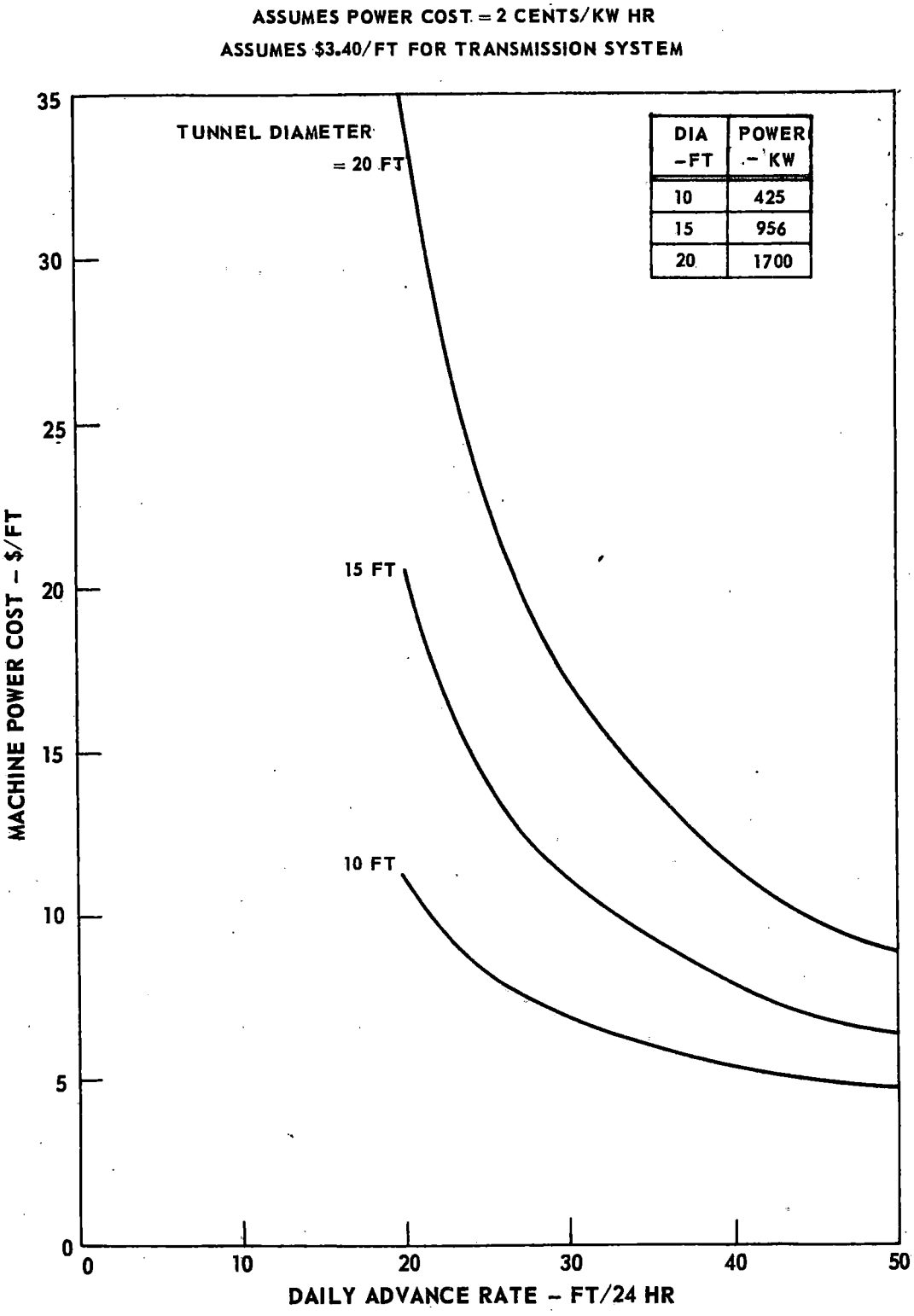

FIGURE 138 COST OF TUNNELING MACHINE POWER

TABLE 17

TUNNELING MACHINE COST

No.	Date	Tunnel Job	Diameter - ft in.	Max. Rock Compressive Strength - psi	Machine Power - hp	Machine Thrust - lb	Machine Weight - tons	Total Machine Cost - $	Total Machine Cost (Adjusted to 1969 Costs) - $
1	1964	Richmond, N.Y.	12' 0"	35,000	600	1,900,000	71	500,000	612,500
2	1960	Tasmania	16' 1"	13,000	626	750,000	115	470,000	633,600
3	1964	Azotea	13' 3"	9,200	400	450,000	85	400,000	490,000
4	1964	Navajo #1	21' 2"	7,000	1,000	1,400,000	280	1,000,000	1,225,000
5	1963	Bessan, France	7' 0"	19,000	150	300,000	36	200,000	250,200
6	1964	Frieburg, Switz.	8' 6"	7,000	200	400,000	40	220,000	269,500
7	1965	Blanco	10' 7"	5,000	300	380,000	60	340,000	406,300
8	1966	Oso	10' 7"	5,000	300	380,000	60	375,000	434,600
9	1965	Lucerne, Switz.	11' 6"	15,000	400	550,000	70	335,000	400,300
10	1965	St. Louis Sewer	8' 0"	17,000	330	559,250	30	330,000	394,400
11	1967	Mather Mine	13' 0"	10,000	540	866,000	80	540,000	608,600
12	1968	BARTD	20' 0"	23,000	825	2,200,000	215	825,000	871,200
13	1965	Phila. Sewer	13' 8"	25,000	540	866,000	80	330,000	394,400
14	1968	Chi. Sewer	13' 10"	15,000	600	890,000	85	560,000	591,400

TABLE 18

MACHINE COST ESTIMATE

Based on data in Table IV-7, and assuming a linear relationship to all variables, a "best fit" equation for machine cost is given by:

$$\text{Machine Cost} = \$384{,}473 - \$34{,}200\,(D) - \$8{,}920\,(psi) + \$99{,}500\,(P) + \$5{,}730\,(T) + \$19{,}850\,(T_o)$$

where D = diameter in feet
psi = rock strength in psi $\cdot 10^{-3}$
P = installed horsepower $\cdot 10^{-2}$
T = machine thrust in lb $\cdot 10^{-5}$
T_o = machine weight in tons $\cdot 10^{-1}$

Machine Cost Data Point (from Fig. IV-7)	Actual Cost (1969) (from Fig. IV-7)	Calculated Cost Using Above Eq.	Error
1	$ 612,500	$ 598,743	$13,746
2	633,600	614,329	19,270
3	490,000	442,595	47,404
4	1,225,000	1,231,060	- 6,060
5	250,200	213,785	36,415
6	269,500	333,300	- 63,800
7	406,300	418,414	- 12,113
8	434,600	418,414	16,186
9	400,300	426,686	- 26,385
10	394,400	379,454	14,945
11	608,600	597,795	10,805
12	871,200	870,760	439
13	394,400	441,137	- 46,736
14	591,400	595,526	- 4,125

Standard error using this formulation is $38,550.

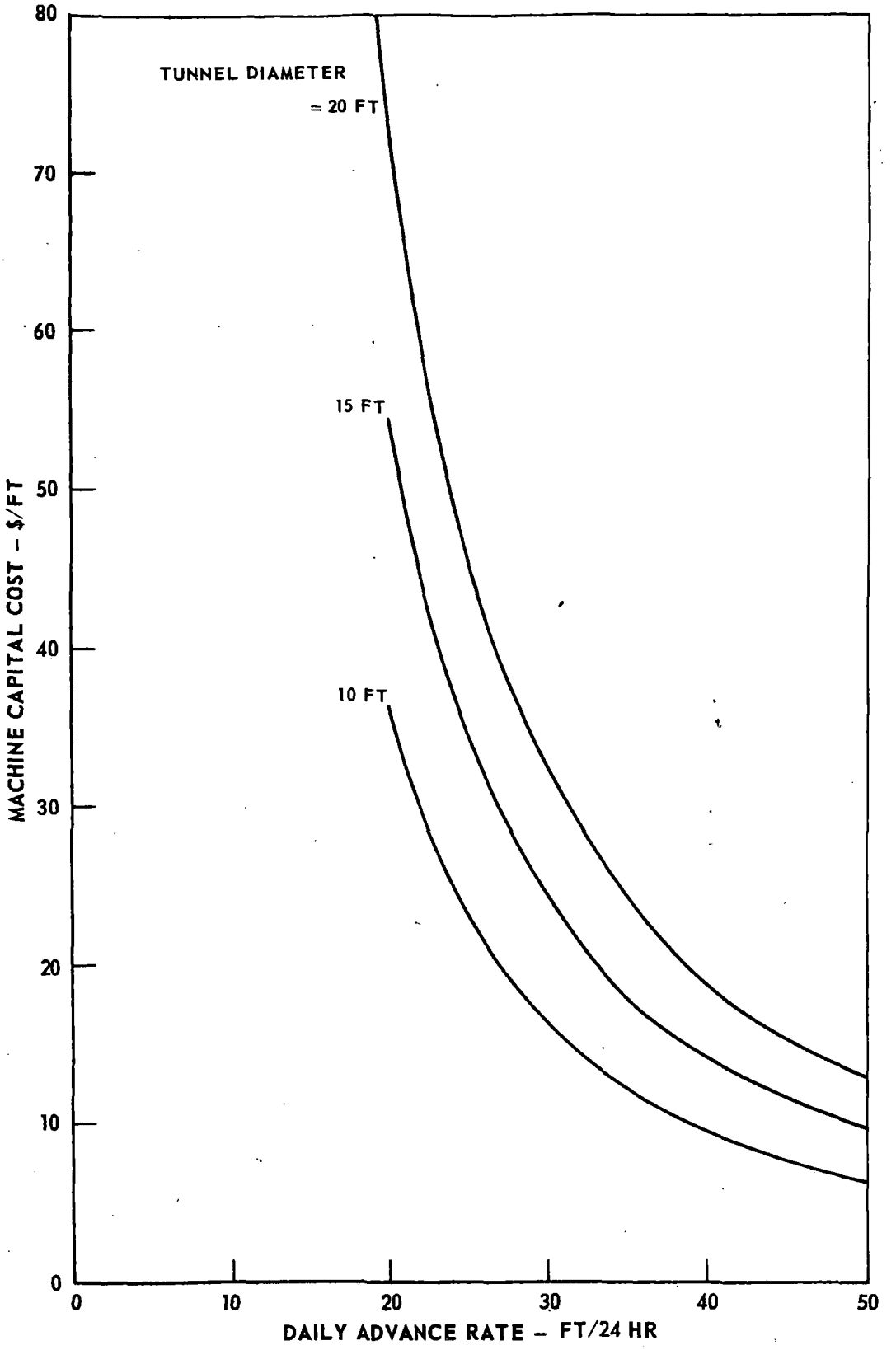

FIGURE 139 BORING MACHINE CAPITAL COST

Boring Machine Parts and Supplies

Repair parts for a boring machine can vary considerably in cost. The amount required is dependent upon many factors, ranging from manufacturing lead times to contractor philosophy of preventive maintenance to machine operator degree of skill, among other factors. For this reason, 20% of machine write-off cost was arbitrarily chosen to represent boring machine parts and supply costs. This figure appears to meet a consensus of machine manufacturers. This value of 20% does not appear on any curve but is included in summing the total costs for plotting the final total costs of conventional machine boring.

Determination of Cutter Cost

To establish cutter cost relationships, data were gathered from every available source including magazine articles, papers, contractors, and foreign machine manufacturers. Pertinent literature is cited in Refs. 36 to 38. Also, and most importantly, extensive discussions were held with manufacturers in this country of cutter bits and tunneling machines for hard rock. The tunneling machine and cutter bit manufacturers contacted are listed in the acknowledgments in the foreword.

After compiling the data available it was clear that the cost trends supported grouping hard rock into three basically different types: igneous types, sandstones, and limestones. All cutter costs were separated into these groupings, and after reducing the cutter costs to a dollars/yd^3 basis, the cutter costs were plotted vs rock compressive strength, as shown in Fig. 140. As in the case of the penetration analysis, it was recognized that rock compressive strength is in all probability not the best overall indicator of cutter cost, and perhaps not even the best single indicator of cutter cost. However, the compressive strengths are the only values of rock characteristics which are available for the various jobs on which cutter costs were reported. An attempt was made to include raise boring cutter costs in the correlations along with tunnel machine cutter costs. However, a wide discrepancy developed between the costs reported for raise boring and those reported for tunneling. In the face of this lack of correlation between these two cases, the raise boring cutter costs were neglected in compiling the final cost correlation.

Cost data on some 45 different tunnel projects were included in developing the curves shown in Fig. 140. A large portion of the data consisted of cutter manufacturers' estimates for projects rather than actual boring experience. There were 21 data points for igneous rock, 8 for sandstone, and 16 from which to develop a curve for limestone. Even after separation into the three rock classes, it was noted that a rather wide range of costs existed within each class. In order to include this variability, and not have the final costs appear to be grossly in error when compared to specific known cases, the method of presentation shown in

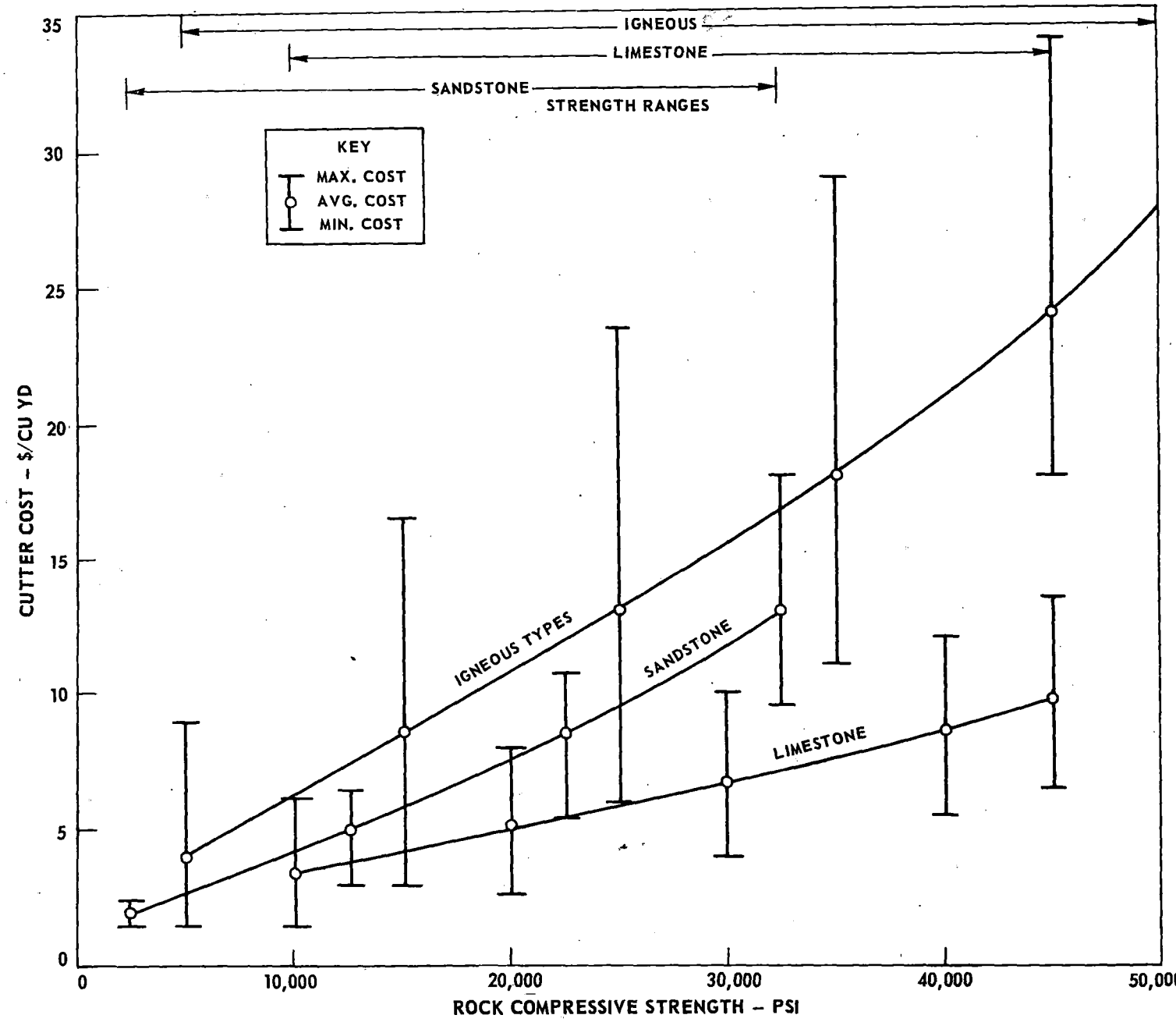

FIGURE 140 HARD ROCK CUTTER BIT COSTS

Fig. 140 was developed to show the upper and lower bounds of the cost for each rock type. For purposes of estimating cutter costs in the present study, the weighted average curves are used. The upper and lower bounds are presented merely as an indication of the extent to which these average cutter costs could be in error, when compared to a specific data point for which only rock strength and rock type are known. Based on the data in Fig. 140, curves of cutter costs per linear foot of completed tunnel can be developed for various tunnel diameters and rock types.

In plotting the cutter cost data, the same problem developed which caused concern in the previously discussed penetration rate curves. Specifically, far too great a percentage of the data upon which the projected curves are based lies in the range of 15,000 to 25,000 psi rock compressive strength, and vary few data points were available in the range of rock strength greater than 25,000 psi. For this reason, it must be realized that in the range of interest for the present study (i.e., rock strenght greater than 25,000 psi) the cost trends are primarily extrapolations of past experience in boring rocks whose strength is on the lower threshold of this range.

Other Cost Components

To the three types of cost mentioned above (variable, fixed, and cutter costs) were added other indirect costs and profit to determine a total tunnel excavation cost. All other indirect costs were assumed to be equal to 5% of all the previously listed fixed and variable costs. This amount, when added to the indirect labor costs, amounts to approximately 20% of the direct cost total, which is considered to be a feasible percentage for indirect costs in the type of work under consideration. An arbitrary figure of 10% of all cost is also included in the total cost chart for profit which, again, is considered reasonable for tunneling operations.

Cost Summary and Total Cost Charts

The preceding cost data can be summarized to determine the total expected cost of machine tunneling as a function of tunnel diameter and rock type and strength. A sample of a form used for calculating the total costs based on this method is shown in Fig. 141. Calculations using this form were made to calculate the total costs of tunneling in igneous rock for tunnels of 10-, 15-, and 20-ft diameter, and for various rock strengths. The results of these calculations are shown in Figs. 142 through 144, which indicate the realtive important of the various cost categories discussed above. The 10% profit mentioned above is not included in these curves.

(DOLLARS PER LINEAR FOOT)

CALCULATIONS FOR _____ FOOT DIAMETER TUNNEL	ROCK COMPRESSIVE STRENGTH (PSI)																				
	45,000			40,000			35,000			30,000			25,000			20,000			15,000		
	DAILY ADVANCE RATE (FT/DAY)																				
FIXED COST																					
INDIRECT LABOR (50,000' TUNNEL) ($3/FT)																					
CONCRETE																					
UTILITIES																					
MISCELLANEOUS EQUIPMENT																					
SUBTOTAL FIXED COST																					
VARIABLE COST																					
DIRECT LABOR																					
INDIRECT LABOR																					
SUBTOTAL LABOR																					
ACCUMULATIVE SUBTOTAL																					
HAULAGE																					
ACCUMULATIVE SUBTOTAL																					
VENTILATION																					
ACCUMULATIVE SUBTOTAL																					
POWER																					
ACCUMULATIVE SUBTOTAL																					
BORING MACHINE																					
MACHINE PARTS (20% MACHINE COST)																					
ACCUMULATIVE SUBTOTAL																					
CUTTERS																					
ACCUMULATIVE SUBTOTAL																					
5% INDIRECT COSTS*																					
ACCUMULATIVE SUBTOTAL																					
10% PROFIT																					
TOTAL COST																					
* INCLUDES ALL INDIRECT COSTS BUT LABOR WHICH IS COVERED ABOVE.	LS	SS	IG	LS	SS	IG	LS	SS	IG	LS	SS	IG	LS	SS	IG	LS	SS	IG	LS	SS	IG

LS = LIMESTONE SS = SANDSTONE IG = IGNEOUS

FIGURE 141 FORM FOR CALCULATING HARD ROCK TUNNELING COST

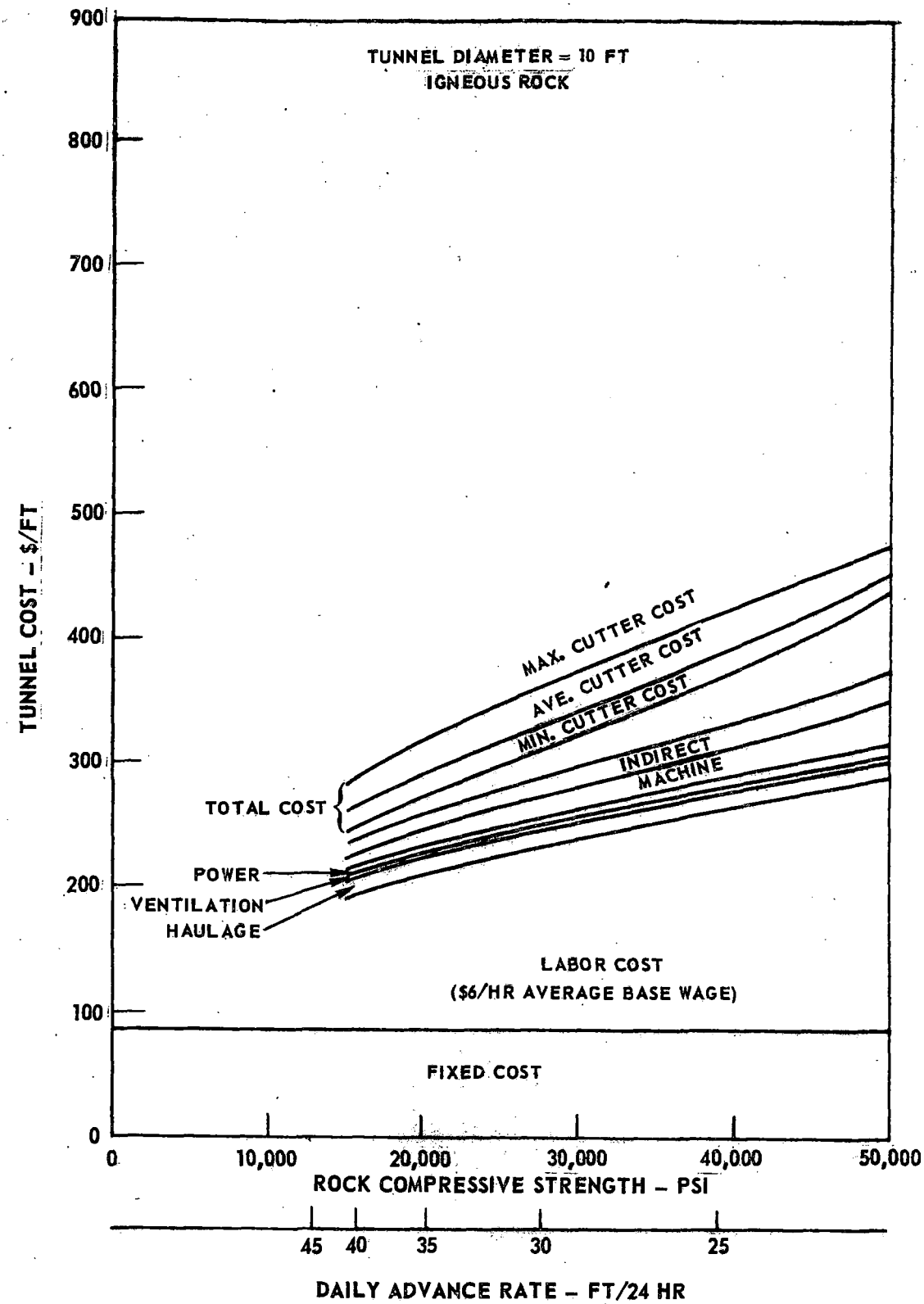

FIGURE 142. HARD ROCK TUNNEL EXCAVATION AND LINING COST

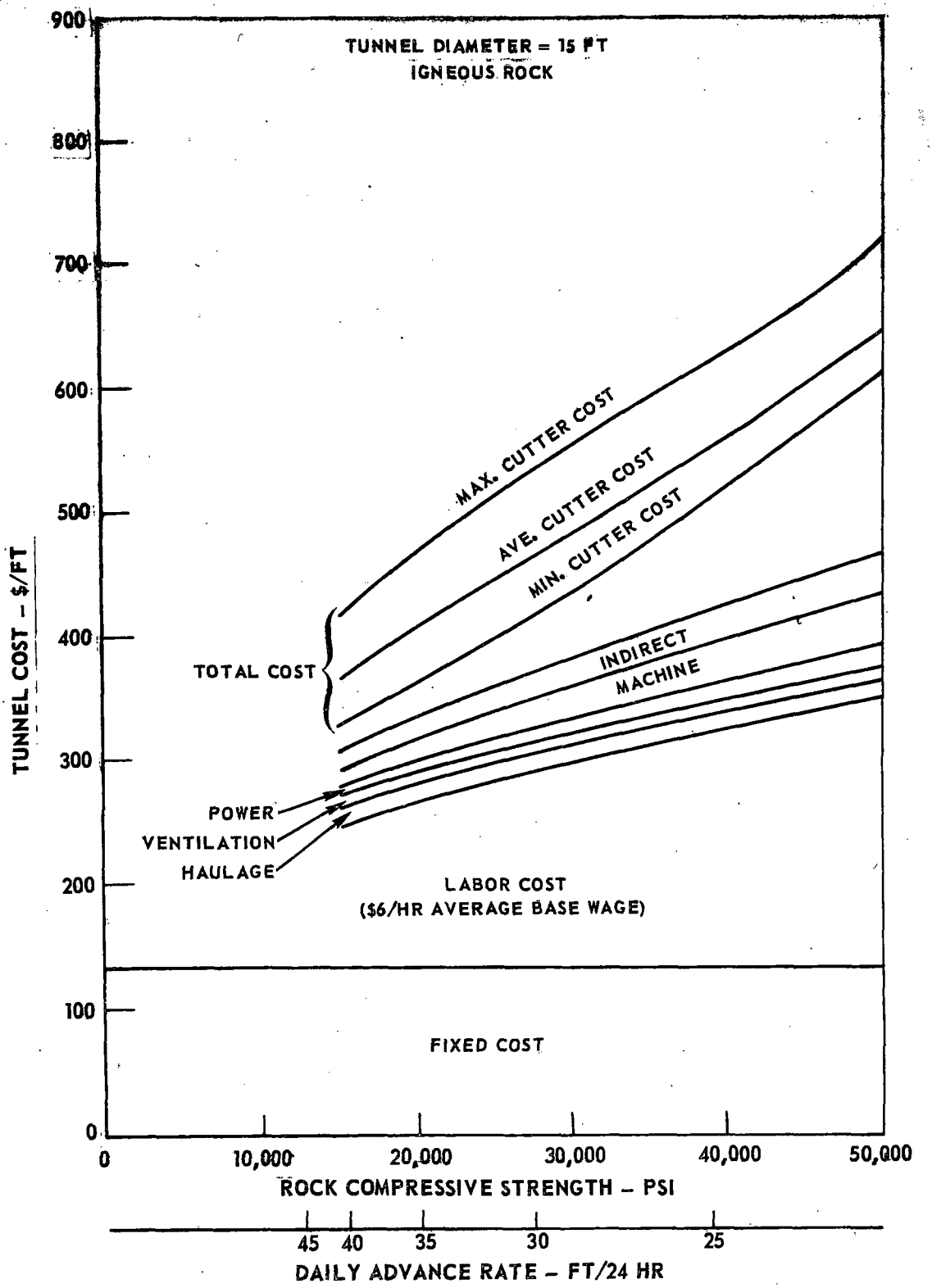

FIGURE 143. HARD ROCK TUNNEL EXCAVATION AND LINING COST

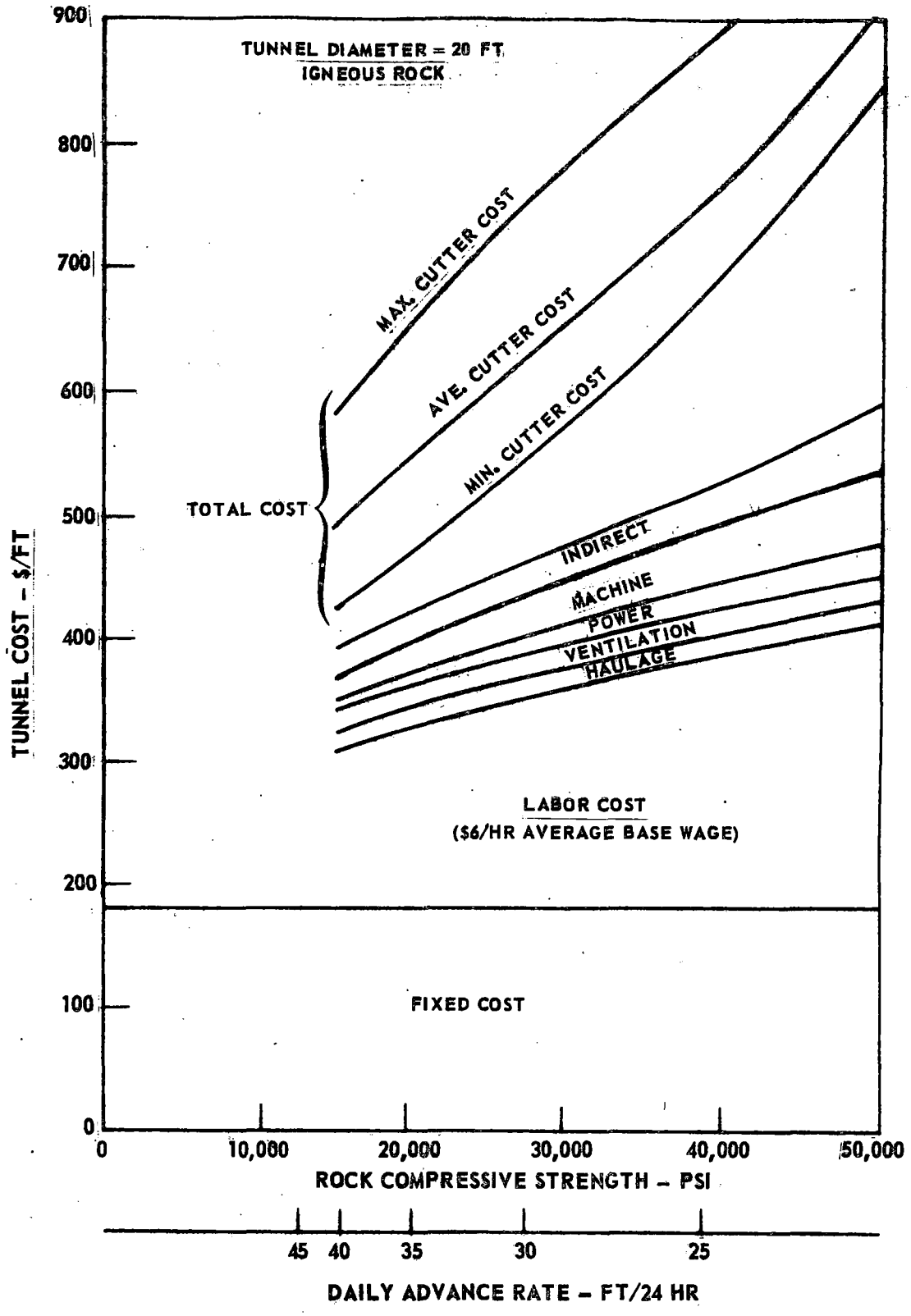

FIGURE 144. HARD ROCK TUNNEL EXCAVATION AND LINING COST

All of these curves are plotted against both daily advance rate and rock strength. This double scale is included as a reminder that the cutter costs were collected and correlated as a function of rock strength, while all the other variable costs were calculated as a function of daily advance rate. Thus, to plot the total costs on a single curve, some relationship between rock strength and daily advance rate is required. This relationship is found in the penetration analysis, as summarized in Fig. 133, which defines the relationship between the two horizontal axes on Figs. 142 to 144 . Use of a different penetration analysis would give a different relationship between cutter costs and all other costs.

The high percentage of the total costs in cutter costs is of interest. As rock strength increases, the cutter costs increase, both absolutely and as percentages of total costs. Also, the cutter costs become more significant for large-diameter tunnels. For 10-ft diameter tunnels, the average cutter costs shown increase from 10 to 15% of the total cost with increasing rock strength. For a 15-ft-diameter tunnel, the average cutter costs account for 15 to 25%, while for a 20-ft-diameter tunnel 18 to 30% of the total cost is in the cutters.

Labor cost is also a large percentage of total cost; it increases as the rock strength increases (advance rate decreases). In contrast to the cutter costs, labor becomes a decreasing percentage of total costs at larger tunnel diameters. Thus, assuming average cutter costs, direct labor charges run from 37 to 42% of the total cost for a 10-ft-diameter tunnel, but are only 23 to 24% of the total cost for a 20-ft-diameter tunnel.

These results are of interest for the evaluation of heat-assisted tunneling, since the application of heat is expected to result in lower cutter costs and/or higher advance rates in very hard rock.

Total costs for sandstone and limestone are not shown. The curves for these rocks would be similar to those shown here for igneous rocks, but with a lesser percentage of cost in the cutter cost, as indicated by Fig. 140. It should be kept in mind that these total costs, which were derived purely as a yardstick against which to measure the effects of adding heat to a tunneling machine for working in very hard rock, are considered to be representative of present-day tunneling technology only in a very rough sense. They can in no way be considered to be cost estimates for any actual tunnel and will, in all probability, require considerable cost updating, even for generalized analyses, within a few years. However, they are believed to represent fairly the characteristics of tunneling costs in hard rock with present-day mechanical tunnel boring equipment.

CHAPTER V - ALTERNATE MODES OF THERMAL ROCK FRACTURE

CONSIDERATION OF VARIOUS MODES OF KERFING

A basic tenet of promoting rock fracture with the heat-weakening mode of using thermal energy, as discussed in the Introduction to this report, and expounded upon in Chapter II, is to avoid melting of the rock surface. The importance of avoiding melting is due to the expected waste of thermal energy in changing the phase of the rock, as well as possible increases in the rock reflectivity in its melted state. During the course of the study of heat-weakening a basically different method of using heat energy for tunneling was conceived; to increase the power density of the heat so as to cause melting of the surface, thereby creating a slot, or kerf, in the rock surface. The basic concept further assumed that making such slots would then allow mechanical energy to be used in such a fashion that rock could be broken in tension rather than in compression. If such slots could be made sufficiently narrow, the total amount of energy used to melt the rock in the slots might be the same order of magnitude as, or even less than, the amount of heat energy needed to weaken the rock enough to allow an equivalent mechnical penetration rate. In considering all of the possibilities of using such a kerfing scheme, three different ways of utilizing a melted kerf for penetrating very hard rock have been defined. These three different modes of using thermal energy for kerfing are indicated in Fig. 145 as (a) low-depth kerfing, (b) keep kerfing, and (c) pure kerfing.

Low-Depth Kerfing (Mode A)

In low-depth kerfing a shallow kerf is provided between the disk cutter paths, thus providing an open channel to which the disks can break the rock spalls. The existence of the small open kerf can hopefully replace some mechanical cutters, so that the mechanical cutter spacing could be increased with no loss in overall advance rate. As indicated on Fig. 145, the spall size with this method of kerfing would be expected to be similar to that with regular mechanical tunneling (i.e., no heat added). Schematically, a heat-assisted boring machine using kerfing in this mode would be exactly similar to the heat-assisted tunneling machines discussed in Chapters II and III. The basic mode of rock fracture would be the same as in present-day (nonheat-assist) tunneling machines; the heat input would simply be concentrated in a sufficiently great power density to cause melting and penetration of the rock surface, rather than merely warming the rock surface as is done in heat-assisted tunneling.

d/w = KERF DEPTH TO WIDTH JUST PRIOR TO MECHANICAL BREAKAGE, OR REMOVAL

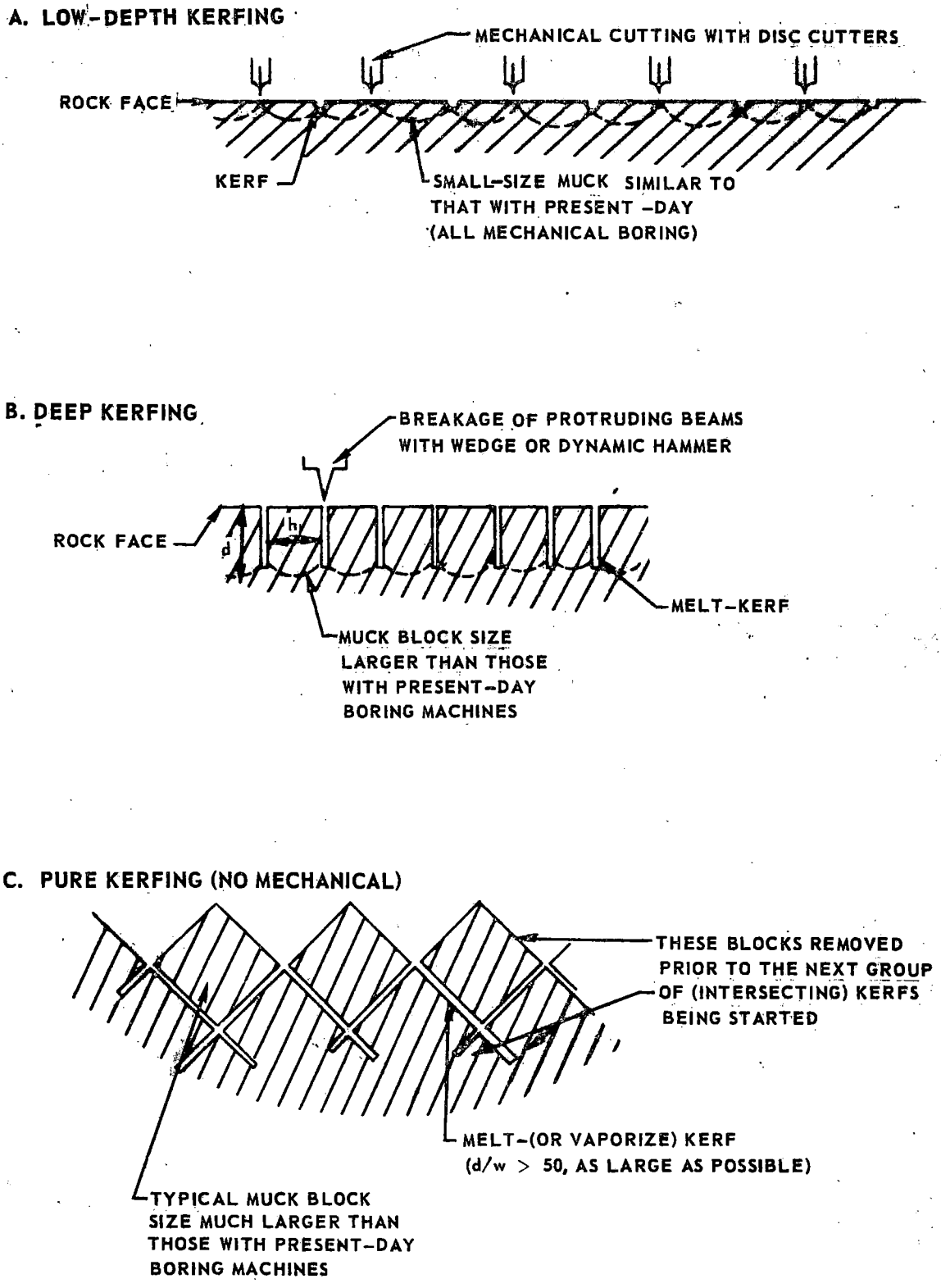

FIGURE 145 MODES OF KERFING

Deep Kerfing (Mode B)

The second mode of using heat energy to make slots in the rock, which is referred to as the keep kerfing mode in Fig. 145 , involves making penetration by melting to a significant depth into the rock such that the rock is left in bars or annuli protruding from the rock face with a height the same order of magnitude as the distance between kerfs (d/h in Fig. 145 = 1.0). The basic advantage of the keep kerfing schemes is that the rock can then be broken off in relatively large blocks, either by forcing a wedge between the protruding rock ridges or by hitting the rock with a dynamic impact device. This form of kerfing is similar to that proposed, on a much larger scale, for tunneling systems involving flame-jet spalling in Ref. 2. The characteristic muck block size with this type of kerfing would be substantially larger than the chips produced by present-day mechanical boring. Substantially less mechanical energy would be used at the same advance rate due to the fact that the rock would be broken in a more efficient manner.

Pure Kerfing (Mode C)

The third manner of employing the kerfing phenomenon in a thermal tunneling machine would be to completely dislodge the rock by means of thermal energy without any mechanical breakage required. One way of arranging the kerfs so this would occur is shown under the mode of pure kerfing in Fig. 145. Typically the block sizes with this mode of kerfing would have to be somewhat larger than for either of the two previous modes, and the melt cuts would have to be very narrow relative to their depth for the energy requirements not to become excessive. On the other hand, this third mode of kerfing does offer the possibility of penetration without any mechanical force other than that necessary to remove the isolated blocks and is therefore of interest to study as an end point in the direction of reduced mechanical effort for tunneling.

ANALYSIS OF KERFING MODES

Basic to all of the forms of thermal kerfing discussed above is the removal of material from a slot by thermal energy impinging on the rock. Therefore to discuss any of these forms of kerfing some basic information was developed on the energy requirments for melting rock. Also of increasing interest in going from modes A through C is the feasible kerf geometry (ratio of depth to width of kerf) which can be made in rock with highly concentrated thermal energy impinging on the rock. To answer these questions some basic critical literature surveys and experiments were undertaken.

Literature Survey of Energy Requirements for Rock Kerfing

The results of pertinent experiments reported in the literature show energy consumption values of 4210 (Ref. 39) and 3860 (Ref. 40) Btu/lb of rock removed when making a slot in the rock face by the impingement of thermal energy. However, design values of 567 and 167 Btu/lb are mentioned in Ref. 39, of the energy required to heat and melt siliceous minerals is reported in Ref. 41 to be roughly 677 Btu/lb. These values of energy requirements cover an exceedingly wide range. Therefore a literature survey was made to determine both the sensible heat and latent heat of fusion of typical igneous rocks in order to form a data base on which to estimate the energy required to cut a kerf in igneous rock with thermal energy.

Since the composition of various igneous rocks is never the same and since the rock thermal characteristics of interst arising from geologic studies do not include energy balances, there is very little data published on the latent heat of rocks. Data on viscosity, density, and thermal conductivity were found in Ref. 12. . Also, data on melting points of minerals and of rocks were found in Ref. 42 and are shown in Tables 3 and 19. One obstacle to the development of a set of thermodynamic data for typical igneous rocks is their wide range of chemical composition, which displays such a diversity of crystalline phases that new forms are still being discovered (Refs. 43 and 44). It is therefore futile to determine a consistent set of thermodynamic data for any "typical" igneous rock type.

However, some thermodynamic data were obtained from Ref. 45 for several common constituent minerals of igneous rock. These data, shown in Figs. 146 through 148, indicate that the heat required to raise the minerals from room temperature to their melting point does not vary (among the various minerals) by more than a factor of 2 (i.e., 500 to 900 Btu/lb). In addition, if the sensible heat above the melting point of the lowest-melting constituent is ignored, and all melting is assumed to take place at the same temperature, the resulting energy requirement for heating and melting of each constituent is close to 600 Btu/lb. Therefore, this value was used for preliminary estimates of the minimum kerfing energy requirements. The use of the value of 600 Btu/lb corresponds to an assumption that the mixture will melt at a temperature near the melting point of the lowest-melting component, that the heat of solution is small enough to be negligible, and that the melting process will be in thermochemical equilibrium.

The assumed energy requirment of 600 Btu/lb compares favorably with the value reported in Ref. 41 (677 Btu/lb) and the first value recommended as a design value in Ref. 39 (567 Btu/lb). The discrepancy with the reported experimental values of 4210 and 3860 Btu/lb (Refs. 39 and 40 for laser and electron beam cutting, respectively) can perhaps be explained by the fact that in both the

TABLE 19

MELTING POINTS OF VARIOUS IGNEOUS ROCKS

Rock	Temperature °C	
	Softens	Becomes Fluid
Granite, Predazzo	1150 - 1160	1240
Monzonite, Predazzo	1115 - 1125	1190
Lava, Vesuvius	1030 - 1060	1080 - 1090
Lava, Etna	962 - 970	1010 - 1040
Basalt, Remagen	992 - 1020	1060 - 1075
Leimburgite	995 - 1000	1050 - 1060
Phonolite	1060	1090
Nepheline Syenite	1040 - 1060	1060 - 1100

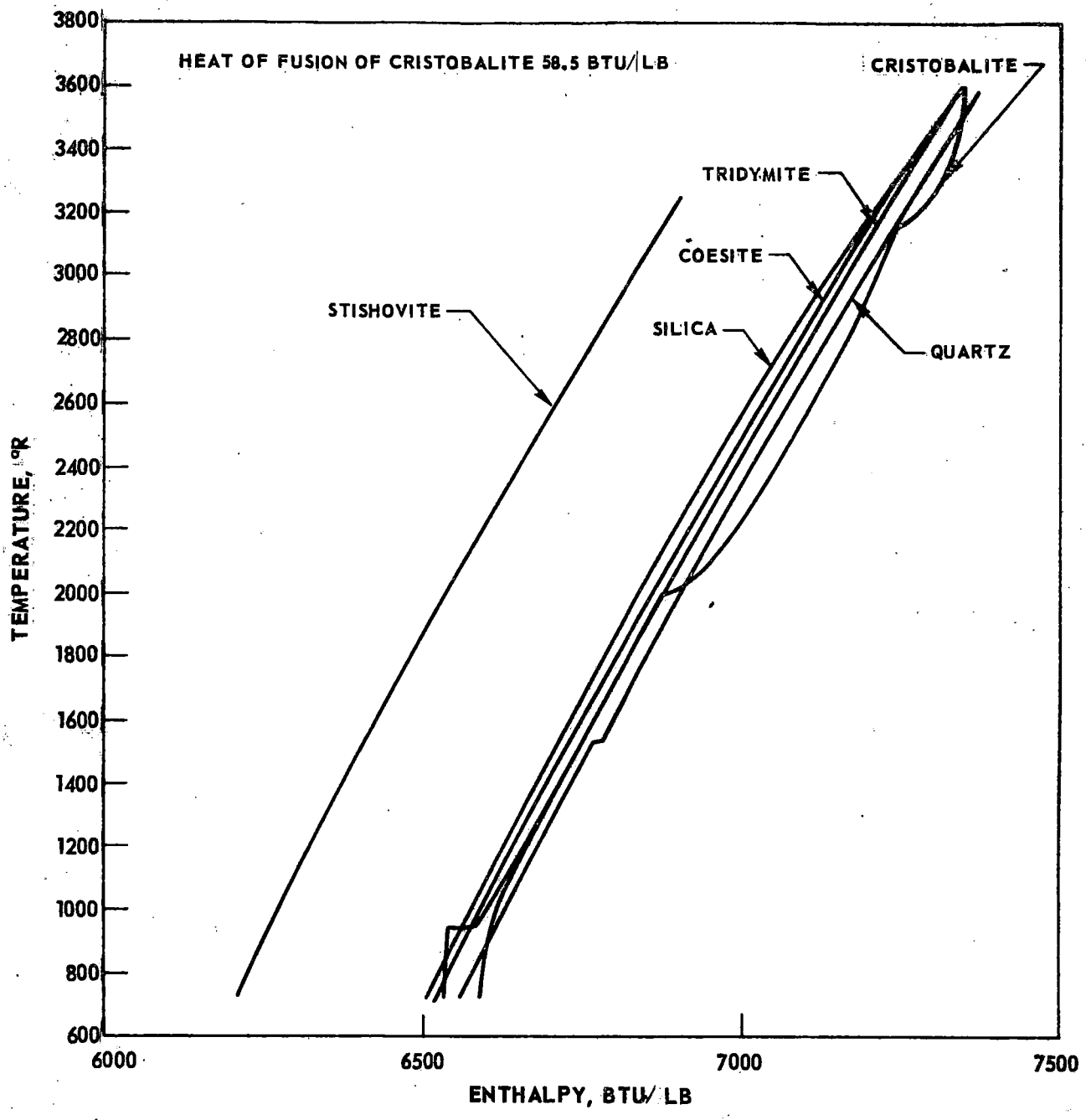

FIGURE 146 ENTHALPY OF VARIOUS FORMS OF SiO_2

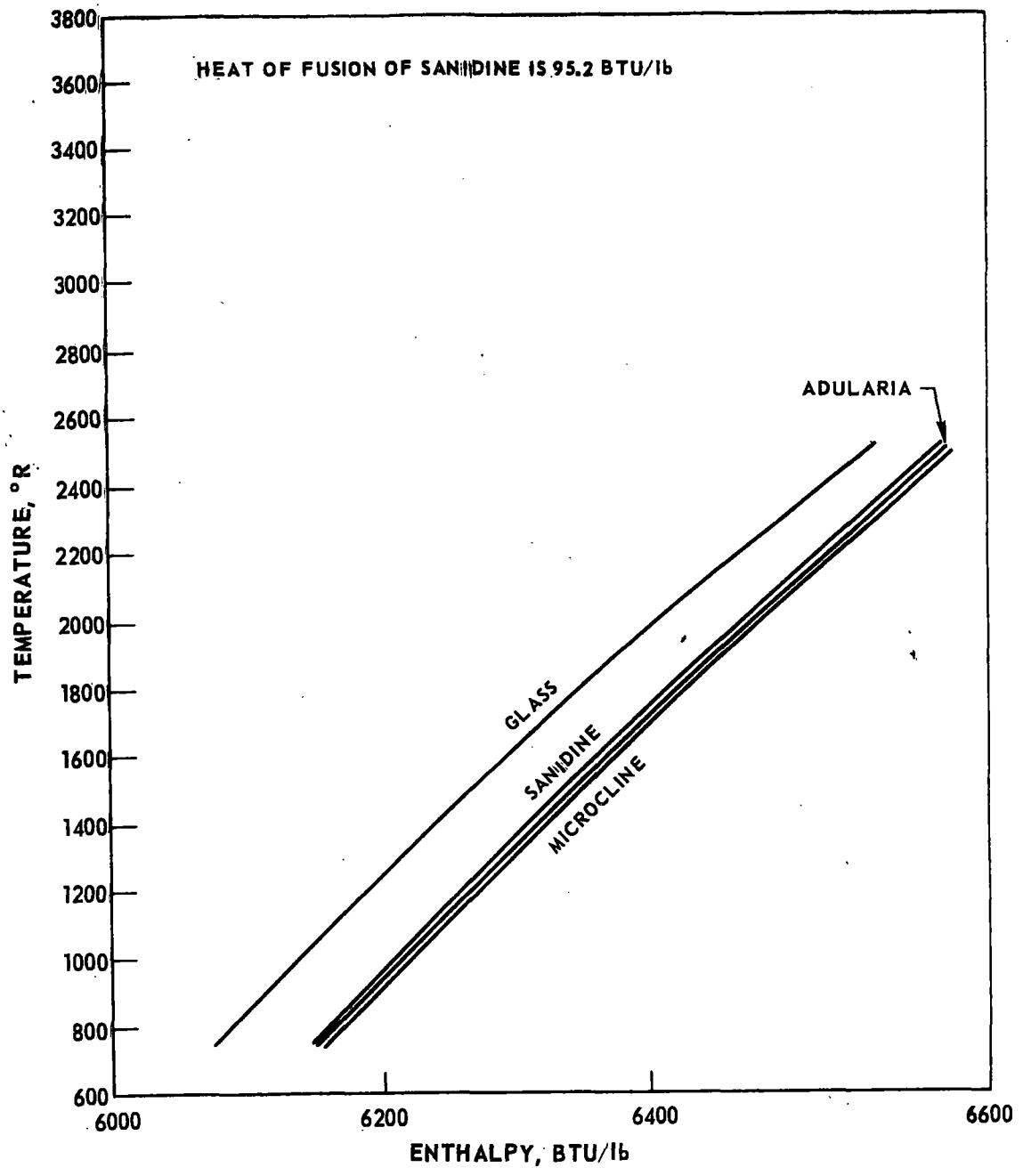

FIGURE 147 ENTHALPY OF VARIOUS FORMS OF $KAlSi_3O_8$

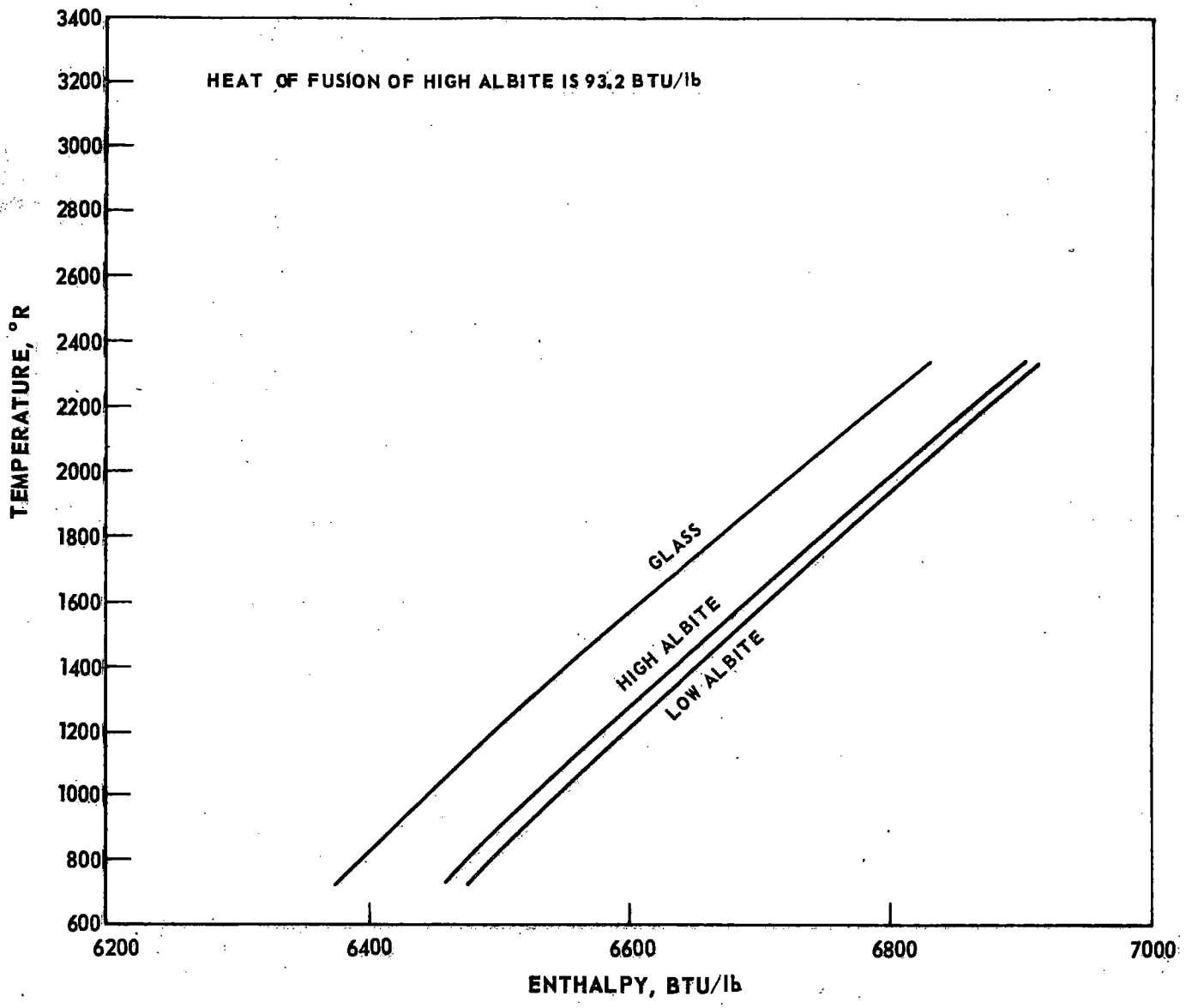

FIGURE 148 ENTHALPY OF VARIOUS FORMS OF $NaAlSi_3O_8$

experiments in Refs. 39 and 40 no attempt was made to remove the melted rock by any mechanism other than natural boiling of the melt. It is likely that considerable melt superheating occurred, and indication of some vaporization was apparent in both cases. It is also possible that the amount of heat lost to the solid rock through the molten zone was very significant over the relatively long heating times reported.

Analysis of Heat Transfer Losses to Solid Rock

This value of melting energy required (600 Btu/lb) was incorporated in an analysis of the power requirements for a kerfing system capable of cutting a kerf 1 in. deep in rock at various speeds and with various kerf widths. This energy requirement for melting was combined with a simplified analysis of the energy loss to the rock mass through heat transfer. The heat transfer loss was calculated on the basis of a kerf made in a semi-infinite rock face, with the wall temperature on both sides of the kerf equal to that of molten rock during passage of the heating beam. Heat is absorbed at each point along the kerf walls only during the time it takes the beam, whose diameter is equal to the kerf width, to pass the point. Heat transfer losses to the bottom and leading edges of the kerf were ignored. The results of these calculations are shown, for a 1-in.-deep kerf in Fig. 149, where the required beam power level and energy fraction lost to heat transfer into the surrounding rock are shown as a function of cutting velocity and kerf width. The heat transfer losses indicated by this analysis are so small, less than 5%, that the energy requirements shown are essentially directly proportional to the rock volume removed. In other words, for cutting speeds greater than 10 in./sec, the power requirements can be determined simply by calculating the mass of rock removed and assuming teh expenditure of the melting energy per unit volume of rock removed. Consideration of the assumptions going into, and the results from, this analysis indicates that the power requirements shown in Fig. 149 represent an absolute minimum estimate of the power required to melt a kerf. Sufficient question still existed concerning the actual power requirements to make a kerf that experiments were run with an electron beam machine to determine both the power required and the maximum ratio of kerf depth to kerf width that could be achieved with this highly concentrated form of thermal energy. These tests and the results therefrom are discussed below.

Experimental Results

Experimental Program

A systematic series of electron beam tests on Barre granite was conducted at the Hamilton Standard Division of United Aircraft. These tests were made with the Hamilton Standard 25-kw nonvacuum electron beam machine, which has an

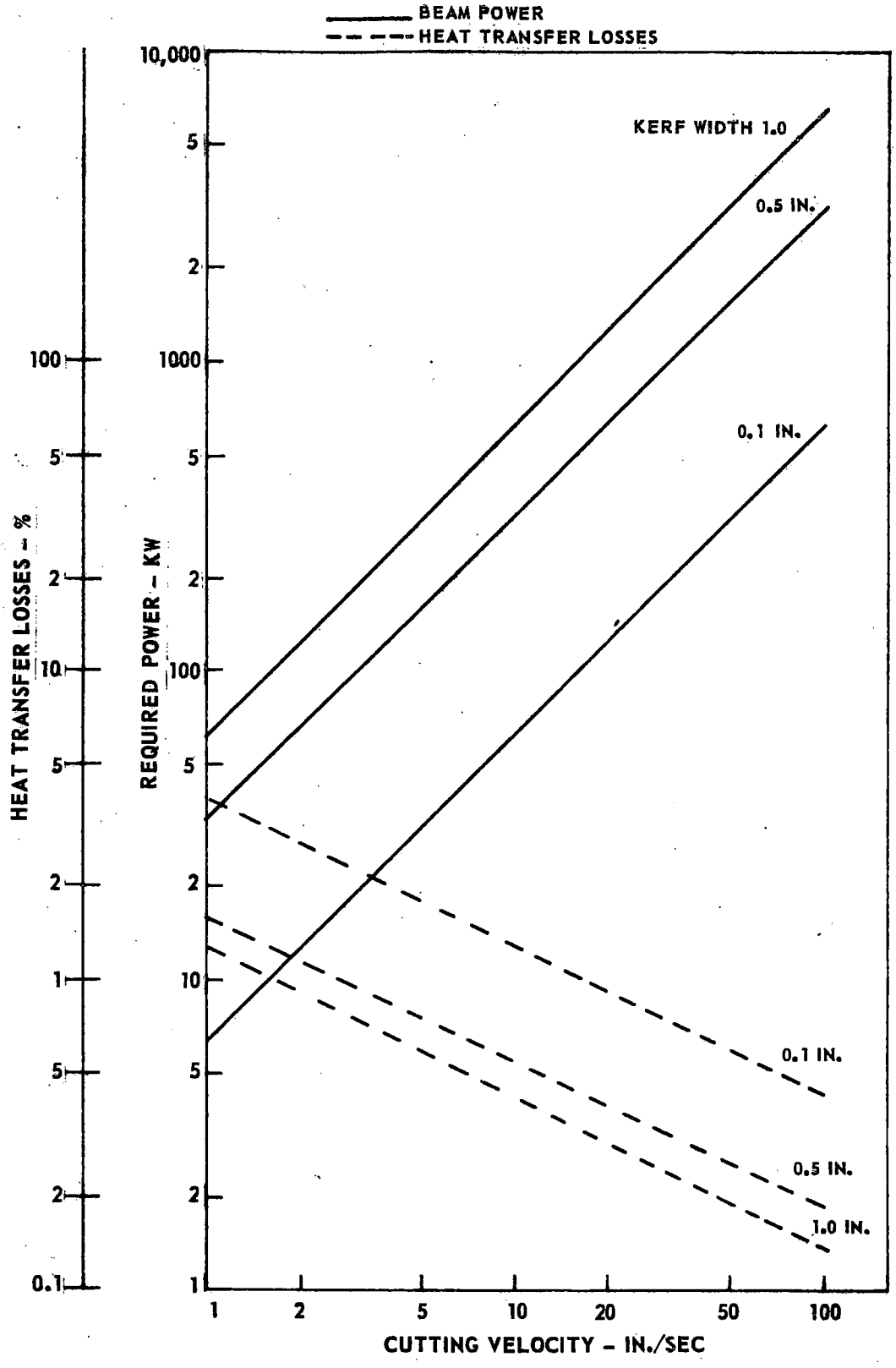

KERFING DEPTH = 1 IN.

FIGURE 149 KERFING ENERGY REQUIREMENTS

accelerating voltage of 175 kv. The test program included irradiation of approximately 30 blocks of granite, each measuring roughly 14 x 13 x 5 in. The test conditions for the first part of this test program and the results, in terms of resulting kerf geomertry, are shown in Table 20. Photographs of three of the test blocks are shown in Figs. 150 through 152.

For these tests, the granite blocks were cut at beam powers of 12, 18, and 25 kw at a constant accelerating voltage of 175 kv. The cutting speed was varied between 500 and 1500 ipm. One to 10 passes were made over a given section. Also, the spacing between cut sections was varied; i.e., some cuts were made 2 in. apart, while others were made with 3-in. spacings. Work distance (distance between the end of the gun and the rock) was usually maintained at 0.25 in. A few tests were made for work distances of 1 and 2 in.

For a second test series, it was found necessary to increase the work distance from $\frac{1}{4}$ to $\frac{3}{4}$ in. to reduce injestion of debris into the electron gun and improve beam stability. The test conditions for, and results from, this test series are shown in Table 21. There was very little rock penetration in this series due to the increased work distance. However, this series also included two special tests; the first involved cutting granite in vacuum, and the second involved cutting granite at ambient pressure in a helium environment. Both tests indicated an increase in penetration, i.e., approximately threefold in vacuum compared to nonvacuum operations, and by approximately 1.5 when substituting helium for air. However, cutting rock in vacuum was very limited because of high outgasing rates when impinging the electron beam on the rock. The vacuum degenerated in a period of 2 to 3 sec such that unsatisfactory performance (arcing) of the electron beram gun would occur.

Analysis of Test Results

Table 22 shows the thermal energy requirements expended in making the slots during tests selected from Table 20. These values are only approximate, due to the difficulty of estimating kerf volume. It can be seen that, for a large variety of power levels and table speeds, the energy per unit volume to cut the rock was approximately in the range of 200 to 300 thousand joules/in.^{3}, which corresponds to a range of 1900 to 2800 Btu/lb of rock (assuming 0.1 lb per cubic inch of granite). Of greatest interest are the tests at relatively high table speeds, since with normal rotation of a mechanical tunneling head, traverse speeds of the order of at least 4 ft/sec are expected on the outer periphery of a conventional tunnel boring machine.

In order to determine the potential capabilities of making a deep slot with repeated passes of a high-power beam at high speed, repeated passes of the 25-kw beam were made over slots with the beam held $\frac{1}{4}$ in. away from the working surface,

TABLE 20

SUMMARY OF ELECTRON BEAM TESTS MADE ON BARRE GRANITE BLOCKS

Made with Hamilton Standard 25 kw nonvacuum Electron Beam

Test No.	Standoff Distance, in.	Traverse Speed, in./min	Beam Output Power Level, Kilowatts	Special Conditions of Test	No. of Passes	Channel Depth (in.)	Channel Width (in.)	Comments
1	0.25	60	25		1	0.50		Excessive melting and cracking of rock near the melt zone.
2	0.25	150	25		1	0.25-0.40		
3	0.25	600	25	Cutting out of beam caused three passes by one side of rock for 1 pass at other side.	1	0.25	0.10	
					3	0.10	0.10	
4	0.25	1,000	25	Cutting out of beam caused three passes by one side of rock for 1 pass at other side.	1	0.05	0.10	
					2	0.10	0.10	
					3	0.15	0.10	
(for subsequent tests, blower was reversed to blow in same direction as rock travel)								
5	0.25	1,000	25		1	0.05	0.10	
6	0.25	1,500	25		1	0.04	0.10	
7	0.25	1,500	25		2	0.05	0.10	
8	1.0	600	25		1	0.05	0.60	
9	2.0	600	25		1	0.05	1.0	
10	0.25	1,500	25	Make successive channels by passing 2, 4, 6, 8, or 10 times over the 1st, 2nd, 3rd, 4th, and 5th channel, respectively.	2	0.09		
					4	0.13	0.08 ave.	
					6	0.16		
					8	0.18	0.17 max. (at top)	
					10	0.23		
11	0.25	1,500	25	3 passes per channel, channels 2 in. apart	3/channel	0.13 0.14 0.12 0.13 0.14	Same as Test #10	Block to be drilled by MIT.
12	0.25	1,500	25	3 passes per channel, channels 3 in. apart	3/channel	0.14 0.14 0.14 0.11	Same as Test #10	Block to be drilled by MIT.
13	0.25	1,500	18	Multiple passes as in Test #10	2	0.08		Roughly same penetration as Test #10, with 2/3 the power.
					4	0.10	= 0.075 ave.	
					6	0.16		
					8	0.19	= 0.10 max.	
					10	0.24		
14	0.25	1,500	12	Multiple passes as in Test #10	2	0.07		
					4	0.10	= 0.06 ave.	
					6	0.12		
					8	0.17	= 0.08 max.	
					10	0.18		
15	1.0	500	25	Single passes, spaced 2 in. apart	1/channel	0.10 max.	0.75-1.0	Rock to be drilled at MIT.
16	2.0	500	25	As in Test #15	1/channel	0.090 max.	1.0-1.25	Rock to be drilled at MIT.

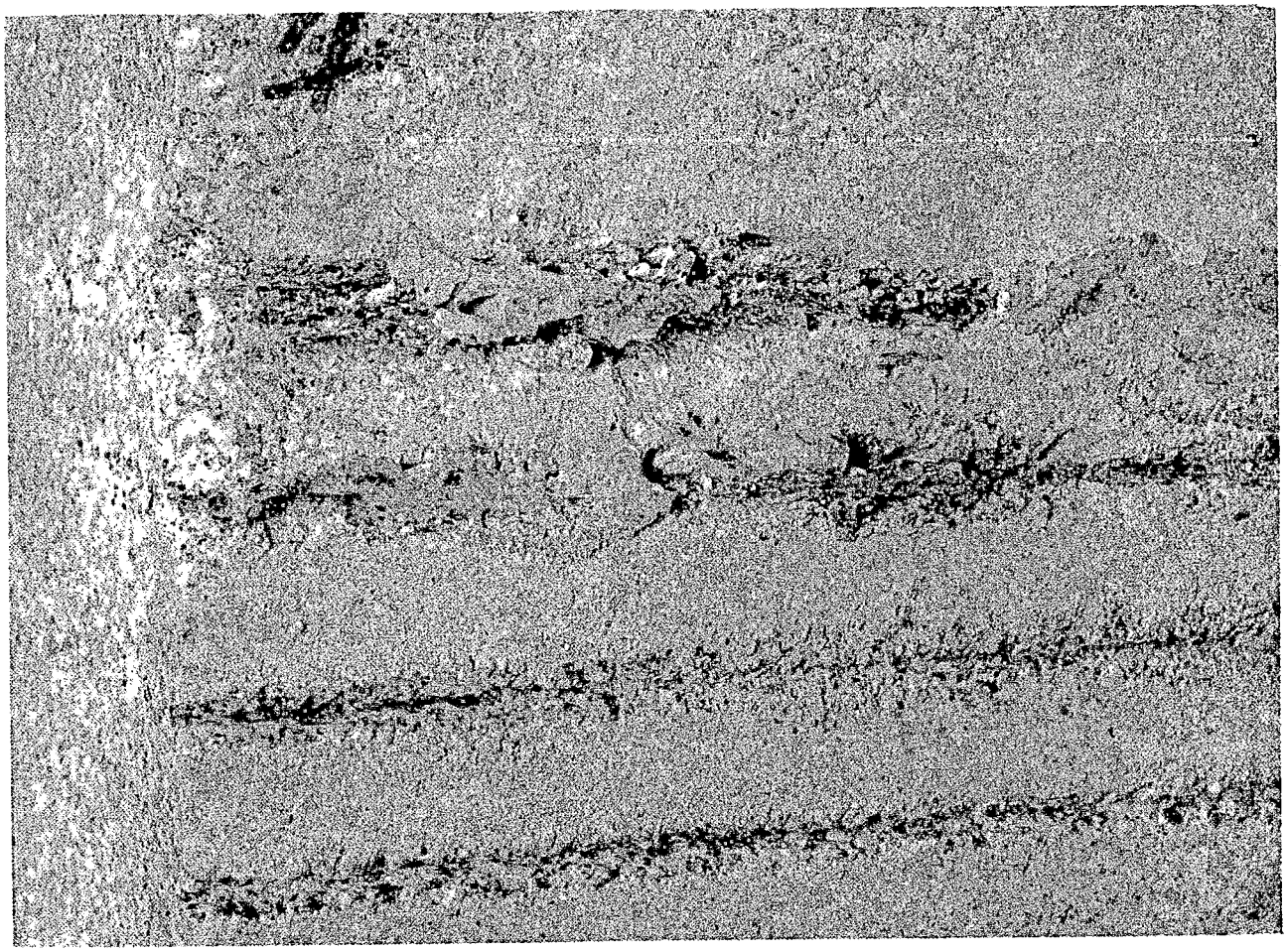

1 PASS PER CUT

RUNS 1 (TOP) THROUGH 4 (BOTTOM) SHOWN

(SEE TABLE 21 FOR IDENTIFICATION OF RUN CONDITIONS AND CUT DIMENSIONS)

FIGURE 150 ELECTRON BEAM CUTS IN ROCK

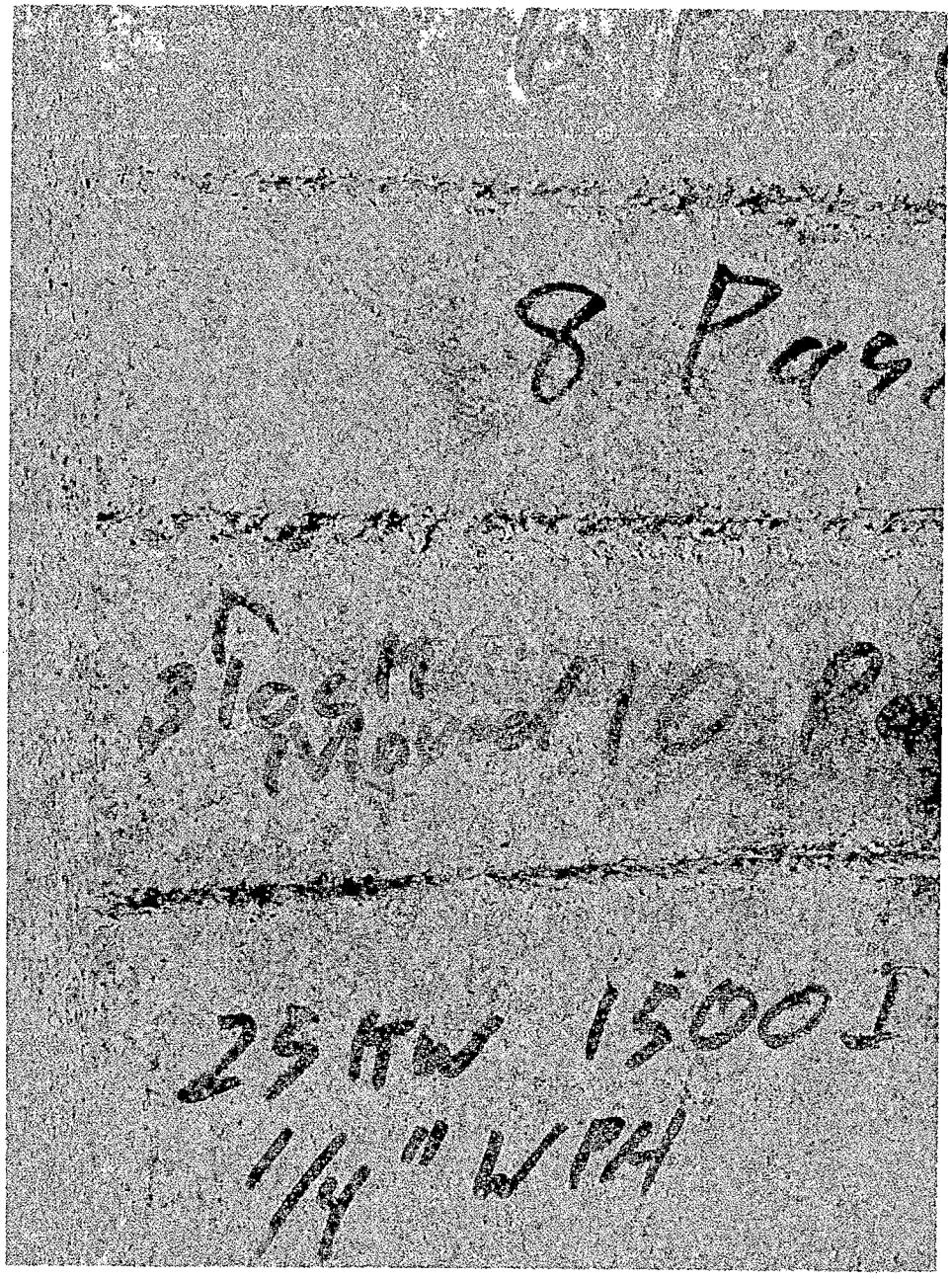

LAST THREE SLOTS MADE IN TEST #10

(SEE TABLE 21)

FIGURE 151 ELECTRON BEAM CUTS IN ROCK

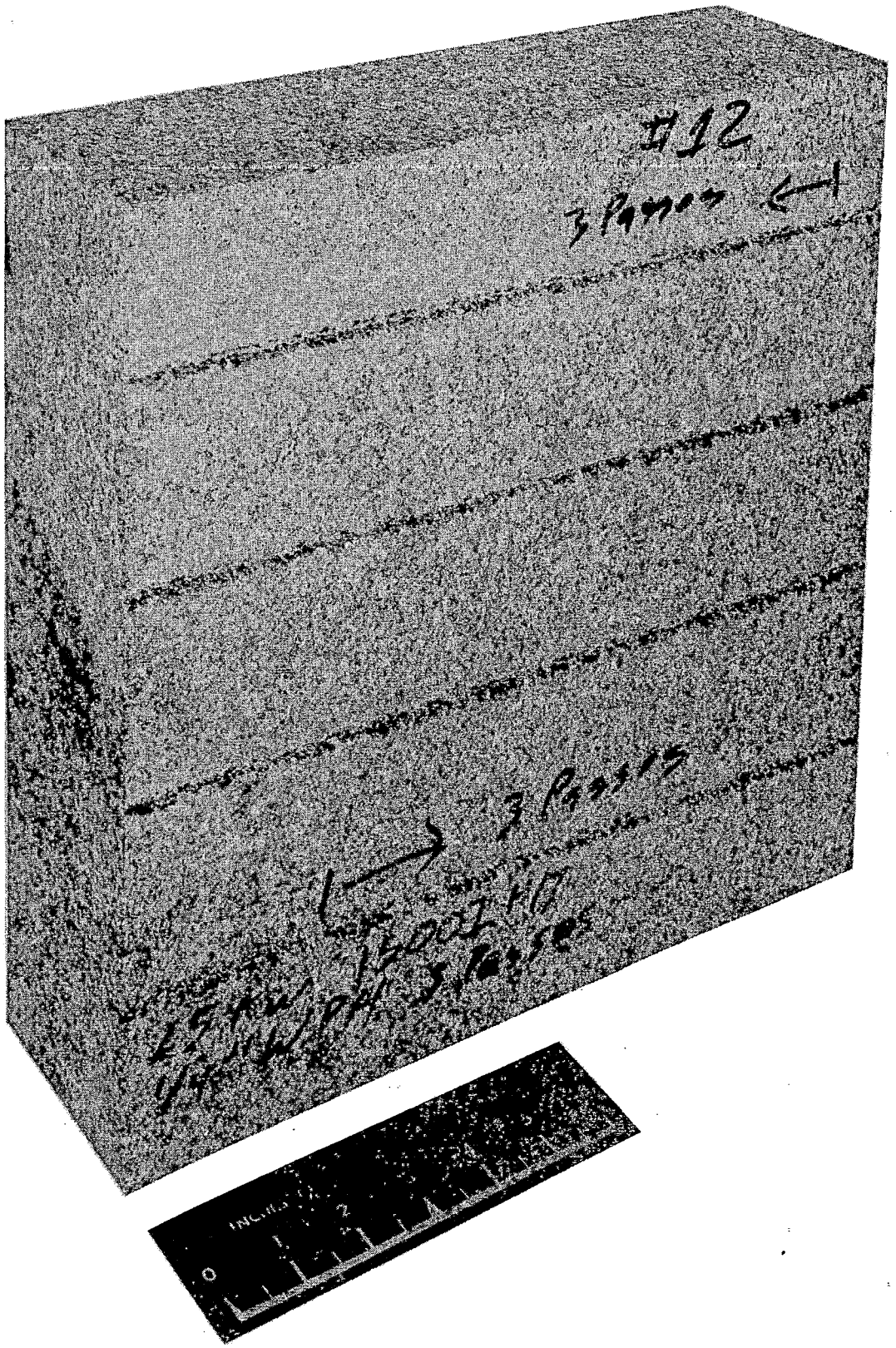

TEST NO. 12 (SEE TABLE 21)

FIGURE 152 ELECTRON BEAM CUTS IN ROCK

TABLE 21

SUMMARY OF ELECTRON BEAM TESTS MADE ON BARRE GRANITE BLOCKS

Made With Hamilton Standard 25 KW Nonvacuum Electron Beam Machine

Test No.	Standoff Distance (in.)	Traverse Speed (in./min.)	Beam Output Power Level (kilowatts)	Special Conditions of Test	No. of Passes	Channel Depth (in.)	Channel Width (in.)	Comments
17	0.75	300	25	3" separation between paths	1	0.06	0.58	Unlabelled block
18	0.75	600	25	3" separation between paths	1	0.05	0.55	
19	0.75	1200	25	3" separation between paths	1	0.06	0.50	
20	0.75	216	18	3" separation between paths	1	0.08 av.	0.50 av.	
21	0.75	432	18	3" separation between paths	1	0.05 av.	0.375 av.	
22	0.75	864	18	3" separation between paths	1	0.05	0.47	
23	0.75	150	12	3" separation between paths	1	0.07	0.50	Two samples labeled "23"; chose wider cut for sample "23"
24	0.75	300	12	3" separation between paths	1	0.05	0.42	
25	0.75	600	12	3" separation between paths	1	0.05	0.45	
26	0.75	432	18	2" separation between paths	1	0.05	0.51	
27	0.75	432	18	4" separation between paths	1	0.06	0.56	
31	0.75	500	18	3" separation between paths; three Helium blowers used, each located 90° apart	1	0.08; 0.05: 0.06; 0.06	0.30 av	
32	0.75	500	18		1	0.08; 0.06; 0.10; 0.05	0.30 av	Direction of travel was into the tri-helium blowers
33	0.75	500	18		1	0.06; 0.06; 0.09; 0.05	0.32 av	
--	~ 15	50	6	Cut in high vacuum environment of $\sim 10^{-4}$ torr	1	1.5 av.	0.2 av.	Excessive melting and cracking of material

TABLE 22

ENERGY REQUIREMENTS FOR MAKING KERFS IN BARRE GRANITE

(From data in Tables 20 and 21)

Test No.	No. of Passes	$in.^3$ removed in. of kerf	joules in. of kerf	joules/$in.^3$ rock removed
3	3	0.025	7500	300,000
	1	0.01	2500	250,000
4	1	0.005	1500	300,000
	2	0.010	3000	300,000
	3	0.015	4500	300,000
6	1	0.004	1000	250,000
7	2	0.05	2000	400,000
10	2	0.0072	2000	278,000
	4	0.0104	4000	384,000
	6	0.0128	6000	469,000
	8	0.0144	8000	555,000
	10	0.0184	10,000	543,000
14	2	0.0042	960	229,000
	4	0.0060	1920	320,000
	6	0.0072	2880	400,000
	8	0.0102	3840	377,000
	10	0.0108	4800	444,000
31 (in Helium)	1	0.015-0.025	2160	86,500-144,000

for three different power levels as reported in tests No. 10, 11, and 14 (see Table 20). From the results in Table 20 it is clear that the beam was incapable of making very deep kerfs, the first few passes being far more efficient than subsequent passes.

This result is shown more clearly by plotting the specific energy of removal as a function of a number of passes as shown in Fig. 153. One reason for the decrease incutting efficiency with increasing number of passes is that after each pass a considerable amount of molten material was left in the kerf, which was not removed mechanically prior to the subsequent passes. Therefore, it is expected that considerable energy was expended in remelting solidified drops of lava, particularly after many passes had been made. Also as the kerf depth increases, the beam-to-rock energy transfer decreased due to increased scattering in the electron beam over the increased distance between the bottom of the kerf and the electron beam gun outlet.

Comparing the results in Fig. 153 with the results reported in the literature which are shown on the vertical axis in Fig. 153, a value of 4000 Btu/lb (422,000 joules/in.^{3}) was assumed for subsequent analysis of the energy required for making kerfs in rock. Also it is clear from the test results in the test program that except for the case of the electron beam working in a vacuum (see Run No. 35 in Table 21) the maximum L/D that can be achieved with an electron beam with an accelerating voltage of 175 kv is roughly 2 to 3.

It is difficult to reconcile this experimental result with the theoretical value of 600 Btu/lb which is almost 7 times less. Remelting of the rock as mentioned above, vaporization of rock particles, energy losses in the beam, heat transfer to and energy reflected from the surface all undoubtedly play some part in this increase in energy over that theoretically required. However, since the experimental values do agree fairly well with those experimental values found in the literature, the 4000 Btu/lb value would appear to be a valid one to use for subsequent design considerations. Perhaps one subsystem which should be provided for future tests of this type would be some sort of scraping mechanism, either an air jet or mechanical scraper, to remove any molten rock as soon as it is formed. (An air blower was in use during the electron beam test discussed above, although it was directed perpendicularly to the exhaust of the electron beam gun, and no particular effort was made to achieve a high scrubbing action at the bottom or walls of the kerf, i.e., the purpose of the jet was to keep rock vapor and particules from entering and/or condensing on the electron beam device.)

Performance Analysis

Based on the energy requirements determined above, some estimates were made of the expected performance of thermal kerfing systems of the three types outlined

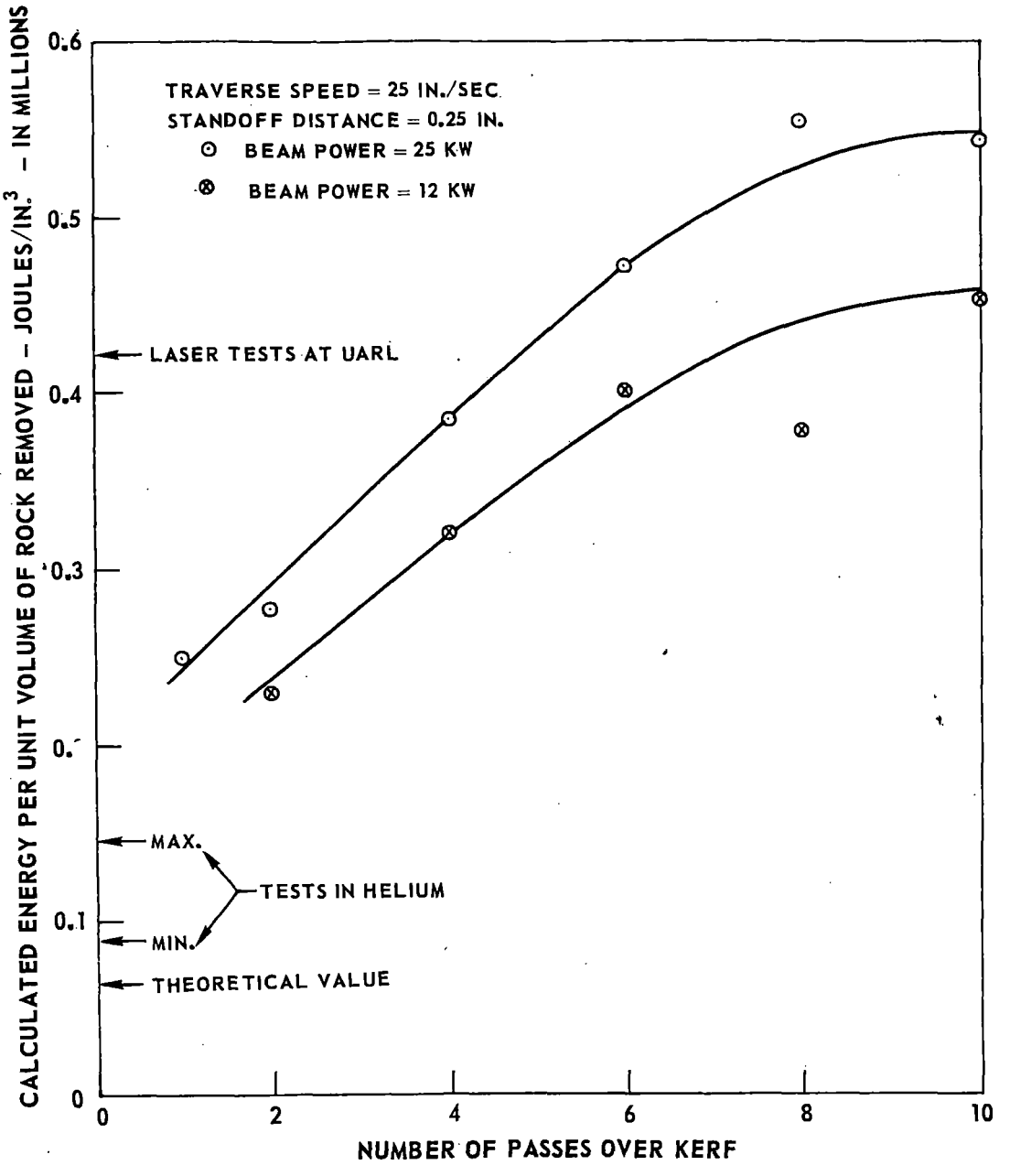

FROM ELECTRON BEAM TESTS

FIGURE 153 THERMAL ROCK REMOVAL EFFICIENCY

in Fig. 145. The object of this analysis was to determine the thermal power requirements of tunnelers employing the three different kerfing concepts.

Low-Depth Kerfing (Mode A)

According to Mode A, the thermal kerfing method would simply be a substitution for the heat-weakening concept. Therefore, instead of heating the rock along a $\frac{1}{4}$-in. band between cutter paths, the rock would be allowed to melt, thus forming a kerf. Such a condition was achieved with test blocks No. 11 and 12 (see Table 20) which were subsequently drilled with the rock-cutting test device at MIT, which was described in Chapter I. Test Block No. 11 was used in calibrating the MIT test rig and determining the optimum separation distance between the cutter bit and the physical kerf. Test Block No. 12 was cut and the data recorded as shown in Table 23.

The specific energy of cutting the electron beam-irradiated block (Block No. 12) is compared in Table 23 to the specific energy of a similar block which was cut after an equal amount of irradiation in the heat-weakening mode with a 650-watt laser beam. Both of the drilling tests were run on cold blocks, and thus the effect of heating is less than it would be if the blocks had been tested while hot (compare Figs. 16 and 22). Substantially more muck was removed from the kerfed block than from the heat-weakened block, even including the melt that was produced by the laser. The muck removed from the kerfed block was even greater than that removed from a lased block tested hot at the same heat input (see Fig. 26 in Chapter I). These results, though fragmentary, indicate such a startling increase in muck removed for the same energy applied that the low-depth kerfing mode appears to warrant further detailed consideration as an alternative to the heat-weakening mode.

No specific design work was done on a tunneler system involving this mode of thermal kerfing because such a system would look entirely similar to the laser systems designed for the heat-weakening mode, as discussed in Chapter III. The restrictions on surface coverage discussed in Chapter II, which limit the amount of laser power that can be installed with the heat-weakening mode, would of course not be a consideration with the kerfing mode. However, the design concept would still be exactly similar with perhaps focusing mirrors in the head to provide a more concentrated beam path than would the plain mirrors as discussed in Chapter III.

Deep Kerfing (Mode B)

Mechanical breakage of rock should be somewhat simpler with this mode of tunneling than for normal mechanical boring; however, no data on the energy requirements to break rock ridges was found or developed. (Reference 46 treats the breaking force required, and expected breaking patterns, but does not

TABLE 23

RESULTS OF DRILLING TESTS

Conditions for drilling tests:

Cutter Thrust = 3000 lb
Cutter Diameter = 4 inches
Cutter offset = 7/16 inch
Independent Cuts
Cutter Table Speed = 2 in./sec
Blocks Tested Cold
Muck Values Normalized to 10-inch Cut
Effective Heat Input (from Laser or Electron Beam) 3000 joules/inch

A. Electron Beam-Treated Rock - Kerfing Mode

Test Block No. 12 from Table 20.

Pass No.	Muck (grams)	
1	11.8	
2	10.9	Average muck removed/pass = 10.52 gm.
3	7.6	(does not include melted rock removed)
4	11.8	

B. Laser-Treated Rock - 600 Watt Focused Beam - Heat-Weakening Mode

Pass No.	Muck* (grams)	
1	4.57	
2	3.57	Average muck removed/pass = 4.46 gm
3	5.57	
4	3.71	including rock melt removed = 7.70
5	4.86	

* Actual cuts were 14 inches long. Data reduced by multiplying by 1/1.4 to agree with other data which are 10-inch cuts.

go into energy requirements.) Much less rock surface area would be formed than in conventional boring (see Fig. 145), and the rock could be more easily attacked. The breaking action may take place only intermittently, with the kerfing going on continuously. No design work was done on this mode, although if a wedging action between rock ridges were used, the tunnel head designs developed in Chapter III would again be similar to the design of a machine using this mode of rock breakage. In this mode, however, the cutters (wedges) would be aligned with the heated rock areas (kerfs), rather than set between them.

Since the expected mechanical power requirements are small relative to the thermal power requirements, it is assumed that the design advance rate of the machine will be determined by the installed thermal power and the specific energy of rock removal.

Referring to Fig. 154, if the tunnel has a radius, R, and the distance between annular kerfs is H, then a total of n = R/H annular kerfs is required. The total length of kerf is equal to the sum of the kerf perimeters, or,

$$\text{Total kerf length} = \Sigma\, \pi\, D_i = 2\pi \sum_{i=0}^{h} (R - iH) = \pi R \left(\frac{R}{H} + 1\right). \qquad (10)$$

Normally R/H will be very large relative to 1.0 (R > 10 ft, H ~ 3 in.), so the total kerf length can be approximated by $\pi R^2/H$. The volume of rock melted (kerf volume) per total volume of rock removed (advance rate x face area) is then given by

$$\frac{\text{Kerf width x Kerf length/ft of Advance}}{\text{Face Area/ft of Advance}} = \frac{w \cdot \pi R\,(R/H)}{\pi R^2}. \qquad (11)$$

If it is further assumed that the kerf depth must be equal to the distance between kerfs for ease of breakage, then

$$\frac{w}{H} = \frac{w}{d} \qquad (12)$$

Taking a value of 422,000 joules/in.^{3} (4000 Btu/lb) as the energy output needed for making this kerf, the thermal power requirements for this mode of kerfing can be easily related to advance rate and kerf w/d, as shown by the solid lines in Fig. 155.

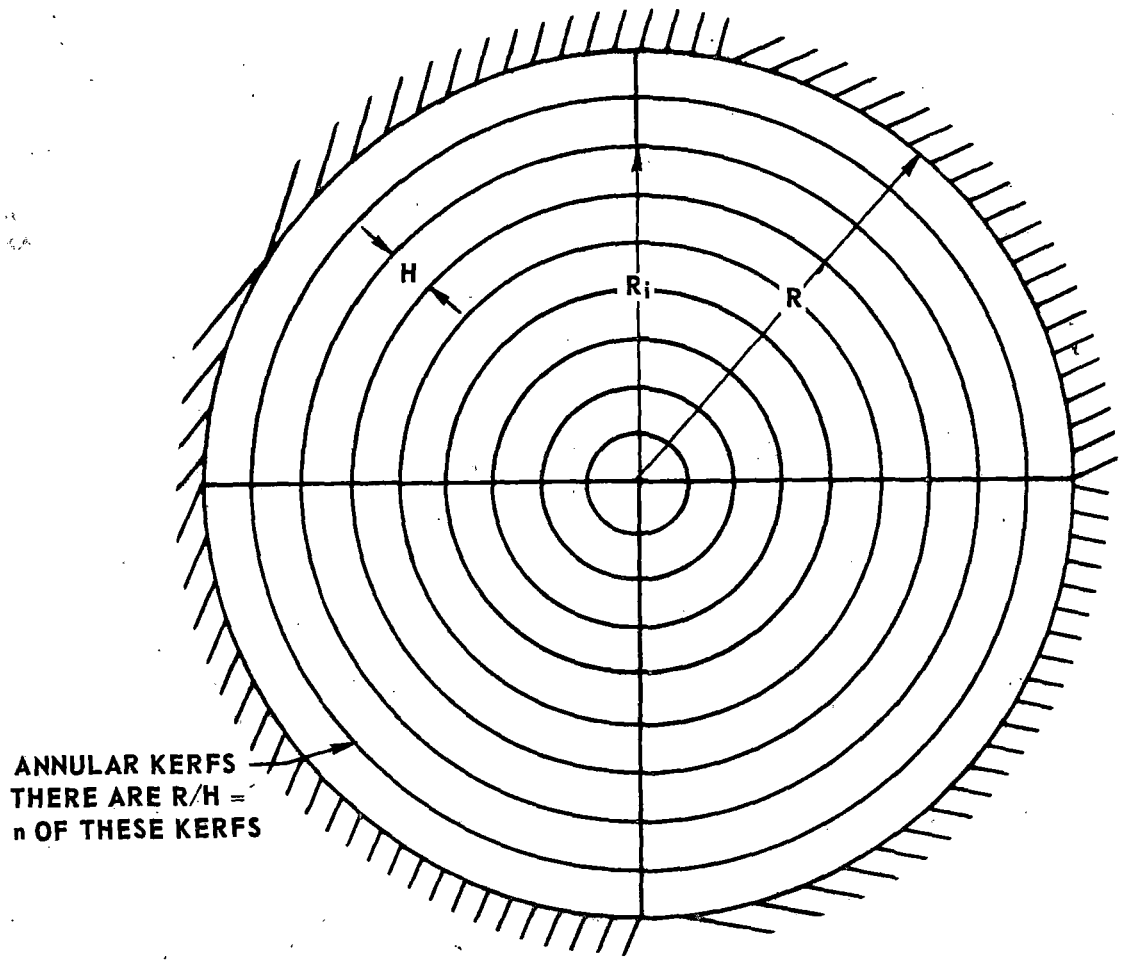

FIGURE 154 GEOMETRY FOR DEEP KERFING

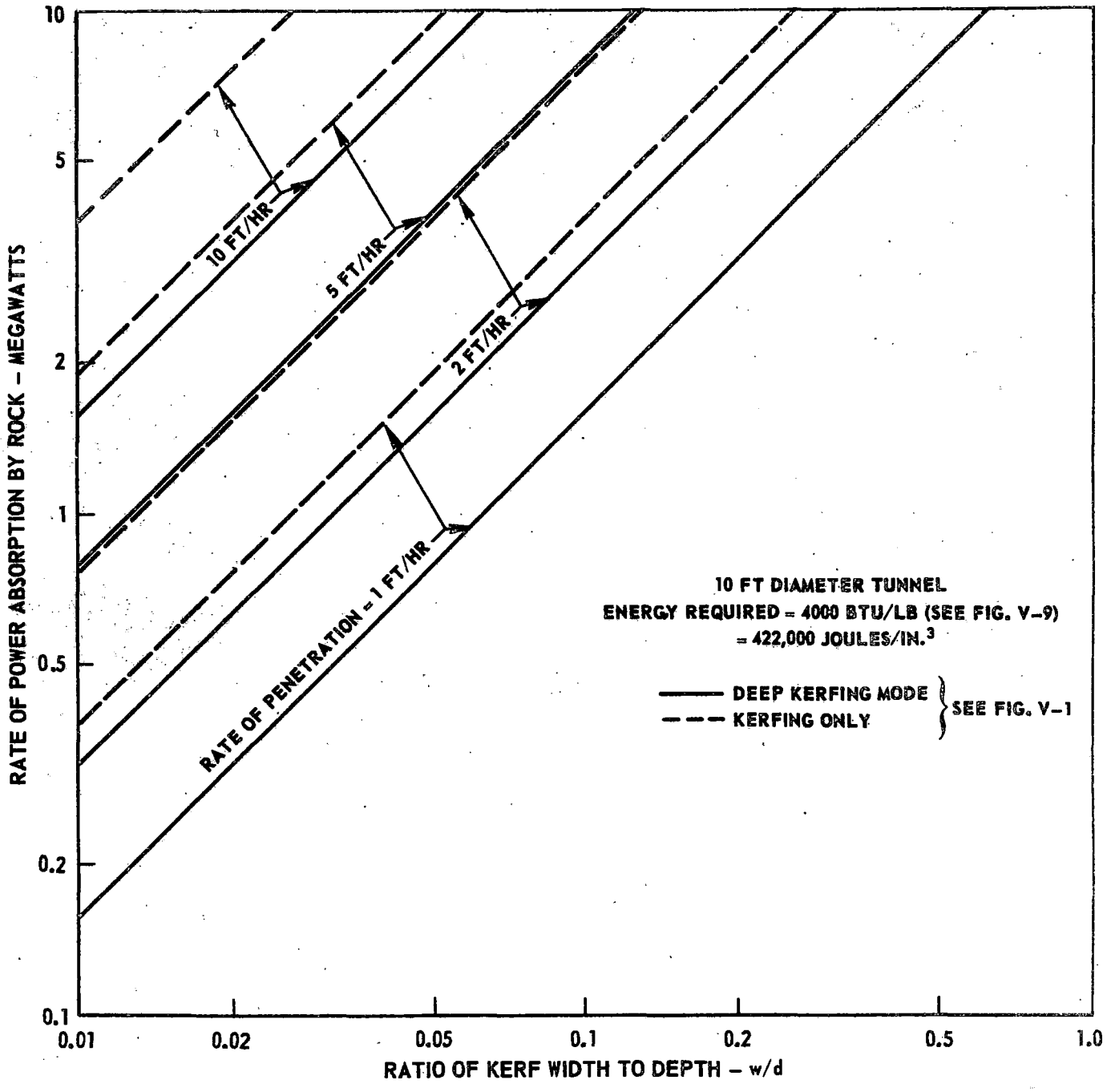

FIGURE 155 POWER REQUIREMENTS FOR THERMAL KERFING OF ROCK

Pure Kerfing (Mode C)

The performance of the pure kerfing mode is determined by the thermal power system output only, since no mechanical power (other than that to constrain and carry the blocks) is necessary for rock removal.

Design Concept

A preliminary sketch of a design concept which incorporates the pure kerfing principle shown in Fig. 145 is presented in Fig. 156. The sketch was made to indicate the potentially light structural arrangement necessary to transmit the laser energy, and the resulting openness in the tunnel near the face. Actually, much of this volume would be filled with the mechanical equipment necessary to convey the rock slabs away from the face in a controlled manner.

As indicated by the mirrors in Fig. 156, a circular mirror would first be traversed around the tunnel gage to isolate the entire tunnel face to a depth of approximately one foot. The mirror head would then be moved vertically, indexing across the tunnel face and isolating long slabs of rock by making intersecting kerf cuts. The power required to remove rock at a given rate with such a technique would depend on the geometry of the blocks removed, the w/d of the metled slot, and the specific energy or removing rock from the kerf. These are discussed below.

Power Requirements

The power requirements are derived by determining the volume of rock that must be melted out of a kerf per unit volume of total rock removed, and then applying some energy per unit time to melt-cut the rock. To determine the volume of rock melted out, an estimate is first made of the kerf wall area per unit length of tunnel.

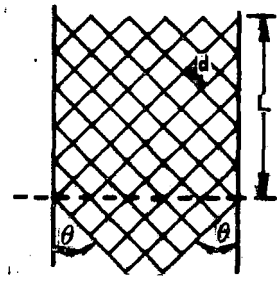

Top View of
Cutting Pattern

Referring to the sketch, if one considers all the cuts in one direction, then one can develop an expression for all the cross-cut areas in a given length L, which is the tunnel length from the beginning to the end of one such cut (see sketch).

$$\text{Cross-cut area per unit length } L = 2\,\frac{D}{d}\,\frac{\pi R^2}{\tan\theta} \qquad (13)$$

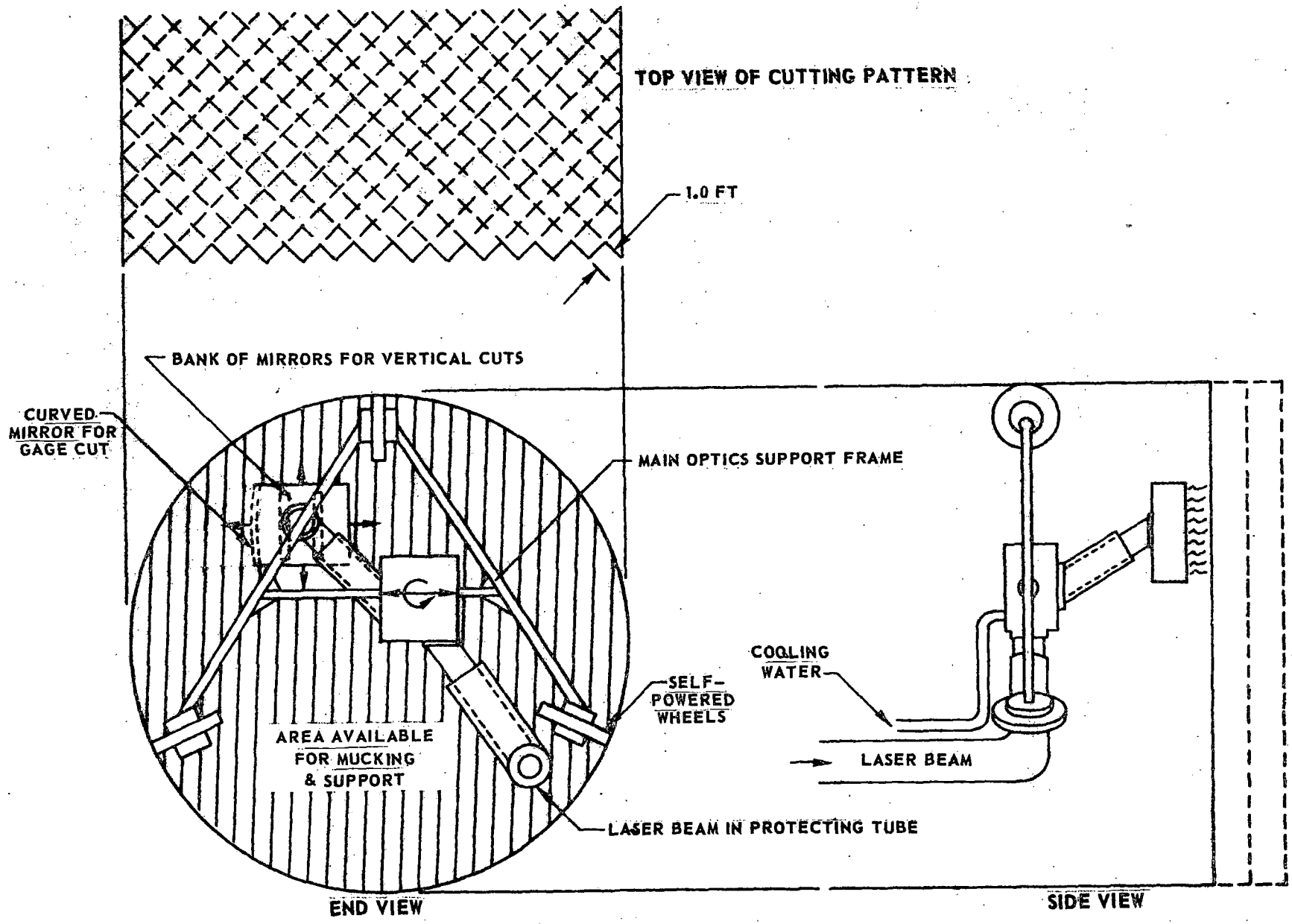

FIGURE 156 SKETCH OF LASER KERFING SCHEME

Also, there is the outside gage area, which is given by

$$\frac{\pi D^2}{\tan \Theta} \cdot \tag{14}$$

Then, dividing the total kerf area per unit length, L (given by Eqs. 13 and 14), by the total volume of rock in this length leads to

$$\frac{A}{V} = \frac{2}{d} + \frac{4}{D} , \tag{15}$$

and the total volume melted out divided by the total volume is then given by

$$\frac{A \cdot w}{V} = \frac{\text{Vol}_{\text{melted}}}{\text{Vol}_{\text{removed}}} = 2\,\frac{w}{d} + \frac{4w}{D} . \tag{16}$$

Using this relationship, and assuming 4000 Btu/lb required energy to make the melt-cut, the thermal power requirements necessary to attain various advance rates in a 10-ft-diameter tunnel are given in Fig. 155, as a function of kerf width to depth ratio, and advance rate.

The power requirements shown in Fig. 155 for the last two modes of kerfing are for a 10-ft-diameter tunnel. For any other tunnel diameter, the power required will go up by $(D/10)^2$ for the same kerf width and advance rate. The economics of employing this mode of hard rock tunneling, and the deep kerfing mode, are considered in Chapter VI.

CHAPTER VI - ECONOMIC ANALYSIS OF HEAT-ASSISTED TUNNEL BORING MACHINES

This chapter contains an estimate of the economic benefits to be derived from the heat-assisted boring machine concepts developed in this report.

Chapters I through III of this report are concerned with the application of the original heat-weakening concept, wherein the rock is thermally stressed prior to mechanical cutting, but melting and/or vaporization is avoided if possible. The first section of this chapter deals with the expected economics of operating either laser- or radiant heater-assisted tunneling machines based on the heat weakening of rock.

An alternative concept, developed in Chapter V, is to form kerfs in the rock to facilitate breakage, as opposed to thermally stressing the otherwise intact rock face. Estimates of the economics of tunnel excavation based on the kerfing concept are presented in the second section of this chapter.

ANALYSIS OF HEAT-WEAKENING BORING MACHINES

Method of Economic Analysis

Data presented in Chapter I show an increase in muck removal from a test block with the application of heat. This increase in muck removal can be exploited in two ways: either by reducing tunneler rpm, thereby increasing expected cutter life, or by increasing the rate of advance, thereby reducing both cutter costs and variable costs, such as labor. These two schemes for estimating the economics of heat weakening are discussed below as Modes 1 and 2. Muck removal data, rather than specific energy data, were used in the economic evaluation since only muck removal data were available for the higher thrust (5000 lb) tests which are felt to be more representative of full-scale boring machine conditions than the data for 3000 lb cutter thrust. The data used are summarized in Fig. 47.

Mode 1 - Reducing Tunneler RPM at Constant Advance Rate

The amount of muck removed per pass, multiplied by the number of cutter passes per unit time (e.g., rpm), is a measure of the tunneler penetration rate. Therefore, if the penetration rate is held constant and the muck removal rate is increased by the addition of heat energy, then the rpm can be reduced according to

$$rpm_h = rpm_o \left[\frac{mr_o}{mr_h}\right], \qquad (17)$$

where mr = muck removal rate per cutter pass

$()_h$ = value with heating

$()_o$ = value without heating.

A reduction in rpm is beneficial, since it will reduce the amount of installed heater power necessary for a given amount of damage to the rock, and it should reduce cutter costs. Cutter costs are assumed to relate to some fixed total distance (cutting path) that the cutters traverse during their lifetime; it is further assumed that this cutting distance is unaffected by the application of heat to the rock. Therefore, if the rpm can be reduced by 50% (without a loss in advance rate) by the addition of heat, then the cutters should last for twice as many linear feet of tunnel, and the cutter costs per linear foot of tunnel are assumed to be reduced by 50%. Thus, for a given rock type, and a fixed penetration rate,

$$cc_h = cc_o \left[\frac{rpm_h}{rpm_o}\right], \qquad (18)$$

where cc = cutter costs in dollars per foot of tunnel

$()_h$ = value with heating

$()_o$ = value without heating.

Nominal rpm values without heating are given in Fig. 52. Figure 157 shows the sensitivities of cutter costs to machine rpm and advance rate for a typical case, employing the above assumptions.

Based on these assumptions, an economic analysis can be performed as outlined in Fig. 158. Choosing a value of joules per inch of heater path (starting in the upper left-hand corner of Fig. 158), the test data can be consulted to find an expected increase in the muck removal rate. Based on this increase in removal rate, the savings in cutter costs can be determined, as discussed above. Also, based on the expected reduction in tunneler rpm, the heating power required can be estimated. Heater system costs and environmental control costs may then be estimated, to determine the total costs of heat generation and control. Note that the base (no heat) penetration rates used in the calculations are those developed as a function of rock strength in Chapter IV. Finally, the heater costs and the cutter cost savings can be compared to determine the desirability of this mode of heat-assisted boring.

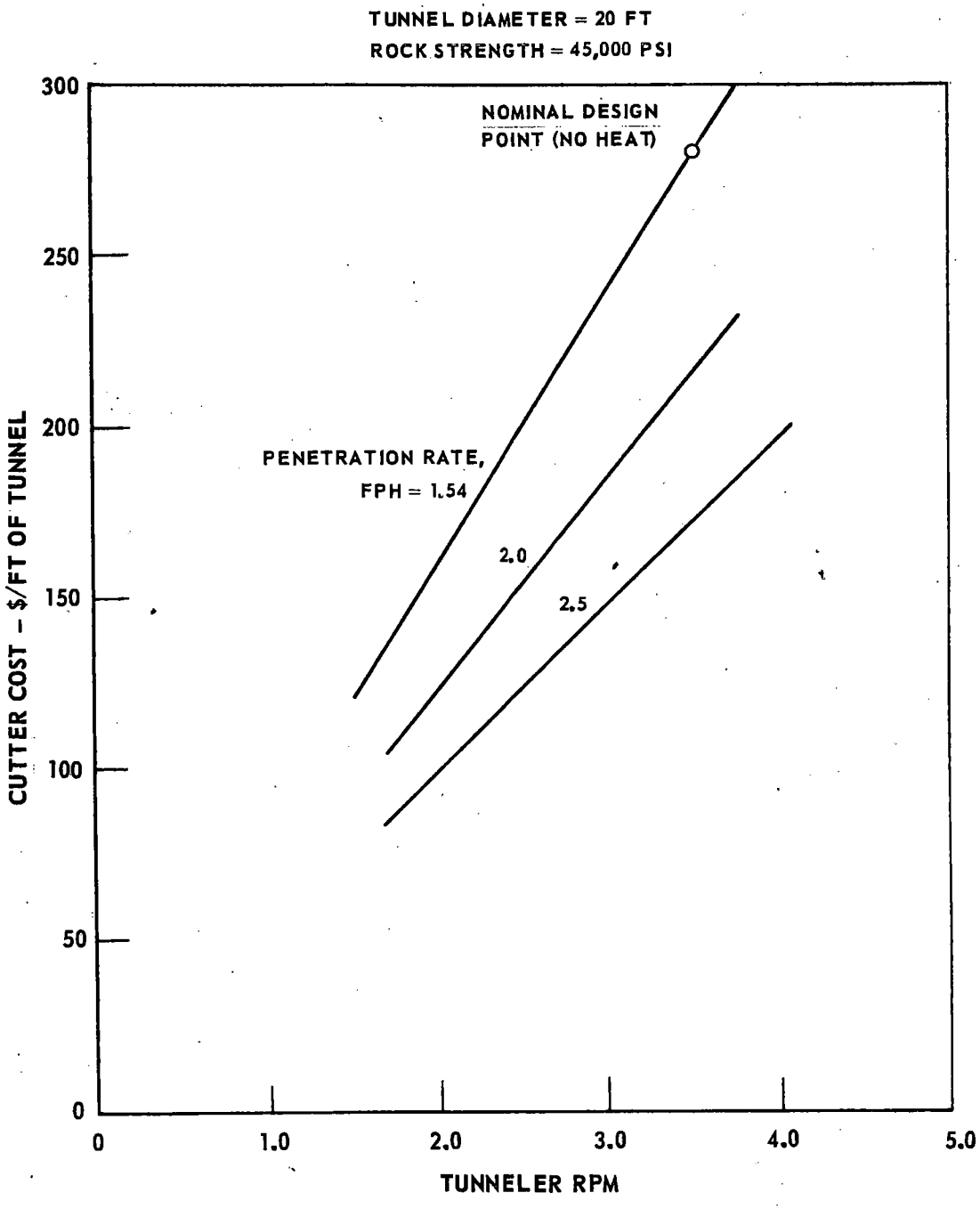

FIGURE 157. EFFECT OF PENETRATION RATE AND RPM ON CUTTER COST

FIGURE 158. EVALUATION OF HEAT-WEAKENING COSTS AND SAVINGS MODE 1 – REDUCTION IN RPM ONLY

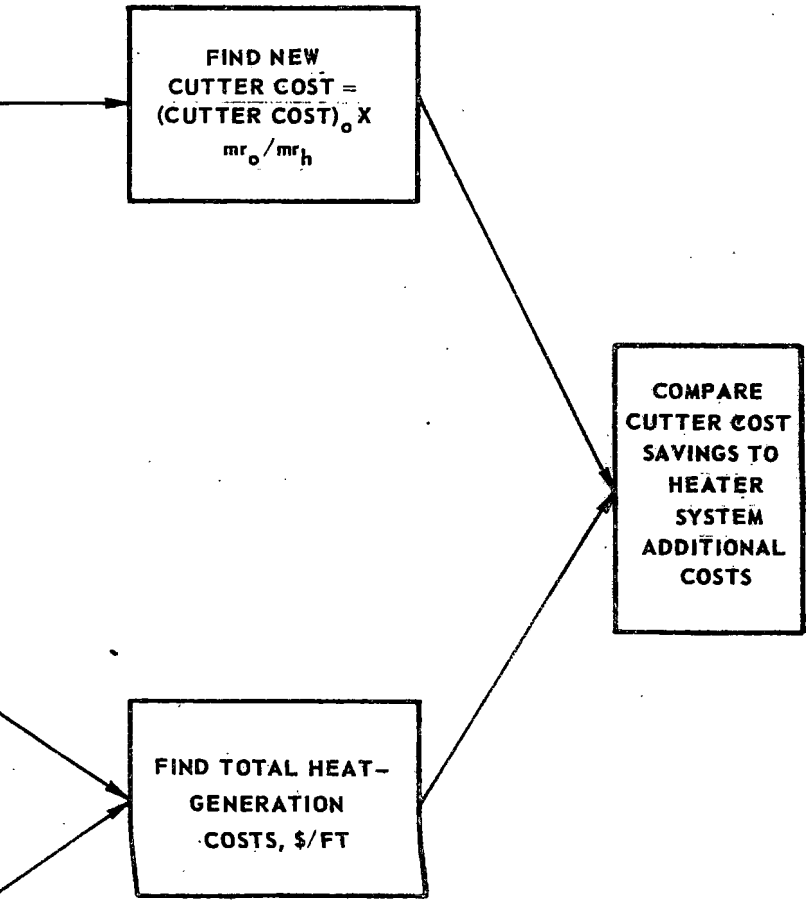
FIND NEW CUTTER COST = (CUTTER COST)$_o$ X mr_o/mr_h
COMPARE CUTTER COST SAVINGS TO HEATER SYSTEM ADDITIONAL COSTS
FIND TOTAL HEAT-GENERATION COSTS, $/FT

Mode 2 - Increasing Advance Rate at Constant RPM

An alternative assumption that can be made regarding the effect of an increase in muck removal rate is that the rpm stays constant, and the penetration rate increases by the same amount as the increase in muck removal rate. For this case,

$$\frac{mr_h}{mr_o} = \frac{PR_h}{PR_o} \tag{19}$$

where mr = muck removal rate

PR = penetration rate

$()_h$ = value with heating

$()_o$ = value without heating

Based on this assumption, the economic analysis for Mode 2 of operation is outlined in Fig. 159. As in Mode 1, an energy input is selected, and an increase in muck removal is established from the test data. An increase in penetration rate is then determined as specified above. The reduction in cutter cost is then calculated, based on the increased muck removal. However, a reduction in the variable costs is also calculated, correspoinding to the increased penetration rate. As in Mode 1, the basic penetration rate (penetration with no heat) is that developed in Chapter IV as a function of rock strength. Penetration rate with heating is based on multiplying this basic penetration rate by the muck removal ratio developed in the test program. Both the cutter costs and the variable costs used in this analysis are those developed in Chapter IV. To determine cutter costs, igneous rock is assumed throughout this chapter. Heating system costs are then calculated assuming no reduction in rpm. (As developed in Chapter II, rpm is taken as 70/D, or 3.5 for a 20-ft-diameter tunnel.) Finally, the total cost savings can be compared to the expected cost reductions, to evaluate the economic efficiency of this mode of operation

Heating System Cost Functions

Heating system hourly cost elements considered include a fuel cost, a yearly capital cost, and a cost for environmental control. Fuel oil is assumed to be available at 80¢ per million Btu. Yearly utilization is assumed at 3000 hours (12 hr of operation per 24 hr operating day, 5 days/week, 50 weeks/yr). A yearly charge of a fixed percentage of the heating system cost is assumed to cover depreciation, interest, and yearly maintenance. With these assumptions, the equation for the heater system hourly cost appears as

FIGURE 159. EVALUATION OF HEAT-WEAKENING COSTS AND SAVINGS MODE 2 - HEAT WEAKENING CAUSES INCREASE IN PENETRATION RATE

$$\$/hr\big|_h = \frac{P_T}{\eta_s}\left[\frac{2.73}{\eta_D} + \frac{C_H\, 10^3\,(P)}{3000} + \frac{F\,(P)}{3000}\right], \qquad (20)$$

where P_T = power into rock, mw

η_s = power into rock/heater device output

η_D = heater device output/fuel rate input

C_H = heater device cost, \$/kw

F = heater system fixed cost

P = fraction of capital cost paid per year to cover capital cost of heater

Power into the rock, P_T, is given by

$$P_T = J_0\ \frac{rpm}{60}\ \frac{\pi\, D^2}{4}, \qquad (21)$$

where J_0 = joules/in.^{2}

D = tunnel diameter, in.

as developed in Chapter II. The test results in Chapter I are presented in terms of joules/in.; to calculate the effective joules/square in., a cutter spacing (full scale) of 3 in. is assumed.

Heater system cost per foot is given by dividing Eq. (20) by the penetration rate. The specific constants, η_s, η_D, C_H, and F used for the two heater systems have nominal values, as determined in Chapter III, as follows:

Heater Type	η_s	η_D	C_H (\$/kw)	F(\$)	P
Laser	0.75	0.06	5000	200,000	0.2
Radiant Heater	0.85	0.225	150	0	0.6

A nominal laser cost of \$5000/kw is assumed. In Chapter III a cost of \$10,000/kw is devloped, based on current laser cost estimates, using a 10% laser efficiency.

Development of higher operating efficiencies, and less expensive components, as mentioned in Chapter III, should lead to the lower specific cost for high-power laser systems. Also, note that a yearly charge of 0.6 times the radiant heater system cost is assumed. This assumes a charge of 20% on the installed system cost plus two replacements of heating elements per year (3000 hours of operation).

Costs and Savings of Heat-Weakening by Lasers

Figure 160 indicates the cutter cost savings, and the cost of installing and operating the heating system for a laser-powered tunneler employing heat-weakening, assuming a reduced rpm in direct proportion to the expected increase in muck removal rate (Mode 1). The dotted line indicates the expected cutter cost savings, in dollars per foot of tunnel, due to decreased rpm. The solid lines indicate the cost per foot of tunnel of the laser heating system and necessary environmental control system, based on laser capital costs of $10,000, $5000, and $2000/kw. The results indicate that the heating system costs are dominated by the laser system capital cost, as indicated by the large change in system costs with changes in the laser capital cost.

Figure 160 also indicates that there is little hope of achieving any excavation economies for this case. The heater costs come close to the cutter cost savings only at the low heating power levels (as would be expected from an examination of the test results used for this figure, which are those of Test 4 in Fig. 47). However, as the heating rate approaches zero, the heat-weakening effect falls off, and the minimum feasible heating power required for this case is about 350 kilowatts.

The economic effect of putting the indicated increase in muck removal rate into an increase in tunneler advance rate is indicated in Fig. 161. The indicated savings are substantially higher here, due to the additional savings in variable cost. Also, the cost of supplying a given rock heating rate, on a per-foot basis, is decreased due to the higher advance rate. This effect more than compensates for the higher power level required to achieve a certain level of weakening due to the higher machine rpm than the previous case.

The indicated increase in penetration rate is from 1.54 ft/hr for the unheated case (see Chapter IV) to 1.85 ft/hr at a heat input level of 440 kw, and to 2.3 ft/hr for 4.4 Mw. The amount of cutter penetration assumed for the highest advance rate is thus only about 0.14 inches per pass, so the increases in advance rate assumed appear to be quite reasonable. Due to the better economic results obtained with the Mode 2 analysis, this method of cost accounting is assumed for all subsequent discussion of laser-assisted tunneling costs.

η_S = 0.75 DECREASING RPM DUE TO HEATING (MODE 1)

η_D = 0.06 USING TEST RESULTS FROM FIG. 47, TEST 4
ROCK STRENGTH = 45,000 PSI
TUNNEL DIAMETER = 20 FT

———— = COST ADDED DUE TO HEATING

— — — = COSTS SAVED DUE TO HEATING

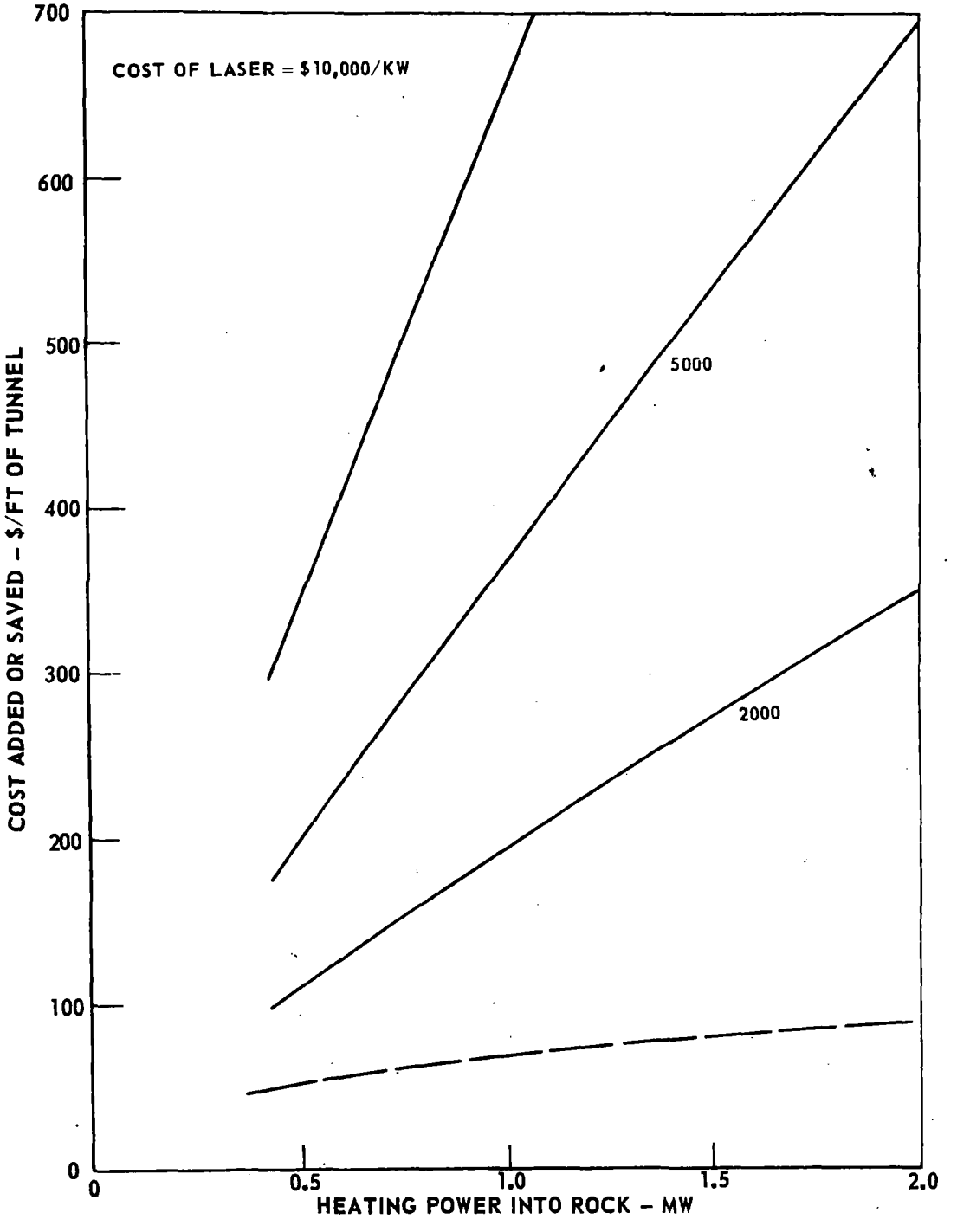

FIGURE 160. INCREMENTAL COSTS AND COST SAVINGS FOR LASER-ASSISTED TUNNELER

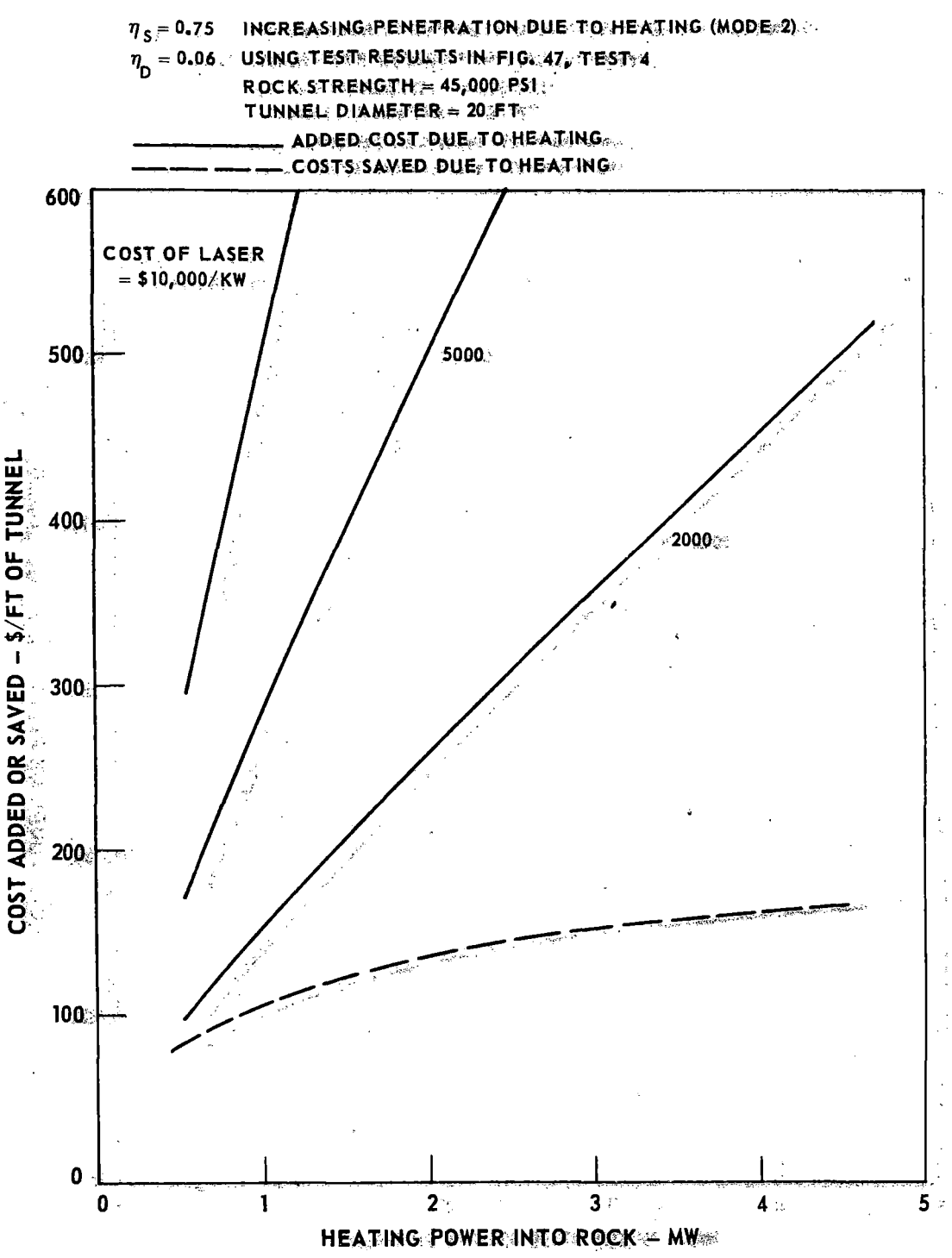

FIGURE 161. INCREMENTAL COSTS AND COST SAVINGS FOR LASER-ASSISTED TUNNELER

Since the capital cost of the laser system predominates, the effect of increasing the laser system transmission efficiency, or the laser efficiency itself on heater system costs, is relatively insignificant, as shown in Fig. 162. Note that this curve assumes a constant laser capital cost of $5000/kw, independent of the system efficiency. To the extent that increasing efficiency could reduce the specific cost of the laser, such an increase in efficiency could affect the economics to a greater extent than that shown in Fig. 162. A strict relationship between laser efficiency and specific cost was not developed during this study, so the two variables are handled separately here.

A comparison of costs and savings incurred in small-diameter tunnels is compared to the 20-ft-diameter case (for a laser cost of $5000/kw and all other parameters as in Fig. 161) in Fig. 163. This curve indicates that the heating power costs per foot are relatively insensitive to tunnel diameter for a given heat flow rate into the rock. As tunnel diameter decreases, the power requirement to do a certain amount of damage is reduced because of the smaller face area, but increased due to the higher rpm (see Eq. (21)). These effects interact and result in little change in hourly cost when plotted as a function of power into the rock, in Fig. 163. The savings, however, are noticeably greater for a large-diameter tunnel for which cutter costs represent a higher proportion of the total costs to begin with, as discussed in Chapter IV. Thus, heat weakening in advance of mechanical drilling probably has greater application to large-diameter ($\sim$ 20 ft) tunnels, for which cutter cost is a more serious problem than in small-diameter ($\sim$ 10 ft) tunnel boring.

The results shown so far are for a basic rock strength of 45,000 psi compressive strength. For a typical case, costs and savings were computed for a range of rock strength, and the results are shown in Fig. 164. The comparison chosen is virtually unaffected by rock strength; the savings are roughly 40% of the costs incurred at all rock strengths.

All cost results shown so far have been calculated using results from the tests incorporating the highest value of cutter thrust (Test 4 in Fig. 47). While this test series is felt to be the most accurate indicator of full-scale boring conditions, it is of interest to determine the effect of using a different set of test results obtained at a lower thrust setting. Going to 3000 lb thrust and multiple cuts gives results similar to, and slightly worse than, those used so far. Calculations made with test results from the 3000 lb cutter thrust tests working on a smooth surface (Test 1 in Fig. 47), which gave the best results of any test series, are shown in Fig. 165. As would be expected, the difference between the heater system cost and the cutter and variable cost reductions, at high heating powers, is less than for the previous test data. It is also of interest to note that, due to the much greater percentage increase in muck removal at high energy inputs shown for Test 1 in Fig. 47, the economics now favor the higher power levels. Also, it

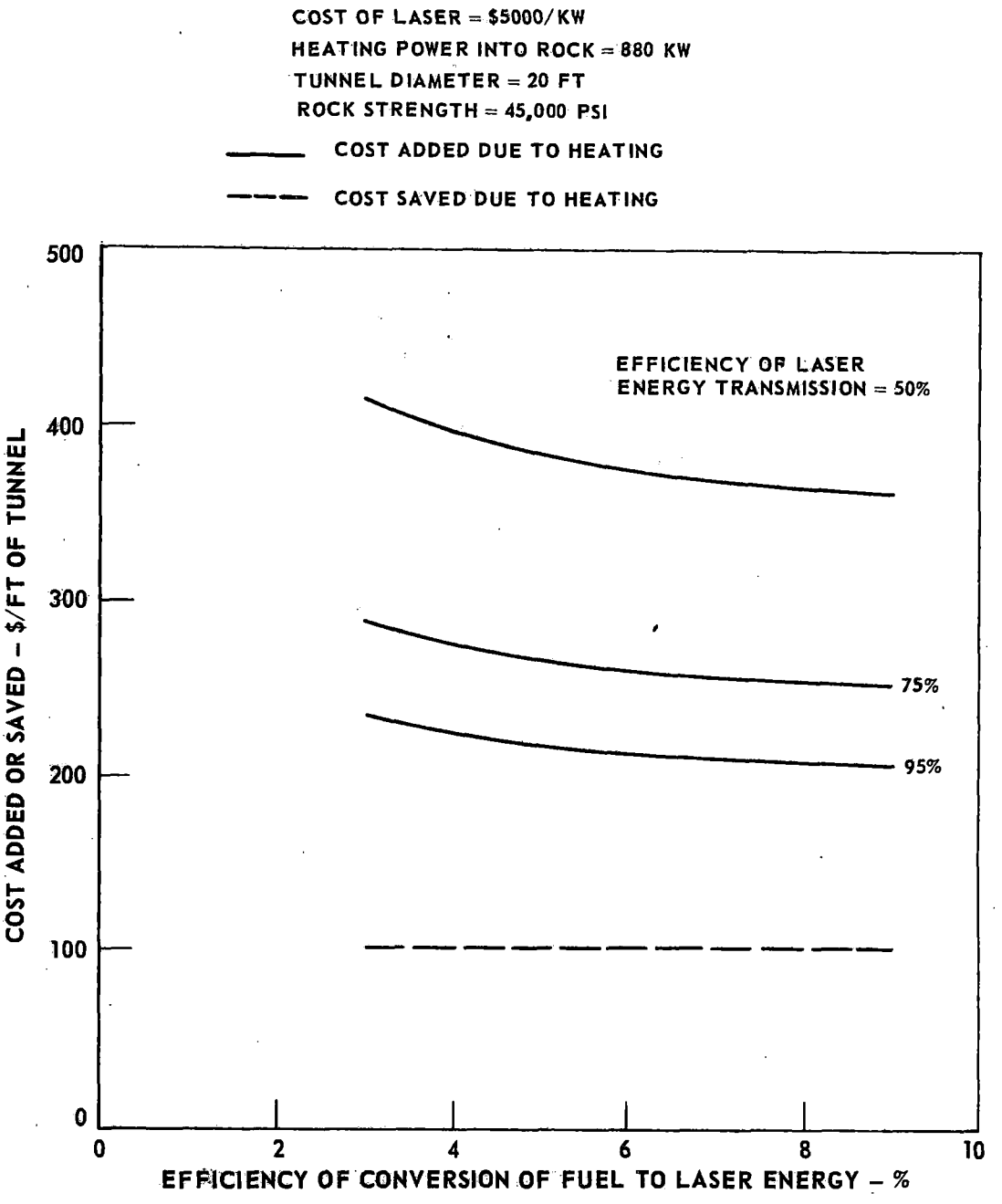

FIGURE 162. EFFECT OF EFFICIENCY OF LASER ENERGY GENERATION AND TRANSMISSION ON LASER-ASSISTED TUNNELING COSTS

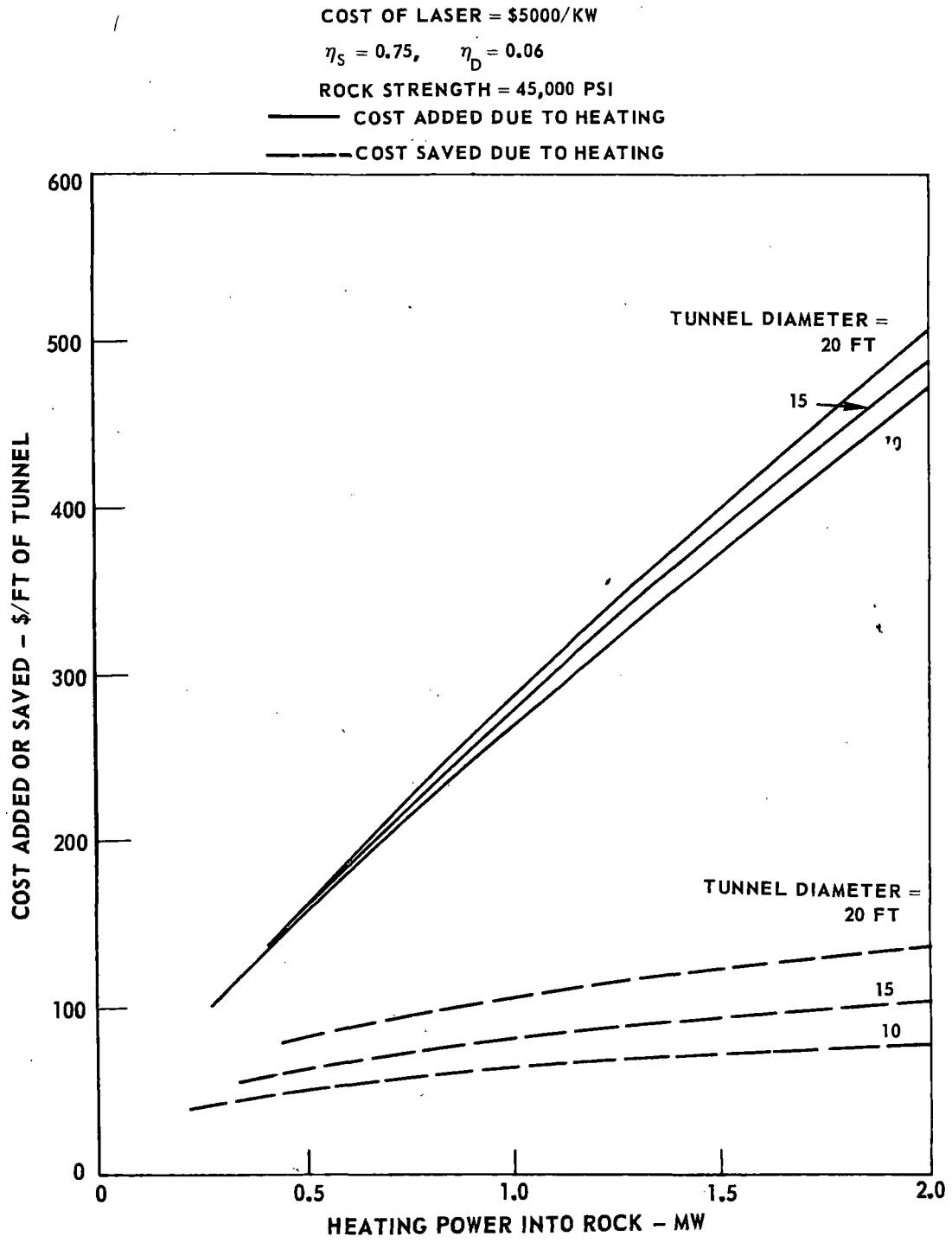

FIGURE 163. INCREMENTAL COSTS FOR LASER-ASSISTED TUNNELERS IN DIFFERENT TUNNEL SIZES

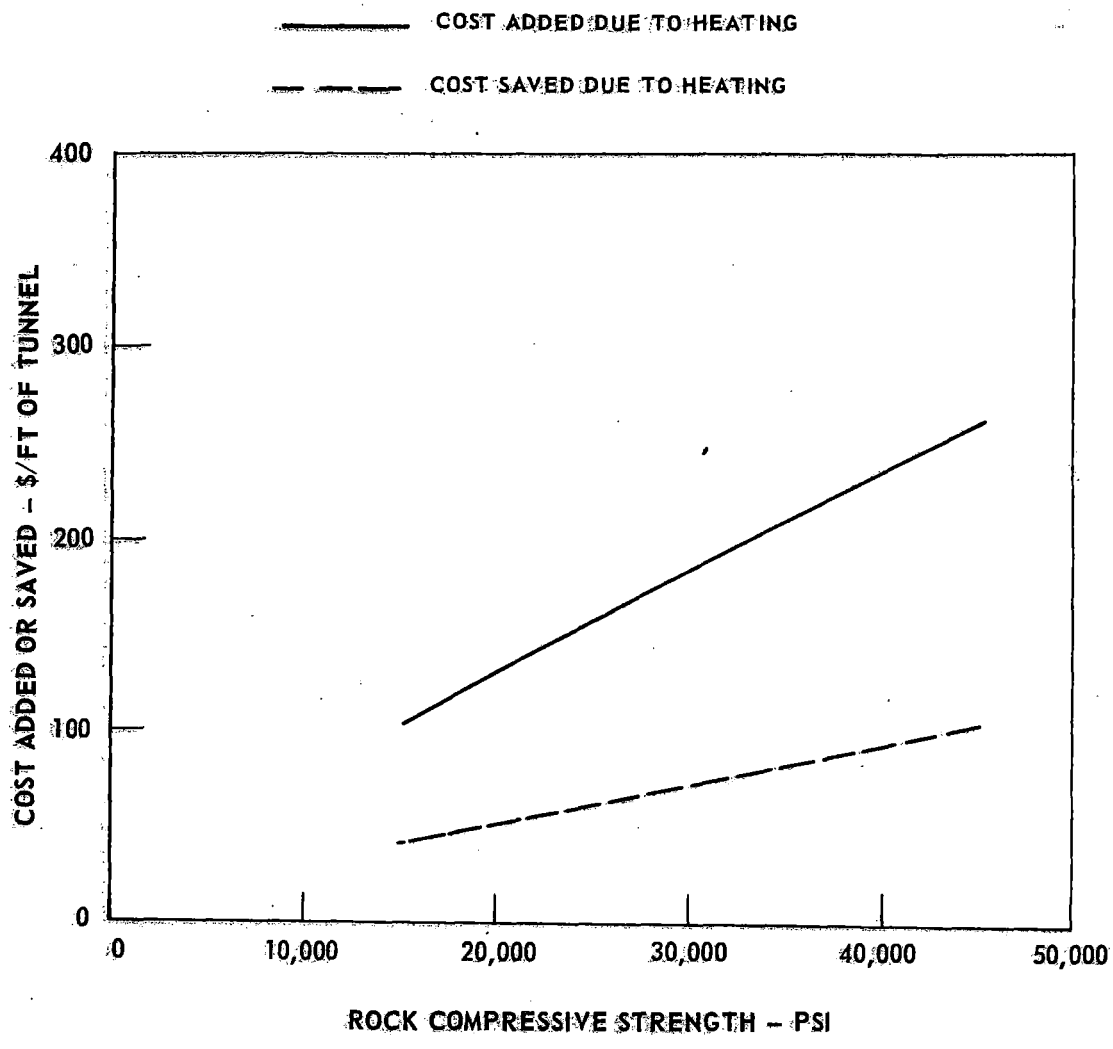

FIGURE 164. INCREMENTAL COSTS AND SAVINGS FOR LASER-ASSISTED TUNNELER

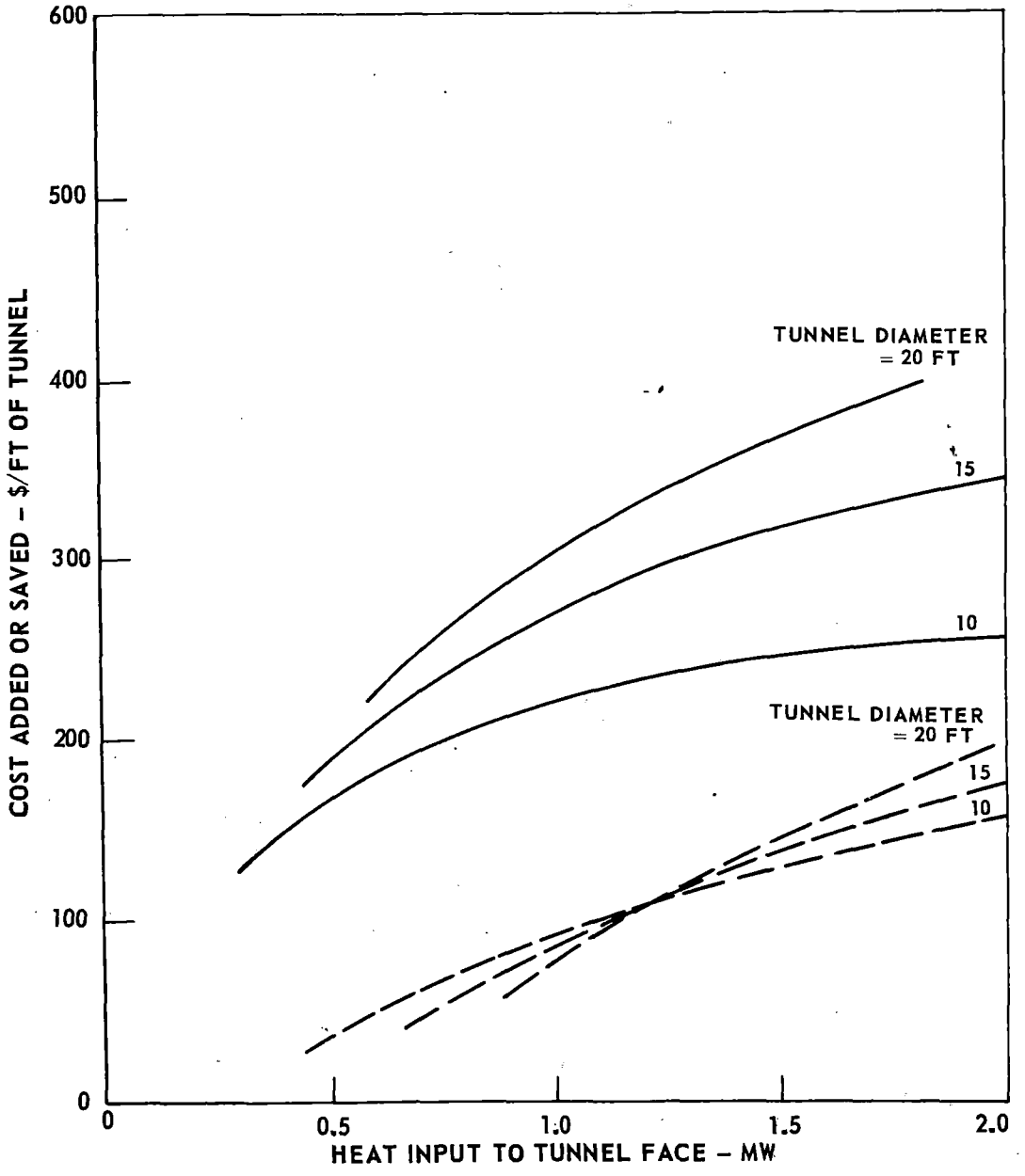

FIGURE 165. INCREMENTAL COSTS AND SAVINGS FOR LASER–ASSISTED TUNNELER

is apparent that, for these test results, the addition of heating power is slightly more efficient in small tunnels. However, even for this most optimistic set of test data, the costs incurred still exceed the costs saved for all conditions.

Figures 166 and 167 allow determination of the laser capital cost levels necessary for the expected savings to be equal to the increased costs at two typical heating levels, 1000 and 4000 joules/in., respectively. For a 20% laser electrical efficiency the break-even laser cost is $1000/kw based on the test results at cutter thrusts of 5000 lb (Fig. 166), and roughly $2800/kw based on the 3000 lb, independent cut tests (Fig. 167). These cross-over costs would vary somewhat with heating power level, but the example cases chosen are of greatest interest based on the previously discussed results.

Costs and Savings of Heat Weakening by Radiant Heaters

Figure 168 shows the additional costs and savings due to adding a radiant heater system to a tunneler, assuming the resulting increase in muck removal rate is used to reduce machine rpm. The test results used for computing this figure are the unfocused laser tests at 5000 lb cutter thrust reported in Fig. 47 as test 3. The cost per foot of the heating system (as before, this includes device capital and power costs, as well as environmental control system costs) is relatively insensitive to changes in tunnel diameter for a given heating power. Cost savings, however, increase markedly with larger tunnel diameter, where the cutter costs represent a larger percentage of the total excavation cost.

As shown on Fig. 168, there are limitations on the analysis which may overlap to prevent the possibility of a successful radiant heater design for a 10-ft-diameter tunnel. As discussed in Chapter III, the radiant heater system is basically a low-power-density device. Limitations on the power that can be installed were established, ranging from about 650 kw in a 20-ft-diameter tunneler, to 160 kw in a 10-ft machine. The heating power into the rock (85% of the heater power output) is therefore limited, as shown by the limitation on the right-hand side of Fig. 168. A second limitation is based on the threshold amount of heat required to significantly damage the rock. Although the data in Fig. 47 indicate a significant effect of rock heating even down to very low values of heat input, detailed examination of the test data indicates that the advantages shown by the curves in Fig. 47 are probably invalid below heat input levels of about 500 joules/inch. This value then forms a boundary as shown on the left-hand side of Fig. 168. Although the exact locations of these boundaries might vary somewhat from those assumed here, based on more detailed analysis, it appears that use of the radiant heater concept may not be possible for 10-ft-diameter tunnels. For 20-ft tunnels, the concept does appear to be feasible but would not result in any net excavation cost savings.

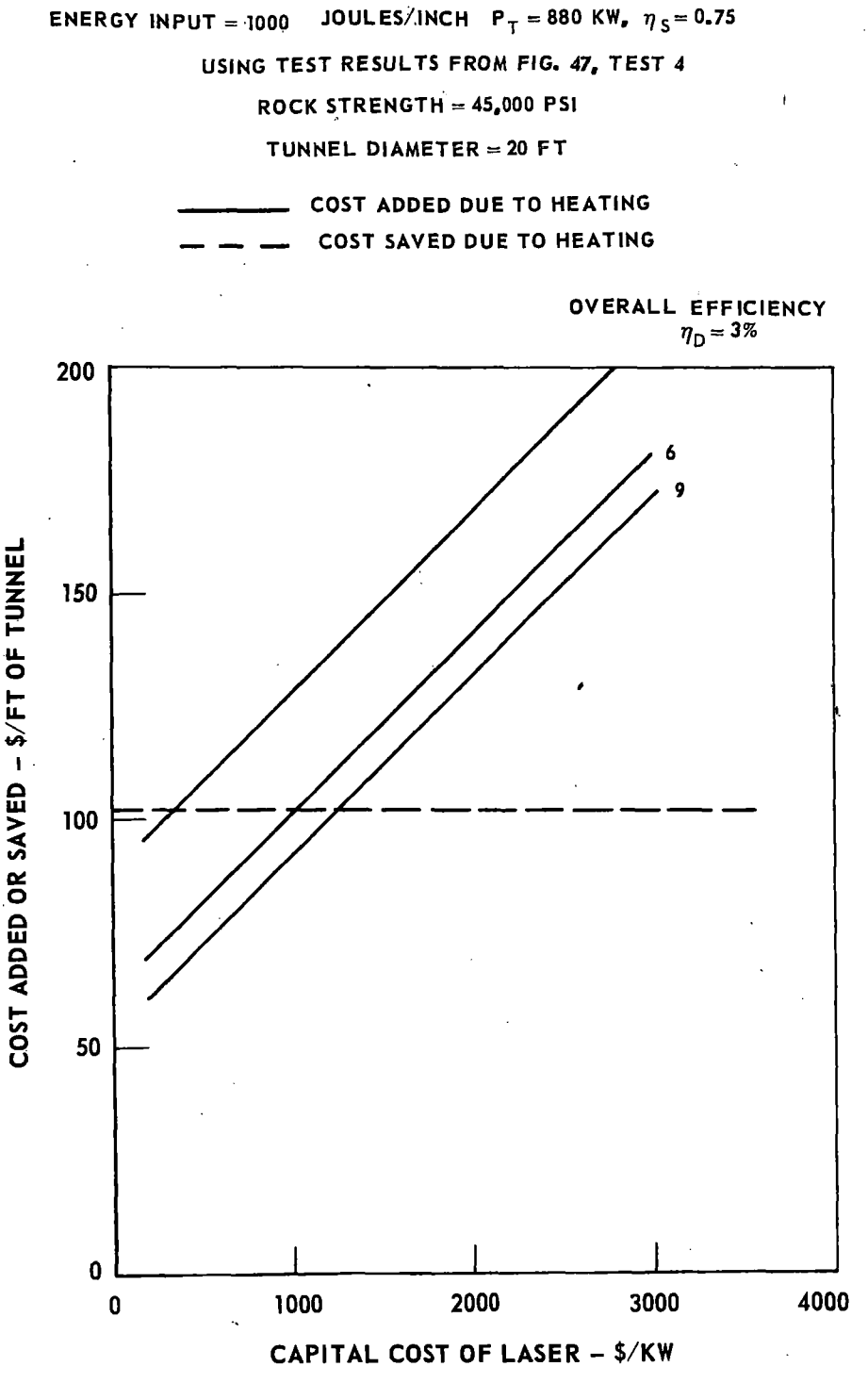

FIGURE 166. DETERMINATION OF "BREAK-EVEN" CAPITAL COST OF LASER DEVICE

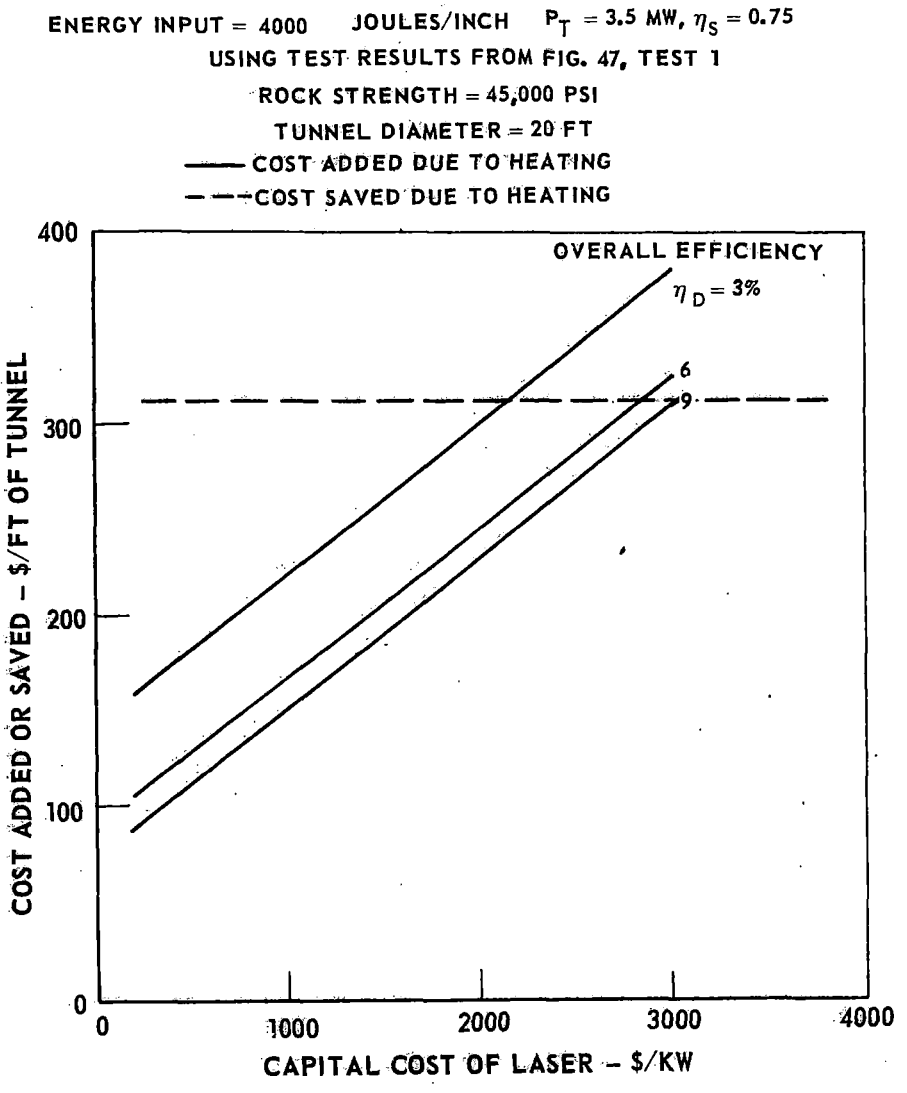

FIGURE 167. DETERMINATION OF "BREAK-EVEN" CAPITAL COST OF LASER DEVICE

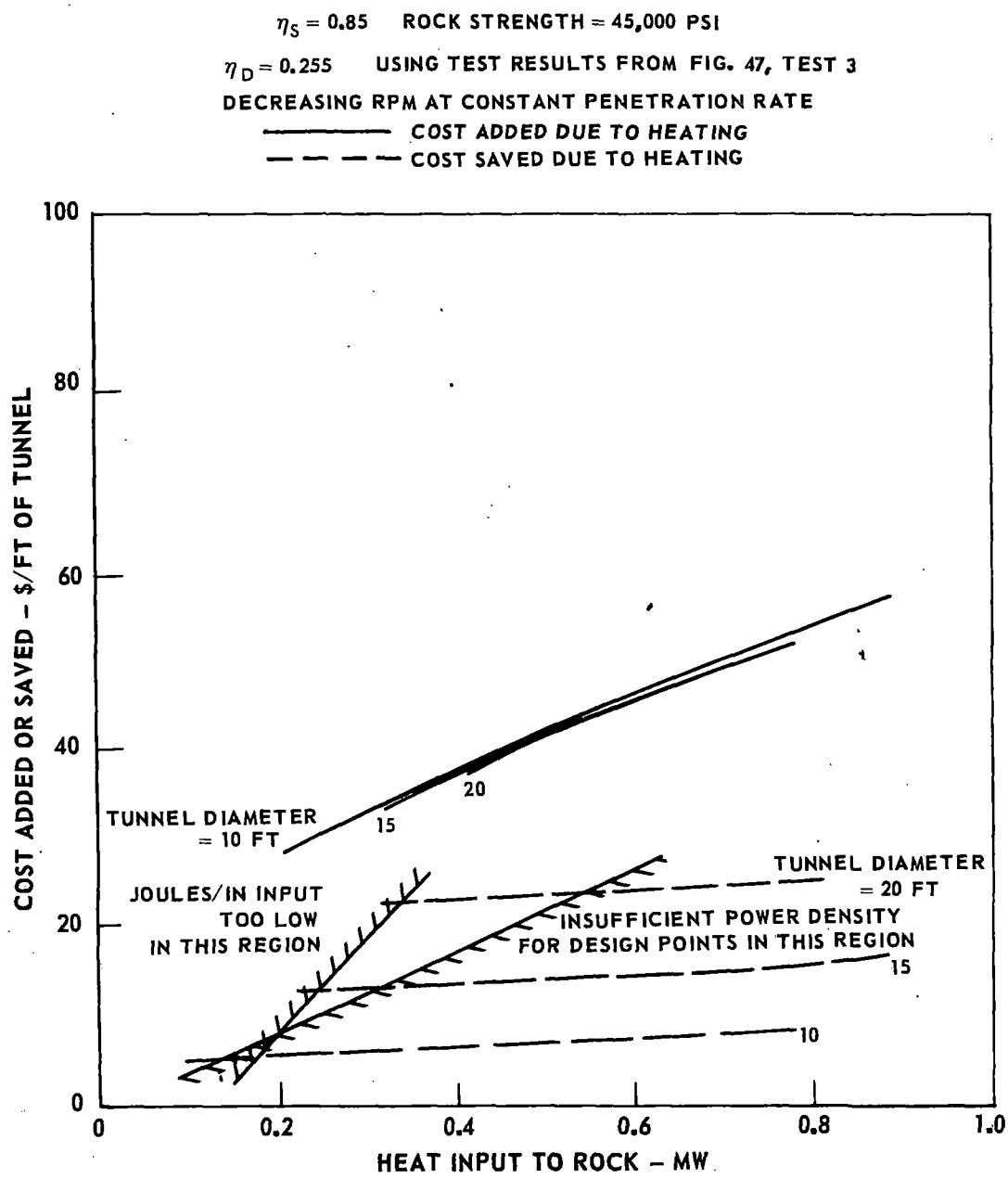

FIGURE 168. INCREMENTAL COSTS AND SAVINGS FOR RADIANT-HEATER-ASSISTED BORING MACHINE

The effect of assuming an increase in machine penetration rate with an increased rock removal rate due to heating is shown in Fig. 169 . Since there is no reduction in machine rpm for this case, a larger installed power is required to deposit a given heat energy per revolution, and the heat input limitation moves to the right. As a result, the concept appears to be feasible only for tunnel diameters greater than 16 to 17 ft, and only a fairly narrow range of design conditions is offered even for a 20-ft tunneler. However, for an installed heater power of roughly 600 kw, the cost of adding the heating system is roughly equal to the expected cost reductions.

These results are all for boring in 45,000 psi rock. As would be expected, relative cost benefits of adding heat are greater in the higher rock strengths, as shown for a typical case in Fig. 170.

The effect of radiant heater capital and operating cost on the heating system cost per foot of tunnel is shown in Fig. 171. Since the radiant heater is relatively inexpensive and efficient, even large changes in the cost and efficiency parameters have little noticeable effect on the system costs. The environmental control costs constitute a large part of the heater system costs with the radiant heater.

The rock-cutting test data used in computing Figs. 168 through 171 was that taken with an unfocused laser, which corresponds to a heated path width of approximately one inch. Consulting the test data, it is noted that if the heating beam could be more sharply focused, an increase in the muck removal ratio from 1.09 to 1.20 would be expected. This increase in the muck removed would cause an increase in the costs saved to about $81/ft, and a net cost saving of roughly $43/ft. However, such good focusing would be impossible, since the heater element diameter (1/2 inch) is greater than the heated path required (3/8 inch). Considering the geometric limitations on reflecting optical systems, it is felt that an effective heated path of 1 in. is probably optimistic.

ANALYSIS OF KERFING CONCEPT

Three modes of thermal kerfing were investigated, as reported in Chapter V. In the first mode, the heat energy was simply assumed to be focused to a sufficiently small path width to cause a small kerf to be formed. Mechanical cutting would then proceed as in the heat-weakening mode. The second mode, which is referred to as deep kerfing, involves making deep slots, with the protruding annuli of rock then being broken off by a wedging or hammering action. Rate of penetration in this deep kerfing mode is assumed to be determined by the thermal power requirements, as outlined in Chapter V. The third mode of kerfing assumes complete removal of the rock by slotting; no mechanical impact or pressure is required for rock removal. This mode is labeled pure kerfing.

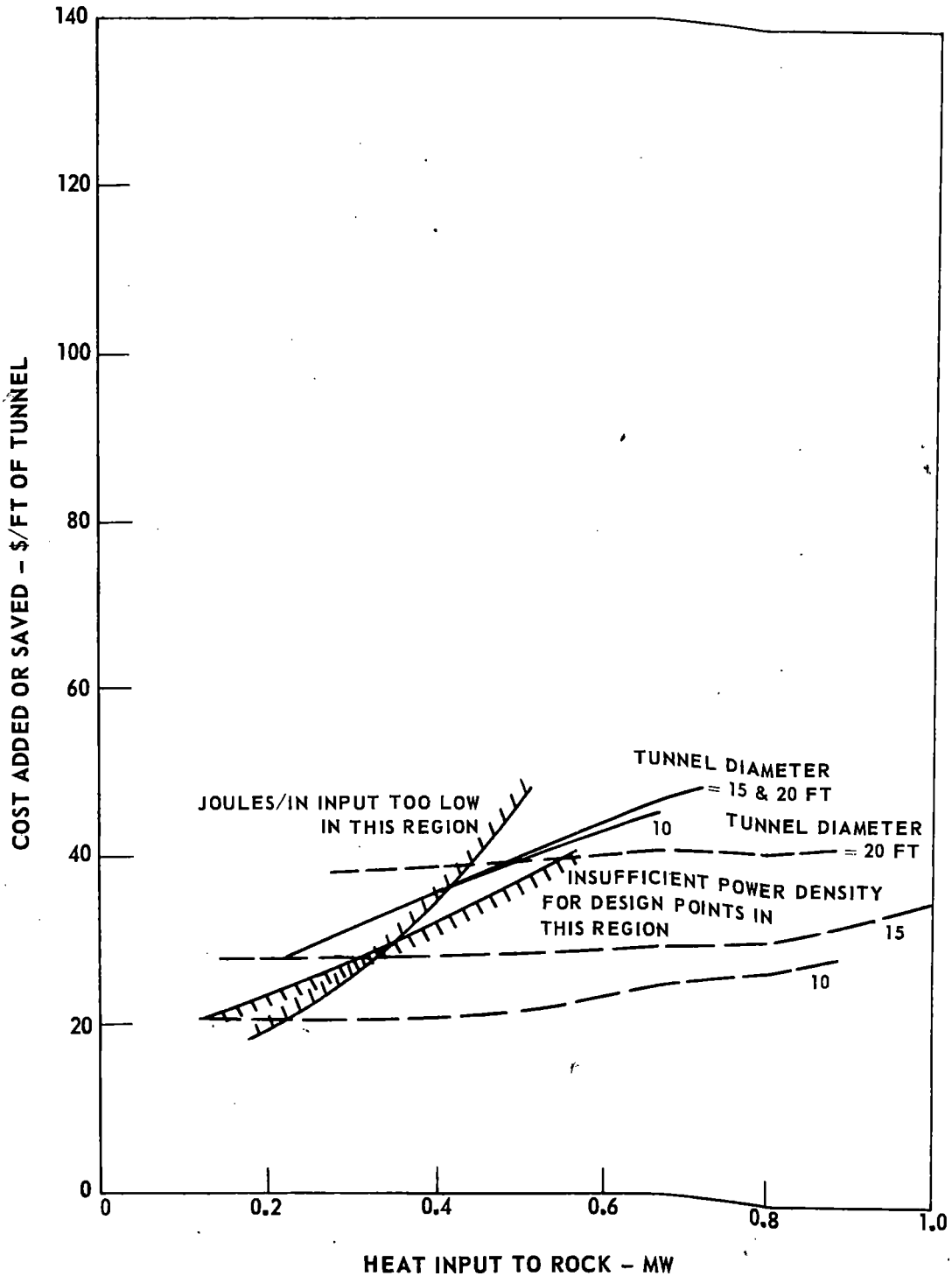

FIGURE 169. INCREMENTAL COSTS AND SAVINGS FOR RADIANT-HEATER-ASSISTED BORING MACHINE

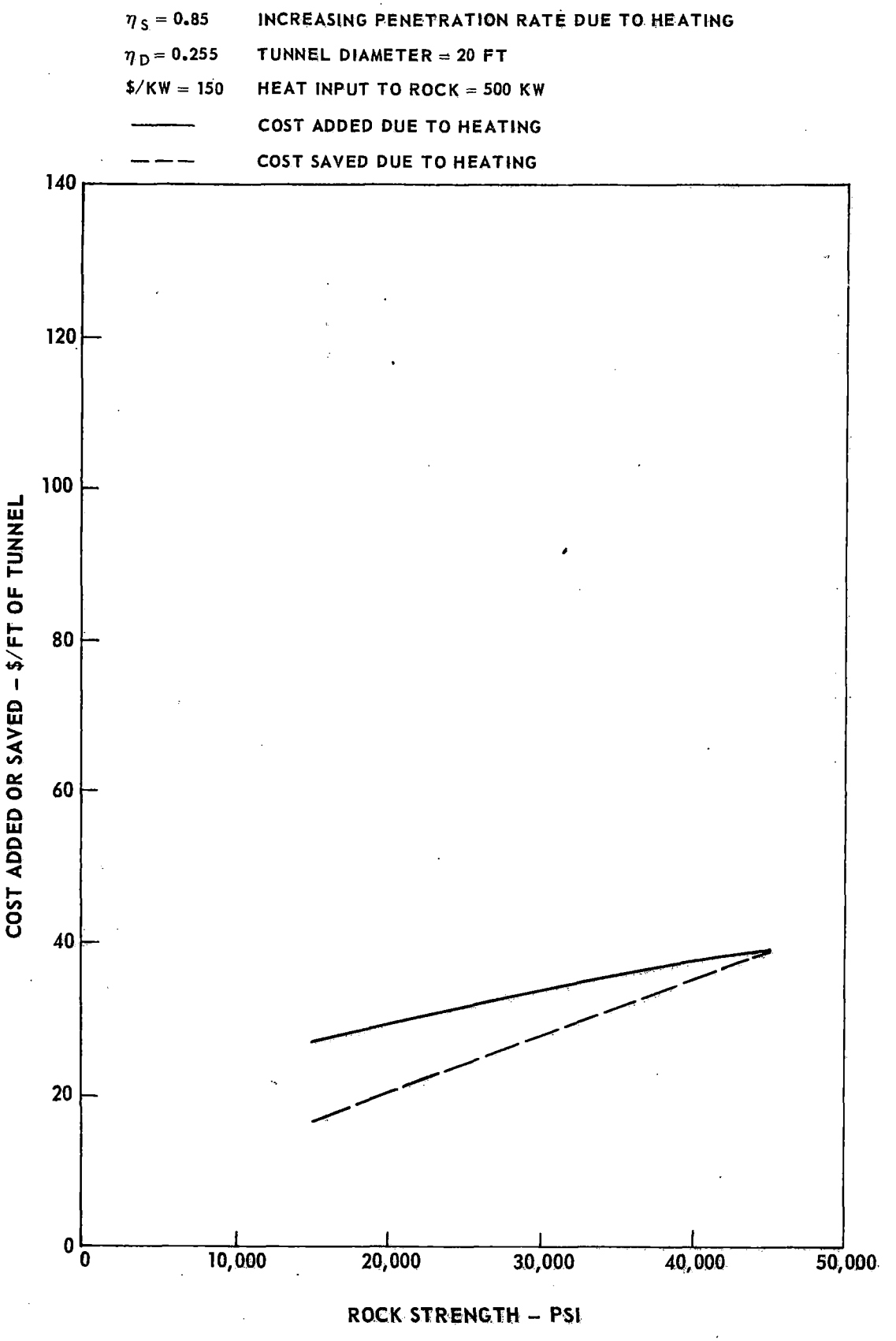

FIGURE 170. INCREMENTAL COSTS AND SAVINGS FOR RADIANT-HEATER-ASSISTED BORING MACHINE

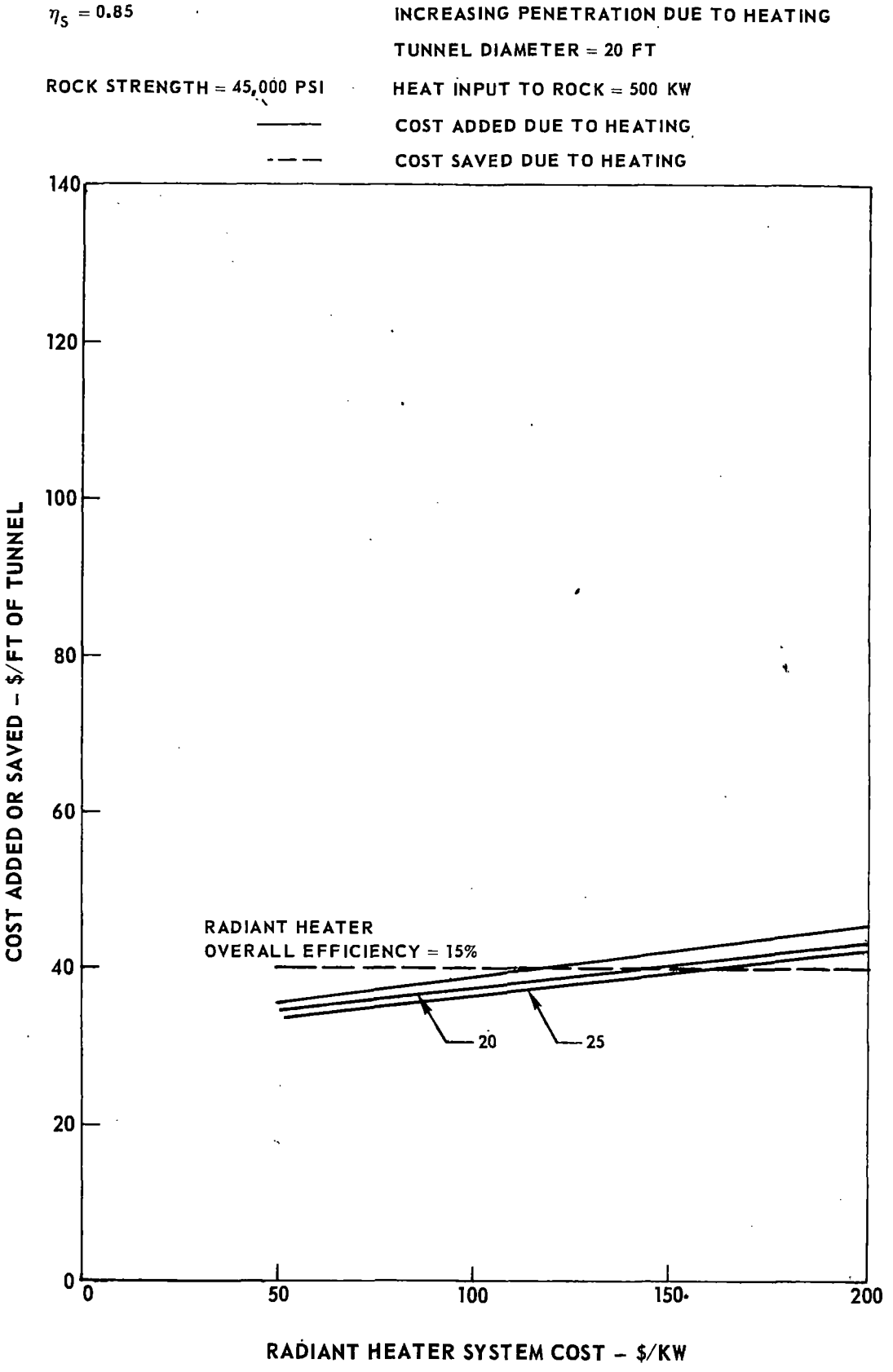

FIGURE 171. INCREMENTAL COSTS AND SAVINGS FOR RADIANT-HEATER-ASSISTED BORING MACHINE

A single test data point was developed for the first mode, which is presented and discussed in Chapter V. For the other two modes of kerfing, some exploratory economic calculations were performed, based on the relationship between thermal power output, advance rate, and kerf geometry discussed in Chapter V.

Deep Kerfing Mode

For the deep kerfing mode, it is assumed that some reduction in cutter cost would be realized, due to the more efficient mode of mechanical cutting expecte . Thus, a saving in cutter cost of 50% was assumed. This reduction is arbitrary, but is more reasonable than assuming no cutter cost reduction. All other costs were calculated as for the heat-weakening case, with the penetration rate being given by the thermal energy analysis (see Fig. 155).

The cost results of this analysis are shown in Fig. 172. This figure is for a thermal kerfing system power output of 1 megawatt. Other power levels would show different relationships between the system cost and the kerf geometry, but 1 megawatt was assumed here as a typical case. The excavation cost plotted in Fig. 172 has the same components as the total costs developed in Chapter IV, less profits and the 5% indirect cost. For reference, the costs based on a similar accounting basis are shown for a nonheat-assisted boring machine. As shown, the costs for deep kerfing are similar to those for mechanical cutting only if the kerf width-to-depth ratio is in the range of 0.015 to 0.025 (kerf d/w = 40 to 67), depending upon the laser cost. Interesting economics are achievable, even for a laser cost of $5000/kw, if kerf w/d can be decreased to 0.01.

The 1 megawatt system is less desirable in a 20-ft-diameter tunnel, as shown in Fig. 173. Here the kerf width-to-depth ratio must be well below 0.01 to show substantial economies over pure mechanical tunneling. A higher power would probably yield better excavation economies at a given w/d for this tunnel size.

Pure Kerfing Mode

Finally, some results were calculated for the pure kerfing mode, for which the cutter costs were assumed to be zero. These results are shown in Fig. 174. The costs in these curves are considered comparable to mechanical boring costs at any rock strength, since it is assumed that the thermal properties of the rock are unaffected by the rock strength. To compete with present-day mechanical tunneling costs in 25,000 psi rock, it is clear that kerf width-to-depth ratios below 0.005 will be required. Again, this is for the particular case of a 1 megawatt heating level in a 10-ft-diameter tunnel, which may not be the best power level. In any event, however, it is probable that a somewhat lower w/d will be required for the pure kerfing mode relative to the deep kerfing mode. The real question remains: what is the feasible depth-to-width ratio that can be achieved?

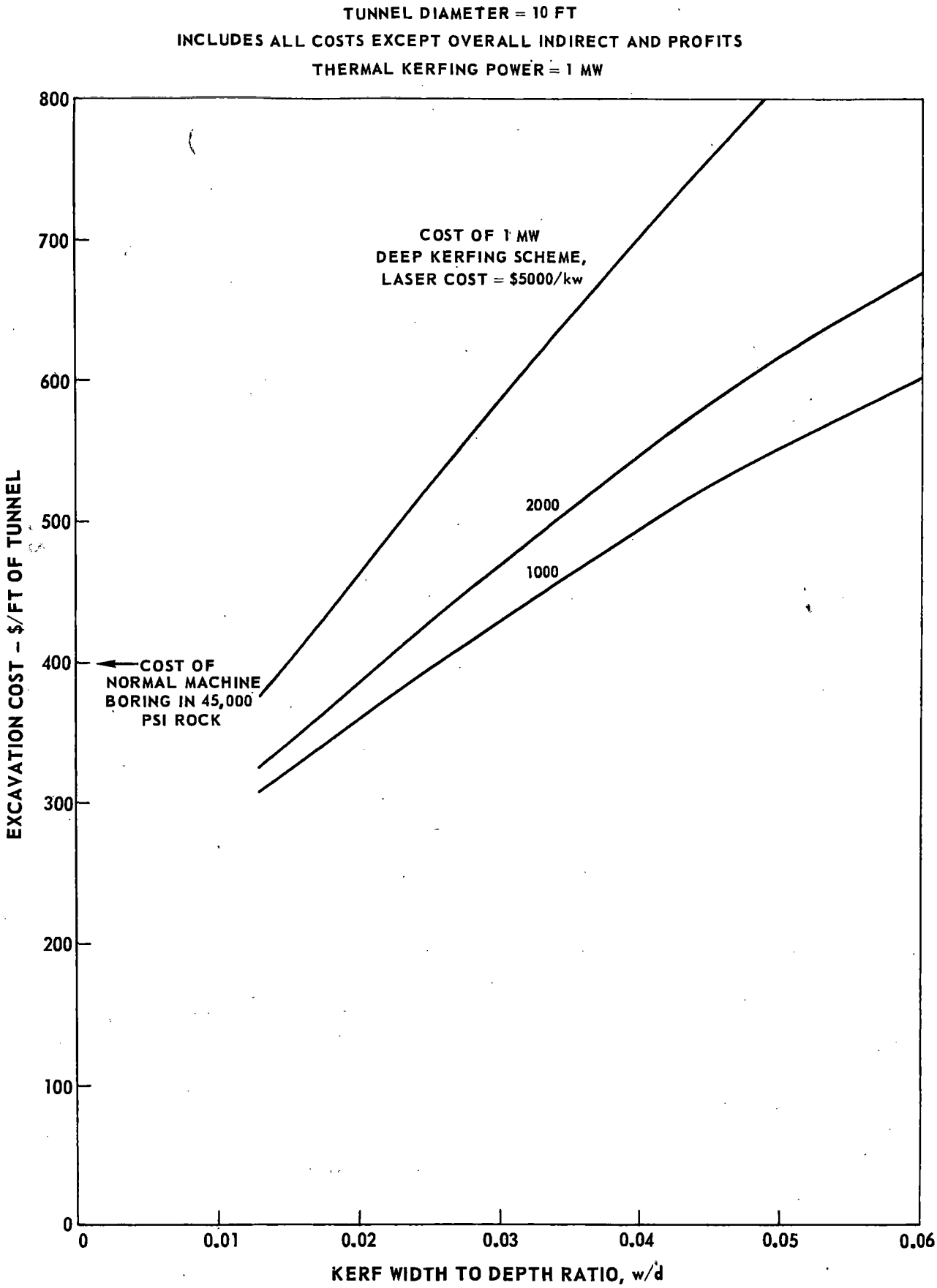

FIGURE 172. COST OF TUNNELING WITH DEEP–KERFING SYSTEM

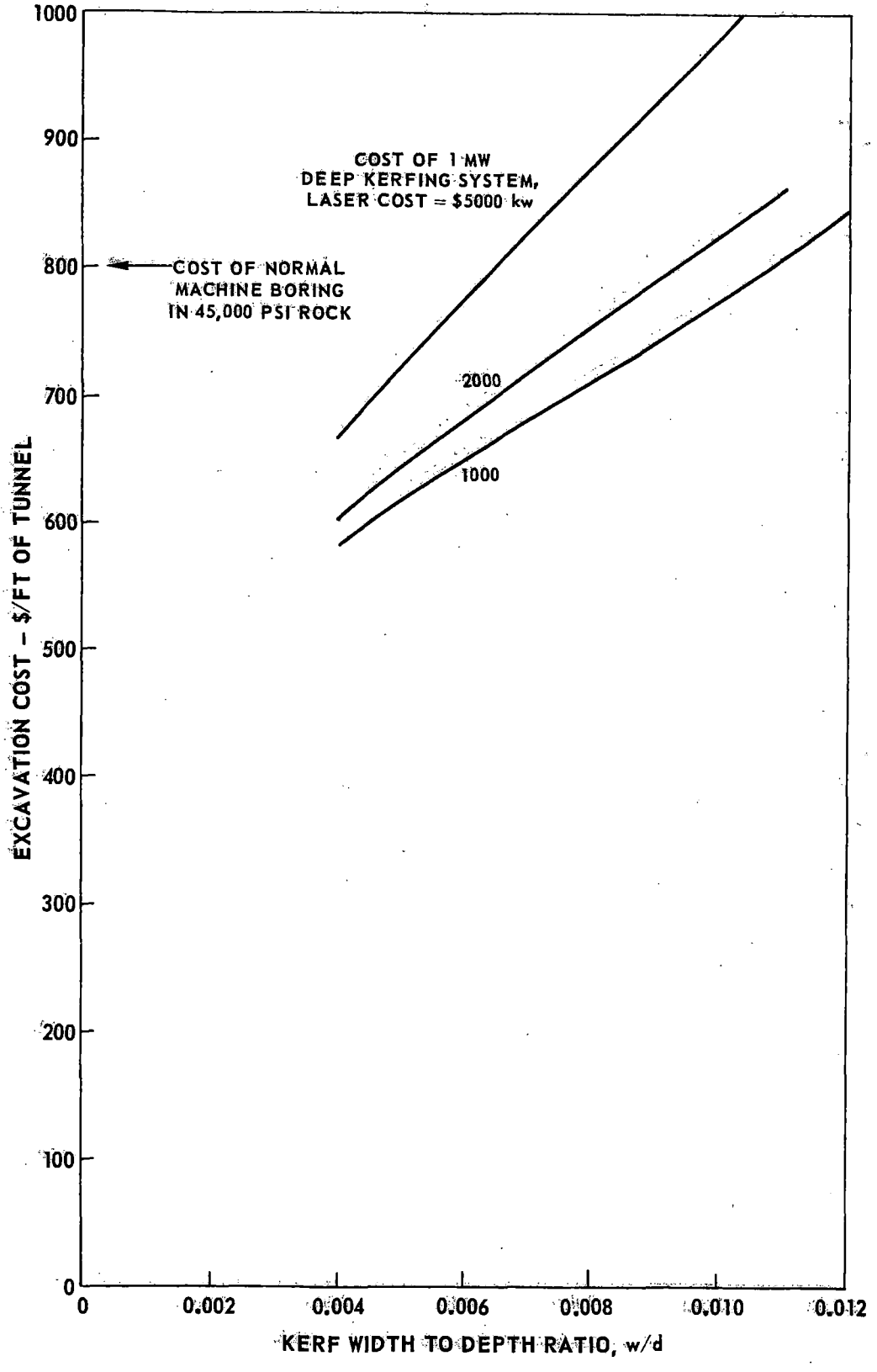

FIGURE 173. COST OF TUNNELING WITH DEEP-KERFING SYSTEM

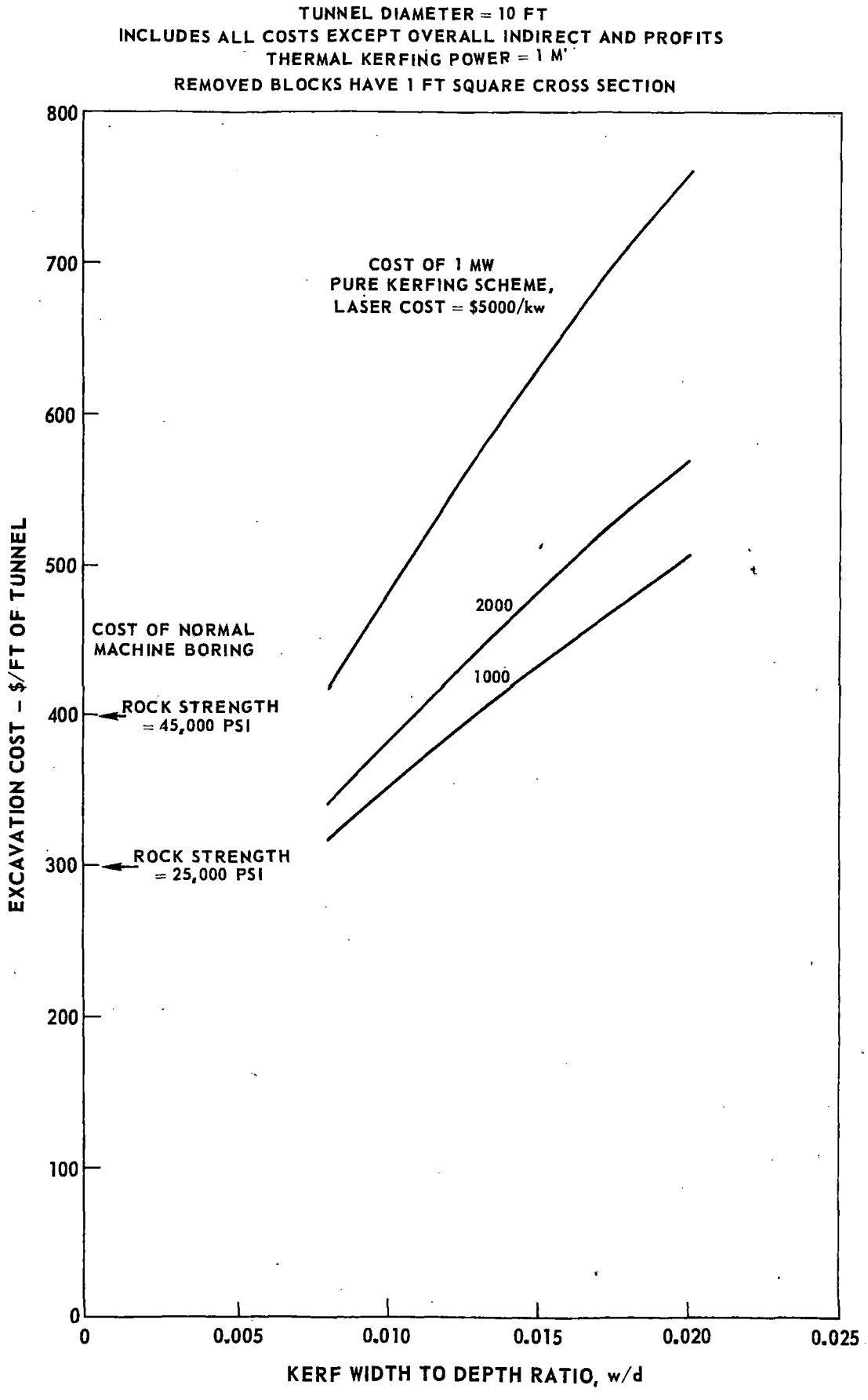

FIGURE 174. COST OF TUNNELING BY PURE KERFING MODE

CONCLUDING REMARKS

It is of interest to review certain limitations on the scope of the analyses leading to the above economic results, and to speculate on the possibilities of their relaxation.

The amount of radiant-heater power that can be installed on a boring machine head is limited by the cutter assembly housing size and muck scoop designs typical of present-day tunneling machines. A complete redesign of a tunneling machine head, with particular emphasis on compact arrangement of cutter housing and muck scoops might well permit a significant increase in the amount of radiant heater units that could be installed. As a result, the right-hand boundaries in Figs. 168 and 169 would be moved to the right, thus making design points in smaller tunnelers more feasible. Also, all the (unfocused laser) data upon which the radiant heater economics are based assume heating along the cutter path. If the heating were done between cutter paths, the indicated benefits may be greater than is shown here. However, it is unlikely that the indicated benefits would be sufficient to justify development of such a machine.

Another area where present mechanical boring technology is restricting the potentialities of heat-assisted boring is through the tunneler rpm. The present tunneler rotation rates, as specified in Chapter II, are those which are felt to be near-optimum considering both rate of penetration and tool wear. If advances in cutter design could be achieved so as to allow efficient cutting at lower tunneler rpm, the heating power required to do a certain amount of damage to the rock in each revolution could be reduced.

A third area into which elements of the analyses in this study could be extended is nonfull-face boring machines. Some tunneler type such as the Greenside-McAlpine machine (in Fig. 55) could be combined with a separate heating source, such as the 150-kw electron beam installation shown in Chapter III. Although the Greenside-McAlpine machine has a basically low penetration rate, there are other existing machines, such as the Habegger Mole, which use multiple separate heads working on the face, and which evidently show some basic advantages over the full-face machines for present-day, nonheat-assist operation.

A final point concerns the possibility of using concentrated heat energy to alleviate the cutter bit problems only at the outside gage of the tunnel. It is a generally accepted fact that the gage cutters account for a greater share of the total cutter cost, on a per-cutter basis, than the interior cutters. Informal estimates of the percentage of total cutter cost represented by the gage cutters range from 30% to 60%. Significant weakening or kerfing of just the gage could be accomplished for far less heating power than has been considered here to heat the entire face. Employing kerfing at only the gage would therefore have a greater effect on cutter cost reduction per unit of heat added than would the other concepts considered herein. The economics and performance advantages of applying thermal power only at the gage should therefore be considered further.

CONCLUSIONS

GENERAL CONCLUSIONS

1. The operation of tunneling machines incorporating lasers to heat weaken hard rock in advance of mechanical cutters is technically feasible, but economically unattractive. This result is primarily due to the current very high projected capital cost of large laser units. No commercial lasers have yet been built in the size range treated in this study; however, if such a unit were built, it is estimated it would cost $10,000/kw. This capital cost would have to be reduced to less than $1000/kw before the cost of adding such a heating system would be less than the tunneling cost savings expected from the heat-weakening effect.

2. Tunneling machines employing metal-clad radiant-heater elements to heat weaken the rock generally will also cost more to install than they can save in tunneling costs, although one 20-ft-diameter tunneler configuration was identified for which the excavation cost saved by adding the heater roughly balanced the cost of installing the heating system. The main disadvantages of these heaters are their low power density and poor focusability. Based on present-day tunneling machine characteristics developed in this study, such a heating system is more desirable for a large-diameter (20 ft) tunneler than a small-diameter (10 ft) machine.

3. The use of concentrated thermal energy to melt shallow kerfs in rock to assist mechanical tunnelers can result in the removal of twice as much rock per unit of heat input as in the case of the heat-weakening (nonmelting) concept.

4. Deep thermal kerfing, which would allow a substantial reduction in the mechanical energy requirement and mechanical cutter cost for tunneling even in very hard rock, would require making kerfs in the rock with a depth-to-width ratio on the order of 100 or more to be economically attractive. Whether or not ratios this high could actually be achieved has not been determined.

DETAILED CONCLUSIONS

1. The residual damage due to heating, measured by testing rock that has been heated by the laser and then cooled, does not change the rate of muck removed significantly reduces the specific energy slightly. Similar tests made with the same heat input but while the rock was still hot show an increase in muck removal and a larger decrease in specific energy, indicating the added effect

of the thermal stress field on increasing the mechanical cutter efficiency. These results are for an unfocused laser beam, one inch in diameter.

2. Focusing the laser beam to $\frac{1}{4}$ in. in diameter and offsetting the heating path from the cutter path provides the largest increase in cutting efficiency. For this mode of operation with a 650-watt laser beam, the muck removal rate was increased by as much as 60% relative to the unheated case, at a 5000-lb cutter thrust level.

3. There is a threshold amount of heat energy input to the rock below which there is no detectable reduction in rock cutting specific energy or increase in muck removal. For most tests of interest, this threshold is about 500 joules/inch of heater path, for independent cuts by a 3000-lb-thrust cutter on an initially smooth rock surface.

4. There is an optimum spacing between parallel cutter paths for which the rate of muck removal is a maximum and specific energy of rock removal a minimum. This optimum spacing increases with either increasing cutter thrust or decreasing cutter diameter. The optimum spacing for many repeated cuts is greater than for a single set of cuts made on an initially smooth surface.

5. For the test setup at MIT, increasing the cutter speed causes a noticeable increase in the specific energy required for muck removal and a decrease in the muck produced, both for initial cuts on a smooth surface and for many repeated cuts.

6. Tests run on a smooth block at 5000-lb cutter thrust with a 4-in.-diameter cutter, and repetitive cuts made at 3000-lb cutter thrust gave similar results, and are felt to be the most representative of full-scale rock cutting. Increases in muck removal with heating were limited to under 60% for the heat inputs run under this program.

7. It is technically feasible to modify a full-face rotary tunneling machine to transmit laser energy for heating a rock face. Such an adaptation would be particularly straightforward if the laser energy could be supplied to the center of the rotating head through a tube along the central axis of the boring machine.

8. For a laser-assisted boring machine, the laser itself will most likely be placed outside the tunnel. The laser energy will be delivered to the machine in a protective tube supplied with dry air. Periodic mirror stations will be required for beam pointing and refocusing. The number of these mirrors should be kept to a reasonably low level; laser-assist is therefore less likely to be used in tunnels with many curves.

9. Control of the tunnel environmental temperature increase caused by either a laser or a radiant-heating system should pose no insurmountable environmental temperature problem. Nominal amounts of cooling water, plus 10,000 cfm of cooling air, will keep tunnel temperatures near the face at or below 80 deg F for all design cases considered.

10. Dust regenerated by rock cutting is not expected to cause a major loss of laser power. Rock conditions must be dry or "wet rock" (i.e., no flowing water) for useful heating with a laser beam.

11. The likelihood of flowing water conditions on the tunnel face absorbing laser power, can best be minimized by injecting cooling air on the rock face at the point of laser beam impingement so as to keep large quantities of water out of the beam, and adding cooling water to the muck behind the face area proper.

12. High-temperature jets have substantially lower heat transfer efficiency to a rock face than does radiant energy. Also, flame and plasma jets would pose an extreme air pollution problem in the tunnel which would require a sophisticated, expensive removal system.

13. Electron beam machines are not suitable for heat weakening in conjunction with rotary full-face tunneling machines because of (a) the necessity for a close (less than 2 inch) stand-off distance, (b) the large volume of space required for an electron beam machine, (c) their inability to rotate continuously because of the required vacuum and high-voltage supply lines, and (d) their production of X-rays. They are not suitable for kerfing primarily because of the even closer stand-off distances required.

14. The muck trains for heat-assisted boring operations will likely be shorter than those for normal boring operations, to minimize the heat released to the tunnel by the (potentially) hot rock. The sooner the hot rock is transported from the tunnel, the less of its heat is deposited in the tunnel walls. Alternatively, some form of insulating covers may be employed on the cars.

15. Cutter costs are a significant portion (as much as 30%) of the total costs of machine tunnel boring. Cutter costs increase, both absolutely and as a percentage of total excavation costs, with increasing rock strength and increasing tunnel diameter.

16. The test results do show that the application of heat energy to rock can increase the muck removal rate of subsequent mechanical cutting. The economic analysis indicates that this effect should be employed to increase machine advance rate rather than to reduce machine rpm at a constant advance rate.

17. Present cost estimates for large-size laser systems are in the neighborhood of $10,000/kw. Future increases in laser efficiency (which would reduce the power supply size requirements) and development of less expensive subsystems may allow reduction of this cost to the neighborhood of $5000/kw for very large lasers.

18. Informal estimates made by cutter bit manufacturers suggest that between 30% and 60% of the total cutter cost on large-diameter tunnels can be ascribed to cutting the gage. Therefore, the use of high-density heat from a laser to make a shallow kerf at the gage diameter of the tunnel should yield a greater benefit per unit of heat than would full-face heat weakening.

RECOMMENDATION

Although the results of the present study indicate that the heat-weakening concept is uneconomic, the data developed on the kerfing mode appear to warrant further investigation. In particular, the concept of kerfing only at the tunnel gage, to eliminate the mechanical gage cutters, would appear to cause a maximum reduction in the cutter cost per unit of heat applied, and would result in laser system power requirements which may be satisfied by commercially available systems in the foreseeable future.

A comprehensive program involving kerfing tests, small-scale mechanical tests, and an analysis of the full-scale gage cutter problem is recommended. Kerfing tests should be run on various types of rock, with various laser types and power conditions, to establish laser power and optical system specifications for a mechanical test rig. A mechanical test rig, which allows rock boring both with and without gage kerfing should then be built, and mechanical and mechanical-plus-kerfing tests should be run. These tests will establish the benefits of such a concept at a small scale. Analysis should then be made of the full-scale gage cutter problem, and its importance as a limitation on mechanical tunnel boring. The results of the small-scale tests should then be reviewed in the light of the analysis of the full-scale data, leading to the possible definition of a full-scale test-bed.

APPENDIX A

TEMPERATURE PROFILES IN ROCK

Estimates of the temperature profiles within a semi-infinite rock depend upon determining the heat transfer coefficient adjacent to the rock surface. From Ref. 13 the relationship between Stanton, Reynolds, and Prandtl numbers and model geometry for a circular nozzle is:

$$(N_{St})\,(N_{Re})^{0.434}\,(N_{Pr})^{0.63} = 0.74\,\left(\frac{R}{D}\right)^{-0.434}, \tag{22}$$

where the terms of this and subsequent equations are defined at the end of this appendix. Equation can be rewritten in terms of its basic components in the following manner:

$$\left(\frac{h}{C_p G}\right)\left(\frac{dV\rho}{\mu}\right)^{0.434}\left(\frac{C_p \mu}{K}\right)^{0.63} = 0.74\left(\frac{R}{d}\right)^{-0.434}. \tag{23}$$

By rearranging terms of Eq. (23) and changing the units of R and V to in. and ft/sec, respectively, the heat transfer coefficient can be defined as:

$$h = 0.06225\, C_p G\left(\frac{\mu}{V\rho R}\right)^{0.434}\left(\frac{K}{C_p \mu}\right)^{0.63}. \tag{24}$$

Once this coefficient is established, the temperature at the surface or at any location within a semi-infinite body can be determined from the following expression (Ref. 13):

$$T_x = (T_f - T_R)\left[\operatorname{erfc}\left(\frac{X}{2\sqrt{\alpha t}}\right) - \exp\left(\frac{Xh}{K_R}\;\frac{\alpha t h^2}{K_R^2}\right)\operatorname{erfc}\left(\frac{X}{2\sqrt{\alpha t}}\;\frac{h\sqrt{\alpha t}}{K_R}\right)\right] + T_R. \quad \text{(II-A4)} \tag{25}$$

The heat flow rate into the rock surface then can be calculated for any time from the equation:

$$q = 2\pi R^2 h\,(T_f - T_s), \tag{26}$$

and the total heat flow into the target area is equal to:

$$Q = \int_o^t q \, dt. \tag{27}$$

Equation (27) may be solved explicitly, or the total heat flow may be approximated by calculating the heat flows over short increments of time and then summing these for the total time which a fixed target area is exposed to the jet exhaust. This latter method was selected for the procedure outlined in Appendix B.

NOMENCLATURE

C_p	Specific heat of exhaust gas - Btu/lb-F
d	Exit diameter of jet nozzle ft
G	Mass velocity of exhaust at nozzle exit - $lb/hr\text{-}ft^2$
h	Heat transfer coefficient in wall film - $Btu/hr\text{-}ft^2\text{-}F$
K	Thermal conductivity of exhaust gas - Btu/hr-ft-F
K_R	Thermal conductivity of rock - Btu/hr-ft-F
N_{Pr}	Prandtl number - dimensionless
N_{Re}	Reynolds number - dimensionless
N_{St}	Stanton number - dimensionless
q	Rate of heat transfer into rock surface - Btu/hr
Q	Total heat transferred into rock in time, t - Btu
R	Radius of rock wall target - in.
t	Time - sec
T_f	Exhaust gas temperature at wall - F
T_R	Equilibrium rock temperature prior to heat addition - F

T_x	Temperature in rock at distance x from surface - F
T_s	Temperature at rock surface - F
V	Exhaust gas velocity at nozzle exit - ft/sec
x	Linear distance into rock from surface - ft
α	Thermal diffusivity of rock - ft^2/hr
ρ	Exhaust gas density - lb/ft^3
μ	Exhaust gas viscosity - lb/hr-ft

APPENDIX B

Rock Temperature Profile Fortran Computer Program
Written for GE Time-Sharing Computer

```
10 DIMENSION XX(20)
12 DIMENSION HOLLI1(7),HOLLI2(7)
13 400 CONTINUE
15 READ 401,HOLLI1
16 READ 401,HOLLI2
19 401 FORMAT(4X,7A6)
20 READ,PO,TO,FAR,VAIR,DIST,XKROCK,CPROCK,RHOROCK,TOROCK,VCUT
21 +     ,DELTIM,XN
30 READ,XNX
40 NX=XNX;N=XN
50 READ,(XX(I),I=1,NX)
62 PRINT 63
63 63 FORMAT(//)
70 PRINT,"PROGRAM FOR DETERMINING ROCK TEMPERATURE PROFILES"
75 PRINT 76,HOLLI1
76 76 FORMAT(13H ROCK TYPE-     7A6)
>5 PRINT  -     7A6)
85 PRINT 86,HOLLI2
86 86 FORMAT(15H HEAT SOURCE -    7A6)
90 PRINT 100,PO,TO,FAR,VAIR,DIST,XKROCK,CPROCK,RHOROCK,TOROCK,VCUT
91 +    ,DELTIM
100 100 FORMAT(30H COMUSTION PRESSURE                    F7.2,4HPSIA/
102 +    30H COMBUSTION TEMPERATURE                    F7.1,2H R/
104 +    30H FUEL-AIR RATIO                             F7.3/
106 +    30H BURNER AIR FLOW                           F7.3,5H SCFM/
108 +    30H BURNER-ROCK SPACING                       F7.1,3HIN./
110 +    30H TH. CONDUCTIVITY-ROCK                     F7.4,11HBTU/HR-FT-F/
112 +    30H SPECIFIC HEAT-ROCK                        F7.4,9HBTU/LB-F /
114 +    30H ROCK DENSITY                               F7.2,8HLB/CU.FT/
116 +    30H INITIAL ROCK TEMPERATURE                  F7.1,1HF/
118 +     30H CUTTER SPEED                             F7.1,7HIN./SEC/
120 +     30H TIME INCREMENT                           F7.3,3HSEC/)
130 PRINT 140
140 140 FORMAT(3X,10HROCK DEPTH,9X,4HTIME,9X,9HROCK TEMP,5X,
142 +    14HHEAT FLOW RATE/6X,5H(IN..),11X,5H(SEC),12X,3H(F),11X,
144 +    8H(BTU/HR)    )
150 TOX=TO-460
160 PR=14.7/PO
170 TS=PR*.286*TO
180 A=49.028*SQRT(TS)
190 XM=SQRT((TO/TS-1.)*5)
200 VEXH=A*XM*.98
210 RHOE=39.612/TS
220 WAIR=VAIR/13.6
230 WEXH=WAIR*(1.+FAR)
240 AEXH=WEXH*2.352/(RHOE*VEXH)
250 DEXH=SQRT(AEXH/.785)
260 G=8640*VEX
```

```
270 R=DFXH/2 + DIST*.1051
280 VISFXH =.0000324*TS+.04398
290 XKFXH=.0000175*TS+.0115
300 CPFXH =.310883 -(.105239E-3)*TS+(.8519E-7)*TS↑2-(.278828E-10)
310 +    *TS↑3+(.425577E-14)*TS↑4-(.250341E-18)*TS↑5
320 A1=(VISFXH/(300*R*RHOF*VFXH))↑0.434
325 A2=(XKFXH/(CPFXH*VISFXH))↑.63
330 H=(.06225)*CPFXH*G*A1*A2
340 TSROCK=TS-460
350 ALPHAR=XKROCK/(CPROCK*RHOROCK)
380 TMAX=2*R/VOUT
390 QT=0
400 DO 11 I=1,NX
410 X=XX(I)12
411 IP=0
412 T=.000001
413 IQ=0
422 888 IF(T-TMAX) 40,41,41
424 41 T=TMAX
425 IP=N+1
426 40 IP=IP+1
430 T=T/3600
435 AAA=1-ERFC(X/(2*SQRT(ALPHAR*T)))
440 BBB=EXP(H*X/XKROCK + ALPHAR*T*H*H/(XKROCK↑2))
450 CCC=1-ERFC(X/(2*SQRT(ALPHAR*T))+H*SQRT(ALPHAR*T)/XKROCK)
460 TEMP=(TSROCK-TOROCK)*(AAA-BBB*CCC) + TOROCK
465 T=T*3600
470 IF(X) 55,56,55
472 56 Q1=(3.14159/144)*R*R*H*(TSROCK-TEMP)
474 QT=QT+Q1
480 55 IF(IP-1-N)700,66,66
485 66 IP=1
487 IF(X)680,681,680
488 681 IF(IQ)67,68,67
490 67 PRINT 32,1,TEMP,Q1
491 32 FORMAT(12X,F16.3,F16.1,F16.1)
492 GO TO 700
495 68 PRINT 30,XX(I),T,TEMP,Q1
500 30 FORMAT(F12.2,F16.3,F16.1,F16.1)
515 515 IQ=1
520 GO TO 700
525 680 IF(IQ)685,686,685
530 686 PRINT 30,XX(I),T,TEMP
532 GO TO 515
535 31 FORMAT(12X,F16.2,F16.1)
540 685 PRINT 31,T,TEMP
550 700 IF(T-TMAX+.0000001) 10,11,11
760 10 T=T+DELTIM
565 GO TO 888
580 11 CONTINUE
585 QT=QT*DELTIM/3600
590 PRINT 591,QT,R,AFXH
591 591 FORMAT(13H QT          =  F8.3,4H BTU /
592 +          13H R           =  F8.3,4H IN. /
593 +          15H NOZZLE AREA =  F8.5,7H SQ IN.  /)
610 GO TO 400
620 C
620 END
630 $USE FFBXXS***
640 $DATA
```

APPENDIX C

US ATOMIC ENERGY COMMISSION
STANDARD OPERATING PROCEDURE
NEVADA TEST SITE ORGANIZATION

MAXIMUM PERMISSIBLE EXPOSURE LEVELS TO LASER RADIATION

0570-01 The following laser exposure limits are listed in terms of incident energy/cm^2 or power/cm^2 on the body and are based upon "worst case" conditions in light of present knowledge. Any exposures that result in a persistent after-image should not be repeated.

02 Maximum Permissible Exposure Levels Incident on the Eye

a. For infrared lasers (wave lengths greater than 1.4 μ) the maximum energy incident upon the cornea of the eye is 0.1 joules per square centimeter per pulse or 1.0 watts per square centimeter for continuous lasers.

b. For lasers operating in the ultraviolet (< 0.4 μ) portion of the spectrum, the maximum permissible energy incident on the eye is 5×10^{-7} watts/cm^2 (average power).

c. For a continuous beam laser operated in the visible or near infrared (0.4 μ to 1.4 μ) portion of the spectrum, a corneal illuminance of 3×10^{-6} watts/cm^2 may be used.

d. For a pulsed laser operated in the visible or near infrared portion (0.4 μ to 1.4 μ) of the spectrum with off time between pulses of 100 milliseconds or greater and with a pulse duration shorter than 100 nano-seconds, a corneal illuminance of 0.1 watt per square ceintimeter peak power may be used.

e. Limits for repetitive pulsed lasers operated in the ultra-violet, visible or near infrared portion of the spectrum, with off time between pulses less than 100 milliseconds, cannot be determined at this time because of insufficient biological data. The limits for peak pulse power and average power output, when determined, will be more stringent than either of the limits based on the pulsed or continuous case listed above.

03 Maximum Permissible Exposure Level of Laser Radiation Incident on the Skin

For lasers operating in the visible, near infrared, and infrared portions of the spectrum, the maximum intensity incident on the skin, excluding the eye is 0.1 joules per square centimeter per pulse or 1.0 watts per square centimeter for continuous lasers.

APPENDIX D

DESIGN CONSIDERATIONS FOR ELECTRON BEAM MACHINES

In considering a design approach for an electron beam unit which may be suitable for use on or integration into a tunneling system, various significant design parameters must be reviewed and optimized for the intended environment. Two of the major considerations, which are discussed below for beam-out-of-vacuum equipment, are:

(1) Electron beam column definition, and

(2) Power requirement as a function of beam current and accelerating voltage.

Electron Beam Column

For most electron beam guns, a high vacuum environment of 10^{-4} torr is required for generating an electron beam. The degree of vacuum required depends, in large measure, on the type of cathode being used. For example, in a scanning electron microscope using a field emission source (Ref. 47), the gun requires a vacuum of 10^{-9} torr. Tests have shown that performance of the cathode tip is more dependent on the local gas pressure than on any other parameter. Conversely, for a vacuum melt furnace requiring an electron beam with high power (e.g., > 100 kw) and a large-diameter beam to promote surface heating, the cathode consists of a refractory-type disk having a diameter of $\frac{1}{2}$ inch or greater. The vacuum required for these operations is approximately 10^{-4} torr. For the majority of welding equipment, a vacuum of 10^{-4} torr or higher is also recommended. Directly heated filaments consisting of tungsten or tantalum ribbons or hairpin wire designs generally are used for generating electron beam emission. Some of the more specialized electron beam guns may use indirectly heated filaments. The latter designs are usually limited to specialized systems requiring high beam emission or a quality beam, i.e., an emitter which generates uniform distribution of electrons. For a third type of cathode, commonly referred to as a cold cathode design, electron beam emission can be generated for a vacuum range of approximately 10 to 300 microns; the optimum pressure usually is a function of the high voltage required to accelerate the electrons from the cathode through its fall region to the work-piece.

For each of the above cathode designs, various types of vacuum equipment are required. For the cathode structure requiring 10^{-9} torr, special molecular pumps coupled with diffusion and roughing pumps are needed. In addition, outgassing of

the system by using heat for "baking" is recommended. For the 10^{-4} torr regime, conventional oil diffusion pumps backed with roughing pumps are adequate. Electron beam operation at this vacuum usually can be achieved in a matter of minutes, depending on the amount of vacuum equipment utilized. For vacuum pressures of approximately 100 microns, a roughing pump usually is adequate. The rating (cfm) of the pump will determine system pumpdown time prior to initiating beam-on operations.

It therefore becomes apparent that the selection of the type of cathode will, in large part, determine the amount of vacuum equipment required. Since this vacuum equipment usually is mounted in a fixed position, flexible vacuum lines from the pump to the gun are required. These lines in turn must be effectively coupled to the out-of-vacuum electron beam column. The number and size of the lines are dependent not only on the cathode design but also on power output (gun), orifice (transmission) diameters, number of orifice stages, and operating high voltage. In brief, the cathode geometry, gun geometry, and beam power selected for impingement on the target determine the electron beam diameter.

The high voltage or accelerating potential particularly influences the beam diameter, since the voltage determines the speed of the electron or its effective probability of interaction with an air molecule, viz., the higher the voltage the less the probability of collision or interaction between elements.

To successfully transmit an electron beam from a vacuum to an ambient environment, one or more orifices are required. The openings of these orifices must be optimized so that the transmission efficiency is high (viz., > 90%), and influx of air through the orifices into the filament region is minimal. If transmission efficiencies are not maintained at a proper value, loss in beam intensity and/or overheating of the orifice structure can occur. Restated, a balance in orifice size and vacuum pumping must be maintained for effective electron beam out-of-vacuum transmission. Finally, laboratory tests have shown that electron beam transmission accomplished at accelerating voltages in excess of 100 kv produces electron velocities which have a longer mean free path and smaller beam diameter than an electron beam transmitted at lower accelerating voltages. For example, beam spot diameter can be related to accelerating potential by the following approximation (Ref. 48):

$$d = k\left(\frac{i}{v}\right)^{3/8}$$

where k is a function of the system spherical aberration and point of maximum beam constriction

i is the beam current

v is the beam accelerating potential.

For accelerating potentials of 100 and 150 kv, the approximate mean free paths for air are 0.063 and 0.100 cm, respectively (Ref. 49). The average distance traversed by an incident electron before an interaction occurs is the mean free path; this distance is a function of the gas atomic number, the gas density (vacuum), and the momentum (mass-velocity) of the incident electrons. Finally, transmission through the orifices as well as the air gap from orifice to workpiece can be enhanced by using an accelerating potential as high as possible to suppress spreading of the beam due to multiple scattering of the electron beam by air molecules. Using classical physics, Williams (Ref. 50) has derived the following expression for the mean square scattering angle for a collimated beam incident on a thin laminative scattering medium:

$$\theta^2 = \left\langle \frac{C}{E^2} \right\rangle$$

where C is a constant depending on the scattering medium, and

E is the energy of the incident beam.

Thus as high an accelerating potential as possible must be chosen to prevent the beam from fanning out and scarfing the orifice system.

Taking into consideration the above dependent design considerations, the approximate beam column dimensions for a 25-kw out-of-vacuum machine, including the electron optics and orifice assembly, are a cylinder of 12 inches in diameter a length of 30 inches. A directly heated tungsten filament is used for this gun. Weight of the gun assembly is estimated at 200 pounds; this weight estimate includes the optical column, the orifice staging assembly, and the interconnections to the gun for the required roughing and/or diffusion vacuum lines.

The use of a single gun rather than a number of multiple guns mounted on a large tunnel cutter is suggested; the limitations imposed by the need of supporting equipment, i.e., power supplies and vacuum equipment, required for each individual gun assembly preclude the use of multiple guns or the "Gatling" arrangement.

Power Relationships

Present out-of-vacuum electron beam equipment is rated at 25 kw. For this power, the vacuum pumps are two 300-cfm roughers used in conjunction with two 240-cfm

blowers; a 6-inch diffusion pump also is required to maintain the necessary vacuum in the upper electron optical column. For higher power systems, increased vacuum equipment will be required. To obtain higher powers, either the accelerating voltage or the beam current must be increased. The optimum solution would be to select an optimal accelerating voltage and beam current (power level) which would dictate the need for minimum vacuum equipment and also generate minimal X-radiation during beam impingement on the workpiece.

When beam power is increased from 25 to 300 kw and the accelerating voltage is kept constant, the beam diameter increases by a factor of approximately two-and-a-half, as given by the above equation for beam diameter.

When operating at higher powers, the orifice diameters must increase. For example, the normalized area ratio value increases from 0.5 at 6 kw and 200 kv to approximately 8 at 300 kw and 200 kv. Expressed more simply, the orifice openings must be approximately 16 times larger in area at 300 kw than at 6 kw. The ratios referred to for the various beam powers and accelerating voltages are based on an experimental 12-kw, 175-kv machine which uses a 0.06-inch diameter orifice having an efficiency of approximately 95%. The efficiency referred to is defined as that of beam energy which is transferred from the gun through the orifices to a target.

Further analyses indicate that at 150 kw the beam diameter is estimated at 0.075 to 0.100 inch for an accelerating potential of 150 kv. At higher accelerating potentials, or specifically at 350 kv and for a beam power of 150 kw, the beam diameter is estimated at 0.050 inch. It should be stated that the above reference values are analytical estimates. The total width of the beam may actually be larger if the fringes are added out to 2 σ which accounts for approximately 70% of the total beam energy.

For application of an electron beam to rock cutting, advantages in penetration and efficiency are obtained at the higher accelerating voltages. Minimal beam diameter and maximum kinetic energy thus are maintained. However, there are design limitations for the upper bound. These limitations are concerned with the designs of the high voltage insulators and the number of orifice stages required to transmit the beam from a high vacuum environment into a working ambient pressure. A preliminary study indicates that a prototype system should include a filament capable of delivering approximately 750 ma at an accelerating voltage of 200 kv. Such a system should provide 150 kw of power and possibly meet the power requirements for tunneling operations.

REFERENCES

1. Norman, N. E., and R. Stier: Economic Factors of Mechanical Rock Tunneling. Mining Engineering, June 1967, p. 75.

2. Carstens, J. P., et al: Feasibility of Flame-Jet Tunneling. Final Report to OHSGT on Contract No. 7-35126, May 1968. PB No. 178198, 178199, 178200.

3. Moavenzadeh, F., R. B. Williamson, and F. J. McGarry: Laser-Assisted Rock Fracture. MIT Department of Civil Engineering, R67-3, January 1967 (Clearinghouse No. PB-174 245).

4. Moavenzadeh, F., R. B. Williamson, and F. J. McGarry: Thin Disk Technique for Analyzing Rock Fractures Induced by Laser Irradiation. MIT Department of Civil Engineering, R68-21, May 1968 (Clearinghouse No. PB-179 205).

5. Williamson, R. B., F. Moavenzadeh, and F. J. McGarry: Some Relationships Between Power Level, Exposure Time, Sample Size and Weakening in Laser-Assisted Rock Fracture. MIT Department of Civil Engineering, R68-30, August 1968.

6. Farra, G., C. R. Nelson, and F. Moavenzadeh: Experimental Observations of Rock Failure Due to Laser Radiation. MIT Department of Civil Engineering, R69-16, April 1969 (Clearinghouse No. PB-187 274).

7. Moavenzadeh, F., R. B. Williamson, and A. E. Z. Wissa: Rock Fracture Research. MIT Department of Civil Engineering, R66-56, November 1966 (Clearinghouse No. PB-173 368).

8. Forootan-Rad, P., and F. Moavenzadeh: Crack Initiation and Propagation in Rock. MIT Department of Civil Engineering, R68-29, May 1968 (Clearinghouse No. PB-178 987).

9. Green, S. J.: Uniaxial Compression Tests on Three Geologic Materials. General Motors Corporation, Report No. MSL-68-6.

10. Williamson, T. N.: Tunneling Machines of Today and Tomorrow. Paper presented to Highway Research Board, Washington, D. C., January 14, 1970.

11. Banas, C. M.: The Role of the Laser in Material Processing. Presented at the Canadian Materials and Processing Technology Conference, Toronto, Canada, September 29-October 2, 1969.

12. Clark, S. P., Jr.: Handbook of Physical Constants. The Geological Society of America, Inc., 1966.

13. Metzger, D. E.: Spot Cooling and Heating of Surfaces with High Velocity Impinging Air Jets. Technical Report No. 52 for ONR Contract NONR 225(13). Stanford University, April 1962.

14. Rohsenow, W. M., and H. Y. Choi: Heat, Mass, and Momentum Transfer. Prentice-Hall, Inc., Englewood Cliffs, New Jersey, 1961.

15. Hovis, W. A., and W. R. Callahan: Infrared Reflectance Spectra of Igneous Rocks, Tuffs, and Red Sandstone from 0.5 to 22 μ. Journal of the Optical Society of America, Vol. 56, No. 5, May 1966.

16. Schumacher, B. W.: A Review of the (Macroscopic) Laws for the Electron Penetration Through Matter. First International Conference on Electron and Ion Beam Science and Technology. R. Bakish, Editor. John Wiley and Sons, Inc., New York, 1965.

17. Baddour, R. F., and R. S. Timmins (Editors): The Applications of Plasmas to Chemical Processing. The MIT Press, Cambridge, Massachusetts, 1967.

18. Lohs, K.: Toxology of Motor Vehicle Exhaust Gases. Zeitschrift Militar Med. Moscow, 1964.

19. Buscek, et al: Characteristics of Cross-Field Convectively Cooled CO_2 Lasers. Paper given at the 4th DOD Conference on Laser Technology, San Diego, California, January 1970.

20. Denes, L. J.: Surface Reflectivity at 10.6 Microns. United Aircraft Research Laboratories Report to be published.

21. Harrigan, F. A., et al: High Power Gas Laser Research. UA Army Missile Command Contract No. DA-AH01-1589. Raytheon Research Division, Waltham, Massachusetts, September 1968.

22. McCoy, John H.: Atmospheric Absorption of Carbon Dioxide Laser Radiation Near Ten Microns. Technical Report 2476-2, Electroscience Laboratory, Ohio State University, September 10, 1968.

23. Smith, D. C., and F. G. Gebhardt: Saturation of the Self-Induced Thermal Defocusing of Laser Radiation in a Wind. United Aircraft Research Laboratories Report UAR-H296, November 1969.

24. Carstens, J. P.: Trip to Sewer Tunnel Being Drilled in Chicago. United Aircraft Research Laboratories Report UAR-J57, March 5, 1970.

25. Hartman, H. I.: Mine Ventilation and Air Conditioning. Ronald Press Co., New York, 1961.

26. Sheehy, S. P., et al: Handbook of Air Pollution. Public Health Service Publication No. 999-AP-44, Bureau of Disease Prevention and Environmental Control, Public Health Service, US Department of Health, Education, and Welfare, 1969.

27. Van De Hulst, H. C.: Light Scattering by Small Particles. John Wiley & Sons, New York, 1957.

28. Krascella, N. L.: The Absorbtion and Scattering of Radiation by Small Solid Particles. Journal of Quantitative Spectros copy and Radiative Transfer, Vol. 5, 1965.

29. Krascella, N. L.: Extinction Scattering and Absorbtion of 10.6μ Electromagnetic Radiation by Spherical Water Droplets. United Aircraft Research Laboratories Report UAR-G7, January 16, 1968.

30. Simon, I: Spectroscopy in Infrared by Reflection and Its Use for Highly Absorbing Substances. Journal of the Optical Society of America, US/41, No. 5, May 1951, pp. 336-345.

31. Wisner, G. R., and L. J. Denes: Absorptance and Reflectance of Mirrors at 10.6 Microns. United Aircraft Research Laboratories Report UAR-G229, November 1, 1968.

32. Aries, R. S., and R. D. Newton: Chemical Engineering Cost Estimation. McGraw-Hill, New York, 1955.

33. Zimmerman, O. T., and I. Lavine: Chemical Engineering Costs. Industrial Research Service, Dover, New Hampshire, 1950.

34. Greer, C. M.: Letter to J. P. Carstens dated April 2, 1970, from Dittinger and Greer, Inc., as representatives of Edwin L. Wiegand Co.

35. Connecticut Law Journal, p. 7, Section 19-13-E45.

36. Barendsen, P.: Mechanized Drifting by the Full-Face Method. Tunnels and Tunneling, Part I, July 1969; Part II, September 1969.

37. Bruce, W. E., and R. J. Morrell: Principles of Rock Cutting Applied to Mechanical Boring Machines. Proceedings, Eleventh Symposium on Rapid Excavation. Sacramento State College, Sacramento, California, October 1969.

38. Robbins, R. J.: Robbins Tunnel Boring Machines - A Status Report with an Eye to the Future. Paper presented at Conference on Tunnel and Shaft Excavation, University of Minnesota, Minneapolis, Minnesota, May 1968.

39. Schumacher, B. W.: Electron Beams...A New Tool for Cutting Rock. Yale Scientific Magazine, March 1969.

40. Banas, C. M.: Preliminary Laser Rock Cutting Experiments. Memorandum to J. W. Davis, United Aircraft Research Laboratories, August 22, 1968.

41. Armstrong, D. E., et al: Rock Melting as a Drilling Technique. Report LA-3243, Los Alamos Scientific Laboratory, Los Alamos, New Mexico, March 1962.

42. Clarke, F. W.: The Data of Geochemistry. US Geological Survey Bulletin 770, Government Printing Office, Washington, 1924.

43. Tuttle, O. F., and N. L. Bower: Origin of Granite in the Light of Experimental Studies in the System $NaAlSi_3O_8$-SiO_2-H_2O. Memoir 74, The Geological Society of America, New York, 1958.

44. Deer, W. A., et al: Rock Forming Minerals. Volume 4 Framework Silicates. John Wiley & Sons, New York, 1963.

45. Robbie and Waldbaum: Thermodynamic Properties of Minerals and Related Substances at 298.15 K and One Atmosphere Pressure and at Higher Temperatures. US Geological Survey Bulletin 1259, Government Printing Office, 1968.

46. Teale, R.: The Breakage of Ridges of Rock. Published in Mechanical Properties of Non-Metallic Brittle Materials, W. H. Walton, Ed., Proceedings of a Conference organized by the Mining Research Establishment of the National Coal Board. Held in London, April 1958.

47. Crewe, A. V., et al: Electron Gun Using a Field Emission Source. Review of Scientific Instruments, Volume 39, No. 1, April 1968.

48. Schwarz, H.: Trans. 2nd Int'l. Vac. Cong., Washington, D. C., October 1961.

49. Goudsmit, S., and J. C. Saunders, Phys. Res., Vol. 57, No. 24 (1940).

50. Williams, E. J., Rev. Modern Phys., 17, 217 (1945).

GPO 904.231